APT2024

The 9th Asian Particle Technology Symposium

Engineering a Sustainable Future

Sydney, 1 – 4 December 2024

Amora Hotel Jamison Sydney

Contents

Cutting-edge discrete element methodologies for digital twin integration

Mikio Sakai[a]

[a]The University of Tokyo, Tokyo, Japan
*Corresponding author: mikio_sakai@n.t.u-tokyo.ac.jp

In the era of Industry 4.0, the concept of a digital twin has been proposed. Simulation-based digital twins are anticipated to be widely employed in future manufacturing processes. Naturally, this trend will extend to the powder industries. In the simulation-based digital twin of the powder process, the discrete element method (DEM) will be extensively utilized due to its high accuracy and reasonable computation costs. Our research group has developed core technologies for DEM-based digital twins. Our implicit algorithm [1] for the solid-fluid interaction term has significantly enhanced the calculation efficiency of DEM-CFD simulations. Additionally, our capillary force model [2], based on the toroidal approximation, has improved the accuracy and robustness of DEM simulations for wet particles. Our scalar-field-based wall boundary model enables the capture of minute changes in domain shape in DEM simulations. Furthermore, our surrogate model [3-5], composed of a reduced order model based on proper orthogonal decomposition, can successfully predict macroscopic particle behavior. We believe that advanced modeling and surrogate models will become essential technologies for establishing digital twins in the powder industries.

References

[1] Y. Mori, M. Sakai, Chem. *Eng. J.* **2021**, 406 126841.

[2] K. Tamura, Y. Mori, K. Takabatake, M. Sakai, *Phys. Fluids* **2022**, 34, 023319.

[3] R. Li, G. Duan, D. Yamada, M. Sakai, *Ind. Eng. Chem. Res.* **2023**, 62, 17008−17018.

[4] Kai-en Yang, Shuo Li, Guangtao Duan, Mikio Sakai, *J. Chem. Eng. Jpn* **2024**, 57, 2316155.

[5] Shuo Li, Guangtao Duan, Mikio Sakai, *Physics of Fluids* **2024**, 36 033340.

Numerical prediction on frictional characteristics of binary mixtures consisting of flexible cylindrical particles and rigid spheres

Yanping Zhu,[a] Xiwen Mu,[a] Pengyue Guo,[a] Hao Zhang,[a,*]

[a]Key Laboratory for Ecological Metallurgy of Multimetallic Mineral of Ministry of Education, School of Metallurgy,
Northeastern University, Shenyang, 110819, PR China
*Corresponding author: zhangh@mail.neu.edu.cn

A Discrete Element Method (DEM) model for deformable cylindrical particles is established to investigate the Jenike shear process of binary mixtures consisting of flexible cylindrical particles and rigid spheres[1]. The effects of the shape of flexible cylindrical particles and the proportion of cylindrical particles to spherical ones on the friction behavior of the mixture are discussed. Numerical results show that both the shear stress and internal friction angle increase with the aspect ratio (Ar) of the flexible cylindrical particles but decrease with the increase of the proportion of spherical particles. For the mono-system containing flexible cylindrical particles of Ar=6 but without spheres, the strong interlocking packing structure leads to high shear stress and internal friction angle. It is indicated that the inclusion of rigid spheres disrupts the interlocking structure between flexible cylindrical particles and acts as a lubricant during the shear process. Based on the numerical results, a predictive correlation is established to predict the frictional characteristics of binary mixtures consisting of flexible cylindrical particles and rigid spheres considering the effect of particle shape and proportion. The capability of the correlation is demonstrated via a comprehensive numerical study of a rotating drum based on DEM and two fluid flow, respectively. Furthermore, through a microscopic analysis of the numerical results, a deeper understanding of this phenomenon is gained. It is confirmed that the spherical particles can fill the voids between the flexible cylindrical particles, increasing the compactness of the mixture and promoting lubrication effects. The current research contributes to the better understanding of the mechanism of particle flow and is of paramount importance to improve the kinetic theories for complex granular flows.

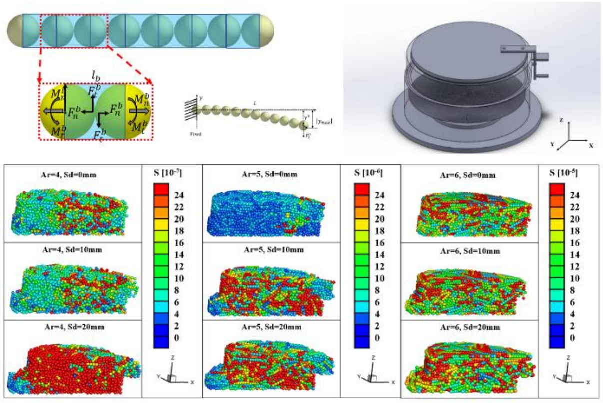

Figure 1. Distributions of S of flexible particles under different Sd and γ. (a) Ar=4; (b) Ar=5; (c) Ar=6.

References

[1] Y. Zhu, H. Zhang, P. Guo, X. An, S. Jiang, *AIChE J* **2024**, 70, 18296.

A study on the dynamics of steel frames with damping particles

Yun-Chi Chung*, Chun-Cheng Yang

Department of Mechanical Engineering, National Central University, Jhong-Li, 32001, Taiwan

This study introduces particle damping technology to mitigate the vibration of 5-story steel frames during earthquakes. A coupled discrete element method (DEM) and finite element method (FEM) were utilized to analyze the dynamic response of steel frames with damping particles. The study investigates the effects of filling ratio and cavity design of particle dampers on the corresponding dynamic characteristics. Furthermore, an actual earthquake scenario was simulated on the 5-story steel frame. The numerical results demonstrate that as the filling ratio decreases, the damping effect diminishes as well. Interestingly, maintaining the same cavity volume and particle mass, dividing a single cavity into several smaller ones can enhance the contact frequency between the particles and cavity walls, thereby resulting in a higher damping effect. During the simulated two-directional earthquake, it was observed that the first three modes exhibit significant vibration attenuation effects. This serves as validation that particle dampers offer effective vibration attenuation across a broad frequency range and in various directions.

Coarse grained DEM with rolling resistance and particle size distributions

Kimiaki Washino,[a,]* Yuze Hu,[a] Ei L. Chan,[a] Jun-ichi Watanabe,[b] Masahiro Takezawa,[b] Takuya Tsuji,[a] Toshitsugu Tanaka[a]

[a] Department of Mechanical Engineering, Osaka University, Suita, Osaka 565-0871, Japan
[b] Manufacturing Innovation Division, Panasonic Holdings Corporation, Kadoma, Osaka 571-0056, Japan
*Corresponding author: washino.k@mech.eng.osaka-u.ac.jp

Powders and granular materials are ubiquitous and play a crucial role in many industries. It is of paramount importance to understand macroscopic powder characteristics such as bulk density and angle of repose for better control and optimisation of industrial processes. However, little is known about the relationship between macroscopic powder characteristics and microscopic properties of particles (e.g., particle size, sliding friction and rolling friction). Therefore, empirical knowledge is often used in practical applications today to determine the design of equipment and process conditions, which necessitates an enormous number of trial-and-errors and costs time and money.

Discrete Element Method (DEM) has been extensively used for simulation of various particulate processes. It is a Lagrangian model and directly calculates the particle interactions using the microscopic properties to track the motion of individual particles. Therefore, it may be an ideal tool to help understand the so-called micro-macro transitions. However, one of the major challenges in DEM is the immense computational cost which increases rapidly as the number of particles in a system increases. Coarse grain models are particularly attracting attention as a way to reduce the computational cost in DEM. Coarse grain models employ artificially scaled-up particles that replicate bulk behaviour of the original particles. The Scaled-Up Particle (SUP) model, which is proposed in the authors' previous work [1-4], is a promising coarse grain model based on a set of universal scaling laws.

The present work is dedicated to investigating the validity of the SUP model for particle bed and heap formation where rolling resistance is exerted on the particles. An extensive number of simulations have been performed using the SUP model as well as other scaling methods listed in Table 1, and the results are compared with the bulk behaviour of the original particles. It is observed that the SUP model can capture the original bulk density and angle of repose well as shown in Figure 1. It is also proven that the model can be used to simulate the behaviour of particles with size distributions.

Table 1. Three different methods tested in this work. Method 1 is the scaling laws derived from the SUP model. $\boldsymbol{F}_I$, $\boldsymbol{M}_I$ and $\boldsymbol{F}_B$ indicate arbitrary inter-particle force, inter-particle torque and body force, respectively. The subscripts S and O stand for scaled-up and original particles, respectively.

Method 1	Method 2	Method 3
$\boldsymbol{F}_{IS} = l^2 \boldsymbol{F}_{IO}$	$\boldsymbol{F}_{IS} = l^2 \boldsymbol{F}_{IO}$	$\boldsymbol{F}_{IS} = l^3 \boldsymbol{F}_{IO}$
$\boldsymbol{M}_{IS} = l^2 \boldsymbol{M}_{IO}$	$\boldsymbol{M}_{IS} = l^3 \boldsymbol{M}_{IO}$	$\boldsymbol{M}_{IS} = l^3 \boldsymbol{M}_{IO}$
$\boldsymbol{F}_{BS} = l^3 \boldsymbol{F}_{BO}$	$\boldsymbol{F}_{BS} = l^3 \boldsymbol{F}_{BO}$	$\boldsymbol{F}_{BS} = l^3 \boldsymbol{F}_{BO}$

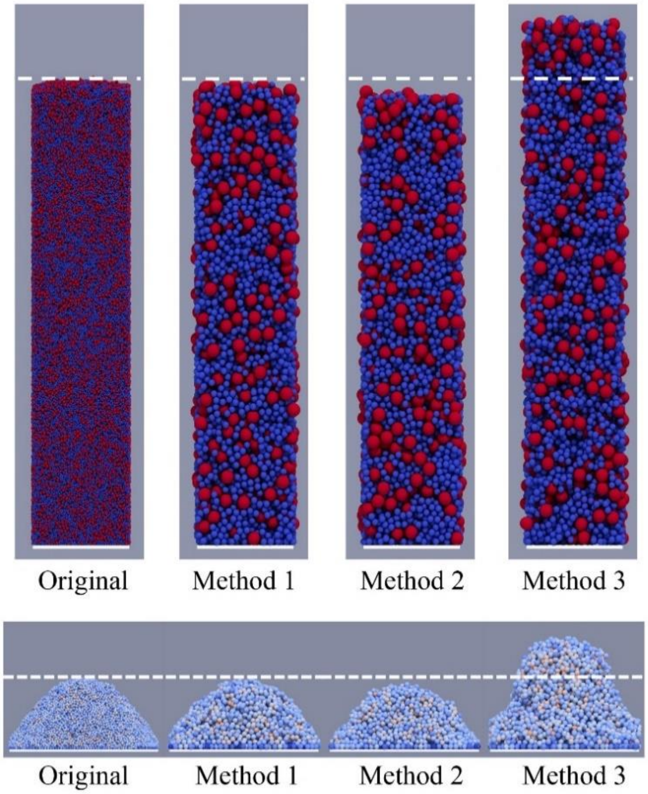

Figure 1. Bulk density (top) and angle of repose (bottom) of original and coarse grained particles. Method 1 is the scaling laws derived from the SUP model.

References

[1] E. L. Chan, K. Washino, *Chem. Eng. Res. Des.* **2018**, 132, 1060-1069.

[2] K. Washino, E. L. Chan, T. Kaji, Y. Matsuno, T. Tanaka, *Particuology* **2021**, 59, 2-15.

[3] Y. Hu, E. L. Chan, T. Tsuji, T. Tanaka, K. Washino, *Powder Technol.* **2022**, 404, 117483.

[4] K. Washino, E. L. Chan, Y. Nishida, T. Tsuji, *Powder Technol.* **2023**, 426, 118676.

CPFD prediction of coal-ammonia co-firing in a 550 MWe USC CFB boiler for carbon-free power generation

Joonwoo Kweon,[a] Byoung-Hwa Lee,[b] Chung-Hwan Jeon [a,b,*]

[a]School of Mechanical Engineering, Pusan National University, Busan, Republic of Korea
[b]Pusan Clean Energy Research Institute, Pusan National University, Busan, Republic of Korea
*Corresponding author: chjeon@pusan.ac.kr

Ammonia is a carbon-free fuel that reduces CO_2 emissions by replacing fossil fuels. While coal-ammonia co-firing decreases CO_2 emissions, leads to increased NOx and N_2O emissions. Therefore, it is necessary to study the combustion characteristics of co-firing. In the present study, CPFD simulations for coal-ammonia co-firing were performed to predict gas-solid flow, combustion characteristics and NOx and N_2O emissions in a 550 MWe ultra-supercritical (USC) circulating fluidized bed (CFB) boiler using CPFD Barracuda VR. The CPFD simulations were calculated using the energy minimization multiscale (EMMS) model, which considers the asphyxiation and drag reduction characteristics of gas-solid fluidization systems [1]. Prior to co-firing case study, a simulation for coal-fired was implemented and validated by comparison with the experimental data (e.g., pressure and temperature profile, gas composition at the cyclone outlet) [2].

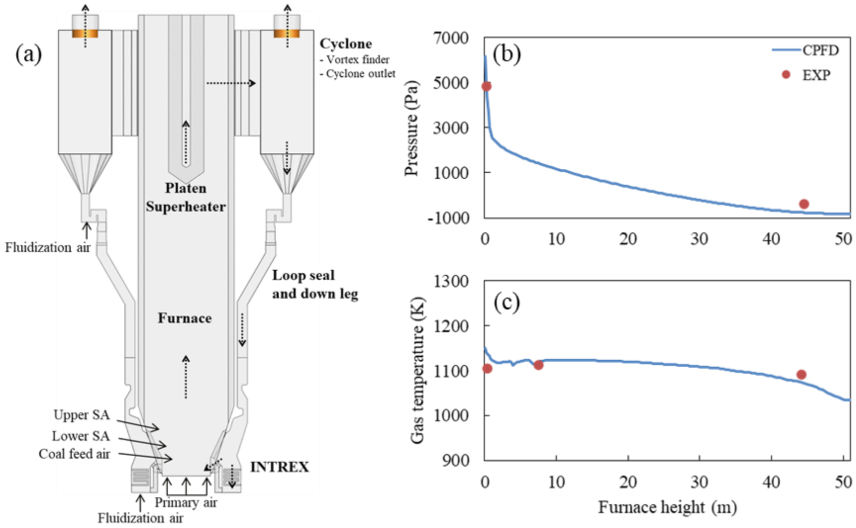

Figure 1. (a) Schematic of 550 MWe USC CFB boiler, (b) pressure and (c) temperature profiles

Acknowledgement: This work was supported by the "National Research Foundation of Korea" funded by the Ministry of Science, ICT, and Future Planning (grant number 2022K1A4A8A01080312)

References

[1] N. Yang, W. Wang, W. Ge, L. Wang, J. Li, *Industrial & Engineering Chemistry Research* **2004**, 43, 5548-5561
[2] B. H. Lee, Y. H. Bae, K. M. Kim, Y. Jiang, Y. H. Ahn, C. H. Jeon, *Fuel* **2023**, 342, 127878.

Characterisation of granular flows using MRI

Maral Mehdizad,[a] Daniel Clarke,[b] Petrik Galvosas,[b] Daniel Holland,[a*]

[a]University of Canterbury, Christchurch, New Zealand
[b]Victoria University of Wellington, Wellington, New Zealand
*Corresponding author: daniel.holland@canterbury.ac.nz

Establishing and validating models for granular flows is challenging because granular flows are inherently opaque. They also exhibit complex and varied mechanics owing to the different conditions these flows maybe found in, from "gaseous" in one limit to "solid-like" motion in the other. Magnetic Resonance Imaging (MRI) is a promising tool for characterising granular flows as it permits visualisation of the flow structure in opaque three-dimensional (3D) systems. Flow MRI is now quite well established and can be used to study both steady and unsteady flows. However, a full description of the flow mechanics requires the knowledge of the solid volume fractions (3D density maps) as well. The aim of this work is to establish methods for mapping solid volume fractions and flow fields of the same systems.

The systems studied include silos and Couette cell devices. Measurements are shown to be quantitative by determining the mass flow rate and comparing these with macroscopic measurements of the mass flow rate (Figure 1, [1]). The resulting data were then used to examine models of the flow in hoppers [2] and Couette cells (Figure 2, [3]), thus providing cross-validation to simulations and guidance for future research.

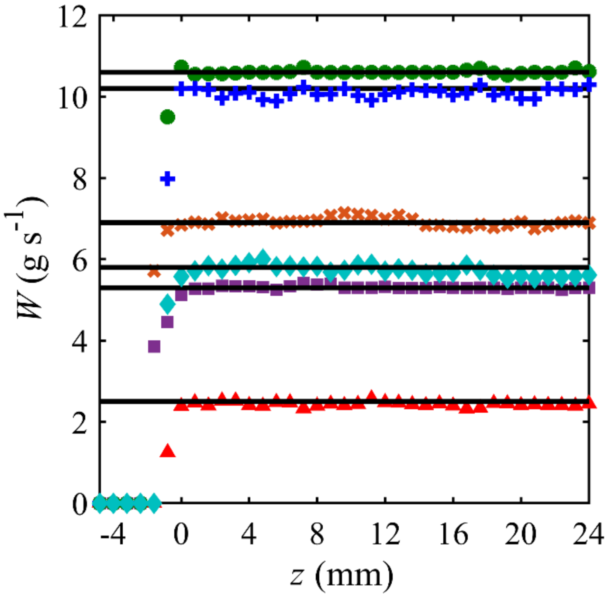

Figure 1. MRI (symbols) and gravimetric (black lines) mass flow rate measurements for silos with half angles and diameters of 10° (D = 9.5 mm) (✚), 30° (D = 9.5 mm) (✖), 60° (D = 7.5 mm) (▲), 60° (D = 9.5 mm) (■),60° (D = 11.5 mm) (●), and 90°(D = 9.5 mm) (◆).

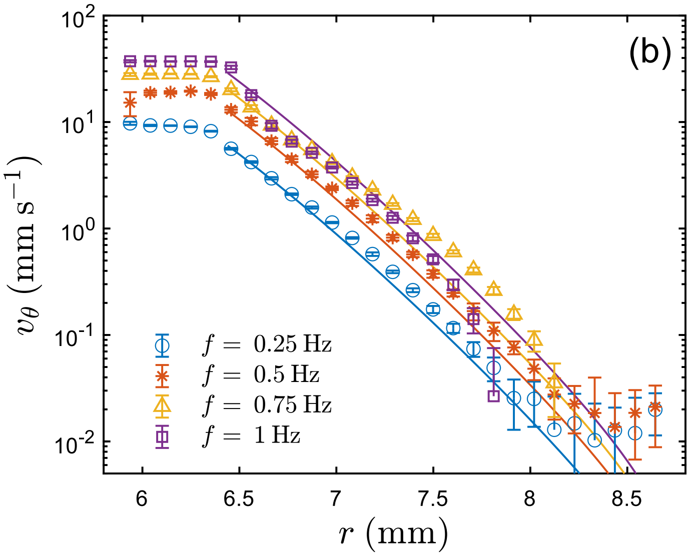

Figure 2. Velocity profile across the annular gap in a Couette cell. Markers denote experiments, solid lines denote numerical solution to the nonlocal granular fluidity equation.

References

[1] M. Mehdizad, L. Fullard, P. Galvosas, D.J. Holland, J. Magn. *Reson* **2021,** 325 106935.

[2] M. Mehdizad, L. Fullard, P. Galvosas, D.J. Holland, *Powder Technol* **2021,** 392 69–80.

[3] D.A. Clarke, J. Poata, P. Galvosas, D.J. Holland, *Phys. Fluids* **2024**, 36 053317.

CFD-DEM model development and applications in polydisperse solid-fluid systems

Zhouzun Xie, Yansong Shen*

School of Chemical Engineering, University of New South Wales, Sydney, NSW 2052, Australia,

This report introduces the development and application of a CFD-DEM model in polydisperse solid-liquid systems. Polydisperse particle systems are widely present in industries such as chemical engineering, metallurgy, and energy. However, due to the complex interactions and heterogeneity among particles, simulating their flow, heat and mass transfer behaviours poses significant challenges. Based on the CFD-DEM coupling method, this study develops a collection of numerical models tailored for polydisperse particles, capable of accurately simulating the hydrodynamics, heat and mass transfer processes between solid and liquid phases.

The report focuses on the key techniques in model development, including handling particle size distribution, particle-fluid coupling methods, model validation, and parameter optimization. It also presents case studies demonstrating the application of the CFD-DEM model in various engineering scenarios such as water treatment, fluidised reactors, blast furnace and nanomedicine in cancer treatment. These examples showcase the effectiveness of the model in simulating the dynamic behaviours of polydisperse particle systems.

This model serves as reliable tools for the design and optimization of multiphase flow systems, helping to improve industrial process efficiency and resource utilization while advancing sustainable engineering technologies.

2-D simulations of fibrous particle penetration through mesh screens: a hybrid lattice-Boltzmann Lagrangian method

Thanh-Phat Duong[a], Yen-Hsi Li[a], Sheng-Yao Chou[a], Hairong Tao[c], Kuang C. Lin[a,b,*]

[a]Department of Engineering and System Science, National Tsing Hua University, Hsinchu 30013, Taiwan [b]Institute of Nuclear Engineering and Science, National Tsing Hua University, Hsinchu 30013, Taiwan [c]College of Chemistry, Beijing Normal University, Beijing 100875, China *Corresponding *Corresponding author: kclin@umich.edu

Inhalation of airborne fibers such as asbestos has been the concern for toxicological response that can affect lung tissues. It has been known that fiber nylon mesh screens are one of inexpensive and easily disposable filtration medium for separating nanoparticles and micron particles in gas streams. This study aims at developing a first-ever computational model (Fig. 1) that predicts experimental measurements for fibrous particle filtration (Fig. 2) in nylon mesh screens with 20, 30, 41 and 60 μm [1,2]. The mean particle lengths investigated are 11.4, 15.3, 24.8, 54.3 microns and particle aerodynamic diameters are 0.8 to 10 microns. The aerodynamic diameter for the particle ranges from 0.4 □m to 10 □m. The complex filtration physics is modelled by a hybrid lattice Boltzmann-Lagrangian scheme. The fluid motion, in a nearly creeping flow field, is driven by the gas speed of 7 cm/s. The mesh structures and the particles are simplified from 3-D into 2-D via the mapping process that adopts the modified cross-sectional pore-size based model previously developed by our group. Based on our previous studies [3,4,5], the 2-D model describing a semi-infinite array of clean fibers represents a cross-sectional domain of a 3-D mesh screen. For the particle dynamics, the 2-D particle equations consider shape factors for fibrous particles and instantaneous orientation of each fibrous particle is computed. The predicted screen filtration efficiency values well agree with experimental measurements for 20- and 30-μm screen pore sizes that capture particles of 0.8- to 10-□m aerodynamic diameter with particle length 11 and 15 μm. For the relatively coarse screen pore sizes (41, 60 μm), the computational results show good agreement with the experimental screen collection efficiency which is dominated by the interception mechanism for the aerodynamic diameter between 0.8 and 4 μm. The present study further proves that the large discrepancy between computed and measured screen filtration efficiency is caused by the insufficient particle samples used in experiments. Furthermore, the particle distributions along the fiber surface are analysed (Fig. 3) to unveil the details of particle capture mechanisms. This study is expected to become the foundation for improving fibrous particles filtration and air purification devices.

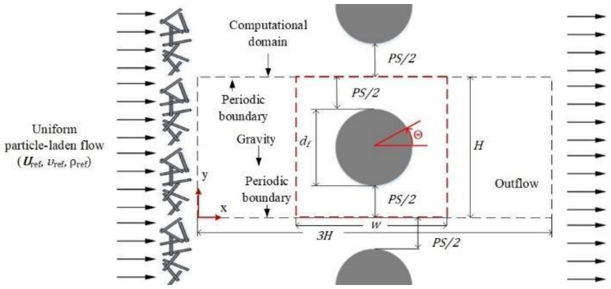

Figure 1. Schematic of physical model and boundary conditions.

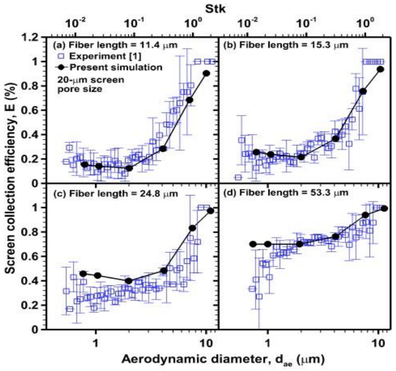

Figure 2. Comparison between measured [1] and computed screen collection efficiency as a function of aerodynamic diameter (0.4-11 μm) for the screen pore size at 30 μm with different particle lengths: (a) 11.4 μm (b) 15.3 μm (c) 24.8 μm and (d) 53.3 μm.

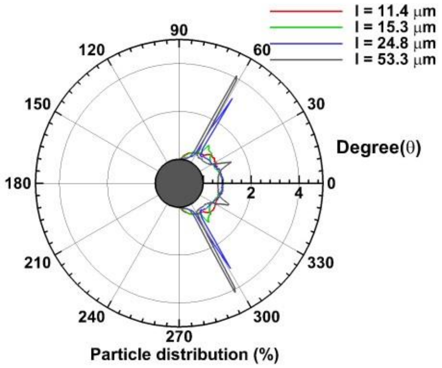

Figure 3. Distribution of particle numbers capture on a fiber screen pore size of 20 μm and aerodynamic diameter of 10 μm for various fiber lengths.

References

[1] B.K. Ku, G. Deye, L.A. Turkevich, *Journal of Aerosol Science* **2017,** 114: p. 250-262.
[2] B.K. Ku, G. Deye, *Journal of Aerosol Science* **2019**, 53(10): p. 1217-1227.
[3] K.C. Lin, H. Tao, K.W. Lee, *Aerosol Science and Technology* **2014**, 48 (12), p. 1299-1307.
[4] K.C. Lin, J.S. Tsai, *Journal of Aerosol Science* **2018**, 124, p. 146-159.
[5] J.H. Li, T.H. Yu, K.C. Lin, *Aerosol Science and Technology* **2022**, 56 (12), 1174-1189.

Super-quadric CFD-DEM-VOF modelling of gas-solid-liquid systems

Xinxin Tang, Shuai Wang, Yansong Shen*

School of Chemical Engineering, University of New South Wales, Sydney, NSW 2052, Australia
*Corresponding author: E-mail: ys.shen@unsw.edu.au

In many chemical engineering processes, gas-solid-liquid flow involving nonspherical solid particles is commonly practised and should be modelled for process understanding and optimisation; however, reliable modelling along with parallelization is still lacking. This work combines an unresolved CFD-DEM-VOF coupling framework, featuring a super-quadric particle shape model to model the gas-nonspherical particle-liquid flow and a “ghost domain” algorithm to improve the parallelization efficiency. The model is applied to two cases – cuboid particle sedimentation and dambreak formation, for model effectiveness demonstration. According to the simulation results, the model effectively captures the interactions between particles and phases in the relevant scenarios. This is reflected by the agreements of numerical simulations and experimental or analytical data in these two cases. Moreover, the parallelization technique utilizing the "ghost domain" displays remarkable steadiness and noteworthy efficiency. As the processor increases from 2, 4, 8, 16, to 32 processors, the running time obviously decreases almost linearly. This research introduces an innovative computational approach for simulating systems containing gas, non-spherical particles, and liquid. It demonstrates the method's potential to analyze interactions between particles and fluids in the unresolved framework.

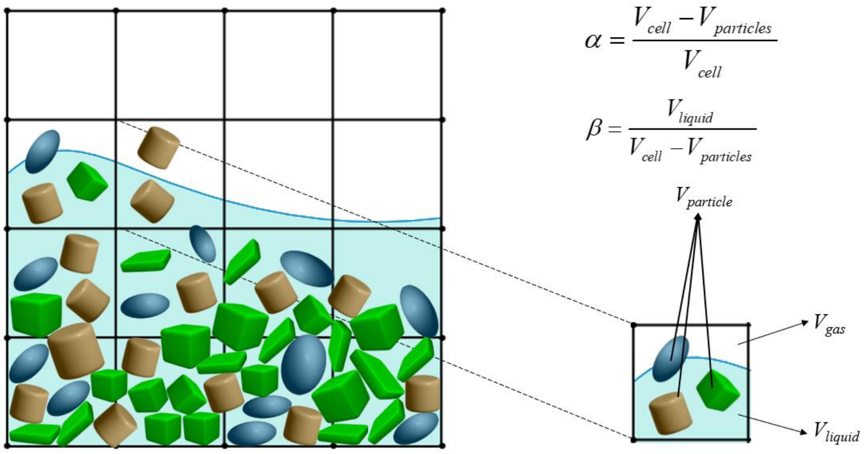

Figure 1. The depiction of the CFD-DEM-VOF model utilized for gas-nonspherical particle-liquid modelling

Simulation analysis of particle behavior during wet ball milling

Kizuku KUSHIMOTO,[a,]* Junya KANO,[a]

[a]Institute of Multidisciplinary Research for Advanced Materials, Tohoku University, Sendai, Japan
*Corresponding author: kizuku.kushimoto.d2@tohoku.ac.jp

A wet ball mill is a type of the milling method, and solid particles are mixed in liquid and are ground by the collisions of balls. The wet ball mill is characterized by its high milling speed, its ability to be scaled up, and the small size of the particles that can be ground. Conversely, the challenge of the wet ball mill is that it is difficult to control the grinding behavior of the particles. This is because there are not only many parameters for wet ball milling, such as ball amount, ball type, and particle concentration, but also the effects of these parameters on milling are not comprehended sufficiently. In particular, the influences of the ball collision conditions, such as relative velocity, rotational speed, and ball diameter, have not been elucidated because it is difficult to change only the collision conditions in experiments. On the other hand, the simulation could be effective to analyze the influences of the collision conditions on milling because the simulation can analyze the particle behavior when the collision conditions are only changed. Furthermore, we developed the simulation method for analyzing the particle behavior during the wet ball milling, which is called Advanced Discrete Element Method coupling with Computational Fluid Dynamics (ADEM-CFD) [ref]. **Figure 1** shows a snapshot of the behavior of particles sandwiched and ground by two balls in liquid using ADEM-CFD. Therefore, this presentation reports the results that the influences of the collision conditions of the balls on the grinding behavior of the particles during the wet ball milling are analyzed by the simulation using ADEM-CFD.

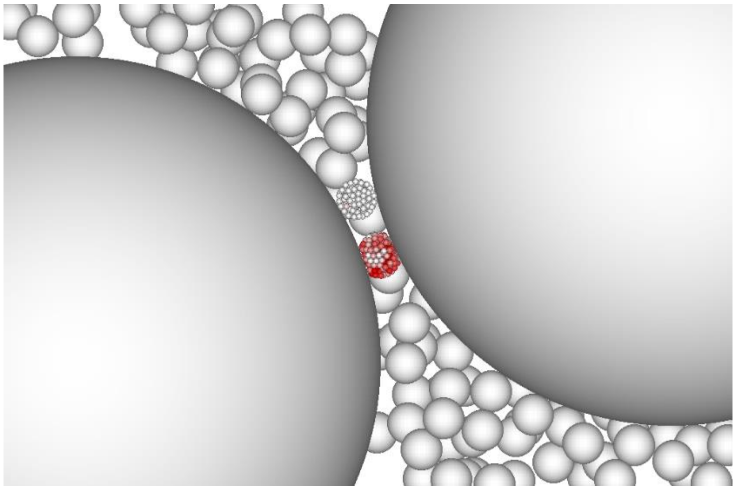

Figure 1. Grinding behavior of particles between two balls represented by ADEM-CFD (The color means the damage degrees of the particles).

References

[1] K. Kushimoto, S. Ishihara, J. Kano, *Adv. Poweder Technol.* **2019**, 30, 1131-1140.

The efficient calibration and industrial application of discrete element method

B.D. Jenkins[a,b], A.L. Nicuşan[a], A. Neveu[b], G. Lumay[b, c], F. Francqui[b], J.P.K.
Seville[a], C.R.K. Windows-Yule[a]

[a]School of Chemical Engineering, the University of Birmingham, Edgbaston, Birmingham, B15 2TT, UK
[b]Granutools SPRL, Rue Jean Lambert Defrˆene 107, 4340 Awans, Belgium
[c]Grasp laboratory, ^{CESAM} research unit, University of Li`ege, Place du 20 Aouˆt 7, 4000 Li`ege, Belgium

Discrete element method (DEM) – a type of numerical granular simulation – is a powerful tool that can accurately model complex granular dynamics. DEM is currently being utilised to better understand the complex behaviour of granular materials in industrial equipment and can be partnered with modern machine learning techniques to automatically explore and test new designs.

As with anything, modelling or experimental, there are limitations with DEM. One of the most important is the requirement to meticulously calibrate the particle material properties. These are the properties that define how individual particles interact such as the force of friction due to particles moving past each other and the cohesive forces that particles experience due to van der Waals, liquid bridging, or electrostatic forces. Not being able to accurately define these properties in a DEM simulation leads to inaccurate simulations that would not replicate the behaviour of a physical material [1].

Two approaches to calibration are currently employed, direct and indirect calibration, but both are either time-intensive and/or inaccurate. The first, direct calibration, is an approach where the properties of a granular material are experimentally measured on a single particle scale. This is a time-intensive approach that yields values that may not correspond to the values required for DEM to produce quantitatively accurate results. The second, indirect calibration, makes use of bulk measurements of granular materials to back compute particle properties. The indirect calibration approach, however, requires many simulations to be run to back compute the particle properties [1].

This work presents a new method for DEM calibration that builds on the indirect calibration method. Using symbolic regression and big data, a micro-macro mapping is created that allows simulations to be calibrated without requiring huge computational resources. Micro-macro mapping, as the name suggests, is a method of mapping the properties of particles at the microscopic level to bulk measurements at the macro level. Put simply, one could determine the precise DEM particle properties for a powder by directly calculating a range of bulk measurements of the powder that were measured experimentally within in a few seconds.

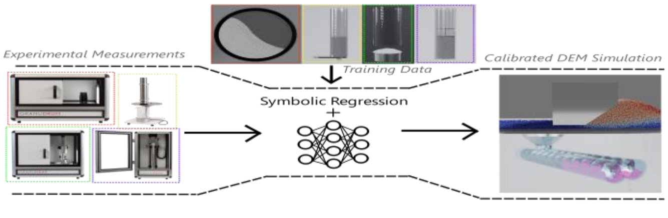

Figure 1. Diagram of the novel calibration approach methodology.

In addition to this new efficient calibration approach, the application of it to calibrate simulations of industrial systems will be shown in addition to the validation of these simulations to the ground truth of experimental results.

References

[1] C.R.K Windows-Yule and Aurelien Neveu. *Papers in Physics* **2022,** 14, 140010.

Evaluation and correction of systematic errors in unsteady cavitation flow visualization experiments

Longhao Xiang,[a,b] Songying Chen,[a,b,*]

[a]Key Laboratory of High Efficiency and Clean Mechanical Manufacture, Ministry of Education,
School of Mechanical Engineering, Shandong University, Jinan 250061, China
[b]National Demonstration Center for Experimental Mechanical Engineering Education,
Shandong University, Jinan 250061, China
*Corresponding author: chensy66@sdu.edu.cn

Flow visual experiment is an effective method to investigate the characteristics of unsteady cavitation flows. However, assembly errors of high-speed cameras can cause image distortion, and refraction through different media can prevent light from focusing on the optical center, reducing image quality. This paper establishes a scientific procedure for camera calibration and multi-layer planar refraction imaging distortion correction to minimize system errors in flow visualization experiments. A nonlinear camera model is used to analyse the causes of lens distortion in high-speed cameras and the necessity of correction. Radial and tangential distortions of the lens are corrected based on Zhang's method[1]. A multi-layer planar refraction imaging model is established to discuss the prerequisites for applying camera calibration parameters in air to underwater calibration. Using the Pinax model[2], the forward projection equation of air-glass-water multi-layer planar refraction is derived to achieve the transformation between physical camera image points and virtual camera image points. By comprehensively considering the results of camera calibration and multi-layer planar refraction imaging distortion correction, the system error of flow visualization experiments is reduced by 3%, and the absolute error in spatial scale measurement is reduced by 70%.

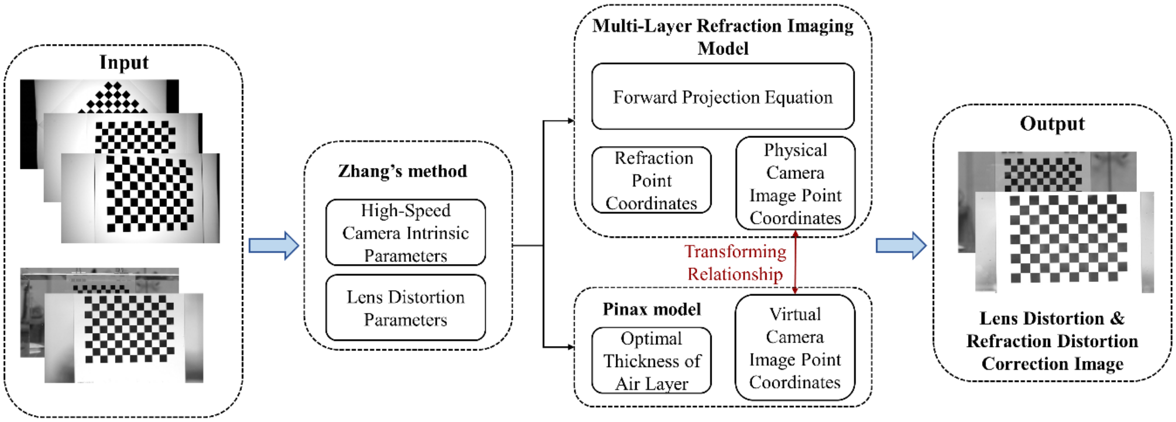

Figure 1. Graphical Abstract

References

[1] Zhang Z. *IEEE Transactions on pattern analysis and machine intelligence* **2000**, 22(11), 1330-1334.

[2] Łuczyński T, Pfingsthorn M, Birk A. *Ocean Engineering* **2017**, 133, 9-22.

Accurate and efficient realization of stress jump condition in the IB-LBM modelling of flow around and through porous bodies

Xiaowen Liu,[a, b,] * Qingang Xiong,[a,b]

[a] State Key Laboratory of Pulp and Paper Engineering, South China University of Technology, Guangzhou, 510640, China
[b] School of Light Industry and Engineering, South China University of Technology, Guangzhou, 510640, China
*Corresponding author: liuxw2021@scut.edu.cn

An immersed boundary-lattice Boltzmann method (IB-LBM) is proposed to simulate the incompressible flow around and through homogeneous porous bodies with stress jump condition. The flow in the porous domain as well as the pure-fluid domain is governed by the generalized Navier–Stokes equations [1] which is solved using the LBM. At the porous-fluid interface, a shear stress jump together with a continuity of normal stress [2] is imposed. The effects of the viscous and inertial jump parameters are both taken into account. These physical boundary conditions are implemented through the immersed boundary method where the fourth-order Runge-Kutta scheme is embedded. The proposed IB-LBM is validated by carrying out several test cases. Good agreements with literature on numerical results demonstrate its accuracy and reliability. This numerical method is easy to implement and efficient in terms of CPU cost and memory management. It thus has great potential to be executed on multi-GPU to simulating flows through moving porous bodies.

Table 1. The wake length and separation angle for flow around and through a porous circular cylinder at $\varepsilon = 0.7$ and $Da = 1\times10^{-4}$.

Re	**Reference**	L_f/D[a]	θ_s **(deg)**[b]
20	Yu et al. [3]	0.884	42.0
	Chen et al. [4]	0.867	42.6
	Present	0.883	42.2
40	Yu et al. [3]	2.196	53.0
	Chen et al. [4]	2.145	52.8
	Present	2.233	51.4

[a] *Wake length normalized by the diameter of circular cylinder.*

[b] *Separation angle from the rear stagnation point of the cylinder.*

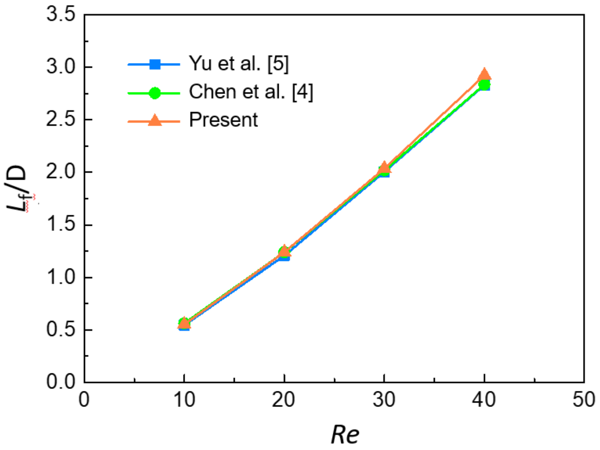

Figure 1. Variation of the wake length as a function of *Re* for the flow around and through a porous square cylinder at $\varepsilon = 0.7$ and $Da = 5\times10^{-4}$.

References

[1] L. Wang, L. P. Wang, Z. Guo, and J. Mi, *Int. J. Heat Mass Transfer* **2015**, 82, 357.

[2] J. A. Ochoa-Tapia and S. Whitaker, *J. Porous Media* **1998**, 1, 31.

[3] P. Yu, Y. Zeng, T. S. Lee, X. B. Chen, H. T. Low, *Comput. Fluids* **2011**, 42(1), 1.

[4] H. Chen, P. Yu, C. Shu, *Phys. Fluids* **2021**, 33(8), 083603.

[5] P. Yu, Y. Zeng, T. S. Lee, H. X. Bai, H. T. Low, *Int. J. Heat Fluid Flow* **2010**, 31, 141.

A SPH-DEM-FEM coupled model for non-regular particle-fluid-structure interactions based on geometric solid-liquid boundary condition

Jie Wu, Lu Liu, Shunying Ji*

State Key Laboratory of Structural Analysis, Optimization and CAE Software for Industrial Equipment, Dalian University of Technology, Dalian 116024, China
* Shunying Ji: jisy@dlut.edu.cn

In natural and engineering applications, granular materials often have irregular shapes, leading to common scenarios where irregular particles, fluids, and structures interact. As a result, the analysis of interactions between these components has always been a prominent topic in the field. In dealing with complex fluid-structure coupling interfaces involving irregular particles, fluids, and structures, the key challenge lies in efficiently handling the variability while maintaining accuracy. This study is based on an algorithm for coupling irregular particles to fluids[1], utilizing the dilated polyhedron discrete element method[2] to simulate irregular particles, an explicit incompressible smoothed particle hydrodynamics method[3] for the fluid phase, and a fitted boundary model to analyze the interaction between irregular particles and fluids[4]. In addition, finite element methods are utilized to create a structural response analysis model and develop coupling algorithms between irregular particles and structures, as well as between fluids and structures, thereby completing the coupling algorithm among the three elements. Regarding the interaction between irregular particles and structures, the interaction forces and points are calculated directly based on the extended discrete element algorithm. These are then interpolated onto the finite element mesh nodes as external loads for finite element analysis[5]. For the interaction between fluids and structures, the original fitted boundary model's limitations in determining the pressure distribution on the finite element mesh faces are addressed. This study incorporates the construction of a level set function to replace the original polynomial fitting. This function takes into account the mesh area and relative positions to calculate the fluid pressure on each mesh face. Validation models are then constructed based on the above techniques, comparing the finite element calculation results with theoretical solutions or results from commercial finite element software to verify the accuracy of the model. Finally, the model is applied to the coupling interaction of offshore wind turbines with sea ice and currents. This generates preliminary simulation results of the turbine's dynamic response.

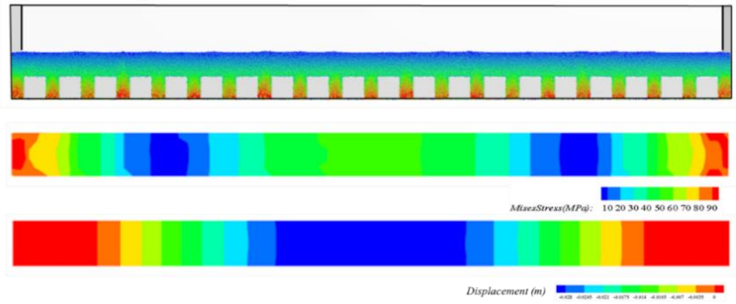

Figure 1. The simulation of elastic plates in three-dimensional solid-liquid two-phase media.

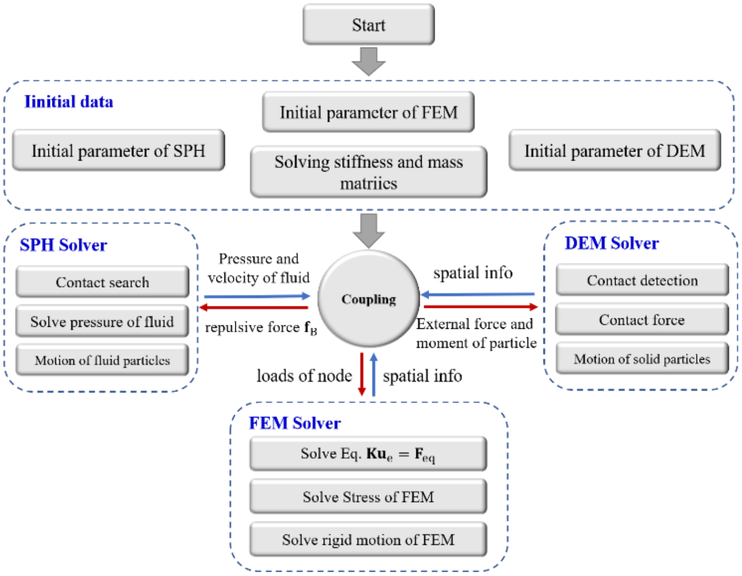

Figure 2. Simplified flowchart of coupled DEM-SPH-FEM model.

References

[1] L. Liu, J. Wu, S. Y. Ji, *Powder Technology*, **2022**, 400, 117249.

[2] L. Liu, S.Y. Ji, *Applied Ocean Research* **2018**, 75, 53-65.

[3] Nomeritae, E. Daly, S. Grimaldi, H.H. Bui, *Advances in Water Resources* **2016**, 97, 156-167.

[4] A. Eitzlmayr, G, Koscher, J. Khinast, *Computer Physics Communications* **2014**, 185 (10), 2436-2448.

[5] D. B. Yang, L. Liu, S. Y. Ji, *Ocean Engineering* **2023**, 268, 113469.

Discrete element methods for largely deformed granular materials with arbitrary morphologies

Shunying Ji

State Key Laboratory of Structural Analysis, Optimization and CAE Software for Industrial Equipment, Dalian University of Technology, Dalian 116024, China

The numerical simulation of deformable granular materials with arbitrary morphologies remains a challenge for the Discrete Element Method (DEM). To address this, we develop a Minkowski sum model for calculating collision forces and large deformations of arbitrarily shaped granular materials and structures. In this model, dilated superquadrics, spherical harmonics, and polyhedrons are employed to construct particles with convex and concave shapes. Each solid particle is divided into a series of tetrahedral elements, with dilated triangular elements on the surface used for contact detection and collision force calculations. Additionally, the granular skeleton is constructed using cylinders and nodal spheres corresponding to these tetrahedral elements. The chain-linked skeleton method enables the transfer of external forces from surface nodes to the interior of the particle, leading to the relative motion of the internal nodal spheres under internal forces and resulting in large deformations. To verify the conservation, accuracy, and robustness of this model, several numerical examples are conducted and compared with theoretical and finite element results, demonstrating good agreement. This model allows for the simulation of complex granular systems involving various dilated DEM models, capturing both the flow and elastic-plastic deformation of granular materials in deformable structures.

GPU-accelerated CFD-DEM modeling of gas-solid reacting flow with complex geometry

Dazhao Gou, Yansong Shen*

School of Chemical Engineering, UNSW Sydney, NSW 2052, Australia
*Corresponding author: ys.shen@unsw.edu.au

The coupling of Computational Fluid Dynamics (CFD) and Discrete Element Method (DEM) is a widely used approach for simulating gas-solid reacting flows in various industrial processes, yet its high computational cost has limited applications to large-scale systems involving numerous particles and complex geometries. This work presents a robust, highly efficient GPU-powered CFD-DEM coupling approach, which, for the first time, effectively simulates large-scale gas-solid reacting flow systems with intricate geometries. In the developed model, fluid flow calculations are performed using CPU parallelization, while particle flow simulations leverage GPU parallelization, and the coupling between CFD and DEM is fully implemented on GPU to enhance computational efficiency. A novel coupling strategy between the CFD solver and DEM solver has been developed, featuring advanced techniques for improved numerical stability, particularly for systems involving unstructured CFD meshes and complex geometries.

The developed model is validated through experimental measurements [1], showing good agreement with experiments, and its computational performance is compared to previous GPU-based CFD-DEM simulations [2, 3], demonstrating superior efficiency. The model is subsequently applied to simulate the dynamic behavior of gas-solid flow, coke combustion, and raceway dynamics in industrial-scale blast furnaces, considering the influence of complex tuyere structures. The results indicate that the largest and most stable raceway volume can be achieved with a 5° downward tuyere, although the -5° tuyere nose experiences greater wear compared to a 10° downward tuyere. This work demonstrates the capability of the model to handle large-scale, dense gas-solid systems with high particle numbers and intricate geometries, providing an efficient and robust solution for simulating industrial applications of gas-solid reacting flow systems.

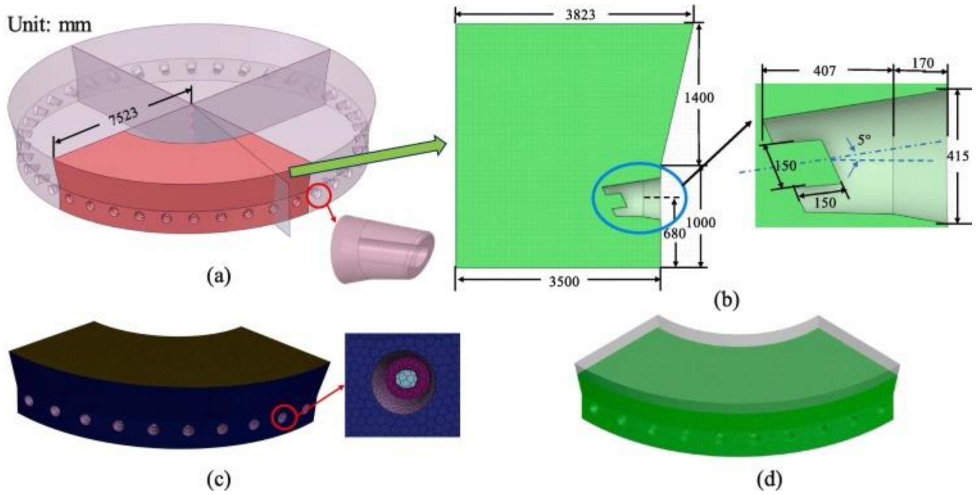

Figure 1. Geometry and initial settings of the raceway for the industrial blast furnace.

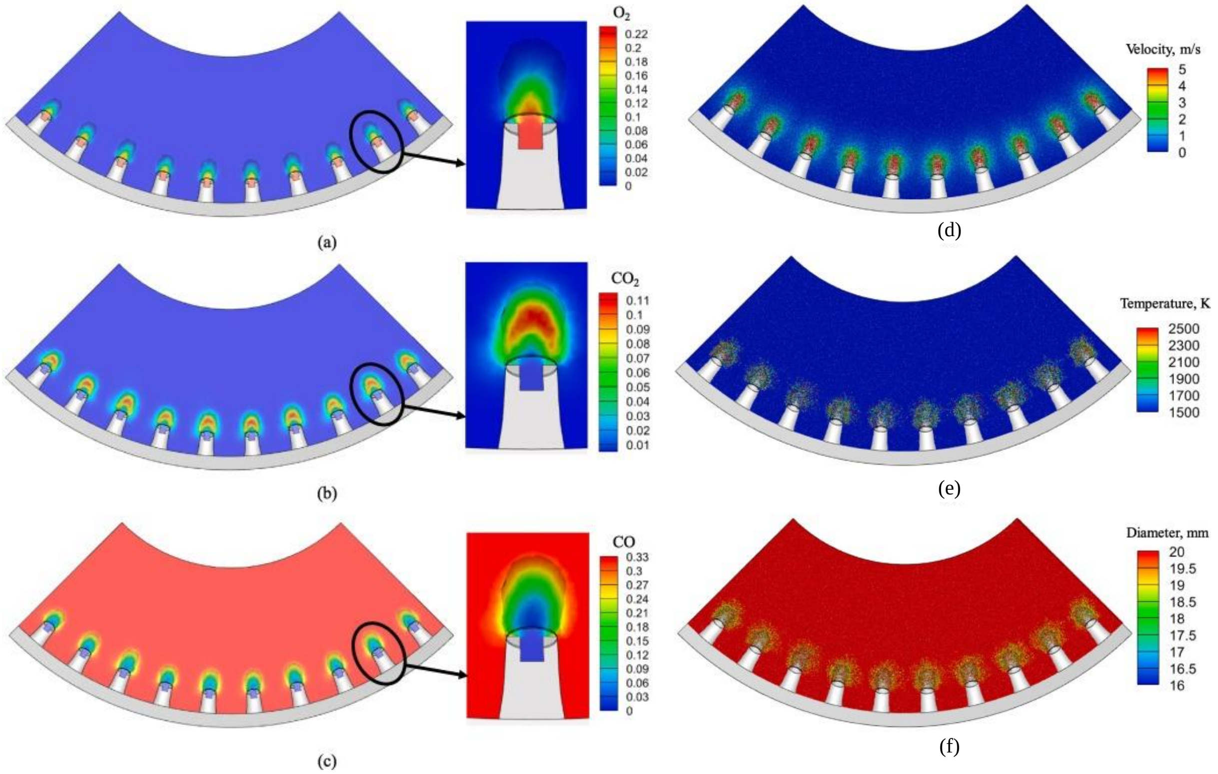

Figure 2. (a-c) Distribution of O_2, CO_2, and CO; (d-f) distribution of particle velocity, particle temperature, and particle diameter at the cross-sectional plane of the tuyere center at 20 s.

References

[1] Nogami, H., H. Yamaoka, and K. Takatani, *ISIJ International* **2004**, 44(12), 2150-2158.
[2] Wang, S. and Y. Shen, International Journal of Heat and Mass Transfer **2022**, 184, 122302.
[3] Porcu, R., et al., *Chemical Engineering Science* **2023**. 273, 118614.

Influence of the calculation method of liquid bridge force model on DEM simulation of wet powder behavior

Tomotaka Otsu, Hideya Nakamura*, Shuji Ohsaki, Satoru Watano

Osaka Metropolitan University, Sakai, Japan
*Corresponding author: hideyanakamura@omu.ac.jp

Wet powders are widely used in various fields. Thus, there is a great need for simulation technology that can accurately calculate the wet powder behavior. The discrete element method (DEM), which solves the equations of motion of individual particles to obtain the behavior of the entire powder, has proven to be able to accurately calculate the dry powder behavior. For DEM simulation of the wet powder behavior, the calculation of the interparticle liquid bridge force is important. To calculate the liquid bridge force, the liquid bridge characteristics, such as the bridge formation distance, liquid bridge volume, and minimum bridge distance, should be defined. In addition, the calculation methods for the liquid bridge force during particle contact should be defined. However, treatment of these characteristics and calculation methods in DEM simulations is not standardized [1-3], which prevents accurate DEM simulations for wet powders.

In this study, we focused on the two calculation methods for DEM simulation of wet powder: calculation methods of bridge formation distance and liquid bridge force during particle contact. By combining the two types of calculation methods for the bridge formation distance [1-2] and the liquid bridge force during particle contact [2-3], respectively, a total of four calculation methods were evaluated. First, microscopic adhesion energy acting between the two particles was evaluated for each calculation method. Then, influence of the calculation methods on the DEM simulation of wet powder behavior was investigated by comparing the results of the drawdown test and rotating drum test.

The liquid film contact method (LFC) [2] and the solid contact method (SC) [1] were investigated to calculate the bridge formation distance (Fig. 1). The LFC considers that liquid bridges are formed between solid particles when the liquid film layer covering the particle comes into contact. In contrast, the SC assumes that the liquid film layer is thin and the liquid bridge force acting during the approach of two particles is ignored, whereas the liquid bridging force only acts when the solid surfaces of the particles come into contact. In addition, the Hertzian-and-liquid-bridge force method (H-LB) [3] and JKR model [2-3] were examined to calculate the liquid bridge force during particle contact (Fig. 1). In the H-LB, the liquid bridge force at zero interparticle distance is added to the Hertzian contact force. In the JKR model, the interparticle contact force with liquid bridge adhesive force is calculated by using the surface tension coefficient of the bridging liquid as the interparticle surface energy. In this study, four types of implementations combining the LFC, SC, JKR, and H-LB, namely LFC-JKR, LFC-H-LB, SC-JKR, and SC-H-LB, were investigated.

Firstly, we calculated the adhesion energy E_{ad} acting between two particles bonded by a liquid bridge to analyze the microscopic difference in the four types of calculation methods. E_{ad} was defined as the value obtained by integrating the inter particle liquid bridge force from bridge formation to its rupture over the interparticle distance. Fig. 2 shows E_{ad} at each calculation method. Focusing on the calculation methods for the bridge formation distance (LFC and SC), LFC, which considers the liquid film, showed larger E_{ad} than that at SC. On the other hand, focusing on the calculation methods for liquid bridge forces during particle contact (JKR and H-LB), E_{ad} at JKR and H-LB was almost equal. This is attributed to the fact that the distance δ_0, at which the interparticle force becomes zero ($\delta_0 = 10^{-6}$ times the particle diameter), was much smaller than the liquid bridge length δ_{rup} ($\delta_{\mathrm{rup}} = 10^{-3}$ times the particle diameter), resulting in little difference between JKR and H-LB.

Next, DEM simulation of wet powder behavior was performed. Fig. 3 shows the height of the powder heap obtained by the drawdown test. Regardless of the calculation methods, the heap height was almost the same. Therefore, it was found that in the drawdown test, where particle motion is static, the calculation method for wet powder does not significantly impact on the DEM simulation results. Fig. 4 shows the averaged kinetic energy of powder flow (K_{E}) obtained by the rotating drum test. Focusing on the calculation methods for bridge formation distance (LFC and SC), K_{E} at LFC was smaller than that at SC. This is because the liquid bridges are more likely to be formed at the LFC than SC due to the thicker liquid film, leading to more pronounced particle motion dissipation. This trend is consistent with the higher E_{ad} at LFC shown in Fig. 2. On the other hand, in the calculation method for liquid bridge force during particle contact (JKR and H-LB), K_{E} at H-LB was smaller than that at JKR. This is because the adhesion force of H-LB is larger than that of JKR, leading to higher dissipation of the particle motion.

In summary, it was found that the calculation method of liquid bridge force has almost no influence on the DEM simulation of static drawdown test, whereas it significantly influences on the DEM simulation of the dynamic rotating drum test. For the static powder behavior, differences in the calculation methods of the liquid bridge force did not lead to significant differences in the DEM simulation results. On the other hand, for the dynamic powder behavior, even in the minor differences in the calculation methods, it significantly impacts on the DEM simulation results.

References

[1] S. Gong, Z. Zuo, G. Xie, H. Lu, J. Zhang, *Powder Technology* **2019**, 346, 301–315
[2] Y. Tsunazawa, D. Fujihashi, S. Fukui, M. Sakai, C. Tokoro, *Advanced Powder Technology* **2016**, 27, 652–660
[3] S. Li, J.S. Marshall, G. Liu, Q. Yao, *Progress in Energy and Combustion Science* **2011**, 37, 633–668

Measurement on the Plane Strain Deformation of Sand Based on Digital Image Correlation Technology and Its DEM Numerical Simulation

Xiaoxia Guo*, Pengpeng Wang

State Key Laboratory of Structural Analysis, Optimization and CAE Software for Industrial Equipment, Dalian University of Technology, Dalian 116024, China
* Corresponding author: hanyuer@dlut.edu.cn

The Digital Image Correlation (DIC) method can be used to observe both the overall and local deformation processes of a soil specimen in plane strain tests [1,2]. However, due to experimental constraints, the soil specimen is encased within a specimen membrane, and the deformation of the specimen is represented through the deformation of the membrane. After the formation of shear bands, the sample is divided into two parts that slide along the shear band, making it impossible to directly observe the movement of particles. With the help of PFC software and after calibrating the discrete element parameters based on experimental data, it is possible to observe the movement of soil particles [3]. In plane strain tests, the deformation used by DIC technology can calibrate micro-structural parameters of discrete element models. The numerical simulation model of a plane strain specimen is shown in Figure 1. To ensure the accuracy of the simulation results, flexible boundaries are applied to the specimen's edges. The deformation fields of the plane strain test and simulation are shown in Figure 2. Figure 2(a) is the axial displacement diagram of the plane strain specimen under 100kPa lateral pressure obtained from numerical simulation. Since the upper and lower loading plates simultaneously load towards the center of the specimen, the displacement values of the specimen have both positive and negative values. Figure 2(b) is the axial displacement diagram under 100kPa lateral pressure after the formation of shear bands in the Euler coordinate system obtained from the plane strain test. During the test, loading is applied from top to bottom, and the displacement values are considered positive in the downward vertical direction. From Figures 2(a) and 2(b), it can be seen that the shear band inclination angles are basically the same, and the displacement trends are quite consistent. The deformation of the flexible boundaries in the numerical simulation is also similar to the test. Therefore, this also indicates that the determined micro-structural parameters are accurate. It is undeniable that due to the precision of sample preparation and the non-ideal uniformity of the soil material, the X-shaped shear bands obtained from the simulation do not completely match the single shear band that appears in the test. This is also the direction for further improvement of the computational theory and enhancement of sample preparation accuracy.

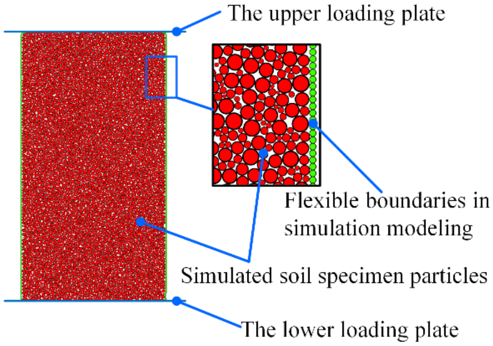

Figure 1. Discrete element model (DEM) of plane strain specimen

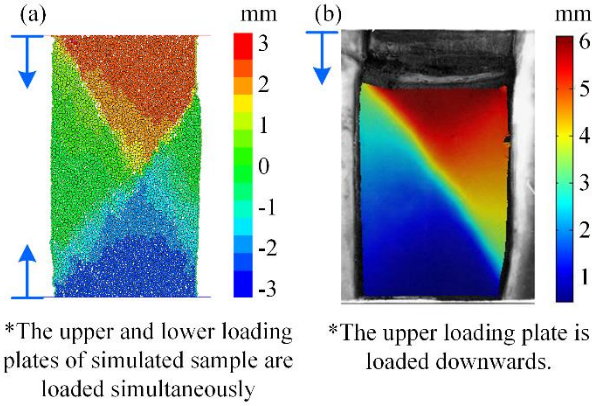

*The upper and lower loading plates of simulated sample are loaded simultaneously

*The upper loading plate is loaded downwards.

Figure 2. Discrete element simulation result compared with plane strain test result

References

[1] Tang Y, Okubo S, Xu J, et al. *Engineering Geology* **2019**, 249(31), 172-185.
[2] Yang C, Wei J, Huang H, et al. *Cement and Concrete Composites* **2018**, 86, 178-189.
[3] Zhang F, Li M, Ming P, et al. *Acta Geotechnica* **2019**, 14(2), 487-503.

Numerical simulation of the evolution of the funicular liquid bridge in a three-particle system

Fengjie Yao, Yinyi Xue, Di Wu, Liu Liu, Ping Zhou, Dongling Wu *

School of Energy Science and Engineering, Central South University, Changsha, Hunan, China
Corresponding author: dongling.wu@csu.edu.cn

The study of particle-liquid bridge interactions in the granulation process at the microscopic scale can help to understand more profoundly the influence of wet inter-particle motions on the agglomerate structure and to promote the development of the granulation process in the iron and steel industry as well as energy saving and emission reduction. To analyze the morphology of the liquid bridge between wet particles and its evolution, this paper, based on the principle of energy minimization, applies the gradient descent method to numerically simulate the evolution of the morphology of the three-particle separation process with the ring and rope liquid bridge under the premise of considering the role of gravity and researches the influences of the factors of the particle spacing, the particle-size ratio, the volume of the liquid phase, the solid-liquid contact angle, and so on on the morphology of the bridge, the force of the bridge, and the bridge breakage distance.

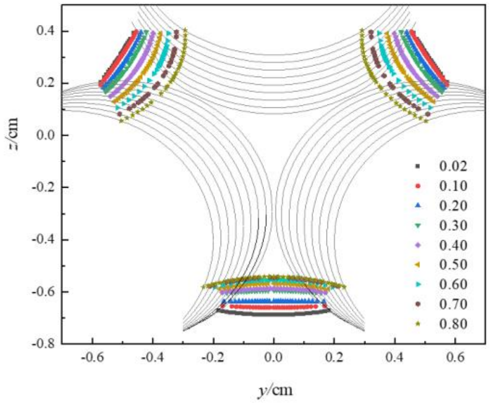

Figure 1. Contours of the longitudinal section of the centre of the liquid bridge at different particle spacings（$\theta = 50°$、$V = 0.277cm^3$）

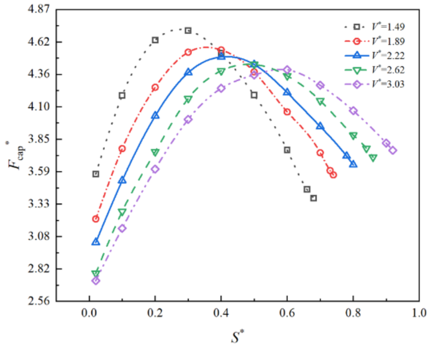

Figure 2. Variation of dimensionless capillary force with particle spacing for different liquid volumes

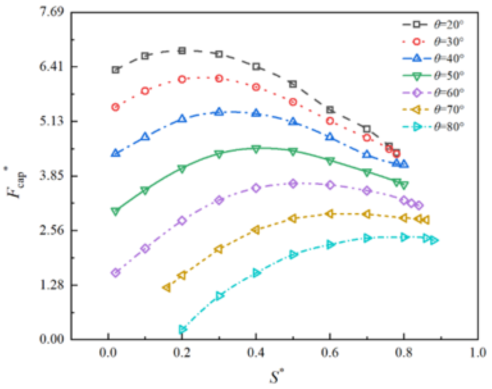

Figure 3. Variation of dimensionless capillary force with particle spacing at different contact angles

The results show that the maximum bridge force positively correlates with the liquid-phase volume and contact angle, while the fracture distance negatively correlates with the liquid-phase volume and contact angle. Finally, the explicit functional equations of the liquid bridge force and the liquid bridge fracture distance with the contact parameters were established by data fitting.

References

[1] Butt, M. Kappl, Normal capillary forces, *Adv. Colloid Interf. Sci*. **2009**, 146 (1–2), 48–60.

[2] G. Lian, J. Seville, *Adv. Colloid Interf. Sci*. **2016**, 227, 53–62.

[3] N.P. Kruyt, O. Millet, *J. Fluid Mech*. **2017**, 812, 129–151.

[4] Koromila I A , Spandonidis C C , Spyrou K J . *The 13th International Ship Stability Workshop* **2013**.

3D cell-split failure model in polyhedron DEM for modeling breakable granular materials

Ting Qiao,[a] Shunying Ji[a],*

[a]Dalian University of Technology, Dalian, the People's Republic of China
*Corresponding author: jisy@mail.edu.cn

Particle size distribution variation and particle position rearrangement caused by particle fragmentation are important reasons for the evolution of physical and mechanical properties of granular materials. In order to effectively simulate the macroscopic and microscopic mechanical behavior of crushable granular materials, specific destruction schemes are established for different types of granular materials. A contact bonding model for cemented granular materials, a 3D cell-split failure model for continuous materials, and a hybrid implementation of the above two are developed based on polygon mesh discrete element method(DEM)[1,2]. In 3D cell-split failure model, once the internal stress state of the particle meets the failure criterion, the proposed 3D subset splitting method is used to cut and separate polyhedral particles of arbitrary shape. For the particles of linear elastic materials, the contact detection and movement updating of the particles are realized by polygon mesh DEM firstly[1,2]. On this basis, the cell-split failure model consists of four main parts: calculation of internal stress field, failure criterion, failure mode and particle segmentation. The approximate calculation scheme of the internal stress field based on the 3D analytical solution and superposition principle[3] can maintain a certain calculation accuracy while meeting the requirement of computational efficiency. Energy based-failure criteria are used to evaluate when a particle fails, and the corresponding failure mode is used to describe how the particle fails[4]. Finally, particle segmentation adopt 3D subset splitting method to ensure the specific technical realization of the particle fragmentation[4]. Compared with the DEM-based bonded particle model and fragment replacement model, the cell-split failure model has no restrictions on the shape, size and number of descendant particles. Descendant particles are generated directly at the location of parent particles at the moment of destruction, and the mass and volume of granular materials are conserved throughout the destruction process. Therefore, the cell-split failure model can not only reflect the actual shape and size distribution of the descendant particles, but also avoid the problem that the geometric constraints of the descendant particles after the fragment replacement are unrealistic.

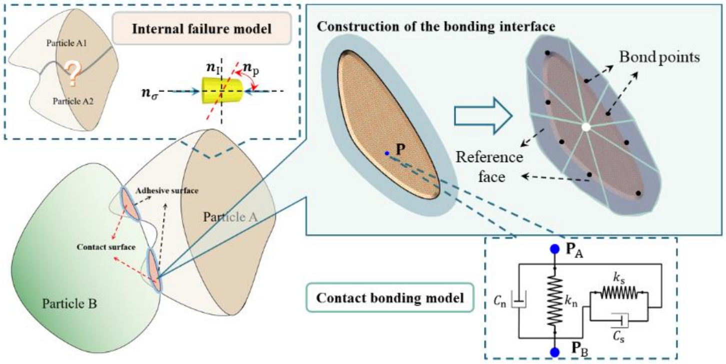

Figure 1. The hybrid implementation of the contact bonding model and cell-split failure model in crushable polygon mesh discrete element method.

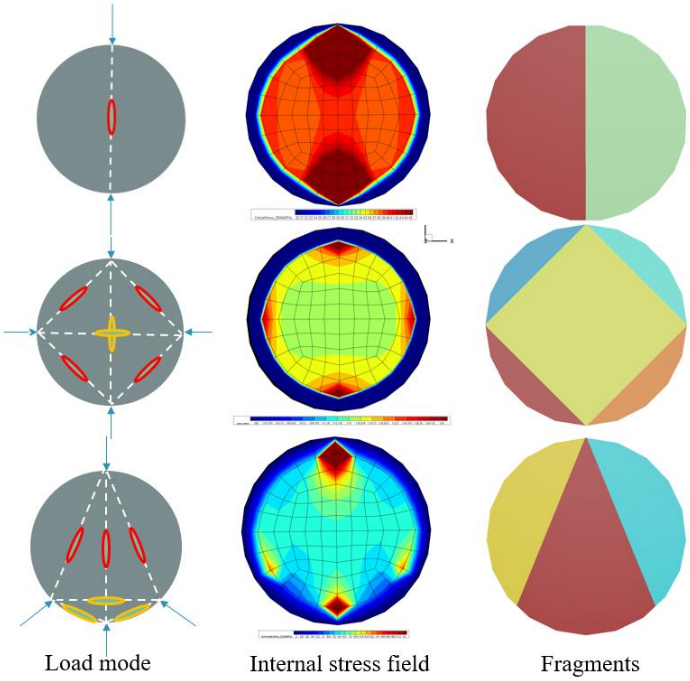

Figure 2. Failure simulation of quasi-two-dimensional disk under different loading modes using cell-split failure model.

References

[1] L. Ji, Q. Ting, J. Shunying, *Acta Mechanica Sinica.* **2023**, 39, 722245.

[2] Y.T. Feng, *Computer Methods in Applied Mechanics and Engineering*. **2021**, 373, 113493.

[3] A. E. Danilo, E. C. Luciano, *International Journal of Rock Mechanics & Mining Sciences.* **2013**, 60, 125-133.

[4] J. Yupeng, M. Peter,J. H. Hans, and A. M. Fernando, *Physical Review E*. **2021**, 104,045311.

Predicting liquid-liquid phase separation in small-molecule crystallization using Phase-Field simulations

Kazunori Kadota,[a]* Yuhei Tsugawa,[b] Mikio Yoshida,[b] Yoshiyuki Shirakawa,[b]

[a] Wakayama Medical University, Wakayama 640-8156, Japan
[b] Doshisha University, Kyotanabe, Kyoto, 610-0321, Japan
*Corresponding author: kazunori-kadota@wakayama-med.ac.jp

Small-molecule compounds often exhibit poor water solubility, leading to LLPS during cooling and anti-solvent crystallization, known as "oiling-out" [1]. LLPS, observed in small-molecule solutions besides proteins and polymers, divides the solution into solute-rich and solute-poor phases, impacting crystal quality. It affects particle size, polymorphism, and impurity levels, sometimes halting crystallization. Crystals formed during oiling-out contain impurities, fragile agglomerates, and partial amorphous characteristics, making it crucial to avoid in crystallization processes. Several studies explore the advantages use of LLPS in crystallization. Additionally, the operating strategy for crystallization involving LLPS is a major concern. Utilizing Process Analytical Technology (PAT) tools is deemed valuable in this context. Studies aim to prevent oiling-out and understand crystallization mechanisms by monitoring system states. Predicting changes in each phase's structure and concentration can support process design. The present study focused on the Phase-Field method, valued for predicting LLPS generation and state changes accurately.

A ternary system comprising butylparaben (solute), ethanol (good-solvent), and water (anti-solvent) was employed at a temperature of 323.15 K. To represent spinodal decomposition in the ternary anti-solvent, good-solvent, and solute system, a multi-component Cahn-Hilliard model was applied [2]. The simulation model used in the calculations was a two-dimensional lattice model, and periodic boundary conditions were applied to all boundaries. The calculation time interval was set to 5×10^{-4}. Phase-Filed simulations were performed for three compositions (α, β, and γ) in each zone in **Fig. 1**. The variance of the solute fraction across all grid points at dimensionless time is expressed. When the phase separation occurs, transitioning from a single-phase to a two-phase state, the solute fraction distribution across all grid points within the computational domain shifts from unimodal to bimodal. Consequently, the variance of the solute fraction escalates rapidly. The induction time is defined as the inflection point at which the temporal change in variance adheres to the subsequent equation; $\frac{\partial^2 V_{c_S}}{\partial t'^{\,2}} = 0$

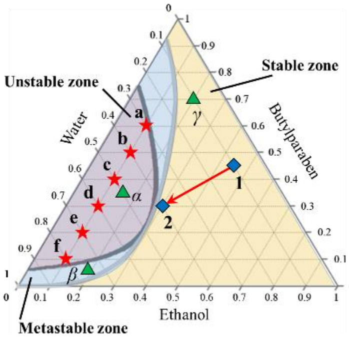

Figure 1. Average compositions of individual simulation systems are presented. These systems include Validity Simulation scenarios denoted as α, β, and γ, Spinodal decomposition simulations labeled from a to f, and Anti-solvent addition simulations identified as 1 and 2

Figure 2 depicts the solute fraction distribution, with red indicating higher solute concentration and purple indicating lower concentration. Validation was conducted for compositions α, β, and γ across unstable, metastable, and stable zones, respectively. In the unstable zone, phase separation was observed in simulations from both homogeneous and dispersed states, confirming validity. In the metastable zone, phase separation did not occur with small fluctuations but progressed when a dispersed phase was present. In the stable zone, phase separation did not occur with small fluctuations, and the dispersed phase disappeared over time, supporting validity.

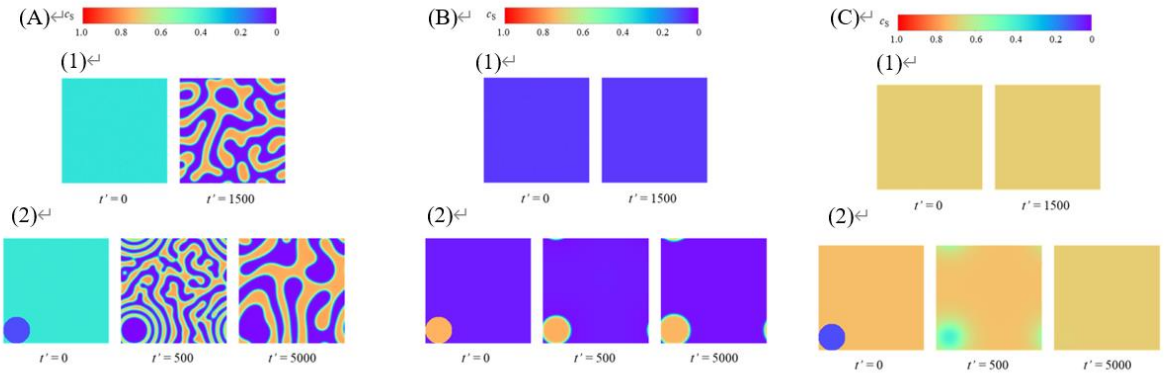

Figure 2. Color maps of solute fraction c_S at (A) composition α in the unstable zone, (B) composition β in the metastable zone, and (C) composition γ in the stable zone. (1) ±1% initial fluctuations. (2) Dispersed phase arrangement of 50 cells in diameter. As the color shifts towards red, the solute fraction increases, while it decreases towards purple.

Figure 3 illustrates phase separation dynamics for compositions a-f, displaying the solute-rich and solute-poor phases evolving over time. Varied phase separation states are observed, with compositions near the spinodal line forming circular dispersed phases while those farther exhibit bi-continuous phases characteristic of spinodal decomposition. The induction time for solute-rich phase formation was analyzed, revealing an increase as compositions approach the spinodal line, suggesting prolonged induction times. Dimensionless time against solute mole fraction variance was analyzed, with rapid increases indicating phase separation onset. Induction times showed prolonged durations closer to the spinodal line. Phase separation mechanisms vary based on composition, affecting phase structure and induction times. Understanding these dependencies is crucial for LLPS-based crystallization process design. Further analysis focuses on compositions with differing volume fractions of the minor phase, emphasizing their influence on phase separation structures.

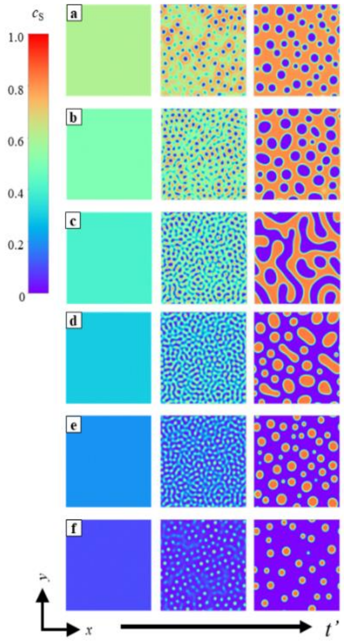

Figure. 3 Temporal changes in the color map during spinodal decomposition across compositions a-f.

References

[1] S. Amari, A. Okude, S. Kudo, H. Takiyama, *ChemistrySelect* **2022**, vol 7 45

[2] J.W. Cahn, J.E. Hilliard, J. Chem. Phys. **1958**, vol 28, 258-267.

High speed simulation of powder mixing in bi-disperse particle systems

Naoki Kishida, Hideya Nakamura*, Ohsaki Shuji, Satoru Watano

Department of Chemical Engineering, Osaka Metropolitan University, Japan
*Corresponding author: hideyanakamura＠omu.ac.jp

Powder mixing is ubiquitous in a wide variety of manufacturing sectors, including chemical industries. In the mixing process, multiple components with different physical properties, such as particle size, are usually treated. Under these conditions, powder segregation can occur due to differences in particle properties. The degree of segregation in a powder mixture significantly affects the quality of the final product derived from powder processing, necessitating the development of methods to predict segregation.

Computer simulation using the Discrete Element Method (DEM) is a powerful tool for the analysis of the powder mixing process. In DEM, the dynamics (position and velocity) of individual particles are numerically solved. These calculations are performed at extremely small time steps (microseconds order). Therefore, a large number of iterations are required to calculate the entire powder mixing process, and it is difficult to predict practical mixing in an actual process.

Recently, we developed an original machine learning model, namely Recurrent Neural Network with Stochastically calculated Random motion (RNNSR), which allows long time-scale powder mixing simulation with low computational cost and high accuracy [1]. RNNSR learns individual particle dynamics from short-time DEM simulation results and predicts powder mixing over a long time. However, RNNSR was only verified for monodisperse particles and has not been applied to bi-disperse particle systems that exhibit segregation. In this study, we expanded RNNSR to handle bi-disperse particles and evaluated its effectiveness in simulating segregation phenomena. The performance of expanded RNNSR was evaluated in terms of particle velocities, mixing behavior, and computing speed. As a result, expanded RNNSR was able to predict powder segregation phenomena due to the differenced in particle size with fast speed. In addition, the segregation phenomena of bi-disperse particle systems was predicted regardless of the initial filling conditions by expanded RNNSR.

References

[1] N. Kishida, H. Nakamura, S. Ohsaki, S. Watano, *CEJ* **2023**, 475, 146166.

Valuations of charging efficiency and critical gap under contact electrification model

Zhen Tan[a,*], Zhonghua Yu[b]

[a]Jiangsu Shipping College, Nantong, China
[b]Zhejiang University, Hangzhou, China
*Corresponding author: ztan@jssc.edu.cn

The electrification mechanism during particle fluidization is complex, and developing a reliable contact electrification model requires addressing many issues, especially the valuations of the charging efficiency and the critical gap for the electron tunnelling. This work aims to utilize the modelling of the simplest normal contact electrification between insulator particle and metal surface as an attempt to explore methods for the valuations of the critical gap and charging efficiency. A contact electrification model is developed based on the condenser model. The appropriate expressions for the contact potential difference and charge relaxation are discussed by reviewing previous works; the valuations of critical gap and charging efficiency are implemented by analysing the effect of initial charge and impact velocity on the transferred charge. The model is validated by the published experimental results, and accurately predicts the electrification during the normal collision of the insulator particle on the metal surface.

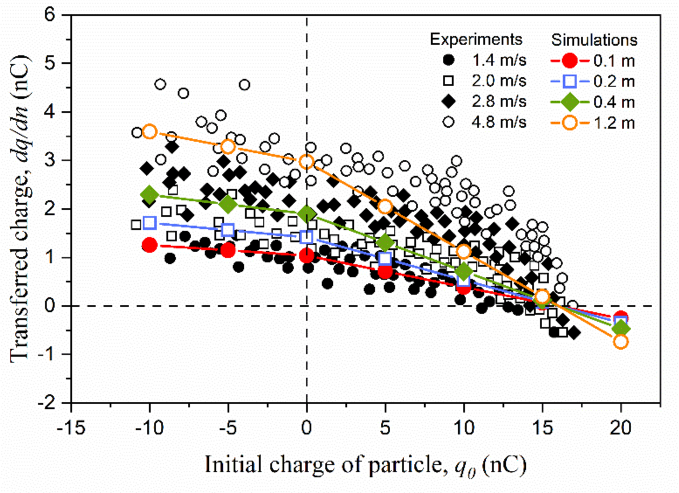

Figure 1. Effect of the initial charge of the sphere on the electrification.

ADEM simulation validation for the construction of grinding theory

Haruki Mochizuki,[a,]* Kizuku Kushimoto,[b] Junya Kano,[b]

[a]Graduate school of Environmental Studies, Tohoku University, Japan
[b]Institute of Multidisciplinary Research for Advanced Materials (IMRAM), Tohoku University, Japan
*Corresponding author: haruki.mochizuki.q8@dc.tohoku.ac.jp

Industrial grinding efficiency is as low as about 1%[1]. The reason is that grinding is operation used to produce powders and granules from ancient times. Grinding is a simple operation of breaking down particles, and empirical use of grinding became active before theoretical considerations. Even today, grinding conditions are determined by trial and error. For these reasons, several studies have been conducted to increase and estimate grinding efficiency. In the study on the energy of grinding, Lewis proposed a general equation for the energy required for grinding and the change in particle size. The energy required for grinding can be calculated as follows:

$$\boldsymbol{dE = -Cx^{-n}dx} \tag{1}$$

where $\boldsymbol{E}$ is the energy required for grinding, $\boldsymbol{C}$ is the correction factor, $\boldsymbol{x}$ is the particle size variation, and $\boldsymbol{n}$ is the power number. Furthermore, Rittinger, Kick, Bond, and others proposed several theoretical equations by varying the power number $\boldsymbol{n}$ in Lewis' equation. The reason why several theoretical equations are proposed is that the power number $\boldsymbol{n}$ in Lewis' equations vary depending on the particle size and material, and other factors. The scope of application of these theoretical equations is limited. Theoretical equations must be uniquely obtained to determine grinding efficiency in industrial applications. Thus, studies have been done to make the theoretical equation unique by verifying Lewis' equation. However, in the experimental verification, it is difficult to make the equation unique for wide particle size range and various materials because the power number $\boldsymbol{n}$ is a parameter depending on the particle characteristics.

In such a situation, we considered that the use of simulation would be effective. Simulation has the advantage that parameters can be easily obtained, identical particles can be used, and multiple experimental trials can be omitted. Among the simulation models that represent grinding, we focused on ADEM(Advanced Discrete Element Method)[2]developed by Ishihara et al. ADEM simulation is useful for detailed observation of particle grinding behavior, and ADEM is effective in identifying factors that affect grinding due to the small number of simulation parameters that need to be set. Therefore, in this study, the power number $\boldsymbol{n}$ by simulation was compared by experiment. ADEM simulation reproduced experimental particle grinding, and qualitative and quantitative agreement of particle grinding characteristics with experiment was confirmed. The power number $\boldsymbol{n}$ in Lewis' equation was calculated by simulation and experiment, and the two were compared. As a result, the power number $\boldsymbol{n}$ by the simulation was in quantitative agreement with the power number $\boldsymbol{n}$ by experiment. This indicates the validity of ADEM in the construction of grinding theory and in the calculation of grinding efficiency.

References

[1] D.W Fuerstenau, A.-Z.M Abouzeid, *International Journal of Mineral Processing* **2002**, 67, 161-185.

[2] Shingo Ishihara, Junya Kano, *ISIJ Int*. **2019**, 59, 820-827.

Granular shear flow criteria for accuracy of coarse-grained DEM

Kyota Mitsunashi, Shota Yokokawa, Hideya Nakamura*, Naoki Kishida,
Shuji Ohsaki, Satoru Watano

Department of Chemical Engineering, Osaka Metropolitan University, Japan
*Corresponding author: hideyanakamura@omu.ac.jp

A discrete element method (DEM) is a numerical simulation method which computes the equations of motion for individual particles consisting of a bulk powder, thereby, simulating the bulk powder behavior. DEM has been employed for modelling and simulation of powder handling processes. However, a computational load of the DEM is extremely high due to its Lagrangian approach. This hinders the large-scale DEM simulation of a powder handling process at the manufacturing scale, where the required number of particles is over a billion or more. Thus, high computational load of the DEM is a major issue for its practical application. To address this issue, the coarse-grained DEM (CG-DEM) is a promising approach. In the CG-DEM, the bulk powder behavior is computed by using artificially up-scaled particles representing a group of original particles. This leads to reduction of the number of particles and computational load. Our research group has developed a new CG-DEM method, termed CGSF (coarse-grained method for granular shear flow). We demonstrated its effectiveness for coarse-grained DEM simulation of powder mixing processes with granular shear flow [1,2]. As with other coarse-graining methods, CGSF was derived based on an idealized granular shear flow including several simplifying assumptions. Thus, it is expected that there are criteria for granular shear flows which can be successfully coarse-grained by the CGSF. However, such flow criteria were unknown. In this study, a coarse-grained DEM simulation of a granular shear flow in rotating drum mixer was performed with the CGSF. Accuracy of the CGSF was systematically investigated under various flow regimes and intensities of the granular flows in a rotating drum mixer. Finally, flow criteria for successful coarse-graining with CGSF were clarified.

Accuracy of the CGSF was expected to depend on the regime and intensity of the granular shear flow. To simulate the granular shear flow with various regimes and intensities, DEM simulations of granular flow in a rotating drum were performed under combinations of various particle-particle and particle-wall friction coefficients (μ_{PP} and μ_{PW}) and various rotating speeds of the drum. Particle diameters in the original and coarse-grained systems were 0.5 mm and 2.0 mm (i.e. coarse-graining ratio of 4), respectively. Accuracy of the CG-DEM was evaluated using the relative error of the total particle kinetic energy in the CG system to that in the original system.

First, relationship between relative error of the CG-DEM and inertial number I was investigated (**Fig. 1**). The inertial number I is a dimensionless number representing the magnitude of the granular shear flow [3]. The inertial number I in a rotating drum can be calculated by the following [3]:

$$I = \frac{\sqrt{2}\,\dot{\gamma} d}{\sqrt{gh\cos\theta}} \tag{1}$$

where, $\dot{\gamma}$ is the shear rate [1/s], d is the particle diameter [m], g is the gravitational acceleration [m/s^2], h is the thickness of

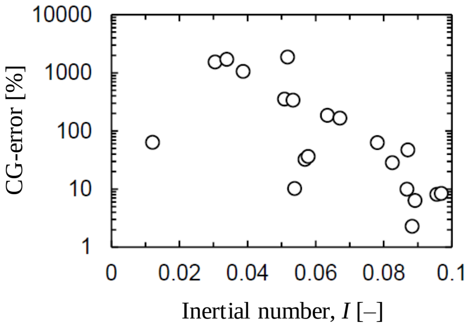

Figure 1. Coarse-graining error (CG-error) as a function of the inertial number I.

shear zone [m] and θ is the dynamic angle of repose [rad]. I represents the ratio of the "inertia force" to the "compressive force" acting on the particles under the shear flow [3]. Higher I corresponds to that the particles in the shear flow are more likely to move in the direction of its translational velocity. **Fig. 1** shows that the coarse-graining error (CG-error) decreased with an increase in the inertial number, indicating higher CG-accuracy at higher shear flow intensity. The scaling law of the CGSF was derived under an assumption that a constant particle velocity gradient occurs permanently in the coarse-graining region [1]. Thus, the CG-error was considered to be higher at smaller inertial number, where the velocity gradient was non-uniform and intermittent, whereas the CG-error became lower at higher inertial number, where the velocity gradient was uniform and nearly constant. Nevertheless, even at the same inertial number I (ex. $I \approx 0.05$ and 0.085), some simulation results exhibited significantly different CG-errors. This suggested that CG-accuracy cannot be characterized solely by the magnitude of the granular shear flow.

To investigate another critical flow characteristic other than the inertial number, we then focused on the velocity gradient at the wall boundary. We analyzed velocity profile in the radial direction. The particle velocity profile in the original system was averaged (i.e., coarse-grained) within the CG-particle size, and averaged (i.e., coarse-grained) velocity profile in the radial direction was extracted. Then, the translational particle velocity gradients at the vicinity of the moving wall ($\dot{\gamma}_{\mathrm{wall}}$) and at the bulk powder bed ($\dot{\gamma}_{\mathrm{bulk}}$) was calculated, and their ratio ($\dot{\gamma}_{\mathrm{wall}}/\dot{\gamma}_{\mathrm{bulk}}$) was quantified. The $\dot{\gamma}_{\mathrm{wall}}/\dot{\gamma}_{\mathrm{bulk}}$ means a discontinuity of the translational particle velocity at the vicinity of wall boundary. Similarly, gradients of the particle angular velocity were also calculated, and their ratio ($\omega_{\mathrm{wall}}/\omega_{\mathrm{bulk}}$), corresponding to a discontinuity of the particle angular velocity at the wall boundary, was also quantified. **Fig. 2** summarized the CG-error as functions of $\dot{\gamma}_{\mathrm{wall}}/\dot{\gamma}_{\mathrm{bulk}}$ and $\omega_{\mathrm{wall}}/\omega_{\mathrm{bulk}}$. The color of the plot indicated the CG-error at each condition. The CG-error tended to increase as the discontinuities in the velocities near the wall boundary increased. The CGSF was derived under an assumption that the velocity gradient within the coarse-grained particle (i.e., averaged volume element) was constant [1]. Higher discontinuities in the particle velocity near the wall deviates from this assumption, leading to higher CG-error.

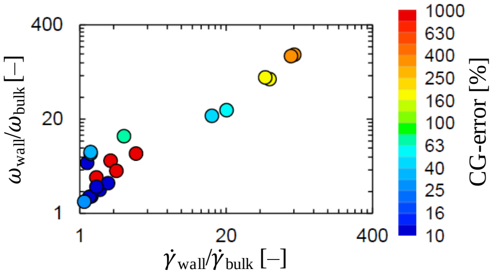

Figure 2. Coarse-graining error (CG-error) as functions of ($\dot{\gamma}_{\mathrm{wall}}/\dot{\gamma}_{\mathrm{bulk}}$) and ($\omega_{\mathrm{wall}}/\omega_{\mathrm{bulk}}$).

Finally, the CG-error was summarized by both the magnitude of the shear flow (inertial number I) and discontinuity of the particle velocity at the wall boundary ($\dot{\gamma}_{\mathrm{wall}}/\dot{\gamma}_{\mathrm{bulk}} + \omega_{\mathrm{wall}}/\omega_{\mathrm{bulk}}$) (**Fig. 3**). It was found that the CG-error was successfully characterized by using both the inertial number I and $\dot{\gamma}_{\mathrm{wall}}/\dot{\gamma}_{\mathrm{bulk}} + \omega_{\mathrm{wall}}/\omega_{\mathrm{bulk}}$. **Fig. 3** also revealed that the CG-accuracy can be sufficiently high (CG-error < 10%, shaded region in **Fig. 3**) in the range of $I > 0.085$ and $(\gamma_{\mathrm{wall}}/\gamma_{\mathrm{bulk}}+\omega_{\mathrm{wall}}/\omega_{\mathrm{bulk}}) < 4.5$, clarifying the flow criteria for successful coarse-graining by CGSF.

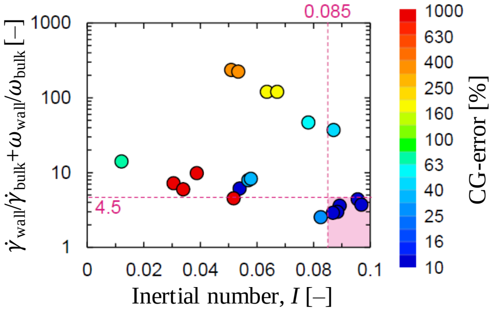

Figure 3. Coarse-graining error (CG-error) as functions of dimensionless magnitude (the inertial number I) and discontinuity near wall boundary ($\dot{\gamma}_{\mathrm{wall}}/\dot{\gamma}_{\mathrm{bulk}} + \omega_{\mathrm{wall}}/\omega_{\mathrm{bulk}}$).

References

[1] H. Nakamura, H. Takimoto, N. Kishida, S. Ohsaki, S. Watano, *Chem. Eng. J. Adv.* **2020**, 4, 100050.

[2] M. Saruwatari, H. Nakamura, *Chem. Eng. J.* **2022**, 428, 130969.

[3] G. D. R. Midi, *Eur. Phys. J. E.* **2004**, 14, 341–365.

Optimization of media size combination and agitator geometry for high grinding efficiency agitated media mill by DEM

Ryo Miyazawa,[a] Yutaro Takaya,[b] Susumu Gunji,[c] Kenichi Momota,[c] Satoshi Shiina,[c] Kyoko Okuyama,[c] Hidehiro Kamiya[d] Chiharu Tokoro [b,d,*]

[a]Graduate School of Creative Science and Engineering, Waseda University, Okubo 3-4-1, Shinjuku-ku, Tokyo, Japan, 169-8555
[b]Graduate School of Engineering, The University of Tokyo, Hongo 7-3-1, Bunkyo-ku, Tokyo, Japan, 113-8656
[c]NIPPON COKE & ENGINEERING CO.LTD., Toyosu 3-3-3, Koutou-ku, Tokyo, Japan, 135-6007
[d]Faculty of Science and Engineering, Waseda University, Okubo 3-4-1, Shinjuku-ku, Tokyo, Japan, 169-8555
*Corresponding author: tokoro@waseda.jp

An agitated media mill is capable of fine grinding by impact, shear, and frictional forces due to the media by the rotation of stirring shaft. In the agitated media mill, since the particle size of the grinding product is greatly affected by the rotational speed, the shape of agitator, the geometric structure of the mill, and the media size, the determination of optimum condition is much difficult compared with container driven type mill, such as vibration or planetary mill. Furthermore, in the case of dry grinding condition, since the input energy is often converted into thermal energy, which often reduces the grinding efficiency, the selection of optimal grinding conditions is important. In addition, the experimental optimization of geometrical structure of agitator shaft required a great cost and time, because the decision of optimum structure has been often made by trial and error. Therefore, there is room for further improvement of grinding performance by improving the equipment geometry and operating conditions. In previous studies of the agitated media mill, uniform size media have been generally focused, there are few studies focused under the conditions of media with different sizes. The discrete element method (DEM) is one of the great tools that can evaluate the grinding performance inside a mill for the purpose of optimizing the grinding process and elucidating the mechanism. The objective of this study is to investigate the effects of different feed ratios and size ratios of different sized media on impaction energy and impact frequency of media by DEM for elucidating the grinding mechanism and the optimal feed conditions for media with different diameters.

Experiments and simulations were conducted using model A, which has eight stirring blades at 90°. In the experiments, the grinding speed was evaluated by Alyavdin-Chujo equation. Simulations were also conducted using model B, which has eight stirring blades slightly deviated from 90°.The conditions of the stirring shaft are shown in Figure 1. Experiments and simulations were performed using zirconia as the medium. The comparison was made under the condition of a 1:1 as number-based ratio of large to small media with a packing volume fixed at 70% of the mill volume. The size of the small medium was used as a parameter for comparison. Large media with a diameter of 10 mm and small media with diameters of 3 mm and 2 mm were used. The media conditions and kinetic constant are shown in Table 1.

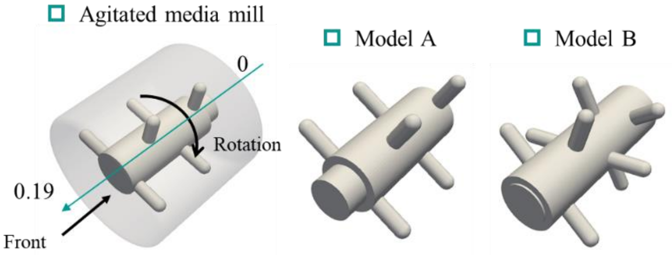

Figure 1. .Agitator geometry of conventional model A, model B.

Table 1. Number of media put into agitated media mill used for simulation and experiment.

	Number of large/small media	**Small media size**	**Agitator Geometry**	**Kinetic constant Early stage**	**Kinetic constant Late stage**
Case A-1	4006/4006	3 mm	Model A	0.51 min^{-1}	0.085 min^{-1}
Case A-2	4006/4006	2 mm	Model A	0.49 min^{-1}	0.088 min^{-1}
Case B-1	4006/4006	3 mm	Model B	-	-

The experimental results of the grinding experiment showed that the grinding speed in Case A-2 with 2 mm small media was slower and the particle size distribution was wider than that in Case A-1.

Figure 2(a) shows the simulation results of collision energy. Case A-2 was lower collision energy than that in Case A-1. DEM simulation results showed that the number of collisions was increased by increasing the contact surface due to the smaller media used at Case A-2, but the collision energy was reduced, which may indicate that the experimental grinding speed was lowered. The grinding speed is considered to have decreased due to the decrease in the collision energy. Figure 2(b) shows the simulation results of the distribution of the media position in the mill. It is thought that small media accumulated to the front and back of the mill. Therefore, the accumulation of small media at the front and back of the mill is thought to reduce the collision energy, resulting in a reduction in grinding speed. In Case B-1, where the arm shape was changed to Model B, the number of small media at the front of the mill decreased compared to Case A-1. This suggests that the use of the Model B arm improves the uniform distribution of small media and enhanced the grinding speed.

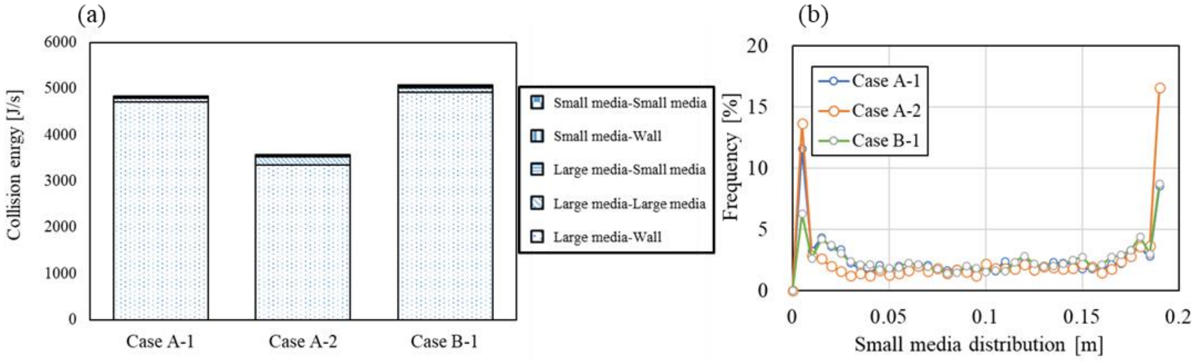

Figure 2. Simulation result of (a) Collision energy and (b) Media distribution in the direction of the rotation axis.

Numerical analysis on dominant factors affecting flowability of composite particles

Atsushi Omori,[a] Shuji Ohsaki,[a] Hideya Nakamura[a] and Satoru Watano[a*]

[a]Depertment of Chemical Engineering, Osaka Metropolitan University, Japan
*Corresponding author: watano@omu.ac.jp

Powders are used in many fields, including pharmaceuticals, cosmetics, foods, daily necessities and industrial products. Since more than 50% of all products in the global chemical industries are in particle state, the use of powders has attracted much attention [1]. In general, specific surface area of particles increases with decreasing particle size, which is expected to improve their disintegration and solubility. On the other hand, powder behavior is dominated by adhesive force on the particle surface rather than gravity force acting on the particles, when particle size becomes small. Many methods have been proposed to improve the flowability of powders by the surface modification of cohesive particles. For example, it has been shown that the flowability of cohesive particles (host particles) can be improved by coating the host particles with nanoparticles (guest particles), which are widely used as a flow aid [2]. It is generally understood that particle surface properties change the flowability by increasing the distance between the host particles and decreasing the van der Waals forces. However, theoretical analysis of the change in flowability is not sufficient, and the mechanism has not yet been elucidated.

In this study, numerical simulation using the discrete element method (DEM) was conducted to analyze kinetic behavior of the composite particles. A bonding model was used to simulate a composite state in which the guest particles are stuck onto the surface of the host particles. In addition, JKR model was used to describe the adhesion between the particles by surface energy. The flowability of the composite particles was assessed by the static angle of repose under different physical properties of the host and guest particles. Figure 1 shows the composite particles. A particle size ratio of host : guest = 10 : 1 was used, which has been reported to be the necessary condition to form ordered mixture (complete mixing). A lifting cylinder was used to measure the static angle of repose.

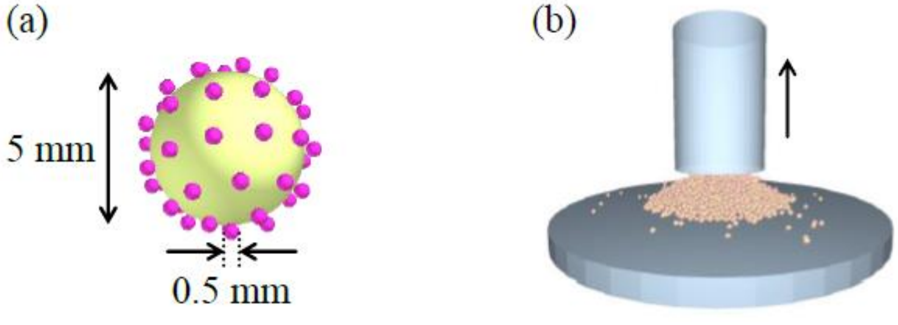

Figure 1. (a) Composite particle and (b) Lifting cylinder of angle of repose measurement.

References

[1] M. Han et al., *Powder Technology* **2020**, 365, 208–214.

[2] J. Visser, *Powder Technology* **1989**, 58, 1–10.

Sensitivity analysis of DEM parameters on bulk powder properties

Kinuko Hayashi, Hideya Nakamura*, Shuji Ohsaki, Satoru Watano

Department of Chemical Engineering, Osaka Metropolitan University, Japan
*Corresponding author: hideyanakamura@omu.ac.jp

A discrete element method (DEM) is a numerical simulation method which simulates various powder behaviors by solving the equations of motion for individual particles consisting of the bulk powder. DEM is widely applied to a numerical analysis of various powder handling processes. To accurately simulate the behavior of a real powder using the DEM, it is essential to adequately determine the DEM parameters for the particle contact forces, such as friction coefficients, restitution coefficients, stiffness, and so on. Methods for determining input DEM parameters are classified into the direct measurement and bulk calibration approach. In the direct measurement, microproperties for the individual particle are measured experimentally, and the measured microproperties are directly used as the DEM parameters. Nevertheless, the direct measurement of powders with non-spherical, smaller particle size (less than sub-millimeter) and inhomogeneous properties is challenging. Therefore, the bulk calibration approach is often selected. In the bulk calibration approach, firstly, a specific bulk powder property (e.g., angle of repose, compactability of powder bed, internal friction angle, etc.) is measured experimentally by using a specific testing system. The DEM simulation for the testing system is then performed by iteratively changing the DEM parameters until the bulk powder property in the DEM simulation matches to that measured experimentally. To efficiently determine the DEM parameters in the bulk calibration approach, the use of numerical optimization methodologies such as neural networks [1], genetic algorithms [2], and Bayesian optimization [3] are effective. For efficient calibration, it is necessary to select not only a numerical optimization methodology but also a suitable testing system to calibrate the target DEM parameters with high sensitivity. However, sensitivity of the DEM parameters (microscopic properties) on the bulk powder properties (macroscopic properties) has not been revealed, resulting in the empirical selection of the testing system.

In this study, we performed sensitivity analysis of DEM parameters on various bulk powder properties measured by different testing systems. DEM simulations were performed by varying DEM parameters for typical testing systems, which were the lifting cylinder test, uniaxial compression test, and rotational shear test. Total of eleven DEM parameters for particle-to-particle and particle-to-wall, including sliding friction coefficients, rolling resistance coefficients, restitution coefficients, Young's modulus, Poisson's ratio, and particle density, were varied. To efficiently analyze the correlation between eleven DEM parameters and bulk powder property, we employed the Plackett-Burman design. The range of each DEM parameter was determined with reference to nine existing literatures. Multiple regression analysis was then performed with the bulk powder property value as the objective variable and DEM parameters as the dependent variables to investigate the sensitivity of each DEM parameters on the bulk powder property. We here focused on monodisperse, cohesionless, and spherical particles.

Fig. 1 shows the results of sensitivity analysis at each testing system. In the lifting cylinder test (Fig. 1(a)), the static angle of repose $\theta_{!}$ was measured as the bulk powder property. Sensitivity analysis revealed significance of the sliding friction coefficient between particle and wall ($\mu_{"\#}$) and particles ($\mu_{\#\#}$), whereas the sensitivity of the rolling friction coefficient between particle and wall ($\mu_{\$"\#}$) was low. In the uniaxial compression test (Fig. 1(b)), the elastic modulus G of the compacted powder was taken as the bulk powder property. Sensitivity analysis showed that the Young's modulus of the particles ($E_{\#}$) had a significant impact compared with other parameters. In the rotational shear cell test (Fig. 1(c)), the internal friction angle $\theta_{\%}$ was measured as the bulk powder property. Sensitivity analysis showed significance of the sliding friction coefficient between particles ($\mu_{\#\#}$) and Young's modulus of the particles ($E_{\#}$). The coefficient of restitution between particles (e_{pp}) did not have a significant impact on the all bulk powder properties investigated in this study, although it slightly affected the static angle of repose in the lifting cylinder test. The p-values of the parameters with high sensitivity in each test were less than 0.050, indicating that they were significant variables. Furthermore, all the data suggested that the bulk powder properties can be influenced by multiple DEM parameters, rather than by any specific parameter. From these results, we can select appropriate testing systems and powder properties for calibration. For example, if we want to calibrate the friction coefficient ($\mu_{\#\#}$, $\mu_{"\#}$), the lifting cylinder test would be suitable. In summary, this study can identify DEM parameters with significant influence on various bulk powder properties. This can contribute to perform more efficient parameter calibration.

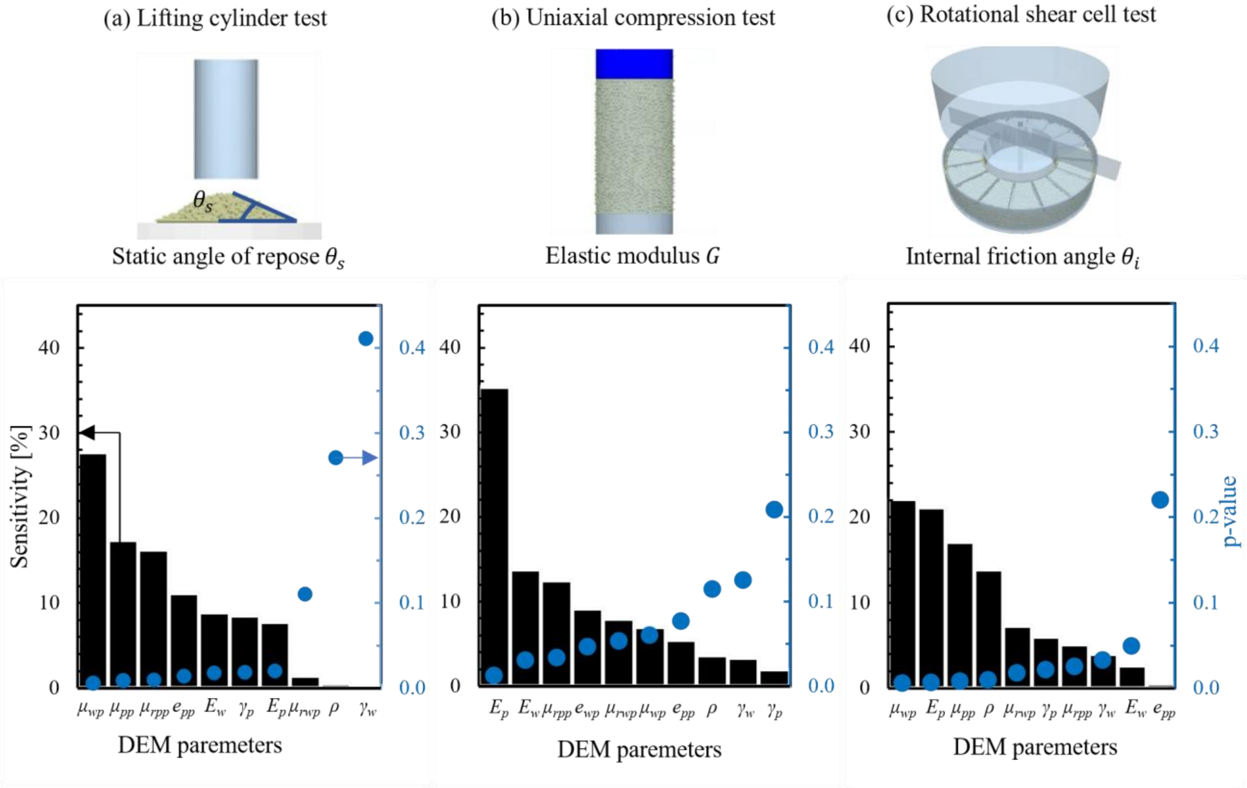
(a) Lifting cylinder test

(b) Uniaxial compression test

(c) Rotational shear cell test

Static angle of repose θ_s

Elastic modulus G

Internal friction angle θ_i

Figure 1. Testing systems and sensitivity analysis results. (a) Lifting cylinder test. (b) Uniaxial compression test. (c) Rotational shear cell test. $\mu_{!!}$ and $\mu_{"!!}$ denote sliding friction coefficient and rolling resistance coefficient between particles. $\mu_{\#!}$ and $\mu_{"\#!}$ denote sliding friction coefficient and rolling resistance coefficient between particle and wall. $E_{!}$ and $E_{\#}$denote Young's modulus of particle and wall. $\gamma_{!}$ and $\gamma_{\#}$ denote Poisson's ratio of particle and wall. ρ denote the particle density.

References

[1] F. Westbrink et al., *Powder Technology*, **2021**, 379, 602–616

[2] C. Richter et al., *Minerals*, **2021**, 11, 848

[3] W. Dhaouadi, et al., *Granular Matter*, **2022**, 24, 1–20

Simulation Research of the Impact of pressure on the Gasification Performance of Pet-Coke Slurry in an Entrained-Flow Gasifier

Hyung-Tae Kim,[a] Ji-Hwan Lee,[a] Hyeong-Bin Moon,[a] Jin-Wook Lee, [b] Byoung-Hwa Lee,[c] Chung-Hwan Jeon [a,c,]*

[a]School of Mechanical Engineering, Pusan National University, Busan, Republic of Korea
[b]Plant Process Development Center, Institutefor Advanced Engineering, Yongin-si, Gyeonggi-do, Republic of Korea
[c]Pusan Clean Energy Research Institute, Pusan National University, Busan, Republic of Korea
*Corresponding author: chjeon@pusan.ac.kr

Petroleum coke (pet-coke), a cost-effective byproduct of heavy crude oil refining, has potential as an alternative fuel source. This study utilizes three-dimensional computational fluid dynamics (CFD) simulation to optimize hydrogen (H_2) and carbon monoxide (CO) production from pet-coke slurry gasification in a 2-ton-per-day (2TPD) entrained-flow gasifier. Additionally, an research of internal phenomena was conducted under various pressure conditions (11 bar, 16 bar, 21 bar, and 26 bar). The results indicate that higher pressures lead to reduced particle flow and decreased internal velocity. Moreover, increasing internal pressure correlates with higher CO levels and lower H_2 concentrations. The objective of this analysis is to enhance production efficiency by understanding and optimizing the effects of operational parameters on fluid dynamics, temperature profiles, particle behavior, carbon conversion efficiency, and syngas composition, providing valuable insights for improving pet-coke gasification technology.

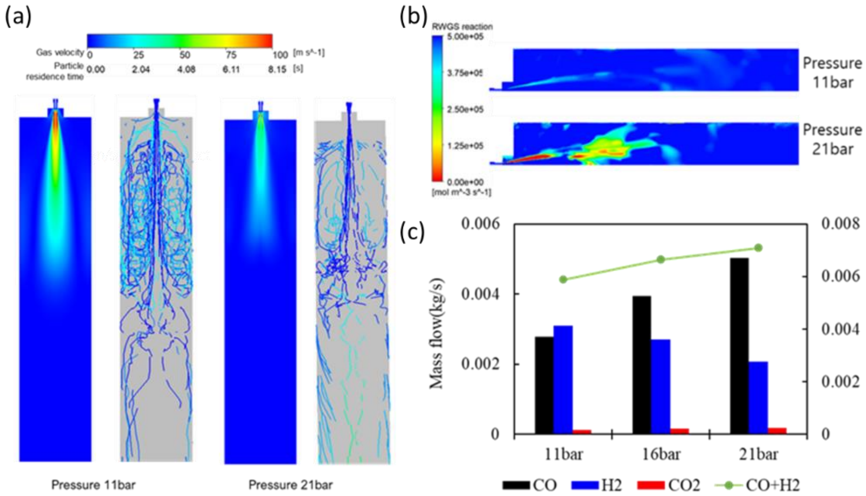

Figure 1. (a) velocity&particle trajectories, (b) reaction rate and (c) species distribution of outlet

Acknowledgement: This work was supported by the Institute for Advanced Engineering (grant number 21PCHG-C163217-01)

References

[1] Kim, H. T., Lee, J. H., Lee, J. W., Lee, B. H., & Jeon, C. H., *ACS omega*, **2023**, 8.48, 45922-45941
[2] Wu, Y., Zhang, J., Smith, P. J., Zhang, H., Reid, C., Lv, J., & Yue, G. ,*Energy & Fuels*, **2010**, 24.2: 1156-1163.

A Macro-dynamic Analysis of the Density Induced Segregation in a Rotating Drum Based on CFD Simulation

Rezwana Rahman,[a] Haiping Zhu,[a,*] Yang Xiang,[a] Aibing Yu[b]

[a]School of Engineering, Design and Built Environment, Western Sydney University, Penrith NSW 2751, Australia
[b]Faculty of Engineering, Monash University,14 Alliance Lane (Engineering 72), Clayton Victoria 3168, Australia
*Corresponding author: h.zhu@westernsydney.edu.au

Segregation of granular materials caused by particle properties such as size and density in rotating drums has been a significant research topic in the recent decades. Most earlier investigations in the area focused on size induced particle segregation. Some studies have addressed the density effect in the segregation process in rotating drums, but mainly at a microscopic scale based on the discrete element method simulations. Very little attention has been paid to the macro-dynamic analysis of particle density induced segregation.

To understand the density segregation of particles at a macroscopic scale, the CFD simulations of the solid–gas flow in a horizontal rotating drum have been conducted. The Eulerian-Eulerian multiphase model with the kinetic theory of granular flow (KTGF) was used in the simulations. Three different combinations of three materials with spherical shape (glass – poly propylene, steel – glass and steel – poly propylene) have been considered. The three materials (glass, steel and poly propylene) have different densities (2500, 7800 and 1160 kg/m^3) and the same size (0.775 mm). Physical experiments under similar conditions have also been carried out to validate the applicability of the simulation models. The research focused on the radial and axial segregations of the particles and impacts of two key properties, rotational speed and fill level of the drum.

The results indicate that CFD simulation can reproduce the flow patterns shown in the physical experiments. Further, for all cases considered in the simulations, the higher density particles tend to move into the particle bed and form a core, while the lower density particles create a band near the drum wall during the segregation process due to buoyancy effect. As the density ratio of particles increases, segregation becomes more pronounced in the radial direction, but less noticeable in the axial direction. Increasing rotational speed could promote the formation of the radial segregation, but would cause the vanishing of the axial segregation. Fill level exhibits a complex effect on the segregation. Both low and high fill levels (10% and 50%) have more prominent segregation patterns than the middle fill level of 25%. The middle fill level has more noticeable axial segregation. The formation of segregation is related to the profile of the particle velocity.

Numerical modelling of raw material effects in ironmaking blast furnaces

Kailai Chen,[a], Shibo Kuang,[a,*], Lulu Jiao [b], Aibing Yu [a,d]

[a]ARC Industrial Transformation Research Hub for Smart Process Design and Control, Department of Chemical and Biological Engineering, Monash University, Clayton, VIC 3800, Australia
[b]School of Energy and Environment, Southeast University, Nanjing 210096, China
[c]Center for Energy and Environment, Southeast University-Monash University Joint Research Institute, Suzhou 215123, China
*Corresponding author: Shibo.Kuang@moansh.edu

The optimization of raw materials and burden structures is usually done empirically in the blast furnace (BF). Thermal and chemical properties of raw materials measured in lab-scale experiments are important indicators for such an optimization. However, general methods of selecting ore/coke of various types and proportions in real BFs are still lacking. In this work, a 2D unsteady numerical model based on the softening-melting under load test is developed and validated. The correctness of reaction kinetics is verified by comparing the predicted and measured results. Moreover, various types of raw materials are evaluated in this experiment and the corresponding model. The specific rate constant of indirect reduction kinetics for each type of ore is determined by such a method. And the application of these rate constants for various burden structures is verified. All this thermal and chemical information can be incorporated into the 3D BF process model. Thus, raw material effects on the BF performance can be evaluated quantitively, which can provide guidance for raw material optimization in real BFs.

Combined DEM-LSTM-CNN modelling to predict mill load and particle size in ball mills

Yudong Zou,[a,*] Yaoyu Li,[b] Jie Bao,[c] Runyu Yang[a]

[a] School of Materials Science and Engineering, University of New South Wales, Sydney, 2052, Australia
[b] School of Chemical Engineering, The University of Queensland, Brisbane, 4072, Australia
[c] School of Chemical Engineering, University of New South Wales, Sydney, 2052, Australia
*Corresponding author: yudong.zou@unsw.edu.au

Ball mills are essential for particle size reduction in industry, but the random and complex motions of particles within the mill make predicting and controlling the grinding process challenging [1, 2]. The microscopic properties of particles, such as breakage behaviour and energy changes, play a crucial role in optimising production. Although numerical approaches like DEM can capture the complexity of particle behaviour, their high computational effort makes real-time monitoring and prediction of the internal-external relationship impractical in actual production. Therefore, a more efficient tool is needed to quickly establish and monitor this relationship to improve product quality and process efficiency [3, 4].

Previous research has been shown that machine learning methods are an effective solution for achieving rapid prediction [4, 5]. Li et al. [4] proposed an artificial neural network (ANN) model, trained on DEM simulation data and externally accessible information (acoustic emission (AE) signals, power draw), to quickly predict particle flow within a rotating drum. They later developed a three-phase modelling framework using a convolutional neural network (CNN) model to predict ball mill performance. The model data included AE signals, power draw, and grinding rate, and could be quickly applied to predict larger mill systems through transfer learning with limited new training data. However, their studies did not consider the breakage of particles and the evolution of particle size distribution (PSD) with grinding time. As particle size continue to decrease in grinding, the AE signals also change with time. In addition, while their CNN model was able to link the AE signals with PSD, it cannot predict the future grinding performance and PSD, thus limiting its applications to the control of grinding processes.

Previous studies have demonstrated the effectiveness of Long Short-Term Memory (LSTM) models in handling temporal dependencies in data, leading to a deeper understanding of process evolution [6]. LSTM models effectively address and alleviate the challenges of exploding and vanishing gradients commonly encountered in traditional time series prediction models, resulting in improved performance in long-term forecasting. Through its unique cell structure consisting of input gate, output gate, and forget gate, the LSTM model efficiently processes input data, capturing long-term dependencies within sequential data. In the context of temporally driven processes such as grinding operations, the LSTM model can dynamically account for variations in particle size, strength, and breakage probability across different grinding durations, accurately simulating extended grinding processes and predicting future changes.

This work aims to purpose a combined DEM-LSTM-CNN modelling frame to predict future particle breakage behaviour and size distribution by training a long grinding process data. As illustrated in Fig. 1. grinding process in a ball mill under different operation conditions will be simulated using the DEM model, and the evolutions of power draw, PSD as well as the internal particle-wall collision energy with grinding time will be extracted. The collision energy is then converted into AE signals using the AE model developed by Li et al. [4]. LSTM models are trained with AE signals and power draw data to predict future AE signals and power consumption. Subsequently, a pre-trained CNN model [5] will use the predicted AE signals and power draw from the LSTM model to predict future PSD. Finally, the predicted PSD and power draw are compared with the PSD obtained from the DEM simulations. It is expected the model will accurate prediction on the grinding performance of a ball mill under different condition, thus providing guidance on the control and optimisation of the mill.

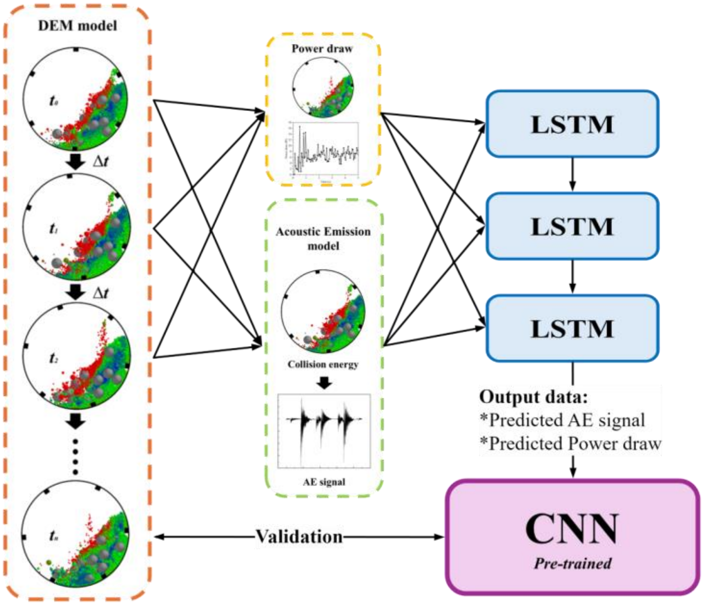

Figure 1. Flowchart of the data-driven DEM-LSTM-CNN modelling framework.

References:

[1] K. Schönert, *Int. J. Miner. Process.* **1988,** 22, 401-412.
[2] Y. Zou, C. Zhang, D. Gou, G. Cheng, and R. Yang, *Miner. Eng.* **2023,** 204, 108401.
[3] L. Zhao, X. Jin, and X. Liu, *Eng. Fail. Anal.* **2020,** 109
[4] Y. Li, J. Bao, A. Yu, and R. Yang, *Chemical Engineering Science* **2021,** 246, 117012.
[5] Y. Li, J. Bao, T. Chen, A. Yu, and R. Yang, *Powder Technol.* **2022,** 403, 117409.
[6] Y. Han, N. Ding, Z. Geng, Z. Wang, and C. Chu, *A*, *Journal of Process Control* **2020** 92 161-168.

Numerical modelling of particle transport and retention in porous media

Sagar G. Nayak,[a,b,c] Prapanch Nair,[b] Zhenjiang You,[c] Geoff Wang[c,*]

[a]UQ-IITD Research Academy (UQIDRA), Indian Institute of Technology Delhi, New Delhi, India
[b]Department of Applied Mechanics, Indian Institute of Technology Delhi, New Delhi, India
[c]School of Chemical Engineering, The University of Queensland, Brisbane, Australia
*Corresponding author: gxwang@uq.edu.au

The performance of a porous medium is often impaired by infiltration of foreign particles or by unanticipated transport of suspended particles during fluid flow through it. This phenomenon, popularly known as formation damage, is prevalent in several energy applications including carbon sequestration, flow in geothermal reservoirs, and in H_2 storage. Particulates encountering a pore can get strained, form a bridge, get attached to or detached from the substrate or even pass through it (see figure 1). The fate of the particulate depends on factors like the size of the particle and pore-throat, ionic strength and pH of the host fluid, temperature, flow rate etc.[1] and has profound implications on the performance of the porous media. Given the complexity of the phenomenon and its relevance, a systematic study of the underlying mechanisms is necessary for possible control. This study proposes the use of fidel and efficient numerical models to simulate hydrodynamic and mechanical processes behind the transport and retention of particles in porous media. The ability to simulate such phenomena enables one to study the contributing mechanisms in isolation. An algorithm involving immersed boundary method (IBM) alongside distributed Lagrangian multipliers (DLM) for rigidity constraints is used to model the fluid-particle and fluid-porous media interactions. Mechanical and electrostatic interactions among particles and between particles and porous media are also modelled. Results of the study can be used to draw conclusions on dominating parameters thus helping in the mitigation and control of performance decline.

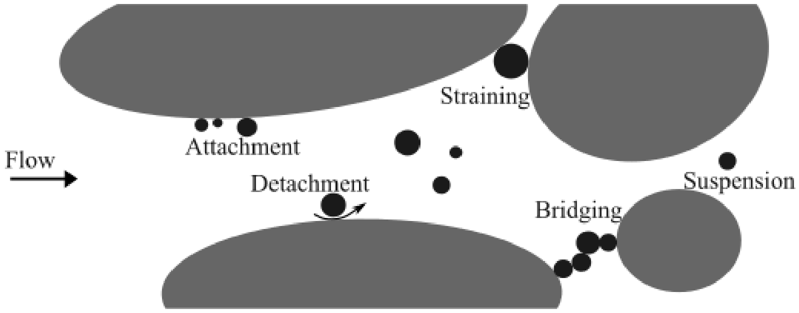

Figure 1. Fate of the indigenous and suspended particles in a pore.

References

[1] Y. Yang, W. Yuan, J. Hou, Z. You, *Water Research* **2022**, 214, 118172.

Two-phase flow analysis on particle motion in blast furnace raceway

Hiroshi Nogami,[a],* Ryusei Matsuda,[b] Shungo Natsui[a]

[a]Institute of Multidisciplinary Research for Advanced Materials, Tohoku University, Sendai, Japan
[b]Department of Metallurgy, Graduate School of Engineering, Tohoku University, Sendai, Japan
*Corresponding author: nogami@tohoku.ac.jp

The raceway is an important region in the blast furnace because it has great effects on the efficiency and stability of the blast furnace operation. The raceway is a cavity that is formed due to the coke consumption and the drag force, and the coke particles circulate inside due to interaction between particles and high-velocity blast gas. The raceway is the space for the combustion of coke and auxiliary reducing agents, and is deeply related to the operation status of the blast furnace. Therefore, a quantitative understanding of the raceway behavior is indispensable for designing a highly efficient and stable operation of a blast furnace. In this study, the multi-phase flow behavior in the raceway was discussed through the three-dimensional mathematical simulation.

The mathematical model tracks the particle motion by the Lagrangian method and the gas flow by the Eulerian computational fluid dynamic method, under the isothermal and non-reactive conditions. These two methods are combined by exchanging the distribution of the voidage and the drag force.

The model was applied to a small-scale cold-model condition. The plastic beads of 3 mm in diameter were packed in a vessel of which thickness was 20 mm. A slot tuyere is settled at a height of 45 mm from the bottom. Air was horizontally introduced from the tuyere. **Figure 1** shows a variation of forces acting on a single particle in the raceway. At the time 0.584 and 0.594 s, the particle is located in the gas stream from the tuyere and receives strong rightward drag force. The particle reaches the end of the raceway cavity and collides with the packed particle at 0.584 s. With this collision, the particle received a strong leftward contact force. Afterward, the particle climbs up along the cavity edge receiving an upward drag force around 0.614 s. Then move toward the tuyere wall around 0.738 s. During these movements, the particle is densely surrounded by the other particles and receives contact forces in various directions from the surrounding particles.

This numerical simulation successfully evaluates the multi-phase dynamics in the raceway.

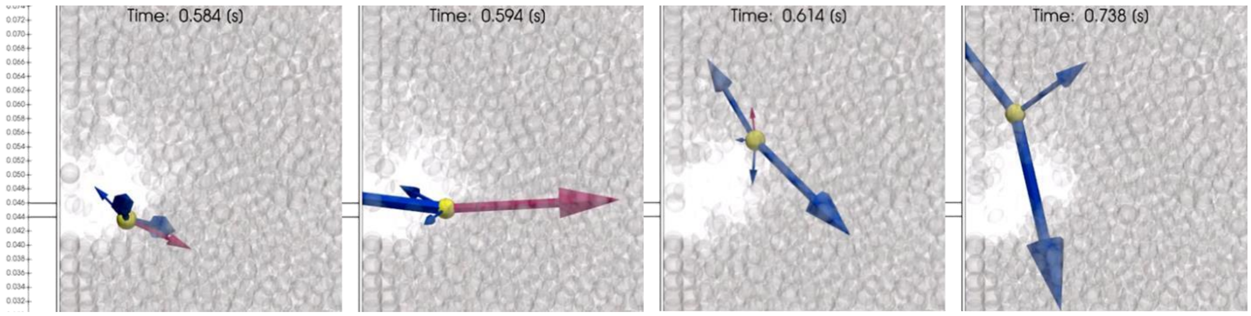

Figure 1. Variation of forces acting on a particle in the raceway. (Blue: Contact force, Red: Drag force).

POD-based reduced-order model for dense particulate flow

Shuai Wang,[a,b,]* Kun Luo,[a,b] Jianren Fan[a,b]

[a]State Key Laboratory of Clean Energy Utilization, Zhejiang University, Hangzhou, China
[b]Shanghai Institute for Advanced Study of Zhejiang University, Shanghai, China
*Corresponding author: wshuai2014@zju.edu.cn

Simulation of dense gas-solid flow in fluidized beds is computationally intensive, and current speedup methods remain insufficient. Proper Orthogonal Decomposition (POD) addresses this challenge by decomposing the original flow field into spatial modes and corresponding temporal coefficients. A data-driven Reduced-Order Model (ROM) integrating POD and machine learning was proposed for high-efficiency modeling in fluidized beds. Radial Basis Function Neural Networks (RBFNN) and Temporal Convolutional Neural Networks (TCN) were employed for real-time prediction of time evolution coefficients. A parameterized intrusive POD-Galerkin ROM was developed for rapid parametric prediction in dense gas-solid flow. The ROM results demonstrate that the temperature exhibits an obvious periodic characteristic, highlighting its potential for long-term prediction and digital-twin system establishment.

Brief Biography

Dr. Shuai Wang is currently serving as an assistant professor at Zhejiang University. He completed his B.E. and Ph.D. degrees from the College of Energy Engineering at Zhejiang University in 2014 and 2019, respectively. Following this, he worked as a postdoctoral fellow at the School of Chemical Engineering at the University of New South Wales from 2019 to 2022. His research interests include i) multi-scale CFD-DEM simulation of dense gas-solid reacting flow; ii) high-efficient utilization of renewable energy resources, e.g., biomass, hydrogen; iii) high-performance parallelization computation; iv) thermochemical processes in ironmaking blast furnaces; v) phase change in additive manufacturing. He has made substantial contributions to the field of energy and environmental science with over 70 peer-reviewed publications and approximately 2000 citations, holding an impressive H-index of 28. He has been recognized for his research excellence with the "Wu Chung-hua Outstanding Graduate Student Award" in 2019 and the "Excellent Doctoral Thesis of the Chinese Society of Particles" in 2020. Additionally, he serves as a guest editor for the Frontiers in Energy Research and an editorial board member for Energies and Journal of Environmental Materials and Sustainable Energy.

Pyrolysis behavior of thermally thick biomass particles: A modelling study

Xiaoke Ku,* Jin Wang

Department of Engineering Mechanics, Zhejiang University, Hangzhou, China
*Corresponding author: xiaokeku@zju.edu.cn

In view of the growing public awareness of global warming, reducing CO_2 is becoming more urgent. As one of the most promising renewable energy resources, biomass has attracted much attention worldwide due to its carbon neutrality and wide availability. In terms of modelling thermo-chemical conversion of biomass at particle scale, the most-often-used model is the thermally-thin model, which is also called the isothermal model. The thermally-thin model is based on the assumption that the temperature gradient inside a particle can be neglected. This assumption is not applicable to large biomass particles. Therefore, in this presentation, we will describe two different thermally-thick particle models. The first one is a one-dimensional thermally-thick model, which is used to investigate biomass pyrolysis in a rotary drum reactor. Results show that increasing the rotating speed increases the particle accumulated displacement; Increasing the rotating speed or filling level shortens the average particle residence time at the wall, reduces the heat conduction rate, and delays the particle heating-up and reaction processes. The second one is a three-dimensional thermally-thick model, which is applied to study the pyrolysis characteristics of a large biomass particle. Results show that increasing the operation temperature enlarges the internal temperature gradient, reduces the mass of solid residue, and generates a higher internal gas velocity.

Impact of flow on the distribution of particle agglomerate impurities and the development of an associated model

Yiting Xiao,[a] Zhengbin Pan,[a] Bo Kong[a,b,]*

[a]Department of Chemical Engineering, Guangdong Technion Israel Institute of Technology, Shantou, 515063, China
[b]Guangdong Provincial Key Laboratory of Materials and Technologies for Energy Conversion, Guangdong Technion – Israel Institute of Technology, Shantou, Guangdong 515063, China
*Corresponding author: bo.kong@gtiit.edu.cn

Lithium salts with high purity standards (greater than 99.5%) are in increasing demand in the lithium battery industry. The high production efficiency of lithium salts makes dynamic crystallization a desirable process. However, during dynamic crystallization, the crystals are affected by shear, turbulence, and impurities in the flow field to form dense, solid spherical aggregates. Consequently, it is difficult to remove the impurities incorporated into the aggregates, resulting in a low purity of the final product. Despite this, few studies have been conducted on the internal relationship between impurity incorporation and crystal aggregation and breakage. Furthermore, a mathematical model for aggregation and breakage under solvent inclusion has not yet been developed. This study used the cooling crystallization of potassium chloride as a model system to conduct real-time data collection using high-speed visualization methods, which allows a detailed analysis of the transition process in aggregate size and morphology. Then flow characteristics and impurity incorporation were investigated to determine how they influence the aggregation, breakage, and coarsening of crystals quantitatively. Incorporating the diffusion mechanism of impurities on crystal planes into the process of aggregation, breakage and coarsening as well as building sub-models of PBE aggregation, breakage, and coarsening under solvent inclusion.

CFD analysis of raceway dynamics and emission control with COG and RCOG injection in an ironmaking blast furnace

Ehsan Farajzadeh, Yuting Zhuo, Yansong Shen*

School of Chemical Engineering, University of New South Wales, Sydney, New South Wales 2052, Australia
*Corresponding author: ys.shen@unsw.edu.au

The ironmaking industry, heavily dependent on blast furnaces (BFs), accounts for approximately 7% of global CO2 emissions, driven by high fossil fuel consumption. This study develops a three-dimensional (3D) transient computational fluid dynamics (CFD) model to investigate the effects of injecting coke oven gas (COG) and reformed coke oven gas (RCOG) on raceway evolution within BFs. The analysis focuses on key performance indicators, including raceway shape, size, gas species distribution, combustion behavior, and temperature profiles, across three injection rates: 100, 150, and 200 Nm^3/t-HM. The results show that RCOG injections lead to a 3% increase in molar fractions of H_2 and O_2 and a 10% reduction in CO_2 emissions compared to COG. COG models, however, produce larger raceway areas by approximately 5%, attributed to delayed methane combustion. Temperature comparisons indicate that the highest raceway temperatures (up to 2200 K) occur in COG models at 200 Nm^3/t-HM injection rates, while RCOG models exhibit more uniform temperature profiles. Furthermore, COG injection results in 30% CO and 15% CO_2 emissions along the tuyere centerline. These findings highlight the varying operational impacts of COG and RCOG injections, with RCOG offering better temperature management and lower carbon emissions. This study provides a detailed framework for optimizing COG and RCOG utilization to enhance BF efficiency, reduce environmental impact, and maintain operational stability.

Physics-informed dynamic mode decomposition for short-term and long-term prediction of gas-solid flows

Dandan Li[a,b], Bidan Zhao[a,c], Shuai Lu[a,b], Junwu Wang[a,c]*

[a]State Key Laboratory of Multiphase Complex Systems, Institute of Process Engineering, Chinese Academy of Sciences, P. O. Box 353, Beijing 100190, PR China
[b]School of Chemical Engineering, University of Chinese Academy of Sciences, Beijing 100049, PR China
[c]College of Mechanical and Transportation Engineering, China University of Petroleum, 102249 Beijing, PR China
*Corresponding author: jwwang@cup.edu.cn

Integration of physics principles with data-driven methods has attracted great attention in recent few years. In this study, a physics-informed dynamic mode decomposition (piDMD) method, where the mass conservation law is integrated with a purely data-driven DMD method, is developed for fast prediction of the spatiotemporal dynamics of solid volume fraction distribution in bubbling fluidized beds. Assessment of the prediction ability using both piDMD and DMD is performed using the CFD-DEM results as the benchmark: Both DMD and piDMD can predict the short-term behaviour of solid volume fraction reasonably well, but piDMD outperforms the DMD in both qualitative and quantitative comparisons; With respect to their long-term ability, the piDMD-based prediction of the instantaneous solid volume fraction distributions is qualitatively correct although the accuracy needs to be improved, and the predicted time-averaged radial and axial profiles are satisfactory; Whereas the DMD-based prediction of instantaneous snapshots and time-averaged results is completely nonphysical. Present study provides a fast and relatively accurate method for predicting the hydrodynamics of gas-solid flows.

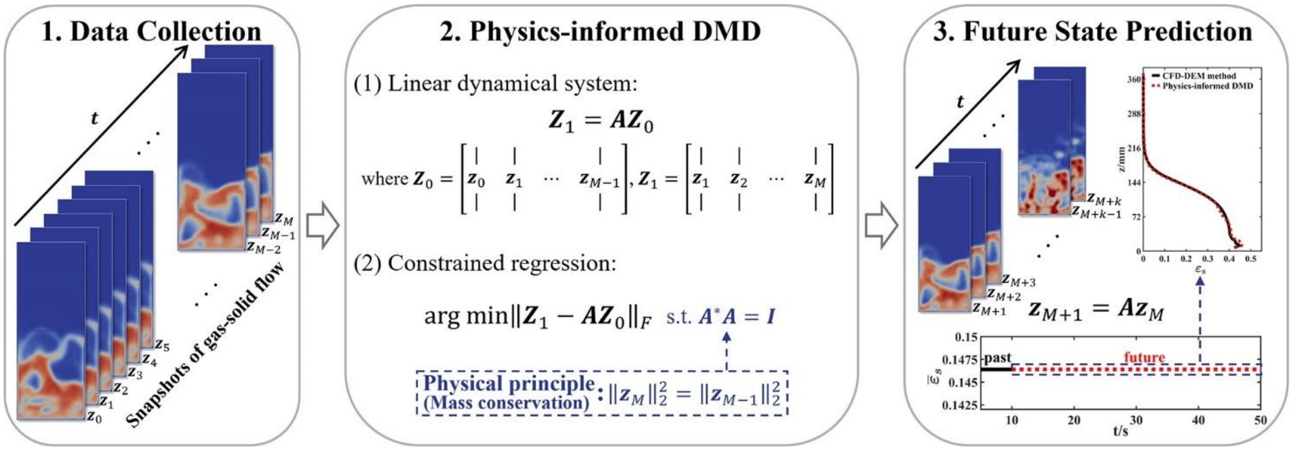

Figure 1. The conceptual illustration of prediction of dense gas-solid flow using physics-informed dynamic mode decomposition (piDMD).

Lattice Boltzmann method for modeling gas-solid fluidization

Limin Wang,* Wei Ge

Institute of Process Engineering, Chinese Academy of Sciences, Beijing, China
*Corresponding author: lmwang@ipe.ac.cn

Two kinds of coupled lattice Boltzmann method and discrete element method (LBM-DEM) approaches were developed for modeling gas-solid fluidization at different levels (different time-spatial scales and accuracy), namely lattice Boltzmann based particle-resolved direct numerical simulation (LB-based PR-DNS) [1] and lattice Boltzmann based discrete particle simulation (LB-based DPS) [2]. LB-based PR-DNS where particle size is much larger than lattice size, can directly simulate the flow and detailed dynamic interaction at gas-solid interface, while LB-based DPS where lattice size is much larger than particle diameter, achieves a good balance between computational accuracy, time consumption and computational efficiency, and it can obtain local information such as particle trajectories, as well as the macro information such as time-averaged flow field (Figure 1). Finally, both LB-based DNS and DPS are powerful tools in exploring gas-solid fluidization, which enabled development of lattice-based multi-fluids dynamics (LMFD) simulation software and a new drag correlation is proposed with consideration of scale-dependence [3].

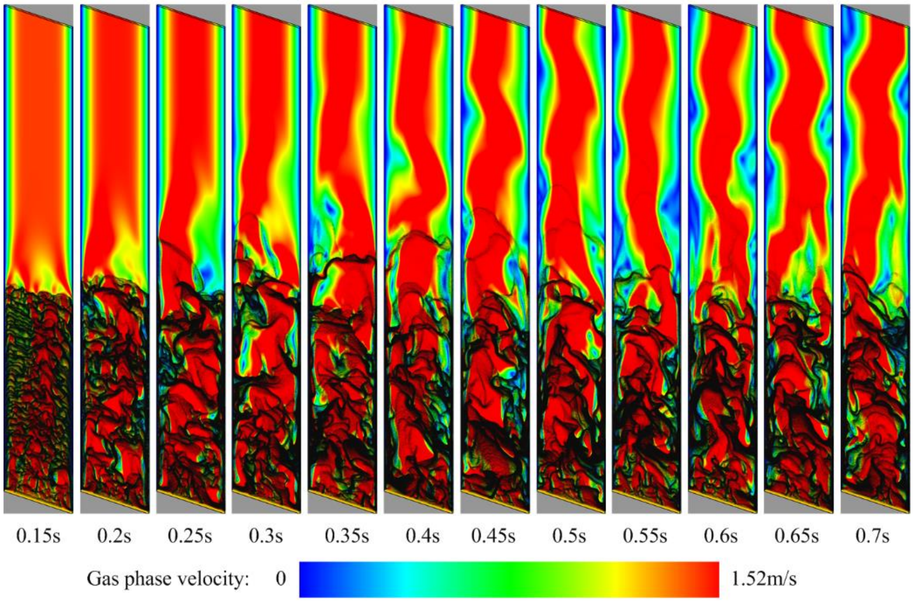

Figure 1. Snapshots of LBM-DEM simulated gas-solid fluidization.

References

[1] L.M. Wang, G.F. Zhou, X.W. Wang, Q.G Xiong, W. Ge, *Particuology* **2010**, 8, 379-382.

[2] L.M. Wang, B. Zhang, X.W. Wang, W. Ge, J.H. Li, *Chem. Eng. Sci.* **2013**, 101, 228-239.

[3] X.W. Liu, W. Ge, L.M. Wang, *AIChE J*. **2020**, 66, e16883.

The fluctuating characteristics of particle flow during silo discharge

Xiaoxing Liu,* Dancheng Zhang, Xiaodong Yang, Hui Guo

Institute of Process Engineering, Chinese Academy of Sciences, Beijing 10090, China
*Corresponding author: xxliu@ipe.ac.cn

Although resonant motion of particles during mass flow discharge from silos has been extensively investigated by earlier researchers, the appearance of such phenomenon during funnel flow discharge has not been emphasized. In this work, the flow behavior of particles during funnel flow discharge from flat-bottomed silos has been investigated by conducting 3D Discrete Element Method (DEM) simulations. It is found that particles in the upper part of flowing zone move collectively, manifested by the oscillatory fluctuations of the velocity and the non-Gaussian characteristics of the fluctuations of individual velocity around the average. Correlation analysis and discrete Fourier transform have been performed to characterize the emission and propagation of velocity fluctuation. It is found that the observed resonant motion of particles is induced by the regular fluctuation of contact force between particles, and there exists an intermediate region in the converging part of the flowing zone. The bottom boundary of this region corresponds to the emission source from which the velocity wave propagates upwards and downwards. Its upper boundary coincides with that of the converging part of the flowing zone and is featured by the most violent fluctuation of contact force. The simulation results thus suggest that the discharge of granular assembly seems to be determined by the rheological behavior of particles in this intermediate region.

No-affine displacement field

The variations of the delayed time between the time signals of particle velocity monitored at different positions

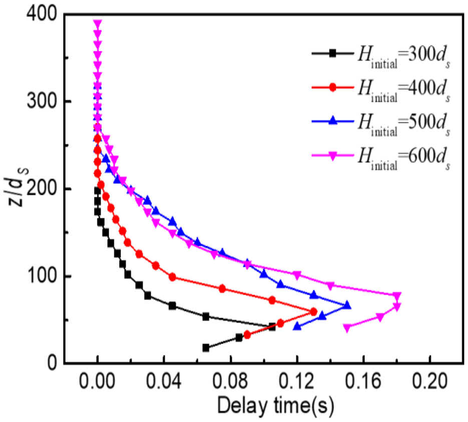

Distributions of particle compressive force along the silo wall

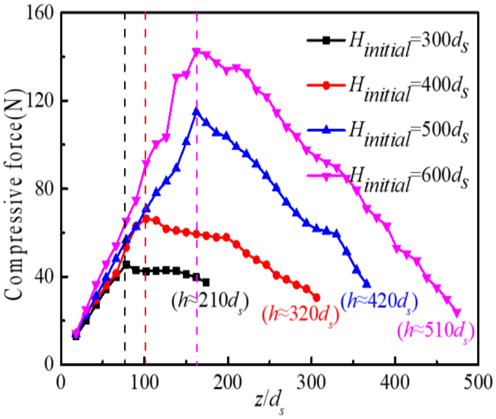

Collaborative modelling of gas-solid reacting flow in a fuel reactor equipped with process controllers in chemical looping combustion

Guoyin Yu, Yuting Zhuo, Shuyue Li, Yansong Shen*

School of Chemical Engineering, University of New South Wales, Sydney, NSW 2052, Australia
*Corresponding author: ys.shen@unsw.edu.au

Chemical reactors usually feature complex internal reacting flows, and they are usually equipped with process controllers to stabilise their operations, especially for highly dynamic reactors including chemical looping combustion/conversion (CLC). However, their dynamic internal states are not well understood due to the lack of reliable research tools. In this work, for the first time, an innovative numerical collaborative model is developed to describe the reacting flow details and simulate the response to a process controller. The collaborative model is applied to a fuel reactor (FR) in a CLC to demonstrate its effectiveness. The detailed internal flow patterns in the FR are obtained and described by the three-phase reacting flow CFD model, and the circulating rate of oxygen carrier (OC) is controlled and optimised by the fuzzy logic controller (FLC). The controller is designed to operate at varying control time intervals, 1 s, 2 s, and 5 s, to study the optimal frequency for data sampling and feedback. The efficiency of the controller to the FR is tested in terms of OC circulation, gas components and the general performance of the reactor. The results show that the stability of OC circulating rate and performance are effectively improved by the process controller; among the three control intervals, the 2 s interval shows the highest feasibility and capability of maintaining stable OC circulation and CO2 yield in the FR. Quantitatively, compared to the base case without a controller, the deviation of the OC circulating rate values has decreased from 0.123 to 0.058, and the CO2 yield has increased from 86.93 % to 88.16 % in the control case with a 2 s interval. This work provides a new cost-effective tool for real-time simulating and controlling the reacting flow system including CLC for clean combustion and solid wastes conversion.

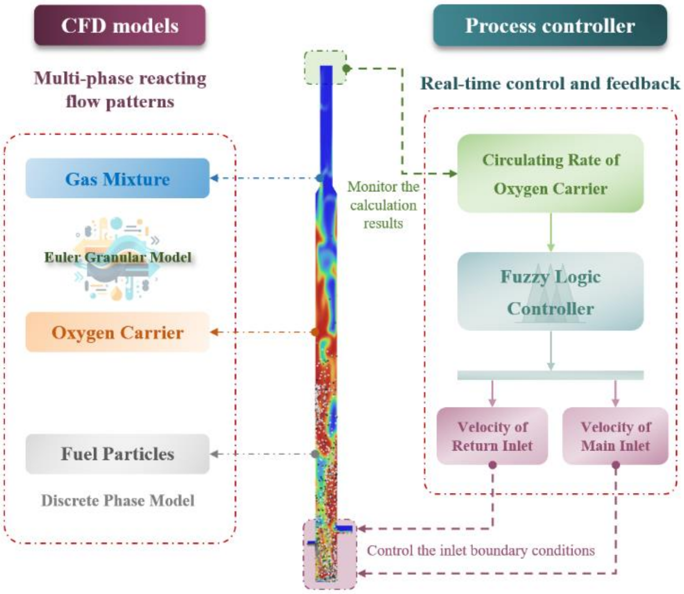

Figure 1. Graphical abstract.

Application study on a coarse-grained DEM-CFD to a wet bead mill simulation

Yuki Tsunazawa,[a,]* Mikio Sakai[b]

[a]Geological Survey of Japan, National Institute of Advanced Industrial Science and Technology (AIST),
Ibaraki, Japan
[b]Department of Nuclear Engineering and Management, School of Engineering, The University of Tokyo,
Tokyo, Japan
*Corresponding author: tsunazawa-y@asit.go.jp

A wet bead mill, also known as a wet stirred media mill, is commonly employed in various chemical engineering processes such as pharmaceuticals, ceramics, and minerals. Achieving highly efficient fine grinding requires a deep understanding and appropriate control of particle behavior. For this purpose, the discrete element method (DEM) coupled with computational fluid dynamics (CFD) has been extensively utilized in solid-fluid mixture systems. However, the existing DEM-CFD method [2] faces significant challenges, including limitations on the number of computational particles, stability issues, and difficulties in modeling rapidly moving structures. To address these challenges, this study investigates the applicability of a numerical model that combines the coarse-grained DEM-CFD [3], an implicit algorithm for the drag force term [4], and a scalar field-based wall boundary [5] in simulating a wet bead mill. Visualizing particle behavior in the wet bead mill using the coarse-grained DEM-CFD allows for the accurate reproduction of original particle behavior. A good agreement is observed for macroscopic characteristics, including particle velocity and total kinetic energy, between the original particle and coarse-grain particle systems. Conversely, simulations conducted with simply large particles, without employing the coarse-grain model, exhibit quite different results from those of the original particle system. Consequently, this study demonstrates the applicability of combining the coarse-grained DEM-CFD, an implicit algorithm for the drag force term, and a scalar field-based wall boundary in simulating industrial wet bead mills. Furthermore, stable calculations cannot be achieved in the simulation of the bead mill without the implicit algorithm for the drag force term. These valuable results will contribute significantly to the numerical investigation aimed at optimizing the scale-up of bead mills.

Acknowledgement

This work was partially supported by JSPS KAKENHI Grant Number (21H04870).

References

[1] P.A. Cundall, O.D.L. Strack, *Geotech.* **1979**, 29, 47-65.

[2] Y. Tsuji, T. Kawaguchi, T. Tanaka, *Powder Technol.* **1993**, 77, 79–87.

[3] M. Sakai, H. Takahashi, C.C. Pain, J.-P. Latham, J. Xiang, S, *Adv. Powder Technol.* **2012**, 23, 673–681.

[4] Y. Mori, M. Sakai, *Chem. Eng. J.* **2021**, 406, 126841.

[5] Y. Shigeto, M. Sakai, *Chem. Eng. J.* **2013**, 231, 464-476.

VOF-DEM investigation of the wet grinding process in a SAG mill

Qixuan Zhu,[a] Yuqing Feng,[a,]* Peter Witt,[a] Warren Bruckard,[a] Runyu Yang[b]

[a]CSIRO Mineral Resources, Victoria 3169, Australia
[b]School of Materials Science and Engineering, University of New South Wales, Sydney 2052, Australia *Corresponding author: Yuqing.Feng@csiro.au

Semi-autogenous grinding (SAG) mills are essential for cost-effective ore beneficiation, primarily utilizing wet milling processes [1]. Although the milling process has been extensively studied by DEM modelling, the effect of slurry is frequently neglected due to its complex interactions with the charge. This paper presents a coupled CFD-DEM model to simulate the wet grinding process in a SAG mill. The model, which adopts a VOF approach to simulate the gas and liquid slurry phase, was validated by comparing theoretical and experimental data of particle sedimentation, phase conservation, as well as the flow and particle patterns in a lab-scale wet drum. The model was then utilized to simulate interactions between ore, steel ball, gas, and slurry in a SAG mill at various rotation speeds. Fig. 1 illustrates the fluid and particle dynamics within the mill at 40 s. The analyses consider the angle of repose, power draw, particle collisions, and velocity distributions. The findings elucidate the multiphase interaction mechanisms in the SAG mill and underscore the necessity of including slurry in simulations to accurately model the milling dynamics.

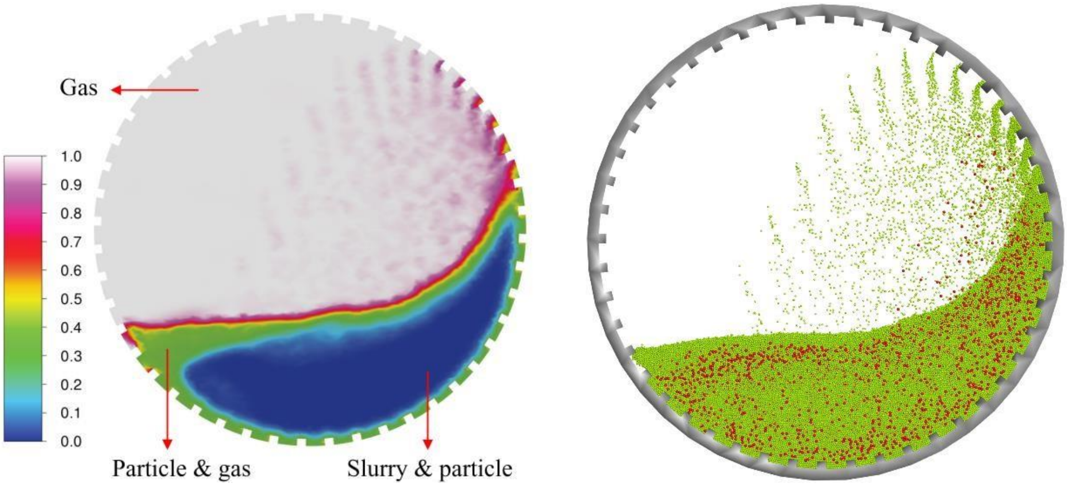

(a) (b)

Figure 1. (a) Gas volume fraction; (b) Particle dynamics with steel ball particles in red and ore particles in green.

References

[1] P.W. Cleary, R. Morrisson, S. Morrell, *Int. J. Miner. Process.* **2003**, 68 129-165.

Prediction of flow through packed beds using machine learning

Sagar G. Nayak,^{a,b,c} Hariprasad Kodamana,^{d} Prapanch Nair^{b,*}

[a]UQ-IITD Research Academy (UQIDRA), Indian Institute of Technology Delhi, New Delhi, India
[b]Department of Applied Mechanics, Indian Institute of Technology Delhi, New Delhi, India
[c]School of Chemical Engineering, The University of Queensland, Brisbane, Australia
[d]Department of Chemical Engineering, Indian Institute of Technology Delhi, New Delhi, India
*Corresponding author: pnair@am.iitd.ac.in

Flow through packed beds, is ubiquitous in the energy industry. A packed bed is typically understood as a porous medium. The prediction of single and multiphase flows through the packed bed is not feasible unless the scales ranging from the pore scale to the reactor scale are considered and their effects are coupled. This is because the direct numerical simulations (DNS) of reactor flows (typically involving millions of particles) are beyond the reach of modern supercomputers. Traditional multiscale techniques which assume separation of phenomena across scales cannot account for the influence of particle shape and arrangement in a general manner. To address the predictions at larger scales, we propose the use of machine learning based tools for prediction of flows at larger scales that are trained with data from simulations at smaller scales.

Firstly, we use Fourier Neural Operators (FNO) to generalize the flow through arbitrary arrangement of particles for single and multiple phases. We use simulations from a Cartesian grid based finite volume solver to generate flow data at particle scales to train Neural Operators [1]. We show that the Neural operators generalize the prediction of flows through porous media with impressive accuracy. We then use the same data to show that multiphase flow through much larger domains (up to 16 times the number of particles) can be predicted with more than 90% accuracy. We also present techniques for improving the accuracy with a few large-scale simulations. In the Fig. 1 we show the FNO predictions of two-phase flow for a small cell containing 3 particles and predictions using the same for flows through 48 particles (a 16x domain).

Secondly, we introduce a graph based neutral network to encode flow through a packed bed. The relevant flow scales are considered, and the time evolution of the two-phase flow interface is predicted. The results are then compared against classical dispersion studies.

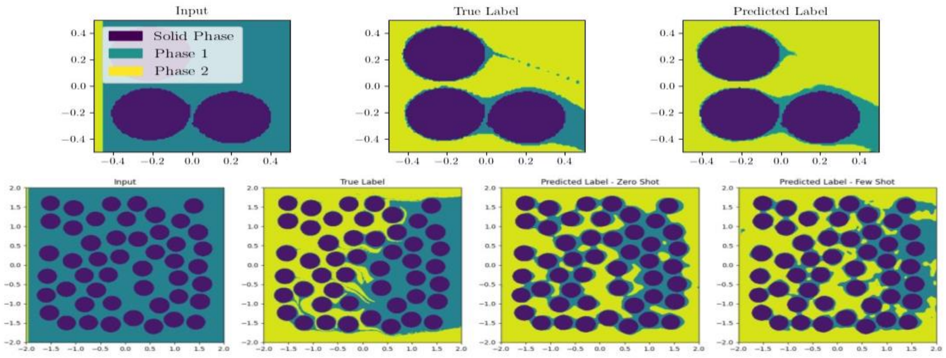

Figure 1. Top row: FNO predictions of flow through an arbitrary arrangement of 3 particles. Bottom row: Flows predicted using the top row data, for flow through a 16x domain. True label refers to the simulation result, zero shot is trained purely from 3 particle configurations and few shot uses 10% samples from the large scale.

References

[1] P. Nair, S. Mühlbauer, S. Roy, T. Pöschel, *Phys. Fluids* **2023,** 33, 042010.

Research on drag force of bubble swarms based on direct numerical simulation

Zhendong Li,[a,b] Fan Duan,[a,b] Xiao Chen,[a,b] Qiang Zhou[a,b,c,]*

[a]School of Chemical Engineering and Technology, Xi'an Jiaotong University, Xi'an, China
[b]Engineering Research Center of New Energy System Engineering and Equipment, University of Shaanxi Province, Xi'an, China
[c]State Key Laboratory of Multiphase Flow in Power Engineering, Xi'an Jiaotong University, Xi'an, China
*Corresponding author: zhou.590@mail.xjtu.edu.cn

An accurate drag force model of bubble swarms is essential for predicting gas-liquid two-phase flows. In the literature, the drag force of bubbles is generally calculated based on macroscopic force balance [1], which introduces not only the force balance assumption but also the equivalent bubble diameter. In such studies, bubbles are often simplified as spherical bubbles [2], or the aspect ratio is used to consider the nonsphericity of bubble shape [3], resulting in inaccurate calculation of the bubble drag force. In this paper, the drag force is obtained by directly integrating the stress on bubble surface based on the VOF method, which avoids introducing the force balance assumption and can handle bubbles of arbitrary shapes. Firstly, numerical simulations of the free rise of a single spherical bubble at low Reynolds numbers are carried out, and the calculated drag force results are compared with the theoretical solution, verifying the accuracy and applicability of the proposed method. Then, direct numerical simulations are performed for bubble swarms with different inlet gas velocities. The drag force values obtained from the simulations are made dimensionless using the buoyancy force acting on a single bubble, and the correction coefficient for bubble swarms is fitted using the Reynolds number and gas holdup, establishing a drag force model for bubble swarms with gas holdups ranging from 0.1 to 0.4. Finally, the established drag force model is applied to the simulation of air-water two-phase flow in a sieve tray distillation column. The results show good consistency between the simulation results and experimental data.

References

[1] W. Dijkhuizen, E. I. V. van den Hengel, N. G. Deen, M. van Sint Annaland, J. A. M. Kuipers, *Chem. Eng. Sci.* **2005**, 60(22), 6169-6175.

[2] I. Roghair, Y. M. Lau, N. G. Deen, H. M. Slagter, M. W. Baltussen, M. Van Sint Annaland, J. A. M. Kuipers, *Chem. Eng. Sci.* **2011**, 66(14), 3204-3211.

[3] A. Tomiyama, G. P. Celata, S. Hosokawa, S. Yoshida, *Int. J. Multiph. Flow* **2002**, 28(9), 1497-1519.

Diffusion and dissolution of oil droplet in supercritical water

Qiuyang Zhao, Lichen Zheng, Xuetao Wang, Yu Dong, Liejin Guo*

State Key Laboratory of Multiphase Flow in Power Engineering, Xi’an Jiaotong University, Xi’an, PR China
*Corresponding author: lj-guo@mail.xjtu.edu.cn

Introduction

Supercritical water (SCW) is proposed as a promising agent for heavy crude oil recovery [1]. Extensive studies have shown that SCW can be miscible with most organic compounds and gases, and the miscibility of heavy oil and SCW was the key mechanism for enhanced recovery [2]. In this paper, MD simulation was employed to study the dissolution and miscibility characteristics of heavy oil in SCW.

Result and discussion

With the increase of simulation time, the lighter oil molecules with smaller molecular masses were rapidly and uniformly dissociated in the solvent environment, while the remaining asphaltene molecules with higher molecular masses formed clusters. Clusters of different sizes are further disordered accumulations of monomers and nanoaggregates. SHS and SCW were all capable of dissolving heavy oil droplets. The increase in density slowed down the dissolution rate of oil droplets. When the solvent ambient density was 0.1 g/cm^3, the heavy oil droplets were completely dissociated in SCW after only 50 ps of simulation time. When the solvent ambient density increased to 0.5 g/cm^3, the dissolution rate of oil droplets became significantly slower. The complete dissociate state was reached only at about 600 ps.

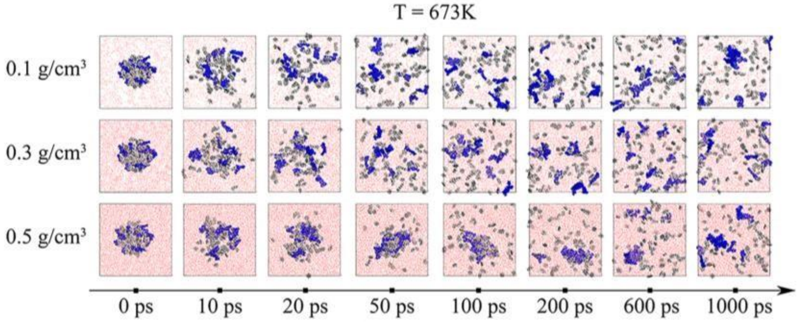

Figure 1. Dissolution process of heavy oil droplet in superheated steam and supercritical water.

The dissolution characteristics of heavy oil in SCW were mainly determined by the temperature and density of the solvent environment and the structure of oil molecules. The increase in solvent density inhibited the dissolution of heavy oil, while the effect of temperature was determined by the competitive relationship between the decrease in solubility of heavy oil in SCW and the increase in dissociation between heavy oil molecules. Therefore, raising the temperature and lowering the pressure are effective means to improve the solubility of heavy oil in field applications. For the oil molecule structure, SCW showed the best solubility for light aromatic hydrocarbon molecules due to polar effects, followed by non-polar chain alkanes, and the worst solubility for cycloalkanes due to stronger oil intermolecular interactions. The asphaltene molecules exhibited better solubility than cycloalkanes due to electrostatic attraction interactions with the solvent, but simultaneously showed poorer solubility than chain alkane molecules due to poor dissociation. The increase in the number of carbon atoms was detrimental to the solubility of the oil molecule, while the isomeric phenomenon of chain alkanes and the change in the heteroatom species in asphaltenes did not significantly affect the solubility characteristics of the oil molecule.

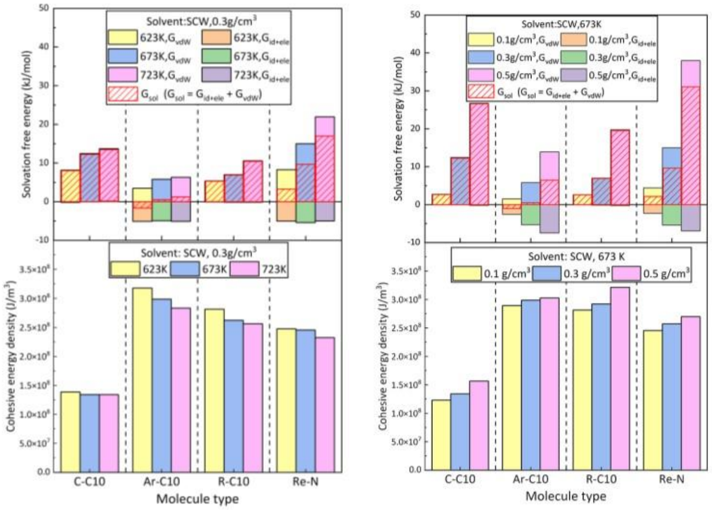

Figure 2. Effect of temperature and pressure on SFE of heavy oil components in SCW, and CED of heavy oil components.

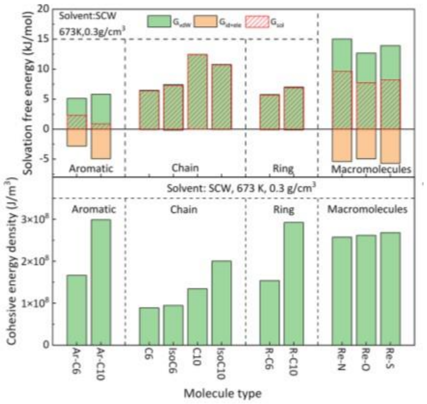

Figure 3. Influence of molecular structure on the SFE and CED of heavy oil molecules in SCW.

Conclusion

The results indicated that the dissolution characteristics of heavy oil were mainly determined by the density, temperature, and oil molecule structure. The increase in solvent density inhibited the dissolution of heavy oil, while the effect of temperature was determined by the competitive relationship between the decrease in solvent solubility and the increase in solute dissociation. The increase in carbon atoms was detrimental to the solubility of the oil, while the isomerization of chain alkanes and the change in the heteroatom in asphaltenes did not significantly affect the solubility. Electrostatic attraction interaction was the main cause of poor dissociation of polar oil molecules.

References

[1] Q.Y. Zhao, L.J. Guo, Y.C. Wang, et al., *Energy Fuel* **2020**, 34, 360-367.

[2] H. Jin, Y. Wang, H. Wang, et al., *Phys. Fluids* **2021**, 33, 023313.

Intelligent virtual process engineering: modelling, computing and analysing

Haolei Zhang,[a,b] Aiqi Zhu,[a,b] Ji Xu,[a,b] Wei Ge[a,b]*

[a]State Key Laboratory of Mesoscience and Engineering, Institute of Process Engineering, Chinese Academy of Sciences, Beijing 100190, China
[b]School of Chemical Engineering, University of Chinese Academy of Sciences, Beijing 101408, China
*Corresponding author: wge@ipe.ac.cn (W. Ge)

Virtual process engineering (VPE) [1] aims to allow chemical engineers to design, scale-up, optimize, or control processes online and in real-time, without the need for extensive, stage-by-stage experimental trials and errors. VPE requires high accuracy, capability and efficiency of the numerical simulation methods, in the example of gas–solid systems widely present in chemical, mineral and power industries, the coupling of discrete element method (DEM) with computational fluid dynamics (CFD), namely CFD–DEM, is becoming an effective simulation method for this purpose.

Traditionally, the computational cost of the DEM part in CFD-DEM is much higher than the CFD part as many more solid particles are tracked than the CFD grids. But with coarse-graining of the particles and heterogeneous high-performance computing, the CFD part becomes the wall-time bottleneck in many cases. To boost the performance of the CFD part, a dual-grid approach [2] is proposed, where the pressure is solved on a coarse grid to ensure mass conservation, while the fluid velocity and particle-fluid interactions are computed on a fine grid to retain accuracy, achieving one order of magnitude speedup. To further speed up the CFD part, a fluid-dynamics prediction method (FPM) [3] is proposed to predict the gas phase flow dynamics in the gas–solid flow systems. Using the dataset from accurate CFD–DEM simulations, the artificial neural networks (ANN) and the UNet architecture are constructed by analyzing the influence of the flow dynamics at different spatio-temporal scales. The FPM can again be an order faster than the CFD for flow prediction. Integrating the FPM into the CFD–DEM framework, long-time simulation of the gas–solid system is achieved, which enables VPE to optimize industrial reactors with in-depth analysis of the huge volume of simulation data based on artificial intelligence. [4]

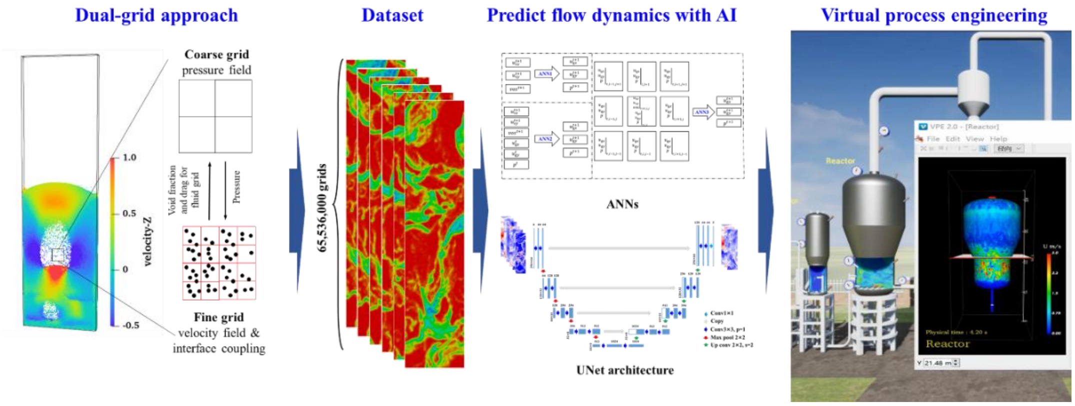

Figure 1. Schematic of the intelligent virtual process engineering.

References

[1] W. Ge, et al., *Chem. Eng. Sci.* **2011**. 66(19), 4426-4458.

[2] A. Zhu, Q. Chang, J. Xu, W. Ge, *Chem. Eng. J.* **2024**, 492, 152218.
[3] H. Zhang, J. Xu, L. Guo, L. Gao, J. Ye, W. Ge, *Phys. Fluids* **2024**, in revision.
[4] H. Zhang, A. Zhu, J. Xu, W. Ge, *Particuology* **2024,** 89, 131-143.

Development of advanced models for blast furnace ironmaking: analysis of operational dynamics and process optimization

Xiaobing Yu, Yansong Shen*

Chemical Engineering School, University of New South Wales, Sydney, NSW 2052, Australia
*Corresponding author: ys.shen@unsw.edu.au

This study presents the development and application of novel models, including several integrated multi-fluid blast furnace (BF) models [1-12], with a focus on burden layer structure and innovative operations [13], and a localised region model studying raceway behaviours of a packed bed reactor. The model integrates multiphase flow and key thermochemical processes within the chemical reactors.

A gas residence time distribution (RTD) model was developed to better understand gas flow patterns and RTD formation within a BF. The results indicate that the gas flow in the BF is predominantly piston-type, while flow in the stagnant regions contributes to the RTD tail. Additionally, several innovative operations were systematically investigated using BF models, coupled with relevant sub-models. These include sub-models for central coke charging (CCC), nut coke charging, carbon composite briquette (CCB) charging, burden batch weight selection, oxygen enrichment, and hydrogen shaft injection. These operations are aimed at reducing fuel consumption, improving productivity, and enhancing the environmental sustainability of BF operations. The influence of shaft angle on BF performance was also examined, revealing mechanisms by which the shaft angle affects in-furnace behaviour. Furthermore, hydrogen injection via the shaft was theoretically explored, and its RTD was systematically analysed. The findings show that hydrogen flow rate has a more pronounced effect on RTD than injection temperature, deepening our understanding of hydrogen behaviour within the BF.

For the first time, a transient-state BF (TBF) model was developed to capture dynamic in-furnace phenomena, including flow, thermal, and chemical behaviours, alongside chemical reactions in specific burden layers. This TBF model was applied to a commercial, industry-scale BF to simulate the time evolution of velocity fields, cohesive zone profiles, thermal fields, and gas utilisation efficiency from the initial to the steady state. The model's capabilities were demonstrated through its application to hot burden charging, capturing time-evolving in-furnace phenomena at specific intervals. Moreover, the TBF model was used to investigate the dynamic responses of various BF regions to changes in burden temperature (BT), quantitatively showing that regions near the gas inlet exhibit faster and more significant responses compared to other areas.

In addition to the integrated multi-fluid BF models, an advanced 3D multi-fluid model was developed using the Eulerian-Eulerian method. This model, coupled with heat transfer and heterogeneous reactions, simulates reacting flow behaviours within and around raceways for a slow-moving packed bed chemical reactor. The results show that raceway behaviours are more symmetrical on horizontal cross-sections compared to other orientations. Specifically, probability theory and statistical analysis were employed to quantitatively evaluate raceway characteristics.

Overall, these models offer valuable insights into fundamentals, novel operations and provide cost-effective tools for understanding the evolution of in-reactor behaviours during operational changes. They also lay the foundation for real-time monitoring and control of packed bed reactors, contributing to the broader knowledge of in-reactor phenomena.

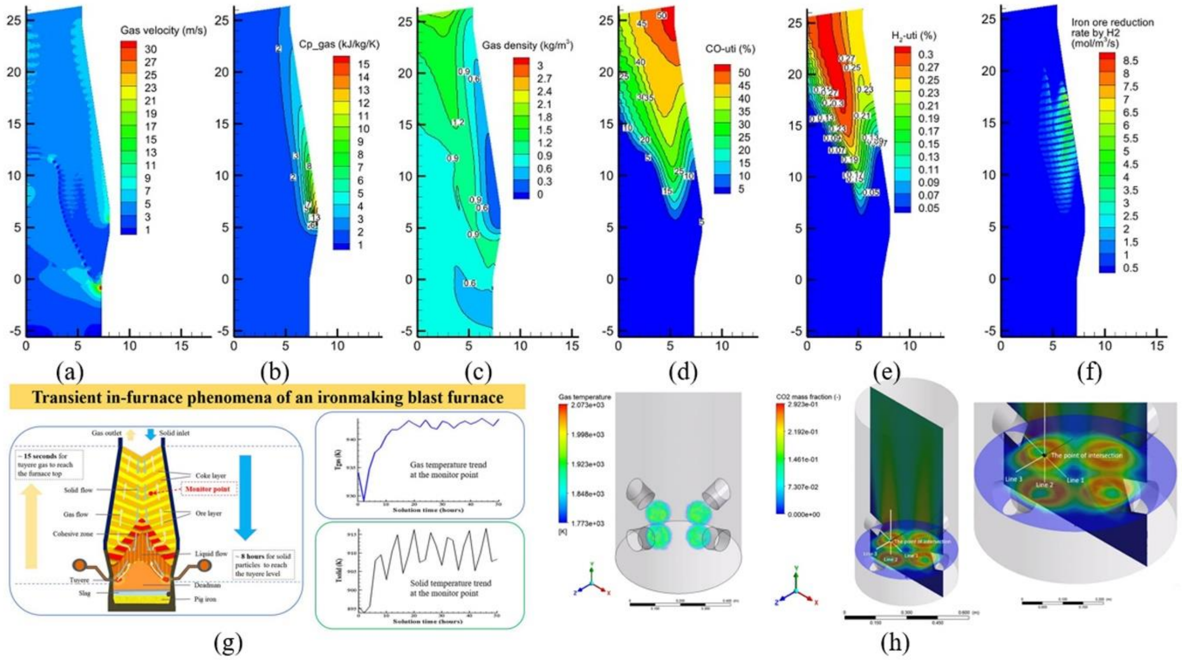

Figure 1. Typical results of in-reactor phenomena: _BF adopting hydrogen shaft injection_: (a), gas velocity; (b), heat capacity of gas; (c), gas density; (d), carbon monoxide utilisation efficiency; (e), hydrogen utilisation efficiency; (f), iron ore reduction rate by hydrogen; _BF adopting hot burden charging_: (g), gas and solid temperature trends with time at monitoring point; _Raceway study of a packed bed reactor_: (h), raceway profiles and CO2 distribution.

References

[1] X. Yu, Z. Hu, Y. Shen, *Fuel* **2021**, 302, 121092.

[2] X. Yu, Y. Li, H. Xu, Y. Shen, *Powder Technol.* **2022**, 407.

[3] X. Yu, Y. Shen, *Metall. Mater. Trans. B* **2018**, 49(5), 2370-88.

[4] X. Yu, Y. Shen, *Chem. Eng. Sci.* **2019**, 199, 50-63.

[5] X. Yu, Y. Shen, *Powder Technol.* **2019**, 361, 124-35.

[6] X. Yu, Y. Shen, *Energ Fuel* **2019**, 33(11), 11603-16.

[7] X. Yu, Y. Shen, *Metall. Mater. Trans. B* **2019**, 50(5), 2238-50.

[8] X. Yu, Y. Shen, *Metall. Mater. Trans. B* **2020**, 51(5), 2079-94.

[9] X. Yu, Y. Shen, *Metall. Mater. Trans. B* **2020**, 51(4):1760-72.

[10] X. Yu, Y. Shen, *Chem. Eng. Sci.* **2022**, 248.

[11] X. Yu, Y. Shen, *Fuel* **2023**, 348.

[12] X. Yu, Y. Shen, *Fuel* **2024**, 372.

[13] X. Yu, Y. Shen, *Fuel* **2024**;367.

Towards pore-scale simulation of multiphase flows in porous media

Zhisong Ou,* Qiang Xue

State Key Laboratory of Geomechanics and Geotechnical Engineering, Institute of Rock and Soil Mechanics, Chinese Academy of Sciences, Wuhan 430071, China
*Corresponding author: zsou@mail.whrsm.ac.cn

Modelling multiphase flow in porous structures remains a challenge due to the complexity of handling multiple interfaces. This paper presents a one-domain pore-resolved simulation approach for immiscible two-phase flows in porous media, using a monolithic fluid-solid coupling framework to implicitly consider the existence of solid objects. The fluid-fluid interfaces are captured through solving an algebraic volume of fluid equation, with the fluid interfacial tension considered by integrating a continuum surface force. Wall wettability condition is imposed by modifying the contact angle of the fluid interface at the embedded solid surface. The resulting equations are simple and stable, as there are no empirical models or parameters involved for the interface representation. This approach has been validated through performing a series of test-case simulations, including capillary-dominated flow, capillary rise with gravity, Taylor film formation, and finally two-phase flow in a heterogeneous porous structure. The numerical approach is demonstrated to be well suitable for investigating pore-scale two-phase flows in realistic porous media.

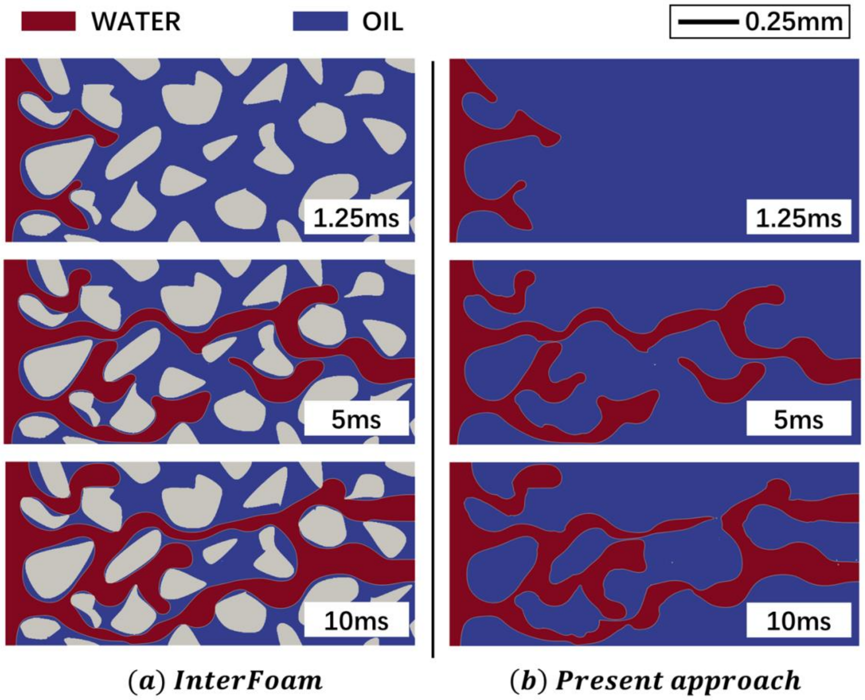

Figure 1. Saturation field of oil drainage in a complex pore network, as predicted by (a) *interFoam* and (b) the present approach.

References

[1] Z. Ou, C. Chi, L. Guo, D. Thévenin, *J. Comput. Phys.* **2022**, 468, 111447.

A corrected solid stress closure considering the effect of the wall boundary in gas-particle fluidized bed

Shouzheng Yuan,[a] Qiang Zhou[a,b,*]

[a]School of Chemical Engineering and Technology, Xi'an Jiaotong University, Xi'an, China
[b]State Key Laboratory of Multiphase Flow in Power Engineering, Xi'an Jiaotong University, Xi'an,China
*Corresponding author: zhou.590@mail.xjtu.edu.cn

Filtered two-fluid models (fTFMs) are usually employed to predict the flow behavior in large fluidized bed reactors. In fTFMs, the filtered drag forces and filtered solid stresses hold great importance and are significantly influenced by heterogeneous structures. A recent study[1] showed that the forces due to filtered solids stresses, although smaller than the filtered drag forces, are considerable at larger filter sizes. Many previous filtered closures are developed based on full-periodic domain datasets. The wall boundary in practical fluidized reactors can impact the evolution of heterogeneous structures, thereby affecting the accuracy of these closures. This work aims to further enhance the performance of existing filtered solid stress closure by introducing the influence of the wall boundary.

In this work, the fine-grid discrete element method (DEM) is utilized to simulate gas-solid beds with various solid volume fractions. A filtering technique, combined with Cloete's anisotropic solid stress closure[2], is applied to obtain the solid stress of the xy and yy components in the flow direction y. We propose two correction coefficients, denoted as H_{rxy} and H_{ryy}, which correlate with the distance from the grid to the wall boundary. To extend the corrected closure, the influence of local solid volume fraction and filter size are additionally introduced. Subsequently, simple coarse-grid posteriori validations are conducted. The filtered drag model in Ref.[3] is used and abbreviated as Gao model. Figure 1 presents the radial distributions of solid volume fraction obtained from the coarse-grid ($72d_p$) results by Gao model and the corrected stress closure at the bed height of 2.31m in the Wei's fast bed[4]. As opposed to previous closure (Gao-cloete), the corrected closure (Gao-cloete-corrected) exhibits a trend that closely aligns with the experimentally measured values. This figure provides evidence that the modification of the existing solid stress closure is effective.

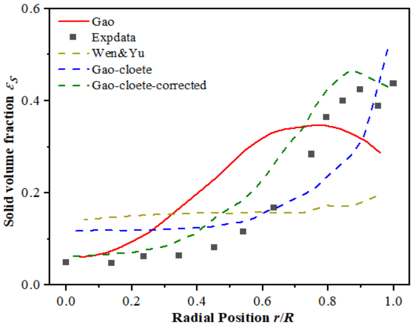

Figure 1. The radial profiles of solid volume fraction at a bed height of 2.31 m in the Wei's fast bed.

References

[1] S. Schneiderbauer, *AICHE J* **2017**, 63, 3544-3562.
[2] J.H. Cloete, S. Cloete, S. Radl, S. Amini, *Chem. Eng. Sci.* **2018**, 192, 906-929.
[3] X. Gao, T. Li, A. Sarkar, L. Lu, W.A. Rogers, *Chem. Eng. Sci.* **2018**, 184, 33-51.
[4] F. Wei, H.F. Lin, Y. Cheng, Z.W. Wang, Y. Jin, *Powder Technol.* **1998**, 100, 183-189.

Analysis of simulated metal powder distribution in new design DED nozzle out flow field

Bing-Zhi Wang,[a] Li-Tsung Sheng,[b] Shu-San Hsiau[a,]*

[a]Department of Mechanical Engineering, National Central University, Zhongli, Taoyuan, Taiwan
[b]Department of Mechanical and Electro-Mechanical Engineering, National Ilan University, Yilan, Taiwan
*Corresponding author: sshsiau@cc.ncu.edu.tw

The powder utility efficiency in DED processes is important to the parts makers in reducing cost. In this research, we intend to construct a new-structure nozzle and analyze the powder distribution in cladding zone to confirm getting higher efficiency producing procedure is possible which is benefit to the cost saving.

Regular DED nozzle structures usually contain three different passage channels: laser protect gas, powder carrier gas and shielding gas. In this study, the new-designed nozzle is one with some gas bypass branches connecting powder channel and shielding channel before the powder ejecting into cladding zone. The bypass branches can lead a portion of the powder carrying gas into shielding channel result in decreasing of the gas mass fraction in the exit of powder channel into the cladding zone. This can be helpful to make powder concentration increase in the central portion of cladding zone. The higher powder concentration implies the raising of the powder utility efficiency.

A structure of regular nozzle without bypass branches is analyzed to examined to verify the powder distributed conditions in cladding zone. The ejected powder concentration from nozzle in cladding zone is analytically calculated according to both radical distance and vertical distance. Meanwhile, the new design structure nozzle’s powder density distribution is checked in this similar manner and procedures and get the corresponding data. Both structures are applied to many different operative conditions, the results of operative conditions are collected. The comparison between those two structures can be held after both nozzle structures results obtained, and we can conclude from these two concentration DED nozzles structures the higher efficiency one. In this way, the better conditions can be picked out to setup routine working conditions.

Investigation the gas-solids two-phase flows in fluidised bed with different scale based on MP-PIC approach

Haigang Wang[a,b]

[a]State Key Laboratory of Coal Conversion, Institute of Engineering Thermophysics, Chinese Academy of Sciences, Beijing 100190, China
[b]School of Engineering Science, University of Chinese Academy of Sciences, Beijing 100049, China

Gas-solids fluidsed beds are typical used in coal combustion and gasification process in energy related industry. The flow hydrodynamic behavior in the reactor is complex and unsteady. The flow dynamic affects the combustion and gasification efficiency as well as the emission, likes Co2, SOx and NOx. Especially, with the increase in dimensions and scales, the effect becomes more serious. Therefore, it is important to investigate the flow dynamics changes with the scale up of the dimensions. In this research, MP-PIC approach will be used to simulate the gas-solids two phase flow in different scale of circulating fluidised beds. Details model including drag model between gas and solids will be given. The dimensions effect on the flow dynamic will be given and compared with available reference measurement, likes pressure drop measurement and process tomography. The challenge will be given in the end of the paper.

Numerical simulation of the decarboxylation process of powdered $CaCO_3$ in the pilot jet flame

Susumu Tsuchiya,[a] Masaya Muto,[b,]* Yuta Umeno,[c] Takayuki Nishiie,[c] Noriaki Nakatsuka,[d]
Fumiteru Akamatsu,[d] Ryoishi Kurose[e]

[a]Yabashi Industries CO., LTD., Ogaki, Japan
[b]Meijo University, Nagoya, Japan
[c]Numerical Flow Designing CO., LTD., Tokyo, Japan
[d]Osaka University, Osaka, Japan
[e]Kyoto University, Kyoto, Japan
*Corresponding author: mutom@mejo-u.ac.jp

Quicklime, which is widely used in steel production, exhaust gas treatment, soil stabilization treatment, and raw materials for building materials, is obtained by firing limestone $CaCO_3$ at a high temperature. The gas flow field inside the rotary kiln, which has a length of several tens of meters, is kept at a high temperature by the spray flame, and the limestone is calcined while flowing down in the kiln. However, the details of the gas temperature distribution inside the kiln, the behaviour of the flowing limestones, and the effect of the residence time on the quality of the obtained quicklime have not been fully clarified. Therefore, in our previous study, a numerical simulation was conducted to clarify the gas temperature distribution in the kiln and the behaviour of limestones flowing down in the kiln by performing a numerical simulation of the combustion field in the actual rotary kiln [1].

The purpose of this study is to investigate in detail the decarboxylation process of $CaCO_3$ by a numerical simulation using powdered lime powder $CaCO_3$ rather than relatively large diameter limestone like those used in actual rotary kilns, aiming to achieve more uniform decarboxylation of $CaCO_3$ and to investigate the decarboxylation process in more detail. Large-eddy simulation is applied to a laboratory-scale jet flame formed in an upright cylindrical furnace in which powdered $CaCO_3$ is injected and a three-stream flamelet/progress-variable approach [2-4] is employed as turbulent combustion model. The LES solver used in this study is the FrontFlow/red developed by the CRIEPI, Kyoto University, Kyushu University, and NuFD (Numerical Flow Designing Co., Ltd.). The governing equations for the gas phase are the conservation equations of mass, momentum, energy, mixture fraction of fuel, mixture fraction of CO_2 generated by the limestone calcination, and progress variable. For the powdered $CaCO_3$ flowing in the combustion field are tracked in a Lagrangean manner using the Particle-Source-In-Cell (PSI-Cell) model. The upright cylindrical furnace length and inner diameter are around 1.2 m and around 0.2 m, respectively. Powdered $CaCO_3$ are injected from the top of the furnace and flow down inside of the furnace. The arithmetic mean value of powdered $CaCO_3$ injected is approximately 20 μm.

As a snapshot of the present simulation of decarboxylation process, Figure 1 shows instantaneous distribution of particle temperature, mass fraction of $CaCO_3$ in each particle and residence time of each particle. In each figure, particles present in a thin region including the center cross section in the depth direction are visualized. From Figure 1(a), it is found that powdered $CaCO_3$ particles are injected into the furnace from the top of the furnace at room temperature and then rapidly heated by the jet flame. Also, particles kept at a low temperature can be seen in the center of the jet. This is because relatively largediameter particles are not sufficiently heated and penetrate downstream while maintaining large inertia due to the jet flow. As shown in Figure 1(b), the decarboxylation reaction of the heated $CaCO_3$ powder particles progresses, and many particles with a $CaCO_3$ mass fraction of almost zero are dispersed from the longitudinal center of the furnace to the downstream. However, particles with a relatively large mass fraction of $CaCO_3$ can be seen near the center of the jet. This is considered to be because the temperature of the particles kept low at the center of the jet, and there is not enough residence time for decarboxylation to proceed. As seen in Figure 1(c), the residence time of particles passing through the center of the jet is short. On the other hand, particles with a long residence time are dispersed around the middle of the longitudinal direction of the furnace, especially near the wall. The possible reasons for this are as follows. Relatively small $CaCO_3$ particles do not have much inertia when they are injected into the furnace, so they decelerate as they pass through inside the furnace and are also entrained by the recirculating flow generated inside the furnace by the jet.

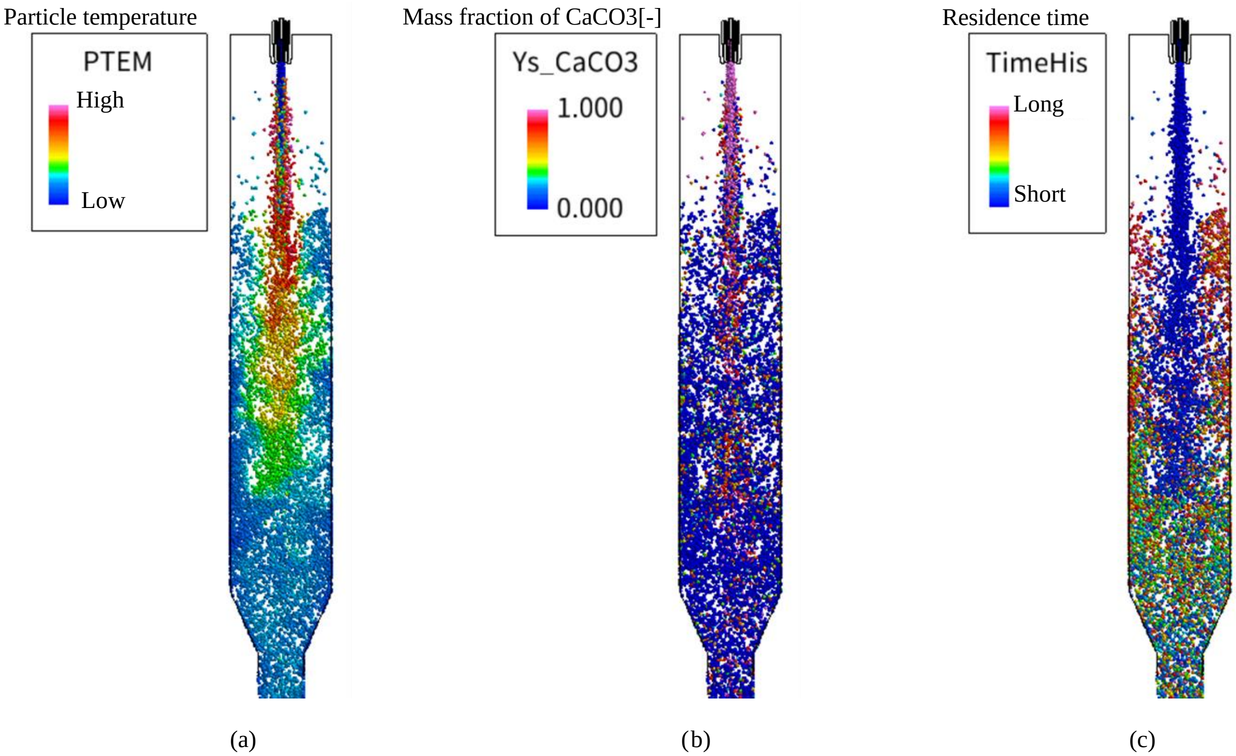

Figure 1. Instantaneous distribution of (a) particle temperature, (b) mass fraction of $CaCO_3$ in each particle, (c) residence time of each particle.

References

[1] S. Tsuchiya, M. Muto, Y. Umeno, T. Nishiie, R. Kurose, *Proc. ICCCI 2022*. **2022**.
[2] M. Ihme, Y.C. See, *Proc. Combust. Inst.* **2011**, 33, 1309–17.
[3] T. Honzawa, R. Kai, K. Hori, M. Seino, T. Nishiie, R. Kurose, *Energy AI.* **2021**, 5, 2666-5468.
[4] H. Kasuya, Y. Iwai, M. Itoh, Y. Morisawa, T. Nishiie, R. Kai, R. Kurose, *Appl. Energy Combust. Sci*. **2023**, 12, 100083.

A numerical simulation study of particle flow and reaction flow in H_2 shaft furnace

Zhengjian Liu,[a,*] Shaofeng Lu,[a] Yaozu Wang,[b,c] Jianliang Zhang[a]

[a]School of Metallurgical and Ecological Engineering, University of Science and Technology Beijing, Beijing 100083, China
[b]School of Intelligence Science and Technology, University of Science and Technology Beijing, 100083 Beijing, China
[c]Institute of Artificial Intelligence, University of Science and Technology Beijing, 100083 Beijing, China
*Corresponding author: liuzhengjian@ustb.edu.cn

Iron and steel industry is an important basic industry for economic development. At present, the emission of steelmaking is about 1.9t-CO_2/ t-steel. Total direct emissions in 2020 are about 2.6 billion tons, accounting for 7 to 9 percent of global anthropogenic CO_2 emissions [1]. Agreement adopted in 2015 sets the goal of controlling the temperature rise below 2°C in 2100 compared with that before industrialization [2,3]. At present, the vast majority of crude steel is produced through the BF/BOF route. In order to achieve carbon emission reduction goals, "breakthrough innovation" low-carbon development technologies need to be developed in the future. However, due to the characteristics of the BF's high-carbon energy structure, its CO_2 emissions It accounts for about 70% of the entire BF/BOF long process [4], so the CO_2 emission reduction potential of the BF/BOF route is limited. As an alternative to the long process, the short process of direct reduction (DR)/electric arc furnace (EAF) can reduce CO_2 emissions by 40-60% compared with the long process [5,6].

In DR process, the direct reducing iron (DRI) produced by hydrogen-based shaft furnace accounts for more than 75% of the global DRI production. This process mainly uses natural gas as feed gas and produces reducing gas with a high proportion of H_2 through reforming reaction to achieve further carbon reduction. With the wide application of hydrogen energy, H_2 shaft furnace uses pure H_2 to reduce iron oxide, which can further reduce CO_2 emissions. Although large-scale hydrogen production is limited by environmental protection and economic factors, with the development of hydrogen production technology from renewable energy, H_2 shaft furnace has a broad development prospect in the future. Therefore, some major companies are scrambling to carry out H_2 shaft furnace research projects, such as HYBRIT of SSAB and LKAB cooperation[7], H2H project of ArcelorMittal, MIDREX and Paul Wurth's H_2 Green Steel, etc.

Since there is a complex energy and mass transfer process in the H_2 shaft furnace and it is a black box model, it is difficult to use experimental instruments to reproduce the shaft furnace production process. Therefore, we can establish a mathematical model of the shaft furnace and obtain different results in a short time through numerical simulation. The spatial distribution of physical quantities in the shaft furnace under the conditions more accurately reflects the actual situation.

At present, numerical simulation on shaft furnaces mainly uses pseudo fluids to replace actual burden particles, which cannot reflect the specific flow state of the burden in the shaft furnace and the interaction between burden and reducing gas. Therefore, this work established a 3D model of H_2 shaft furnace based on CFD-DEM two-way coupling, simulated the flow of burden particles in the shaft furnace and the interaction between gas and burden particles. Obtained the gas distribution and the movement of burden particles. The flow state in the furnace was discussed, and the influence of the reducing gas flow rate on the falling process of burden was discussed. Finally, a CFD-DEM chemical reaction 3D model of the H_2 shaft furnace was further established, and the detailed distribution of temperature, metallization degree, etc. in the shaft furnace was obtained. Provides corresponding information for the operation of H_2 shaft furnace.

References

[1] M. Flores-Granobles, M. Saeys, *Energy Environ. Sci.* **2020**, 13(7), 1923-1932.

[2] C. Bataille, M. Åhman, K. Neuhoff et al, *J. Clean. Prod.* **2018**, 187, 960-973.

[3] L. Belkhir, A. Elmeligi, *J. Clean. Prod.* **2019**, 214, 185-194.

[4] T. Ariyama, K. Takahashi, Y. Kawashiri et al, *J. Sustain. Metall.* **2019**, 5, 276-294.

[5] K. Rechberger, A. Spanlang, A. Sasiain Conde et al, *Steel Res. Int.* **2020**, 91(11), 2000110.

[6] P. E. Duarte, J. Becerra, Reducing greenhouse gas emissions with Energiron non-selective carbon-free emissions scheme. **2011**.

[7] M. Pei, M. Petäjäniemi, A. Regnell et al, *Metals* **2020**, 10(7), 972.

CFD-DEM study of the effect of lump ore on in-furnace phenomena in an ironmaking blast furnace

Peng Zhou,[a,b] Shibo Kuang,[c,*] Dianyu E,[d] Ruiping Zou,[c] Wenqi Zhong,[a] Aibing Yu [b,c,*]

[a]School of Energy and Environment, Southeast University, Nanjing, 210096, China
[b]Center for Energy and Environment, Southeast University-Monash University Joint Research Institute, Suzhou, 215123, China
[c]ARC Research Hub for Computational Particle Technology, Department of Chemical Engineering, Monash University, Clayton, Melbourne, VIC, 3800, Australia
[d]Jiangxi Provincial Key Laboratory for Simulation and Modelling of Particulate Systems, Jiangxi University of Science and Technology, Nanchang 330013, PR China
*Corresponding author: aibing.yu@monash.edu
*Corresponding author: shibo.kuang@monash.edu

Natural lump ore can be used directly in a blast furnace (BF) smelting to replace part of the sinter and pellets, which can effectively reduce BF production costs and CO2 emissions and is therefore regarded as a very promising ferrous material. The mechanism of the effect of lump ore in the mixed burden on the in-furnace phenomena is still not well understood. In this study, a validated computational fluid dynamics-discrete element method (CFD-DEM) model is employed to investigate the thermo-chemical behaviours of lump ore in a BF. The effect of the sinter-lump ratio on typical in-furnace phenomena is comprehensively explored and analysed under various operating conditions. The numerical results show that the use of lump ore in the mixed burden has a significant influence on the formation of the cohesive zone (CZ) as well as on the gas distribution and permeability of the upper of the BF. As the ratio of lump ore increases from 0% to 30%, the CZ becomes thicker and taller. Additionally, the gas porosity in the upper part of the furnace decreases, leading to a decline in the permeability of the BF, which results in a significant increase in the gas pressure drop. On the other hand, the increase in the proportion of lump ore leads to a decrease in top gas utilization while improving productivity. These results provide theoretical guidance for the use and control of lump ore in BFs.

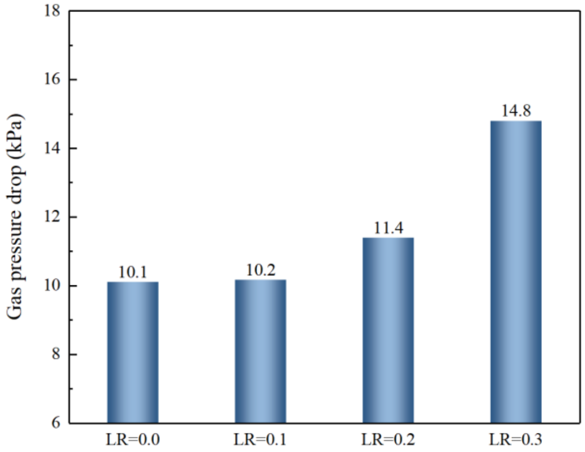

Figure 1. Effect of lump ratio on gas pressure drop in the BF.

Numerical investigation of motion of a pellet-shaped particle placed in uniform flow

Kenji Tanno,* Toshiaki Fukada

Central Research Institute of Electric Power Industry, Yokosuka, Japan
*Corresponding author: k-tanno@criepi.denken.or.jp

Gasification is a promising technology for high-efficiency power generation using biomass and for recycling carbon resources such as plastics. In those systems, biomass and plastics are expected to be used in centimeter-order pellet form, without being pulverized into fine particles. Haider and Levenspiel [1] studied drag coefficient (C_D) of non-spherical particles by investigating the relations between C_D, particle Raynolds number Re_p and sphericity. Non-spherical particles placed in flow may move with rotating, but their results do not include the effect of rotation. Zhang et al. [2] performed numerical simulations using the Arbitrary Lagrangian-Eulerian (ALE) method for a single pulverized coal particle to evaluate the effect of rotational motion of a non-spherical particle on drag coefficient. However, the size of pulverized coal particle they targeted was about 40μm, and the range of particle Reynolds numbers is very different from that of the pellet-shaped feedstocks. Here in this study, numerical simulation with six degrees of freedom motion of a pellet-shaped single particle of centimeter order is performed by employing the ALE method. The flow velocity was set to 10 m/s, and the particle was placed in the upward flow at the beginning of the computation (Figure 1). Numerical results showed that the drag coefficient varies with particle rotation motion. Pressure drag dominantly affects drag force, drag force decreases as projected area decreases and increases as projected area increases. As a result, the curve of the drag coefficient exhibits up and down fluctuating behaviour (Figure 2).

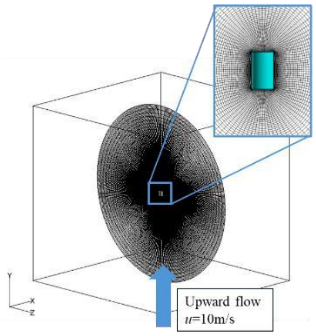

Figure 1. Computational domain and pellet-shaped particle.

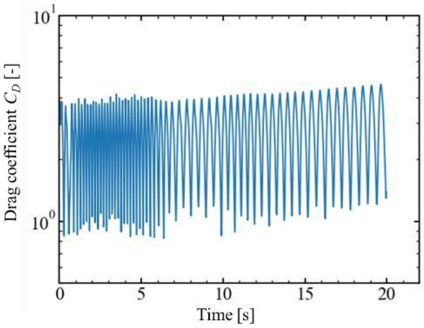

Figure 2. Temporal variation of drag coefficient.

Acknowledgement

This work is based on results obtained from a project, JPNP16002, commissioned by the New Energy and Industrial Technology Development Organization (NEDO).

References

[1] A. Haider, O. Levenspiel, *Powder Technol.* **1989**, 58(1), 64-70.
[2] W. Zhang, H. Watanabe, T. Kitagawa, *Adv. Powder Technol* **2018**, 29, 2048-2060.

Validation study on the coarse graining DEM-CFD simulation for large-scale industrial liquid–solid flow systems

Nobutaka Kitsunai,[a] Mikio Sakai[b]

[a]Murata Manufacturing Co., Ltd., Kyoto 617-8555, Japan
[b]Department of Nuclear Engineering and Management, School of Engineering, The University of Tokyo, Tokyo 113-8656, Japan

Large-scale liquid-solid flow systems, such as planetary mixer and inline mixer, are often employed in chemical engineering. Numerical modeling is widely applied for the design and the better understanding of complex phenomena. The discrete element method (DEM) coupled with the computational fluid dynamics (CFD) is applied to simulate the liquid-solid dispersion systems for the optimization of the particle design and operating conditions. However, application of the numerical simulations for these systems is still limited because the number of the particles becomes small comparing with the required one in the industrial processes. This makes difficult to understand the complex behavior in these processes. The coarse-grained DEM was developed to resolve the problem for the simulation of the real industrial processes. Adequacy of the coarse-grained DEM has been proven for simple systems so far. In the present study, applicability of the coarse-grained DEM is examined to simulate the liquid-solid flow in a planetary mixer. It is demonstrated that the coarse-grained DEM can simulate the industrial liquid-solid flow systems.

Numerical study on the dynamic behaviors of shear-thinning droplets impacting on a hydrophobic spherical surface

Jialiang Cai, Jiliang Ma,* Xiaoping Chen, Cai Liang

School of Energy and Environment, Southeast University, Nanjing, China
*Corresponding author: jlma@seu.edu.cn

During the process of fluidized bed spray granulation, the particles are partially wetted by a non-Newtonian binder, which forms a “liquid cap” at the steady state on the particle surface [1]. The way the droplet spreads on the particle surface will also impact the strength of the liquid bridge force between particles. This, in turn, determines the size, structure, and strength of the agglomerates during granulation [2, 3]. Hence, it is crucial to elucidate the collision-wetting-deposition characteristics of non-Newtonian droplets on a particle surface.

In this study, the dynamic behavior of shear-thinning droplets impacting on a hydrophobic spherical surface is numerically investigated using the Volume of Fluid (VOF) method coupled with dynamic contact angle and a power-law model. The differences in dynamic behaviors between shear-thinning and Newtonian droplets are first studied. By analyzing the distribution of pressure and shear rate inside the droplet, it is found that the shear-thinning behavior of the droplets leads to an uneven distribution of apparent viscosity upon impact, which in turn prevents droplet rebound. The effects of various impacting conditions, such as apparent viscosity, impact velocity, surface tension and dynamic contact angle, on the spreading factor and liquid film thickness of shear-thinning droplets are investigated. According to the behaviors of droplets, the impacting process can be divided into three phases: (I) initial deformation, (II) inertia-dominated, and (III) viscosity-dominated phases. In order to reveal the physical mechanisms that prevent shear-thinning droplets from rebounding on the hydrophobic particle surface, the conversion of kinetic energy, viscous dissipation, surface energy and potential energy during the three phases of the impact process is also analyzed in detail.

References

[1] K. Terrazas-Velarde, M. Peglow, E. Tsotsas, *Chem. Eng. Sci*. **2009**, 64, 2631-2643.

[2] A. Burggraeve, T. Monteyne, C. Vervaet, J.P. Remon, T.D. Beer, *Eur. J. Pharm. Biopharm*. **2013**, 83, 2-15.

[3] R. Andrade, O. Skurtys, F. Osorio, *Food Res. Int*. **2013**, 54, 397-405.

A mPOD-based reduced-order modelling approach for fast gas-solid flow simulations

Huiting Chen,[a] Wangyan Li,[b,a] Jie Bao,[a] Yansong Shen[a,]*

[a]School of Chemical Engineering, University of New South Wales, NSW 2052, Australia
[b]College of Science, University of Shanghai for Science and Technology, Shanghai 200093, China
*Correspondence author: ys.shen@unsw.edu.au

Gas-solid flow systems are widely practised in chemical engineering and known for their multi-scale and intricate complexity, and thus their simulations are usually time-consuming and computationally demanding. To address this long-standing challenge, a novel non-intrusive reduced-order modelling (ROM) approach for gas-solid flow simulations is introduced and applied to a fluidised bed for demonstration. For the first time, a multi-scale proper orthogonal decomposition (mPOD) is applied to decompose the gas-solid data into a set of spatial and temporal bases that are spectrally cleaner and energetically more relevant than those produced by other decomposition methods. To tackle the complexities of high-dimensional data and long-term dependencies encountered in prior approaches, a hybrid deep learning framework, i.e., the transformer encoder–long short-term memory decoder model, is employed for the ROM prediction. The proposed method demonstrates excellent performance in balancing accuracy and efficiency for capturing the complex dynamics of gas-solid flows. The mean absolute percentage error between the proposed ROM and full-order model is as small as 10% in this fluidised bed case, demonstrating high accuracy. Additionally, it achieves a 1000-fold speedup in efficiency, providing a cost-effective tool for practical applications in real-time monitoring and control of gas-solid systems.

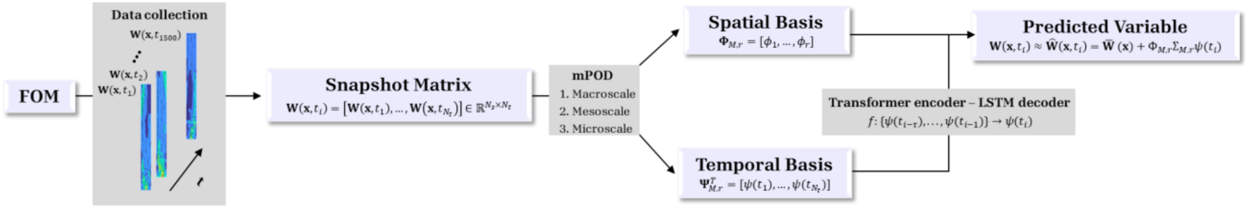

Figure 1. The modelling approach of mPOD-based ROM proposed in this work.

Super-quadric CFD-DEM study of spout deflection behaviour of non-spherical particles in a spout fluidized bed

Zhan Luo, Shuai Wang, Yansong Shen*

School of Chemical Engineering, University of New South Wales, Sydney, NSW 2052, Australia
*Correspondence author. ys.shen@unsw.edu.au

Non-spherical particles are commonly encountered in chemical engineering processes including fluidization processes, yet their instability phenomena still lack understanding. In this study, the spout deflection – a typical instability phenomenon of non-spherical particles in a pseudo-two-dimensional (pseudo-2D) spout fluidized bed is first studied by a super-quadric computational fluid dynamics-discrete element method (super-quadric CFD-DEM) model. The intensity of spout deflection is quantified by the spout deflection angle concept. The effect of particle shape (i.e., sphere, cubic, ellipsoid, and cylinder) on the flow in terms of flow pattern, spout deflection, pressure drop, particle orientation, and normal contact force is systematically studied and compared by the time- and frequency-domain analysis. It shows that the spout channel becomes narrower for cubic, ellipsoid and cylinder particles where the particle aspect ratio increases. With the increase of spouting gas velocity, the median value of the spout deflection angle decreases and increases for cubic and ellipsoid particles, respectively. Furthermore, the pressure drops in the vertical and horizontal directions of the cubic, ellipsoid, and cylinder particles are different from each other. At last, In the bed of cubic particles, the ordered arrangements appear close to the wall region and random arrangements occur in the other regions. This work reveals the influences of non-spherical particles on spout deflection and offers insights into practical applications through optimal operation.

Numerical simulation of immersed tube bubbling fluidized bed in calcium-based thermochemical energy storage system: influence of key parameters

Xiaodie Guo,[a] Wenjing Zhou,[a,]* Jinjia Wei[a,b]

[a] School of Chemical Engineering and Technology, Xi'an Jiaotong University, Xi'an, 710049, P. R. China
[b]State Key Laboratory of Multiphase Flow in Power Engineering, Xi'an Jiaotong University, Xi'an 710049, P. R. China
*Corresponding author: wj.zhou@mail.xjtu.edu.cn, jjwei@mail.xjtu.edu.cn

Thermochemical energy storage (TCES) applied in concentrated solar power (CSP) holds promise for the large-scale deployment of solar energy and offers solutions to energy shortages and environmental concerns. Among the various TCES systems, the $CaO/CaCO_3$ system stands out as the most promising energy storage system currently due to its low cost and high energy density characteristics. However, its widespread application faces challenges due to the lack of efficient reactors. In recent years, efforts have been devoted by researchers to the development of chemical reactors that can be effectively integrated with solar thermal power generation systems. Among the various reactors, fluidized bed reactors are noted for their excellent heat and mass transfer performance and the advantage of continuous operation, making them a more suitable choice as reaction vessels for TCES systems. However, research on the application of the $CaO/CaCO_3$ TCES system in fluidized bed reactors is relatively scarce. This scarcity may be attributed to the higher temperature range and operational complexity associated with this system compared to other forms of TCES. As an important supplementary tool for experimental measurements, computational fluid dynamics (CFD) can efficiently and intuitively capture the gas-solid flow, heat and mass transfer, and chemical reaction characteristics within fluidized bed reactors, thereby providing valuable insights for optimizing reactor design and its industrial applications.

In this study, the calcium looping energy release process in a bubbling fluidized bed reactor was numerically simulated using an Eulerian-Eulerian two-fluid model, and the validity of the model was verified. The effects of the presence or absence of immersed tubes, particle diameter, CO_2 mole fraction, and gas velocity on the fluid dynamics and thermochemical performance of the carbonation process were comprehensively investigated. The research findings indicate that the presence of immersed tubes improves flow characteristics and effectively controls the bed temperature rise rate. Compared to the absence of immersed tubes, the conversion rate increased by 29.3%. The influence of particle diameter on the conversion rate is not significant, attributed to the competitive effect between particle concentration and CO_2 concentration. When the CO_2 molar fraction was increased to 0.65 and 0.8, the conversion rates within the same time frame improved by 31.1% and 63.3% respectively. However, excessively high CO_2 molar fractions can lead to an increased likelihood of the upper part of the immersed tubes being exposed to air, resulting in a sudden drop in heat transfer coefficient (HTC). Compared to the velocity of 0.35 m/s, the conversion rates increased by 31.8%, 57.5%, 77.0%, and 88.7% at the other four velocities, respectively. However, excessively high gas velocities lead to increased bed instability and result in a decrease in the bed to wall HTC. Additionally, an analysis of energy utilization during the carbonation process was conducted. The study suggests that enhancing the heat transfer between the immersed tubes and the bed will be a focal point for future reactor optimization designs.

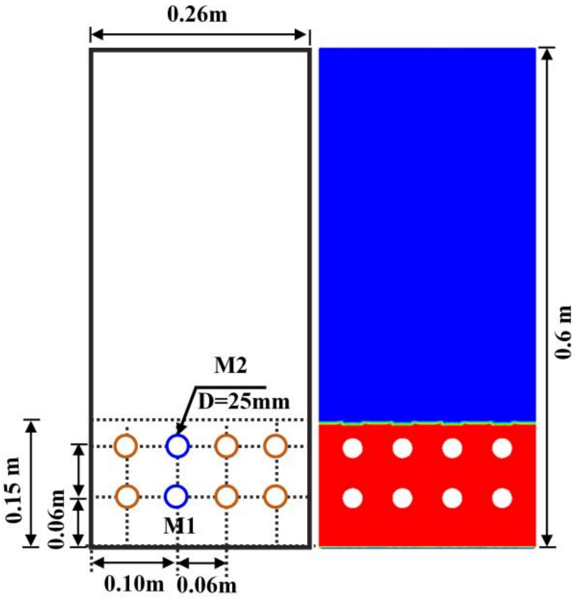

Figure 1. Schematic diagram of bubbling fluidized-bed reactor for Carbonation reaction.

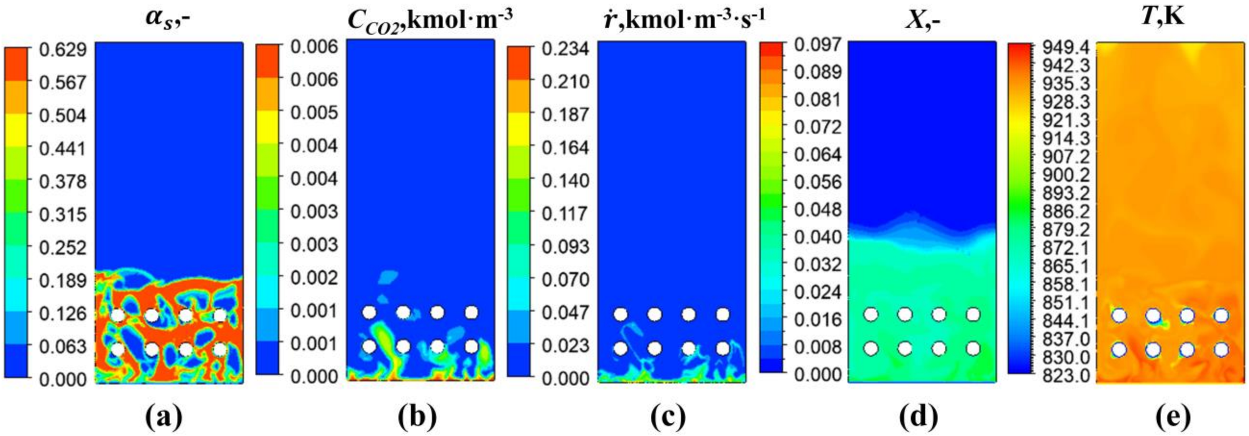

Figure 2. Distribution of physical quantities during carbonation in fluidized bed reactor, t = 20 s: (a) solid volume fraction; (b) CO2 concentration; (c) Heterogeneous reaction rate; (d) conversion rate;(e) gas temperature.

Promotion of particle agglomeration by different vortex generator angles based on PIV-PDPA experiment

Hainuo Wang,[a] Yumeng Zhang,[a,b,*] Shijun Yan,[a] Wenhao Ding,[a] Pengfei Lv,[a] Bo Wang[a,*]

[a]Key Laboratory of Western China's Environmental Systems (Ministry of Education) and Engineering Research Center of Fine Particle Pollution Control Technology and Equipment, Gansu Province, College of Earth and Environmental Sciences, Lanzhou University, Lanzhou 730000, PR China
[b]College of Atmospheric Sciences, Lanzhou, 730000, PR China
*Corresponding author: Name: Yumeng Zhang Email: zhangyumeng@lzu.edu.cn
Name: Bo Wang Email: wangbo@lzu.edu.cn

Turbulent agglomeration is a promising pretreatment technology aimed at enhancing fine particles removal efficiency. Recent studies suggested that V-structure vortex generators are effective in improving turbulence to promote particle collisions and size increase. However, the experimental studies on flow fields and particles induced by V-structure vortex generators with different angles are still insufficient. To this end, this study investigated the effect of the angle of V-structure vortex generators on particle agglomeration based on the experimental approach. More specifically, the flow field dynamics were obtained directly from a Particle Image Velocimetry, while the particle behavior and size variation were investigated by a Phase Doppler Particle Analyzer. The results of the Phase Doppler Particle Analyzer showed that the addition of the vortex generator and its angle increase led to an increase in average size as well as cross-particle size, while a decrease in number concentration of smaller particles, which confirmed the collisions between smaller particles. Through Particle Image Velocimetry experiments, it was found that a wider range of recirculation regions and counter-rotating eddies were generated. Furthermore, by analyzing particle distribution and tracking single particle trajectory through numerical simulation, two kinds of agglomeration mechanisms were proposed. One being the trajectory crossover of smaller particles triggered by recirculating vortex, and the other is the preferential concentration of larger particles. The results of this study can provide a theoretical basis for the design of V-structure vortex generators and particle agglomeration techniques.

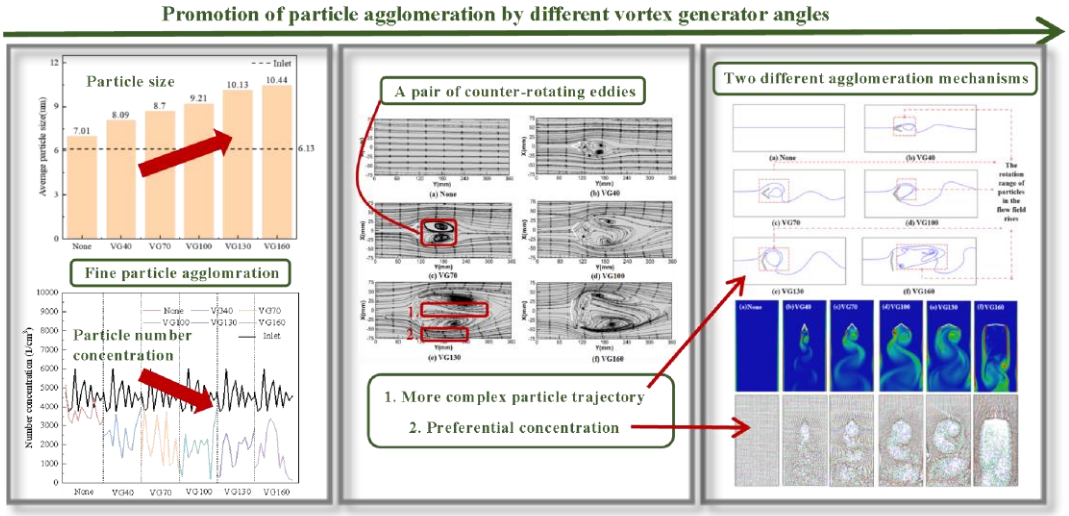

Figure 1. Graphical abstract.

CFD investigation of the structural effects of internal gas intake on powder conveying performance in fuel supply systems for aerospace engines

Guanlong Ren, Qingang Xiong,* Fangjun Chen

South China University of Technology, Guangzhou, China
*Corresponding author: qingangxiong@scut.edu.cn

Optimal design of gas intake in powder fuel supply systems is crucial for the performance of aerospace engines [1]. There is little research on the impact of intake structure on powder conveying performance [2]. Three novel internal intakes were proposed, which are spherical, cube-shaped, and dome-shaped. After validation, CFD simulations demonstrate that the fluctuation of the mass flow rate of powders in the domeshaped intake is reduced by about 73.3% compared with the annular external one. Variation trends of phase velocities are similar for the spherical and cube-shaped intakes, while those are similar for the annular external and dome-shaped internal intakes. The fluctuation of the area of gas zone for the annular external and spherical internal intakes is larger than that for the cube-shaped and dome-shaped internal intakes.

Pressure and relative pressure drop in the fluidization chamber have a stable stage, and the fluctuation of the relative pressure drop is small when dome-shaped internal intake is used.

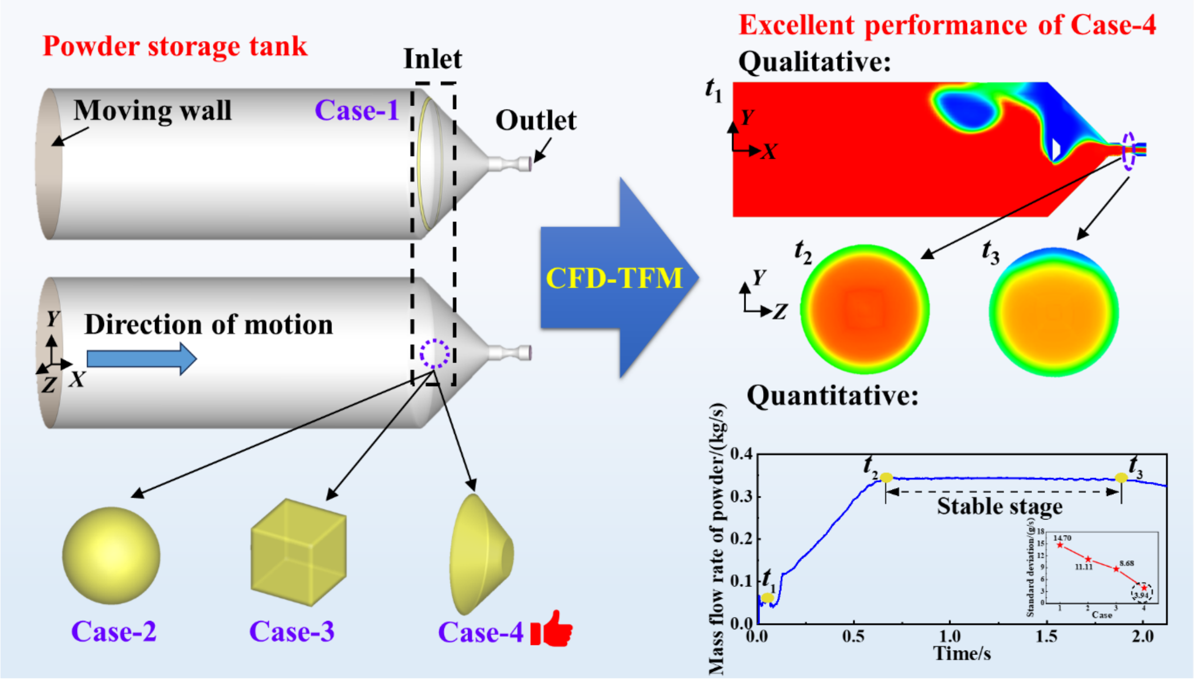

Figure 1. The different powder supply system structures and the presentation of qualitative and quantitative results under optimal structures.

References

[1] J. Tang, Y. Yang, Z. Wang, H. Lu, H. Liu, *Powder Technol.* **2023**, 420, 118406.

[2] J. Liao, K. Xia, J. Song, S. Luo, D. Xu, Y. Feng. *Adv. Powder Technol.* **2022**, 33, 103790.

Mechanical behavior analysis of vertical ocean structures based on DEM-FEM-SPH coupling method

Haoyi Zhang, Lu Liu, Shunying Ji*

State Key Laboratory of Structural Analysis, Optimization and CAE Software for Industrial Equipment, Dalian University of Technology, Dalian 116024, China
*Corresponding author: jisy@dlut.edu.cn

Vertical ocean structure in ice area plays an important role in the field of ocean engineering, and are widely used in oil and gas exploration and exploitation, ocean wind energy utilization, ocean observation and scientific research, etc. The safety of vertical ocean structure in ice area is directly affected by sea ice load and seawater lashing. Therefore, this study aims to explore the load characteristics and dynamic response characteristics of deformable structures under the combined action of sea ice and sea water by establishing a multi-medium coupled numerical model of ice-water-structure. This coupling methods include discrete element method(DEM), smoothed particle hydrodynamics method(SPH) and elastic-plastic finite element method(FEM). The damage and failure behavior of sea ice are described by spherical discrete elements with cohesion-breaking properties [1], the liquid is represented by explicit incompressible smooth particle fluid mechanics [2,3], and the structure is represented by finite elements [4]. The interactions between particle, liquid and solid phase, the entrainment between particle phase and liquid phase and the dynamic response of the structure are analyzed. The accuracy of the numerical algorithm is verified by comparing the basic simulation results with the dam break model experiment and the loading experiment results of sea ice sample and deformable stiffened plate. Finally, rigid materials, linear elastic materials, elastic-plastic materials and elastic materials considering geometric nonlinearity are used to model and simulate the structure of the offshore vertical wind turbines, and compare the load conditions of the wind turbines and the differences in the mechanical behavior of the particle and liquid under different conditions. The results show that a smaller sea ice load and a larger displacement amplitude at the top of the wind turbines tower can be obtained by using geometrically nonlinear elastoplastic materials to model the wind turbines. Different materials of the wind turbines will also respond to the failure model affecting sea ice and the behavior of sea ice entrain.

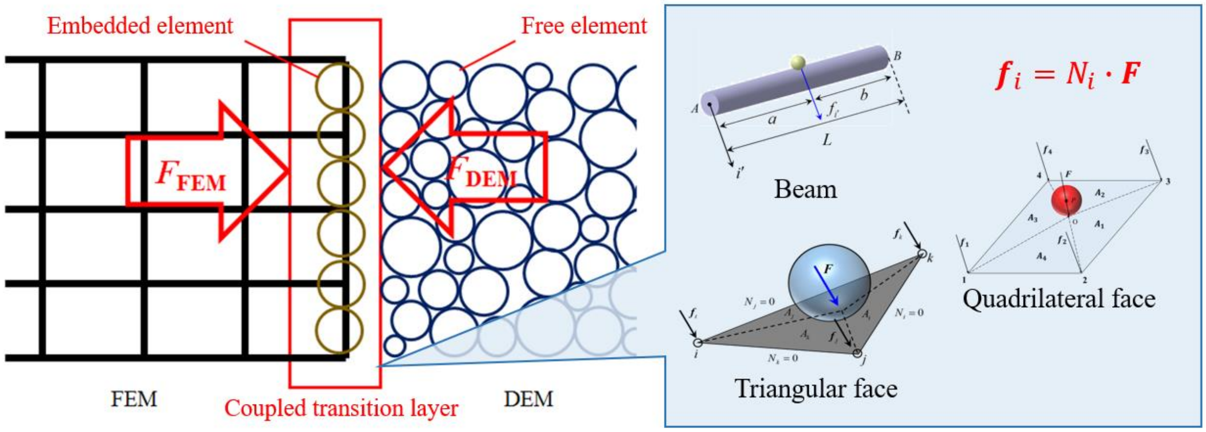

Figure 1. DEM-FEM Coupling strategy.

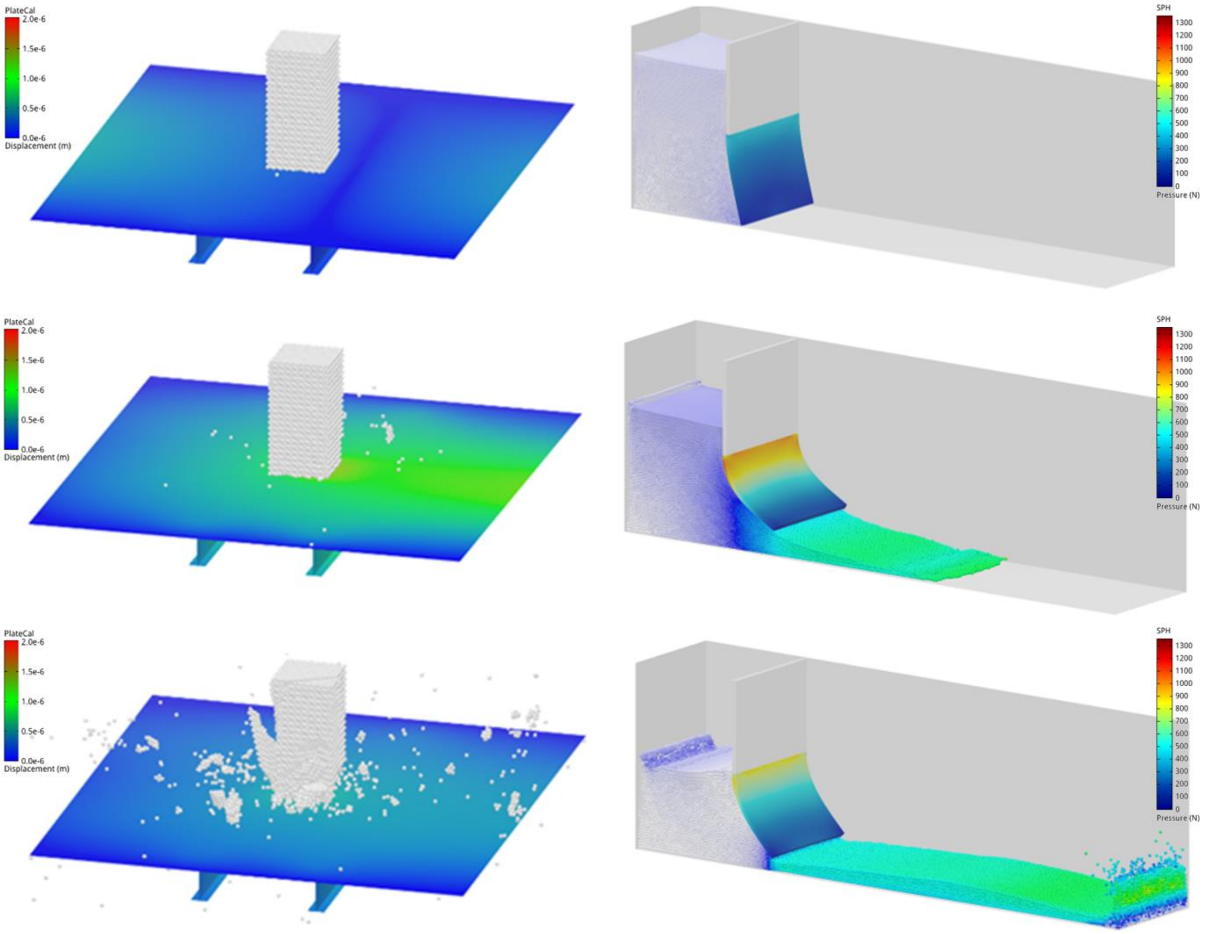

Figure 2. Numerical simulation for experimental verification.

References

[1] X. Long, S. Ji, Y. Wang, *Part. Sci. Technol.* **2019**, 37(5): 550-559.

[2] L. Liu, J. Wu, S. Ji, *Powder Technol.* **2022**, 400: 117249.

[3] G. Fourey, C. Hermange, D. Le Touzé et al, *Comput. Phys. Commun.* **2017**, 217: 66-81.

[3] D. Yang, L. Liu L, S. Ji, *Ocean Eng.* **2023**, 268: 113469.

Chemical evolution of reactive particle aggregates in fluids

Shuaiqi Zhao, Han Huang, Rui Zhang, Kunpeng Zhao, Bofeng Bai*

State Key Laboratory of Multiphase Flow in Power Engineering, Xi’an Jiaotong University, Xi’an 710049, China
*Corresponding author: bfbai@mail.xjtu.edu.cn

Agglomeration of reactive porous particles in fluids leads to the formation of flocs with complex structure, severely limiting the fluid-solid reaction rate in chemical industry. For example, particle agglomeration in the supercritical water gasification technology significantly decreases the carbon gasification efficiency. Here, we propose a three-dimensional diffusion-reaction model, and investigate the fluid-solid reaction of char particle flocs with different structure in the supercritical water. The reaction process of 102 randomly generated flocs with fractal dimension ranging from 1 to 2.33, floc porosity ranging from 0.35 to 0.78 and newly introduced surrounding factor ranging from 2 to 12 that represents the local compactness are numerically simulated. We observe an intraparticle porosity increase stage, followed by a floc deformation stage and a floc breakage stage. Before the floc breakage stage, the floc porosity tends to decrease while the fractal dimension tends to increase. The fluid-solid reaction rate is directly proportional to the initial floc porosity, and inversely proportional to the initial fractal dimension. However, during the floc breakage stage, both the floc porosity and fractal dimension decrease rapidly, and the fluid-solid reaction rate is inversely proportional to the initial surrounding factor. A simple analytic correlation is thereby proposed to evaluate the complete reaction time of flocs with different structure. Moreover, the looser flocs of lower fractal dimension and higher floc porosity tend to break into a smaller number of larger sized sub flocs during the breakage stage. The present numerical method can be further developed to describe common fluid-solid reaction issues.

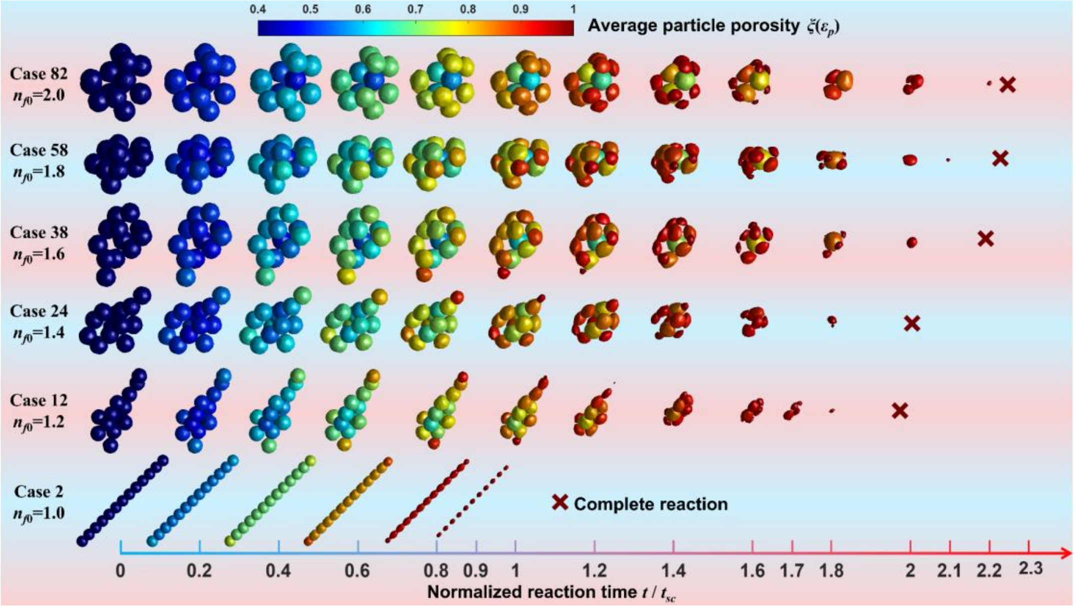

Figure 1. Typical evolution of structure of flocs with different initial fractal dimension n_{f0}. The initial surrounding factor F_{s0} of these flocs is all equal to 5 (Case 2 is 2) and the initial floc porosity ε_{f0} is around 0.55 (Case 2 is 0.3139). The reaction time t is normalized by the complete reaction time of a single isolated particle t_{sc}.

CFD study on reducing microfiltration membrane fouling with hemispherical promoter

Yuan Xi,* Wanyi Xu

Panjin Institute of Industrial Technology, Liaoning Key Laboratory of Chemical Additive Synthesis and Separation,
Dalian University of Technology, Panjin, China
*Corresponding author: xiyuan@dlut.edu.cn

For the microfiltration process, the membrane fouling causes the membrane flux to abruptly decay as the filtration progresses. It also increases the system energy consumption and reduces the service life of the microfiltration membrane. In this paper, a new type of hemispherical turbulence promoter was designed and its effect was analyzed by using computational fluid dynamics (CFD). The turbulence promoter could improve the fluid velocity gradient, the degree of turbulence and the wall shear stress. It also could suppress the formation of the boundary layer on the membrane surface. The cost-benefit approach and multiple linear regression analysis were used to analyze the three parameters, such as the central rod diameter, hemispherical diameter and hemispherical center distance. The degree of turbulence and wall shear stress of the internal flow field were proportional to the diameter of the hemisphere and the diameter of the central rod, and inversely proportional to the distance between the center of the hemisphere. It was suggested that the hemisphere ball center distance, the hemisphere diameter and the center rod diameter were 19mm, 9mm and 7mm respectively. The average wall shear stress on the membrane surface was 3.452Pa, which increased by 16.6% compared with that before optimization. While the average dissipation rate of turbulent kinetic energy was 7.667m2/s3, which was 7.9% lower than that before optimization.

Numerical simulation of upper airway in sleep apnea

Ami Takahashi, Shuji Ohsaki, Hideya Nakamura, and Satoru Watano*

Osaka Metropolitan University, Osaka, Japan
*Corresponding author: watano@omu.ac.jp

Obstructive sleep apnea (OSA) is a disease where breathing repeatedly stops during sleep. Symptoms include severe daytime drowsiness, chronic fatigue, and the prevalence of many unaware patients, which has become a significant social issue. Therefore, there is a demand in the medical field for indicators that can easily assess a patient's symptoms. One of the causes of OSA is the relaxation of muscles around the upper airway during sleep, leading to the collapse of the base of the tongue. However, the detailed mechanisms of fluid dynamics and obstruction have not been fully elucidated. Therefore, the purpose of this study was to elucidate the fluid dynamics within the upper airway and propose a simple symptom prediction index.

Using Computational Fluid Dynamics, a numerical analysis method, the pressure in the patient's upper airway 3D CT models (Figure 1 (a)) were analyzed. The results are shown in Figure 2, revealing that pressure loss increases with the decrease in cross-sectional area around the obstruction site. Furthermore, the simplified upper airway models (Figure 1 (b)) were analyzed and elucidated the shape parameters influencing pressure loss. Subsequently, using these parameters, dimensional analysis was conducted. Upon substituting the obtained predictive equation with the results from Figure 1 (a) and calculating the error between the predicted values and the actual values, it was found that the error was minimized in Eq. (1).

$$\frac{\Delta P}{\rho u^2} = 0.771\left(\frac{h' u \rho}{\mu}\right)^{-0.235}\left(\frac{h'}{h}\right)^{0.0772}\left(\frac{h'}{L}\right)^{-0.488}\left(\frac{S}{h'^2}\right)^{-0.607} \tag{1}$$

In Eq. (1), each parameter represents: ΔP: pressure loss, ρ: fluid density, u: flow velocity at the obstruction, μ: viscosity, h': height of the obstruction, h: height of the inlet, L: length of the flow path and S: crosssectional area of the obstruction. Figure 3 demonstrates the high accuracy of Eq. (1), showing that pressure loss prediction became possible with Eq (1).

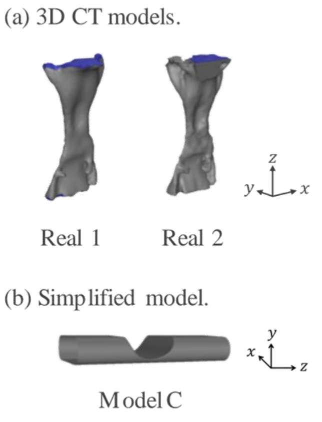

Figure 1. The models used for the analysis.

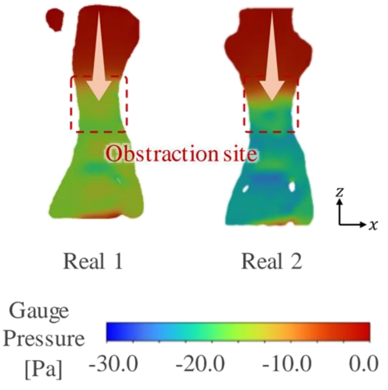

Figure 2. Analysis results of pressure in the 3D CT models.

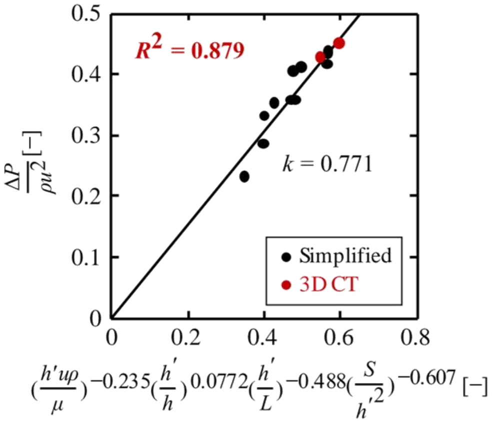

Figure 3. The optimal predictive equation for ΔP expressed using shape parameters.

Simulation of slurry filling in cosmetics manufacturing

Momoko Sugimoto,[a] Shuji Ohsaki,[a] Hideya Nakamura,[a] Satoru Watano,[a,*] Keisuke Terada,[b]
Kazuhiro Nishimi,[b] Shuji Hasegawa[b]

[a]Osaka Metropolitan University, Osaka, Japan
[b]Shiseido Co., Ltd, Tokyo, Japan
*Corresponding author: watano@omu.ac.jp

Wet-molding processes are widely used for powder solid cosmetics such as eye shadow and foundation. This wet molding process consists of agitation, filling, pressing, and drying operations. Cosmetics obtained by this molding process are characterized by their ability to have unique usability and texture. However, in actual production, cracks or uneven surfaces may appear on the finished product, which may be judged as defective. Therefore, there are many issues to be solved regarding the problems caused in each process.

The purpose of this study is to clarify the causes of surface irregularities and cracks, focusing on the filling process of the wet molding process of eye shadow. Since it is difficult to experimentally confirm the conditions inside the slurry, numerical simulation was used in this study. An overview of the geometry is shown in Fig 1. Numerical simulation was conducted using Computational Fluid Dynamics (CFD), which allows for the analysis of fluids. A Level set method was also used as a gas-liquid interface capture method because air exists in the vessel and accurate analysis of the air-slurry interface is necessary to accurately understand the behavior of the slurry. As shown in Fig 2, a comparison of numerical simulation of the gas liquid two-phase and experimental results confirmed that the slurry filling process could be well reproduced. Furthermore, as a numerical simulation method, the Discrete Element Method (DEM) was used to analyze the behavior of particles in the slurry, which enables the analysis of particles. Then, CFD, DEM, and the Level set method were studied by numerical simulation of three phases of solid-liquid-gas. As a result, the cause of the uneven surface of eye shadow could be proved.

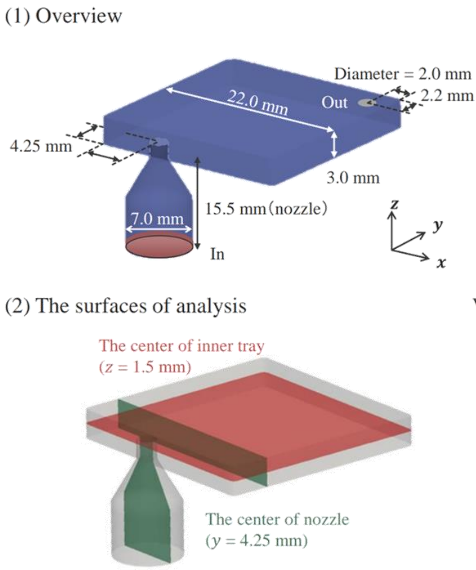

Figure 1. Geometry of calculation domain:
(1) Overview and (2) the surfaces of analysis.

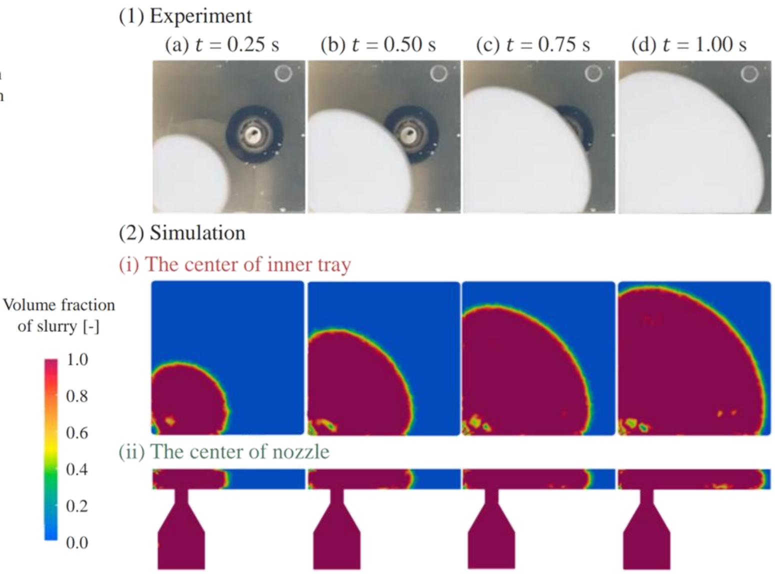

Figure 2. Pictures of slurry filling process with different times:
(1) Experiment and (2) Simulation.

Elucidation of granulation mechanism of pressure swing granulation: A combined experimental and simulation study

Tomoyuki Hirota, Shuji Ohsaki,* Hideya Nakamura, Satoru Watano

Department of Chemical Engineering, Osaka Metropolitan University, Osaka, Japan
*Corresponding author: shuji.ohsaki@omu.ac.jp

1. Introduction

Fine powders are increasingly utilized in various fields including pharmaceuticals, although the granulation should be necessary due to issues with flowability. Wet granulation, one of the granulation processes, primally requires binders to enhance particle cohesion, leading to drawbacks such as decreased product functionality. On the other hand, dry granulation can be performed without a binder. This study focused on pressure swing granulation (PSG), which is one of dry granulation methods. In PSG, it is assumed that granules are formed by adhesion of fine particles during the repetition of the three processes of compression, crushing, and fluidization of the powder. However, the detailed granulation mechanism remained unclear. Therefore, the objective of this study is to elucidate the granulation mechanism of PSG through experimental and numerical analyses. In the experiments, the powder height lifted during the crushing process was observed under the different air flow rates. In the calculations, the crushing and fluidization processes were calculated with different air velocities using a coupled model with discrete element method (DEM) and computational fluid dynamics (CFD). In addition, the compression process was computationally improved based on the Courant number.

2. Method

2-1. Experimental Method

Calcium carbonate with a medium diameter of 3.4 μm was used as a model fine powder. 100 g of calcium carbonate was granulated by PSG using a vessel with dimensions depicted in Fig. 1(a). The operating conditions for the PSG experiment were set to a compression pressure of 100 kPa, a fragmentation pressure of 150 kPa, and air flow rates of 250 and 0 L/min. The change over time of the maximum height reached by the powder during the fragmentation process was evaluated with an image analysis.

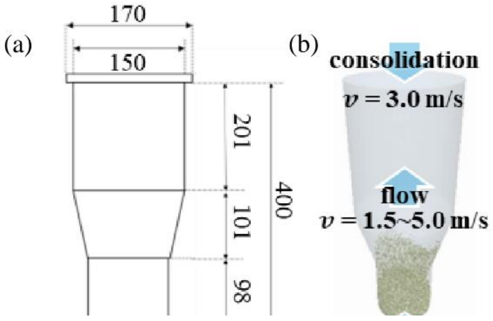

Figure 1. (a) Size of vessel for PSG and (b) calculation conditions for each process in DEM simulation.

2-2. Calculation Method

The numerical simulation was performed by a coupled model with DEM and CFD. Two-way calculations were conducted to account for the interaction between particles and fluid. In this study, as shown in Fig. 1(b), compression was conducted by flowing air from the top surface of the geometry, while fluidization and fragmentation were achieved by flowing air from the bottom surface of the geometry. The calculation times were set to 0.3, 0.5, and 1.0 seconds, and the outlet was set to atmospheric pressure release.

3. Results and Discussion

3-1. Experimental Results

The calcium carbonate was granulated by PSG with/without fluidization process. Fig 2 shows the relationship between the number of cycles of three processes and $H_{\max}/L$ which is the ratio of the length at the bottom of the vessel to the maximum height of powder layer. In the case of the inclusion of the fluidization process (Fig. 2(a)), the maximum height decreased as the cycle number increased. This was due to the difficulty of lifting the large granules by air as the granulation progressed. On the other hands, in the case of the PSG without the fluidization process (Fig. 2(b)), the maximum height remained unchanged regardless of the cycle number. This was because the no fluidization process resulted in

little change in granule size and weight changed during L/min and (b) 0 L/min granulation. These results indicate that the fluidization process played a significant role in PSG.

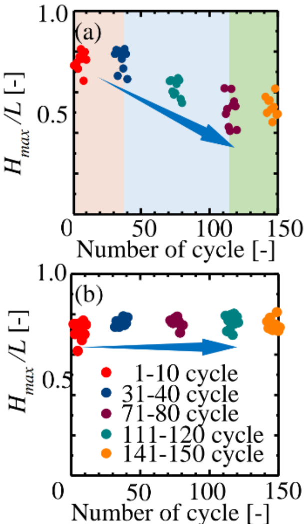

Figure 2. Experimental maximum height of powder during PSG at air flow rates of (a) 250 L/min and (b) 0 L/min.

3-2 Calculation Results

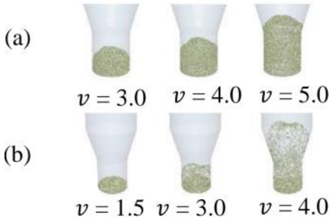

$v = 3.0$ $v = 4.0$ $v = 5.0$

$v = 1.5$ $v = 3.0$ $v = 4.0$

Figure 3. Calculated maximum height of particles during (a) crushing and (b) fluidization processes.

The DEM-CFD simulations were performed for the crushing and fluidization processes for different air velocities. Fig. 3(a) and (b) show snapshots of the maximum height reached by particles at different air velocities during the crushing and fluidization processes. The particle lifting height increased with increasing air velocity for both crushing and fluidization processes. It was found from Fig. 3 that, at the same air velocity, the maximum height of particles in fluidization process was higher than that in crushing process. This was because the length of time for air to flow differed compression between the two processes, with the crushing process taking less time. In addition, the compression process was calculated under the condition of air inflow from the top surface at 3.0 m/s. Fig. 4 shows the snapshots of the particle behavior in the compression process calculated with different time step. A time step of 0.003 resulted in particles ascending, while a time step of 0.00025 resulted in a compression of particles. The appearance of calculation was improved by reducing the time step. This improvement was related to the Courant number. Specifically, the vessel used in this study acted as a reduction tube during the compression process, causing the flow rate to exceed the inlet one. Therefore, the time step should be set to keep the coolant number below 1. According to these results, the simulations for the three processes were successfully performed by a DEM-CFD method.

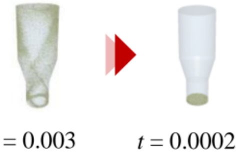

$t = 0.003$ $t = 0.00025$

Figure 4. Snapshots of particle behavior in compression process calculated with different time step.

4. Conclusion

This study investigated the granulation process in PSG through the experimental and numerical analyses. It was revealed from the experiments that the fluidization process had a significant impact on granulation. Computational analysis confirmed variations in particle lifting height with different air flow velocities during crushing and fluidization. Improvements in calculation accuracy in compression were achieved by reducing the time step to maintain a Courant number below 1.

A surrogate prediction model for air core prediction of hydrocyclones to stabilize operation

Qing Ye,[a] Shibo Kuang,[a,*] Peibo Duan,[b] Ruiping Zou,[a] Aibing Yu,[a,c]

[a]ARC Research Hub for Smart Process Design and Control, Department of Chemical & Biological Engineering, Monash University, Clayton, Victoria, 3800, Australia
[b]Department of Data Science and Artificial Intelligent, Faculty of Information Technology, Monash University, Suzhou, 215123, China
[c]Center for Energy and Environment, Southeast University-Monash University Joint Research Institute, Suzhou, 215123, China
*Corresponding author: Shibo.Kuang@monash.edu

Hydrocyclones are used to separate particles by size across diverse industries. The operation stability inside the hydrocyclone is identified using discharge types linked to air core profiles characterized by their shape and diameter. This study introduces a machine learning model meticulously crafted the instant prediction of air core profiles. The model is constructed based on a modified graph neural network (GNN). It is rigorously trained with the data generated from the well-validated computational fluid dynamics (CFD) models. To enhance prediction accuracy, two key modifications are applied to this GNN-based surrogate model. One is the data smoothing to decrease the drastic changes in data. The other is the loss function modification to incorporate air core information. Comparative analyses involving this novel model, the original GNN, and RF models in predicting air core profiles demonstrates the superior accuracy of our proposed model in spatial distribution, radial distribution and air core type results. Additionally, a series of studies have been conducted to underscore the efficacy of our proposed model, including the distribution prediction of air core type and quality and air core optimization by combining the modified GNN and genetic algorithm (GA).

Numerical simulation on powder die-filling in a rotary tablet press

Arata Hashimoto, Mikio Sakai

School of Engineering, The University of Tokyo, Tokyo, Japan
*Corresponding author: mikio_sakai@n.t.u-tokyo.ac.jp

In the large-scale manufacturing of pharmaceuticals, a rotary tablet press is essential for producing medical tablets. The tablet fabrication process mainly consists of three steps: granulation, die-filling, and compression, among which the die-filling determines the weight of the tablets. Hence, this process has been extensively investigated in recent years. The existing experimental study reveals that a downward motion of lower punches and the depth of this downward motion are key factors for the efficiency of the die-filling process. Unfortunately, due to the limitations of experimental techniques, the mechanisms and physical phenomena behind the die-filling process have not yet been systematically investigated. Numerical simulations such as the discrete element method (DEM) coupled with the computational fluid dynamics (CFD), termed as to the DEM-CFD, are widely employed to facilitate the understandings of die-filling process. However, in the conventional DEM-CFD, the intricate fluid-particle interactions cannot be accurately calculated in a rotary tablet press due to a rotary motion of the disc. To address this critical issue, recently, the author's group has developed a novel DEM-CFD method, which has enabled to conduct numerical simulations in the systems involved with arbitrary-shaped walls and complexly moving walls. In this method, the wall boundary conditions are modelled by the combination of the signed distance function (SDF) and the immersed boundary method (IBM). The adequacy of this approach has been validated in so many industrial processes including various scenarios of die-filling. In this study, this newly developed DEM-CFD method is adopted to simulate powder die-filling process in a rotary tablet press, and the interactions between particles and fluid will be systematically investigated. Through thus study, the relationship between the motion of the lower punch and fluid dynamics, the disc rotation speed, and their effect on the filling ratio are clearly revealed for the first time.

Part of this study is financially supported by JSPS KAKENHI (Grant Nos. 21H04870).

References

[1] A. K. Schomberg, A. Kwade, J. H. Finke, *Pharmaceutics* **2020**, 12, 3.

[2] C. Zheng, E. Yost, A. R. Muliadi, N. Govender, L. Zhang, C. Wu, *Particuology* **2024**, 88, 107-115.

[3] Y. Shigeto, M. Sakai, *Chem. Eng. J.* **2013**, 231, 464-476.

[4] X. Sun, M. Sakai, *J. Chem. Eng. Japan* **2017**, 50, 161–169.

[5] H. Yao, Y. Mori, K. Takabatake, X. Sun, M. Sakai, *J. Taiwan Inst. Chem. Eng.* **2018**, 90, 9–17.

Mass transfer enhancement in liquid−liquid extraction with discrete liquid film flow

Chao Chang,[a] Qijun Zheng,[b] Yong Wang,[c,]* Shibo Kuang,[a,]*

[a]ARC Research Hub for Computational Particle Technology, Department of Chemical & Biological Engineering,
Monash University, Clayton, Victoria 3800, Australia.
[b]Centre for Simulation and Modelling of Particulate Systems, Monash-Southeast University Joint Research Institute,
Suzhou, China
[c]National Engineering Research Center of Green Recycling for Strategic Metal Resources, Institute of Process
Engineering, Chinese Academy of Sciences, Beijing 100190, China
*Corresponding author: wangyong@ipe.ac.cn
*Corresponding author: shibo.kuang@monash.edu

This work presents a method to enhance the mass transfer rate in the liquid−liquid extraction process. In this method, discrete liquid films were realized by controlling the flow of the dispersed phase along a wire immersed in the continuous phase. An experimental setup was built to quantify the mass transfer of the liquid film. The results showed that liquid films increased the mass transfer efficiency by 40−65% compared to liquid droplets, enlarged the specific surface area by 53.3%−69.7%, and extended the residence time by 27.6%−51.9%. Additionally, the effects of the wire height were examined under two different wire diameters to confirm the feasibility of the new extraction method. Finally, based on the experimental data of liquid films, correlations were formulated to predict the overall mass transfer coefficient. This study opens a new direction for the development of liquid−liquid extraction technologies.

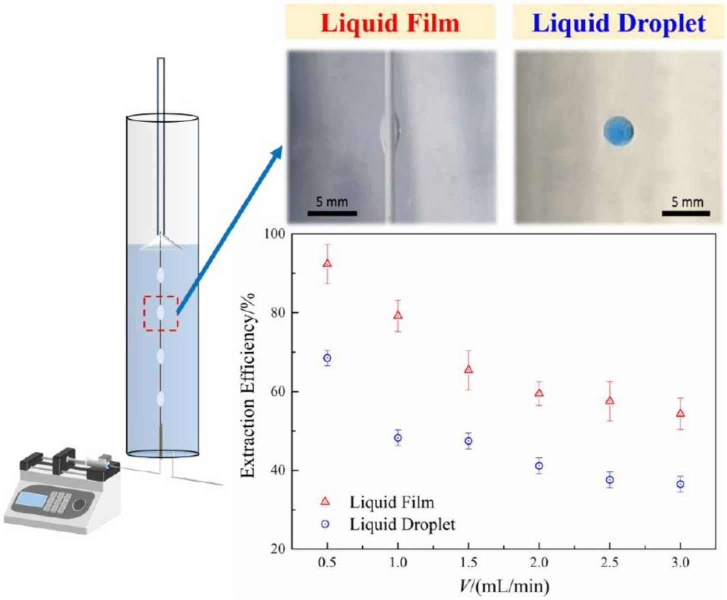

Figure 1. Abstract Graphics.

References

[1] C. Chang, Q. Zheng, Y. Wang, Z. Su, B. Wang, S. Kuang, *Ind. Eng. Chem. Res.* **2023**, 62, 17297-17305.

An intraparticle model for simulation of biomass conversion: the effect of temperature inhomogeneity on heat capacity, heat transfer, drying and pyrolysis

Qiang Zheng,[a,*] Yujie Tian,[b,c,*] Wei Wang,[b,c] Qijun Zheng,[a] Shibo Kuang[a]

[a]ARC Research Hub for Smart Process Design and Control, Department of Chemical Engineering, Monash University, VIC, Australia
[b]State Key Laboratory of Mesoscience and Engineering, Institute of Process Engineering, Chinese Academy of Sciences, Beijing, China
[c]School of Chemical Engineering, University of Chinese Academy of Sciences, Beijing, China
*Corresponding author: qiang.zheng@monash.edu (Q. Zheng), tianyj@ipe.ac.cn (Y. Tian)

Thermally-thick biomass conversion exhibits intraparticle temperature inhomogeneity, which significantly influences the surface-to-core temperature equilibration and conversion time [1]. Computational fluid dynamic (CFD) simulations of the reactor-scale biomass conversion generally do not account for the effect of intra-particle temperature inhomogeneity. As a result, it overestimates heating and conversion rates, and causes a sudden release of volatiles [2]. However, the direct multiscale simulation method for considering the effect of intraparticle temperature inhomogeneity—coupling the particle-scale simulation and the reactor-scale simulation simultaneously—is computationally impractical [3]. Recently, researcher [4] have developed the indirect multiscale simulation method, which considers the effect of intraparticle temperature inhomogeneity, while ensuring computational efficiency. In this work, we improve this indirect multiscale simulation method by proposing a new intraparticle model, which comprehensively considers the effect of temperature inhomogeneity on heat capacity, heat transfer, drying, and pyrolysis. First, we derive the non-isothermal model using the space averaging method on the particle-scale transport equations. Second, by comparing the non-isothermal and isothermal models, we identify correction factors that evaluate the effects of temperature inhomogeneity on heat capacity, heat transfer, drying, and pyrolysis. Third, particle-scale simulations provide the evolution of intra-particle temperature and species concentration, allowing us to solve the correction factor functions **(Figure 1)**. Finally, these correction factors are integrated into CFD simulations of reactor-scale biomass conversion. The model validation are carried out over both particle-scale and reactor-scale levels by comparing the predictions against experimental data (**Figure 2**). Finally, we further apply this improved indirect multiscale simulation method to the simulation of an industrial-scale cement pre-calciner using coal and biomass as fuels. The simulation results indicate that the intra-particle temperature inhomogeneity significantly influences the cement pre-calciner performance (**Figure 3**). This improved indirect multiscale simulation method is expected to achieve both accurate and efficient predictions on thermally-thick biomass conversion over industrial-scale reactors.

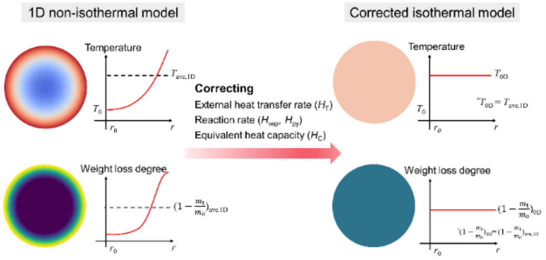

Figure 1. Schematic of corrected isothermal model derived from 1D non-isothermal model.

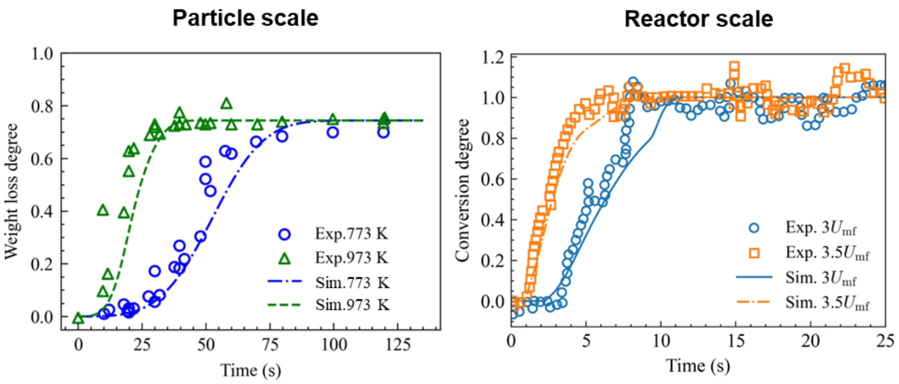

Figure 2. Model validation over particle scale and reactor scale under various operating conditions.

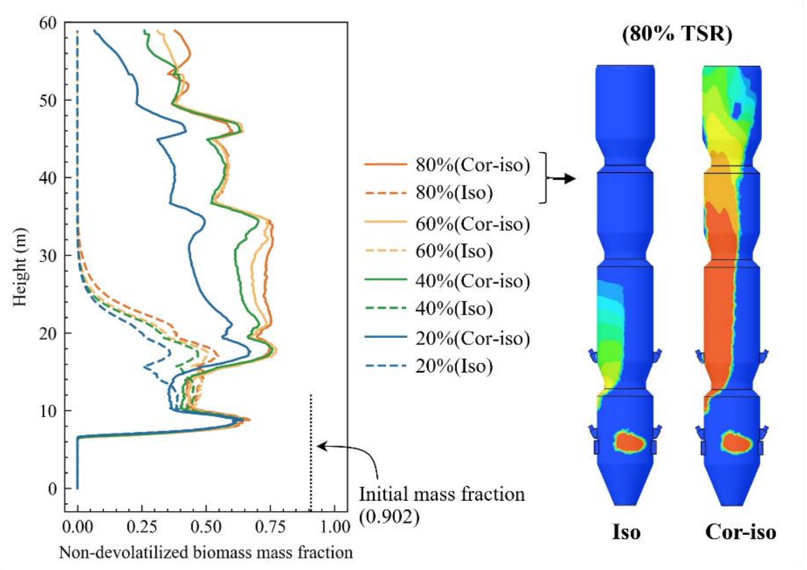

Figure 3. Comparison of non-devolatilized biomass predictions between the isothermal (Iso) and corrected isothermal (Cor-iso) models for industrial-scale cement pre-calciner at different thermal substitution rates (TSR).

References

[1] X. Ku, F. Shen, H. Jin, J. Lin, H. Li, *Ind. Eng. Chem. Res.* **2019**, 58, 1720-1731.

[2] M.P. Remacha, S. Jiménez, J. Ballester, *Fuel* **2018**, 234, 757–769.

[3] M.A. Gómez, C. Álvarez-Bermúdez, S. Chapela, A. Anca-Couce, J. Porteiro, *Energy* **2023**, 281, 128243.

[4] H. Luo, W. Lin, K. Dam-Johansen, H. Wu, *Energy Fuels* **2020**, 34, 9620–9631.

CFD-DEM-DPM modelling of fluid-particles-fines reacting flows in blast furnace

Dan Xu, Yansong Shen*

School of Chemical Engineering, University of New South Wales, Sydney, NSW 2052, Australia
*Corresponding author: ys.shen@unsw.edu.au

The complex fluid-particle-fine (FPf) reacting flows have been widely practised in many energy-intensive engineering processes, yet numerical methods capable of comprehensively describing the particle-scale thermochemical behaviours related to the FPf reacting flows were still lacking. In this work, a novel CFD-DEM-DPM model is developed, for the first time, to describe the fluid, particles and fines reacting flows and their interactions. Then, to demonstrate its effectiveness, it is employed to simulate the co-combustion of coke and pulverized coal in a dynamic raceway in ironmaking blast furnaces (BFs). After model validation, the complex in-furnace phenomena related to the co-combustion of coarse coke particles and fine coal particles are comprehensively captured. Particularly, instead of the pre-set raceway treatment in the previous raceway simulations, a dynamic raceway cavity is predicted explicitly driven by the fluid-particle-fine interactions and further, inside the dynamic raceway, the combustion of coal fines including moisture evaporation, devolatilization and char reactions are presented in detail. Subsequently, the impact of operations with and without coal injections are quantitatively compared, showing that both the reducing gas and reaction heat from the coal combustion contribute to an expansion of the raceway cavity. Further, the effects of pulverized coal rate on the in-furnace phenomena are studied. The present work represents a significant breakthrough in the explicit modelling of FPf reacting flows, and provides a cost-effective tool for understanding FPf-related processes and developing new technologies including carbon–neutral ironmaking technologies.

Simulations of ethylene oxychlorination in a catalyst pellet packed reactor of dual space resolutions

Cheng-En Li,[a] An-Ni Huang,[b] Wan-Yi Hsu,[b] Tsuo-Feng Wang,[a] Hsiu-Po Kuo[a,*]

[a]Department of Chemical Engineering, National Taiwan University, Taipei, Taiwan
[b]Green Technology Research Center, Chang Gung University, Taoyuan, Taiwan
*Corresponding author: hsiupokuo@ntu.edu.tw

The fast development in micron-scale computed tomography (micro-CT) technology has revolutionized our ability to distinguish the intricate interior structure of porous catalysts. Ethylene oxychlorination is a pivotal process in the production of vinyl chloride monomer (VCM), which is the precursor for the manufacturing of polyvinyl chloride (PVC). In this study, we conduct dual-resolution simulations based on the catalyst pellet's inner pores and the cylindrical pellets packing's interstitial voids. In the first stage, we unveil the microstructural intricacies of a porous pellet employing micro-CT. In the second stage, Discrete Element Method (DEM) is applied to construct the packed bed structure at pellet level. The information acquired in the first stage is integrated into the packed bed structure and the dual-resolution reactor model is obtained. Reaction kinetics coupled Computational Fluid Dynamics (CFD) is then used to approach the intricate flow and reaction characteristics therein the dual-resolution model. The comprehensive flow patterns, heat and mass transfer phenomena, as well as the intricate details of reaction behaviours are initially conducted. The pellet's coking phenomena observed in practice are well described by the current dual-resolution reaction-CFD modelling.

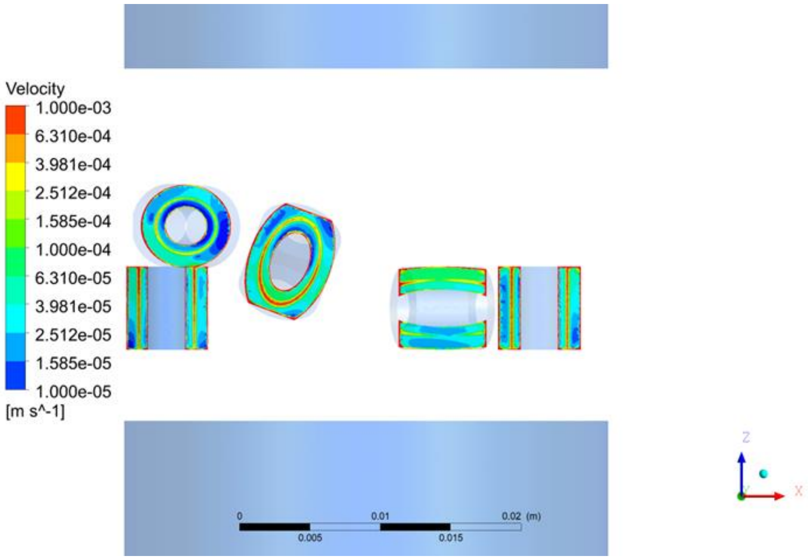

Figure 1. The velocity distribution contours in the selected catalyst pellets.

References

[1] N. Jurtz, M. Kraume, G. D. Wehinger, *Rev. Chem. Eng.* **2019**, 35, 139-190.

[2] H. Ma, Y. Wang, Y. Qi, K. R. Rout, D. Chen, *ACS Catal.* **2020**, 10, 9299-9319.

Development of a filtered reaction rate model for a non-equimolar reaction

Lingxue Wang,[a] Zheqing Huang, [a] Qiang Zhou[a,b]*

[a]School of Chemical Engineering and Technology, Xi'an Jiaotong University, Xi'an, China
[b]State Key Laboratory of Multiphase Flow in Power Engineering, Xi'an Jiaotong University, Xi'an, China
*Corresponding author: zhou.590@mail.xjtu.edu.cn

Gas-solid flows with non-equimolar reactions are frequently observed in numerous applications. Such reactions change the number of moles of the gas phase, consequently influencing the structures of gas-solid flows and the behavior of the reactions [1]. The coarse-grid simulation is extensively employed to model industrial-scale reactors, with their accuracy largely dependent on meso-scale models. However, existing meso-scale reaction rate models do not consider the influence of non-equimolar reactions. Addressing this limitation, this work introduces a novel reaction rate model that corrects the model established by Huang et al. [2], which only equimolar reaction is involved. MFiX software was utilized to simulate a series of high-resolution fine-grid simulations of isothermal, solid-catalysed non-equimolar reactions within the reactor, and the ratio of the number of moles of the product gas to that of the reactant is set to be 2. The Morris analysis [3], filtering technique, conditional average and correlation analysis [4] are applied to scrutinize the results from these fine-grid simulations. The research explores the potential to correct the model using new markers such as the surrounding solid volume fraction, gas phase density gradient, velocity divergence, the Reynolds number derived from the filtered gas-solid slip velocity, and other variables as new markers are explored. The results indicate that the Reynolds number, based on slip velocity, is a critical marker. Then the Reynolds number is used as a unique variable to formulate the correction coefficient. The effectiveness of the new model is verified through both prior and posteriori tests in fluidized beds.

References

[1] T. W. Li, A. Mahecha-Botero, J. R. Grace, *Ind Eng Chem Res* **2010**, 49 (15), 6780-6789.

[2] Z. Q. Huang, L. X. Wang, Q. Zhou, *AIChE Journal* **2021**, 67(5): e17185.

[3] M. D. Morris, *Technometrics* **1991**, 33(2):161–174

[4] Y. Igci, A. T. Andrews, S. Sundaresan, S. Pannala, T. O'Brien, *AIChE Journal* **2008**, 54 (6), 1431-1448.

Enhanced powder properties of nano/micro particles enabled by atomic and molecular scale coatings

Fuweng Zhang[a.b]

[a]Qingyuan Innovation Laboratory, Quanzhou, China
[b]College of Chemical Engineering, Fuzhou University, Fuzhou, China *Corresponding author: zfw.ustb@hotmail.com

A dry inhalation drug powder, Budesonide, is often used to treat asthma and chronic obstructive pulmonary disease by respiratory inhalation. In this study, we demonstrate how to alter the powder properties (flowability, entrainment behavior, wettability) by surface modification of inhalation drug powders via atomic layer deposition (ALD) and molecular layer deposition (MLD). Different nanofilms were successfully deposited onto the Budesonide powders (size range of 0.1 to 10 μm). Specifically, Nano-scaled layers of inorganic (SiO2, TiO2, and Al2O3), organic (PET), and hybrid inorganic-organic (tatanicone) were coated on the surface of Budesonide particles via ALD, MLD, and combined ALD-MLD processes. The effects of different coating materials and coating cycles (thickness) on the wettability, flowability, and entrainment behavior of drug powders were investigated.

Uncoated Budesonide powder is classified as a very hydrophobic material with poor flowability. The improvement in powder flow is reflected by the decrease in the angle of repose and minimum pick-up velocity, as well as promoting the pneumatic delivery of a much higher amount of drug powders after ALD or hybrid coating treatments. In contrast, organic-coated budesonide via MLD exhibits comparably poor flow as uncoated one. Rather than being transported in individual particles, the uncoated and PET-coated powders are pneumatically delivered in form of large clusters with a size of over 500 μm, whereas the ALD budesonide is dispersed in small agglomerates (<100 μm). The inorganic nanofilm deposited on the drug particles alters the surface chemistry to reduce the inter-particle forces measured by atomic force microscopy, giving rise to an improved drug delivery performance.

Improvements in the wettability of drug powders coated with inorganic nanofilms via ALD are also observed, and the positive effect can be further enhanced by increasing the number of coating cycles. In contrast to ALD-coated Budesonide, PET-coated budesonide via MLD becomes super-hydrophobic compared to uncoated Budesonide.

Knowledge gained from this study connects several key powder material length scales that provide a basis for a more mechanistic understanding of dry particle surface modification on bulk powder functionality.

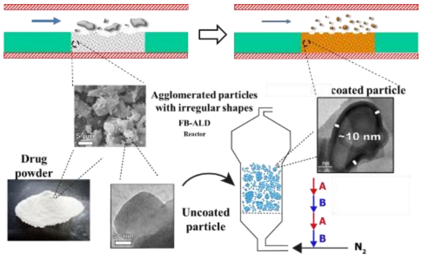

Figure 1. The improved flowability of drug particles enabled by FB-ALD coating.

References

[1] F. Zhang, K. Wu, D. La Zara, F. Sun, M. J. Quayle, G. Petersson, S. Folestad, J. W. Chew, J. R. van Ommen, *CEJ* **2023**, 142131.

Mixing/segregation behaviours for density difference binary particle bed in a vibrating fluidized bed

Yoshihide Mawatari,* Naoki Iwamura, Yuki Ishiyama

Department of Applied Chemistry, Kyushu Institute of Technology, Kitakyushu, Japan
*Corresponding author: mawatari.yoshihide675@mail.kyutech.jp

This study investigated the fluidization characteristics under mechanical bed vibration for binary particle bed. In this study, the density difference particles with almost equal size were used as binary particle bed. The fluidized bed was made of transparent acrylic resin and its internal diameter was 65 mm. A sintered stainless plate was used as a gas distributor. The fluidizing gas was dry nitrogen and its flow rate was controlled with a mass flow controller. The bed pressure drop was measured with a differential manometer and the relationship between superficial gas velocity and bed pressure drop was obtained by the decreasing gas velocity method (de-fluidization method) to evaluate the minimum fluidization velocity (u_{mf}). A sinusoidal vertical vibration was added with a vibrator and the vibration frequency and the vibration amplitude were set with a function generator. The particles used in this study were spherical and their sizes and the true densities were varied from 30 to 100 μm and from 2500 to 8000 kg/m^3 respectively. Initially, the bed was fluidized with enough high gas velocity to mix the binary particles. Then the gas velocity and the vibration conditions were fixed for 5 minutes. After the fixed vibrating and fluidization conditions for 5 minutes, the gas velocity and the vibration were simultaneously stopped to form the fixed bed. The particles were sampled from the bed surface with a certain height and the weight of the sample was measured. The measured sample weight and the height obtained by the height difference before and after the sampling can evaluate the average density profile in the axial direction. Figure 1 shows the map of the flow pattern related to the operation conditions such as the superficial gas velocity and the vibration amplitude (vibration frequency was kept constant). With the lower vibration amplitudes, the bed was not segregated but mixed well. However, with larger vibration amplitudes than a certain magnitude, the bed was segregated and the boundary between upper and lower layers was recognized. In the conditions where the segregation occurred, the segregated bed turned into a mixed bed again as the gas velocity decreased. The vibration enhanced the migration of both different densities of the particle in the whole bed regularly, and it caused the diminishment of the upper/lower boundary.

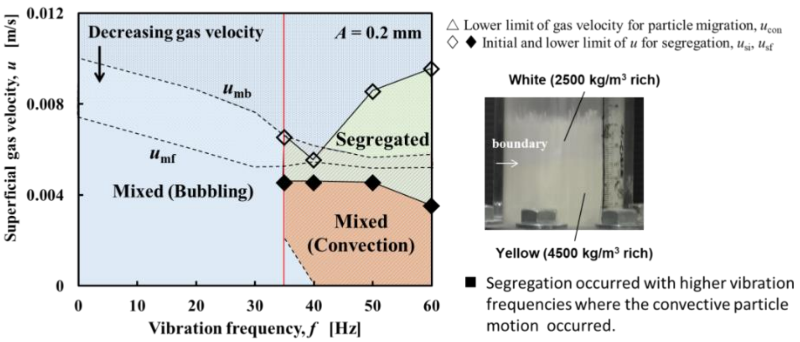

Figure 1. Map of flow patterns for binary particle bed related to the gas velocity and the vibration amplitude.

Insights into the gas-solid hydrodynamics and thermochemical mechanisms in calcium-looping energy storage using CFD-DEM

Hongchuan Jiang,[a] Cai Liang[a,*]

[a]Key Laboratory of Energy Thermal Conversion and Control of Ministry of Education, School of Energy and Environment, Southeast University, Nanjing, China
*Corresponding author: liangc@seu.edu.cn

Calcium looping thermochemical energy storage (CaL-TCES) based on dense particle flow is a promising technology for large-scale long-duration energy storage and industrial decarbonization. In this work, the fluidization and thermochemical behaviors in the CaL-TCES reactor were investigated, using CFD-DEM coupled with a comprehensive heat transfer and inhomogeneous reaction models. Moreover, the effects of operating parameters on particle dispersion, heat transfer and heat storage performance were systematically explored. The results show that wall-particle conduction and radiation are main heat transfer modes in near-wall zone, while central zone is an essential reaction site despite poor heat transfer performance. The reaction rate magnitude is mainly influenced by particle temperature T, while CO_2 partial pressure ratio R_{PCO2} near particles dominates reaction homogeneity. High T in bubbling phase and low R_{PCO2} in intermediate phase as well as reactor bottom induced them as main reaction sites. A certain range of fluidization number and particle diameter has a greater effect on dispersion coefficient, improving heat transfer and reaction homogeneity. Furthermore, high T decreases chemical heat storage ratio and increases sintering probability.

Numerical simulation on the fluidization-atomic layer deposition of the nanoparticle agglomerates under the scale of agglomerate and fluidized bed

Zuyang Zhang[a], Daoyin Liu[a,*]

[a]Key Laboratory of Energy Thermal Conversion and Control of Ministry of Education, School of Energy and Environment, Southeast University, Nanjing 210096, Jiangsu, China
*Corresponding author: dyliu@seu.edu.cn

The atomic layer deposition (ALD) modification on nanoparticles shows potential application. Fluidized-bed ALD is an efficient technology of nanoparticle dispersion and modification. We employed several forms of numerical simulations to investigate the ALD behaviour of nanoparticle agglomerates at different scales.

Due to its cohesion, the nanoparticles are fluidized in the form of hierarchical agglomerates. Based on the Gordon`s diffusion and reaction model[1] for simple straight pores and trenches and Jin`s work[2], we developed a zero-dimensional diffusion-reaction model to simulate the coverage behaviour of primary agglomerations of nanoparticles. On this basis, we used computational fluid dynamics (CFD) to study the relationship between ALD coating behaviour and cluster structure (size, fractal dimension) of complex agglomerates composed of primary agglomerates. On the other hand, we used an adhesive CFD-DEM model[3] to study the impact of fluidization behaviour in the fluidized bed on the fluidization-ALD behaviour of the nanoparticle agglomerates. According to the simulation results, for each primary agglomerate, its saturation time scales with the number of particles contained in the agglomerate as a power-law relationship, and the power exponent is a function of the agglomerate fractal dimension. For the fluidized bed, as the utilization rate of precursor is high, the overall saturation time of the bed is mainly limited by stoichiometry, and the coverage uniformity among the particles is related to the fluidization state, and the best coverage uniformity of particles is achieved under the most homogeneous fluidized condition.

References

[1] R.G. Gordon, D. Hausmann, E. Kim, J. Shepard, *Chemical Vapor Deposition* **2003**, 9(2), 73-78.
[2] W. Jin, J.R. van Ommen, C.R. Kleijn, *Chemical Engineering Science* **2019**, 206, 180-186.
[3] D. Liu, B.G.M. van Wachem, R.F. Mudde, X. Chen, J.R. van Ommen, *AIChE Journal* **2016**, 62(7), 2259-2270.

The influences of the inlet and outlet designs on the performances of a cyclone separator

Chung-Min Wang,[a] An-Ni Huang,[b] Ruey-Chi Hsu,[c] Tsuo-Feng Wang,[a] Hsiu-Po Kuo[a,]*

[a]Department of Chemical Engineering, National Taiwan University, Taipei, Taiwan
[b]Green Technology Research Center, [c] Department of Chemical and Materials Engineering, Chang Gung University, Taoyuan, Taiwan
*Corresponding author: hsiupokuo@ntu.edu.tw

Cyclone separators have been widely utilized in the industry for decades. Classic Stairmand cyclone designs show good performances and are almost the standards in industry. However, the Stairmand cyclone designs do not consider the inlet and outlet geometries, which vary in various fields depending on the site spaces and applications. Here, Computational Fluid Dynamics (CFD) is employed to study the performances and hydrodynamics of Stairmand cyclones with different inlet and outlet designs. The effects of different types of inlet and outlet geometries on the separation efficiency, pressure drop, and vorticity distribution inside the cyclone separator are evaluated. The discrete particle phase is also considered by a two-way coupling technique. A more complex outlet design would increase pressure drop, while the separation efficiency depends on different modules. This work also focuses on the vortex core center positions inside the cyclone, which present higher eccentricity at the conical part and top of the cylindrical part.

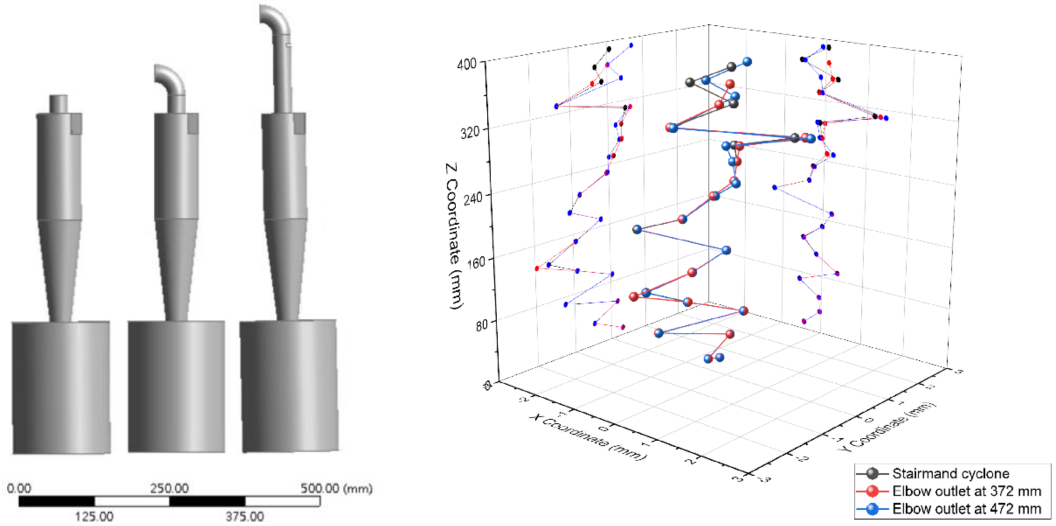

Figure 1. (a) The geometry of different outlet designs. (b) the vortex core center diagram.

References

[1] L.H. Yang, C.Y. Chen, W.Y. Hsu, K. Fukui, T. Fukasawa, A.N. Huang, H.P. Kuo, *Adv. Powder Tech.* **2022**, 33, 103791.

[2] A.N. Huang, K. Ito, T. Fukasawa, K. Fukui, H.P. Kuo, *Journal of the Taiwan Institute of Chemical Engineers* **2018,** 90, 61-67.

Towards the influence of fluid convection on filtered drag in fluidized gas-particle flows

Ju Jiang, Xiao Chen, Qiang Zhou*

State Key Laboratory of Multiphase Flow in Power Engineering, Xi'an Jiaotong University, Xi'an, China
*Corresponding author: zhou.590@mail.xjtu.edu.cn

Most of the mesoscale drag modelling processes for gas-solid two-phase flow are based on periodic systems. However, in such systems, the flow field is statistically homogeneous and isotropic, whereas the real fluidized bed presents a heterogeneous and anisotropic distribution. The influence of convective transport on mesoscale drag has been seldom considered in periodic systems as the convection term of momentum equations only varies within a limited range. However, in real fluidized beds, the fluid convection may play a significant role and have a notable impact on the drag force.

This study conducts a series of numerical simulations for fluidized beds with different sudden expansion sections using a highly resolved two fluid model (TFM). Flow field data containing acceleration zones are then collected. Based on a priori analysis, it is observed that convection terms in acceleration zones are much larger in magnitude with those in periodic systems, and the convection transport has a notable impact on the heterogeneous drag. In general, the presence of convection facilitates the formation of mesoscale structures, further reducing the filtered drag force compared to the uniform state. The heterogeneous characteristics intensifies as convective transport of the fluid increases, while the influence of convection will gradually vanish as the local solid volume fraction increases. Previous researches [1] have reported a linear relationship between the filtered gas-phase pressure gradient and the filtered drag in periodic systems. With a force balance analysis of the momentum equations, it is found that this linear relationship still holds in the acceleration zones where significant convection occurs. Both priori and posteriori analyses of the filtered drag in the acceleration zones indicate that predictive capability of drag models constructed solely with solid volume fraction and gas-solid slip velocity can reduce significantly in the acceleration zones, suggesting that additional markers may need to be introduced to consider the impact of convection. While the gas-phase pressure gradient implicitly contains the effects of local convection, models incorporating this physical quantity also demonstrate good accuracy for the flow behaviour in the sudden expansion fluidized beds.

References

[1] Jiang M, Zhang Y, Yu YX, Zhou Q, *Powder Technology* **2021**, 394, 1050-1076.

Numerical Simulation Study on Multi-Component Gas Sulphur Reduction of Phosphogypsum

Leilei Zhang, Yanxin Chen*, Bo Zhao

College of Materials Science and Engineering, Xi'an University of Architecture and Technology, Xian 710055, China
*Corresponding author: yx_ch@126.com

Under the context of "carbon peaking and carbon neutrality" and "resource utilization," the coproduction of sulfuric acid and cement from phosphogypsum through Sulphur reduction is crucial for the sustainable development of the phosphorus chemical industry. This study employs a combination of numerical simulation and experimental methods to analyse the reaction process of Sulphur vapor in different forms (S_6, S_4, S_2) during the pre-reduction of phosphogypsum in a reduction furnace. This approach compensates for the single limitation of Sulphur vapor participating in reactions only in the form of S_2, thereby making the reaction mechanism of gaseous Sulphur reduction of phosphogypsum more closely aligned with actual production conditions.

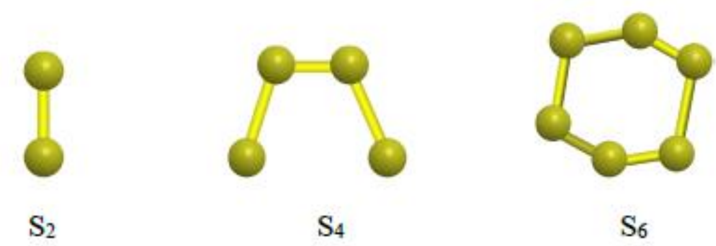

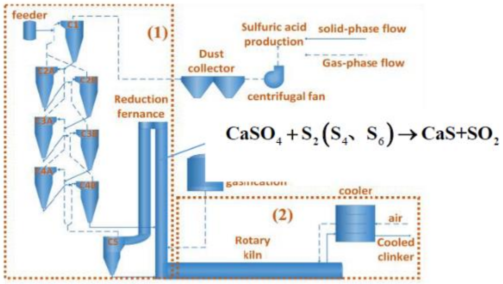

Figure. 1 Pilot test system of dilute phase fluidization

Figure. 2 Process Flow Diagram of pilot test

Numerical simulation of a secondary separation cyclone separator

Jingyi Chen,[a] Yanxin Chen,[a,*] Leilei Zhang [a]

[a]College of Materials Science and Engineering, XI’AN university of architecture and technology, Xian 710055, China
*Corresponding author: yx_ch@126.com

The efficient separation of particles smaller than 10 μm in flue gas poses a significant challenge in industries such as petroleum, chemical, and environmental sectors. This study employs the Eulerian-Lagrangian method to conduct numerical simulations of a novel secondary separation cyclone separator. Specifically, the research investigates the influence of the number of narrow slots in the secondary separation structure and the inner cylinder's radius on the separation efficiency of fine particles and the resulting pressure drop. The results demonstrate that the new design enhances the separation efficiency of particles smaller than 10 μm by 8-10% compared to conventional cyclone separators. Importantly, particles separated by the secondary separation structure contribute 5.54% to the overall separation efficiency, while the associated increase in pressure drop remains within an acceptable range. These findings offer valuable insights for enhancing the separation of fine particles in gas-solid separation processes.

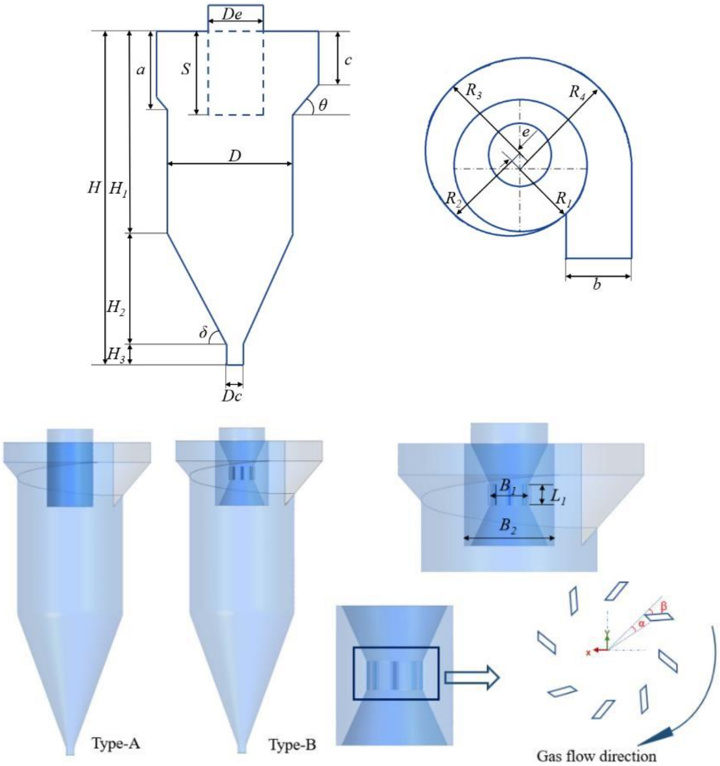

Figure 1. The three dimensional models and the structure diagrams.

Based on A spiral cyclone (Type-A) structure with high separation efficiency, a secondary separation structure is proposed as shown by Type-B in Fig 1. Table 1. shows the basic dimensions of the cyclone precipitator corresponding to Fig 1.

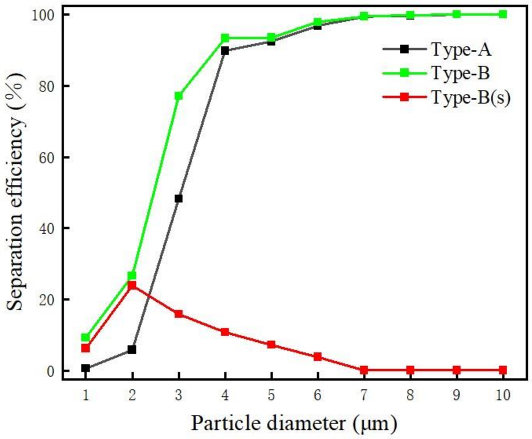

Figure 2. The separation efficiency of three cyclone separators.

Table 2. The total separation efficiency of three cyclone separators.

Cyclone separators	**Total separation efficiency (%)**
Type-A	70.00
Type-B	79.10
Type-B(s)	5.54

Fig 2 shows the classification separation efficiency of the two cyclone separators.Compared to the Type-A cyclone separator, the Type-B cyclone separator demonstrates a significantly improved separation efficiency for fine particles (particle diameter less than 5 μm). In particular, the secondary separation structure notably enhances the separation efficiency of fine particles with a particle size of 3 μm, achieving an impressive 28.96% improvement.

Simulation of the biomass gasification process of cubic particles in a fluidized bed using the superquadric method

Jun Xie,[a,]* Hao Xu,[a] Xinhe Shen[b]

[a]School of Energy and Mechanical Engineering, Nanjing Normal University, Nanjing, PR China
[b]Southeast University, City, Nanjing, PR China
*Corresponding author: xiejun0218@126.com

An efficient biomass gasification process requires a comprehensive understanding of the physical and chemical phenomena occurring at multi-length and time scales. The non-spherical shape of biomass particles increases the difficulty of multi-scale simulation. In this study, a multiscale computational approach was developed and validated for cubic biomass by integrating a superquadric particle method with chemical reaction kinetics and computational fluid dynamics in open-source code MFiX [1]. The recently developed superquadric DEM model was employed to describe the non-spherical particle-particle contact and gas-particle interaction [2]. The De Felice-Holzer/Sommerfeld hybrid model was used to calculate the drag force on particles, and Richter & Nikrityuk correlation was employed for gas-solid heat transfer [3]. Drying, pyrolysis, gasification, combustion, water-gas shift reactions were considered for gasification process. In the particle reaction model, it is assumed that the size of cubic particle shrinks with the constant density and particle shape (same aspect ratio).

The established model was first validated by comparing with experimental data for the combustion of a single cuboid particle. Then the gasification process of cubic biomass in a bubbling fluidized bed is simulated. The cubic biomass particles were continuously fed from the inlet of left wall. The flow pattern, temperature and gas component distributions inside the bed are presented, as shown in Figures 1 and 2. The effects of key operating parameters on product gas compositions are studied in terms of biomass size, bed temperature, and air equivalent ratio. The particle-scale characteristics such as the evolution process of particle size, temperature, and component were emphatically analyzed.

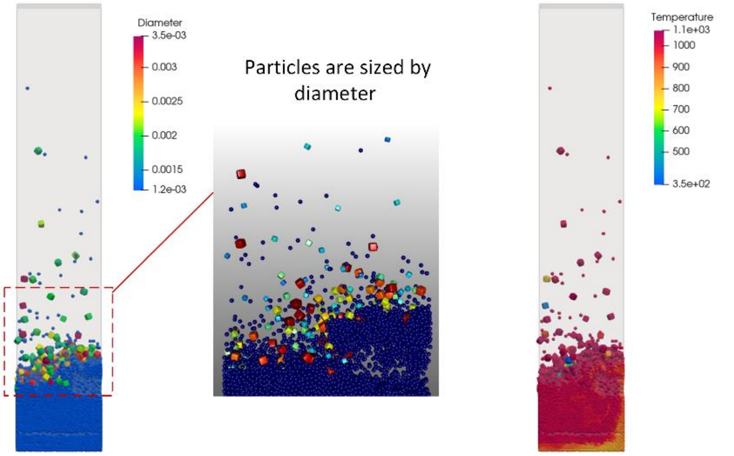

(a) Particle diameter (b) Particle temperature

Figure 1. Particle size and temperature inside the bed.

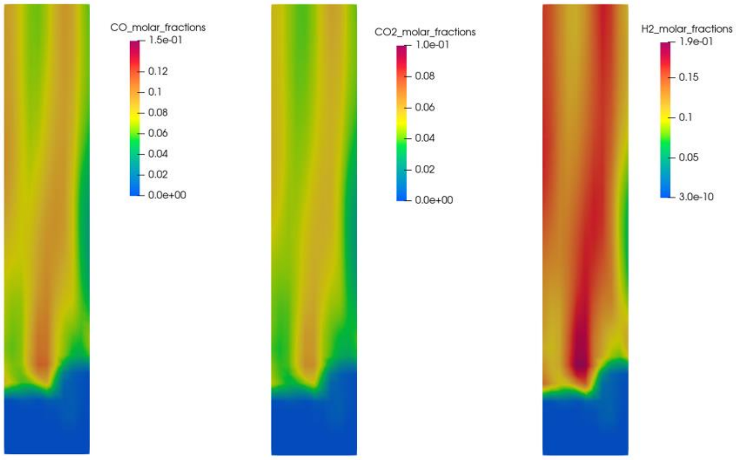

(a) CO (b) CO_2 (c) H_2

Figure 2. Distributions of gas compositions inside the bed.

References

[1] Lu, L., X. Gao, J.-F. Dietiker, et al., *Chem. Eng. Sci.* **2022**, 248, 117131.
[2] Gao, X., J. Yu, L.Q. Lu, et al., *Aiche J.* **2021**, 67(4).
[3] Gao, X., J. Yu, L. Lu, et al., *Chem. Eng. J.* **2021**, 420, 127654.

Interaction Force Analysis in the Binary Nuclear Fuel Particle Co-fluidization Simulations in Spouted Bed using CFD-DEM Method

Yu Tian, Lin Jiang, Rongzheng Liu, Youlin Shao, Xu Yang, Bing Liu, Malin Liu*

Institute of Nuclear and New Energy Technology, Tsinghua University, Beijing 100084, China
*Corresponding author: liumalin@tsinghua.edu.cn

In the preparation of tristructural-isotropic (TRISO) coated nuclear fuel particles by fluidized bed-chemical vapor deposition (FB-CVD) technology, UO_2 kernels are fluidized in the spouted bed and coated with pyrolysis carbon and silicon carbide. According to Geldart classification of powders, particles are classified into four groups (A, B, C, D), as shown in Figure 1(a) [1], and the high-density particle like UO_2 kernel is characterized as group D, which requires a high gas flow in a spouted bed [2]. Since its invention in 1955, the spouted bed, a unique type of fluidized bed designed for handling Geldart D-type particles, has been utilized in various applications including particle coating, drying, and surface modification [3]. In the conventional spouted bed, particles have stable circulations, and undergo three distinct regions: the spouting region, fountain region, and annulus region [4], as can be seen in Figure 1(b).

In a newly designed dispersed nuclear fuel, big nuclear coated particles are mixed with small coated nuclear particles together, then compressed into fuel element matrix to increase the particle packing fraction [5]. Therefore, large and small nuclear kernels are fluidized together in the coated particles preparation process, which is a hot topic in nuclear fuel research. Computational fluid dynamics-discrete element method (CFDDEM) is used to simulate the co-fluidization behaviours of binary particle systems in the spouted bed [6]. Liu et. al. studied the segregation directions of binary mixtures of Geldart B particles in bubbling fluidized beds and a combined model was proposed [7]. Under suitable conditions, both particles can achieve good fluidization states, as shown in Figure 2. However, the unstable states are obtained in fluidization behaviours of only small particle system. It can be found that the spouting region deviations, leading to unstable circulations and particle fluidization vibrations, as shown in Figure 3. The particle trajectories in the cases above are obtained, as shown in Figure 4 and Figure 5. It can be found that the trajectories in binary particle systems are more regular than those in single small particle systems.

There are some previous researches about this topic. Yue et. al. studied the spout deflection in the spouted bed using CFD-DEM method, and the deflection angle was defined and quantitatively studied to provide a method to characterize and quantify spout deflection [8]. Zhou et. al. studied the effects of particle density on particle movements in the spouted bed using CFD-DEM method, and analysed particle drag, pressure gradient force, gravity, and contact force [9]. Here, the underlying mechanisms of binary particles cofluidization are investigated based on analysis of particle-particle interaction forces. The fluidization behaviours of a series of single and binary particle systems were obtained. In the fluidization processes of binary particle system, the transition point from stable to unstable fluidization with the increase of large particle number was found, as shown in Figure 6. The forces between particles were obtained and compared between single and binary particle systems, as shown in Figure 7. Normal and tangential contact force in binary particle systems were drawn, and the distribution of intensity of particle normal and tangential contact forces were obtained, as shown in Figure 8. The evolution of particle forces with increasing large particle numbers were given. It can be found that the large particle-small particle interaction force is the dominate factor for maintaining the stable spouted state in binary particle spouting behaviour.

In this research, the fluidization mechanism of varying particle systems was studied in detail, and the reasons for the establishment of stable circulations in binary particle systems were revealed from the view of force analysis. These findings will be beneficial for the fluidization research of binary particles, such as nonspherical particles or even two-dimensional flakes fluidization with spherical particles in the future, and also give some guidance for coating technology parameters of nuclear fuel particles, aimed at increasing the particle packing fraction in preparing the dispersed nuclear fuel elements.

References

[1] D. Geldart, *Powder Technol* **1973**, 7, 285-292.

[2] Ray Cocco, Jia Wei Chew, *Powder Technol* **2023**, 428, 118861.

[3] K.B. Mathur, P.E. Gishler, *AIChE J*, **1955**, 1(2), 157-164.

[4] T. Kawaguchi, M. Sakamoto, T. Tanaka, Y. Tsuji, *Powder Technol* **2000**,109, 3-12.

[5] R.N. Morris, P.J. Pappano, *J. Nucl. Mater* **2007**, 361,18-29.

[6] O.O. Olaofe, A.V. Patil, N.G. Deen, M.A. van der Hoef, J.A.M. Kuipers, *Chem. Eng. Sci* **2014**, 108, 258-269.

[7] C. Liu, Y. Zhao, Y. Li, Y. Feng, C. Duan, C. Zhou, L. Dong, *Particuology* **2024**, 90, 340-349.

[8] Y. Yue, T. Wang, M. Sakai, Y. Shen, *Chem. Eng. Sci* **2019**, 205, 121-133.

[9] L. Zhou, Z. Zhao, W. Li, L. Bai, K. A. Ramesh, *Phys. Fluids* **2023**, 35(12), 123345.

Dispersion and flocculation transition of alumina slurries as temperature changes evaluated by a combined OCT and rheometer system

Junichi Tatami,[a]* Miyu Nakamura,[a] Motoyuki Iijima,[a] Takuma Takahashi[b]

[a]Yokohama National University, Yokohama, Japan
[b]Kanagawa Institute of Industrial Science and Technology, Ebina, Japan
*Corresponding author: E-mail tatami-junichi-xv@ynu.ac.jp

Although the internal structure of slurries is generally evaluated through rheological properties, this does not always provide correct results. Direct observation of the internal structure, performed simultaneously with rheological properties, is an effective solution to this problem. In this study, in-situ observation of the internal structure and rheological characterization of alumina slurries as the temperature increase were carried out simultaneously using a combined optical coherence tomography (OCT) and rheometer system. OCT images showed that the temperature increase resulted in inactive particle motion, meaning that the slurry flocculated. The storage modulus increased with this internal structural change. This transition temperature increased with as the amount of dispersant added, which dominates the dispersibility of the particles, increased, but the tendency was founded to be consistent. The change in the adsorption state of the dispersant on the particles with increasing temperature is considered to have caused the slurry to agglomerate.

The study of particle size and morphology changes of metal powders on the same shear energy and impaction with DEM simulation

Heekyu Choi,[a,c,d,e,]* Khulan Uranchimeg,[a] Amgalan Bor,[b] Kyung Sung Kim[c,d]

[a]Graduate School of Material Science Engineering, Changwon National University, Changwon, Gyoungnam 641-773, Republic of Korea
[b]Department of Chemical and Biological Engineering, School of Engineering and Applied Sciences, National University of Mongolia, Ulaanbaatar, Mongolia
[c]Department of Mechatronics Convergence Engineering, College of Future Convergence, Changwon National University, Changwon, Gyoungnam 641-773, Republic of Korea
[d]Research Institute of Future Convergence, Changwon National University, Changwon, Gyoungnam 641-773, Republic of Korea
[e]Graduate School of Convergence on Culture Technology, Changwon National University, Changwon, Gyoungnam 641-773, Republic of Korea
*Corresponding author: hkchoi99@changwon.ac.kr

In this study, the influence of the contact number, the contacts of the ball-to-ball and ball-to-wall, shear energy, and impaction on the evolution of metal powder characteristics was studied with DEM simulation. The characteristics of metal powders were studied in a planetary ball mill under various experimental conditions, such as three different ball sizes, rotation speeds, and milling times, using a discrete element method (DEM) simulation. The particle morphology and size evolution of metal powders were determined using scanning electron microscopy (SEM) and particle size analyzer (PSA). To determine the contact number between the ball and the wall as well as the motion of the ball within the planetary ball mill, the shear end impact energy produced during the collision was examined using the DEM simulation. When compared under the same experimental conditions and energy, the morphologies of metal powder particles were radically different. The characteristics of raw metal powder were found to have an impact on the experimental results.

Keywords: metal powder, particle morphology, particle size, shear energy, impaction.

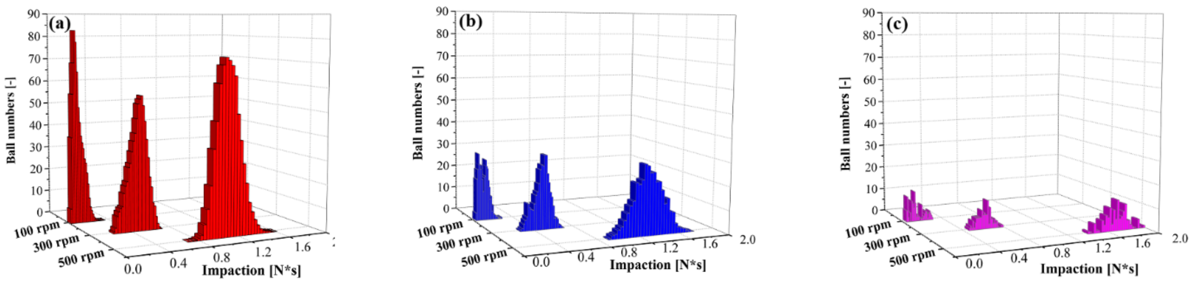

Figure 1. Histogram of ball impaction distribution per moment of ball diameter with (a) 1 mm, (b) 3 mm, and (c) 5 mm during the ball milling process at different rotation speeds [1].

References

[1] B.Jargalsaikhan, A.Bor, K.S.Kim, H.Choi, *Particuology* **2024**, 90, 41-50.

Non-parametric evaluation for particle size distribution analysis

Tatsushi Matsuyama

Faculty of Engineering, Soka University, Hachioji Tokyo Japan

How many particles have to be measured is a traditional question in general in powder technology. In the particle size distribution analysis, various conditions such as sampling and dispersion can affect measurement errors or variations. One important factor is sample size (the number of particles involved in a single measurement), which leads statistical error, also known as fundamental error. The study of the requir3d number of particles for precise measurement has a long history. Recently the concept of 'metrological traceability' has become important, the original question has to be rephrased, requiring an estimate of uncertainty of measurement due to fundamental error, although the basic mathematics remain same.

Traditionally, a parametric analysis based on a mathematical distribution function was used. The advantages of using a parametric distribution are: (1) Many mathematical theories are available, (2) Few parameters are needed to describe the entire distribution, and (3) Probability charts can be used. However, real sample populations do not exactly follow a mathematical distribution. Therefore, non-parametric analysis methods are needed. The bootstrap method is one such non-parametric method and is simple to use. With a dataset of sample size N, re-sampling with replacement is conducted to obtain a bootstrap sample of the same size. Repeating the bootstrap sampling gives a set of bootstrap samples, which approximate real samples well. This method simulates real samples using a computer instead of repeating actual measurements multiple times.

In this presentation, the bootstrap method will be introduced, and its performance using mathematical simulations with log-normal distribution will be shown for number-based distribution. Additionally, the conversion from number-based to mass-based distribution in data processing and the use of the Hatch-Choate formula will be discussed.

Photocurable aqueous suspension design for greener additive manufacturing process of alumina ceramics

Motoyuki Iijima,[a],* Bohua Ma,[b] Junichi Tatami [a]

[a] Faculty of Environment and Information Science, Yokohama National University, Yokohama, Japan
[b] College of Engineering Science, Yokohama National University, Yokohama, Japan
*Corresponding author: iijima@ynu.ac.jp

Additive manufacturing of ceramic components has attracted wide attention due to its possibility to shape on-demand structures which are difficult to be realized using conventional processing methods. Vat photopolymerization using photocurable suspension is one of the promising additive manufacturing methods which can achieve high resolution printing, and therefore, ceramic components with various structures have been demonstrated to be printed up to date [1]. However, most processes require the usage of organic solvents and involves long debinding due to the exceeded amounts of monomers/polymers treated in the photocurable suspensions. Herein, in order to develop a greener and efficient additive manufacturing route for ceramics, we design a new photocurable alumina suspension which is aqueous and can be photocured by interparticle photo-cross-linking reactions using reduced amounts of monomers.

For the design of the suspension, briefly, alumina particles were dispersed in an ion-exchanged water with the aid of L-asparagine and ball milled for 24 h. Then, photo-radical initiator and water-soluble bi-functional acrylate (BA, 5-20 vol% to particles) was added to the suspension. The flowing behavior and photocuring behavior were characterized by a rheometer equipped by a photo-illuminating apparatus. The microstructures of photocured bodies were evaluated by FE-SEM. The designed photocurable alumina suspension was applied to 3D structuring process using a digital light processing (DLP) based 3D printer.

Figure 1(a) presents the flow curves of the designed alumina aqueous suspension (30 vol%) with various amounts of BA. All suspensions possessed flow curves without having a hysteresis character in the course of increasing and decreasing of the shear rates. This result indicates that no strong aggregates were present in the designed suspension. The changes of storage modulus (G') of the suspension before and after photo-irradiation is shown in Figure 1(b). It was confirmed that the G' values of the suspension effectively increased after photo-irradiation which indicates that the designed suspension is photocurable. The suspensions containing higher BA content possessed lager changes in G' due to higher concentration of interparticle cross-links. By comparing the FE-SEM images of raw alumna particles and the microstructures of photocured bodies, it is confirmed that polymer networks were formed among the particles. Figure 3 presents an example of the DLP-3D printed alumina parts by using the designed aqueous suspension. Interestingly, an over-hanged 3D structure was printable without an addition of UV adsorbers and/or polymerization inhibitors. Due to the reduced amounts of monomers used in the suspension, the photocured bodies were de-bindable/sinterable into dense alumina through rapid firing (10ºC/min) without occurring any structural collapse.

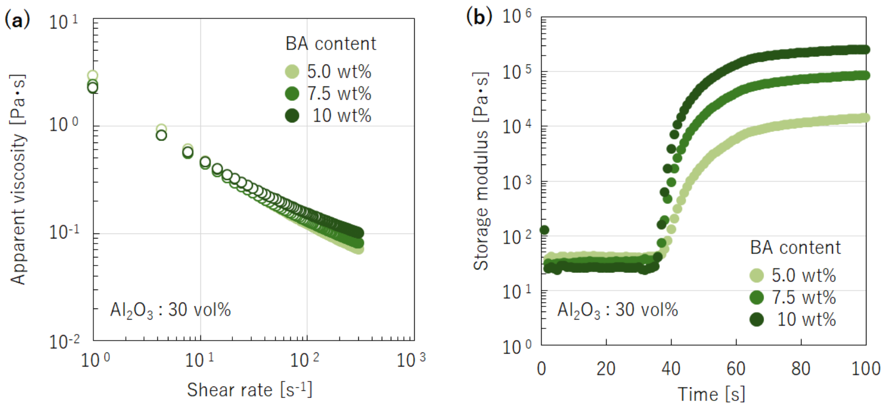

Figure 1. Flowing behaviour of photocurable aqueous alumina suspension:
(a) flow curve and (b) storage modulus before and after photo-irradiation (UV light irradiated at 30 s).

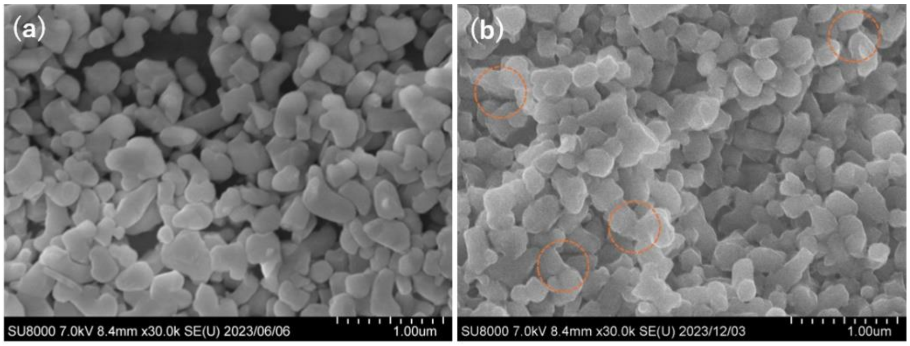

Figure 2. FE-SEM image of (a) raw alumina particles and (b) photocured alumina body (BA content: 7.5 wt%).

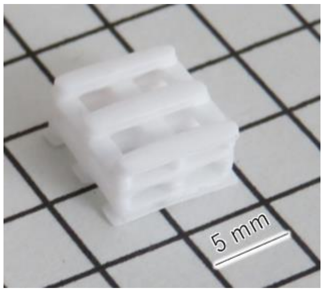

Figure 3. Sintered body of DLP-3D printed alumina body.

References

[1] Z. Chen et al., *J. Eur. Ceram. Soc.* **2019**, 39, 661-687.

Elucidation of influence of saponification degree of added PVA on internal structural changes during drying of SiO2 slurry by operando OCT observation

Hiromasa Kuroda,[a] Junichi Tatami,[a]* Motoyuki Iijima[a], Takuma Takahashi[b]

[a]Yokohama National Univ., Yokohama, Japan
[b] Kanagawa Institute of Industrial Science and Technology, Ebina, Japan
*Corresponding author: tatami-junichi-xv@ynu.ac.jp

Although it is generally considered that in the wet forming of ceramics, lower viscosity slurries yield denser green bodies, this correlation does not always apply. Furthermore, inhomogeneity such as density distribution that occur during drying can lead to cracking and deformation. To accurately address this issue, it is important to understand the internal structural changes and the development of inhomogeneities during the drying process of the slurry. In this study, the internal structure of slurries during drying was observed using optical coherence tomography (OCT), which allows high-speed and high-resolution observation of the internal structure of opaque bodies, to visualize the effect of the saponification degree of polyvinyl alcohol (PVA) added to the slurry on the change in internal structure.

SiO_2 powder (KE-S-30, Nippon Shokubai Co., Ltd.) was added to ion-exchanged water at 45 vol%, and polyethyleneimine (PEI1800, Fuji Film Wako Chemicals Co., Ltd.) was added as a dispersant. Thereafter, PVA (Fujifilm Wako Chemicals Co., Ltd.) with different saponification degree (99.27, 81.32 and 65.53%) was added, and three types of slurries (Slurry A, B, and C in descending order of saponification degree of PVA) were prepared by ball milling. The absence of hysteresis in the flow curves evaluated using a rheometer indicates that the SiO2 particles in the slurry are highly dispersed. The slurries were formed into sheets and the cross-section of the sheet slurry during the drying process was observed using a combined OCT-TG system, consisting of an SS-OCT (IVS-2000-WR, Santec Corporation, 3.7 µm resolution) and an electronic balance (UX1020H, Shimadzu Corporation) equipped with an infrared heater. The heating was continued at an ambient temperature of 50°C until there was no change in weight.

Figure 1 shows the relationship between the apparent viscosity of the slurries and the relative density of the green bodies. Although the apparent viscosity of slurry C was lower than that of slurry A, the relative density of the green body made from slurry C was lower. There is a possibility that the dispersion of the particles during the drying process depends on the degree of saponification of the added PVA.

Figure 2(a) shows OCT images of the cross-section of slurry A in the early stages of the drying process. The speckle pattern in the images changed with time. This is because the particles in the slurry are well dispersed, and the internal structure is constantly changing due to Brownian motion of particles. Subsequently, as the slurry dried, areas of different contrast appeared on the slurry surface. The degree of change in the speckle pattern was evaluated using the motion detection method [1], which confirmed that there were few pixels determined to be in motion in these area (Figure 2(b)). This resulted from the decrease in the quantity of dispersing medium as drying, which reduce the distance between the particle surfaces and caused particle agglomeration, thus suppressing Brownian motion of particles. As drying progressed, the agglomerated area developed toward the bottom of the slurry. Figure 3 shows the relationship between the ratio of the agglomerated area and the dry basis moisture content in the slurry. The ratio of agglomerated areas decreased with an increase of the moisture content, independent of the type of slurry, i.e. the degree of saponification of the added PVA. In the early stages of drying, the degree of saponification of the added PVA had no effect on the development of the agglomerated areas.

Thereafter, agglomeration progressed from the surface and also from the edges of the slurry. At this time, deformation occurred because of the volume change during agglomeration. Figure 4 shows OCT images and displacement in the agglomerated areas estimated by digital correlation method. The magnitude and distribution of the displacement depended on the slurries. This is attributed to the difference in the mechanical properties of the agglomerated area, which are related to the surface state of the particles, depending on the degree of saponification of the added PVA.

References

[1] H. Kuroda, J. Tatami1, M. Iijima and T. Takahashi, *J. Ceram. Soc. Japan* **2023**, 131[3], 37-41.

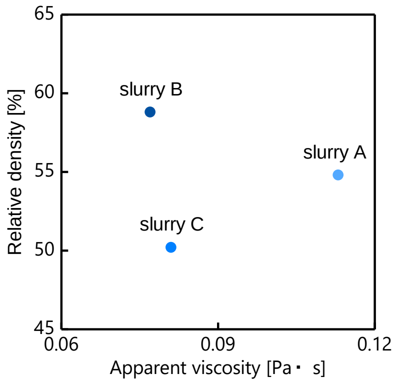

Figure 1. Relation between apparent viscosity of slurries at 10 s^{-1} and relative density of green bodies.

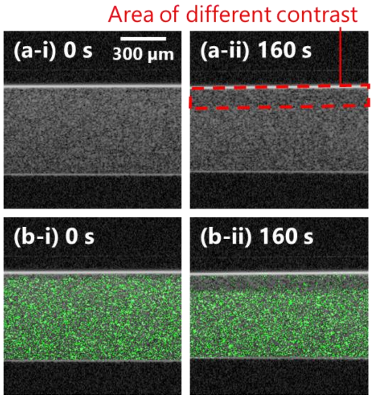

Figure 2. OCT images of cross-section of slurry A, (a): raw image, (b): Result of applying motion detection method.

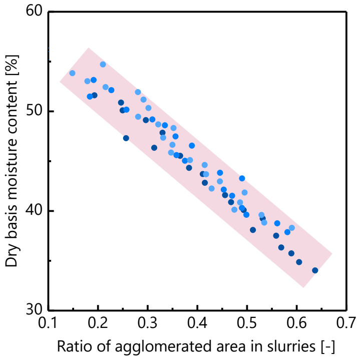

Figure 3. Development of agglomerated areas with the progression of drying

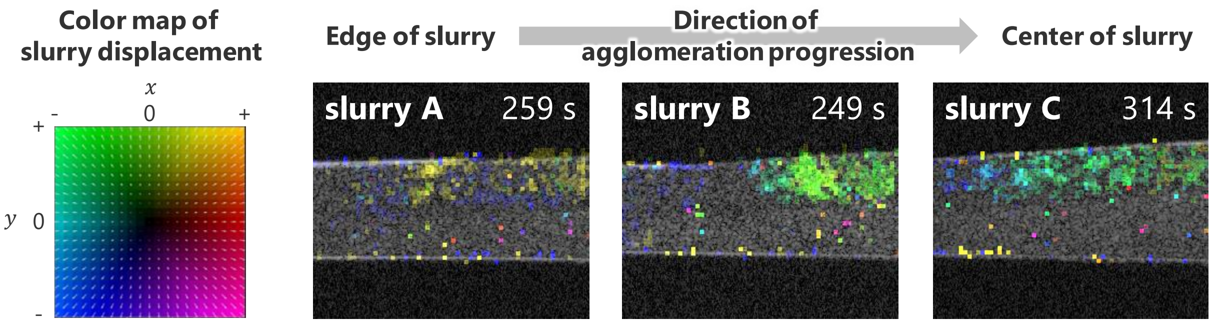

Figure 4. Displacement of agglomerated areas visualized by applying digital image correlation method

Investigation of micronization of TSLP single-domain antibody for pulmonary drug delivery

Jingyu Shi,[a] Hao Miao,[b] Zhenbo Tong[a,]*

[a]Southeast University, Nanjing, China
[b]Monash University, Clayton, Australia
*Corresponding author: z.tong@seu.edu.cn

Pulmonary drug delivery (PDD) is a non-invasive method which leverages the extensive lung surface area to enhance drug absorption and can avoid the first-pass effect. The inhalation of biologics such as proteins and nucleic acids holds great promise for the treatment of both lung and systemic diseases. However, the natural barriers including mucociliary, alveolar macrophage, enzyme, pulmonary surfactant, and epithelium influence the absorption of the inhaled biologics. The drug absorption is also influenced by the aerosol transport and deposition, which varies based on pharmacokinetic (PK) differences in different anatomical positions. Lung deposition is challenging to be controlled due to variations in formulation, devices, usage, and airway geometry. Compared with small molecules, biomacromolecules are more unstable especially during the preparation and usage of inhaled drugs. The atomization and micronization processes can introduce shear stress and dehydration, potentially compromising the efficacy of the drugs. These processes will impact microstructures of drugs, which can further affect their properties and functionalities. As a result, the research focused on investigating the two critical processes to develop a platform for inhaled biomacromolecules in both solution and powder forms.The inhalable human TSLP single-domain antibody dry powder was prepared via spray drying (SD) for decreasing aseptic and cold chain requirements. The results showed that drug aerosol performance is linked to their microstructure. In addition, redissolved human TSLP single-domain antibody exhibited promising blocking activity compared to commercialized Tezepelumab and CSJ-117-FAB.

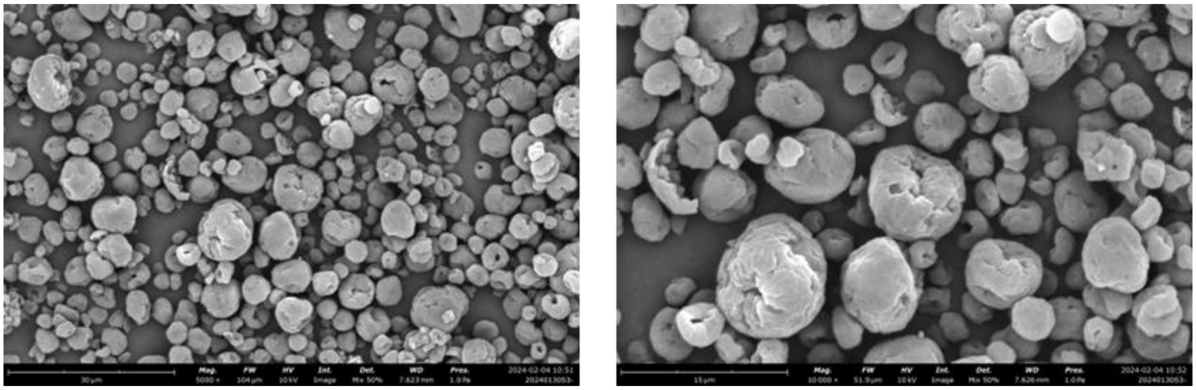

Figure 1. SEM images of SD dry powder of TSLP Single-domain Antibody.

Table 1. NGI results of SD dry powder of TSLP Single-domain Antibody.

Gly:Leu	**1:1**	**3:1**	**1:3**
D50/µm	9.12	6.18	5.29
FPF/%	26.174	45.171	47.238
MMAD/µm	5.034	4.953	4.203
GSD/µm	1.969	1.894	1.904
R2	0.993	0.999	0.966

References

[1] H. Miao, K. Huang, Y. Li, R. Li, X. Zhou, J. Shi, Z. Tong, Z. Sun, A. Yu. *Int J Pharm* **2023**, 640, 123050.

Effective prevention of palladium metal particles sintering by histidine stabilization on silica catalyst support

Harry Cahyanto,[a,b] Xuanming Chen,[c] Frank L. Y. Lam,[c] Ploychanok Iadrat,[d] Chularat Wattanakit,[d] Pinit Kidkhunthod,[e] Varinder Singh,[b,f] Sally Brooker,[b,f] Shusheng Pang,[a] Jungkyu Choi,[g]* Alex C. K. Yip[a,b]*

[a]Department of Chemical and Process Engineering, The University of Canterbury, Christchurch, New Zealand
[b]The MacDiarmid Institute for Advanced Materials and Nanotechnology, New Zealand
[c]Department of Chemical and Biological Engineering, The Hong Kong University of Science and Technology, Hong Kong, China
dDepartment of Chemical and Biomolecular Engineering, Vidyasirimedhi Institute of Science and Technology (VISTEC), Rayong, Thailand
[e]Synchrotron Light Research Institute, Nakhon Ratchasima, Thailand.
[f]Department of Chemistry, University of Otago, Dunedin, New Zealand
[g]Department of Chemical and Biological Engineering, Korea University, Seoul, Republic of Korea
*Corresponding authors: jungkyu_choi@korea.ac.kr and alex.yip@canterbury.ac.nz

A robust method for enhancing the dispersion and stabilization of small metal nanoparticles in heterogeneous catalysts is developed. It involves in situ complexation of palladium(II) by histidine, in water, prior to impregnation in fumed silica. TEM images show that the histidine facilitates dispersion of the Pd(II) into finer nanoscale particles (~2 nm) uniformly distributed on the support, rather than the large clusters (~5 nm) seen in the absence of histidine. After hydrogen reduction, assessments using CO chemisorption and propylene hydrogenation indicate that the coordinated histidine might obscure the active sites on the Pd particles. However, as histidine decomposes between 220-300°C in air, these materials were treated at 225°C in air for 48 h. Afterwards the Pd(II) particles remain the same size, but after hydrogen reduction, there is a 2.4-fold increase in CO gas adsorption, indicative of an expanded Pd surface area. Furthermore, superior catalyst stability (activity >200 h) is observed during propylene hydrogenation at 250°C. This is consistent with histidine use having generated widely spaced, uniformly small, Pd nanoparticles on the silica support which is expected to help prevent agglomeration (sintering) during catalysis. This is a convenient low-cost strategy for reducing metal content, preventing sintering and optimizing catalyst performance.

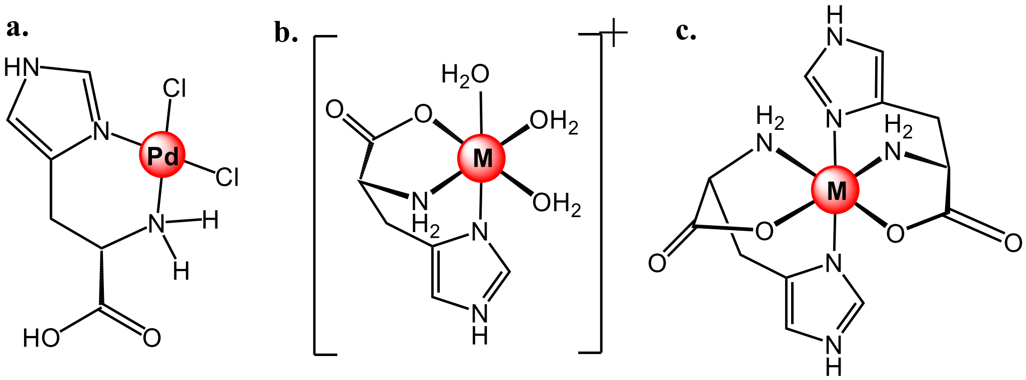

Figure 1. Structures of **a)** square planar 1:1 histidine-palladium complex,[1] **b)** octahedral 1:1 histidine-metal complex, **c)** octahedral 2:1 histidine-metal complex (Note: M = Ni^{2+}, Cu^{2+}, Zn^{2+}).

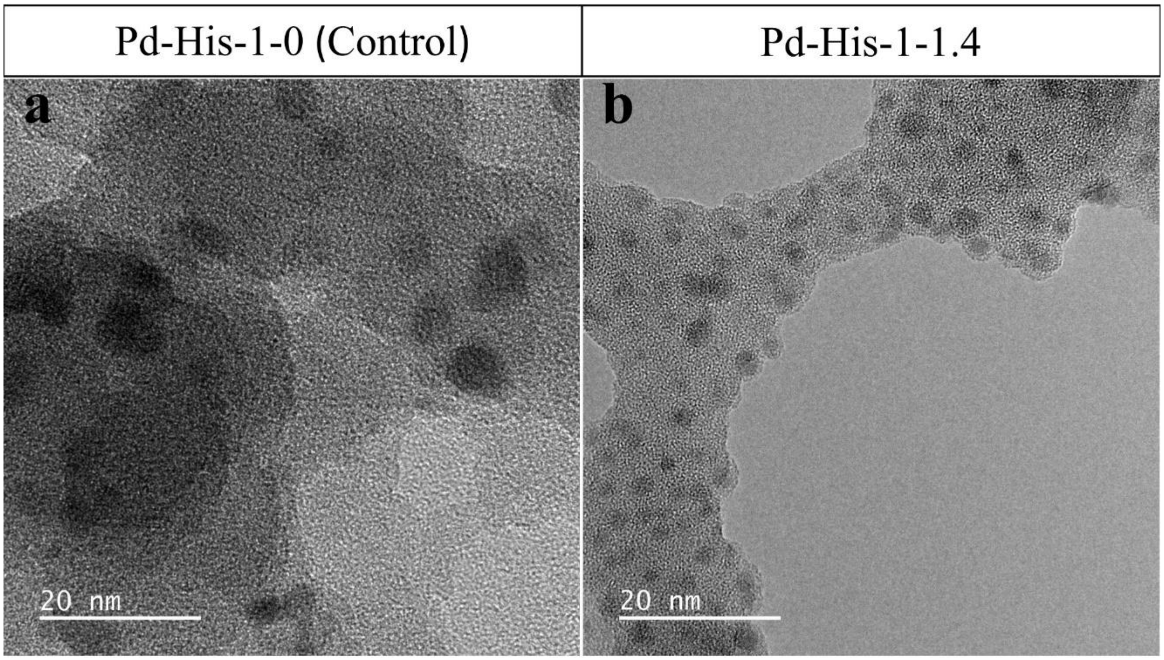

Figure 2. TEM images of: **a)** Pd-His-1-0 (without histidine, control) and, **b)** Pd-His-1-1.4 (with histidine to Pd ratio of 1.4).

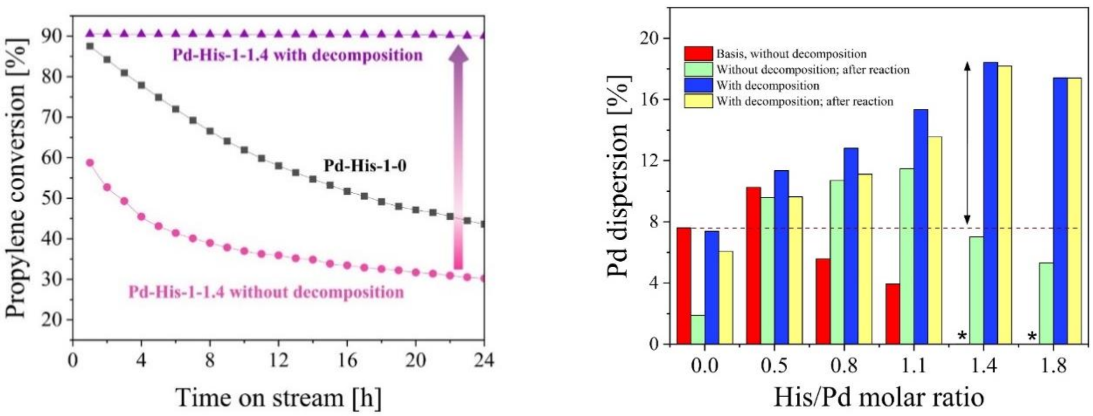

Figure 3. a) comparison highlighting the significant effect of histidine stabilization on Pd nanoparticles on the silica support. Reaction conditions: 0.502 g of catalyst; 3.1 sccm of propylene, 3.1 sccm of hydrogen, and 44 sccm of Ar; T = 250 °C and P = 1.1 bar. **b)** Pd dispersion over silica support prepared at different histidine-to-Pd ratios, with and without subjected to histidine decomposition conditions (225 °C for 48 h) and propylene hydrogenation (250 °C for 24 h). Note: an asterisk indicates the Pd dispersion could not be measured by CO pulse chemisorption due to the coverage of active surface by excessive histidine.

References

[1] A. Caubet, V. Moreno, E. Molins, C. Miravitlles, *J. Inorg. Biochem.* **1992**, *48*, 135.

Automated synthesis of Al-doped ZnO nanoparticles: an online UV-Vis spectroscopy approach

Guohui Yang,[a,]* Marcel Kévin Jiokeng Dongmo,[a] Thomas Meurer,[a] Hermann Nirschl[a]

[a]Karlsruhe Institute of Technology, Institute of Mechanical Process Engineering and Mechanics, Karlsruhe, Germany
*Corresponding author: guohui.yang@kit.edu

Innovative techniques for fabricating and seamlessly integrating customized nano-materials into complex optoelectronic semiconductor systems, such as organic light-emitting diodes and thin-film solar cells, are of paramount significance in the ongoing energy transition. With a surging demand for these technologies and a concurrent scarcity of rare earth materials in semiconductors, aluminum-doped zinc oxide (AZO) nanoparticles have emerged as an economically viable, eco-friendly substitute for indium tin oxide (ITO). [1-2] Our research leverages the versatile sol-gel synthesis method to create homogeneous AZO nanoparticles, allowing precise control over size and morphology through key parameter adjustments, including temperature. These variations impact the transparency and conductivity of solar cells, positioning our research as pivotal in renewable energy (see Fig. 1). To achieve precise control in a batch reactor, we employ a process controller, a model-based soft sensor, and online UV-Vis spectroscopy. This system continuously measures the real-time mass concentration of AZO, providing input for the model-based soft sensor. Leveraging population balance equations (PBE), the soft sensor offers real-time particle size distribution (PSD) data, with model parameters identified through offline Small-Angle X-ray Scattering (SAXS) and Dynamic Light Scattering (DLS) measurements.

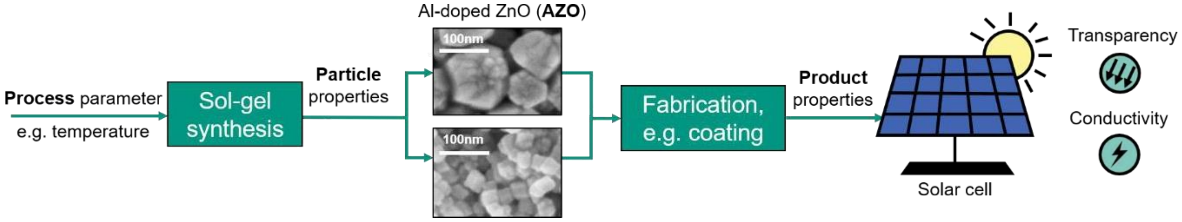

Figure 1. The process temperature is a key control parameter to influence the AZO sizes, as well as the transparency and conductivity of solar cells.

At the upcoming APT 2024 within the sub-theme characterisation, we will present our findings on AZO sol-gel synthesis, elucidate the population balance model parametrized by SAXS and DLS, showcase UV-Vis measurements, and detail an innovative approach for automated AZO production. Our work advances the synthesis of nanomaterials for emerging technologies, promising precise control over AZO particle and product properties.

References

[1] T. Minami, *Thin Solid Films* **2008**, 516, 5822.

[2] K. Ellmer, K. Klein, B. Rech, *Springer Science & Business Media* **2008**.

An approach to automated process optimization in mixing using adaptive and dynamic mixing modes

Benedikt Schwarz,* Johannes Lindner

Technical University of Applied Sciences, Burghausen, Germany
*Corresponding author: Benedikt.Schwarz@TH-Rosenheim.de

Mixing plays a significant role in a broad area of industries e.g. fine- and petrochemicals, food and pharma and mineral processing. The design of mixing processes is usually done using empirical formulations, calculations based on numerical fluid dynamics and experiences with regards to certain mixing applications. Core topics in mixing are homogeneous blending in tanks, dispersion of gases in liquids or liquids in liquids, improvement of heat transfer or suspension and distribution of solids in liquids. The selection of the appropriate stirrer type is done with respect to the desired flow (axial, radial, tangential) and the rheological material properties as it is shown in [1].a. The change of the mixing task or a significant material parameter during the process leads to reduced process efficiency, the need of higher mixing times or lower mixing quality. Changing the tool is often not economically viable due to the changeover costs and production downtime. In order to process different tasks in a wide range of applications in the same mixer, a mixing tank with variable tools was developed in cooperation with the Co. Kniele GmbH. It is shown in [1].b. For highly viscous materials, a close-clearance helical ribbon impeller is implemented (1 in [1].c). The flow pattern of low viscosity fluids can be influenced by a centric stirrer with changeable blade angles 2 in [1] c. An axial flow can be achieved by pitching the blades of the main stirrer. Performing different tasks such as dispersion, aerating and suspending subsequently in the same mixer is hence possible at high efficiency without changing the tool. On top changes the mixing performance due to fluctuating process parameters can be dynamically compensated using an automated design of experiments approach.

Figure 1. a: Classification of stirrers according to predominant flow pattern and range of viscosity (Zlokarnik 2001). b: Multi-purpose mixer developed with Co. Kniele GmbH; c: Actuators of the multi-purpose mixer. (1) helical ribbon stirrer and turbine stirrer with changeable blade angles (2)

The energy introduced into the fluid can be used as target parameter to quantify the quality of a dispersion process. For the stirrer shown in [1],**Error! Reference source not found.** a variety of settings is possible due to the three independent actuators, which can be optimised dynamically to reach an optimum energy input. For the detection of the optimal settings, a control algorithm was developed, which we call automated design of experience. The algorithm changes the speed of main and coaxial stirrer and blade angle in a sequential order and evaluates whether an improvement or degradation regarding energy input results. The current intake of the main stirrer is used as an indicator for the energy input into the fluid.

A test run of the control algorithm applied on the multi-purpose mixer is shown in Figure 2. The target of the algorithm is to make only small changes and determining, whether an improvement is achieved. At the very beginning, the first actuator main stirrer started at a positive speed leading to an increase of current consumption of the stirrer drive. The speed was increased in small steps to increase the energy input in the system. In the second section, the blade pitch was adapted to increase the energy input. After finding the maximum, the variation of the third actuator, the speed of the helical ribbon stirrer started. After a decline of the target value resulted by starting the helical ribbon in positive speed direction, the control algorithm changed the rotational orientation in negative direction which led to a further increase in current intake. The final operating mode was determined with maximum speed of the main stirrer, maximum drag (flow resistance) of the blades and maximum speed of the helical ribbon reversed to the main stirrer. The operating mode can be used for mixing tasks like dispersion or homogenization were a high power input into the fluid is needed.

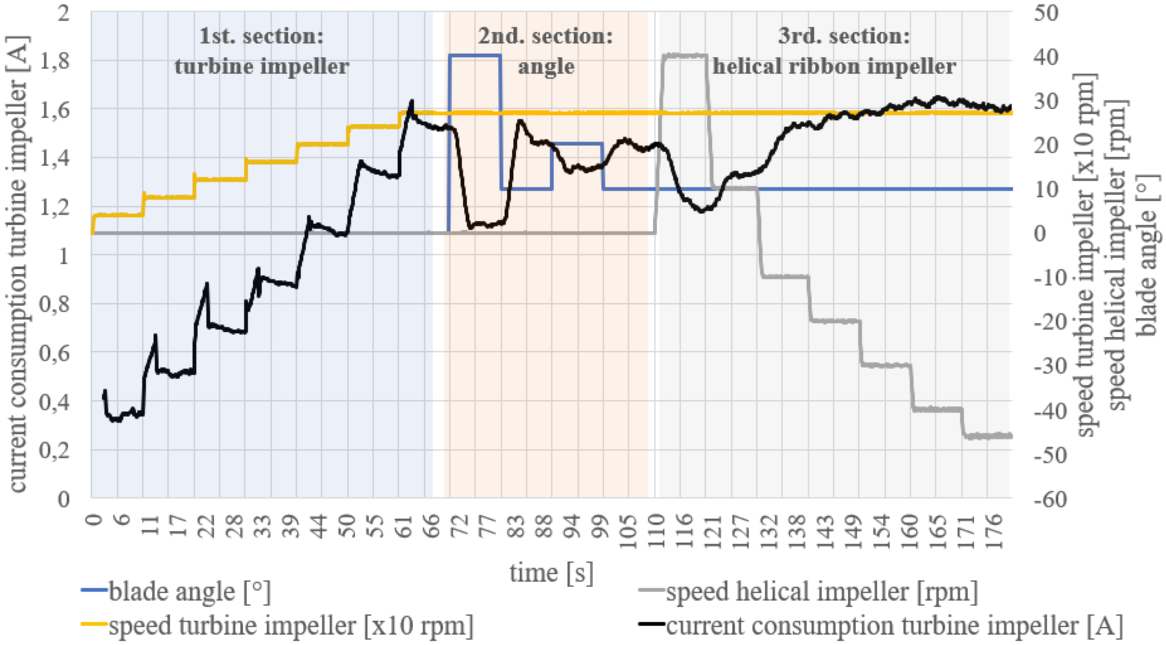

Figure 2. Test run of the automated design of experience applied on the multi-purpose mixer with current intake as target parameter

References

[1] M. Zlokarnik, Stirring: Theory and Practice. *Wiley-VCH* **2001**, Weinheim.

Effective prevention of palladium metal particles sintering by histidine stabilization on silica catalyst support

Harry Cahyanto,[a,b] Xuanming Chen,[c] Frank L. Y. Lam,[c] Ploychanok Iadrat,[d] Chularat Wattanakit,[d] Pinit Kidkhunthod,[e] Varinder Singh,[b,f] Sally Brooker,[b,f] Shusheng Pang,[a] Jungkyu Choi,[g]* Alex C. K. Yip[1,2]*

[a]Department of Chemical and Process Engineering, The University of Canterbury, Christchurch, New Zealand
[b]The MacDiarmid Institute for Advanced Materials and Nanotechnology, New Zealand
[c]Department of Chemical and Biological Engineering, The Hong Kong University of Science and Technology, Hong Kong, China
[d]Department of Chemical and Biomolecular Engineering, Vidyasirimedhi Institute of Science and Technology (VISTEC), Rayong, Thailand
[e]Synchrotron Light Research Institute, Nakhon Ratchasima, Thailand.
[f]Department of Chemistry, University of Otago, Dunedin, New Zealand
[g]Department of Chemical and Biological Engineering, Korea University, Seoul, Republic of Korea
*Corresponding authors: jungkyu_choi@korea.ac.kr and alex.yip@canterbury.ac.nz

A robust method for enhancing the dispersion and stabilization of small metal nanoparticles in heterogeneous catalysts is developed. It involves in situ complexation of palladium(II) by histidine, in water, prior to impregnation in fumed silica. TEM images show that the histidine facilitates dispersion of the Pd(II) into finer nanoscale particles (~2 nm) uniformly distributed on the support, rather than the large clusters (~5 nm) seen in the absence of histidine. After hydrogen reduction, assessments using CO chemisorption and propylene hydrogenation indicate that the coordinated histidine might obscure the active sites on the Pd particles. However, as histidine decomposes between 220-300°C in air, these materials were treated at 225°C in air for 48 h. Afterwards the Pd(II) particles remain the same size, but after hydrogen reduction, there is a 2.4-fold increase in CO gas adsorption, indicative of an expanded Pd surface area. Furthermore, superior catalyst stability (activity >200 h) is observed during propylene hydrogenation at 250°C. This is consistent with histidine use having generated widely spaced, uniformly small, Pd nanoparticles on the silica support which is expected to help prevent agglomeration (sintering) during catalysis. This is a convenient low-cost strategy for reducing metal content, preventing sintering and optimizing catalyst performance.

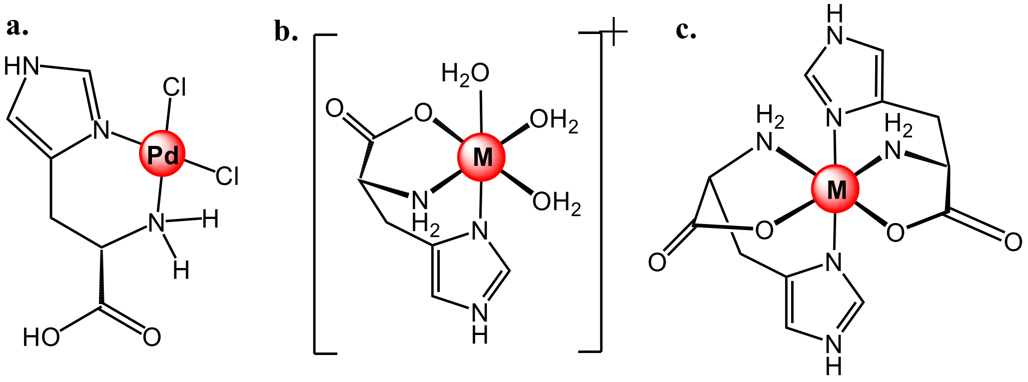

Figure 1. Structures of **a)** square planar 1:1 histidine-palladium complex,[1] **b)** octahedral 1:1 histidine-metal complex, **c)** octahedral 2:1 histidine-metal complex (Note: M = Ni^{2+}, Cu^{2+}, Zn^{2+}).

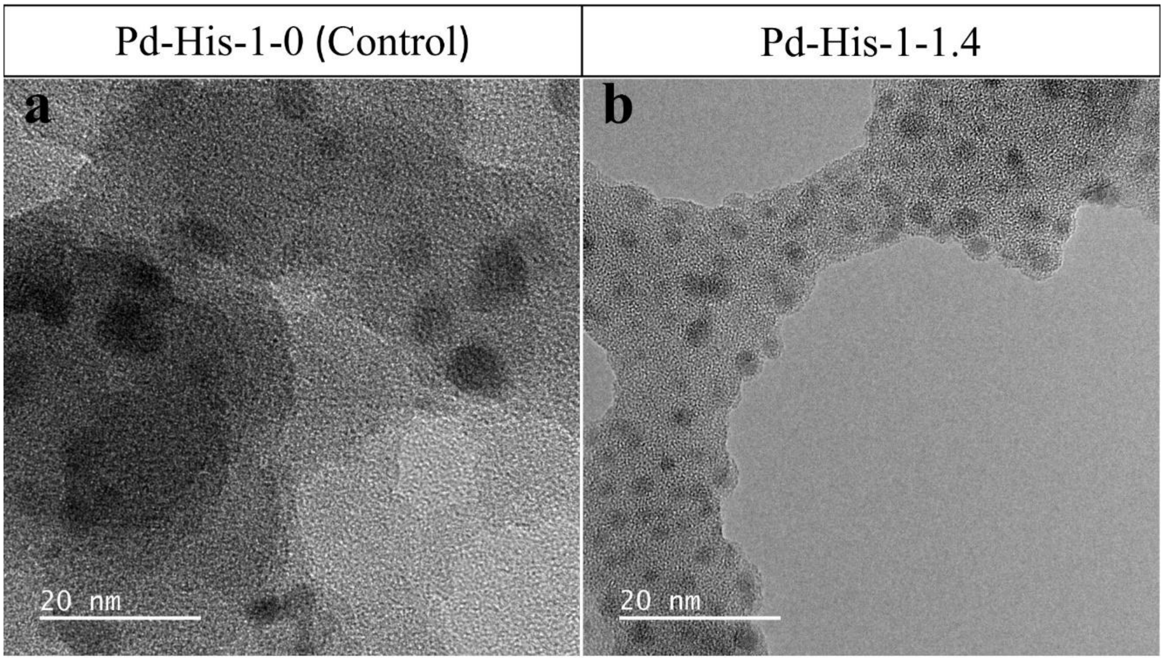

Figure 2. TEM images of: **a)** Pd-His-1-0 (without histidine, control) and, **b)** Pd-His-1-1.4 (with histidine to Pd ratio of 1.4).

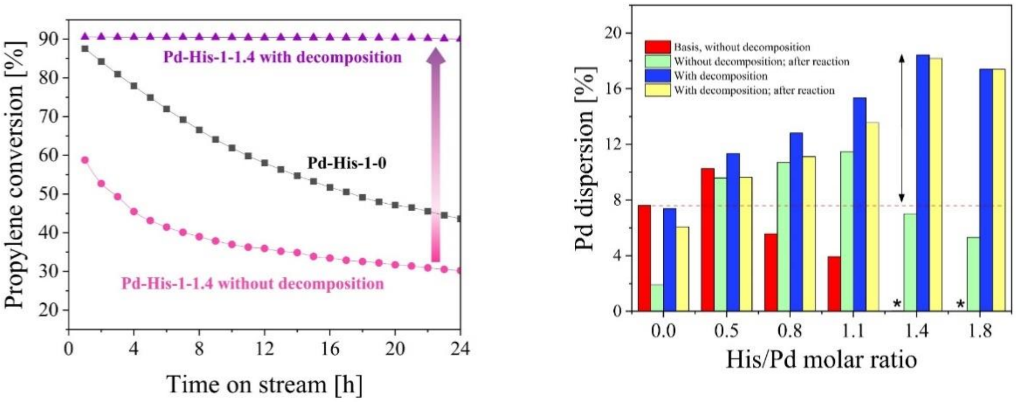

Figure 3. a) comparison highlighting the significant effect of histidine stabilization on Pd nanoparticles on the silica support. Reaction conditions: 0.502 g of catalyst; 3.1 sccm of propylene, 3.1 sccm of hydrogen, and 44 sccm of Ar; T = 250 °C and P = 1.1 bar. **b)** Pd dispersion over silica support prepared at different histidine-to-Pd ratios, with and without subjected to histidine decomposition conditions (225 °C for 48 h) and propylene hydrogenation (250 °C for 24 h). Note: an asterisk indicates the Pd dispersion could not be measured by CO pulse chemisorption due to the coverage of active surface by excessive histidine.

References

[1] A. Caubet, V. Moreno, E. Molins, C. Miravitlles, *J. Inorg. Biochem.* **1992**, *48*, 135.

Effects of a dispersing liquid’s property on an electrically induced fluid flow and particle traps in a self-healing wire system

Kosuke Nakai,[a,]* Masato Adachi,[a]

[a]Kyoto University, Department of Mechanical Engineering and Science, Kyoto, Japan
*Corresponding author: nakai.koske.56s@st.kyoto-u.ac.jp

The development of flexible substrates has been one of the active research fields in recent years. In particular, stretchable wires, which connect these devices and are employed internally, have emerged as critical components. Previous studies have proposed to use conductive elastomers [1] and wavy-structured wiring to achieve stretchability [2]. However, these technologies still have limitations: conductive elastomers have lower conductivity than metal wiring, and wave-structured wiring tends to crack at stress concentrations. As an alternative solution, which focuses on the healing of wires instead of the material itself for longer life cycle, a self-healing wiring system has been developed, as shown in Figure 1 [3]. In this system, the wires are covered with a solution of dispersed metallic nanoparticles. When a crack occurs, an electrostatic field is generated near the cracked area by applying an AC voltage on the cracked electrode. This attracts and traps the dispersed particles due to a dielectrophoretic force, resulting in the bridge of particles that repairs the crack. The morphology of the particle bridge is affected by the amount of particles flowing into the crack under the balance between the dispersion flow generated by the AC electric field and the dielectrophoretic force. In this study, we conducted simulations to investigate the effects of a dispersing liquid’s property on the particle flow rate near the crack and the healing process.

In the simulations of the self-healing wire system, the generated electrostatic field and the induced dispersion flow near the crack were calculated using $\mathrm{COMSOL\ Multiphysics}^{TM}$ software. Due to the symmetry of the wires on either side of the crack, only the right half area is considered, with the corresponding boundary conditions applied as shown in Figure 2. When an AC voltage is applied to one electrode while grounding the opposite electrode in this system, two types of flows occur above the wires: AC electro-osmosis flow (ACEO flow) and electro-thermal fluid flow (ACET flow) [4]. To account for these flows, calculations were performed using the boundary conditions: $v = U_{slip}$ is applied on the electrode surface for the electro-osmotic velocity, and $f = \langle f_{ET} \rangle$ was considered as the volume force driving the electro-thermal fluid flow in the Navier-Stokes equations. From the calculation results, the combined field of drag forces due to the flows and the dielectrophoretic force was obtained under the parameter variations of the dispersing liquid and the applied voltage. The particle flow rate was subsequently calculated from the velocity of the dispersion flowing into the crack area, under the assumption of a constant particle number density. The frequency of the applied voltage is varied from 100 Hz-to 1 MHz at 30 Vp-p. The calculation results are shown in Figure 3. The left figure illustrates the particle flow rate under each condition, while the right one shows the fluid flow at the conductivities of $1.0 \times 10^{-3} \sim 1.0 \times 10^{-6} [S/m]$. The results indicate that a higher particle flow rate is associated with higher conductivity of the dispersion and lower frequency of the applied voltage. As the conductivity becomes smaller, less Joule heat is generated, thus reducing ACET flow, which is induced by the temperature gradient. Moreover, as the frequency decreases, both the ACEO and ACET flow increase [4]. However, if the frequency becomes too low, electrolysis of the dispersion liquid occurs. In addition, the direction of the dispersion flow reverses at high frequencies, although the flow rate becomes smaller, as shown in Figure 3.

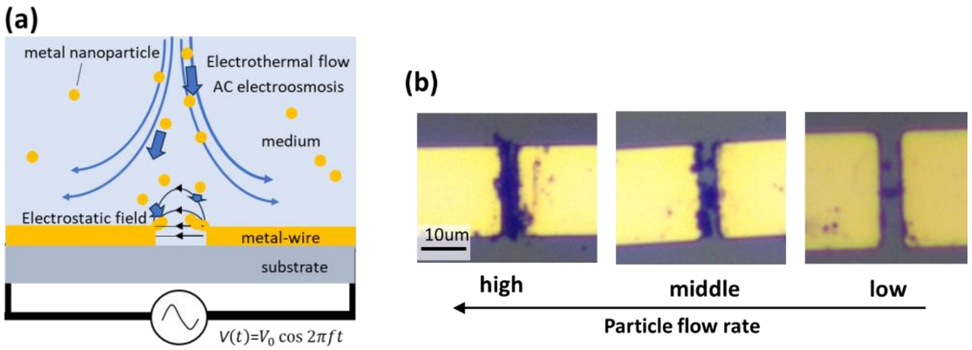

Figure 1. (a) Schematic of the self-healing wire system. When an AC voltage is applied to the electrode at the site of the crack, a dispersion flow is generated, which transports the particles, and particles are trapped at the crack due to dielectrophoretic force. (b) The morphology of the trapped particle bridge varies depending on the particle flow rate.

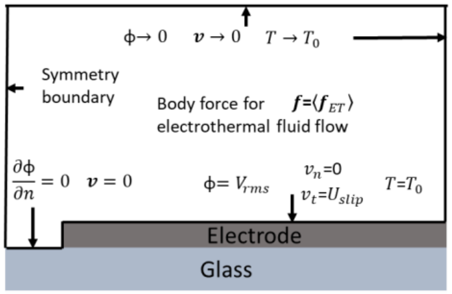

Figure 2. Boundary conditions in simulations.

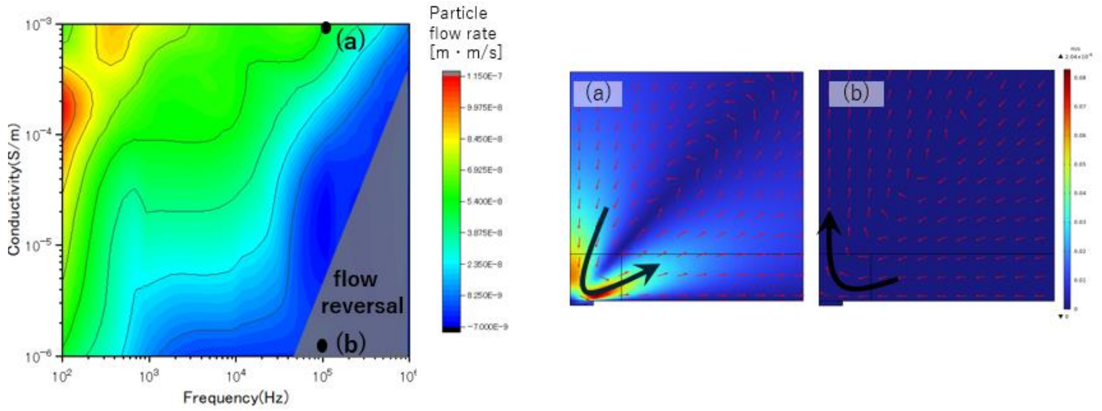

Figure 3. Particle flow rates when the conductivity and the frequency are varied (left side). (a), (b) The fluid flows for (a) $f = 1\times 10^5$[Hz] and $\sigma = 1\times 10^{-3}$[S/m], and $(b) f = 1\times 10^5$[Hz] and $\sigma = 1\times 10^{-6}$[S/m], respectively.

References

[1]T. Sekitani, H. Nakaijima, H. Maeda, T. Someya, *Nat. Mater.* **2009**, 8, 494-499.

[2]D. S. Gray, J. Tien, C. S. Chen, *Adv. Mater*. **2004**, 16, 393-397.

[3]T. Koshi, E.Iwase, *Jpn. J. Appl. Phys.* 2015, 54(no.6S1), 06FP03(6pages).

[4]A. Castgellanos, A. Ramos, A. González, N. G. Green, H. Morgan, *J. Phys. D Appl. Phys.* **2003**, 36, 2584-2597.

Study of particles dispersion change over time for aqueous ceramics slurries

Kenta Kitaumra,[a, b] * Takamasa Mori[a, b]

[a]Department of Chemical Science and Technology, Hosei University, Tokyo, Japan
[b]Hosei University Research Institute for Slurry Engineering, Tokyo, Japan
*Corresponding author: kenta.kitamura.13a@gmail.com

In the wet forming process of ceramics, a slurry is made by mixing raw powders and additives such as dispersants and binders in a solvent. It is known that the product properties depend on the particle dispersion state in the slurry. For this reason, polyelectrolytes are generally added as a dispersing agent in aqueous slurries to control the particle dispersion state. However, it is known empirically that the dispersion state of particles changes over time, and there is a concern that slurries with the same composition may have different product characteristics. In this study, we attempted to elucidate the influence of additive conditions on the change in particle dispersion state over time and the causes of this change.

Alumina powder with MgO contained as a sintering aid (Average particle size 0.44 µm) was used. And , distilled water as a dispersant, ammonium polycarboxylate (Serna D-305, Chukyo Yushi, PCA) as a dispersing agent, polyvinyl alcohol (PVA) as a binder, and amide wax (Nopco 267-A, Sannopco) as an antifoaming agent. The composition of the slurry was determined by setting the particle concentration at 35 vol%, and the amounts of PCA, PVA, and foaming agent added to the slurry were 2.4 - 8.0 mg g^{-1} Al_2O_3, 0.0 and 3.0 mg g^{-1} Al_2O_3, and 0.0 - 3.0 mg g^{-1} Al_2O_3, respectively. The slurry was prepared by dispersing the samples other than PVA in a ball mill for one hour, storing the slurry with stirring, and mixing in PVA at an arbitrary time.

In the general theory of colloid science, the polymer adsorption directly affects the particle dispersion in a slurry. Thus, the PCA adsorption was measured. The slurry was centrifuged at 20150 g for 1 h. The concentration of unadsorbed PCA was measured using a total organic carbon meter (TOC-V, Shimadzu Corporation, Japan). The PCA adsorption amount was calculated using the mass balance equation. The flow curves of the slurries were measured by viscometer. The shear stress was measured changing the shear rate from 0 to 1000 s^{-1}. The temperature of slurry cell was maintained constant at 25 °C. For the sedimentation test, the prepared slurry was placed in a 20 mm diameter sedimentation tube to a height of 150 mm and allowed to settle. The packing fraction of sediment was calculated using the mass balance equation:

$$\Phi_\infty = \frac{h_0}{h_\infty}\phi \qquad (1)$$

where Φ_∞ is final volume fraction of sediment, h_∞ final height of sediment, ϕ is initial volume fraction of slurry, h_0 is initial height of slurry.

Figures. 1 show the packing fraction of sediment of the slurry immediately after ball milling and after 3 days of ball milling. Figures. 1 (a) shows that the packing fraction of sediment of the slurry without PVA was close to that of the slurry immediately after ball milling and after 3 days. In Figures. 1 (b), there is no significant difference in the filling ratio immediately after ball milling the slurry with PVA in the range of PCA dosage 3.6-8.0 mg g^{-1} Al_2O_3. On the other hand, after 3 days, the PCA addition of 6.0 mg g^{-1} Al_2O_3 resulted in a higher packing fraction of sediment. These results indicate that when multiple additives are added, the filling characteristics of the slurry change depending on the timing of the addition.

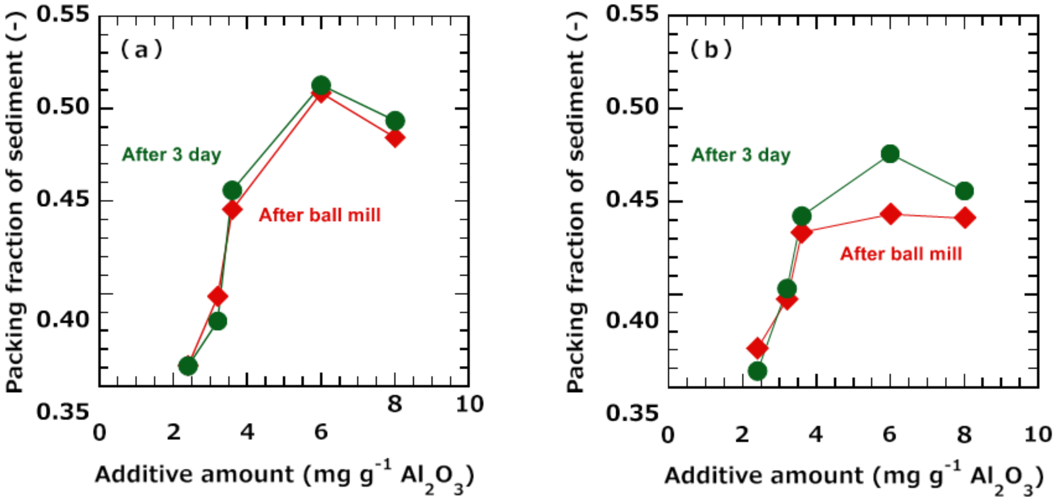

Figures 1. The packing fraction of sediment for each time from ball mill tosettling test as a function of the dditive amoun of PCA; (a) Without PVA, (b) With PVA.

Nomenclature

Φ_∞	Final volume fraction of sediment (–)	ϕ	Initial volume fraction of slurry [–]
h_∞	Final height of sediment (m)	h_0	Initial height of slurry [m]

References

[5][1] L.-C. Guo, Y. Zhang, N. Uchida, K. Uematsu, *J. Am. Ceram. Soc.* **1998**, 81(3), 549–556.
[6][2] X. Li, H. Zhong, J. Zhang, Y. Duan, H. Bai, J. Li, D. Jiang, *Int. J. Appl. Ceram. Technol.* **2020**, 17, 239-247.

Surface Treatments with Linear Alkyl Silane Coupling Agents and Their Effect on Rheological Properties

Taeko Semba,[a,]* Kazuyoshi Yamada,[b] Toshiki Matsuoka,[c] Tsutomu Takahashi[c]

[a] Niigata University of Health and Welfare, Niigata, Japan
[b] University of Hyogo, Himeji, Japan
[c] Nagaoka University of Technology, Nagaoka, Japan
*Corresponding author: taeko-semba@nuhw.ac.jp

Surface treatment was applied to the surface of inorganic particles to improve and stabilize their dispersion characteristics. However, surface treatment can significantly change the rheological properties of particle-dispersion pastes [1]. The key mechanisms are interactions between the surface- treated particles, and between the particles and the dispersant [2], however these are not yet clear. In this study, silane coupling agents with alkyl groups with different carbon numbers were used for the surface treatment of silica. A paste of silica particles dispersed in resin is prepared, and their rheological properties were evaluated.

Silica particles (Seahostar KE-S100, Nippon Shokubai Co., Ltd) were used as inorganic particles. Four silane coupling agents (SCA) with linear alkyl groups (n-propyltrimethoxysilane (C3), hexyltriethoxysilane (C6), octyltriethoxysilane (C8), and decyltriethoxysilane (C10)) were selected as the surface treatment agents [3]. The silica particles were treated using dry mixing method. The surface compositions of the surface-treated silica particles ware analyzed by a Fourier transform infrared spectrophotometer (FT/IR-4200, JASCO Corporation) and an organic carbon-sulfur analyzer (EMIA- 920, Horiba, Ltd.). The surface-treated silica particles were mixed with epoxy resin (EXA-835LV, DIC Corporation) at a volume fraction of 45% and dispersed using a planetary centrifugal mixer (THINKYMIXER, AR-100, THINKY Corporation). The pastes were evaluated using a rheometer (MCR-702, Anton Paar).

A quantitative method for the surface treatment of inorganic particles is described. The carbon mass of each surface-treated silica sample was obtained from organic carbon measurement. The carbon mass per mole is determined from the amount of carbon remaining when the alkoxy groups of the SCA wear completely hydrolyzed. Thus, the number of SCA molecules bound to silica is determined. In contrast, KE-S100 has a specific surface area of 2.9 m^2/g, and the amount required monomolecular coverage of this silica surface was theoretically calculated to be 0.037 mmol/g. The SCA coverage ratio was determined as the ratio of the number of moles of bound SCA to the number of moles of SCA required for monomolecular coverage. When the coverage ratio exceeds 1, the SCA forms a higher-order structure on the silica surface, whereas below 1, it is thought of as monolayer covered state [4].

Table 1. SCA coverage on silica particles.

SCA with linear alkyl groups	C3	C6	C8C10
Carbon mass per 1g silica[mg]	0.81	0.85	1.431.78
SCA moles of bound to silica [mmol/g]	0.022	0.012	0.0150.015
Coverage ratio	0.61	0.32	0.400.40

Figure 1 shows the FT-IR spectra. Evaluation was performed using the diffuse reflection method. The disappearance of the peak attributed to the isolated silanol groups at approximately 3747 cm^{-1} was confirmed. SCA was bounded to the silica and surface treated.

Figure 2 shows the results of the stress-ramp test. The pastes with higher carbon number in the linear alkyl group exhibited greater stress. Yields were observed at C8 and C10. The increased stress values suggested the formation of three-dimensional structures in the paste [5]. A longer carbon number is thought to facilitate the entanglement of the alkyl groups of the surface-treatment agent on the particle surface with the molecules of the epoxy resin, resulting in easier structural formation. By quantifying the amount of bound SCA, the effect of the length of the linear alkyl group on the rheology became more apparent.

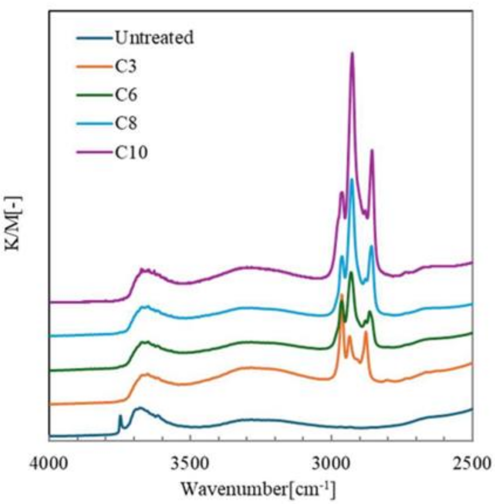

Figure 1. The FT-IR spectra of surface treated silica particles.

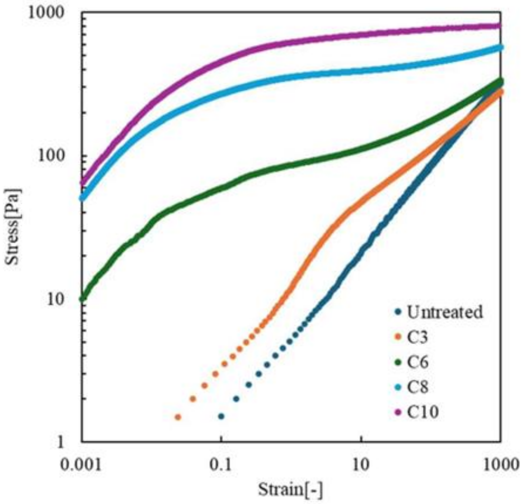

Figure 2. The results of the stress ramp test of pastes.

References

[1] Y. Sato et al., *J. Soc. Rheol. Jpn*. **2021**, 49, 251.

[2] H. Nakamura et al., *J. Soc. Powder Technol. Japan*, **2019**, 56, 438.

[3] Y. Nakamura et al., *J. Adhesion Soc. Jpn.*, **2015**, 51, 42.

[4] T. Nakamura et al., *J. Adhesion Soc. Jpn*., **2020**, 56, 472.

[5] D. J. Klingenberg, C. F. Zukoski IV, *Langmuir*. **1990**, 6, 15-24.

Design of interparticle photo-cross-linkable Pickering emulsions for DLP printing of porous silica components

Shogo Tsutaki,[a] Yoshihiko Yamanoi,[a] Junichi Tatami,[b] Motoyuki Iijima[b,]*

[a]College of Engineering Science, Yokohama National University, Yokohama, Japan
[b]Faculty of Environment and Information Science, Yokohama National University, Yokohama, Japan
*Corresponding author: iijima@ynu.ac.jp

Digital light processing (DLP) printing of porous ceramics using photocurable Pickering emulsions has attracted wide attention due to the flexibility in shaping tailor-made structures. However, the typical photocurable Pickering emulsions contain a large quantity of photocurable monomers to ensure the mechanical strength of printed bodies. This requires long and slow debinding/sintering processes to prevent collapsing of DLP-printed bodies induced by thermal decomposition of photocurable monomers [1]. To realize rapid dewaxing and sintering of 3D printed porous ceramics, herein, we designed a new series of photocurable Pickering emulsion having reduced amounts of monomers. Our proposed system comprises from silica particles whose surface was modified by PEI-mPEG (polyethyleneimine (PEI) partially grafted with polyethylene glycol (PEG) chain), diacrylate monomers (12 wt % to particles), photo radical initiator, photo absorber, polymerization inhibitor, a mixture of dimethyl sulfoxide (DMSO) and water (as continuous phase), and isopropyl myristate (as dispersed phase) [2].

To prepare the interparticle photo-cross-linkable Pickering emulsion, firstly we prepared the stable continuous suspension. Briefly, silica particles were added to DMSO aqueous solvent in which polymer dispersant, photo radical initiator, photo absorber, and polymerization inhibitor were pre-dissolved. After ball-milling for 24 hours, diacrylate monomer was added. Then, IPM was added to continuous phase suspension, followed by vigorous mixing using thin-film swill mixer to obtain interparticle photo-cross-linkable Pickering emulsion. In order to elucidate the proper polymer dispersant structure and their additive content, the apparent viscosity of continuous suspension comprised from different polymer dispersant structure and their additive content were measured using a rheometer. The designed Pickering emulsion was applied to DLP printing to fabricate 3D structured porous silica components. The DLP-printed body was dried at 80°C followed by debinding and sintering at the heating rate of 10°C/min.

Figure 1 shows the effect of additive content of polymer dispersant on the apparent viscosity of continuous phase suspension. When the grafting ratio of PEG chain to PEI was 0 and 40 mol%, the apparent viscosity did not decrease effectively even though the additive content has increased. On the other hand, an effective reduction in the apparent viscosity was measured when the grafting ratio of PEG chain was 20 mol% and the additive content has reached 0.9 mg/m^2. We suspect that the affinity between the continuous phase solvent and the particle surface was appropriate to have stable particle dispersion when the PEG chain grafting ratio was 20 mol%. Figure 2 shows the appearance and inner structure of DLP-printed body using the designed photocurable Pickering emulsion. The results for the sintered body of the corresponding printed parts are also presented. By tuning the content of photo absorber and polymerization inhibitor, a component with fine complex outer structure was successfully printed. Further, SEM observation revealed the presence of porous structure derived from IPM dispersed phase. Owing to the reduced amounts of monomers used in the photocurable Pickering emulsion, the DLP-printed body was rapidly sinterable (10°C/min) without occurring structural collapsing.

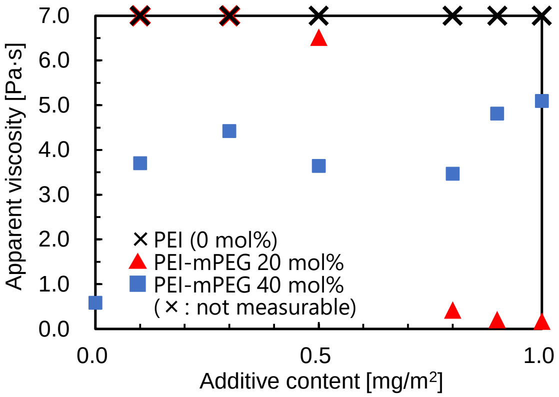

Figure 1. Effect of PEI-mPEG content on the apparent viscosity of the continuous phase suspension.

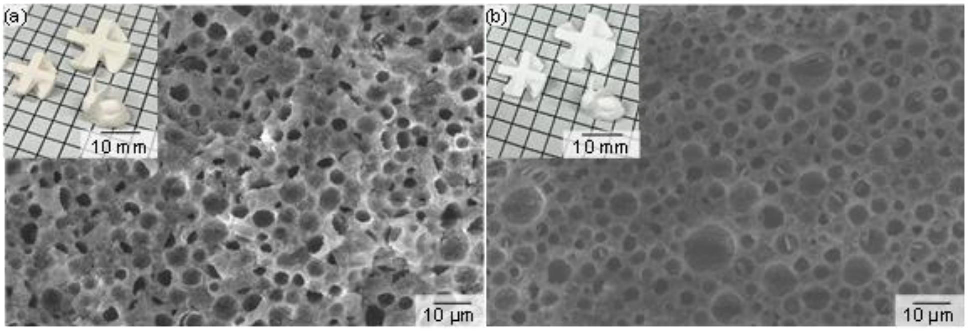

Figure 2. The appearance and inner structure of the DLP-printed (a) dried body and (b) partially sintered body.

References

[1] N. Kleger, et al., *Sci. Rep*., **2021**, 11, 22316.

[2] S. Tsutaki, et al., *Adv. Powder Technol.*, **2024**, 35(5), 104410.

Evaluation of particle concentration dependent stability of silica slurries by 1H pulsed NMR

Yuki Imai,[a] Junichi Tatami,[b] Motoyuki Iijima[b,]*

[a] Graduate School of Environment and Information Sciences, Yokohama National University, Yokohama, Japan
[b] Faculty of Environment and Information Sciences, Yokohama National University, Yokohama, Japan
*Corresponding author: iijima@ynu.ac.jp

The control of dispersion stability of concentrated slurries in the production of ceramics is an essential issue to improve the reliability of final products. Notably, since the wet processing involves drying, which particle concentration gradually increases upon processing, understanding the particle concentration dependent stability of the slurries is essential. Up to date, many discussions on particle interactions and particle dispersion states in concentrated slurries were conducted based on flow characterizations using a rheometer. Since these discussions are based on macroscopic characterizations, methods to understand the particle dispersion behaviour from the microscopic point of view, by an in-situ process, should play an important role to understand the nature of particle stability in concentrated slurries. 1H pulsed NMR technique is a method to measure the relaxation process of protons excited by radio waves. By taking advantage of the phenomenon that the relaxation rates of excited protons become faster when a proton-containing solvent molecules interact with solid surfaces, the dispersion state of fine particles in concentrated slurry should be possible to be evaluated from the perspective of the solvent molecule level by characterizing the relaxation properties of excited protons. Here, using silica slurry as a model, we aim to evaluate the dispersion state of the slurry from a microscopic viewpoint using 1H pulsed NMR and correlate with macroscopic flowing properties.

For the preparation of the silica slurries, polyethyleneimine (PEI, Mw 1800) was pre-dissolved in butylcarbitol (BC) to achieve saturated adsorption conditions. Then, silica particles (220 nm) were added to the solution (2.5-57 vol%) and further planetary mixed, ultrasonicated, and stirred for 24 hours. The flow curves and 1H relaxation curves were evaluated by a rheometer and 1H pulsed NMR, respectively.

The relationship between silica particle concentration and apparent viscosity of the slurries at a shear rate of 300 s^{-1} is shown in Fig. 1. The open and closed keys denote the slurries having flow curves with and without hysteresis characters, respectively. Compared to silica suspension without PEI, the particle concentration where the apparent viscosity increases and a hysteresis character started to appear in the flow curves were found to be lower for those treated with PEI. To examine this phenomenon, the maximum packing fraction (Φ_m) of silica particles in each slurry was estimated by fitting to the Krieger-Doughtery model [2]. Assuming that silica particles were rigid spheres, and the differences between Φ_m and random packing fraction (for spheres, 0.64) were due to the presence of PEI adsorption layer, the dispersant layer thickness on the particles were determined to be c.a. 4.5 nm. This value was similar to the average particle surface distance where the hysteresis character started to appear, which can be calculated from Woodcock model [3]. These facts suggests that interparticle network structures, that can be collapse by shearing, generates in concentrated slurries when the adsorption layer is superimposed.

The relaxation curves measured by 1H pulsed NMR for the slurry and solvent at each particle concentration are shown in Fig. 2. The relaxation time of the slurry was shorter than that of the BC, and this trend was more pronounced with increasing particle concentration. This may be due to the increase of surface area in the slurry where BC can be interacted. Furthermore, it was found that the relaxation curve measured in the slurry could be fitted to exponential decay model with two component relaxation processes ($y(t) = a_1 e^{-t/T_{2,1}} + a_2 e^{-t/T_{2,2}} + y_0$) including extremely short relaxation processes. Under the environment in which adsorption and desorption of BC on silica particles were occurring, BC molecules in the local field are likely to be collided with silica particle surface more frequently than those in the bulk environment and the relaxation progresses faster. Therefore, it is suspected that the component with short relaxation time ($T_{2,1}$) was due to the BC in the local region of the silica interparticle gaps formed in BC. Fig. 3 shows the effect of particle concentration in the slurry on the relaxation time constant $R_{sp,1}$($R_{sp} = \{(1/T_2)-(1/T_b)\}/ (1/T_b)$), which is calculated from $T_{2,1}$ and T_b (solvent relaxation time). $R_{sp,1}$, which is the component attributed to BC in the silica particle interstitial space, showed an inflection point at the particle concentration where a hysteresis character was observed in the flow curves. These results suggest that there is possible correlation between $R_{sp,1}$ value measured by 1H pulse NMR and macroscopic flow properties.

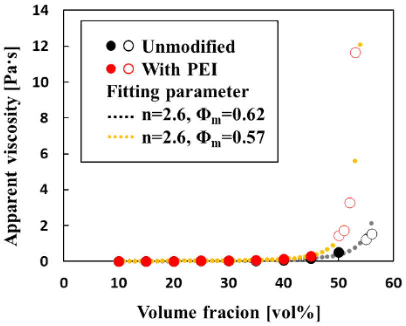

Figure 1. Relationship between particle concentration and apparent viscosity at the shear rate of 300 s^{-1} and curves fitted to the Krieger-Doughtery model.

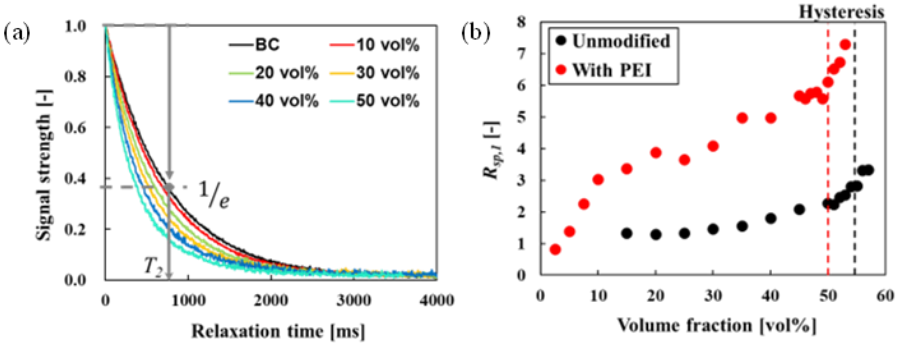

Figure 2. (a) 1H relaxation curves of BC and silica/BC slurries and (b) effect of particle volume fraction on $R_{sp,1}$ (dashed line presents the volume fraction where a hysteresis character appeared in the flow curve measurement)

References

[1] F. Ito et al., *Powder Technol.* **2023**, 423, 118473.

[2] I. M. Krieger et al., *Trans. Soc. Rheol.* **1959**, 3, 137.

[3] L.V. Woodcock, *Lecture Note in Phys.* **1987**, 277, 113.

Design of interparticle photo-cross-linkable slurries treated with silane alkoxides for DLP-3D printing of transparent silica components

Sayaka Yamada,[a] Junichi Tatami,[b] Motoyuki Iijima[b,]*

[a]College of Engineering Science, Yokohama National University, Yokohama, Japan
[b]Faculty of Environment and Information Science, Yokohama National University, Yokohama, Japan
*Corresponding author: iijima@ynu.ac.jp

Hybrid manufacturing (a combination of photocuring/vat photopolymerization and green machining) of complex-shaped ceramic components using photocurable slurries have attracted wide attention toward productive processing. Conventional photocurable slurries contain large amounts of binders to ensure the strength of the photocured body. Therefore, a long processing time is required in the debinding process to prevent structural collapse induced by decomposed gas generation. Reducing the binder content can be a possible approach to shorten the debinding process, however, the lack of binders results in a structural collapse during the machining of the photocured bodies. To solve this dilemma, we have recently designed an interparticle photo-cross-linkable slurry in which very small amounts of acrylates can directly crosslink the particles modified by a reactive polymer dispersant to ensure mechanical properties of photocured bodies [1]. The addition of silane alkoxide functionalized with acryloyl groups (A-Si) was further found to be effective to realize the production of complex-shaped silica glass components via the combination of photocuring and green machining followed by a rapid debinding. This was due to the generation of siloxane bridges among the particles during debinding [2]. On the other hand, the addition of A-Si resulted in poor stability against time, which was a challenge for applying the designed slurries to vat photopolymerization. Here, we design a new interparticle photo-cross-linkable slurry using A-Si as reactive binder and having improved stability against time for rapid 3D structuring of transparent silica glass components through digital light processing (DLP) printing.

In brief, SiO_2 particles, reactive polymer dispersant, photo-radical initiator, phenoxyethanol and butylcarbitol was mixed by ball milling. Then, A-Si (5-20 vol% to solvent) was added as a cross-linking agent to form photocurable slurry. The viscosity curves of the slurry were measured by a rheometer immediately after preparation and after one week storage to assess the dispersion stability. The microstructures of photocured silica bodies after rapid debinding and sintering process (20ºC/min.) were evaluated by FE-SEM. Complex shaped silica compacts were further fabricated from the designed slurry using a DLP-based 3D printer.

Fig. 1 shows the viscosity curves of the slurries with different amounts of A-Si just after preparation and after one week storing. No hysteresis character was observed in the viscosity curves for all A-Si addition conditions, indicating that the amount of A-Si did not affect the flowability in the newly designed slurry. Further, the viscosity curve did not change significantly after one week storing. Fig. 2 shows the changes in the appearance and microstructures of the photocured bodies in the course of rapid debinding and sintering. While the slurry containing 10 vol% A-Si showed a uniform distribution of cross-links among the particles before and after heat treatment, an excess addition of A-Si (20 vol%) found to induce segregation of the cross-links. By selecting an optimum content of A-Si, a complex-shaped transparent silica components were successfully processed through DLP printing and rapid firing, owing to improved stability of the slurries against time (Fig. 3). We believe that the proposed photocurable slurry should play an important role for hybrid manufacturing of transparent silica glass components.

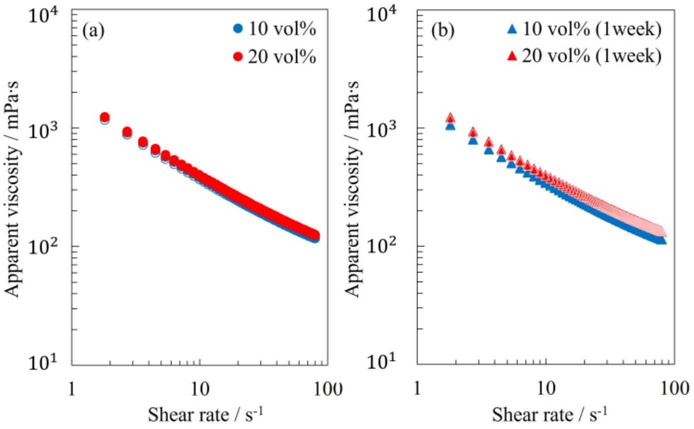

Figure 1. Flow curves of photocurable slurries (a) after preparation and (b) after 1 week storage

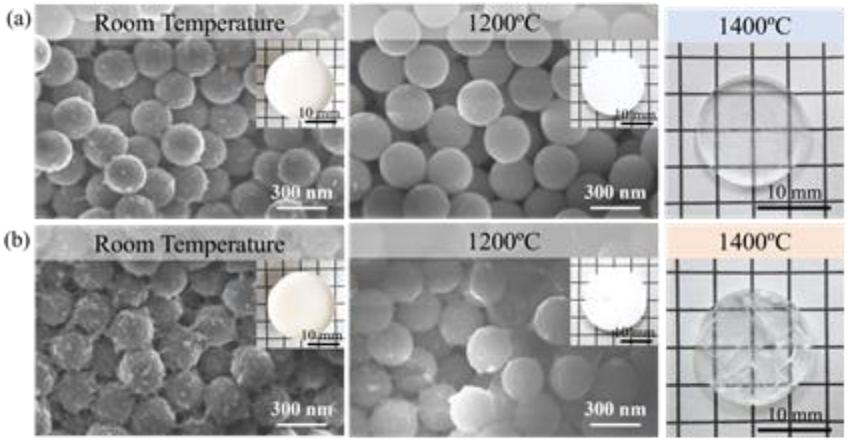

Figure 2. Appearance and microstructures of photocured bodies before and after heat treating at 1200℃ and 1400℃ (A-Si content was (a) 10 vol% and (b) 20 vol%)

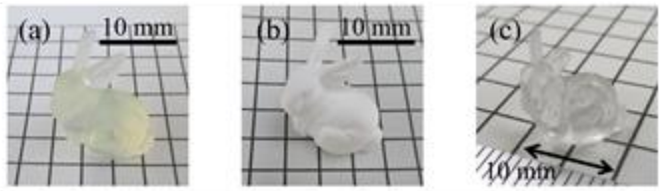

Figure 3. Appearance of silica bodies printed by DLP 3D printer ((a) photocured body and (b) dried body)

References

[1] R. Arita, M. Iijima, Y. Fujishiro, S. Morita, T. Furukawa, J. Tatami, S. Maruo, *Commun. Mater.*, **2020**, 1(1), 30.

[2] R. Sato, T. Yahagi, J. Tatami, M. Iijima, *ACS. Appl. Mater. Interfaces* **2022**, 14, 16445-16452.

MRI and NMR evaluations of pickering emulsions stabilized by cellulose nanofibers

Noriko Kanai,[a,b] Scott A. Willis,[b] Abhishek Gupta,[b] Izuru Kawamura,[c,*] William S. Price [b,*]

[a]Graduate School of Environment and Information Sciences, Yokohama National University, Yokohama, Japan
[b]Nanoscale Organisation and Dynamics Group, School of Science, Western Sydney University, Penrith, Australia
[c]Graduate School of Engineering Science, Yokohama National University, Yokohama, Japan
*Corresponding authors: kawamura-izuru-wx@ynu.ac.jp / w.price@westernsydney.edu.au

Pickering emulsions (PEs) are system stabilized by solid particles instead of molecular-based surfactants. Cellulose nanofibers (CNFs), isolated from plant-based food/agricultural waste, are renewable stabilizers/emulsifiers for oil-in-water (o/w) PEs for their potential use in food, cosmetic, and pharmaceutical industries. Characterizing instability behavior and droplet size distributions (DSDs) are essential to evaluate the quality of PEs. However, commonly used microscopy observations limited the number of droplets in the measurement area, and the laser scattering method for DSDs may include artifacts due to the droplet clusters counting as a single droplet.

Magnetic resonance imaging (MRI) can non-invasively provide deep insight into the internal microstructure and dynamics in spatially inhomogeneous samples. Nuclear magnetic resonance (NMR) diffusometry can determine DSDs based on the translational motion of molecules in a droplet for concentrated emulsions without dilution. This study used MRI and NMR techniques to evaluate instability mechanisms, relaxation/diffusion properties, and DSDs of PEs stabilized by CNFs derived from waste hop stems [1,2]. High-resolution MR images of the 'entire' PEs with 100 μm isotropic voxel resolution were obtained using a 500 MHz (11.7 T) NMR spectroscopy. Voxelwise longitudinal relaxation (T_1), transverse relaxation (T_2), and apparent diffusion coefficients (ADCs) of dodecane or olive oil-in-water PEs stabilized by CNFs were investigated over one month. The DSDs of PEs were estimated from NMR diffusion measurements in conjunction with cogent mathematical modelling.

The three-dimensional MRI provided excellent visualization showing flocculated/coalesced droplets packed near the surface of the emulsions one month after emulsification (**Figure 1**). The T_1 maps were reflected the microstructural changes such as flocculation and coalescence, suggesting the useful marker of relaxation and instability. The NMR diffusion data of the dispersed oil (various *n*-alkanes) were well-described by the Gaussian phase distribution (GPD) approximation with a monomodal log-normal distribution.

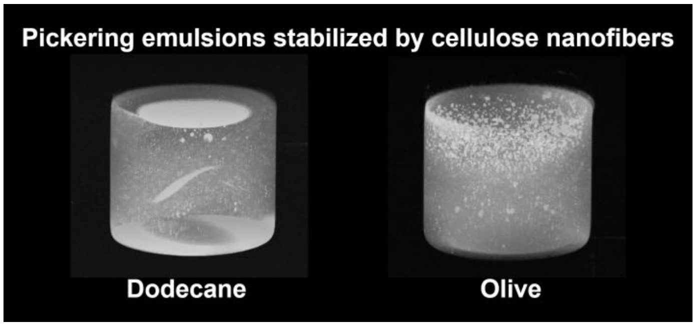

Figure 1. 3D volume rendering of dodecane and olive oil Pickering emulsions stabilized by 1% CNF after one month storage.

References

[1] N. Kanai et al. *Langmuir.* **2023**, 39, 3905.

[2] N. Kanai et al. *J. Mol. Liq.* **2024**, 403, 124793.

The influence of intruder geometry on the segregation phenomenon in a vibrated particle bed

Shu-San Hsiau,[a]* Li-Tsung Sheng,[b] Jia-Jung Wu[a]

[a] Department of Mechanical Engineering, National Central University, Jhongli, Taiwan, R.O.C.
[b] Department of Mechanical and Electro-Mechanical Engineering, National Ilan University, Yilan, Taiwan, R.O.C.
*Corresponding author: sshsiau@cc.ncu.edu.tw

This study investigates the phenomenon of segregation when square intruders with identical mass, volume, density, and different geometry are set into a quasi-two-dimensional vibrated bed. To capture the experimental images of the particles and intruders for analysis purposes, a high-speed camera along with Particle Tracking Velocimetry (PTV) was employed for subsequent analyses. This study also explores particle transport properties such as rise time of intruder, velocity field, granular temperature, and diffusion coefficient of particles.

According to results, it was confirmed that changing the aspect ratio of the intruders significantly impacts particle segregation behaviour. Intruders with larger aspect ratios find it more difficult to rise, thereby requiring more time to reach the free surface of the bed. This phenomenon is also reflected in the rising speed of intruders. This is because intruders with a longer horizontal length create a larger space at the bottom with each round of vibration, requiring more background particles to fill in from above. Furthermore, larger aspect ratios not only affect the bottom region and the number of particles but also hinder the vertical-exchange motion of particles. These two mechanisms explain why intruders with the same volume and density exhibit different rising behaviours. Additionally, we measured the granular temperature to determine whether the introduction of different intruders affects the overall kinetic energy of the system, and found that the overall energy remains unchanged regardless of the intruder's shape. Finally, to better understand the variations introduced by different intruders, we measured the self-diffusion coefficient at the region of the bottom of the intruders. Although the internal energy received by the system is the same, the influence of the aspect ratio leads to varying degrees of fluidization of background particles at the region of the bottom of each intruder, thus causing differences in their rise times.

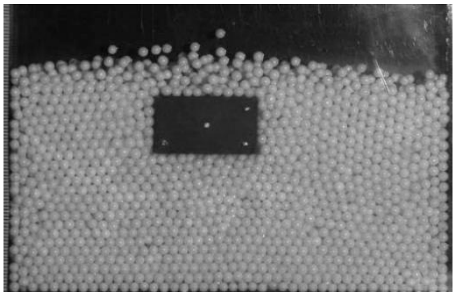

Figure 1. The image during the experiment. The white small particles are the background particles, and the black square block is the intruders. The intruder is set at the bottom of the bed, which consists of background particles. And it will rise to the free surface of the bed at the end of experiment.

Experimental study the combine the effects of density and shape on the dynamic properties and segregation mechanisms of granular material in a rotating drum

Chun-Chung Liao,* Zhe-Hao Zhang

Department of Mold and Die Engineering, National Kaohsiung University of Science and Technology, Kaohsiung, Taiwan
*Corresponding author: liao0910@nkust.edu.tw

Granular materials are found in many natural and industrial processes, ranging from avalanches and landslides to the handling of grains, powders, and other bulk materials in industries like pharmaceuticals, mining, food and agriculture [1-2]. In this study, the dynamic characteristics and segregation behaviors of binary density combined with cubic-shaped particles were investigated by mixing various granular materials in quasi-two-dimensional rotating drums. The experimental results indicate that as the rotation speed increases, the time for the granular mixture to reach a steady state is shortened, and the average velocity, average granular temperature, and dynamic repose angle increase. The results demonstrated that particle shape has a significant influence on density-induced granular segregation behavior. When the shape effect is combined with the density effect, the segregation intensity no longer increases with the density ratio. The addition of non-spherical particles not only impacts segregation behavior but also significantly affects the dynamic characteristics of granular mixtures. The cubic-shaped particles have a larger contact area, thereby increasing frictional contact and enhancing interlocking effects, which reduce particle movement. Furthermore, when the filling level decreases, the granular flow layer becomes thinner, resulting in a decrease in average velocity, average granular temperature, dynamic repose angle, and segregation index. This study provides a better understanding of non-spherical granular flow behavior in rotating drums and confirms the significant influence of the cubic shape effect within the density-induced granular segregation mechanism**.**

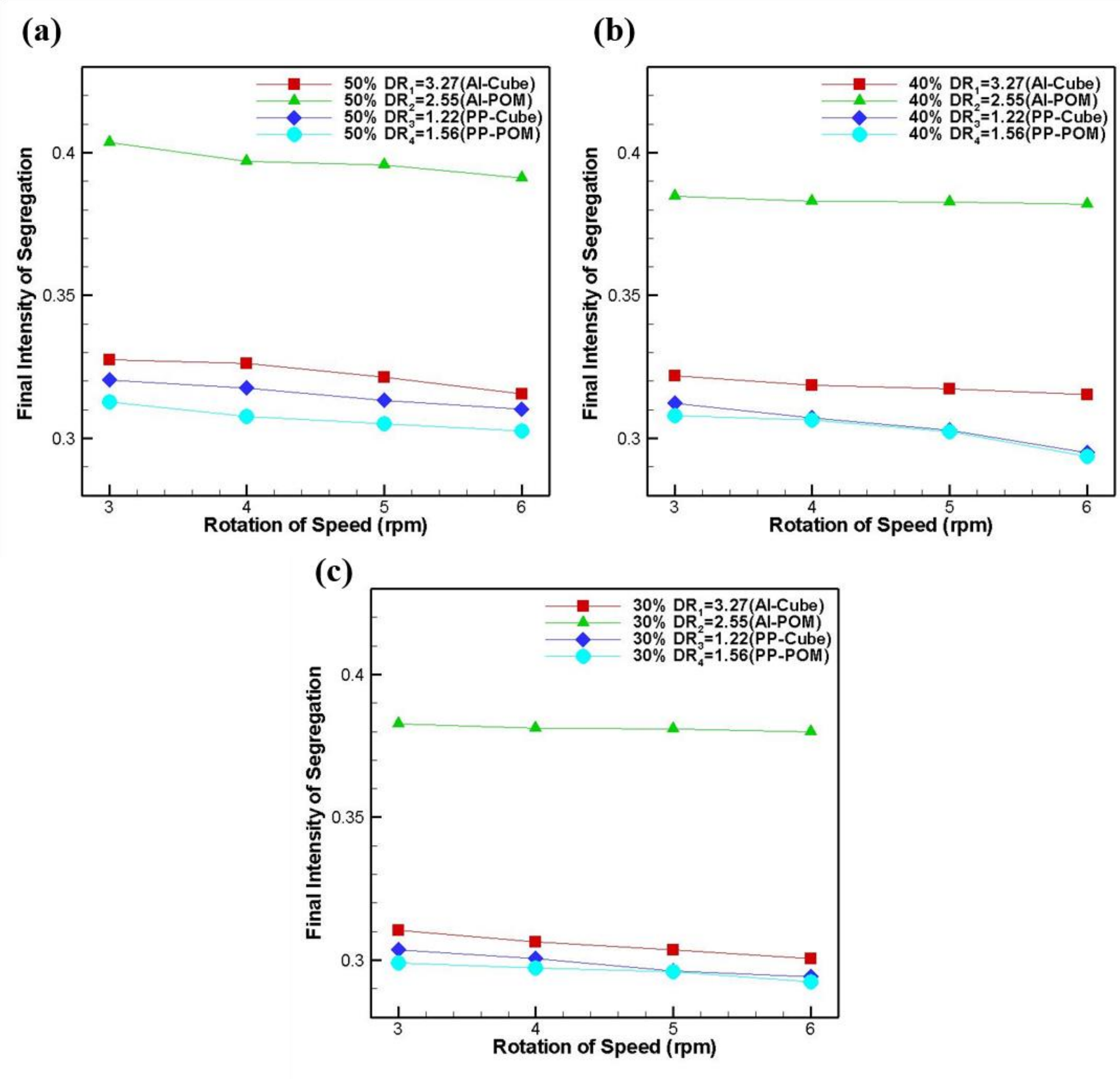

Figure 1. Final steady-state segregation intensity as a function of rotation speed, combining the effects of density and shape at filling rates of (a) 50%, (b) 40%, and (c) 30%.

References

[1] Y. C. Chung, M. L. Hunt, J. N. Huang, C. C. Liao, *Physics of Fluids* **2024**, 36, 023342.

[2] C. C. Liao, M. L. Hunt, H. L. Sun, *Physics of Fluids* **2024**, 36, 073315.

Prediction and optimization of particulate processes using physics augmented machine learning approach

Chengbo Liu,[a,b] Tingting Liu,[a] Kun Hong,[b] Xizhong Chen[a]*

[a]School of Chemistry and Chemical Engineering, Shanghai Jiao Tong University, Shanghai, PR China
[b]Faculty of Chemical Engineering, Huaiyin Institute of Technology, Huaian, China
*Corresponding author: chenxizh@sjtu.edu.cn

Particulate flow plays a critical role in a wide range of industrial processes and natural phenomena, posing significant challenges for rapid and accurate simulation. Traditional simulation techniques, particularly those using the Discrete Element Method (DEM), are notorious for their high computational demands, often balancing precision and efficiency at a cost. The advent of artificial intelligence heralds a transformative shift, sparking interest in leveraging machine learning to simulate particle flow. In this study, we explore the application of cutting-edge machine learning methods, such as Graph Neural Networks (GNNs), to learn interactions between particles and establish corresponding reduced-order models to efficiently simulate particle flow. The developed method reduces computational requirements, significantly enhances efficiency compared to DEM simulations, and maintains a high level of accuracy in predicting particle flow properties. Due to its strong generalization ability, it can handle even more complex conditions not previously encountered with ease. Machine learning excels not only in solving the forward problems of particle flow but also in reverse engineering, surpassing traditional physical simulations and empirical models. For instance, with the aid of machine learning, optimization of geometric structures in fluid-solid coupling conditions can be achieved more easily and efficiently. Meanwhile the inversion evaluations of complex particulate fluid behavior properties is something that previous methods could not achieve. Further exploration of machine learning methods in applications such as liquid-solid stirred tanks and gas-solid fluidized beds demonstrates the versatility and potential of machine learning-based alternative models in capturing the complex dynamics of particle systems.

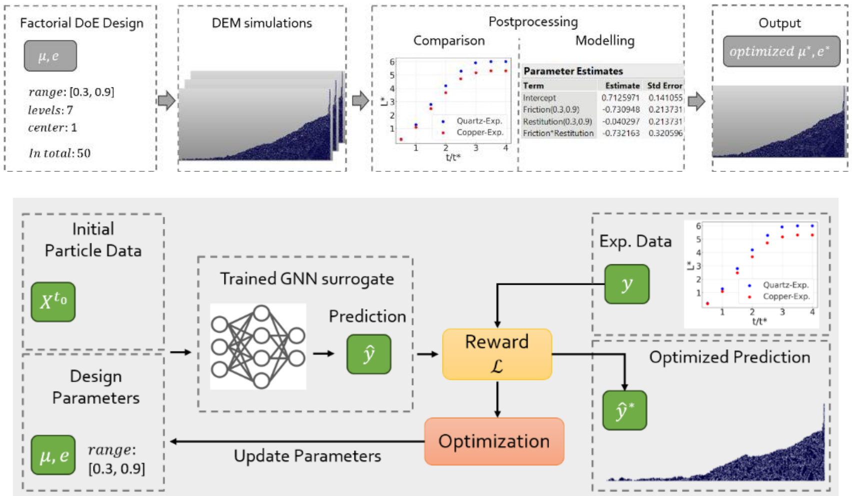

Figure 1. Schematic of DoE for optimizing and the machine learning inverse design procedure for simulations.

References

[1] Y. Jiang, E. Byrne, J. Glassey, X. Chen, *Chem. Eng. Res. Des.* **2023**, 196, 40-51.

[2] Yongjin Choi, Krishna Kumar, *Comput. Geotech.* **2024**, 171, 106374.

[3] A. Sanchez-Gonzalez, J. Godwin, T. Pfaff, R. Ying, J. Leskovec, P. W. Battaglia. *arXiv:2002.09405v2*.

PTFE fibrillation by dry powder mixing and its application to electrode fabrication for all-solid-state battery

Hideya Nakamura,* Shota Miyake, Motoshi Iwao, Shuji Ohsaki, Satoru Watano

Osaka Metropolitan University, Sakai, Osaka, Japan
*Corresponding author: hideyanakamura@omu.ac.jp

All-solid-state lithium-ion batteries (ASSLIBs) are highly promising candidates of the advanced secondary batteries for electric vehicles. One of the key challenges regarding ASSLIBs is development of their manufacturing process. Currently, a mainstream process expected for manufacturing ASSLIBs is a wet process [1]. However, the wet process suffers from disadvantages such as high energy consumption and high environmental load. To address this issue, a dry process, in which ASSLIBs can be produced without solvent, has attracted much attention [2]. In the dry process, the raw powders are mixed with binder particles by a dry mixing process, and the electrode sheet is then fabricated from the powder mixture. A key to the fabrication of electrode sheets in the dry process is the use of binder particles. Polytetrafluoroethylene (PTFE) is a typical binder particle. Morphology of the PTFE can be changed from particulate form to fiber by applying external force and/or heat. Once the PTFE fibers are dispersed in the powder mixture, the PTFE can bind the particles together like a spider's web, resulting in a freestanding electrode sheet even without solvent [3]. This PTFE fibrillation mainly proceeds in the dry mixing before sheet fabrication, however, its mechanism is unclear. In particular, key factors to control the PTFE fibrillation are not identified. It is also unclear that which dry mixing process, and which specific features, are suitable for the PTFE fibrillation. Furthermore, the relationship between the PTFE fibrillation state and the properties of the final electrode sheet also remains unclear. The objective of this study is to identify the key factors for PTFE fibrillation in dry powder mixing and to clarify the specific features of an optimal mixing process for PTFE fibrillation. Furthermore, electrode sheets and all-solid-state half-cells were fabricated using the powder mixtures with different PTFE fibrillation states. The correlation between the PTFE fibrillation states and physico-electrochemical properties of the electrode sheets was investigated.

We investigated three types of dry mixing equipment, which were horizontal high-shear mixer (HSM), planetary ball mill (PBM), and twin-screw hot kneader (TSHK). Generally, in these processes, the dominant external forces exerting the powder are as follows: shear force in the HSM; shear and compressive forces in the PBM; shear and compressive forces with heat in the TSHK. By comparing these different mixing processes, effects of the type of external forces and processing temperature on the PTFE fibrillation were investigated. A cathode active material (LiNi0.5Co0.2Mn0.3O2), sulfide solid electrolyte, and PTFE were used as experimental materials.

Fig. 1 shows appearance of the powder mixture prepared by each equipment and the fine particle fraction (mass fraction of particles less than 250 μm) in the powder mixture. Appearance of the powder mixture prepared by the HSM was almost same as the original raw powder (Fig. 1b), and large amount of the fine particle fraction still remained (more than 70%) (Fig. 1e). In contrast, the powder mixture prepared by PBM and TSHK exhibited large agglomerates over 0.5 cm and fine particle fraction decreased significantly from the original powder. Among these, the TSHK showed the smallest fine particle fraction. These results indicate that the TSHK is the most effective in fibrillating the PTFE. In other words, it was found that mixing equipment capable of applying shear, compressive force, and heat to the powder is suitable for the fibrillation of PTFE.

Influence of the PTFE fibrillation states on physico-electrochemical properties of the electrode sheets was investigated. The electrode sheets were prepared using a powder mixture prepared by the TSHK under various processing temperatures. Fig. 2 shows the tensile strength of sheet as a function of the number density of PTFE fibers in the prepared mixture. Processing temperature was also displayed at each plot. The tensile strength increased with an increase in the number density of PTFE fibers, indicating that a sheet with high strength can be fabricated by using a powder mixture in which PTFE fibrillation proceeds more. Fig. 3 shows the 2C discharge capacity of the half-cell prepared from each mixture as a function of the number density of PTFE fibers in the mixture. The results exhibited that the maximum electrochemical performance was achieved at 30 mm^{-2}, indicating that the relationship between the number density of PTFE fibres and battery performance is not a simple linear relationship, and there is an optimum fibrillation state which maximizes battery performance. Detailed discussion on this non-linear relationship between the PTFE fibrillation states and battery performance will be presented in the symposium.

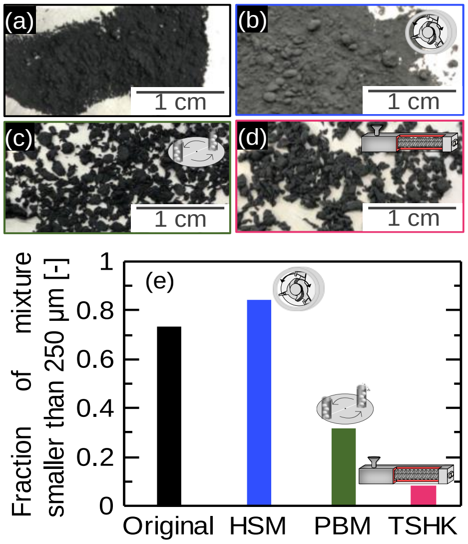

Fig. 1. Appearance of (a) original powder and mixtures prepared by (b) HSM, (c) PBM and (d) TSHK. (e) Mass fraction of mixtures smaller than 250 μm prepared by each mixing equipment.

In summary, it was found that a dry mixing process which can apply shear force, compressive force, and heat to the powder was suitable for the PTFE fibrillation. It was also determined that temperature during mixing is a key factor in the PTFE fibrillation. The relationship between the PTFE fibrillation state and the physico-electrochemical properties of the electrode sheet was then investigated. The sheet with higher tensile strength was fabricated from the powder mixture in which PTFE fibrillation proceeded more. It was also found that there is an optimum fibrillation state which maximizes the ASSLIB performance.

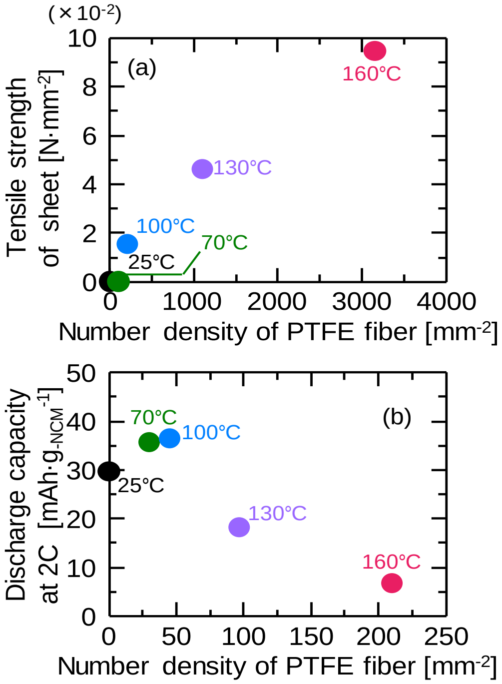

Fig. 2. Correlation between (a) tensile strength of sheet, (b) discharge capacity at 2C and the number density of PTFE fiber.

References

[1] M. Batzer et al., *Batter. Supercaps.* **2022**, 5, e20220032.

[2] Y. Li et al., *Mater. Today.* **2022**, 55, 92–109.

[3] F. Hippauf et al, *Energy Stor. Mater*. **2019**, 21, 390-398.

The rapid prediction of pulverized coal MILD combustion field: CFD + ensemble learning

Hang Shu,[a,b] Wenqi Zhong,[a,b,]* Xuejiao Liu,[a,b] Xi Chen[a,b]

[a] School of Energy and Environment, Southeast University, Nanjing, PR. China.
[b] State Key Laboratory of Low-carbon Smart Coal-fired Power Generation and Ultra-clean Emission, Southeast University, Nanjing, PR. China.
*Corresponding author: wqzhong@seu.edu.cn

Moderate or Intense Low-Oxygen Dilution (MILD) combustion, marked by uniform heat flow, high stability, and low pollution emissions, is a highly promising new efficient clean combustion technology. However, the comprehensive understanding of the complicated combustion laws and mechanisms remains a significant challenge. The combination of CFD and machine learning presents an efficient strategy to expedite research and development, while also owning potential in industrial applications. This study aims to develop a "CFD + machine learning" rapid prediction method for the pulverized coal MILD combustion field. Regarding this method, the combustion field data of a 0.58MW pulverized coal MILD boiler under the varying operating parameters were gathered by the high-precision CFD simulations. Then the efficient Proper Orthogonal Decomposition (POD) algorithm was developed to process these massive original CFD data to the low-dimensional feature projection coefficients, and lastly the regression model between the operating parameters and the feature coefficients was established by the ensemble learning algorithm. In this study, the CFD data construction strategy, and the optimal regression model for the strong turbulent MILD combustion were carefully evaluated and discussed. The results suggest that the most effective combination of model construction parameters for temperature prediction involves half of the combustion field data and a K value of 5 in the K-fold cross-validation procedure, in conjunction with the CATBoost model. As for CO prediction, the optimal approach is to employ the CATBoost algorithm with a quarter of the data and an optimal K value of 10. The final models for both parameters exhibit outstanding performance, with determination coefficients (R^2) surpassing 0.997 for each model, relative absolute errors (RAE) below 0.03, and root relative squared errors (RRSE) under 0.06. Compared to the conventional CFD simulation, the "CFD+Machine learning" can achieve the acceleration of five-order-of-magnitude, demonstrating its significant potential for industrial applications.

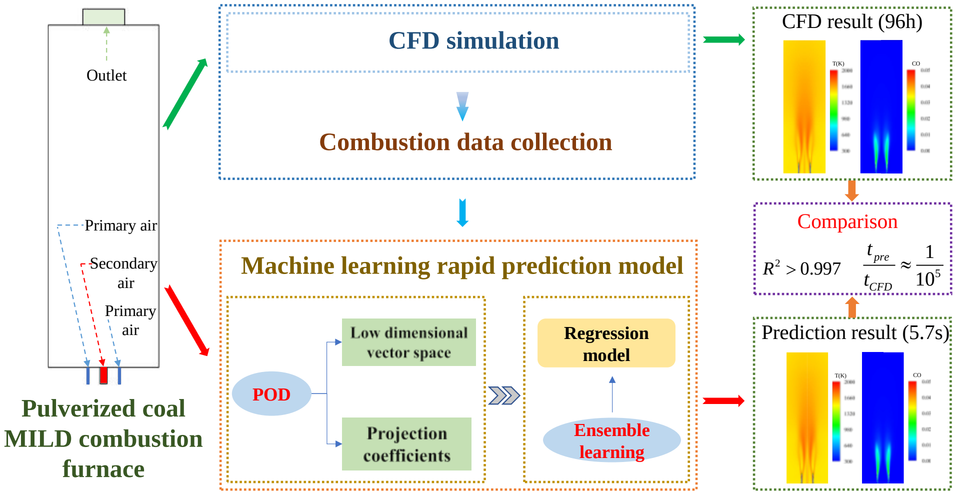

Figure 1. Schematic of CFD + machine ensemble learning

Towards the influence of fluid convection on filtered drag in fluidized gas-particle flows

Ju Jiang,[a] Xiao Chen,[a] Qiang Zhou[b,*]

[a] State Key Laboratory of Multiphase Flow in Power Engineering, Xi'an Jiaotong University, Xi'an, China
[b] State Key Laboratory of Multiphase Flow in Power Engineering, Xi'an Jiaotong University, Xi'an, China
*Corresponding author: zhou.590@mail.xjtu.edu.cn

Most of the mesoscale drag modelling processes for gas-solid two-phase flow are based on periodic systems. However, in such systems, the flow field is statistically homogeneous and isotropic, whereas the real fluidized bed presents a heterogeneous and anisotropic distribution. The influence of convective transport on mesoscale drag has been seldom considered in periodic systems as the convection term of momentum equations only varies within a limited range. However, in real fluidized beds, the fluid convection may play a significant role and have a notable impact on the drag force.

This study conducts a series of numerical simulations for fluidized beds with different sudden expansion sections using a highly resolved two fluid model (TFM). Flow field data containing acceleration zones are then collected. Based on a priori analysis, it is observed that convection terms in acceleration zones are much larger in magnitude with those in periodic systems, and the convection transport has a notable impact on the heterogeneous drag. In general, the presence of convection facilitates the formation of mesoscale structures, further reducing the filtered drag force compared to the uniform state. The heterogeneous characteristics intensifies as convective transport of the fluid increases, while the influence of convection will gradually vanish as the local solid volume fraction increases. Previous researches [1] have reported a linear relationship between the filtered gas-phase pressure gradient and the filtered drag in periodic systems. With a force balance analysis of the momentum equations, it is found that this linear relationship still holds in the acceleration zones where significant convection occurs. Both priori and posteriori analyses of the filtered drag in the acceleration zones indicate that predictive capability of drag models constructed solely with solid volume fraction and gas-solid slip velocity can reduce significantly in the acceleration zones, suggesting that additional markers may need to be introduced to consider the impact of convection. While the gas-phase pressure gradient implicitly contains the effects of local convection, models incorporating this physical quantity also demonstrate good accuracy for the flow behaviour in the sudden expansion fluidized beds.

References

[1] Jiang M, Zhang Y, Yu YX, Zhou Q, *Powder Technology* **2021**, 394, 1050-1076.

On the cemented carbide powder forming process based on the discrete element simulation

Yuanqiang Tan,[a]* Chao Liu,[b] Jie Li,[a] Wenqing Zheng,[b]

[a] Institute of Manufacturing Engineering, Huaqiao University, Xiamen, China
[b] Xiamen Tungsten Co., Ltd, Xiamen, China
*Corresponding author: tanyq@hqu.edu.cn

The Discrete Element Method (DEM) simulation was employed to study the effects of powder properties, process parameters, and mold structure on the powder spreading and pressuring process of WC-Co powder. By calibrating parameters such as the physical properties, contact, and breakage of WC-Co powder, a DEM model of crushable WC-Co powder particles was established. The powder spreading process was divided into two stages: bulk materials dropping and powder filling. The bulk density and particle segregation were used as quality evaluation indicators of the powder spreading in the mold cavity. The influence of powder properties, cavity geometry, and spreading process on the powder bed quality was analyzed. For the pressing process, the compaction density uniformity index and the relative density at the blade tip were defined as quality evaluation indicators. The influence of different process parameters on the pressing and forming process was investigated. The results showed that When the powder filling ratio in the shoe is 46.7%, the filling effect and quality within mold cavity was the best, with a relative bulk density of powder up to 57.87%, and the compacting quality was optimal. When the punch stroke ratio decreased from 5:2 to 5:4, the uniformity of the compacting density distribution was significantly improved.

On the electrostatics of granules and granular flows

Yanlin Zhao,[a] Jun Yao [a]*

[a] International Joint Laboratory on Clean Energy Science and Technology, China University of Petroleum-Beijing,
Beijing 102249, People's Republic of China
*Corresponding author: yaojun@cup.edu.cn

In past decades, the electrostatics of granules and granular flows has obtained more and more attention due to many industrial problems and the associated development of new technologies[1-3]. Granule-wall collision causes electrification, where charge transfer can be characterized by work function, electron transfer, ion transfer, and material transfer. Electrification is affected by many factors [4-6]and increases with granule processing, and the charge amount can reach a saturated state where electrification no longer increases, which has been confirmed by single granule and granule conveying systems. In addition, the presence of electrostatic charges has profound influences in relevant areas, including chemistry, chemical engineering, energy, pharmaceuticals, and so on. The measurement technology of electrostatics [1,4,5,8-10] used in granule conveying systems has been improved with the continuous progress of industry. Furthermore, electrostatics of granules and granular flows will be developed into a more accurate area together with other subjects as an interdisciplinary problem to be concerned [9,11]. In addition, in the pneumatic conveying system, granule-wall and granule-granule collision or friction can cause material transfer due to material breakage[3,11]. The working mechanism of the material transfer due to collision or friction has never been fully understood. Such problems will be solved gradually in the future.

References

[1] J. Yao, Y. Zhang, C.H. Wang, S. Matsusaka, H. Masuda, *Ind. Eng. Chem. Res*. **2004**, 43,7181–7199.

[2] J. Yao, Y. Zhang, C.H. Wang, Y.C. Liang, *AIChE J.* **2006**,52, 3775–3793.

[3] J. Yao, C.H. Wang, *Chem. Eng. Sci*. **2006**, 61,3858–3874.

[4] S. Matsusaka, H. Fukuda, Y. Sakura, H. Masuda, M. Ghadiri, *Chem. Eng. Sci*. **2008**, 63, 1353–1360.

[5] C. He, X.T. Bi, J.R. Grace, *Particuology* **2015**,21, 20–31.

[6] J. Yao, J.Z. Li, Y.L. Zhao, *Adv. Powder Technol*. **2020**,31 1543–1555.

[7] J. Yao, S. Cong, Y.L. Zhao, C.H. Wang, Z.L. Ji, *Adv. Powder Technol*. **2017**, 28, 2003–2014

[8] P. Bunchatheeravate, J. Curtis, Y. Fujii, S. Matsusaka, *AIChE J*. **2013**,59,2308–2316.

[9] S. Matsusaka, H. Maruyama, T. Matsuyama, M. Ghadiri, *Chem. Eng. Sci*. **2010**, 65, 5781–5807.

[10] S. Matsusaka, Control of particle tribocharging, *KONA Powder Part. J*. **2011**,29.

[11] Y. L. Zhao, M. Liu, C.H. Wang, S. Matsusaka, J. Yao, *Adv. Powder Technol*. **2023**, 34, 103895

Granular mixing and segregation: continuum modelling and processes optimization

L.Y.M. Yang,[a]* X.Y. Liu,[b] Q.J. Zheng[2] and A.B. Yu[2]

[a] Ganjiang Innovation Academy, Chinese Academy of Sciences, Ganzhou, China
[b] ARC Research Hub for Computational Particle Technology, Monash University, Clayton, Australia
*Corresponding author: lymyang@gia.cas.cn

The feeding hopper is frequently used in grinding cement clinker to ensure a stable and homogeneous feed of particles. However, due to the large variances in size, the clinker particles can segregate significantly and cause undesirable fluctuations in the subsequent grinding process. This work investigates the flow and segregation of particles in mill-feeding hoppers using the experimental PIV technique and the FEM simulation. The results demonstrate the different zones of fine and coarse particles, corresponding to the flow patterns of the hopper, are affected by the material parameters. Particularly, it is found that the geometric design of the hopper also has a great influence on the flow and segregation. An optimized hopper design using FEM is shown to effectively alleviate the segregation problem in the mill feeding hopper.

References

[1] K. Van der Vaart, P. Gajjar, G. Epely-Chauvin, N. Andreini, J. Gray, C. Ancey, *Phys. Rev. Lett*. **2015**, 238001.

[2] P. Gajjar, J. Gray, *J. Fluid Mech* **2014**, 757, 297-329.

[3] P. Jop, Y.l. Forterre, O. Pouliquen, *Nature* **2006**, 441, 727-730.

[4] Y. Fan, P. B. Umbanhowar, J. M. Ottino, R. M. Lueptow, *Phys. Rev. Lett.* **2015**, 115(8), 088001.

[5] C. P. Schlick, Y. Fan, P. B. Umbanhowar, J. M. Ottino, R. M. Lueptow, *J. Fluid Mech* **2015**. 765, 632-652.

Inorganic-organic hybrid porous ceramics using non-firing solidification and functionalizing starch template method

Kento Ishii,[a] Tetsuo Uchikoshi,[b] Masayoshi Fuji[a,]*

[a] Nagoya Institute of Technology, Tajimi, Japan
[b] National Institute for Materials Science, Tsukuba, Japan
*Corresponding author: fuji@nitech.ac.jp

A porous material is a material that has many pores intentionally and actively introduced into its structure. By selectively introducing pores with specific sizes and shapes into structures, porous materials can be used as lightweight materials, heat insulators, adsorbents, filters, gas sensors, catalyst support, and electrochemical device electrodes [1]. A sacrificial template method is the most simple and common to fabricate porous ceramics [2]. First, resin powder is added as a pore-forming agent to ceramic powder. Then, after the mixed powder is molded and fired, the porous ceramic can be obtained in which the traces of the pore-forming agent are reflected in the pore shape. The finally formed porous structure is determined by the shape of the pore-forming agent, and the distribution of the pore-forming agent in the process from mixing to molding. When applying a porous ceramic body as a filter or an adsorbent, it is desired that all the pores are continuous without being isolated.

We have developed the fabrication process of porous materials with continuous pores by using starch as a pore-forming agent and utilizing gelatinization and retrogradation phenomena [3–5]. Since starch is burned out at a firing temperature of about 500°C without forming residues, it has been widely applied to the fabrication of porous ceramics as a pore-forming agent [6]. Starch is a natural polymeric compound particle extracted from plants and is composed of α-glucose-based polysaccharides such as amylose and amylopectin [7,8]. **Fig. 1** shows a schematic illustration of the starch gelatinization and retrogradation process. The gelatinization phenomenon is that when starch is heated with water, the starch granules absorb water and swell, and a highly viscous sol is formed. Additionally, the gelatinized starch paste forms a gel when the heating is stopped. The retrogradation phenomenon is that the water inside the swollen starch exudes to the outside and separates so that the starch eventually returns to a crystalline state close to its original state. Applying a shearing force to the gelatinized starch can form a three-dimensional network structure in which the starch particles are connected to each other. Furthermore, exudate water clusters form inside the microstructures while the starch network is coarsened by controlling the amount of water separation from starch during the retrogradation process. This allows control of the pore size in the network. The wet starch body after gelatinization and retrogradation is processed by the freeze-drying method to produce a dried body without significantly damaging its microstructure.

The sintering process for burnout of the pore-foaming agent and solidifying the ceramics consumes the most energy in ceramics manufacturing. The ceramics non-firing solidification process is one of the most promising methods for drastically reducing energy consumption in ceramics production [9]. This method enables composites of ceramics with organic and metallic materials. This study reports the effects of various gelatinization and aging conditions on forming starch network structures and applying starch network structures to pore former templates for porous ceramics. We report the results of applying silica-based ceramics-residualized starch hybrid porous materials as bioreactors, utilizing the non-firing ceramics solidification and starch morphology control methods.

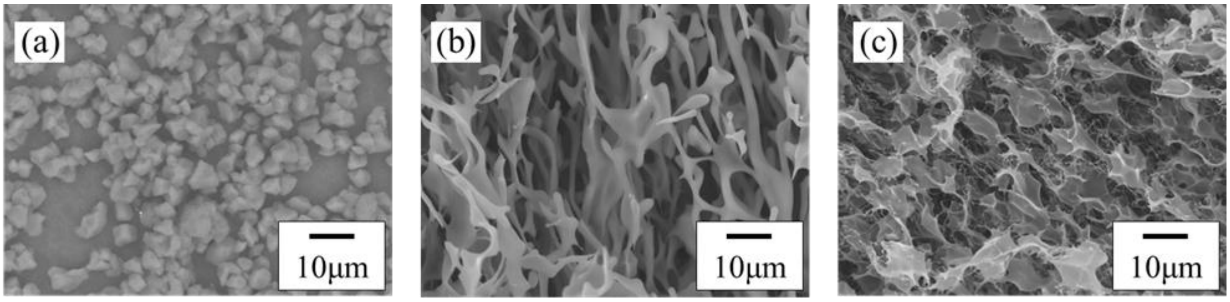

Figure 1. Morphology of (a)as-received rice starch powder, (b) the gelatinized starch network, and (c) the retrograded starch network.

References

[1] K. Ishizaki, S. Komarneni, M. Nanko, Porous Materials: Process technology and applicatoins, Springer Science+Bussiness Media, **1998**.

[2] T. Ohji, M. Fukushima, *Int. Mater. Rev*. **2012**, 57, 115–131.

[3] K. Ishii, M. Shimizu, H. Sameshima, S. Samitsu, T. Ishigaki, T. Uchikoshi, *Ceram. Int.*, **2020**, 46, 13047–13053.

[4] M. Uematsu, K. Ishii, S. Samitsu, E. Bin Ismail, I. Ichinose, N. Ohashi, D. Berthebaud, J.F. Halet, T. Ishigaki, T. Uchikoshi, *Adv. Powder Technol.*, **2022**, 33, 103626.

[5] M. Uematsu, K. Ishii, H. Sameshima, M. Ito, T. K. N. Nguyen, T. Ishigaki, T. Uchikoshi, *Mater. Lett*., **2022**, 326, 132939.

[6] T. T. Dele-Afolabi, M. A. A. Hanim, M. Norkhairunnisa, S. Sobri, R. Calin, *Ceram. Int.*, **2017**, 43, 1633–1649.

[7] M. Schirmer, M. Jekle, T. Becker, *Starch*, **2015**, 67, 30–41.

[8] E. Gregorová, W. Pabst, I. Bohačenko, *J. Eur. Ceram. Soc.*, **2006**, 26, 1301–1309.

[9] Y. Nakashima, H. Razavi-Khosroshahi, C. Takai, M. Fuji, *Adv. Powder Technol.*, **2018**, 29, 1900-1903.

Effects of dispersants and floc formation on yielding phenomena for concentrated silica slurry

Tomonori Fukasawa,* Tatsuhiko Murakami, Mayuna Oka, Yuki Nishimura,
Toru Ishigami, Kunihiro Fukui

Graduate School of Advanced Science and Engineering, Hiroshima University, Higashi-Hiroshima, Japan
*Corresponding author: fukasawa@hiroshima-u.ac.jp

The effects of electrolyte species, electrolyte concentration, and pH of the dispersant on the yield stress of concentrated slurries have been reported, focusing on the particle interaction forces [1]. That is, at the isoelectric point (i.e., the pH at which the net surface charge of the particle is zero) of the particle, the inter-particle attraction was maximum and the yield stress was maximum. In our preliminary experiments, however, the pH at which the yield stress was maximum did not always correspond to the isoelectric point obtained by zeta potential measurement of the particles.

We consider that the yielding phenomena of concentrated slurry is affected by the behaviour of formation and deformation of floc deform depending on changes in electrolyte species, electrolyte concentration, and pH of the dispersant. In this study, we performed sedimentation experiments to evaluate the aggregate structure (size, fractal dimension, and mechanical strength) under various dispersant conditions to investigate their effect on yielding phenomena. Silica particles (average diameter: 0.6 μm) were used as model particles. Five electrolytes (LiCl, NaCl, KCl, CsCl, and GdmCl (guanidium chloride)) were used, focusing on the hydration radii of the cations. The silica concentration of the slurry was adjusted to 35 vol%. In this study, the vane method was employed to evaluate yield stress [2].

Figure 1 shows the effects of electrolyte species, electrolyte concentration, and pH on yield stress. The yield stress increased with increasing electrolyte concentration and pH. Focusing on the cation species, the yield stress was higher for smaller hydration ion radius regardless of pH.

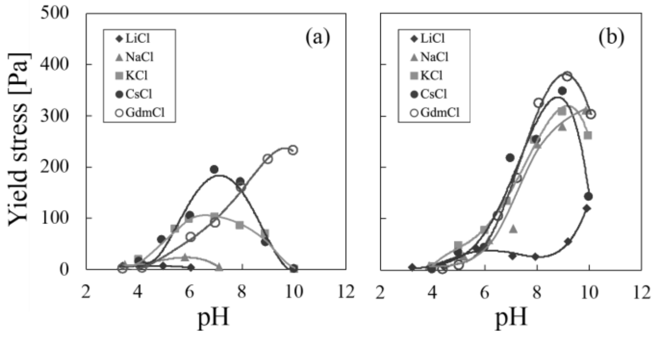

Figure 1. Yield stress of silica slurry as a function of pH for various electrolyte dispersant (a) 0.4 M and (b) 1.0 M.

References

[1] G. V. Frank, *Colloid Interface Sci.* **2002**, 249, 44-51.

[2] P. V. Liddell, *J. Nonnewton. Fluid Mech.* **1996**, 63, 234-261.

Effects of particle charge variation on the cleaning performance of an electrodynamic dust shield under ion irradiation

Shunsuke Mitsunaga,[a,] * Masato Adachi[a]

[a]Kyoto University, Department of Mechanical Engineering and Science, Kyoto, Japan
*Corresponding author: mitsunaga.shunsuke.86a@st.kyoto-u.ac.jp

Granular materials are ubiquitous in nature and industrial sites. These include small particles that can easily become airborne and accumulate on devices and equipment, such as solar panels, leading to their malfunction and performance degradation. While accumulated particles can be easily removed in areas where people have daily access, this problem is severe in harsh environments like desert regions and space environments, such as the Moon and Mars, where numerous technical constraints exist. Thus, the development of particle removal technology that can adapt to these harsh environmental conditions is indispensable [1,2]. Existing techniques include the use of brushes or fluids such as water and air, but many challenges remain for their long-term usage in harsh environments (e.g. water is a precious resource in desert, and it cannot be used in vacuum). As alternatives, electrostatic-based technologies have been developed, with particular attention drawn to the electrodynamic dust shield (EDS). In this system, the traveling wave of an electrostatic field is generated on cleaning target surfaces, enabling the removal of deposited particles with the resulting electrostatic force [3]. The system does not require fluid material or even mechanically moving parts, allowing for small design, lightweight construction, and automation. Numerous researches have been reported on the system, such as investigations of electric parameters on the cleaning performance [4]. In this study, we aimed to investigate the effects of the particle charge on the cleaning efficiency of EDS by introducing a particle charging mechanism.

Fig. 1 depicts the experimental setup. The EDS system consisted of a power supply for generating an electrostatic traveling wave and a substrate on which spiral electrodes made of Indium Tin Oxide (ITO) were printed. The cleaning substrate was insulated and protected by an adhesive insulator and thin glass sheet. When high voltages of phase-shifted rectangular waves were applied to the ITO electrodes, the generated electrostatic traveling wave moved particles radially from the center of the substrate. As shown in Fig. 1, the micro-ionizer (KEYENCE, SJ-M030) was installed on the upper part of the cleaning substrate as the particle charging mechanism. This device can charge or discharge the target object by irradiating ions generated from corona discharge. The ionizer had an internal sensor to detect an external electrostatic field and adjust the ion generation rate to achieve the desired ion balance in the surrounding area. If the EDS is used for space applications, a discharge mechanism which can work in a vacuum is required. In this study, we investigated the fundamental effects of the ionizer on the variation of the particle charges and the removal efficiency of the lunar regolith simulant particles, which mimic the real lunar soils. During the experiment, particles were deposited onto the EDS substrate, followed by ion irradiation, and subsequent removal experiments were carried out. The removal efficiency was assessed based on the weight ratio of particles before and after removal. Additionally, parameters such as the surface potential and charge quantity of the particles upon ion irradiation were evaluated.

Fig. 2 shows the removal of deposited particles using the EDS simultaneously with and without the ionizer. In the case without the ionizer, particles were irradiated with ions for a brief period of 10 seconds immediately prior to activating the EDS. As shown in Fig. 2, the EDS with the ionizer removed particles approximately four times faster than when used without the ionizer. Thus, the combination of the EDS with charging mechanism of particles realizes the better cleaning performance. Fig. 3 displays the surface potential of the particles when they were irradiated with ions for 60 seconds under different humidity conditions, after which the ionizer was turned off. Although the surface potentials increased in a low humidity environment of RH 10 % due to the ionizer, the particles did not charge significantly in a wet condition (RH 40%). This result indicates that environmental conditions influence particle charging. While the charges escape from the particles soon after the irradiation in wet condition, given charges stayed on the particles in dry condition. If the EDS is used in wet condition, it would be better to combine the charging simultaneously, realizing the better removal efficiency of particles.

Figure 1. Experimental setup of the EDS combining a particle charging mechanism

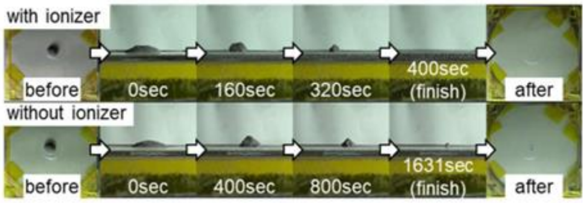

Figure 2. Removal of particles over time when the EDS was activated with and without ionizer

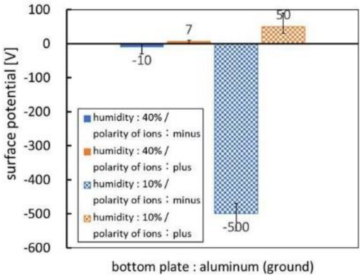

Figure 3. Measured surface potentials of the particle layer

References

[1] J. R. Gaier, *Nasa. TM.* **2005**, 213610, 1–74.

[2] H. Kawamoto, B. Guo, *J. Electrost.* **2018**, 91, 28–33.

[3] S. Masuda, K. Fujibayashi, K. Ishida, H. Inaba, *Electr. Eng. Jpn.* **1972**, 92, 43–52.

[4] H. Kawamoto, K. Seki, N. Kuromiya, *J. Phys. Appl. Phys.* 2006, 39, 1249–1256.

Internal structure evaluation during tablet compaction using multiparticle finite element method

Natsuki Miura,[a] Yusuke Imayoshi,[a] Shuji Ohsaki, [a,]* Hideya Nakamura,[a] Satoru Watano[a]

[a]Osaka Metropolitan University, Osaka, Japan
*Corresponding author: shuji.ohsaki@omu.ac.jp

Introduction

Powder compaction is one of the most widely used production process. The factors affecting the tablet performance include not only the compression pressure and speed, but also the powder properties, such as adhesion force and plastic deformability. The tableting mechanism has not yet been completely clarified despite the enormous studies for powder compaction. The compression conditions are, therefore, mainly determined by empirical knowledge. To solve this problem, quantitatively understanding the internal structure of tablet should be needed. Recently, a multi-particle finite element method (MPFEM) was used as the novel computational method to simulate the powder compression process. This study focused on rotary tableting machines among powder compaction methods. In rotary tableting machines, the punch reportedly tilted during compression and unloading due to roll rotation [1]. In this study, the effect of the punch inclination on the powder compaction and unloading processes was investigated through MPFEM analysis.

Methods

As a preliminary experiment, tablets produced by a rotary tableting machine (Virgo, 0506SS, Kikusui Seisakusho Ltd., Japan) were analyzed using X-ray computed tomography (CT) (Nano3DX, RIGAKU Corp.). Lactose (Pharmatose®80M) was used as a model particle. In this experiment, the compression pressure and rotation speed were set at 20 kN and 19 rpm, respectively. The SRC type tablets with a mass of 200 mg and a diameter of 8.0 mm were obtained. In the numerical analysis, the discrete element method (DEM) was used to perform the filling process. Microcrystalline cellulose (PH-101, Asahi Kasei Corp.), which was spherical particles with a median diameter of 430 μm, was used as a model particle. The filling method was slit filling. The sliding speed was 50 mm/s. The millstone diameter was 2.5 mm and the millstone height was 7 mm. The surface energy was 0.002219 J/m^3. The coefficient of rolling friction was 0.01195. All the DEM simulations were performed using EDEM 2021 (Altair Engineering Inc.). Moreover, the obtained the positional information of particle from the DEM was used to calculate the compaction process using MPFEM. The MPFEM analysis was enlarged to 1000 times scale to reduce the computational cost. The compression distance was set to 1300 mm. Compression time and unloading time were set to 0.01 s and 0.005 s, respectively. The mesh size was 80.0 mm, and the shape was tetrahedral. The shape of the upper punch was an R tablet. In the MPFEM simulation, the different inclination angles of upper punch were set as 0 and 1° to investigate the effect of the punch inclinations on the tableting process. All the MPFEM simulations were performed using Ansys 2022 R1 (Cyber Net Inc.)

Results and discussion

Fig. 1 shows the X-ray CT images of tablets compressed by a rotary tableting machine. The gaps, where cracks occurred, were indicated in gray. The cracks were distributed semi-circularly from the tablet edges.

One of the factors contributing to segregation at crack sites was presumed as stress segregation due to the punch inclination during the rotary tableting process. Numerical analysis was thus conducted to investigate the effect of the punch inclination on the powder compression process. Fig. 2 shows the temporal change in equivalent stress during compression/unloading in MPFEM analysis under the different punch inclination angles. Here, equivalent stress is the absolute value of stress acting per element. The average value of equivalent stress (Fig. 2(a)) reached its maximum at maximum compression, regardless of the punch inclination angles. On the other hand, the maximum value of equivalent stress (Fig. 2(b)) varied significantly during the unloading process depending on the punch inclination angle. To evaluate the stress distribution during the unloading process, the stress distributions from a side view at 0.0125 seconds are shown in Fig. 3. Regardless of the inclination of the punch, the stress values on the sides were almost the same. However, it was found that the punch inclination caused segregation in the powder mass, as shown in Fig. 3(b). Furthermore, the stress distribution on the top surface during maximum compression and unloading was evaluated (Fig. 4). At maximum compression (0.01 s), stress was highest at the center of the upper surface under all conditions under all conditions (Fig. 4. (a)(c)). This indicated that the stress during compression depended on contact with the punch, and the punch inclination had little impact on the stress distribution. On the other hand, the stress increased at the edges during the unloading process for the both punch inclination angles (Fig. 4. (b)(d)). This was due to the contact of elastic recovered particles with the die. However, the stress at inclination angle of 0° (Fig. 4. (b)) was spread across the entire edge during unloading, whereas the stress at inclination angle of 1° (Fig. 4. (d)) was concentrated on one side of the edge. This would be because the punch inclination contributed to bias in the elastic recovery of the particles during unloading. Thus, it was suggested that the punch inclination should be one of the factors contributing to tableting failure.

Fig. 1. X-ray CT images of the tablet.

(a) Average equivalent stress

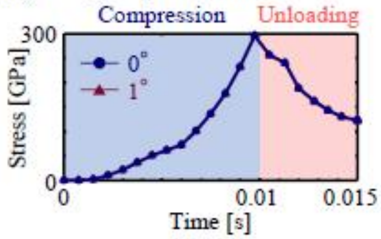

(b) Maximum equivalent stress

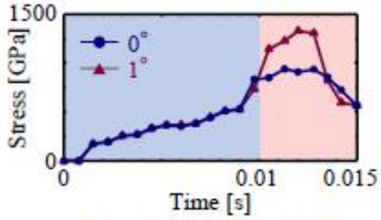

Fig. 2. The temporal variation of equivalent stress.

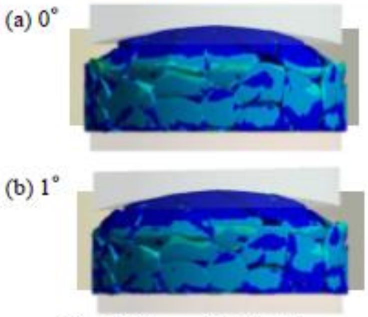

Fig. 3. Stress distribution on the side view.

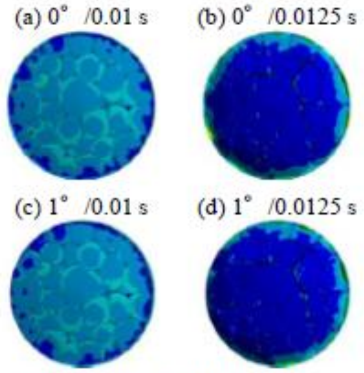

Fig. 4. Stress distribution on the upper surface.

Conclusions

In this study, a multi-particle finite element method was performed to evaluate the internal structure of tablets during tableting process. When compression and unloading were conducted with the upper punch inclination, stress segregation occurred during unloading. It was suggested that the punch inclination generated by the rotary tableting machine should be one of the factors causing tableting failure.

References

[1] M. Cespi, M. Misici-Falzi, G. Bonacucina, S. Ronchi, G. F. Palmieri, *Pharm. Technol.* **2007**, 57, 1277–1284.

Relationship between powder rheology of wet iron ore powder and its granule strength

Kensuke Kumeda[a], Hideya Nakamura[a]*, Shuji Ohsaki[a], Satoru Watano[a], Shohei Fujiwara[b], Yuji Iwami[b], Akinori Murao[b]

[a]Osaka Metropolitan University, Sakai, Japan
[b]JFE Steel Corporation, Fukuyama, Japan
*Corresponding author: hideyanakamura@omu.ac.jp

In recent years, supply of the high-grade iron ore with high Fe-content has declined rapidly, leading to an increased demand for the use of low-grade iron ores containing impurities. In order to utilize low- grade iron ores as raw materials, impurities have to be removed to increase the Fe concentration in the raw ores 1,2). An impurity removal process usually involves grinding and chemical reduction of the raw iron ore. However, such grinding and chemical reduction processes significantly change other physico- chemical properties of the raw iron ore. In particular, fine ore particles after grinding significantly reduce the gas permeability through the ore powder bed in the sintering process and the blast furnace, leading to significantly low productivity of the entire pig iron production process. To avoid such a negative impact, it is necessary to properly design the wet granulation process to agglomerate the milled fine ore particles. In particular, it is particularly important to understand the optimum water content in the wet granulation process. In previous studies3,4), we have demonstrated that an agitation torque, which correlates to a rheological property of wet powders, is effective in determining the optimal water content in the wet granulation of fine iron ore particles. However, the previous studies have only focused on typical raw ore powders, which mainly consist of $Fe2O3$, without chemical reduction treatment, therefore the agitation torque of reduced iron ore powder after chemical reduction treatment has not been investigated. Furthermore, the objective variable for the optimum water content estimated from the agitation torque profile is only the mass fraction of fine particles, while the relationship between this profile and granule strength has not been studied. In this study, the relationship between the agitation torque of wet iron ore powder and its granule strength was investigated. A hematite ($Fe2O3$) and magnetite ($Fe3O4$) powders were selected as model powders of unreduced and reduced iron ore powders, respectively. Mixtures of the hematite and magnetite powders were prepared as model powders for iron ore powders with different degrees of chemical reduction and used in the experiments. Using the mixtures with various mass fractions of hematite and magnetite (i.e., with different degrees of reduction), measurement of the agitation torque and experiments of a wet granulation by using a rotating drum mixer were conducted to study the effects of the degree of the reduction. We then investigated a correlation between the agitation torque of the ore powder rheology with degrees of reduction and the strength of the granules.

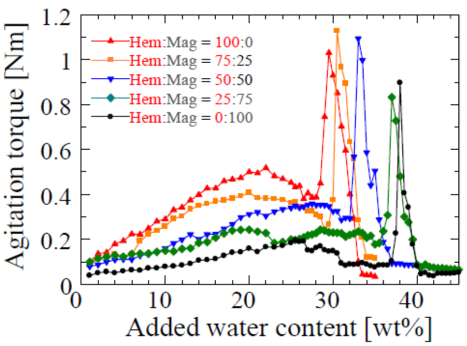

Fig. 1. Agitation torque of ore powders with various blending ratios as a function of water content.

First, the agitation torque of mixture of hematite and magnetite powders was measured to determine the effect of the blend ratio (i.e. degree of chemical reduction of raw ore powders) on the rheological properties of the wet powder Figure 1 shows the results of the agitation torque measurements. It was found that as the ratio of the magnetite increased, the increase in the torque with increasing water content became smaller. It was also found that a mixture with higher magnetite fraction showed a narrower range of water content over which high torque values exhibited. This indicates magnetite powder has lower plasticity.

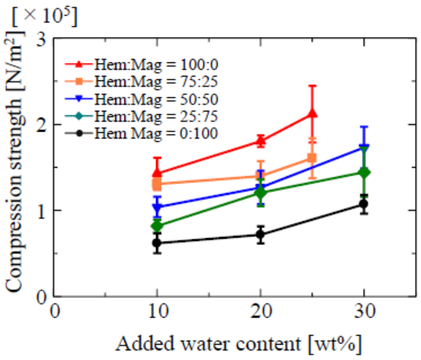

Fig. 2. Compressive fracture strength of granules as a function of added water content.

Wet granulation of hematite-magnetite powder mixture was then conducted. Effects of mass fraction of hematite and magnetite and water content on the compressive strength of the granules were investigated. Figure 2 shows the correlation between the water content and compression strength of the granules. The results showed that the granule strength increased with an increase in the water content. This is likely due to the increased tumbling time and collisions between particles during granulation in a rotating drum, resulting in consolidation. Moreover, it was found that the granule strength decreased as the magnetite ratio increased.

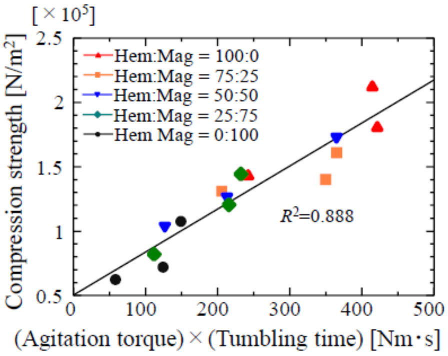

Fig. 3. The correlation between compression strength of z granules and the product of agitation torque at the net water content of granules and tumbling time.

Finally, the relationship between the agitation torque of a mixed powder and its granule strength was investigated at various hematite-magnetite blend ratios. Figure 3 shows a correlation between the agitation torque and the granule strength. A good linear correlation between the granulate strength and the product of the agitation torque and tumbling time was found regardless of the hematite-magnetite blend ratio. Here, it was considered that the agitation torque corresponds to the plasticity of wet powder, i.e. ease of the consolidation of the wet powder. As the tumbling time increased, the number of particle-particle and particle-granulator wall collisions increased. Therefore, it was found that the tumbling time corresponds to the accumulation of external force acting on the granules. Thus, the product of the agitation torque and tumbling time corresponds to the time-integral value of the stress for consolidation, resulting in a good correlation with the granule strength.

In summary, as the magnetite blending ratio of the raw ore powder increased, i.e., the degree of reduction increased, the raw powders exhibited less plasticity, and the granules became less compact. From the comparison of the agitation torque measurement and granulation experiments, it was found that the granule strength can be estimated from the agitation torque regardless of the mixing ratio of the raw material.

Acknowledgments

This work is based on the results obtained from project JPNP12004, subsidized by the New Energy and Industrial Technology Development Organization (NEDO).

References

2. [1] M. Omran, T. Fabritius, A. M. Elmahdy, N. A. Abdel-Khalek, S. Gornostayev, *Sep. Purif. Technol*. **2015**, 156, 724.

3. [2] H. Kubo, N. Maruoka, Y. Sato, *ISIJ Int.*, **2019**, 105, 871.
4. [3] T. Otsu, H. Nakamura, S. Ohsaki, S. Watano, S. Fujiwara, T. Higuchi, *ISIJ Int.*, **2022**, 62, 1381.

[4] S. Yokokawa,.H. Nakamura, T. Otsu, S. Ohsaki, S. Watano, S. Fujiwara, T. Higuchi, *ISIJ Int.*, **2023**, 63, 670

DEM modelling of the effect of triboelectric charging on the mixing of fine powder

Yurui Wang,* Yudong Zou, Runyu Yang

School of Materials Science and Engineering, University of New South Wales, Sydney, Australia
*Corresponding author: yurui.wang2@student.unsw.edu.au

Fine powders ranging in particle size from 1 to 10 micrometres find widespread applications in industries such as pharmaceuticals, cosmetics, coatings, food processing, and chemical manufacturing. The mixing of these fine powders is essential to achieve uniform and homogeneous blends necessary for product consistency and performance. However, due to their small particle size and large surface area, fine powders exhibit high surface energy and strong interparticle forces, including electrostatic, capillary or van der Waals forces. These characteristics can impair flowability, leading to issues like powder aggregation and segregation, thereby affecting the precise composition and consistency of powder mixtures. Understanding and optimizing the flow behaviour of fine powders are crucial for enhancing processing performance and ensuring product quality across these industries.

The accumulation of electrostatic charges on insulating fine powders significantly impacts their flowability during mixing processes, primarily due to triboelectrification or triboelectric charging where charges transfer between materials with different electrical potential upon contact and separation accompanied by friction [1]. In the tribo-charging process, charge transfer may involve electron, ion, and material transfer [2]. During each charge transfer, the materials develop charges of equal magnitude but opposite polarity, which subsequently relax or dissipate. The charged particles experience attractive or repulsive electrostatic forces, affecting their flow behaviours. Furthermore, the level and polarity of electrostatic charges on particles are influenced by operational conditions, particle characteristics (such as size, composition, and surface properties), and environmental factors (especially humidity) [3].

This noticeable electrostatic effect on insulating fine powders stems from their high resistivity, prolonging charge decay times, coupled with their high surface area-to-mass ratio and light weight, which increase susceptibility to accumulating charges and influence from electrostatic forces. These electrostatic charges can cause various issues, including increased particle cohesion leading to reduced flowability, enhanced adhesion to equipment surfaces resulting in higher material losses and compromised equipment efficiency and cleanliness [4]. Additionally, they can contribute to potential equipment failures, inhomogeneous mixing, variability in product quality, measurement errors, and even safety hazards such as dust explosions or fires [5]. Therefore, studying the impact of electrostatics on powder flowability is crucial for maintaining consistent product performance during processing.

The Discrete Element Method (DEM) provides a profound understanding of powder rheology at the microscopic level, making it a useful tool for further investigation of triboelectric charging phenomena in fine particles. By applying Newton's second law, DEM can dynamically track and analyse the motion of individual particles within bulk materials [6]. DEM models that incorporate triboelectric charging (capacitor) and electrostatic interactions have also been developed and widely used to study particle charging and flow behaviours in various processing scenarios [7]. Mehta et al. used DEM to investigate segregation and powder adhesion due to triboelectric charging in different V-blenders, and after comparing with experimental results, they confirmed that DEM can capture the overall charging dynamics [4].

This work is to study how triboelectric charging affects the flow properties of fine powders during the mixing process. A DEM model is developed to investigate the impact of varying particle size, mass ratio, blade tip speed, mixing time, and mixer size on the triboelectric charging process, and explore the influence of these electrostatic charges on the flow and mixing. This investigation enhances fundamental understanding and offers practical insights for optimizing mixing in industries.

The DEM model of a blade mixer has been constructed, integrating both triboelectric charging and electrostatic interaction models. This model is to study the triboelectric charging behaviours of lactose and mannitol fine powders under various conditions. The DEM model has been validated by comparing with experiments using the dynamic testing of a Freeman FT4 powder rheometer. This apparatus measures the variation of flow energy with blade penetration depth at blade tip speeds of 100 mm/s, 70 mm/s, and 40 mm/s.

Experimental and simulation setups are shown in Figure 1 (a). The expected analysis entails measuring axial forces and torques on the impeller during downward blade rotation to calculate flow energy for simulation validation like Figure 1 (b). Flow energy also serves as a metric for particle flowability; higher flow energy indicates lower flowability. By controlling influencing factors, the accumulation of electrostatic charges during mixing quantified as specific charge (charge per unit mass) is studied. Besides, the coordination number, representing the number of contacts per particle, will be used to further analyse the tribo-charging process and the Lacey mixing index of mixtures will be computed to examine mixing uniformity and investigate the impact of charging on product quality.

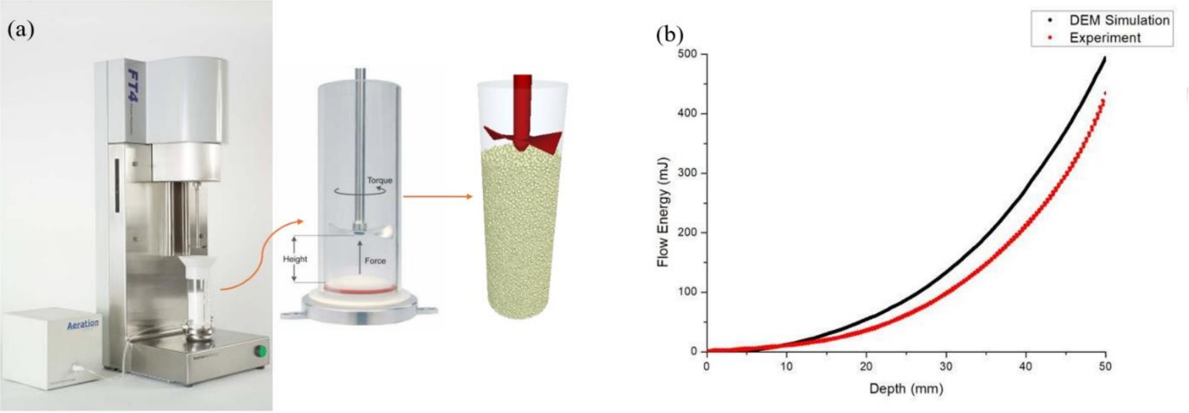

Figure 1. (a) Diagram of FT4 rheometer equipment and simulation; (b) flow energy vs penetration depth of mixture in DEM simulation without electrostatics and experiment.

References

[1] J. Wong, P. C. L. Kwok, H.-K. Chan, *Chem. Eng. Sci.* **2015**, 125, 225-237.

[2] M. U. Ghori, B. R. Conway, *Br. J. Pharm.* **2018**, 3, 1-18.

[3] S. Matsusaka, H. Maruyama, T. Matsuyama, M. Ghadiri, *Chem. Eng. Sci.* **2010**, 65, 5781-5807.

[4] T. Mehta, R. Mukherjee, A. Shah, T. Mastriani, T. Duran, B. Chaudhuri, *Pharm. Res.* **2023**, 40, 2371-2381.

[5] M. Beretta, T. R. Hormann, P. Hainz, W. K. Hsiao, A. Paudel, *Int. J. Pharm.* **2020**, 591, 120014.

[6] F. O. Alfano, A. Di Renzo, F. P. Di Maio, M. Ghadiri, *Powder Technol.* **2021**, 382, 491-504.

[7] C. Pei, C.-Y. Wu, M. Adams, *Powder Technol.* **2016**, 304, 208-217.

Spray freeze granulation drying of non-aqueous Si_3N_4 slurry-effect of the amount of OA in added PEI-OA complex -

Riko Yamazaki,[a] Junichi Tatami,[a*] Motoyuki Iijima,[a] Shinya Kawaguchi,[b] Naoki Kondo[c]

[a]Yokohama National University, Yokohama, Japan
[b]PRECI Co., Ltd., Kawasaki, Japan
[c]National Institute of Advanced Industrial Science and Technology, Nagoya, Japan
*Corresponding author: tatami-junichi-xv@ynu.ac.jp

Spray freeze granulation drying (SFGD) is a granulation technique, in which granules are produced by sublimating solvent from frozen bodies obtained by spraying a slurry. Granules produced by this technique are purported to have a homogeneous internal structure, good flowability owing to their spherical shape, and low strength owing to these porous structure, which provide various oxide ceramics having better properties. However, compounds that react with water to form oxides or hydroxides on the surface of the raw powder, such as nitrides (Si_3N_4), have been little studied in SFGD. In our previous study, SFGD was carried out using nonaqueous Si_3N_4 slurry to obtain granules. Solvent mixtures of *tert*-butyl alcohol and cyclohexane were used to prepare the Si_3N_4 slurries. As a result of in situ optical coherence tomography (OCT) observation of the freezing behaviour of the slurry, it was found that the solvent mixture of the eutectic composition yielded a homogeneous internal structure with fine pores in the freeze-dried body. The granules of that composition prepared by spray freeze granulation drying had a smaller size and a narrower size distribution, which resulted in a homogeneous internal structure of silicon nitride ceramics. The amount of OA in PEI-OA complex should also be an important factor in better ceramics. In this study, the Si_3N_4 slurries were prepared using various amount of OA in PEI-OA complex added as a dispersant. The freezing behaviour was evaluated by applying motion detection method of OCT images obtained from in situ observations as in previous studies.

Fig. 1 shows the OCT images of the freezing behaviour of the Si_3N_4 slurry. By comparing OCT images of the same position at different time in Fig. 1(a) and (b), the pixels determined to be in motion was obtained (Fig. 1 (c)). They expanded from the cooling surface and then the OCT images became stationary. Time dependence of the fraction of the pixels determined to be in motion indicated that the slurry with the higher amount of OA froze faster, which also had lower freezing initiation temperature because of the better affinity between the solvent and the particles. From the SEM images of the freeze-dried bodies, it was found that the higher amount of OA, the finer pores, i.e. the finer solid formed by freezing (Fig. 2). Such more homogeneous internal structure resulted in the higher compressive strength of the Si_3N_4 granules. Although the morphology of the granules obtained was spherical, the granule size were smaller for those prepared from the slurries with lower viscosities (Fig. 3). In addition, the higher the OA amount in PEI-OA complex, the smaller the Hausner ratio. This means that OA plays a role of lubricant, resulting in better flowability of granules.

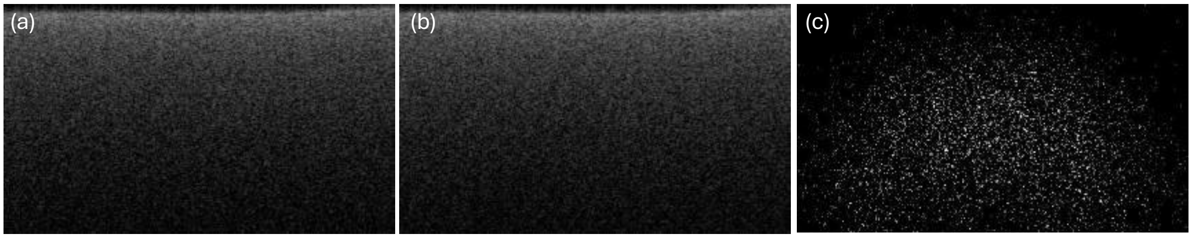

Figure 1. (a) OCT images of the Si_3N_4 slurries prepared by adding the PEI-OA complex containing 10 mol% OA. (b) is the image

obtained 0.04 s after (a). (c) is the result of the motion detection between (a) and (b).

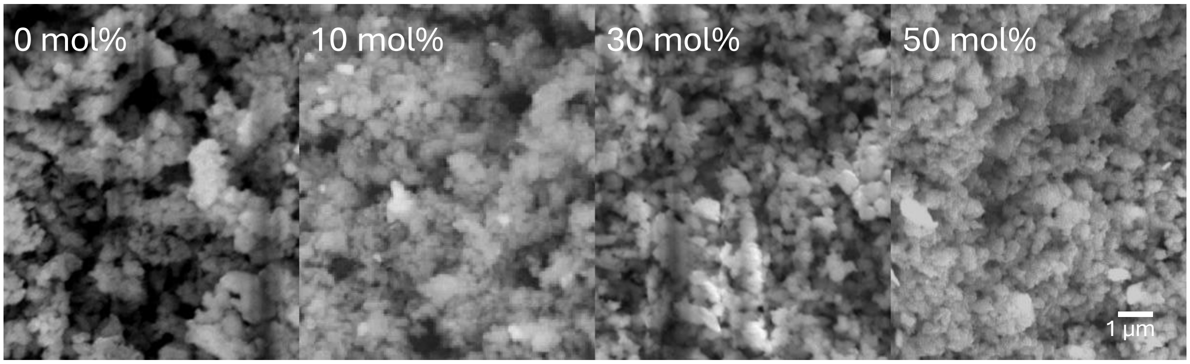

Figure 2. SEM images of freeze-dried bodies prepared using Si_3N_4 slurry with various amount of OA in PEI-OA complex.

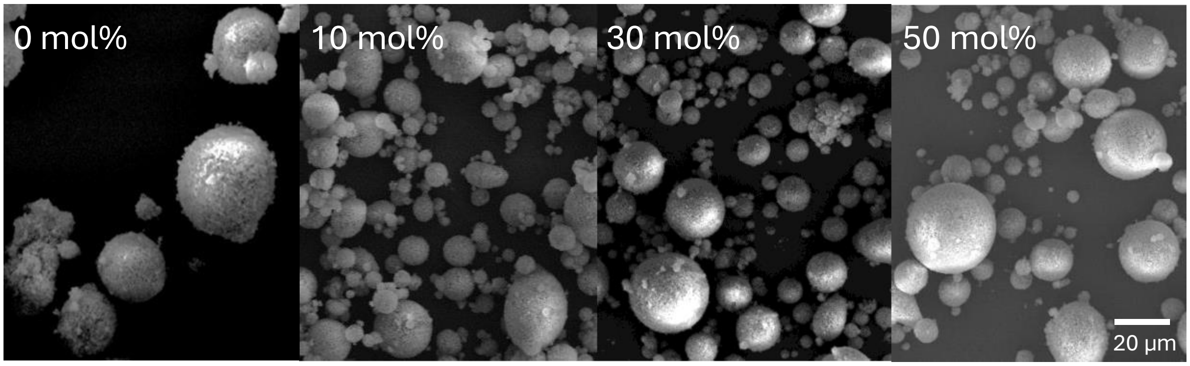

Figure 3. SEM images of SFGD granules prepared by using Si_3N_4 slurry with various amount of OA in PEI-OA complex.

Preparation of arsenic, boron and radioactive cesium adsorbent powder

Nagatomo Mononobe,[a] Hiroaki Minamisawa,[b]* Sakiyori Mononobe,[a] Taizou Uchimura,[a] Masakazu Matsumoto,[b] Shinnosuke Kamei,[b] Hiromichi Asamoto,[b] Keisuke Suzuki,[b] Susumu Takahashi[b]

[a] Monobe Engineering Corporation, 149 Hanashima-cho, Hanamigawa-ku, Chiba, Japan
[b] College of Industrial Technology, Nihon University, 2-1-1 Shinei-cho, Narashino, Chiba, Japan.
* Corresponding author: minamisawa.hiroaki@nihon-u.ac.jp

1 Introduction

High concentrations of boron, arsenic and radioactive cesium have serious effects on the human body. Therefore, the development of adsorbents for boron, arsenic and radioactive cesium is very importance. It has already been reported that adsorbents obtained by graft polymerisation of glycidyl methacrylate (GMA) onto nonwoven fabrics followed by adhesive reaction with N-methyl-D-glucamine (NMDG) exhibit high boron adsorption capacity [1]. In this report, the newly prepared cerium hydroxide adsorbed boron well and is described in detail. Similarly, polyurethane-like adsorbent was prepared and adsorbed arsenic well, and the results are also described. Furthermore, adsorbents such as Phospho-ammonium tungsten for radioactive cesium were examined.

2. Results and Discussion

Cerium hydroxide was obtained by mixing of cerium nitrate solution and sodium hydroxide solution from mixing continuous crystallization. A conceptual diagram of the continuous crystallisation system is shown in Fig. 1. The mean particle sizes of Cerium hydroxide was 2.1µm (Fig.2)

Polyurethane form-like adsorbent(PUF) was obtained using polypropylene glycol(PPG), 4,4'-Diphenylemethane diisocyanate(MDI) and Tri-n-octylamine(TnOA), The resulting adsorbent adsorbed arsenic well.

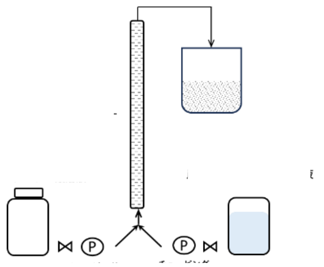

Figure 1. Conceptual diagram of continuous crystals crystallization.

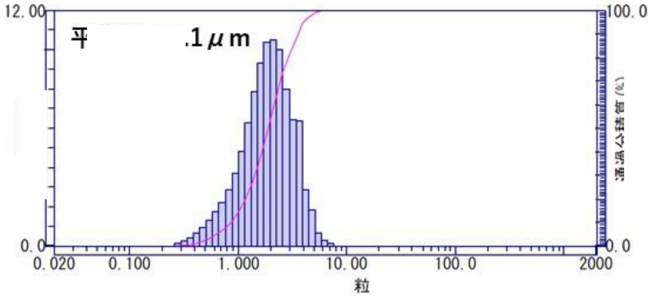

Figure 2. Particle size of Cerium hydroxide

Ammonium phosphotungstate was prepared by continuous crystallisation of aqueous solutions of phosphotungstic acid and ammonium bicarbonate. The resulting adsorbent adsorbed radioactive cesium well. The adsorption isotherms of radioactive cesium on ammonium phosphotungstate are shown in Figure 3. Several adsorbents prepared in this study were pre-coated on spring-type filters(Figure 4) and applied to remove arsenic, boron and radiocesium from seawater and rivers.

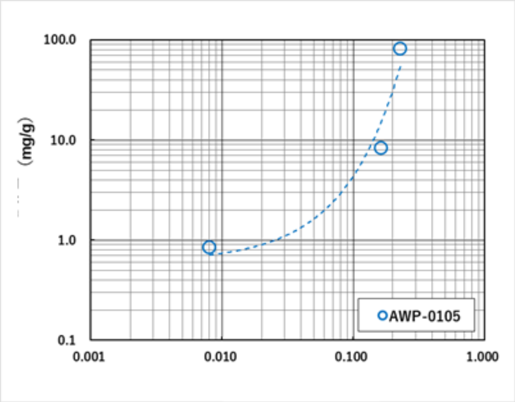

Figure 3. Adsorption isotherms

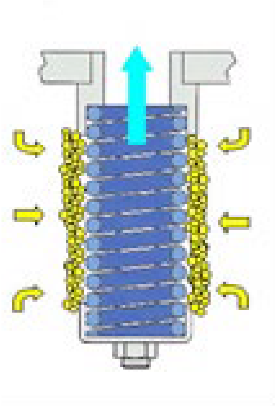

Figure 4. Pre-coated on spring-type filters

3. **Conclusions**

$K_2[CoFe(CN)_6]$ is effective to remove of radioactive cesium from environmetal waters such as sea water and river water, and this study contributes to SDGs NO.7(CLEAN WATER AND SANITATION, Ensure availability and sustainable management of water and sanitation for all).

References

[1] H. Hoshina, J. Chen, H. Amada, *N. Seko, Polymer.* **2021**, 13, 1163-1176.

Macroscopic mixing and segregation behavior of polydisperse spherocylindrical particle mixtures in rotary drums

Qiuhua Miao,[a] Peng Huang,[a]* Runyu Yang,[b] Aibing Yu,[c] Shibo Kuang[c]

[a] School of Mechanical Engineering, Southeast University, Nanjing, China
[b] Department of Chemical Engineering, Monash University, Clayton, Australia
[c] School of Materials Science and Engineering, UNSW Sydney, Australia
*Corresponding author: huangpeng@seu.edu.cn (P. Huang)

The flow behaviour of polydisperse particle mixtures, especially non-spherical particles, is quite complex in rotating drums, making it difficult to understand the mixing and segregation mechanisms. In this work, the combined impact of the large and small particle shapes was thoroughly investigated in detail in bi- disperse particle systems and further verified in polydisperse systems, using various spherocylindrical particles with different aspect ratios (AR). In bi-disperse particle systems, a significant enhancement in the steady segregation degree was observed when the system transitioned from single to double spherocylindrical particles. Besides, in bi-disperse system with double spherocylindrical particles, similar to bi-disperse systems with single spherocylindrical particles, the inclusion of large spherocylindrical particles significantly inhibits the particle percolation process, resulting in better mixing effect. Conversely, the inclusion of small spherocylindrical particles with the higher average packing density requires more energy to overcome inter-locking effect on percolation. Especially the lower the average packing density of small particles, the higher the particle segregation degree. Consequently, the phase diagram was bound to shows two peak regions and one valley region in the interval of 1.0 ≤ LAR, SAR ≤ 4.0 under the combined effect of particle shapes. Additionally, in polydisperse particle systems size-induced particles, with the increasing particle AR value, the steady segregation degree shows the first increasing and then decreasing characteristics, while the initial segregation speed shows the continuous decreasing characteristics.

Table 1. Particle shape parameters used in the simulations.

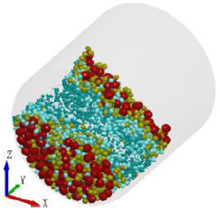	Shape									
	R (mm)	6	5.40	4.98	4.66	4.42	4.05	3.78	3.40	3.14
	A (mm)	6	6.75	7.47	8.16	8.84	10.13	11.34	13.60	15.70
	AR (A/R)	1.0	1.25	1.5	1.75	2.0	2.5	3.0	4.0	5.0
	Sphericity	1.0	0.988	0.968	0.947	0.921	0.878	0.840	0.779	0.730

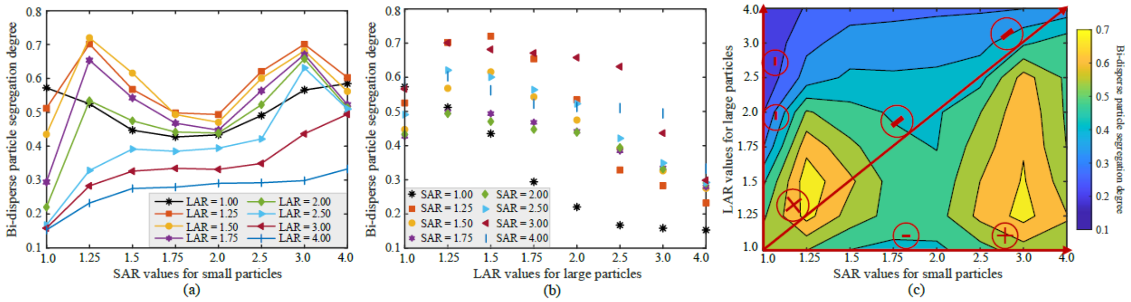

Figure 1. Combined effects of large particle shape and small particle shape:

(a) Effect of small particle shape, (b) Effect of large particles, (c) Combined effects in phase diagrams

Graded porous Al_2O_3 fabrication using electrostatic integrated polymethyl methacrylate (PMMA)-Al_2O_3 composite granules

Wai Kian Tan,* Koki Iwata, Keita Tsuzuki, Go Kawamura, Atsunori Matsuda, Hiroyuki Muto

Toyohashi University of Technology, Toyohashi, Japan
*Corresponding author: tan@las.tut.ac.jp

The unique characteristics of ceramics such as excellent hardness and resistance in heat as well as corrosion have led to their wide usage in many applications. Recently, interest in developing graded porous ceramics for applications such as heat insulation, sound dampening, bio-ceramics and lightweight structural framework for catalyst carriers are increasing [1]. Methods such as sol-gel, organic foam, and freeze-casting are used for fabrication of porous ceramics but still face challenges in forming graded porous ceramic structures.

In this study, fabrication of graded porous ceramics using electrostatically integrated composite granules is demonstrated. Recent reports indicated a feasible fabrication of functional ceramic composites exhibiting desired properties such as enhanced electrical or thermal property using electrostatic integrated composite granules via powder metallurgy [2,3]. By using electrostatic integrated granulation, the heteroaggregation of ceramic and pore-former particles in an aqueous suspension led to the formation of spherical composite granules with a homogeneous distribution of the raw particles while exhibiting improved flowability, and handling ability. The ceramic particles and pore-formers used were alumina (Al_2O_3, average diameter 140 nm) and spherical polymethyl methacrylate particles (PMMA, average diameter 800 nm), respectively. The amount of PMMA incorporated into the composite granules was varied from 0 to 50 vol.%. The microstructures of the porous Al_2O_3 obtained after sintering of pressed PMMA-Al_2O_3 composite granules with different PMMA composition at 1350ºC for 1 h, are shown in Figure 1. These observations indicate a possible porosity control using electrostatic integrated composite granules. By stacking PMMA-Al_2O_3 composite granules in an increasing vol.% of PMMA, a feasible fabrication of graded porous ceramics using is also demonstrated. The findings from this study could benefit the development of a scalable graded porous ceramics manufacturing.

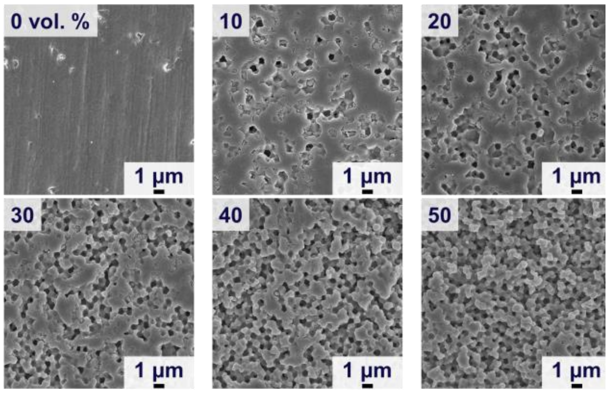

Figure 1: Microstructure of the sintered artifacts (1350ºC ,1 h) obtained using electrostatic integrated Al_2O_3-PMMA composite granules with different vol.% of PMMA

References

[1] W. K. Tan, K. Tsuzuki, A. Yokoi, G. Kawamura, A. Matsuda and H. Muto, *J. Ceram. Soc. Jpn.* **2020**, 128, 605-610.
[2] H. Muto, Y. Sato, W. K. Tan, A. Yokoi, G. Kawamura and A. Matsuda, *Nanoscale* **2022**, 14, 9669-9674.
[3] T. Nakazono, A. Yokoi, W. K. Tan, G. Kawamura, A. Matsuda and H. Muto, *Nanomaterials* **2023**, 13, 199.

Preparation of three-dimensional flowability diagrams for powder beds with different caking behaviours

Yun-Chien Lin,[a] An-Ni Huang,[b] Wan-Yi Hsu,[b] Tsuo-Feng Wang,[a] Hsiu-Po Kuo[a,*]

[a] Department of Chemical Engineering, National Taiwan University, Taipei, Taiwan
[b] Green Technology Research Center, Chang Gung University, Taoyuan, Taiwan
*Corresponding author: hsiupokuo@ntu.edu.tw

Evaluating the flow properties of a powder bed are of practical importance for industrial operations, like silo flows. These properties, including cohesion, unconfined yield strength, major principal stress, flow function, angle of internal friction and bulk density, are typically measured by the shear testers. The flow properties of the testing powders at consolidated, moderately stressed, and initial fluidized conditions are known to be different. Gathering flow property information of the powder bed at different conditions into a flowability diagram is challenging. The traditional Hvorslev surface and the Roscoe/Rendulic surface separated by the critical state line can only consider the flow properties of the compressed powder bed. Here, we prepare the three-dimensional flowability envelope diagrams for different powders using a commercial powder rheometer, FT 4. The normal stress and shear stress acting on the powder, and the bed voidage are the three coordinates. We initially analyse the powder bed flowability under the tensile stress by conducting bed fluidization and shear testing at the same time. The effects of the powder caking on the flowability envelope diagrams' size and shape are systematically studied.

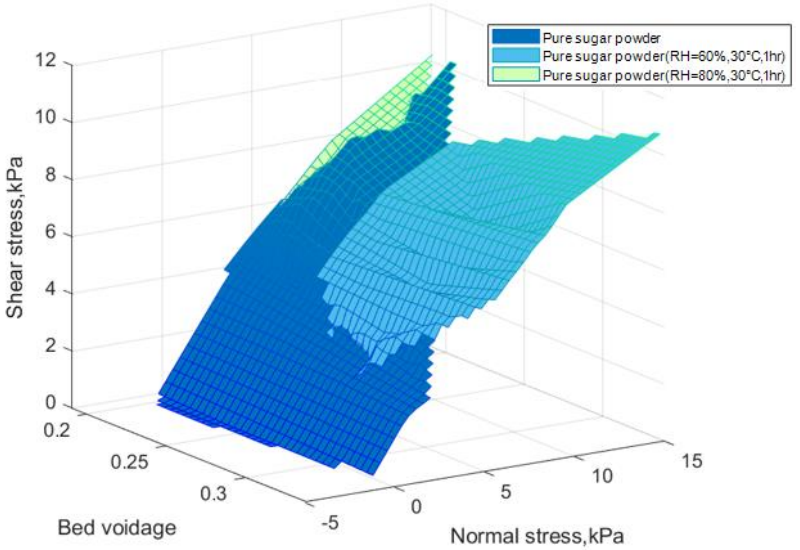

Figure 1. Overlayed Hvorslev diagram of Pure sugar powder

References

[1] W.Y. Hsu, A.N. Huang, H.P. Kuo, *Adv. Powder Tech.* **2020**, 31, 433-438.

[2] Y. Shimada, T. Kawata, S. Matsusaka, *Adv. Powder Tech*. **2018**, 29, 1372-1378.

High sensitive and selective H_2 sensors based on sandwich-structured M_xSn_y-rGO-SnO_2 composites

Yanbai Shen,[a,*] Guodong Li,[a] Sikai Zhao,[a] Cong Han[a]

[a] School of Resources and Civil Engineering, Northeastern University, Shenyang 110819, China
*Corresponding author: shenyanbai@mail.neu.edu.cn

SnO_2 nanoparticles were grown on the surface of reduced graphene oxide (rGO) via a simple reflux reaction, resulting in the formation of rGO-SnO_2 composites with excellent hydrogen (H_2) sensing performance. Noble metal sensitizers, known for their electronic and chemical sensitization effects, have been shown to significantly enhance the sensing performance of metal oxide semiconductor (MOS) based gas sensors. In recent years, intermetallic compounds have gained significant attention in catalysis research due to their tunable electronic structure, excellent stability, and low cost. Especially, intermetallic compounds have demonstrated exceptional catalytic performance. Based on the theoretical basis of the above two aspects, it is hypothesized that intermetallic compounds will offer high sensitization performance in MOS gas sensing. Herein, an in-situ synthetic approach to produce a series of intermetallic sensitizers consisting of three binary M-Sn (M: Au, Pt, Pd) intermetallic compounds were reported. All three intermetallic compounds significantly enhanced the H_2 sensing performance of rGO-SnO_2 composites, with Pd_3Sn_2 exhibiting the most potent sensitizing effect. The 2.0% Pd_3Sn_2-rGO-SnO_2 composites with sandwich structure showed a significant decrease in the optimal operating temperature of rGO-SnO_2 composites in response to H_2 from 225 °C to 90 °C, and its sensor response to 500 ppm H_2 was 250.9, which was 125 times higher than that of rGO-SnO_2 composites.

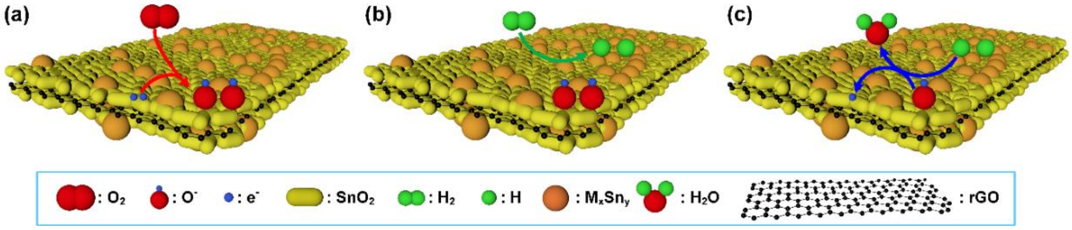

Figure 1. Schematic illustration of H_2 sensing process of M_xSn_y-rGO-SnO_2 composites.

References

[1] G. D. Li, Y. B. Shen, S. K. Zhao, A. Li, C. Han, Q. Zhao, D. Z. Wei, Z. Y. Yuan, F. L. Meng, *Sensor. Actuat. B-Chem.* **2022**, 373, 132656.

[2] G. D. Li, Y. B. Shen, S. K. Zhao, A. Li, S.L. Gao, D. Z. Wei, Z. Y. Yuan, F. L. Meng, D. Meng, *Sensor. Actuat. B-Chem.* **2022**, 368, 132146.

[3] G. D. Li, Y. B. Shen, S. K. Zhao, J. Z. Bai, S. L. Gao, W. B. Liu, D. Z. Wei, D. Meng, X. G. San, *Appl. Surf. Sci.* **2022**, 585, 152623.

Microfluidic-aerosol hyphenated synthesis of metal-organic framework-derived hybrid catalysts for CO_2 utilization

Yi-Hsuan Sung,[a] De-Hao Tsai[a,]*

[a] Department of Chemical Engineering, National Tsing Hua University, Hsinchu City, Taiwan, R.O.C.
*Corresponding author: dhtsai@mx.nthu.edu.tw

A new and efficient technique is developed by combining the hyphenated microfluidic- and aerosol-based synthesis with the coupled differential mobility analysis for the effective and continuous synthesis and simultaneous analysis of metal-organic frameworks (MOFs) derived hybrid nanostructured products. HKUST-1, a copper-based MOF, is chosen as the representative to fabricate Cu-based hybrid catalysts for reverse water-gas shift (RWGS) reaction, an effective route for CO_2 utilization. The effect of precursor concentration and carrier selection on the properties of the resulting products, including mobility size distribution, crystallization degree, surface area and metal dispersion were investigated, as well as the correlation between the material properties of the synthesized catalysts and their catalytic performance in RWGS reaction in terms of conversion ratio/rate, selectivity and operational stability. The results indicated that the continuous microfluidic droplet system can successfully synthesize MOF colloids, followed by the continuous production of MOF-derived hybrid materials through the tandem aerosol spray-drying-reaction system. High catalytic activity and low initiate temperature toward RWGS (turnover frequency = 0.0074 s^{-1}; 450 °C) were achievable. The work facilitates the production and the designed concept of relevant MOF-derived hybrid nanostructured catalysts in the continuous synthesis system and the enhancement of applications in CO_2 capture and utilization.

References

[1] Y.-H. Sung, D. Senthil Raja, J.-H. Huang, D.-H. Tsai, *Small Methods* **2023**, in press, https://doi.org/10.1002/smtd.202301435.

[2] Y.-H. Sung, C.-L. Wu, J.-H. Huang, D.-H. Tsai,Real-Time Quantifying Microdroplet Synthesis of Metal–Organic Framework Colloids Using Gas-Phase Electrophoresis. *Anal. Chem.* **2023**, 95(9), 4513-452.

Functionalization of BTX-derived MWNCTs as a fluorescence sensor hybridized with coumarin for use in metal ion detection

Weerawut Chaiwat,[a,*] Warodom Thepmongkorn,[a] Thanchanok Vettavong,[a]
Pimonpan Inthapat,[a] Phitchawalai Ninthachan,[a] Chawalkul Chotmunkhongsin,[a]
Sirilak Wangngae,[b] Sutthira Sutthasupa[b,**]

[a] Department of Chemical Engineering, Faculty of Engineering, Mahidol University, Nakhon Pathom, Thailand
[b] Division of Packaging Technology, Faculty of Agro Industry, Chiang Mai University, Chiang Mai, Thailand
*Co-corresponding author: weerawut.cha@mahidol.ac.th
**Co-corresponding author: sutthira.s@cmu.ac.th

In this study, functionalized multi-walled carbon nanotubes (f-MWCNT) hybridized with a selected fluorescence dye as coumarin could be developed and used as a fluorescence sensing material for metal ion detection as depicted in Figure 1. MWCNTs with diameters of approximately 30 and 60 nm were synthesized from a mixture of benzene, toluene and xylene (BTX) as a representative of waste plastic pyrolysis products using Fe/b-Al_2O_3 and Fe/SiO_2 as catalysts, respectively. Commercial MWCNTs with a diameter of about 10 nm was also used as a benchmark. One-pot acid treatment at various acid mixture ratios for functionalization and purification of the MWCNTs were conducted in order to add functional groups on and remove catalyst residues out of the MWCNTs. The results showed that f-MWCNTs derived from Fe/b-Al_2O_3 using a 1:3 (v/v) of HNO_3:H_2SO_4 mixture solution resulted in the highest purity at 84%. Microwave digestion was then used to increase MWCNT purity up to 94.6%. For f-MWCNTs derived from Fe/SiO_2, using 25% HF: 75% HNO_3+H_2SO_4 (1:3, v/v) could achieve high-purity MWCNT at 96.7%. Four types of f-MWCNT with low and high purities (84% and 94–97%) and various MWCNT diameters (10, 30, 60 nm), which exhibited photoluminescence with emission in the visible light region, were selected for the selectivity test of metal ion detection. These were compared with those conjugated with coumarin to enhance their fluorescent intensities. The results showed that fluorescent intensity of all fluorescent probes was selectively quenched by Fe^{3+} ions by over 83% as shown in Figure 1. The as-synthesized f-MWCNT successfully achieved comparable good limits of detection (LOD) for Fe^{3+} at 2.20–2.32 μM in a linear concentration range of 0–50 μM, which was further reduced to 1.92–2.21 μM for the coumarin-conjugated f-MWCNTs. The LODs obtained in this study were comparable with those CNT-based fluorescence probes developed in previous studies [1, 2] with 200–1000 times lower concentration of added fluorescence probe in the solution at 0.1 μg/ml. The size and purity of MWCNTs within the ranges of this study did not significantly affect to the performance of the fluorescence intensity and LOD of Fe^{3+} ion. This as-developed f-MWCNT hybridized with coumarin based fluorescence probe could be further applied to environmental and biomedical applications for the detection of Fe^{3+} ion.

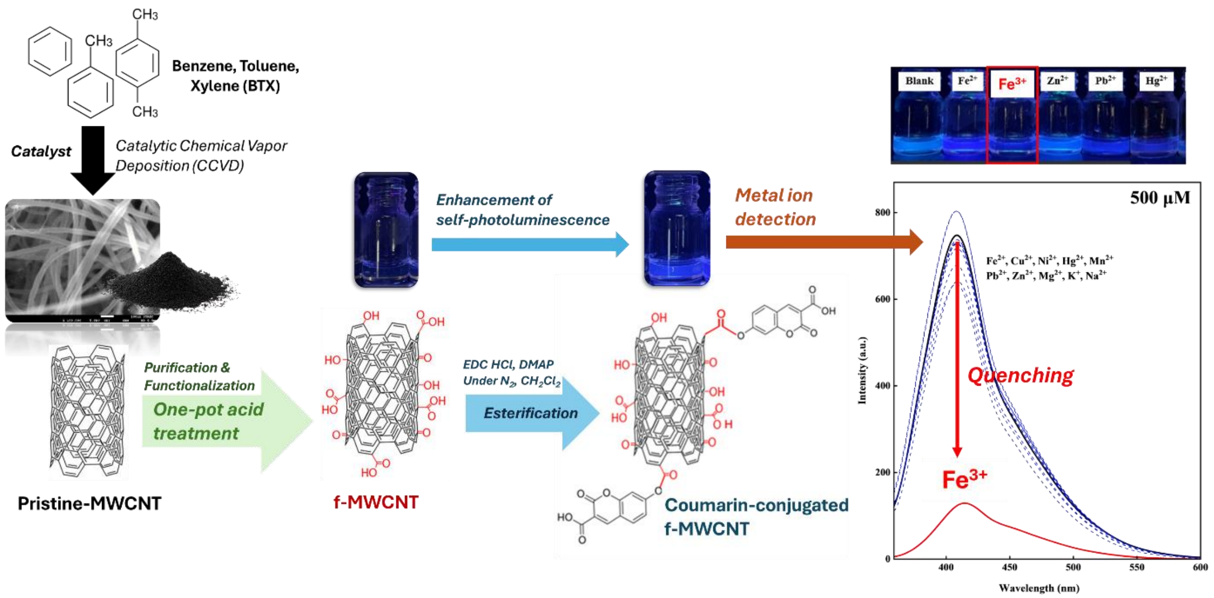

Figure 1. Conceptual study of functionalization of BTX-derived MWNCTs as a fluorescence sensor hybridized with coumarin for use in metal ion detection.

References

[1] K. Rajar, E. Alveroglu, *Mater. Res. Bull.* **2019**, 124, 110748.

[2] Y. Guo, L. Zhang, S. Zhang, Y. Yang, X. Chen, M. Zhang. *Biosens Bioelectron.* **2015**, 63, 61–71.

Synthesis and functionalization of carbon black – silica hetero-aggregates

Simon Buchheiser,[a] * Hermann Nirschl,[a] Frank Rhein[a]

[a]Karlsruhe Institute of Technology, Institute of Mechanical Process Engineering and Mechanics, Straße am Forum 8, Karlsruhe, Germany
*Co-corresponding author: simon.buchheiser@kit.edu

The urgent need for a reduction in the use of fossil fuels in order to reduce CO2-emissions has led to the emergence of electro mobility, e.g., in the form of electric cars. Currently, lithium-ion batteries are the most frequently used component for the needed energy storage. Within batteries a blend of multiple components, including active materials, polymer binders and carbon black, ensures efficient energy storage. Therein, the creation of electrical pathways between the usually non-conductive active material particles is achieved by the addition and homogenous dispersion of carbon black within the electrodes. The formed conductive network of carbon black is supported by a polymeric binder. At the cathode side of lithium (Li) ion batteries, polyvinylidene fluoride (PVDF) is often used as binder which is part of the group of per- and polyfluoroalkyl substances (PFASs). To limit the environmental hazards and subsequent health implications on the basis of the bioaccumulation of these substances, the development and evaluation of alternatives is of the utmost importance. Therefore, this project focuses on enhancing the material properties of carbon black via hetero-aggregation with other additives, to reduce the technical requirements on the binder network and subsequently open up alternatives in binder choice. One material which is well suited for the production of highly ordered composite structures is silica. In addition, the silica particles infiltrate the carbon black structure when the process parameters are well chosen, as demonstrated in a recent publication [1]. Therein, the hetero-aggregation yielded aggregates which consist of the preserved backbone of the fractal carbon structure with silica particles on the carbon black surface for reinforcement as depicted in the transmission electron microscopy (TEM) image in Fig. 1. In order to produce a high amount of hetero- contacts it is necessary to reach high dispersity during the mixing of both nanopowders. Instead of dry mixing where high shear forces are needed, the mixing process is shifted in the gas phase. In a spray the active mixing zone is achieved by high gas velocities above the nozzle. Furthermore, by choosing a burnable liquid as dispersion medium the spray can be ignited, thus creating a turbulent spray flame. The high temperature of the flame as well as the high collision frequency enables the creation of the hetero- aggregates. These hetero-aggregates were produced in a spray flame in which a suspension of a C65 type carbon black and colloidal silica particles was atomized.

A fundamental understanding of hetero-aggregation is only achieved when both, the primary particle properties and their influence on the overarching aggregate structure, is considered. Therefore, a multi-scale approach for the characterization of hetero-aggregates has been applied. The approach includes a combination of small angle X-ray scattering (SAXS), analytical disc centrifugation (ADC) and transmission electron microscopy (TEM) to grant a comprehensive understanding of multiple particle properties by uniting primary particle properties, the fractal dimensions and aggregate properties. Further information on the mixing quality within the hetero-aggregates has been achieved with extensive image analysis of TEM-Images. In order to assess the functionality within batteries, the studied functional properties and relevant material functions include breakage behaviour, dispersion properties and electro-chemical performance. In conclusion, the results connect the process conditions for the hetero-aggregate synthesis with the respective aggregate properties and the resulting functional properties for battery applications.

The presentation will cover results of the multiscale structural characterization of hetero-aggregates consisting of carbon black and silica. Therein the key influences of the experimental conditions on the aggregate structure are characterized. Furthermore, the applicant has developed a method to reproducibly induce stress on aggregates by means of ultrasonic treatment via a sonotrode. In this context, results for varying energy inputs help to understand how the hetero-contact affects the aggregate stability. Afterwards, the aggregate breakage behaviour is characterized with regard to the change in aggregate diameter. Further mixing experiments in a laboratory setup aid to compare network formation and stability with conventional battery mixtures. Subsequently, a defined parameter space for the desired functionalization of the carbon black aggregates is strived for.

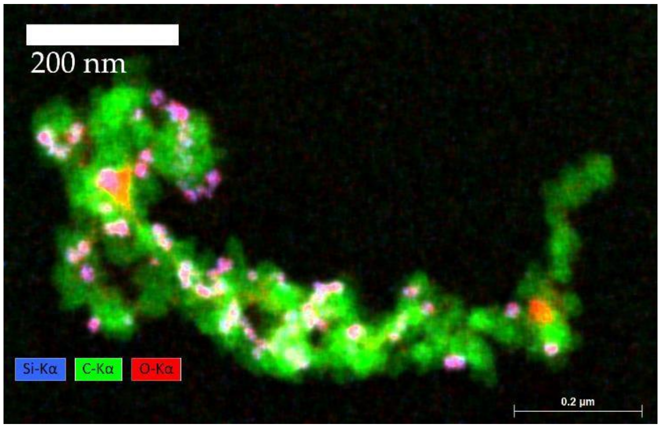

Figure 1. TEM image with energy dispersive X-ray spectroscopy (EDX) of produced hetero-aggregates of carbon black and colloidal silica. Carbon is colored in green and the silica particle appear pinkish.

References

[1] S. Buchheiser, F. Kistner, F. Rhein, and H. Nirschl, *Nanomaterials* **2023**, 13, 1893.

Synthesis and gas sensing properties of semiconducting metal oxide nanostructures

Sikai Zhao,* Yanbai Shen, Wenbao Liu

Northeastern University, Shenyang, China
*Corresponding author: sikaizhao@gmail.com

Gas sensors, the devices that transfer information about the presence and concentration of gases of interest into detectable electrical signals, play an important role in many industries, environmental protection, health and safety, and medical systems, among others. The sensing signal transformation can be achieved by using different principles resulting in various types of gas sensors. Conductometric semiconducting metal oxide (SMO) gas sensors are designed based on the resistance change of a SMO material caused by the interfacial reaction between the gas and the surface of the sensing material, and have captured a large portion of the gas sensing market due to their solid state, low cost, high reliability, and easy operation. As a core part of a SMO gas sensor, sensing materials play a key role in determining the sensing performance of the device, with the microstructure and surface properties being the dominant factors. In this study, SMO nanostructures with different dimensions were designed and synthesized for gas sensing applications. Their gas sensing properties were systematically tested, and the gas sensing mechanism was also investigated and analyzed.

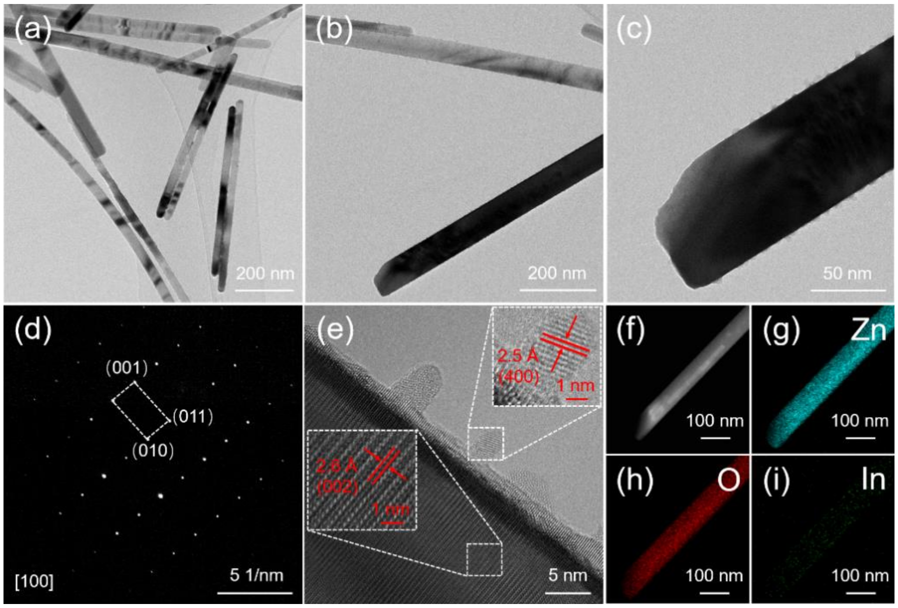

Figure 1. TEM characterization results of the In_2O_3-ZnO heterostructure nanowires

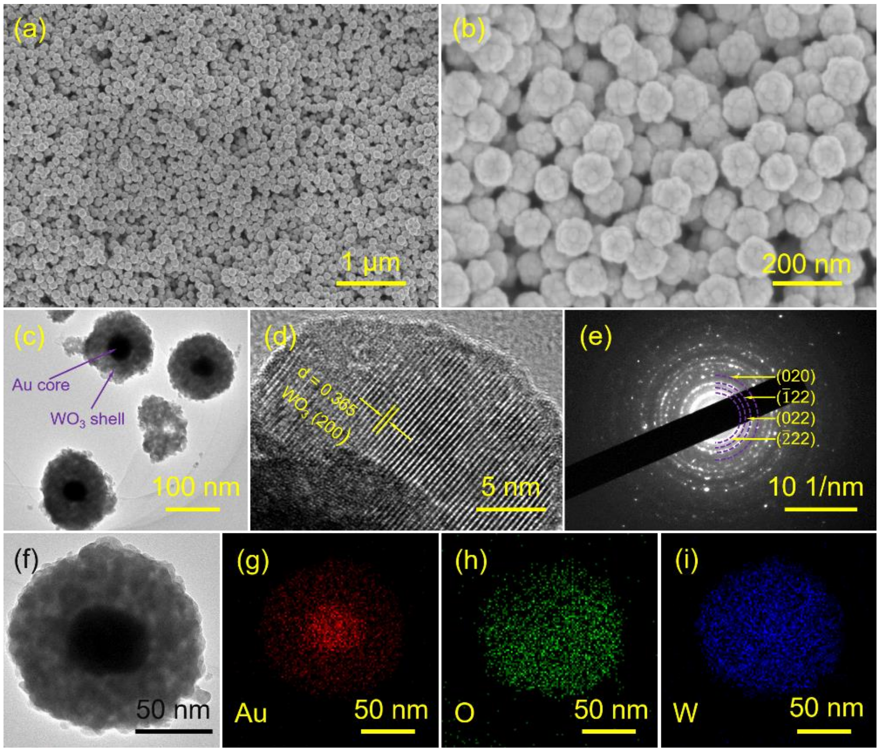

Figure 2. SEM and TEM characterization results of the Au@WO_3 core-shell nanospheres

The role of coating homogeneity for enhanced performance in lithium-ion battery cathodes

Tomoya Ohno,[a,]* Jeevan Kumar Padarti,[a] Shigeto Hirai,[a] Takeshi Matsuda[a]

[a]Kitami Institute of Technology, Hokkaido, Japan

*Corresponding author: ohno@mail.kitami-it.ac.jp

Coating technology for metal oxides on particle materials finds extensive applications in various material research fields, notably in battery materials. Recent focus within lithium-ion batteries (LIBs) research has emphasized the necessity of applying a protective layer onto cathode particles [1-3]. This protective layer not only safeguards the particle surface from degradation during charge and discharge cycles but also facilitates Li-ion and electron pathways. Typically, composite metal oxides serve as ideal coating materials to fulfil these multifaceted requirements, underscoring the critical need for advancing coating processes involving composite metal oxides [4]. In the context of LIBs, the microstructure of resulting core-shell particles, particularly the homogeneity and coverage of the coating layer, profoundly influences cell properties. However, achieving homogeneity at the nanoscale poses challenges due to the precise control required over the deposition phenomenon of the coating material onto core particles' surfaces. In this study, we meticulously regulated process parameters to coat $Li_7La_3(Zr_{1.75}Ta_{0.25})O_{12}$ (LLZTO), a known oxide solid electrolyte, onto cathode particles' surfaces, thereby yielding core-shell particles with varying coating layer homogeneities. Subsequent integration of these core-shell particles into conventional LIBs enabled us to experimentally elucidate the impact of different coating layer homogeneities on cell properties.

Figure 1 illustrates typical observation results obtained via Transmission Electron Microscope + Energy Dispersive X-ray Spectroscopy (TEM+EDS) analysis of LLZTO-coated cathode particles. Detection of Zr, a constituent of the coating material, from nearly identical positions as Co, a constituent of the cathode particles, validates the successful deposition of the target material onto the cathode particle surface. Moreover, slight segregation observed in certain areas indicates partial heterogeneity in the coating layer. Our analysis of coating layer homogeneity extends beyond TEM observations to quantitative assessments using spectroscopic techniques such as X-ray Photoelectron Spectroscopy (XPS).

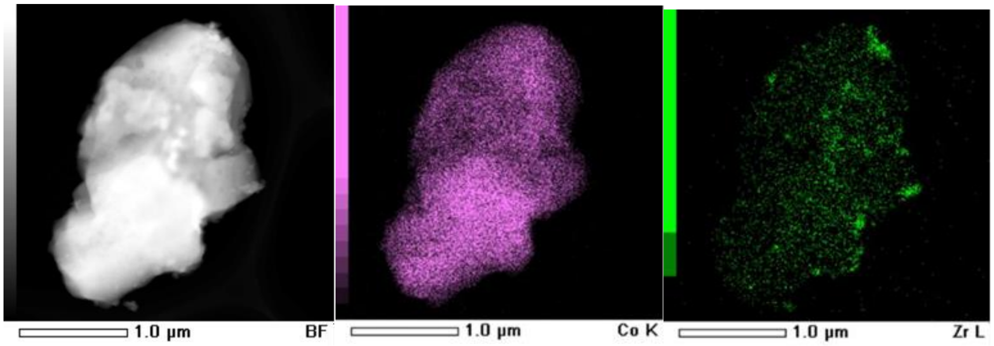

Figure 1. TEM+EDS analysis for $Li_7La_3(Zr_{1.75}Ta_{0.25})O_{12}$ coated $Li(Ni_{1/3}Co_{1/3}Mn_{1/3})O_2$ particle. Co: core part, Zr: shell part

variations in coating amount depending on the electrostatic relationship between homogeneous nucleated coating components and cathode particles.

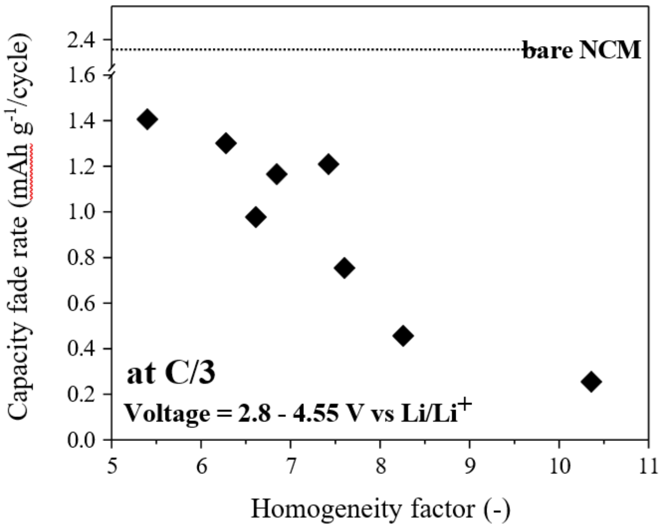

Figure 2. Correlation of coating layer homogeneity on cathode with capacity fade rate

In Figure 2, we illustrated how variations in the homogeneity of the coating layer on cathode particles mitigates the capacity fade rate in conventional LIBs. Through our study, we established an index for the coating layers homogeneity based on the results of XPS quantitative analysis of coating components. A lower homogeneity factor within this index signifies the presence of an island-like structure in the coating layer, while a higher factor suggests a more uniform coverage encapsulating the cathode particles. Our findings confirm that a homogeneous coating relatively protects the cathode particle surfaces against aprotic liquid electrolytes and significantly reducing the capacity fade rate over repeated charge-discharge cycles. Conversely, the presence of a heterogeneous coating layer, resembling an island-like structure, leads to a significant reduction in cell capacity, even when employing the same coating material. These results substantiate the critical role of precisely controlling the homogeneity of the coating layer on cathode particle surfaces in mitigating capacity fade and advancing the performance of LIBs toward greater longevity and reliability.

References

[1] Y. Morino and S. Kanada, *J. Power Sources* **2021**, 509, 230376.

[2] H. Nakamura, T. Kawaguchi, T. Matsuyama, A. Sakuda, T. Saito, K. Kuratani, S. Ohsaki and S. Watano, *J. Power Sources* **2020**, 448, 227579.

[3] J. K. Padarti, Y. Morino, S. Kanada, A. Shiota, S. Hirai and T. Ohno, *Mater. Lett.* **2023**, 347, 134570.

[4] T. Ohno, J. K. Padarti, S. Hirai, T. Matsuda and H. Suzuki, Adv. *Powder Technol.* **2023**, 34, 104247.

Biosynthesis of zinc oxide nanoparticle using clove extract for antimicrobial applications

Tjokorde Walmiki Samadhi,* Vita Wonoputri, Claritta Sukmalovelina, Intan Subadri

Chemical Engineering Department, Faculty of Industrial Technology, Institut Teknologi Bandung, Bandung, Indonesia
*Corresponding author: twsamadhi@itb.ac.id

Biofilm is defined as a collection of microorganisms encased within extracellular polymeric substance (EPS). The presence of biofilm is associated with various problems such as food contamination, fouling of separation membranes, increased resistance to medicine, reduced effectiveness of chlorination in drinking water distribution systems, and others [1-5]. Metal oxide nanoparticles represent a promising tool in overcoming this bacterial resistance due to their antimicrobial and antibiofilm activities [6, 7]. This research investigates the biosynthesis (or green synthesis) of ZnO nanoparticles using aqueous extract of clove flower buds (*Syzygium aromaticum*) and the measurement of their antibiofilm activities. Clove extract is particularly rich in polyphenols [8], which makes it useful as reducing and capping agent in biosynthesis of ZnO via reaction with 0.05 M zinc nitrate solution. The clove extract, prepared by reflux method, showed eugenol peak after 60 mins. Biosynthesis was undertaken at precursor/extract volume ratio of 30/70 and 70/30. A chemical sol-gel synthesized specimen was included for comparison. Dry precipitates produced by the biosynthesis were calcined at 400 °C according to TGA results. Particle morphology and size distribution were characterized by TEM, as presented in Figure 1. Biosynthesized ZnO exhibited severe agglomeration compared to sol-gel ZnO. The smallest nanoparticles were observed for 30:70 biosynthesized ZnO (26.92 nm), followed by 70:30 biosynthesized ZnO (34.98 nm) and sol-gel ZnO (35.69 nm), each with different morphology. Antibiofilm activities were assessed using microtiter plate assay, where 70:30 biosynthesized ZnO indicated the highest activity, producing an approximately 34% reduction of *Escherichia coli* biofilm population. The antibiofilm activity suggested a correlation to different morphologies and ion Zn^{2+} leaching.

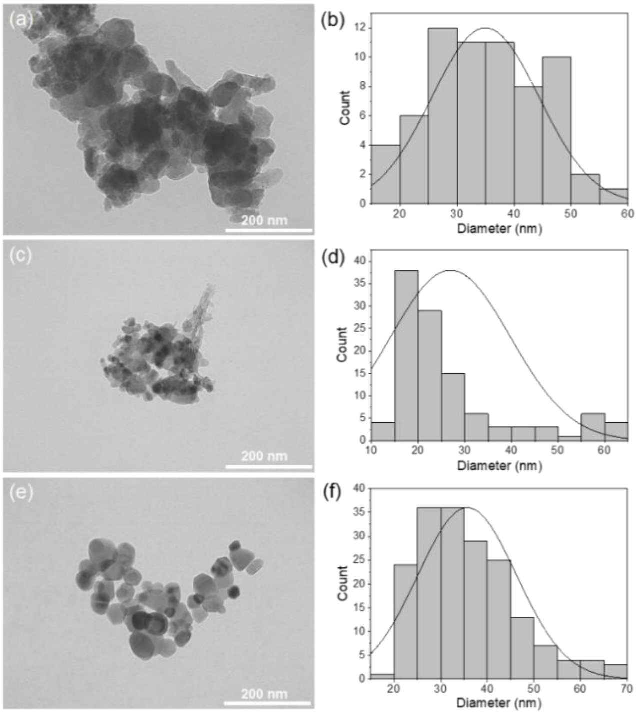

Figure 1. Morphology and size distribution of biosynthesized ZnO nanoparticles (a) precursor/extract = 70/30, (b) precursor/extract = 30/70, and (c) sol-gel

References

[1] G. M. Abebe, *Int. J. Microbiol.* **2020**, 1705814.

[2] T. J. Mpala, A. Etale, H. Richards, L. N. Nthunya, *Env. Sci., Adv.* **2022**, 2013, 39-54.

[3] Y. Xiong, Y. Liu, *Appl. Microbiol. Biotechnol.***2010**, 86, 825-837.

[4] L. Hall-Stoodley, J. W. Costerton, P. Stoodley, *Nat. Rev. Microbiol.* **2004**, 2, 95-108.

[5] V. Wonoputri, C. Gunawan, S. Liu, N. Barraud, L. H. Yee, M. Lim, R. Amal, *ACS Appl. Mater. Interfaces* **2016**, 8, 30502-30510.

[6] A. Raghunath, E. Perumal, *Int. J. Antimicrob. Agents* **2017**, 49, 137-152.

[7] A. Brandelli, A.C. Ritter, F. F. Veras, in M. Rai, R. Shegokar (eds.), *Metal Nanoparticles in Pharma* **2017**, 337-363.

[8] K. I. Ereifej, H. Feng, T. M. Rababah, S. H. Tashtoush, M. H. Al-U'datt, S. Gammoh, G. J. Al-Rabadi, *Food Nutr. Sci.* **2016**, 7, 362-370.

Enhancing the scalability of metal-organic frameworks with copper-crosslinked carboxymethyl cellulose hydrogel support

Paul Kinyanjui Kimani,[a]* Chika Takai-Yamashita,[a,b] Edwin Madivoli[c]

[a]Gifu University, Gifu City, Japan
[b]Institute of Multidisciplinary Research for Advanced Materials, Tohoku University, Sendai City, Japan
[c]Jomo Kenyatta University of Agriculture and Technology, Nairobi City, Kenya
*Corresponding author: paulkimani90.pk@gmail.com

Introduction

Metal-organic frameworks (MOFs) are a category of nanoporous materials formed by the coordination of metal nodes with organic linkers. The easily tuneable porous structure, high crystallinity, large porosity, and high specific surface area of these hybrid materials make them attractive, especially in environmental remediation, including catalysis and adsorption [1].

Metal-organic frameworks (MOFs) have promising potential, but they present certain challenges: their nanoscale dimensions can cause pipe blockages and make recovery processes more complex; their synthesis typically involves the use of toxic chemicals and substantial energy consumption, which restricts their scalability for practical industrial use and commercialisation [2].

Addressing these challenges involves engineering powdered materials into larger architectures, thereby mitigating the shortcomings of MOF materials and rendering them suitable for industrial-scale applications. This enhances their mechanical strength and facilitates easier handling, consequently improving their stability and potential for reuse. Among the methods employed to achieve these macroscopic architectures, supporting MOFs on polymer hosts stands out as a direct, cost-effective, and less complicated approach compared to alternatives such as spray drying and pelletisation [3].

The in-situ growth of MOFs on polymer hosts, though relatively unexplored, is a more environmentally friendly, cheap, and scalable technique compared to directly mixing preprepared MOFs with a suitable polymer. In our study, we explored the potential of carboxymethyl cellulose (CMC) to serve as a platform for the growth of Metal-Organic Frameworks (MOFs). CMC possesses the unique ability to form hydrogels that can be cross-linked by substituting the sodium in CMC with various divalent and trivalent metal ions [4]. We chose CMC for its advantageous characteristics such as biocompatibility, biodegradability, cost-effectiveness, and eco-friendliness. We hypothesised that by crosslinking CMC with copper, the copper ion would provide sites for the nucleation and growth of copper-1,4-benzenedicarboxylate (CuBDC) MOF.

Materials and methods

To initiate the growth of MOFs on the CMC surface, we suspended 4 mmol of terephthalic acid (H_2BDC), and 4 mmol aniline in 40 mL of 2% w/v CMC solution. After vigorous stirring for an hour, the resulting mixture was then slowly added dropwise at a rate of 2 mL/min from a Pasteur pipette nozzle into a 0.2 M copper acetate anhydrous solution. The resulting beads were left in the copper solutions for 24 hrs at room temperature (25°C) before being washed with deionized water and ethanol, and subsequently freeze-dried. We also prepared control beads to evaluate the influence of each component on the hydrogel solution. These included beads made solely from CMC, beads containing CMC and aniline exclusively, and beads composed solely of H_2BDC.

Results and Discussion

The prepared microbeads were spherically shaped but differed in both colour and size (Figure 1). The sky-blue coloured microbeads, typical of copper crosslinked carboxymethyl cellulose, change to a greenish colour with the introduction of aniline moiety. One advantageous aspect of this approach is its ability to regulate the size of the hydrogel beads by adjusting the nozzle size used to dispense the solution.

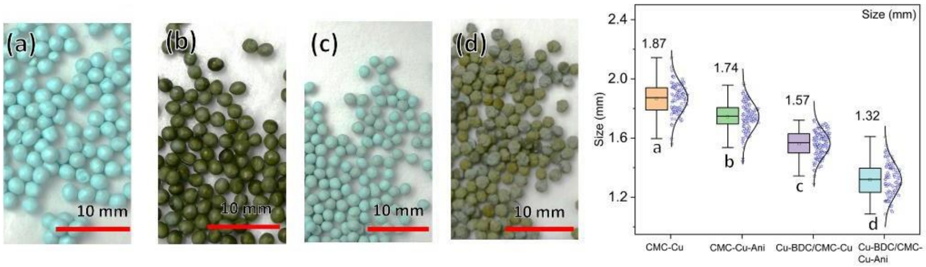

Figure 1. Photographs displaying the prepared beads (a-d) alongside box plots showing their sizes

Only the beads prepared with H_2BDC and aniline exhibited sheet-like folds on their surfaces, decorated with rice-like crystals measuring 483.78±7.29 nanometres (Figure 2b). This indicates that the interaction between aniline and H2BDC molecules facilitated the formation of the crystals. We proposed the idea that the oxidation of aniline on the surface of the beads serves as a template to promote the growth of these crystals. We confirmed these crystals to be Cu-BDC MOF by matching XRD diffraction patterns with the simulated diffraction peaks of Cu-BDC MOF (CCDC No. 687690, Figure 2a). The matched peaks, [0 2 1], [1 3 1], and [2 2 -2] crystallographic planes confirmed the existence of a Cu-BDC layer on the surface of the beads with planes perpendicular to the stacking direction [*5*].

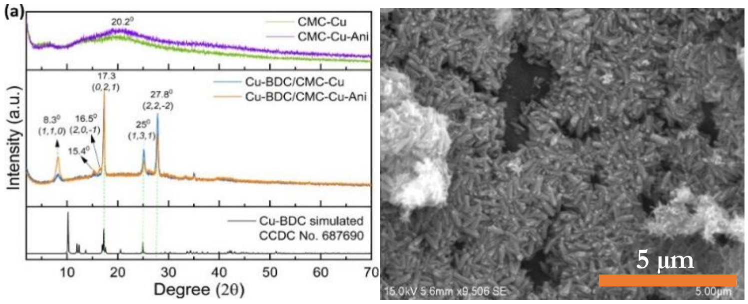

Figure 2. XRD diffraction peaks and SEM micrograph showing the rice-like crystals on the surface of CMC beads

Conclusion

We have developed a method for synthesizing Cu-BDC MOF on carboxymethyl cellulose beads without the use of organic solvents. Aniline played a key role in this process, forming a [Cu-aniline] complex that served as a seeding template for the crystalline material. This method is particularly advantageous due to its scalability, which can be achieved by varying the size of the droplets cast into the copper solution.

References

[1] I. Ihsanullah, *Curr. Opin. Environ. Sci. Health*. **2022**, 26, 100335.

[2] Y. Yao *et al., Small*. **2022**, 18, 2104387.

[3] J. Fonseca, T. Gong, *Coord Chem Rev*. **2022**, 462, 214520.

[4] Z. Ahmadian *et al.*, *Int J Biol Macromol*. **2022**, 253, 126535.

[5] G. Zhan *et al.*, *Adv. Funct. Mater*. **2019**, 29, 1806720.

Enhanced CO_2 hydrogenation performance of modified commercial high entropy alloys

Chunjing Su,[a] Jiaquan Li,[a,] * Jun Huang [a,]*
[a]School of Chemical and Biomolecular Engineering, the University of Sydney, 2008, Sydney, Australia
*Corresponding author: jiaquan.li@sydney.edu.au

The hydrogenation of CO_2 is a crucial process for mitigating anthropogenic CO_2 emissions into the atmosphere and yielding C1 chemicals that can be utilized as fuels and valuable precursors for chemical synthesis. High-entropy alloys (sHEAs) have widespread application across various fields owing to their exceptional thermal stability and tunable microstructure. However, their potential application as catalysts is often limited by the low exposure of active sites. In this study, we utilized commercial CoCrNiFeMn HEAs powder for atmospheric pressure CO_2 hydrogenation reaction and promoted its catalytic performance by a combined treatment of ball milling and high-temperature H_2 reduction. The high-energy ball milling induces a morphological transition in CoCrNiFeMn HEAs, shifting its shape from spherical to irregular. This transformation leads to a significant reduction in particle size and the addition of more surface reactive sites. The subsequent high-temperature H_2 reduction triggers the atomic rearrangement on the CoCrNiFeMn surface, thereby improving its alloy structural homogeneity. These modifications enhance the catalyst's performance in CO_2 hydrogenation. This work introduces a facile modification approach to bolster the catalytic efficiency of commercial HEAs in CO_2 hydrogenation processes with high selectivity.

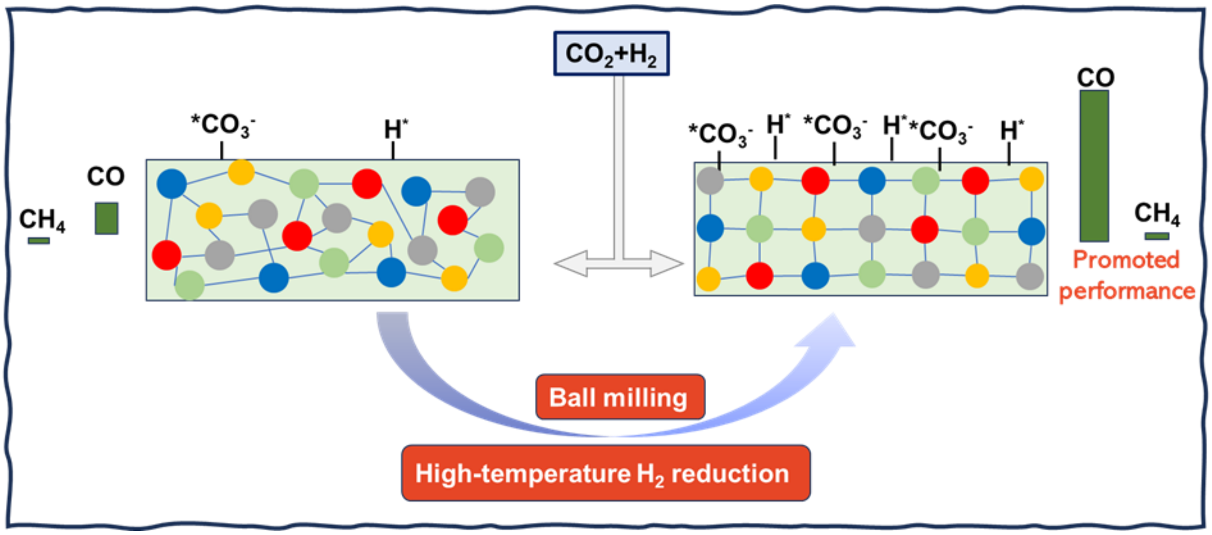

Figure 1. Graphical abstract

Electrostatic particle assembly technique for formation of structurally controlled composite granules

Wai Kian Tan,* Koki Iwata, Keita Tsuzuki, Go Kawamura, Atsunori Matsuda, Hiroyuki Muto

Toyohashi University of Technology, Toyohashi, Japan
*Corresponding author: muto@ee.tut.ac.jp

In fabrication of multifunctional materials exhibiting desired properties, advanced processing technique plays an important role in composite materials design and efficient utilization of additives [1]. A controlled formation and design of composite particles and composite granules using nano- or microscale-sized particles can be achieved using electrostatic assembly of particles. These composite particles and granules exhibit a desired structure, enabling simple processing of via powder metallurgy for fabrication of novel functional composites. Spherical composite granules with improved handling ability are preferred compared to their powder counterpart for rapid and scalable processing. However, it remains a challenge to control the distribution of nanosized particles within composite granules, as this would affect the final microstructure, and hence the properties of the bulk composite.

In this presentation, a feasible controlled incorporation of functional additives at the shell layer of composite granules via electrostatic integrated granulation is demonstrated [2, 3]. The processing of these composite granules led to the formation of connected structural network, enabling the efficient usage of additive materials in bulk composite fabrication. Using carbon nanotubes (CNT), alumina (Al_2O_3) and zirconia (ZrO_2) particles, a feasible controlled formation of core-shell composite granules consisting of a CNT embedded alumina Al_2O_3-ZrO_2 composite shell with a core of Al_2O_3–ZrO_2 were fabricated. The cross-sectional images of a spark plasma sintered artifact obtained using the CNT-incorporated shell-layer Al_2O_3–ZrO_2 composite granules are shown in Figure 1. A mesh-like interconnected network (greyish), which was the CNT-incorporated Al_2O_3–ZrO_2 composite shell can be observed surrounding the Al_2O_3–ZrO_2 granules' core (white). The electrical conductivity of the sintered artifacts obtained using CNT-incorporated shell-layer Al_2O_3–ZrO_2 composite granules was higher (approximately 15 times) than those obtained when CNT was homogeneously distribution within the Al_2O_3–ZrO_2 composite granules (same amount of CNT incorporation at 0.4 vol%). These findings indicate that a feasible formation of structurally controlled composite granules can be obtained using electrostatic particle assembly technique with good prospect for scalable novel composites fabrication.

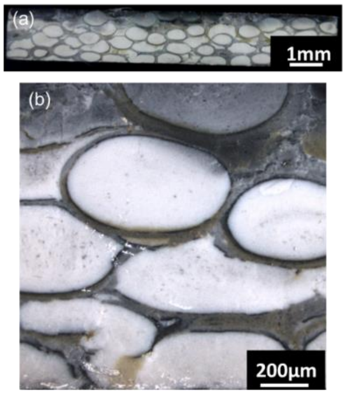

Figure 1: Cross-sectional microscope images of a sintered artifact obtained using the CNT-incorporated shell-layer Al_2O_3–ZrO_2 composite granules at (a) low and (b) high magnification.

References

[1] K. Ishii, A. Yokoi, Y. Sato, K. Hikima, G. Kawamura, W.K. Tan, H. Muto, A. Matsuda, T. Uchikoshi, M. Fuji, *Adv. Powder Technol.* 35, **2024**, 104430.

[2] H. Muto, Y. Sato, W. K. Tan, A. Yokoi, G. Kawamura and A. Matsuda, *Nanoscale*, **2022**, 14, 9669-9674.

[3] T. Nakazono, A. Yokoi, W. K. Tan, G. Kawamura, A. Matsuda and H. Muto, *Nanomaterials*, **2023**, 13, 199.

Spray drying synthesis of alginate particles for enzyme encapsulation

Yilun Weng

The University of Queensland, Brisbane, Australia
*Corresponding author: y.weng@uq.edu.au

Alginate-based materials are widely applied in various industries for the good biocompatibility, bioavailability, non-toxicity, and stability. Food and feed industry are one of the alginate's industrial applications, where alginate can be used as coating materials to encapsulate bio-active ingredients such as enzymes to improve their stability.

In animal feed industry, to reduce animal feed cost, optimize animal performance, and improve process sustainability, exogenous enzymes are frequently utilized as feed additives. Phytase is a common enzyme in animal feed industry, due to its well-recognized ability to enhance the digestion and absorption of phosphorus, by catalyzing the hydrolysis of indigestible phytic acid (inositol hexakisphosphate) in animal feed to a highly digestible form. However, the application of phytase in industry has been greatly limited due to its low thermal stability. Animal feeds are pelleted at temperatures up to 105 °C to kill harmful bacteria. During the steam pelleting process, phytase can lose up to 80% of its activity due to moisture and elevated temperatures.

Enzyme encapsulation in alginate particles via spray drying has shown great potential for improving enzyme thermal stability, however, limited enzyme loading capacities and bioavailability remains a challenge. In the present work, a scalable enzyme encapsulation method was developed to stabilize enzyme against heat, using alginate as the coating material, and the bioavailability of the encapsulated enzyme was studied in vivo. The alginate particles were synthesized using a scalable spray drying method, and the physicochemical properties of the particles were characterized using a range of analysis techniques. The thermal stability of the enzyme was improved by 60%, and a high enzyme loading of 48% (w/w) was achieved.

Novel metal-organic frameworks (MOFs) series: UC-MUFs

Soongseok Yoon[a,b], Agung Bagus Pambudi[b,c], Daisong Chen[d,e], Jin Shang[d,e], Shane G. Telfer[b,f], Ben Hang Yin[b,c], Jungkyu Choi[g], Alex C. K. Yip[1,2*]

[a]Department of Chemical and Process Engineering, The University of Canterbury, Christchurch, New Zealand
[b]The MacDiarmid Institute for Advanced Materials and Nanotechnology, Wellington, New Zealand
[c]Paihau-Robinson Research Institute, Faculty of Engineering, Victoria University of Wellington, Wellington, New Zealand
[d]School of Energy and Environment, City University of Hong Kong, Hong Kong SAR, PR China
[e]City University of Hong Kong Shenzhen Research Institute, Shenzhen, PR China
[f]School of Natural Sciences, Massey University, Palmerston North, New Zealand
[g]Department of Chemical and Biological Engineering, Korea University, Seoul, Republic of Korea
*Corresponding authors: alex.yip@canterbury.ac.nz

The novel metal-organic framework (MOFs) series is developed from the Massey University Frameworks (MUFs) series; the University of Canterbury-Massey University Frameworks (UC-MUFs). Beyond simulation, the UC-MUFs have been investigated through synthesis experiments. The original UC-MUF is composed of copper (II) acetate monohydrate and isophthalic acid as metal ions and organic ligands, respectively. The UC-MUF can be functionalised by using other organic ligands, and two functionalised UC-MUFs (UC-MUF-OH and UC-MUF-CH_3) are found. TGA result shows that the UC-MUF series has thermal stability up to 250 °C, and the decomposition of frameworks starts around 300 °C to 350 °C. The structure of the UC-MUF series is analysed through the SEM, and the hexagonal shape is shown from the three UC-MUF series. In addition, the size of particles of the UC-MUF series is changed depending on functionalised organic ligands in the UC-MUF series. Furthermore, the gas physisorption test is studied to analyse its gas adsorption performance. According to the result, three UC-MUF series show good CO_2/N_2 adsorption selectivity.

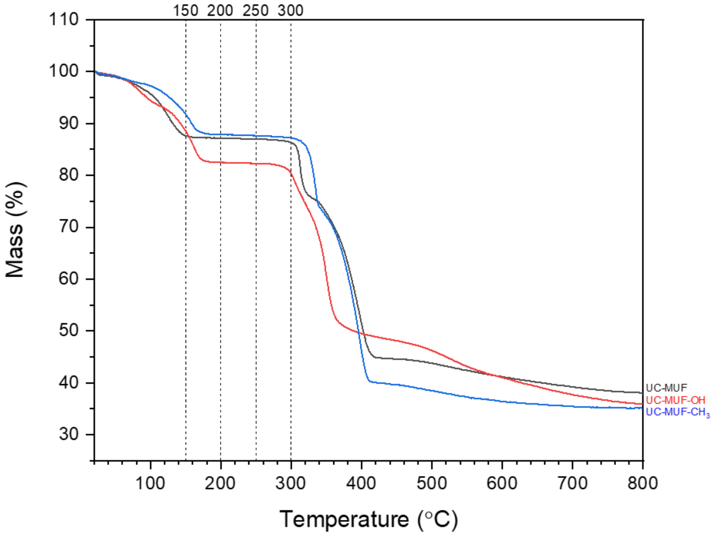

Figure 1. TGA graph of three UC-MUFs in N_2 environment.

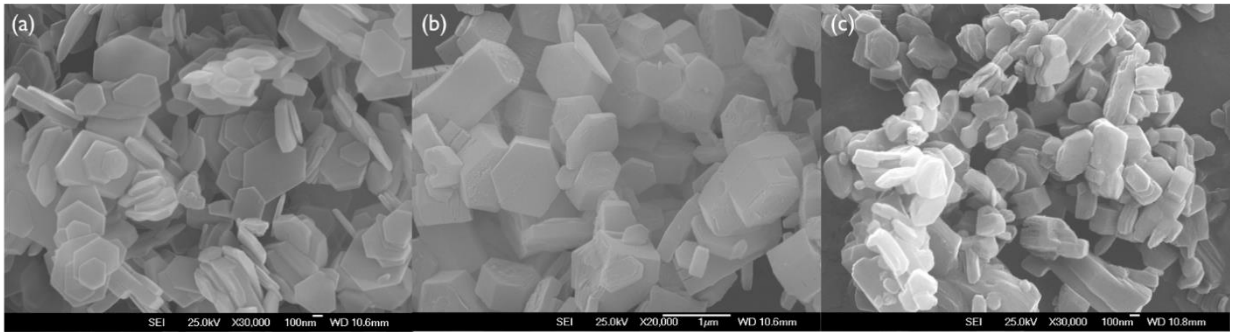

Figure 2. SEM images of the UC-MUFs; **(a)** UC-MUF, **(b)** UC-MUF-OH, and **(c)** UC-MUF-CH_3.

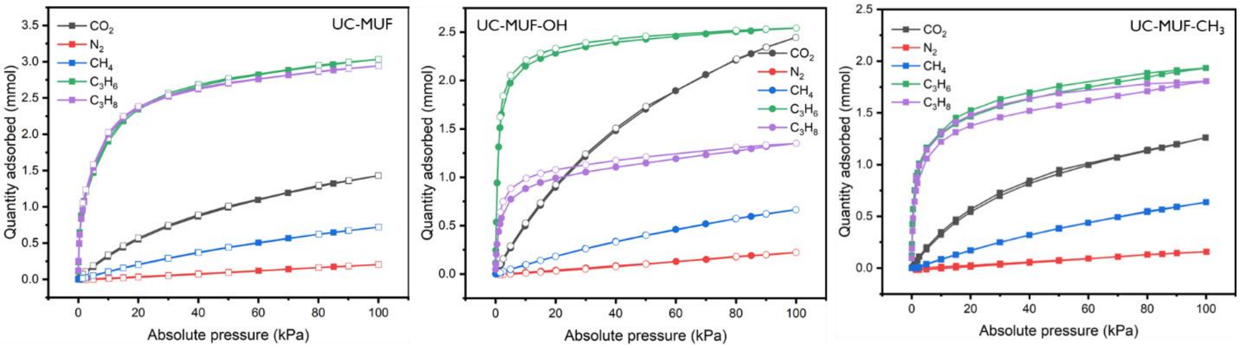

Figure 3. Gas physisorption data of the UC-MUFs.

References

[1] R. K. Deshpande, J. L. Minnaar, S.G. Telfer, *Angew. Chem.*, **2010**, 122, 4702-4706

[2] O. T. Qazvini, R. Babarao, Z.-L. Shi, Y.-B. Zhang, S. G. Telfer, *J. Am. Chem. Soc.*, **2019**, 141, 5014-5020

[3] O. T. Qazvini, L. K. Macreadie, S. G. Telfer, *Chem. Mater.*, **2020**, 32, 6744-6752

[4] O. T. Qazvini, S. G. Telfer, *J. Mater. Chem. A*, **2020**, 8, 12028-12034

0D-2D heterostructures of SnO_2 QDs-metallic sulphide nanomaterials for room-temperature NH_3 sensing

Jinzhou Bai,[a] Yanbai Shen,[a,]* Sikai Zhao,[a] Cong Han[a]

[a]School of Resources and Civil Engineering, Northeastern University, Shenyang, China
*Corresponding author: shenyanbai@mail.neu.edu.cn

Traditional metal oxide semiconductor gas sensors are facing significant challenges for portable devices and integration due to large power consumption caused by high operating temperature. Two-dimensional (2D) nanomaterials with large specific surface areas, rich active sites, and tunable electrical properties are proved to be promising candidates for room-temperature gas sensors. However, several disadvantages including weak response, sluggish response/recovery kinetics, and poor selectivity still need to be overcome for high-performance gas sensors. Rational design of heterostructure between zero-dimensional (0D) quantum dots and 2D nanomaterials may offer a possible way to solve the problems. Herein, SnO_2 quantum dots (QDs) with an average diameter of 3 nm were functionalized with metallic sulphide nanosheets (MoS_2 and SnS_2) via hydrothermal approach. SnO_2 QDs-MoS_2 and SnO_2 QDs-SnS_2 nanocomposites both exhibit excellent sensing properties to NH_3 with fast response speed and good repeatability, high selectivity, and long-term stability at room temperature. Especially, the optimal sensor based on SnO_2 QDs-MoS_2 nanomaterials shows a high response of 8.6 and short response/recovery times of 6 s/121 s to 100 ppm NH_3 at room temperature of 25 °C.

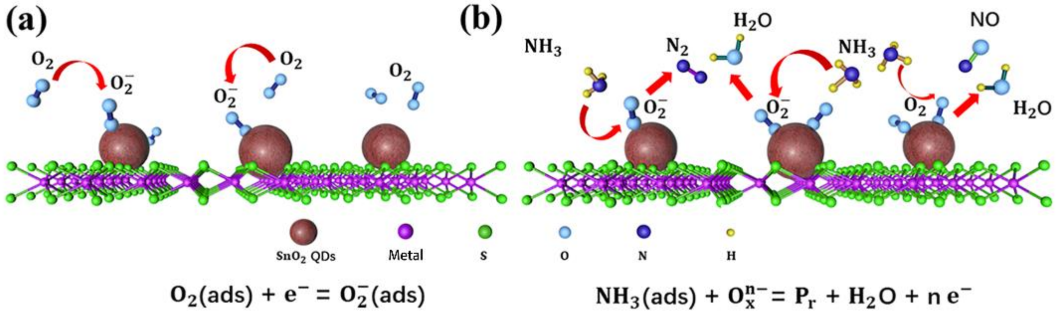

Figure 1. Schematic illustration of NH_3 sensing process of SnO_2 QDs-MoS_2 and SnO_2 QDs-SnS_2 nanocomposites.

References

[1] J.Z. Bai, Y.B. Shen, S.K. Zhao, Y.S. Chen, G.D. Li, C. Han, D.Z. Wei, Z.Y. Yuan, F.L. Meng, *SENSOR ACTUAT B-CHEM* **2022**, 353, 131191.

[2] J.Z. Bai, Y.B. Shen, S.K. Zhao, A. Li, Z.K. Kang, B.Y. Cui, D.Z. Wei, Z.Y. Yuan, F.L. Meng, *ADV MATER TECHNOL-US* **2023**, 8, 220167.

Synthesis of SW/MWCNTs from flare gas: a comparative study on catalyst preparation methods and process optimization

Chawalkul Chotmunkhongsin,[a] Paeka Klaitong,[a] Sunisa Watcharasing,[b] Tawatchai Charinpanitkul,[c]
Sakhon Ratchahat,[a] Weerawut Chaiwat[a,]*

[a]Department of Chemical Engineering, Faculty of Engineering, Mahidol University, Nakhon Pathom, Thailand
[b]Technology Management Division, PTT Exploration and Production Public Company Limited, Bangkok, Thailand
[c]Center of Excellence on Particle Technology and Material Processing, Faculty of Engineering, Chulalongkorn University, Bangkok, Thailand
*Corresponding author: weerawut.cha@mahidol.ac.th

In petroleum and petrochemical industries, flare gas, which consists of methane as its major composition has been abundantly wasted by combustion to largely emit CO_2 to the atmosphere. Recently, conversion of methane and hydrocarbon gases into value-added carbonaceous materials such as carbon nanotubes (CNTs) has been paid attention toward net zero emission policy. In CNT synthesis, well-dispersion of metal catalyst on metal oxide supports is one of key steps in catalyst preparation procedures, leading to the quality of the CNTs synthesized from hydrocarbons through catalytic chemical vapor deposition (CCVD). This study conducted a comparative analysis of three different preparation methods for 10% FeMo/MgO catalysts with Fe:Mo ratio at 2:1 (w/w), namely I. incipient impregnation, II. hydrothermal method, and III. sol-gel method with various additives for synthesis of CNTs from methane as a representative of flare gas as demonstrated in Figure 1. The aim of this study is to achieve optimal performance among three different preparation methods of FeMo/MgO catalyst in order to synthesize single-walled and multi-walled carbon nanotubes (SW/MWCNTs) from methane at various concentrations (25–100 vol% with N_2 balance) through CCVD process at 900 °C by varying reaction time (10–180 min). The CCVD experiments in this study excluded H_2 during reduction of the catalyst by directly utilizing H_2 from CH_4 decomposition, aiming for smaller- diameter CNTs. Techno-economic analysis revealed that the incipient impregnation was considered as the most cost-effective method due to its simplicity, while sol-gel method turned up as the most expensive one with its complexity and environmental concerns. However, despite its affordability, incipient impregnation demonstrated inferior catalyst performance for CNT production compared to that obtained from the hydrothermal method, which exhibited relatively high productivity (>40 wt% in carbon yield) with better SW/ MWCNT's quality (<10 nm in CNT diameter, $I_G/I_D > 3$ in its graphitization analyzed by Raman spectroscopy). Further optimization in CCVD process conditions, including reaction time, catalyst amount, catalyst bed length, and methane concentration was subsequently conducted. It was found that, a longer reaction time led to increases in product yields in terms of gCNT/gCatalyst with lower carbon yields. More loaded catalyst amount resulted in greater gCNT/gCatalyst of CNT products with relatively larger CNT diameter. Moreover, the effect of catalyst bed length showed significant variations in product composition due to H_2 reduction of the catalyst from methane dissociation. This catalyst reduction led to the formation of a metallic structure, resulting in higher yields but larger CNT diameter as discussed in our previous work [1]. Optimal methane concentration at 25 vol% in N_2 was also achieved, resulting in the highest carbon yield and gCNT/gCatalyst without significant changes in SW/MWCNT properties. According to the results in this study, it could be a preliminary guideline for SW/MWCNT production from wasted flare gas in an industrial scale with an appropriate prepared catalyst and CCVD process condition.

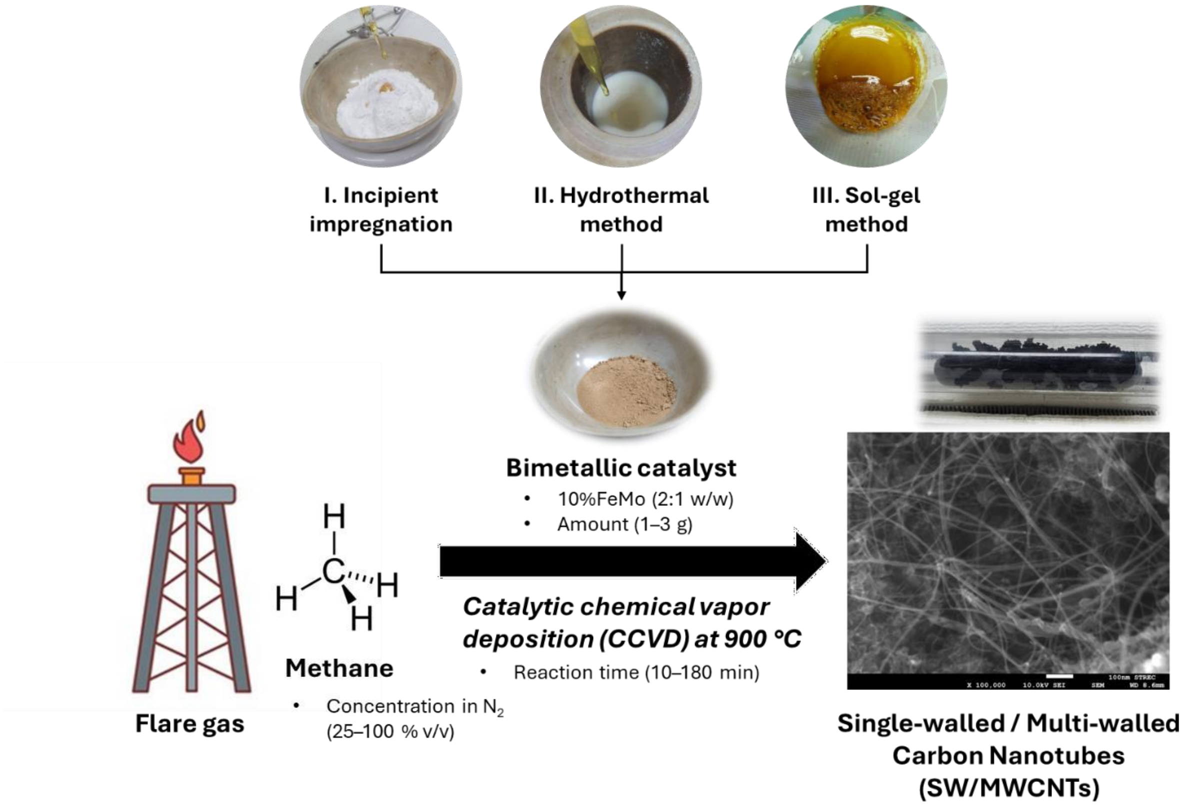

Figure 1. Conceptual diagram of a comparative study on catalyst preparation methods and process optimization for synthesis of SW/MWCNTs from flare gas.

References

[1] C. Chotmunkhongsin, S. Ratchahat, W. Chaiwat, T. Charinpanitkul, A. Soottitantawat *Sci. Rep.* **2023**, 13(1), 21027.

Synthesis of metal-organic framework CALF-20 via mechanochemical route

Shumpei Yonetsu,[a] Shota Kitai,[a] Yuto Higuchi,[a,b,c] Shunsuke Tanaka,[a,b,c]* Saki Moriya,[d] Miki Sugita,[d] Takahiko Takewaki[d]

[a]Graduate School of Science and Engineering, Kansai University, Osaka, Japan
[b]Department of Chemical, Energy and Environmental Engineering,
Faculty of Environmental and Urban Engineering, Kansai Univ., Osaka, Japan
[c]Organization for Research and Development of Innovative Science and Technology, Kansai Univ., Osaka, Japan
[d]Science & Innovation Center, Mitsubishi Chemical Corporation, Kanagawa, Japan
*Corresponding author: shun_tnk@kansai-u.ac.jp

Introduction

Technology to effciently separate and recover CO, has been attracting attention to the great challenge ofclimate change that humanity faces. Curently, the amine liquid-based chemical absorption method is themainstream for CO, capture industy, but this method reguires a large amount of heat energy forregeneration. Recently, solid adsorption processes using pressure swing adsorption (PSA), themal swingadsorption (TSA), and pressure and thermal swing adsorption (PTSA) have attracted attention because thespecific heat of solids is much lowver than that of liquids. Among solid adsorbents, metal-organicfameworks (VOFs) have recently attracted much attention. OFs are porous metal complexes consisingof coordination bonds between metals and organic ligands. It has emerged as an altemnative porous materialto zeolites due to the high stuctural designability based on infmite combination possibilities because theyare composed of metal and organic materials.

H2O molecules normally occupy the CO2 adsorption sites of adsorbents and inhibit CO2 adsorption. Therefore, adsorption processes using zeolites often require a dehydration process before CO2 separation. A material that can selectively adsorb CO2 in the presence of H2O would reduce the energy required for the process. Calgary Framework 20 (CALF-20) , a type of MOFs, has attracted a great deal of attention as an ideal material for next-generation enegy efficient carbon capture.

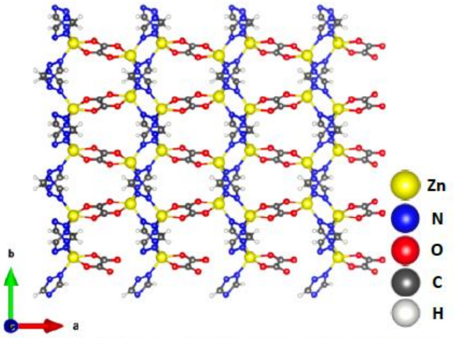

Figure 1 Schematic diagram of CALF-20

We focused on CALF-20 consists of zinc, 1,2,4-tirazolate, and oxalate (Figure 1), which has high durability against steam and does not adsorb much H2O at low relative humidity (<10%). It can selectively adsorb CO2 in the presence of H2O, making it a promising material for carbon capture. In previously reported methods, CALF-20 has been synthesized mainly by a solvothermal method requiring 48 hours [1, 2]. Here, we provide a new route to synthesize CALF-20 with extremely small particle size by mechanochemical treatment.

Experimental section

1.CALF-20-ST synthesis (Solvothermal route: ST): 2.24 mmol of zinc oxalate dihydrate and 24.4 mmol of 1,2,4-triazole were stirred in methanol/H2O mixture (methanol: H2O = 30 : 20 [mL]) for 1 hour. The resulting white suspension was transferred to a Teflon container and placed in an oven at 180 °C for 48 hours. The white powder product was washed and dried.

2.CALF-20-MC synthesis (Mechanochemical route: MC): 2.24 mmol of zinc oxalate dihydrate, 24.4 mmol of 1,2,4-triazole, and 10 mL of methanol were milled with ZrO2 balls (φ10) x 50 in a 250 mL ceramic pot at a rotation rate of 150 rpm for 2 hours at room temperature by using a planetary mill. The white powder product was washed and dried

3.CALF-20-MC-K synthesis (Mechanochemical route assisted by KOH: MC-K): 0.774 mmol of zinc carbonate hydroxide, 4.72 mmol of oxalic acid, 24.4 mmol of 1,2,4-triazole, 4 mL of methanol, and 1 mL of 5M potassium hydroxide were milled with ZrO2 balls (φ10) x 50 in a 250 mL ceramic pot at a rotation rate of 150 rpm for 2 hours at room temperature by using a planetary mill. The white powder product was washed and dried

Results and discussion

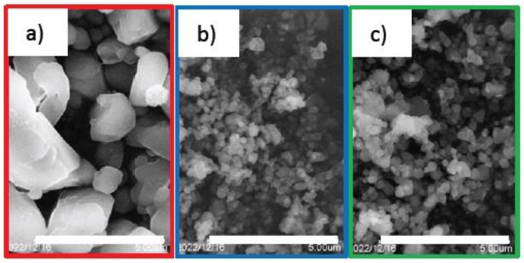

Figure 2 SEM images of the products, a) CALF-20-ST, b) CALF-20-MC, c) CALF-20-MC-K, scale bar: 5 μm

CALF-20-ST was synthesized using the conventional solvothermal method. The crystal structure of CALF-20 was also confirmed in CALF-20-MC and CALF-20-MC-K synthesized via the new mechanochemical route. In the mechanochemical method, the raw material particles collide with other raw material particles and the mill vessel wall to generate a localized and extremely short-lived high-energy reaction field, which is then used to synthesize CALF-20. The mechanical stresses resulted in particle refinement (Figure 2) and also synthesis time was significantly shortened compared to the solvothermal method. It was found to be possible to synthesize CALF-20 without heating and increasing pressure. Although these results demonstrated the possibility of CALF-20 synthesis via the mechanochemical route, to increase the variation of the synthesis process, CALF-20 synthesis using zinc carbonate hydroxide instead of zinc oxalate dihydrate as zinc source was also investigated. When zinc oxalate dihydrate was not used, it was necessary to use an alternative raw material capable of supplying oxalate to construct the framework. Therefore, mechanochemical synthesis was conducted with zinc carbonate hydroxide, oxalic acid, and methanol, but PXRD results showed that

the crystal structure of CALF-20 could not be obtained. When oxalic acid was used, the synthesis was under acidic conditions, and a product different from CALF-20 was obtained. This was because acidic conditions inhibited the deprotonation of 1,2,4-triazole. Therefore, a base was added to bring the reaction closer to the conditions under which 1,2,4-triazole is deprotonated. Here, the addition of KOH gave the final product with crystal structure of CALF-20.

Conclusions

We have provided a new synthetic route for CALF-20 with extremely small particle sizes using mechanochemical treatment. Compared to the previously reported solvothermal method, the synthesis time was reduced to just 2 hours and a simple mechanochemical route was developed.

References

[1] J.-B. Lin et al., *Science* **2021**, 374, 1464-1469.

[2] Y. Wei et al., *RSC Adv.* **2022**, 12, 18224-18231.

Synthesis of gmelinite zeolite particles toward selective CO_2 recovery

Yuto Higuchi,[a,b*] Shunsuke Tanaka[a,b*]

[a]Department of Chemical, Energy and Environmental Engineering, Kansai University, Suita-shi, Japan [b]Organization for Research and Development of Innovative Science and Technology, Kansai University, Suita-shi, Japan
*Corresponding author: yhiguchi@kansai-u.ac.jp, shun_tnk@kansai-u.ac.jp

Introduction

Zeolite, which is one of the microporous materials, has been applied to adsorbents, ion exchangers, and catalysts. Nowadays, zeolites have attractive to capture CO_2 molecules in flue gas emitted from power plants toward carbon dioxide capture, utilization, and storage (CCUS). Zeolites with a low Si/Al ratio can contain a lot of counter-cations in the zeolite framework to maintain charge balance of the framework. These counter-cations cause an electrostatic interaction for molecules with intermolecular polarity such as CO_2, meaning that zeolites have possibility to capture CO_2 molecules selectively. In general, zeolite is crystallized using silicon, aluminium sources and organic-structure directing agent (OSDA), which constructs the ordered zeolite framework but requires OSDA-removing process via calcination using high thermal energy, and then nitrogen oxides produced in calcination must be recovered. Thus, more eco- friendly zeolite synthesis process has been required. Nowadays, interzeolite transformation process, which makes one zeolite be directly transformed into another zeolite, has a possibility to establish OSDA-free zeolite synthesis procedure. In previous, we challenged to synthesize zeolites via OSDA-free interzeolite transformation process [1,2]. In this study, we synthesized gmelinite (GME) zeolite particles, which showed high CO_2 adsorption capacity, using faujasite (FAU) zeolite particles via steam-assisted interzeolite transformation process.

Experimental section

Firstly, 3.0 g of H^+-type FAU zeolite particles with Si/Al = 2.8 and 0.5 g of NaOH granular pellets were placed in a ceramic pot (250 mL) containing five zirconia balls (D = 10 mm) and then they were milled at 150 rpm for 30 minutes at room temperature. The resultant powder was transferred to Teflon-lined stainless-steel autoclave along with 3.0 g of H_2O as steam source separately. The autoclave was heated at 403 K for 4–24 h. The final powder was washed with deionized water to remove excess alkaline compounds until the wash water attained pH = 7 and then dried at 373 K overnight.

Results and discussion

In PXRD patterns of products synthesized at 403 K for 4–24 h via steam-assisted interzeolite transformation process using H^+-type FAU zeolite, the PXRD patterns of GME zeolite raised from 4 h and the PXRD patterns of FAU zeolite disappeared completely after 24 h. In addition, particle morphology of zeolites changed with increase in heating time. Hexagonal prism particles appeared from 4 h, indicating that FAU zeolite with angular particles was transformed into GME zeolite with hexagonal prism particles. After 24 h, the hexagonal prism particles only appeared. The particle morphology of GME zeolite was in accordance with the crystal system of GME framework, which is the hexagonal system. The plane orientation of (002) was parallel to the bottom of the hexagonal prism and (002) plane was assigned to diffraction peak at $2\theta=17.8^\circ$ of GME zeolite (Figure 1). Furthermore, (100) and (101) planes were assigned to the diffraction peaks at $2\theta=7.42^\circ$ and 11.48°, respectively. Therefore, the particle morphology of GME zeolite was in accordance with the plane orientation of GME framework (Figure 1). Finally, Gas adsorption performance of a GME zeolite was investigated. Brunauer-Emmett-Teller surface area (S_{BET}) and micropore volume (V_{micro}) of GME zeolite (S_{BET} = 66 $m^2\ g^{-1}$, $V_{micro} = 2.5\times10^{-2}$ $cm^3\ g^{-1}$) were lower than that of parent FAU zeolite (S_{BET} =

1,132 m^2 g^{-1}, V_{micro} = 0.44 cm^3 g^{-1}). On the other hand, CO_2 uptake of GME zeolite was 6.4 mmol g^{-1} at P_{CO_2} = 100 kPa and higher than that of parent FAU zeolite (Figure 2 left). The position of cation sites in zeolite framework resulted in the CO_2 adsorption performance of each zeolite. In case of GME zeolite, counter-cation influencing CO_2 adsorption existed in the straight channels, which were CO_2 diffusion path of GME framework. Therefore, CO_2 was adsorbed on counter-cations in GME framework and then CO_2 uptake increased sharply. In addition, CO_2 uptake of GME zeolite was higher than N_2 and CH_4 uptakes (Figure 2 right), resulting in that GME zeolite has a possibility to adsorb CO_2 selectively in CO_2/N_2 and CO_2/CH_4 systems. In other words, GME zeolite is expected to be applied to CO_2 recovery system on behalf of previous zeolites.

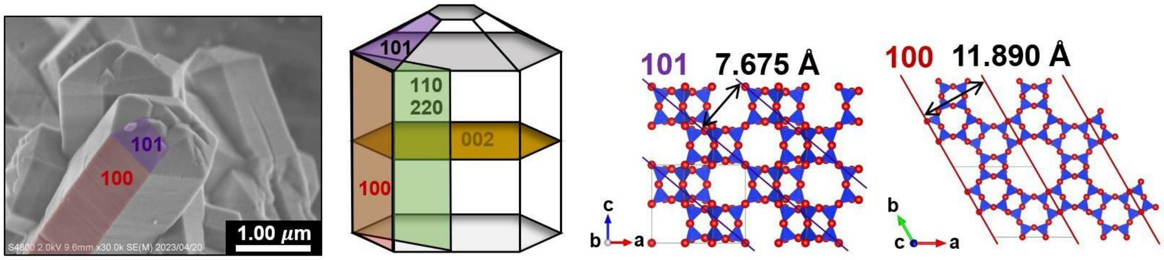

Figure 1. Relationship between particle morphology and crystal plane of GME zeolite.

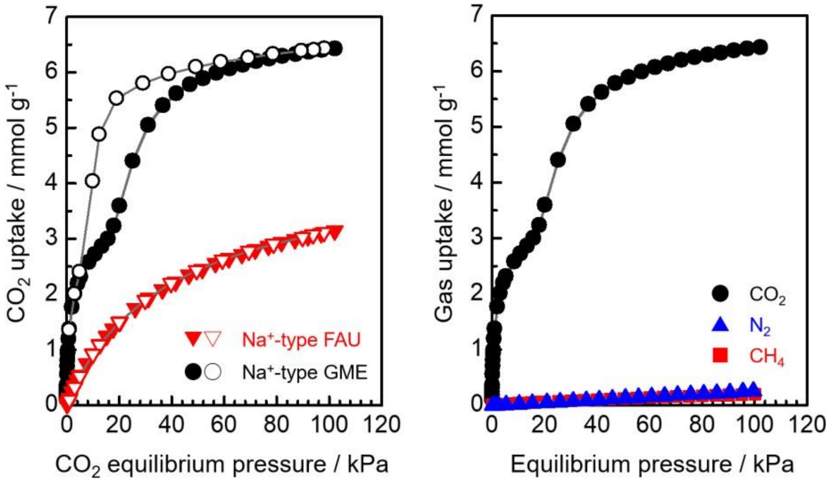

Figure 2. (Left) CO_2 adsorption/desorption isotherms of Na^+-type GME and FAU zeolites, and (Right) CO_2, N_2, CH_4 adsorption isotherms of Na^+-type GME zeolite at 298 K (closed symbol; adsorption, open symbol; desorption).

References

[1] Y. Higuchi, S. Miyagawa, S. Tanaka, *CrystEngComm* **2022**, 24, 3859-3864.

[2] Y. Higuchi, S. Tanaka, *Microporous Mesoporous Mater.* **2023**, 354, 112550.

Synergistic improvement in gas separation performance of MMMs by porogenic action and strong molecular forces of nano particle

Yan Dai,[a,]* Yaping Ding,[a,b] Huahao Wang[a, b]

[a] Liaoning Key Laboratory of Chemical Additive Synthesis and Separation, Panjin Institute of Industrial Technology,
Dalian University of Technology, Liaoning, China
[b] School of Petrochemical Engineering, Shenyang University of Technology, Liaoning, China
*Corresponding author: daiyan@dlut.edu.cn

In the present study, nano particle (ZIF-93 metal–organic frameworks) were prepared. N_2 adsorption tests revealed that the particle size, specific surface area, and pore size of nano particle were 30 nm–45 nm, 869.40 m^2/g, and 0.36 nm, respectively. Pebax-based mixed matrix membranes (MMMs) were prepared using nano particle as the filler. The pore diameters of nano particle lied between the kinetic diameters of CO_2 and N_2; Thus, its pore structure provided a fast transfer channel for CO_2 and increased the permeability of the membrane. Further, X-ray diffraction showed that the membrane became denser upon introducing nano particle because of the formation of a bridging structure between the Pebax molecular chains and nano particle. A denser stacking by moving the Pebax molecular chains closer to each other effectively bettered the CO_2 selectivity of the mixed matrix membrane. The test results showed that when the nano particle loading was 10 wt.%, the CO_2 permeability was 84.85 barrer and the CO_2/N_2 selectivity was 65.76 at 0.4 MPa, which are 51.57 % and 65.50 % higher than those of the pure Pebax membrane, respectively. When the feed pressure was increased to 0.8 MPa, the CO_2 permeability was 94.5 barrer and the CO_2/N_2 selectivity is 87.5, which are 51.57 % and 65.50 % higher compared with those of the pure Pebax membrane, in order. The membrane performance significantly exceeded that of the 2008 Robeson curve.

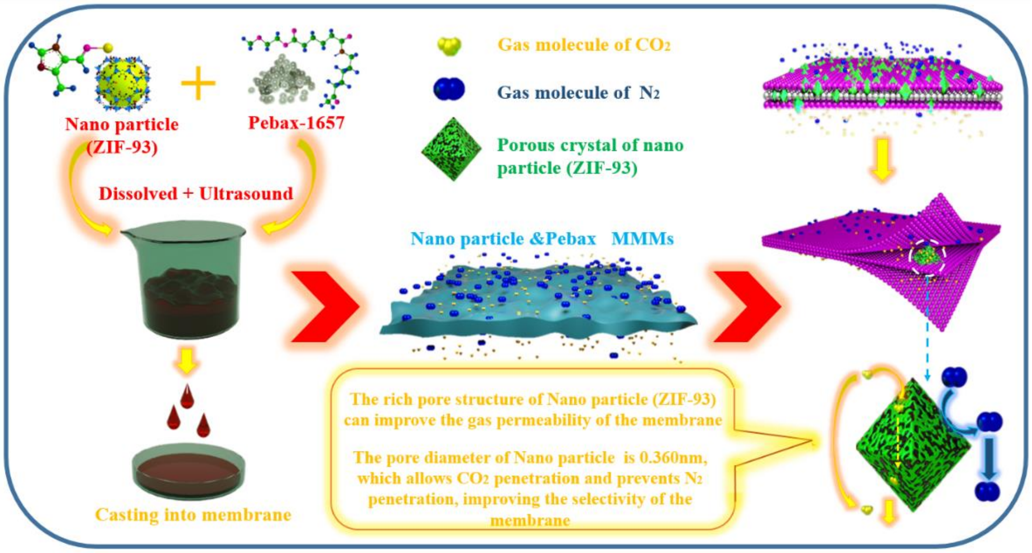

Figure 1. Graphical Abstract

Mechanochemically assisted synthesis of magnetite nanoparticles for the catalytic removal of methylene blue

Takahiro Onizuka,[a] Tomohiro Iwasaki [a,*]

[a] Department of Chemical Engineering, Osaka Metropolitan University, Osaka, Japan
*Corresponding author: tomohiro.iwasaki@omu.ac.jp

1. Introduction

Magnetite (Fe_3O_4) nanoparticles have been actively studied due to its excellent magnetic and catalytic properties [1, 2]. Among such properties, the usage of magnetite nanoparticles as heterogeneous Fenton catalyst, which can degrade organic compounds, has attracted a lot of interest for water purification [3]. However, magnetite nanoparticles prepared via conventional synthesis routes tend to show relatively low catalytic activity. In this work, a novel mechanochemically assisted synthesis of magnetite nanoparticles was conducted. The catalytic degradation of methylene blue by heterogeneous Fenton-like reactions was studied.

2. Experimental

Magnetite nanoparticles can be formed by the following reactions in our process. First, the crystal water of ferric chloride hexahydrate is released by high-energy ball-milling.

$$FeCl_3 \cdot 6H_2O \rightarrow Fe^{3+} + 3Cl^- + 6H_2O \qquad (1)$$

Next, urea is hydrolyzed with the released water in the heating stage.

$$(NH_2)_2CO + 3H_2O \rightarrow 2NH_4^+ + 2OH^- + CO_2 \qquad (2)$$

Simultaneously, Fe^0 is released from steel balls during the milling and then oxidized.

$$Fe^0 \rightarrow Fe^{2+} + 2e^- \qquad (3)$$

Finally, magnetite is formed according to the following reaction.

$$Fe^{2+} + 2Fe^{3+} + 8OH^- \rightarrow Fe_3O_4 + 4H_2O \qquad (4)$$

In the experiments, 2 mmol of $FeCl_3 \cdot 6H_2O$ and 4 mmol of $(NH_2)_2CO$ were placed in a milling vessel with stainless steel grinding balls. The high-energy ball-milling of the starting materials was carried out at 400 rpm for 1 h. After the ball-milling, the vessel was heated at 100 °C for 20 h under static conditions without removing the reactants and grinding balls from the vessel.

Catalytic properties of the magnetite nanoparticles obtained by the mechanochemically assisted synthesis were examined in batch experiments. Typically, 20 mL of 20 mg/L methylene blue solution was mixed with 10 mg of the magnetite nanoparticles. After reached the adsorption equilibrium, 30 wt% H_2O_2 solution was added to the solution for degrading methylene blue. The change in the methylene blue concentration at 40°C was measured to evaluate the catalytic activity.

3. Results and discussion

The XRD pattern of the product shown in **Figure 1a** indicated that the major phase was magnetite. The particle diameter was about 100 nm as shown in Figure 1b.

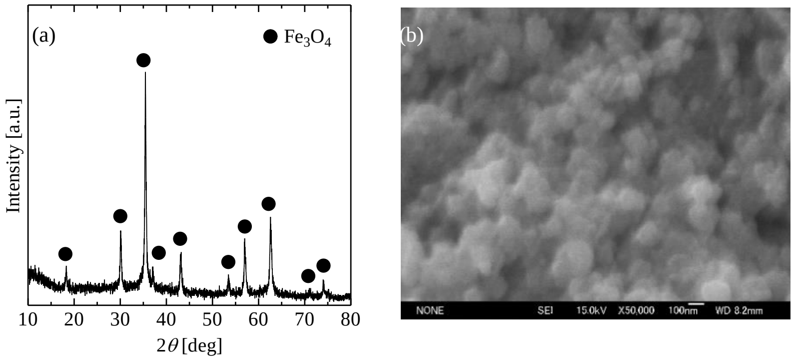

Figure 1. (a) XRD pattern and (b) SEM image of the product obtained by the mechanochemically assisted synthesis

The methylene blue removal (C_t / C_0) was shown in **Figure 2**. The concentration of methylene blue was decreased in the presence of H_2O_2 and magnetite nanoparticles. This suggested that methylene blue was degraded by heterogeneous Fenton-like reactions. These results showed that the magnetite nanoparticles can be used as good heterogeneous Fenton catalyst.

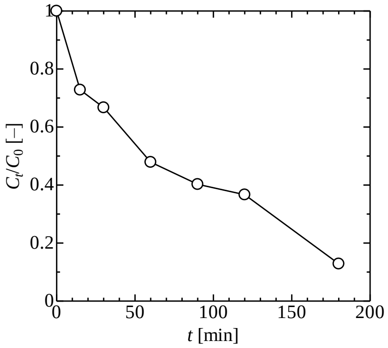

Figure 2. Removal efficiency of methylene blue (Temp. = 40°C, H_2O_2 conc. = 50 mmol/L, pH = natural)

4. Conclusion

The magnetite nanoparticles prepared by the mechanochemically assisted route showed good properties as heterogeneous Fenton catalyst. Our synthesis procedure can provide magnetite nanoparticles with high catalytic activity.

References

[1] C.J. Perecin et al., *Colloid Surf. A* **2021**, 627, 127169.

[2] H. Zhou et al., *Appl. Surf. Sci.* **2022**, 590, 153120.

[3] A. Shokri, M.S. Fard, *Environ. Chall.* **2022**, 7, 100534.

Conversion of flare gas to SWCNTs: a preliminary study on bimetallic catalyst formulas and synthesis condition

Chawalkul Chotmunkhongsin,[a] Paeka Klaitong,[a] Sunisa Watcharasing,[b] Tawatchai Charinpanitkul,[c]
Sakhon Ratchahat,[a] Weerawut Chaiwat[a,]*

[a] Department of Chemical Engineering, Faculty of Engineering, Mahidol University, Nakhon Pathom, Thailand
[b] Technology Management Division, PTT Exploration and Production Public Company Limited, Chatuchak, Bangkok, Thailand
[c]Center of Excellence on Particle Technology and Material Processing, Faculty of Engineering, Chulalongkorn University, Pathumwan, Bangkok, Thailand
*Corresponding author: weerawut.cha@mahidol.ac.th

Flare gas mainly containing methane in its composition has been abundantly wasted from petroleum sites in Thailand. Toward net zero emission policy, carbonaceous materials as carbon nanotubes (CNTs) have been recently focused as a value-added product potentially converted from flare gas as a carbon source aiming to the reduction in greenhouse gas emission. Single-walled carbon nanotubes (SWCNTs) are a special class of nanocarbon materials possessing exceptional properties making them suitable for extensive application. This study aimed to synthesize SWCNTs from methane as a representative of flare gas using iron and molybdenum supported on magnesium oxide (FeMo/MgO) as a bimetallic catalyst at various metal loadings and ratios via catalyst chemical vapor deposition (CCVD) at a constant temperature of 900 °C as a conceptual diagram in Figure 1. In-depth investigation on the effects of CCVD process conditions on the properties of the SWCNTs was also subsequently conducted. The results revealed that SWCNTs with 2–8 nm in diameter as demonstrated in Figure 1 by TEM analysis were best produced using the FeMo/MgO catalyst with the lowest metal loading at 1%, while formation of multi-walled carbon nanotubes (MWCNTs) with 15–30 nm in diameter became more favourable with higher metal loading (5 and 10%).

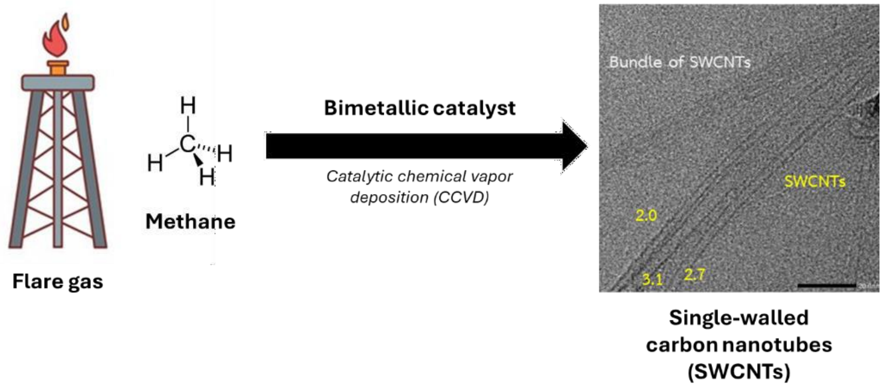

Figure 1. Conceptual diagram of a preliminary study on synthesis of SWCNTs from methane as a representative of flare gas.

The CCVD process without H_2 pre-reduction of the catalyst could produce CNTs with smaller diameters as compared to those obtained with H_2 pre-reduction of the catalyst, consistent with our previous study [1]. The Fe:Mo mass ratio of 1:1 was the optimal ratio producing a substantial carbon yield and the highest ratio of graphitic carbon to amorphous carbon (I_G/I_D). By using the FeMo/MgO catalyst with 1% metal loading with a fixed mass ratio of Fe:Mo at 2:1, CCVD conditions such as the amount of catalyst, reaction time, and the concentration of methane were deeply investigated for SWCNT synthesis. Catalyst amount of 1 g per batch showed the optimum amount in the range of 0.5–3 g used to successfully produce the highest yield in terms of gCNTs/gCatalyst with comparable I_G/I_D. The CCVD reaction time was then varied from 10 to 180 min, it was found that, with a short period of 10 min, the formation of SWCNTs could still possess relatively higher I_G/I_D. With prolonged CCVD reaction time from 20 to 180 min, the formation of SWCNTs and I_G/I_D of the CNT were gradually suppressed, nevertheless, gCNTs/gCatalyst was still continuously increased. Finally, with higher methane concentration (25 to 100%), gCNTs/gCatalyst was considerably increased, while I_G/I_D of the SWCNTs was slightly decreased, suggesting the coating of the SWCNTs by amorphous carbon possibly produced from the consequent conversion of the excessive methane. In brief, this study demonstrates crucial parameters affecting SWCNT production from methane, enabling further development of SWCNTs with desired productivities and properties.

References

[1] C. Chotmunkhongsin, S. Ratchahat, W. Chaiwat, T. Charinpanitkul, A. Soottitantawat, *Sci. Rep.* **2023**, 13(1) 21027.

Synergistic effect of heating rates during plastic pyrolysis and Fe-based catalyst supports on synthesis of MWCNTs from HDPE wastes

Pimonpan Inthapat,[a] Phitchawalai Ninthachan,[a] Thanchanok Vettavong,[a] Warodom Thepmongkorn,[a] Chawalkul Chotmunkhongsin,[a] Maturada Assawagetmanee,[b] Tawatchai Charinpanitkul,[b] Sakhon Ratchahat,[a] Weerawut Chaiwat[a,]*

[a]Department of Chemical Engineering, Faculty of Engineering, Mahidol University, Nakhon Pathom, Thailand
[b]Center of Excellence on Particle Technology and Material Processing, Faculty of Engineering, Chulalongkorn University, Pathumwan, Bangkok, Thailand
*Corresponding author: weerawut.cha@mahidol.ac.th

Nowadays, more than 300 million tons of plastic wastes have been collected globally each year. Among them, high-density polyethylene (HDPE) is also considered one of the most abundant commodity plastic wastes to be recycled and/or alternatively converted to other value-added products. In this study, the production of multi-walled carbon nanotubes (MWCNTs) from HDPE via slow and flash pyrolysis in a two-stage fixed-bed reactor was carried out by varying the heating rate during HDPE pyrolysis and type of Fe-based catalyst supports used in catalytic chemical vapor deposition (CCVD) process, impacting the yields and physicochemical properties of the resulting MWCNT products differently. Using HDPE as a carbon source, slow pyrolysis in the first fixed bed occurred from 300 to 600 °C with heating rates of 5 to 20 °C/min was conducted by comparing with flash pyrolysis at a constant temperature in a range of 450–550 °C. For MWCNT synthesis in the second stage reactor, Fe/Al_2O_3 and Fe/SiO_2 catalysts were comparatively used via CCVD process at a fixed temperature of 800 °C. The results showed that increasing the heating rate from 5 to 20 °C/min significantly reduced the product yield in terms of gCNT/gCatalyst (decreasing from 0.42 to 0.28 for Fe/Al_2O_3 and from 0.31 to 0.15 for Fe/SiO_2) and carbon yields (decreasing from 49.4% to 32.6% for Fe/Al_2O_3 and from 36.3% to 17.4% for Fe/SiO_2). Interestingly, the average diameter of Fe/Al_2O_3-derived MWCNTs exhibited an increasing trend from 29 nm to 37 nm when increasing the heating rate from 5 to 20 °C/min, while it showed an oppositely decreasing trend from 37 nm to 25 nm for Fe/SiO_2-based MWCNTs due to the different compositions of pyrolysis products from HDPE. In recent studies, slower heating rates generally improved the yield and quality of CNTs [1], but the specific catalyst support influenced the diameter and morphology of the resulting CNTs [2]. Meanwhile, increasing the temperature of flash pyrolysis from 450 to 550 °C tended to a decrease in the gCNT/gCatalyst and carbon yields of MWCNTs with the average diameter in a range of 30–40 nm. This could be directly influenced by the effect of temperature during fast pyrolysis of plastic on the product composition [3]. However, in this study, synergistic effects of heating rates during plastic pyrolysis and the type of Fe-based catalyst support have been existed and majorly affected the production yield and properties of MWCNTs from HDPE pyrolysis. Further investigation on kinetics and reaction mechanisms will be necessary to selectively enhance MWCNT production from plastic wastes in related industries.

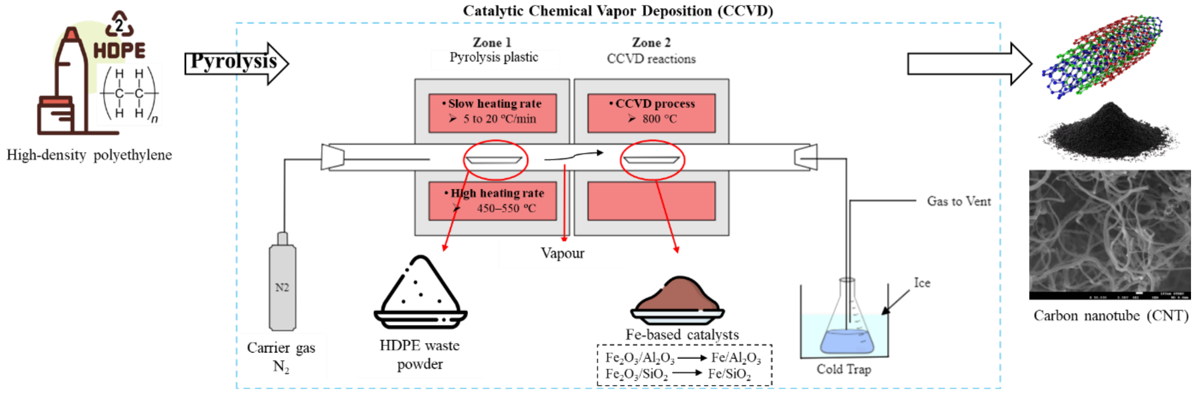

Figure 1. Schematic diagram of CNT production from HDPE pyrolysis via catalytic chemical vapor deposition.

References

[1] A. I. Eldahshory, K. Emara, M. S. Abd-Elhady, M. A. Ismail, *Sci. Eng.* **2023**, 48, 8655–8666.

[2] N. Cai, S. Xia, X. Li, H. Xiao, X. Chen, Y. Chen, P. Bartocci, H. Chen, P. T. Williams, H. Yang, *Waste Manage.* **2021**, 136, 47–56.

[3] G. K Parku, F.-X. Collard, J. F. Görgens, *Fuel Process. Technol.* **2020**, 209, 106522.

Synthesis of nickel supported on mesoporous silica hollow spheres catalysts and their activity for reduction of *p*-nitrophenol

Naoki Toyama,[a,]* Eisaku Kimura,[a] Shinosuke Kamei[a], Masakazu Matsumoto[a],
Shigeki Furukawa[a]

[a] College of Industrial Technology, Nihon University, Chiba, Japan
*Corresponding author: toyama.naoki@nihon-u.ac.jp

p-nitrophenol (*p*-NP) is a toxic, anthropogenic, and carcinogenic organic pollutant generated by industries [1,2]. This compound is reduced to p-aminophenol (*p*-AP), which is non-toxic substance under mild conditions in the presence of the metal catalysts. Several studies using transition metals such as nickel (Ni) as effective catalysts have been reported [3]; the metals have attracted much attention because of their availability, low cost, high catalytic activity, and magnetic properties. Although the nanosized metal catalysts show high activity, the nanosized metal catalysts agglomerate during the catalytic reaction. As a way to solve this problem, there is an approach to immobilize nanosized metal catalysts on supports such as metal oxide, carbon, and others [4]. Therefore, we have focused on mesoporous silica (SiO_2) hollow spheres because of high specific surface area, homogeneous pore structure, and void space. In this study, we synthesized Ni supported on mesoporous SiO_2 hollow spheres catalysts, and investigated influence on reduction of *p*-NP. The mesoporous SiO_2 hollow spheres were prepared by sol-gel method using polystyrene (PS) particles. The mesoporous SiO_2 shell were formed on PS particles, and the PS particles were removed by calcination. Then, Ni catalysts were immobilized on the mesoporous SiO_2 hollow spheres by impregnation method. The ratio of Ni/SiO_2 was adjusted 25 mass%. The activity of Ni supported on the mesoporous SiO_2 hollow spheres catalysts was measured for reduction of *p*-NP. The *p*-NP solution and sodium borohydride were added to the ion-exchange water. Following that, the Ni supported catalysts were added to the mixture, and the mixture solution was withdrawn every 4 min. The adsorption spectra of these solutions were recorded using ultra violet-visible (UV-Vis) spectrophotometer. Firstly, we confirmed the morphology of before and after Ni supported on mesoporous SiO_2 hollow spheres catalysts. Figure 1 shows transmission electronic microscopy (TEM) images of before and after Ni supported on mesoporous SiO_2

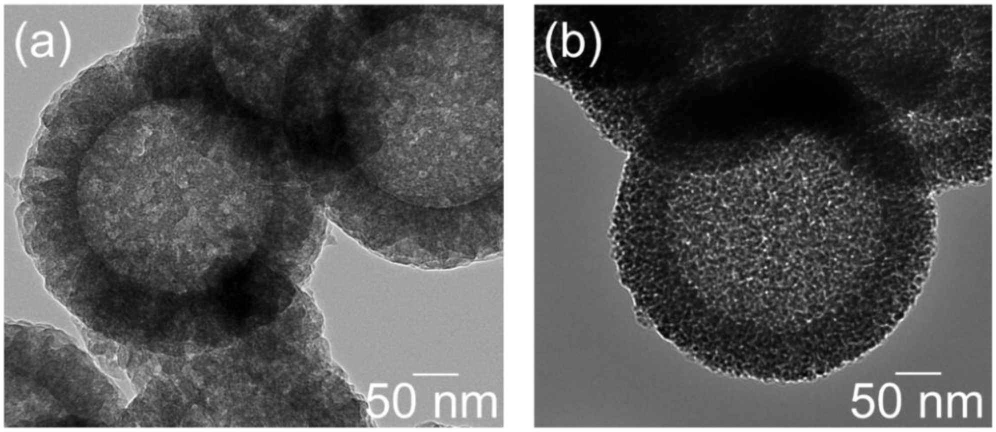

Figure 1. TEM images of(a) before and (b) after Ni supported on mesoporous SiO_2 hollow spheres catalyst.

hollow spheres catalyst. These images demonstrated that the shell thickness was approximately 50 nm. Additionally, there was no change in the morphology before and after Ni supported catalyst. The result of nitrogen adsorption/desorption measurements show that the specific surface areas calculated from BET method of the Ni before and after supported on mesoporous SiO_2 hollow spheres catalysts were 1196 m^2 g^{-1} and 229 m^2 g^{-1}, respectively. In the pore size distribution by the BJH method, a sharp peak at 2.2 nm was observed in the mesoporous SiO_2 hollow spheres. Meanwhile, the peak was not observed in Ni supported on the mesoporous SiO_2 hollow sphere catalysts. This result indicates that Ni catalysts may be supported on the pore of the mesoporous SiO_2 hollow spheres. Next, the Ni supported catalysts were measured the reduction of *p*-NP. Figure 2(a) shows UV-Vis adsorption spectra of the reaction solution with Ni supported on mesoporous SiO_2 hollow sphere catalysts. The adsorption peak at 400 nm, attributed to *p*-NP gradually decreased and disappeared within 8 min. Meanwhile, a new adsorption peak at 300 nm appeared, attributed to *p*-AP. This reaction follows pseudo-first-order kinetics, with the equation $\ln(C/C_0) = kt$. The relative intensity of the absorbance at 400 nm was used to calculate the value of C/C_0, where C_0 and C are the *p*-NP concentrations at the beginning and reaction time, respectively. In this case, the Ni supported on SiO_2 particle catalysts were also evaluated as a comparison as shown in Figure 2(b). From this result, the kinetic rate constant k for the Ni supported on mesoporous SiO_2 hollow sphere catalysts and Ni supported on SiO_2 particle catalysts were calculated at 0.426 and 0.248 min^{-1}, indicating that the Ni supported on mesoporous SiO_2 hollow sphere catalysts has a high activity for this reaction.

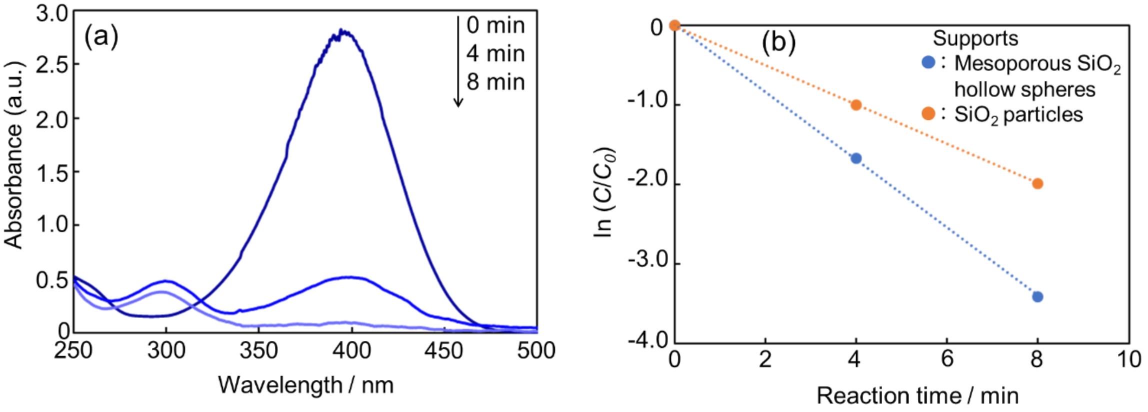

Figure 2. (a) UV-Vis adsorption spectra of the reaction solution with Ni supported on mesoporous SiO_2 hollow sphere catalysts. (b) Relationship between $\ln(C_t/C_0)$ and reaction time for the reduction of *p*-NP in the presence of Ni supported on mesoporous SiO_2 hollow sphere catalysts and Ni supported on SiO_2 particle catalysts.

References

[1] Q. Zhao, D. Bu, Z. Li, X. Zhang, L. Di, *Nanomaterials*, **2021**, 11, 1341.

[2] S. Laha, K.P. Petrove, *Biodegradation*, **1997-1998**, 8, 349-356.

[3] C. Zhang, J. Yang, Y. Liu, Y. Li, Z. Dai, M. Han, J. Bao, *Chemistryselect*, **2019**, 4, 42-48.

[4] R. K. Dhokale, H. M. Yadav, S. N. Achary, S. D. Delekar, *Appl. Sur. Sci.*, **2014**, 303, 168-174.

Synthesis of calcium carbonate using hard clam (mercenaria mercenaria) shells for a source of calcium-based materials

Shinnosuke Kamei,[a],* Takuya Hasegawa,[b] Shu Yin,[b] Naoki Toyama,[a] Takeshi Takemura,[a]
Sigeki Furukawa,[a] Koji Masaoka,[c] Masakazu Matsumoto,[a]

[a] College of Industrial Technology, Nihon University, Narashino, Japan
[b] Institute of Multidisciplinary Research for Advanced Material（IMRAM）, Tohoku University, Sendai, Japan
[c] Research Institute of Salt and Sea Water Science, The Salt Industry Center of Japan, Odawara, Japan
*Corresponding author: kamei.shinnosuke@nihon-u.ac.jp

Hard clams (*Mercenaria mercenaria*) are large filter-feeding bivalve mollusks of the family Marsuprinae. Interestingly, previous studies on the effective use of scallop, cockle, and oyster shells suggest that hard clam shells can also be used as a source of calcium-based materials owing to them being composed of calcium carbonate ($CaCO_3$). Calcium carbonate as materials is one of the most widely used useful materials. It is used in pigments, plastics, wastewater treatment, paper, cement, rubber, and adhesives. To realize the maximum utilization of $CaCO_3$ in industrial applications, obtaining particles with a fine size, narrow size distribution, and uniform morphology and crystal structure (polymorph) is crucial. The synthesizing $CaCO_3$ via a precipitation reaction is a popular topic in chemical engineering. Therefore, the purpose of this study was to investigate the structural properties and chemical composition of hard clam shells in order to examine their potential for practical application. In addition, calcium carbonate obtained via the reprecipitation of dissolved raw shell powder was also investigated.

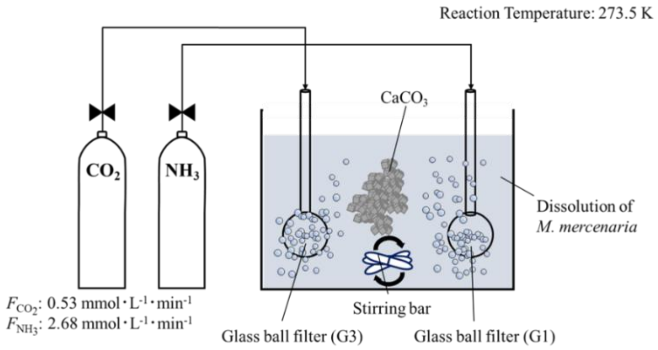

Figure 1. Schematic illustration of the formation process of $CaCO_3$ using hard clams (*Mercenaria mercenaria*). F_{CO_2} and F_{NH_3} refer to the blowing rates of CO_2 and NH_3 gases, respectively.

First, the prepared shell powder was dissolved in hydrochloric acid (35.0–37.0%; Kanto Chemical Co., Inc., Japan) to prepare a calcium solution (200 ml). Reprecipitation was then performed using glass ball filters at CO_2 and NH_3 blowing rates of 0.53 mmol·L^{-1}·min^{-1} and 2.68 mmol·L^{-1}·min^{-1}, respectively. As shown in Fig. 1, a 300 ml beaker was used as a reactor (10 cm in diameter), with a glass ball filter G3 (20-30 μm pores) for CO_2 gas blowing set 3 cm from the bottom on the left side and a glass ball filter G1 (100-120 μm pores) for NH_3 gas blowing set 3 cm from the bottom on the right side, and reprecipitation method were conducted at 100 rpm using a stirring bar (φ; 8 mm, diameter; 30 mm). The calcium solution was reacted with the gases for 5 min under stirring, following which the resulting precipitates were filtered and washed to obtain the final $CaCO_3$ reprecipitates.

As can be seen from the FE-SEM images of the reprecipitates (Fig. 2b), the reprecipitate particles exhibited a uniform spindle shape characteristic to calcite. 20 over particles were picked up from the SEM image (Fig. 2b), and their average diameter was calculated to be approximately 5 μm. We also found that calcium carbonate microparticles can be easily synthesized using glass ball filters at CO_2 and NH_3 blowing method. Furthermore, Fig. 3 shows XRD patterns of the reprecipitated product obtained from the dissolution–reprecipitation process. Calcite, aragonite, and vaterite are marked as “C”, “A”, and “V”, respectively, in the Bragg reflections. The reprecipitates were found to be almost exclusively of the calcite type, which is a highly versatile material in terms of practical application. Fig.4 shows size distribution of reprecipitates particles from the dissolution-reprecipitation process. The standard deviation (σ_p) and the mean diameter were 0.609 and 1.53 μm, respectively. These results show the formation of microsized calcium carbonate, similar to the results of the previous SEM image.

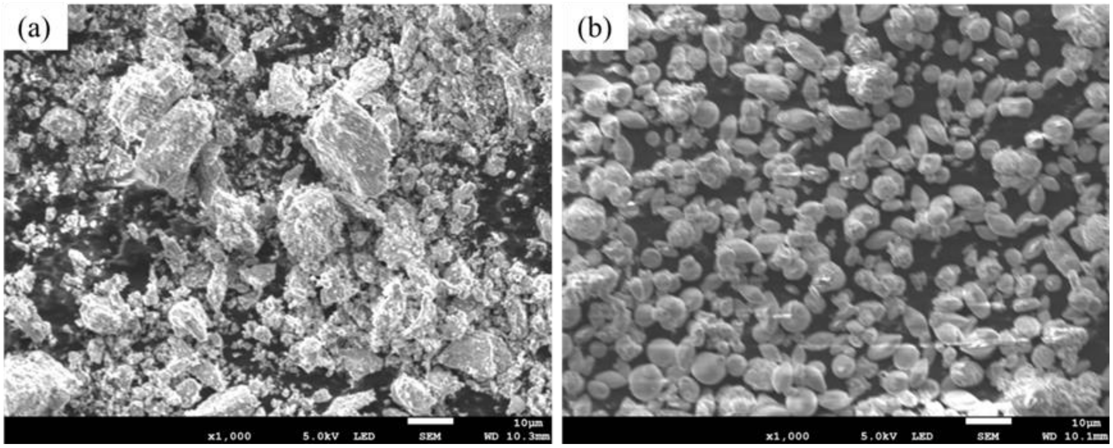

Figure 2. FE-SEM images of raw shell powder (a) and reprecipitates (b).

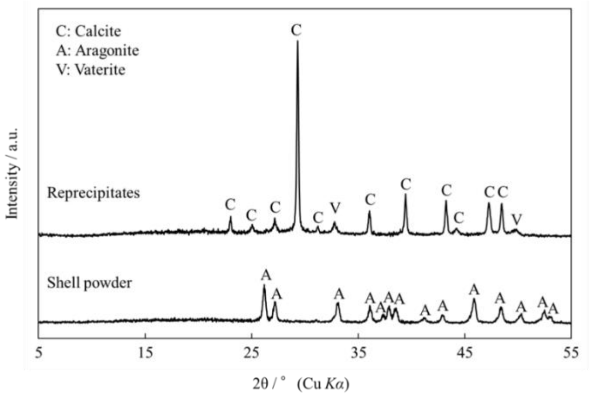

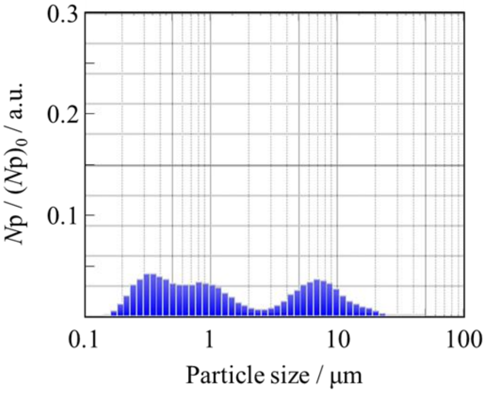

Figure 3. XRD patterns of the product $CaCO_3$ from the dissolution-reprecipitation process.

Figure 4. Size distribution of reprecipitates particles from the dissolution-reprecipitation. process

Reference

[1] S. Kamei, T. Hasegawa, S. Yin, T. Takemura, S. Furukawa, M. Matsumoto, *Salt Seawater Sci. Technol.* **2023**, 3, 58-62.

Synthesis of carbonates by reactive crystallization between Ca·Mg in industrial wastes and CO_2 -controlling the crystal qualities with bubble diameter and $[Mg^{2+}]/[Ca^{2+}]$ ratio in bulk solution -

Masakazu Matsumoto,[a]* Shinnosuke Kamei,[a] Naoki Toyama,[a] Yuzuha Matsuda,[a] Takayoshi Fujii,[a]
Yasushi Noda,[b] Koji Masaoka[a,b]

[a]College of Industrial Technology, Nihon University, Narashino, Japan
[b]Research Institute of Salt and Sea Water Science, The salt Industry Center, Odawara, Japan
*Corresponding author: matsumoto.masakazu@nihon-u.ac.jp

The carbonation process with reactive crystallization between Ca and/or Mg in industrial wastes (waste concrete, steel slug, or concentrated seawater) and CO_2 can be considered as an effective CO_2 recovery/utilization method. In the case where the all of Ca or Mg in waste concrete, steel slug, and concentrated seawater discharged from industry in the world can be converted to carbonates, CO_2 emission reduction is anticipated approximately 1.5 Gt/y which is equivalent to about 38 % of global reduction target (4.0 Gt/y) by 2050 [1-3]. To build up an efficient carbonation process that is adaptable to a carbon neutral society, the increase in conversion ratio of CO_2 and improvement of carbonate crystal qualities are indispensable during the reactive crystallization. In this study, the micron-scale bubble formation technique that enables the generation of regions with a higher ion concentration around the minute gas-liquid interfaces was applied to the reactive crystallization of carbonates from industrial wastes. In the regions near the minute gas-liquid interfaces, Ca^{2+} and Mg^{2+} accumulate because of the negative electric charge on the fine bubble surface, and the concentration of CO_3^{2-} increases because of the acceleration of CO_2 mass transfer caused by minimizing the bubble diameter; hence, local supersaturation increases so that the yield and the crystal qualities of carbonate is expected to improve.

At solution temperature of 298 K, CO_2 bubbles with an average diameter (d_{bbl}) of 40 - 2000 μm were continuously supplied to waste concrete powder extract, steel slug powder extract, or three types of concentrated seawater, i.e., ED brine, concentrated brine, and removed-K bittern, coming from salt manufacture discharge, and carbonates were crystallized within the reaction time (t_{r}) of 90 min. Fine bubbles with a d_{bbl} of 40 μm were generated using a self-supporting bubble generator by the shear of the impeller and a negative pressure owing to high-rotation [4]. The bubbles with a d_{bbl} of 200, 800 or 2000 μm were obtained for comparison using a dispersing-type generator.

Figure. 1 shows the effects of d_{bbl}, and $[Mg^{2+}]/[Ca^{2+}]$ ratio in the industrial wastes solutions on the production rate of carbonates based on unit volume (r_{i}, i: vaterite $CaCO_3$, calcite $CaCO_3$, aragonite $CaCO_3$, and $CaMg(CO_3)_2$). r_{i} was calculated from the gradient of the time change in the concentration of each carbonate produced. Minimizing the bubble diameter led to the increase in carbonate yield based on supplied CO_2 and the uniformization of crystal structure at all industrial wastes solutions used in this work. At a d_{bbl} of 40 μm, the crystal structure of carbonate obtained from industrial wastes solutions changed in the order: vaterite, calcite, aragonite, and $CaMg(CO_3)_2$, with increasing $[Mg^{2+}]/[Ca^{2+}]$ ratio. The results probably resulted from the change in local enrichment of Ca^{2+} and Mg^{2+} in the boundary area of gas-liquid interfaces of fine bubbles. Additionally, the particle size distribution measured using a laser particle size analyzer shifted to a smaller range with decreasing d_{bbl} at all t_{r} values, irrespective of $[Mg^{2+}]/[Ca^{2+}]$ ratio.

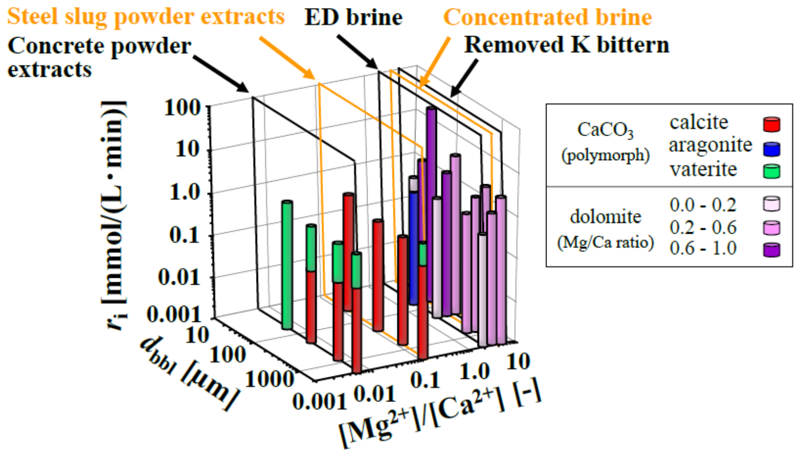

Figure 1. Relation between d_{bbl} or $[Mg^{2+}]/[Ca^{2+}]$ ratio in the bulk solution and r_i (i: vaterite, calcite, aragonite, and $CaMg(CO_3)_2$) from industrial wastes solutions

The nucleation rate (r_n) was determined from the reciprocal of the induction period for nucleation, and the crystal growth rate (r_g) was defined as the average gradient of the particle size curve within t_r of 60 min. The values of r_n and r_g are plotted against d_{bbl} and $[Mg^{2+}]/[Ca^{2+}]$ ratio in **Figure 2**. At all $[Mg^{2+}]/[Ca^{2+}]$ ratio values, r_n increased and r_g decreased with minimizing the bubble diameter. This is because of the growth suppression of the unit crystal owing to the increase in the effective nuclei number with local supersaturation increase at the minute gas-liquid interfaces. Consequently, during the reactive crystallization of carbonates from industrial wastes solutions, the crystal structure can be controlled by $[Mg^{2+}]/[Ca^{2+}]$ ratio in the bulk solution at a d_{bbl} of 40 μm, and d_{bbl} can be an index for the particle size.

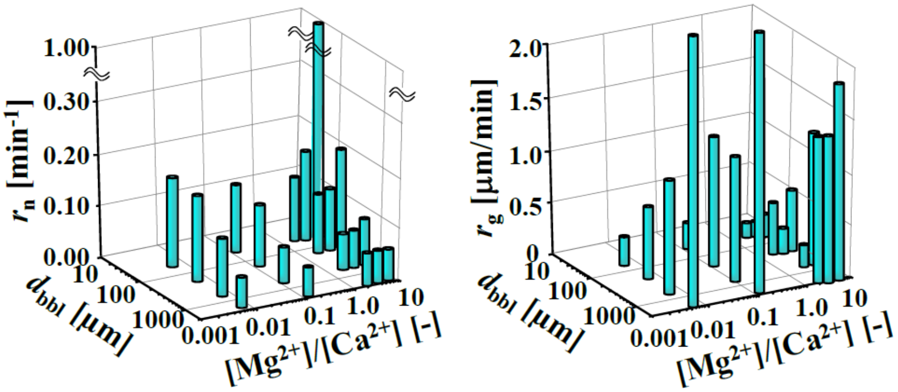

Figure 2. Relation between d_{bbl} or $[Mg^{2+}]/[Ca^{2+}]$ ratio in the bulk solution and r_n or r_g

Reference

[1] E. Jones *et al., Sci. Total Environ.* **2019**, 657, 1343

[2] E. T. Igunnu *et al., Int. J. Low Carbon Technol.* **2014**, 9, 157

[3] M. S. Blondes *et al., Environ. Sci. Low Technol.* **2020**, 54, 13917

[4] M. Matsumoto *et al., Adv. Powder Technol.* **2019**, 30, 707

Enhancing methane production performance by addition of magnetite nano particle doped powdered activated carbon

Ryo Murayama,[a] Stella Chan On San,[a] Kento Nishi,[b] Tatsushi Matsuyama,[b] Junichi Ida[b,*]

[a] Graduate school of Engineering, Soka university, Tokyo, Japan
[b] Department of Science and Engineering for Sustainable Innovation, Faculty of Science and Engineering, Soka University, Tokyo, Japan
*Corresponding author: ida@soka.ac.jp.

Anaerobic digestion (AD) is a microbial process that treats organic wastes by converting them into renewable energy in the form of methane. Recently, the addition of conductive materials (CMs) to the methane fermentation process has been receiving much attention as it could enhance the methane production performance through the direct interspecies electron transfer (DIET) mechanism. In the process of DIET, instead of utilizing hydrogen generated from the breakdown of volatile fatty acids (VFAs) to transfer electrons to methanogens, the added CM works as a bridge to transfer electrons directly from exoelectrogenic bacteria to methanogens without the need to generate hydrogen [1]. Since the electron flow rate is faster than the hydrogen transfer rate, the methane production rate can be improved by using the DIET mechanism [2]. For instance, the addition of powdered activated carbon (PAC) at 5 g/L increased the methane production rate by approximately 2.3 times [3]. However, washout of CMs together with effluent in a continuous operation remains a challenge, thereby CM must be continuously added to compensate the lost leading to increase the running costs [4]. Whilst magnetite nano particle (Mag) has also received great attention due to its recyclability, as it can be recovered from its magnetic properties. Nonetheless, Mag could only improve the methane production rate by half of PAC under the same conditions [3][5]. Therefore, in this study, synthesizing a composite CM that can achieve enhancing methane production performance and facile recovery through doping Mag to PAC was attempted. The objectives of this study are separated into two parts: (1) to evaluate the effect of magnetite doped powdered activated carbon (MDPAC) on the AD performance, and (2) to examine an optimal ratio of Mag to PAC in the MDPAC.

In study 1, the MDPAC was prepared with the ratio of Mag:PAC to 1:2 using the same method described by S. Barua et al., 2019. The AD experiment was performed using the Automatic Methane Potential Test System (AMPTS II) under the following four conditions: (1) Control (no addition of CMs), (2) addition of 10g/L of PAC, (2) addition of 10 g/L of Mag, and (4) addition of 10 g/L of MDPAC. Ethanol was used as substrate with the ratio of sludge to substrate of 2:1 (Volatile Solid-base). All conditions are incubated at 37 ± 2 °C and were carried out in 2 cycles. As analytical parameters, methane production, volatile fatty acids (VFAs), pH, and the microbial community were analyzed. In study 2, three different ratios of Mag:PAC (1:2, 1:1, and 2:1) were prepared in the same way as in the study 1 to evaluate the optimal MDPAC ratio. As for the AD experiment, 10 g/L of each prepared MDPAC was added to the reactor and the effect on methane fermentation was evaluated using the AMPTS II reactor. For comparison, one set of reactors was set in the condition without the addition of MDPAC. Other conditions and analytical parameters for the experiment were the same as in the study 1. Additionally, to evaluate recovery performance of MDPAC, the MDPACs prepared with different ratio conditions were dispersed into the Milli-Q water respectively and mixed for 7 days at 150 rpm. Then, the MDPAC was separated by magnetic sedimentation, the recovered amount of MDPAC was measured.

The result in study 1 shows that the methane production rate for the PAC, Mag, and MDPAC are approximately 2.5, 1.4, and 2.6 times higher than the control condition. It should be noted that even though the actual existing PAC amount in the reactor for the MDPAC condition is much lower than in the PAC condition, the methane production rates for both conditions are comparable. In study 2, the result shows that the methane production rate increased with the increase of Mag content in the MDPAC, where 1:2 MDPAC, 1:1 MDPAC, and 2:1 MDPAC are approximately 1.4, 1.9, and 2.4 times faster than the control condition respectively. Based on the previous report, the effect of pure Mag addition on the enhancement of methane production rate was roughly half of the PAC addition, therefore we expected the opposite result [3][5]. However, in this study, the results showed faster methane production rate for the MDPAC with higher Mag content. This could be the results of synergistic effect from the two materials. As for the recovery performance (data not shown), although the 1:2 MDPAC shows approximately 95% recovery, the 1:1 MDPAC and 2:1 MDPAC showed 100% recovery of the sample. These results indicate that the use of the proposed composite MDPAC could not only effectively enhance the methane production rate but also achieve facile and efficient recovery.

References

[1] G. Martins, A. F. Salvador, L. Pereira, M. M. Alves, *Environ Sci Technol.* **2018**, 52, 10241-10253.

[2] T. Storck, B. Virdis, D. J. Batstone, *The ISME J*. **2016**, 3, 621-631.

[3] J. Ma, H. Wei, Y. Su, W. Gu, B. Wang, B. Xie, *Bioresour. Technol.* **2020**, 313, 123706.

[4] G. Baek, H. Jung, J. Kim, C. Lee, *Bioresour. Technol.* **2017**, 241, 830-840.

[5] Q. Yin, S. Yang, Z. Wang, L. Xing, G. Wu, *Chem. Eng. J.* **2018**, 333, 216-225.

Thermoelectric properties of CoSb3 prepared by solid-state reaction

Bingke Qin,[a] Yizhu Lei,[a]

[a]Liupanshui Normal University, Liupanshui, China
*Corresponding author: qinbingke@126.com

Single-phase Skutterudite thermoelectric materials were prepared by solid-state reaction combined with vacuum ball milling mixtures. The preparation conditions of single-phase thermoelectric compound $CoSb_3$ were as follows: vacuum ball milling time was about 2 h, preparation temperature range was 723-923 K, and holding time was 1-180 min. The undoped sample CoSb3 has higher Seebeck coefficient, higher resistivity and lower thermal conductivity. The preparation method in this study shortened the preparation cycle of $CoSb_3$-based thermoelectric materials to less than 10 hours, greatly accelerating the experimental research cycle of the system. The single phase $CoSb_3$ can be prepared by ball milling combined with solid-state reaction. The samples have many micron-size pores uniformly and the grain was in the nanometer range. The maximum Seebeck coefficient was 222.64 μV/k obtained at the prepared temperature of 863 K. The maximum power factor of 132.17 μW/ (mK^2) at 570 K was obtained and the maximum figure of merit, zT~0.053 at 600 K was obtained by the sample which prepared temperature of 903 K. The $CoSb_3$-based thermoelectric compound $Cu_{0.3}Co_4Sb_{12-x}Te_x$ was prepared by co-doping with Cu,Te using high-temperature solid-state reaction method, and the maximum power factor of ~2,824 μW/ (mK^2) was obtained for the sample $Cu_{0.3}Co_4Sb_{11.5}Te_{0.5}$ @ 769 K while the zT value reaches a maximum value of ~0.83.

References

[1] B. Qin, Y. Ji, Y. Lei, Y. Li. *Ceram. Int.* **2024**, 50, 28296-28300.

[2] Z. Bai, Y. Ji, Y. Li, B. Qin, *Solid State Sci.* **2022**, 132, 106999.

Achieving high syngas/CO_2 conversion into C_{2+}hydrocarbon species over metal oxide nanoparticles as dual-bed catalyst in tandem

Zhaopeng Liu,[a,]* Yizhu Lei,[a,]* Youming Ni,[b] Wenliang Zhu,[b] Zhongmin Liu[b]

[a] Liupanshui Normal University, Liupanshui, P.R. China
[b] Dalian Institute of Chemical Physics, Chinese Academy of Sciences, Dalian, P.R. China
* Corresponding author: liuzhaopeng@tju.edu.cn; yzleiabc@lpssy.edu.cn

With the arrival of the era of carbon neutrality and the depletion of petroleum resources, direct conversion of C1 molecules (such as CH_4, CO, CO_2) into chemicals or fuels has always been of great interest and significance. Achieving a high selectivity of the target product while suppressing the non-selective performance of carbon dioxide could effectively improve the economic value in syngas conversion, and meanwhile reduce carbon emission, which is of great significance for carbon neutrality and carbon peaking, but still challenging. Although C_{2+} hydrocarbon species can be selectively synthesized over oxide molecular sieve composite catalysts, the syngas conversion is low, and CO_2 selectivity is as high as 40-50%. Furthermore, the non-renewable nature of the catalyst in this process limits its industrial application. Based on this, we have developed a two-stage process for efficient synthesis of C_{2+} hydrocarbon products (propane) from syngas (**Fig. 1a**), achieving 95% CO conversion and 80% propane selectivity, with CO_2 selectivity below 15% and propane yield up to 65%, without significant deactivation within 200 hours [1]. This process is not only beneficial for a deeper understanding of the direct synthesis of chemicals from syngas, but also holds the potential to be developed into a new low energy consumption technology for more practical synthesis of chemicals from syngas. Furthermore, we achieved 75% propane selectivity from the by-product CO_2 using a bifunctional catalyst (OX-ZEO) combining In/ZrO_2 and SSZ-13 [2] (**Fig. 1b**), which could further improve carbon atom utilization efficiency. Directly converting CO_2 into propane is challenging, because this process not only needs to overcome the energy barrier of C-C coupling, but also needs to suppress further growth of the carbon chain. The 8-MR micropores and strong acid strength of SSZ-13 are crucial for the high selectivity of propane. Our work shows that high conversion of syngas and further conversion of the by-product CO_2 into propane could be achieved together with excellent stability, exhibiting industrial application potentials.

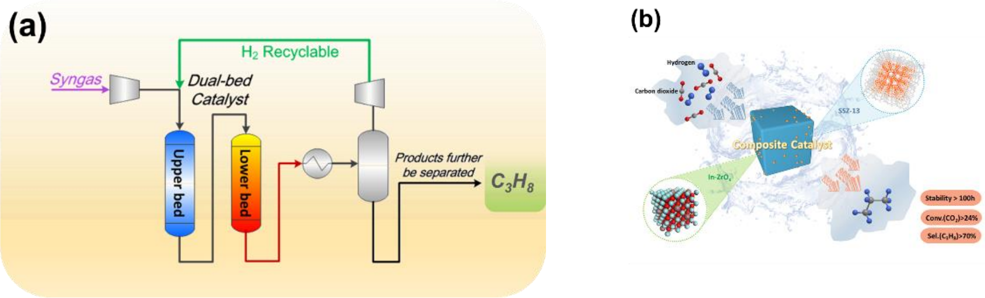

Figure 1. **(a)** Configuration of dual-bed catalyst for syngas to propane; **(b)** Scheme of OX-ZEO catalyst for CO_2 to propane.

References

[1] Z. P. Liu, Y. M. Ni, W. L. Zhu, Z. M. Liu, *J. Energ. Chem.* **2021**, 54, 111-117.

[2] Z. P. Liu, Y. M. Ni, W. L. Zhu, Z. M. Liu, *ACS Catal*. **2022**, 12(7), 3985-3994.

Reactivity and degradation mechanism of metallurgical coke during reaction with H_2O and CO_2 using kinetics modelling and micro-CT analyses

Arash Tahmasebi*, Ai Wang, Behnaz Rahmatmand, Salman Khoshk Rish, David Jenkins

Centre for Ironmaking Materials Research (CIMR), Newcastle Institute for Energy and Resources (NIER), University of Newcastle, Callaghan, NSW 2308, Australia
*Corresponding author: Arash.Tahmasebi@newcastle.edu.au

Partial substitution of coke with hydrogen in the blast furnace is regarded as a promising solution to decrease the carbon intensity of blast furnace ironmaking. Hydrogen gas reduces the ferrous burden while generating H_2O, thus decreasing fossil carbon input, and lowering CO_2 emissions. The altered reaction environment in the hydrogen blast furnace affects coke reactivity and structural evolution, thus influencing coke quality requirements.

This study uses TGA reactivity testing combined with kinetics and Micro Computed Tomography (micro-CT) analyses to improve the fundamental knowledge of the coke reactivity mechanism, microstructural evolution, and degradation mechanism during reaction in conditions relevant to H2-rich blast furnace ironmaking. Two cokes with varying CSR (68.32 and 43.11) were used in the study. Coke reactivity tests were conducted under CO_2 and H_2O at the temperature range of 900-1200 °C. A modified Random Pore Model (RPM) accounting for gas diffusion and the interfacial reaction was developed to evaluate the gasification behaviour of cokes. Micro Computed Tomography (micro-CT) imaging was conducted on partially gasified coke cylinders to 20 wt.% and 40 wt.% conversions. An onion skin analysis method that uses average greyscale intensity at different depths into the coke was developed to calculate reaction progression through individual cokes.

The TGA and kinetics modelling results showed that the initial effective diffusivity coefficient and reaction rate constant of H_2O were approximately 6 and 4.7 times greater than CO_2, respectively. Although both diffusion and reaction rates increased with temperature, the combined effects of the two determined the mechanism of the reaction. Higher temperatures promoted the gasification reaction at the surface of the coke lump compared to the core. Moreover, carbon conversion with H_2O was greater at the surface of the coke, while the reaction between coke and CO_2 took place more evenly throughout the coke volume (Figure 1a). The kinetics modelling results were validated by micro-CT image analysis results shown in Figures 1b and 1c. Dimensional images of the microstructure of coke lumps before and after reaction to 20 wt.% conversion showed that coke reacted with H_2O mostly at the surface, while coke reacted more volumetrically with CO_2.

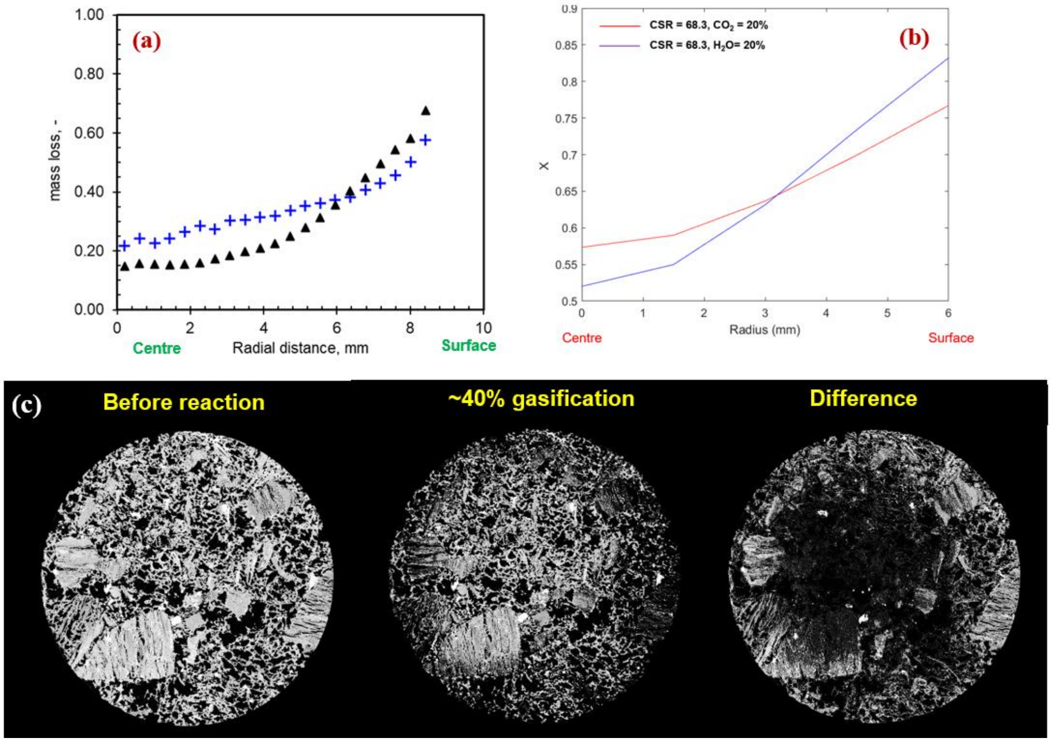

Figure 1. (a) Radial carbon conversion obtained from TGA kinetics modelling; (b) Radial distribution of mass loss after coke gasification to 20 wt.% conversion obtained from CT image analysis; (c) Micro-CT images of coke before and after reaction with H2O to 20% conversion and the difference.

Coproducing biochar pellets and green chemicals from pyrolysis of mallee biomass in Western Australia: A techno-economic analysis

Xiangpeng Gao,[a],* Hongwei Wu[b],**

[a] Centre for Water, Energy and Waste, Harry Butler Institute, Murdoch University, 90 South Street, Murdoch, WA 6150, Australia
[b] Discipline of Chemical Engineering, Western Australian School of Mines: Minerals, Energy and Chemical Engineering, Curtin University, GPO Box U1987, Perth, Western Australia 6845, Australia
*Corresponding author: X.Gao@murdoch.edu.au
**Corresponding author: h.wu@curtin.edu.au

In rural and regional Australia, the local communities are threatened by critical issues including dryland salinity and energy supply [1]. Via integrating with wheatbelt farming systems, mallee plantation is a key strategy for managing dryland salinity to prevent the loss of premium agricultural land in Australia, contributing significantly to instead of competing with food production. Therefore, mallee biomass in the Wheatbelt (with 42 Shires) in Western Australia (WA) is a true second-generation bioenergy feedstock and envisaged to be produced economically at up to ~10 million dry tonnes per annum, with excellent environmental performance [2-5]. These carbon-neutral biomass can play a crucial role in replacing coal for producing metallurgical coke [6], in Australia's heavy industries, particularly steelmaking and mineral processing that are the most difficult to decarbonise, for achieving the target of zero emissions by 2050.

This paper reports a preliminary investigation into a conception of coproducing biochar pellets (as a feedstock for green coke production) and chemicals from mallee biomass in the wheatbelt area of WA. Focuses are particularly on addressing the undesirable biomass properties including being widely dispersed and bulky, of fibrous nature, and having high moisture content (~45 wt%) and low energy density (~5 GJ/m3). The concept includes a combination of employing distributed pyrolysis that converts biomass into biochar and bio-oil in local areas, followed by the production of pellets from biochar and upgrading bio-oil into green chemicals. These addresses not only the dusty and spontaneous nature of biochar [3] that cause concerns for storage and transport, but also the critical phase instability nature of bio-oil that contains 400+ chemical compounds and is of multiphase structure [2]. Techno-economic analysis considered a mobile pyrolyser with a capacity of 40 dry tonnes/day, using mallee biomass as the primary feedstock in WA's wheatbelt. The plant life is 20 years. The project is financed at equity/debt ratio of 40% / 60%. The loan interest rate is 8%, with a loan term of 10 years. The income tax is set at 30%. Following a discount rate of 10%, discounted cash flow analysis was performed to determine the minimum selling price (MSP) of the pellets in the market. The results show that the MSP of the pellets is ~130 and ~90 $A/tonne, without and with the revenues from green chemicals, respectively, which are lower than the price of coking coals (~200 – 300 $A/tonne during 2019 – 2023).

References

[1] Ridley, A. M.; Pannell, D. J., Aus. J. of Experimental Agriculture 2005, 45, 1341-1355.
[2] Bartle, J.; Olsen, G.; Don, C.; Trevor, H., Int. J. Global Energy 2007, 27, 115–137.
[3] Yu, Y.; Bartle, J.; Li, C.-Z.; Wu, H., Energy Fuels 2009, 23, 3290-3299.
[4] Yu, Y.; Wu, H., Energy Fuels 2010, 24, 5660-5668.
[5] Wu, H.; Fu, Q.; Giles, R.; Bartle, J., Energy Fuels 2008, 22, 190-198.
[6] H. Suopajärvi, A. Kemppainen, J. Haapakangas, T. Fabritius, *J. Clean. Prod.* **2017**, 148, 709-734.

Driving the transformation to hydrogen ironmaking: An experimental vertical shaft H_2-DRI reactor facility

Ben Hang Yin,[a,b*] Shaira Mendoza,[a] Chris W. Bumby [a,b]

[a] Paihau-Robinson Research Institute, Faculty of Engineering, Victoria University of Wellington, Wellington, New Zealand.
[b] The MacDiarmid Institute for Advanced Materials and Nanotechnology, Wellington 6012, New Zealand
*Corresponding author: ben.yin@vuw.ac.nz

The iron and steel industry is responsible for approximately 6.3% of global anthropogenic CO_2 emissions, making it a critical focus for decarbonization. One of the promising pathways is the hydrogen-based direct reduction of iron (H_2-DRI), which has been extensively studied at the laboratory scale with iron ores from various regions. However, the challenge remains in scaling these results to continuous, commercial-scale operations. The transition from lab to industry is often hindered by the lack of small-scale continuous reactors that can replicate relevant industrial conditions.

To address this gap, we have successfully commissioned a continuous counter-flow vertical shaft reactor with the capability to process 6 kg/h of iron ore pellets and utilize up to 100 NL/min of hydrogen flow. This reactor, currently the largest H_2-DRI test facility in the Southern Hemisphere, represents a significant advancement in the field. In this presentation, we will outline the entire development process of this reactor, from conceptual design to initial operation. Additionally, we will share our most recent results in the hydrogen reduction of New Zealand titanomagnetite ironsand pellets within this reactor.

This facility provides valuable insights into the scalability of hydrogen direct reduction, identifying potential issues such as ore sticking and operational challenges before commercial implementation. Moreover, it offers a unique platform for producing small quantities of direct reduced iron (DRI) for further downstream investigations, thereby supporting the broader transition toward a more sustainable and green iron and steel industry.

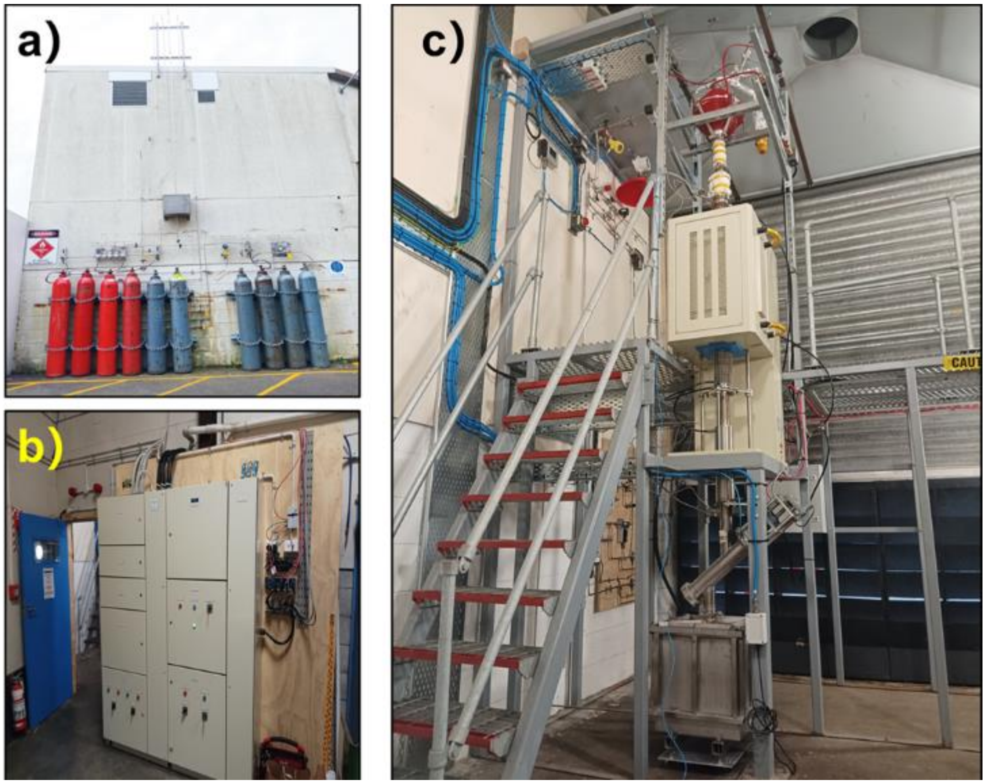

Figure 1. H_2-DRI test facility at the Victoria University of Wellington.

CFD Study of Hydrogen Injection in Blast Furnaces: Tuyere Co-injection of Hydrogen and Coal

Yiran Liu*

School of Engineering, University of Western Australia, Perth, Australia
*Corresponding author: yiran.liu@uwa.edu.au

Hydrogen, sourced through water electrolysis powered by renewables, can replace carbon sources, offering a cleaner alternative. Hydrogen is a carbon-free clean energy and a potential fuel to mitigate CO_2 emission in ironmaking blast furnaces (BFs) where the co-injection of hydrogen/coal is one of the most promising and feasible technologies. In this article, a 3D steady-state industrial-scale CFD model is improved and used for investigating the co-injection of hydrogen/coal in BFs. The model involves gas–particle-solid flow, heat and mass transfer related to the chemical reactions of hydrogen, coal and coke. This model has been validated against the measurements in terms of gas distribution, temperature and burnout. Several injection schemes of the co-injection of hydrogen/coal are designed under the conditions of constant bosh gas volume. The typical in-furnace phenomena, including the interaction between hydrogen and coal, are described, and the effects of the hydrogen injection rate on the co-injection of hydrogen/coal are analysed. The simulation results indicate that hydrogen combustion enhances the devolatilization of coal, but hinders the volatiles combustion. It is found that, as the hydrogen rate increases, the raceway volume-averaged temperature increases, and the raceway peak temperature increases and then decreases; both the raceway surface-averaged burnout and final burnout increase. Such different responses of them to hydrogen injection rates indicate the importance of 3D modelling study. In addition, the higher hydrogen injection rate increases the molar fraction of reducing gas components (H2 and CO) in the coke bed. The model provides a cost-effective tool for the design, optimisation and industrialisation of the co-injection of H_2 and coal.

The reduction kinetic of lump ore by hydrogen

Shuoyang Liu,[a] Helen Tang,[a] Tom Rufford,[a] Geoff Wang,[a] Tim Evans,[b] Xiaodong Ma[a,*]

[a]University of Queensland, Brisbane, Australia
[b]Rio Tinto, Perth, Australia
*Corresponding author: x.ma@uq.edu.au

The transition to fossil fuel-free ironmaking is crucial for reducing CO2 emissions and mitigating the greenhouse effect [1]. Hydrogen-based direct reduction (HyDR) represents a particularly promising approach in this context. Current research predominantly focuses on the reduction of pelletized ores, with comparatively little attention directed towards lump ores. The underlying mechanisms of this process encompass phase transitions, mass and heat transfer, and stress alterations [2]. The interplay among these mechanisms results in the complex composition and microstructure of lump ores. Features such as internal vacancies, cracks, and voids endow massive ores with multiple reactive sites during reduction.

In this study, the reduction behaviour of lump ores in a hydrogen atmosphere was examined using isothermal thermogravimetric analysis (TGA). Reaction rate constants were determined through the application of diffusion and chemical reaction models, which varied according to temperature and the type of iron lump ore used. The findings underscored the predominant influence of chemical reactions in the reduction of lump ores, noting a marked increase in both the rate and extent of reduction with rising temperatures.

Further investigations were carried out to analyse phase changes pre- and post-reduction by Scanning Electron Microscopy (SEM)-Energy Dispersive Spectroscopy (EDS), Electro-Probe Microanalyzer (EPMA) and using X-ray Diffraction (XRD) and. This study aimed to compare the similarities and differences in the reduction processes between lump ore and pellets. The ultimate objective is to develop a comprehensive kinetic model for the reduction of lump ore.

References

[1] Emmanuel Nyankson and Leiv Kolbeinsen, “Kinetics of Direct Iron Ore Reduction with CO-H2 Gas Mixtures,” *International Journal of Engineering Research and*, vol. V4, no. 04, Apr. 2015, doi: https://doi.org/10.17577/ijertv4is040955.
[2] Y. Ma *et al.*, “Hierarchical Nature of Hydrogen-Based Direct Reduction of Iron Oxides,” *SSRN Electronic Journal*, vol. 213, 2021, doi: https://doi.org/10.2139/ssrn.3982257.

Recovery of citric acid-soluble potassium components from biomass combustion bottom ash using both grinding and classification

Fandi Angga Prasetya, Sawa Ishizuka, Tomonori Fukasawa, Toru Ishigami, Kunihiro Fukui*

Chemical Engineering Program, Graduate School of Advanced Science and Engineering, Higashi Hiroshima, Japan
*Corresponding author: kfukui@hiroshima-u.ac.jp

The biomass power plant discharge bottom ash waste where potassium (K^+) component associated with fluidized sand (SiO_2). High K^+ (water- and citric acid- soluble) content is required to fulfill the fertilizer standard [1]. Our previous study has revealed that in the fly ash waste from biomass power generation plant, K^+ component covered fluidized sand, SiO_2 with large particle size [2]. The K^+ component in bottom ash can be assumed to exist in the same form. Therefore, in this study, the surface grinding of bottom ash was proposed to separate K^+ on the surface of bottom ash to obtain particles with high K^+ content. Furthermore, the influence of the grinding conditions on the separation and recovery performance of K^+ content was examined.

Bottom ash waste from a biomass power generation plant equipped with fluidized bed combustion furnace was used as a raw material. The pulverization by ball mill was used as surface grinding of bottom ash. **Table 1** shows the pulverization conditions by ball mill. The sample obtained from the grinding process was classified by using vibration screen with mesh size 75 and 150 µm. The content of citric acid- soluble K^+ was calculated based on the K^+ content in the solution, obtained using 1 g sample was suspended and subjected to extraction in 100 ml of 2.0 mass% citric acid solution for 60 min, then filtrated and measured using pH/Ion meter.

Table 1. Pulverization condition of ball mill.

Sample mass [g]	45
Rotation speed [rpm]	120
Ball size [mm]	Ø9, 15.8
Pulverization time [min]	15, 30, 60, 90

Fig 1(a) shows the citric acid-soluble (CA) K^+ content and yield of the sample passing through screen 75µm as a function of pulverization time. The pulverization process in both ball sizes increased the CA K^+ content from original bottom ash containing 7.1 mg/g CA K^+. However, the pulverization by using ball ϕ 9mm achieved maximum the CA K^+ content at 13.2 mg/g, meanwhile by using ball ϕ 15.8 mm, the CA K^+ always decreased with the grinding time. The pulverization by using ball ϕ 9mm is preferred because it has always the higher CA K^+ content and higher yield, independently of the grinding time. **Fig 1(b)** shows the XRD peak pattern of obtained samples. The original bottom ash and pulverized ash contained crystalline of SiO_2 and $KAlSi_2O_6$ with different peak ratio of these crystals. Namely, the pulverized ash by using ball ϕ 9mm was higher than that of original bottom ash and pulverized ash of ball ϕ 15.8mm. This indicates that potassium components in bottom ash can be concentrated by grinding and classifying Further, concentrated CA K^+ component contains crystalline of $KAlSi_2O_6$.

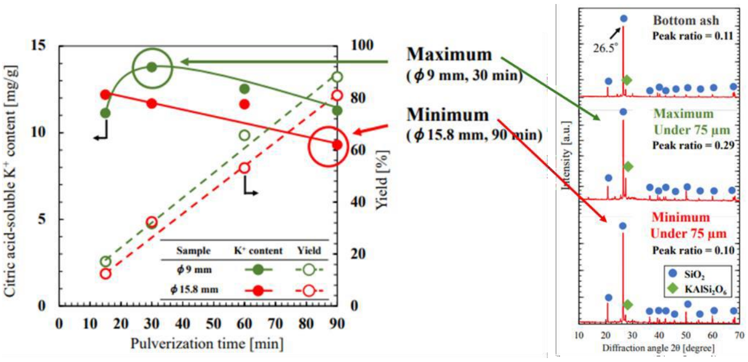

(a) (b)

Figure 1. (a) Citric acid soluble K^+ content and yield as a function of the pulverization time for sample passing through a 75µm screen and (b) its XRD peak pattern

Fig. 2(a) shows the change in the difference in median diameter between ash that passed through 75 µm screen and ash collected on 150µm screen. The pulverized ash sample obtained from ball size ϕ9 mm has higher difference in median diameter than that of ϕ15.8 mm over pulverization time. **Fig 2(b)** schematically illustrates the mechanism by which the broadening of the particle size distribution of pulverized ash affects K^+ enrichment performance. When difference in median diameter is high, the SiO_2 particles is hard to destroy and collected as larger particle on the 150 µm screen and classified small number of SiO_2 that passing through 75µm screen. On the other hand, with the small difference in median diameter, the SiO_2 is pulverized into smaller size and classified higher number of SiO_2 that passing through 75µm screen. This may cause the CA K^+ content that passing through 75µm screen obtained from pulverization using ball ϕ9 mm was higher than that of ball ϕ15.8 mm.

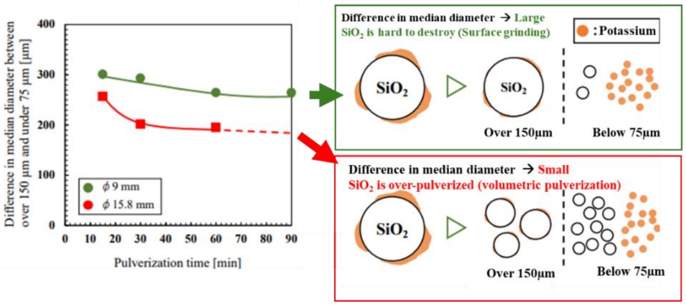

(a) (b)

Figure 2(a) Relationship between pulverization time and difference in median diameter, and **(b)** its mechanism to separate & concentrate potassium components.

K^+ components in bottom ash can be separated and concentrated by grinding and classifying to increase CA K^+ content by forming $KAlSi_2O_6$ which is CA K^+ component. By changing the grinding condition, it may be possible to control the separation and recovery performance of K^+ components.

References

[1] FAMIC, Testing methods for fertilizer, 2020.
[2]. F.A. Prasetya, S. Ishizuka, T. Fukasawa T. Ishigami, K. Fukui., Journal of the Energy Institute, 111, 101396 (2023).

New Frontiers for Electrostatic Separation

Peter M. Ireland*

Discipline of Chemical Engineering, University of Newcastle, University Drive, Callaghan NSW, Australia
*Corresponding author: Peter.Ireland@newcastle.edu.au

A central requirement for an extended human presence in extraterrestrial environments is the ability to use local resources to provide necessities such as drinking water, fuel and metals. In-situ space resource utilisation (ISRU) on the Moon and in other off-Earth environments requires selection of particle processing techniques that will function under those conditions: lack of liquid water, air, and gravity. The most common and popular processing methods used on Earth are heavily reliant on all three, and thus unsuitable for off-Earth applications. One notable exception is electrostatic processing. Comparison of electrostatic separator types (high-tension rolls, screen-plate separators and triboelectric separators) in terms of potential use on the Moon suggests that free-fall plate separators have several advantages over other types. We use new results from a free-fall separator simulator [1] to predict the effect on grade and recovery of reduced gravity on separation of a mixed particle stream in a free-fall separator. We also discuss a novel hybrid conductive parallel plate separator that we are evaluating as an alternative to the type of triboelectric parallel-plate separator that is currently used in the plastics recycling industry. While triboelectric separation is likely to function better in the dry, airless Lunar environment than on Earth, this novel hybrid separator configuration offers potential advantages in terms of effectiveness and reliability in harsh extraterrestrial environments and low gravity.

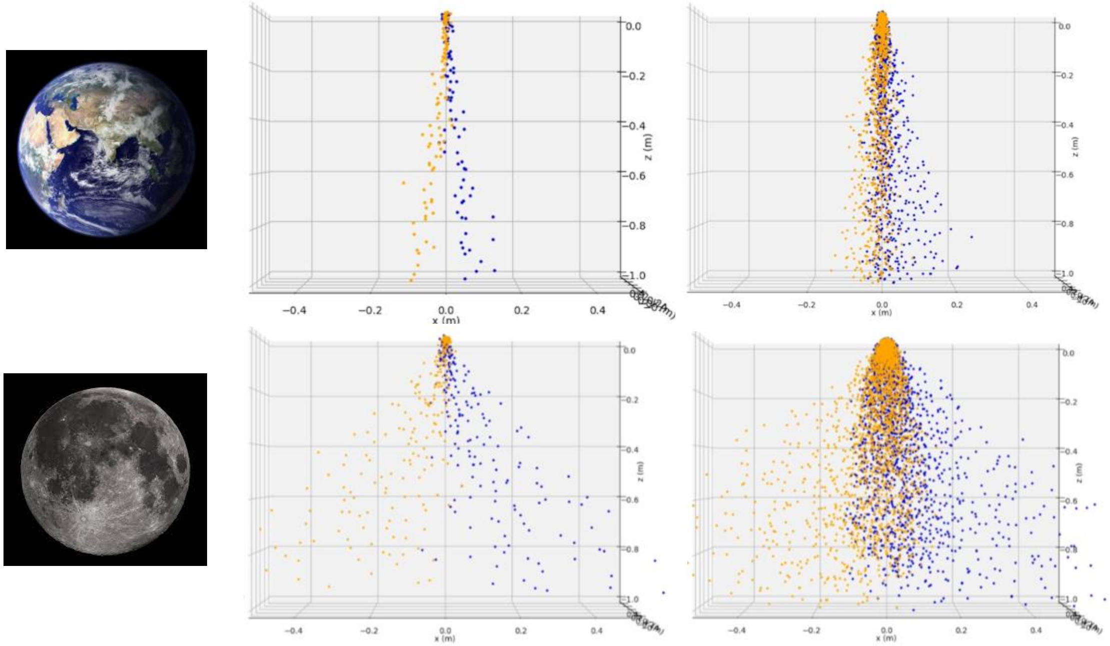

Figure 1. Simulation of free-fall electrostatic separation of a mixed particulate, under both Earth and Lunar gravity.

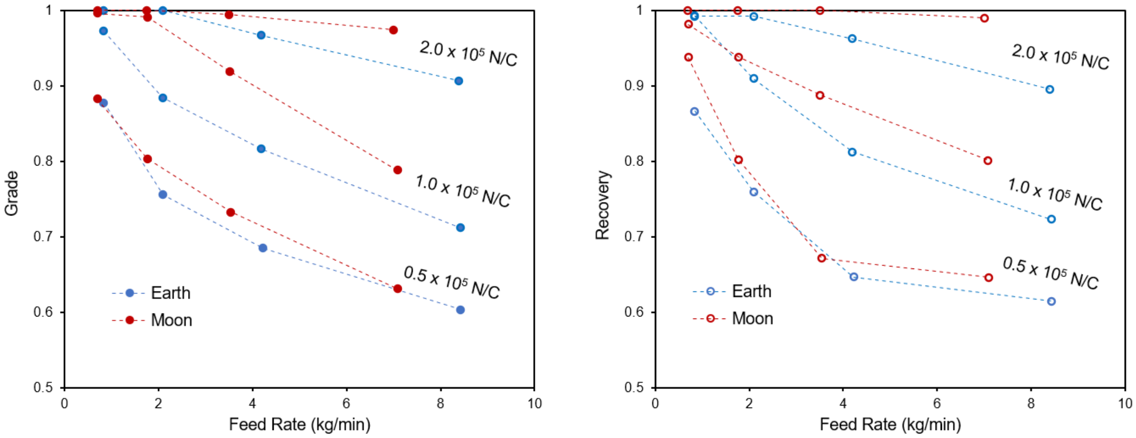

Figure 2. Predicted grade and recovery from simulation of free-fall electrostatic separation of a mixed particulate, under both Earth and Lunar gravity.

References

[1] P. M. Ireland, *Powder Technol.* **2024**, 434, 119290.

How blast rate variation affects dynamic in-furnace behaviours and energy consumption of an industrial-scale blast furnace: A transient-state CFD study

Jin Xie, Xiaobing Yu and Yansong Shen*

School of Chemical Engineering, University of New South Wales, Sydney, NSW 2052, Australia
*Corresponding author: yansong.shen@unsw.edu.au

Blast rate is a key operating parameter affecting the stability and energy consumption of ironmaking blast furnaces (BFs). Understanding the transient in-furnace behaviours resulting from blast rate variations is crucial for optimising BF operations and enhancing energy efficiency in the steel industry. The unplanned change in blast rate may occur sometimes, for example, due to the mechanical failures of blast supply system. However, the time-dependent evolution of in-furnace phenomena due to blast rate variations remains poorly understood. This work employs a transient BF model to numerically investigate the dynamic in-furnace behaviours following blast rate changes and explores potential countermeasures, providing valuable insights for BF operators to maintain furnace stability and performance under varying conditions. First, the impact of blast rate changes on in-furnace phenomena and key performance indicators are studied. The results show that when the bosh gas index decreases by 7 m/min, the top gas temperature decreases by ~67 K and the gas utilization efficiency increases by 1.8% within 20 hours. If ψ increases by 3 m/min, the top gas temperature increases by 23 K, but the top gas utilization efficiency decreases by 0.7% in 20 hours. Then, it is found that it takes nearly 20 hours to recover the in-furnace phenomena after the blast rate is recovered from shortage and if blast rate is insufficient, increasing oxygen enrichment ratio from 1.5% to 5% improves the raceway temperature by 170 K in 40 hours.

The blast furnace (BF) remains the predominant reactor for ironmaking, encompassing both conventional BFs at present and emerging novel BFs in the near term [1]. The blast rate serves as a key parameter in attaining a favorable distribution of in-furnace gas flow and adjusting productivity. In this investigation, we explore the impact of changes in blast rate on transient in-furnace phenomena through the utilization of the transient blast furnace (tBF) model [2]. Additionally, we delve into the efficacy of countermeasures designed to alleviate the adverse effects of low blast rate operation while preserving the thermal field of the blast furnace. These countermeasures have been thoroughly examined to understand their influence on the transient evolution of in-furnace dynamics.

Table 1. Case settings.

	ψ (m/min)	V_{bosh} (m^3/min)	Blast rate (m^3/min)	O_2 enrichment ratio (%)
Case (0)	62	10238.1	7908	1.5
Case (1)	55	9082.1	6960	1.5
Case (2)	65	10733.4	8298	1.5
Case (3)	62	10238.1	7908	1.5
Case (4)	55	9082.1	6802	5

Fig. 1(a) illustrates the top gas temperature evolution after the blast rate is decreased. The top gas temperature exhibits a decreasing trend after the blast rate is decreased and reaches a new stable state at about 20 hours. The decrease in the top gas temperature is attributed to the less heat release due to reducing fuel. **Fig. 1**(b) demonstrates the top gas temperature has an increasing trend after the blast rate is higher, and it reaches stable after about 20 hours. Higher blast rate can introduce higher heat into the furnace and more heat can be released by combustion. **Fig. 1**(c) depicts the top gas temperature evolution after the blast rate is recovered from shortage. The temperature responds fast immediately after the blast rate is restored and the temperature goes back to normal level at about 40 hours. **Fig. 1**(d) presents the RAFT, top gas temperature and top gas utilisation variation after the O_2 concentration in the blast is increased. RAFT and top gas utilization becomes higher, but the top gas is lower since the heat transferred to the upper part of the furnace is reduced.

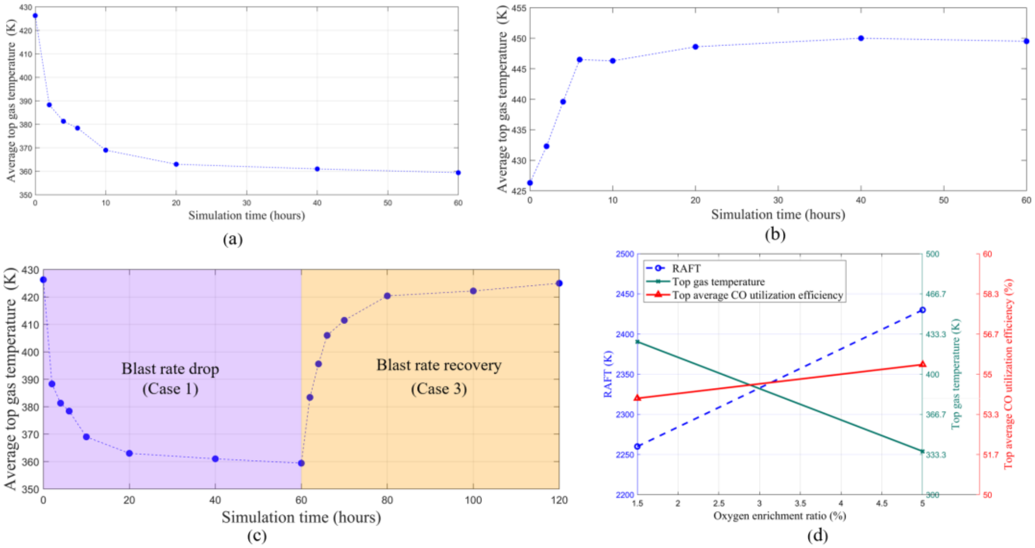

(a) (b) (c) (d)

Figure 1. (a~c) Top gas temperature evolution when blast rate is decreased, increased and recovered respectively, and (d) RAFT, top gas temperature and CO utilisation efficiency when O_2 concentration is increased.

(1) When the blast rate decreases, the gas temperature decreases with time.

(2) If the blast rate is increased, the opposite time-related changing trend in the furnace phenomena can be observed.

(3) After changing the blast rate, the system responds faster in the first 10 hours.

(4) An increase in the oxygen enrichment ratio will improve both BF productivity and hearth temperature while decreasing temperature in the upper part of the furnace.

References

[1] R. C. Zhu. Metallurgical Industrial Press, 2015.
[2] X. B. Yu and Y. S. Shen. Chem. Eng. Sci.2022, vol. 248, p. 117185.

A novel technology of co-injecting hydrogen and biomass in blast furnaces for a sustainable carbon-neutral ironmaking

Ming Jiang Gan, Yiran Liu and Yansong Shen*

School of Chemical Engineering, University of New South Wales, Sydney, NSW 2052, Australia
*Corresponding author Email: ys.shen@unsw.edu.au

We propose a sustainable and feasible carbon-neutral ironmaking technology – the co-injection of hydrogen and biomass in blast furnaces [1,2]. To understand the fundamentals of internal combustion behaviour related to the co-injection of hydrogen and charcoal, a three-dimensional computational fluid dynamics (CFD) model is developed by describing the multiphase reacting flow under the simulated BF conditions. Particularly, the present model features a new treatment of volatile matter and an improved sub-model for hydrogen combustion. The model is validated by two cases of charcoal injection and co-injection of hydrogen and coal. The typical in-furnace phenomena as well as the interaction between the hydrogen and charcoal are analysed comprehensively. The results indicate that the proper injection of hydrogen through the annulus of the charcoal lance is beneficial as high local gas temperatures (1500 K to 1800 K) from hydrogen combustion provided a charcoal burnout enhancement of 6% during the charcoal devolatilisation process. However, char reactions are hindered due to oxygen competition with hydrogen combustion, hence resulting in a slightly reduced final burnout. The optimum conditions to maximise the biochar burnout were explored with a combination of one-factor-at-a-time (OFAT) and design of experiment (DoE) approaches, such that a maximum overall burnout of 51.71% was predicted. This study provides a quantitative tool for the study of this frontier technology, which may serve as a reference to strive toward the net-carbon initiative.

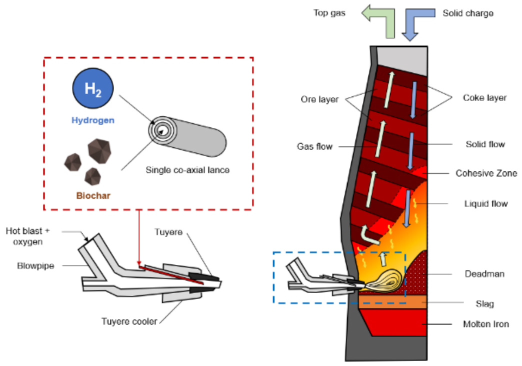

Schematic diagram of the tuyere injection process and the conveyance method through a single co-axial lance

Schematic view of the co-injection of hydrogen and biomass in a blast furnace

Figure 1 Schematic diagram of the novel technology of the CoHB process in a BF.

References

[1]Gan MJ, Liu Y, Shen Y. A novel ironmaking decarbonisation technology — co-injection of hydrogen and biochar (CoHB): A CFD study of combustion in the raceway under simulated blast furnace conditions. Fuel 2023;350:128745. https://doi.org/https://doi.org/10.1016/j.fuel.2023.128745.

[2]Gan MJ, Liu Y, Shen Y. Co-injection of hydrogen and biomass in ironmaking for decarbonisation. International (PCT) Patent Application No. PCT/AU2023/051167, 2023.

Disassembling silica green bodies photocured from interparticle photo-cross-linkable suspension

Yuki Hiroshige,[a] Junichi Tatami,[b] Motoyuki Iijima [b,*]

[a] Graduate School of Engineering Science, Yokohama National University, Japan
[b] Faculty of Environment and Information Sciences, Yokohama National University, Japan
*Corresponding author: iijima@ynu.jp

Additive manufacturing of ceramic materials using photocurable suspensions has garnered wide attention due to its ability to manufacture on-demand structured components which are difficult to be shaped by conventional methods. Although various ceramic components have been structured up to date [1], most studies primarily focuses on the ability of shaping. Therefore, the manufacturing process have not been proactively designed from the perspective of resource recycling. Recently, we have designed a new series of photocurable suspension which raw silica particles were directly crosslinked by small amounts of acrylate-based monomers. The designed suspension was applicable to additive manufacturing process of complex-structured silica components using vat photopolymerization and the photocured bodies were found to have nanoscaled interparticle crosslinks [2]. Inspired from the unique and fine polymer crosslinks formed among the particles, herein, we aim to propose a new disassembling process of the photocured bodies, obtained from interparticle photo-cross-linkable suspension, nearly to primary particle sizes.

In brief, interparticle photo-cross-linkable suspension were designed according to our previous report [2] using butylcarbitol and phenoxyethanol as solvent. Multifunctional acrylates (MA), which penta/hexa-functional acrylate and bi-functional acrylate were mixed in various ratios, were used as a source of interparticle crosslinks. The photocured green bodies were immersed in an aqueous ammonia solution (1.4 wt.%) for a certain period, and then ultrasonicated for disassembling.

Fig. 1 shows the aggregate size distribution of the particles obtained after the immersion of photocured bodies in an aqueous ammonia solution for 5 days, followed by ultrasonic treatment. The photocured bodies having interparticle crosslinks originated from different multifunctional acrylate (MA) mixture ratios was considered. While coarse aggregates were remained when the ratio of penta/hexa-functional acrylate was high in the MA mixture, the photocured bodies gradually disassembled nearly to primary particles as the ratio of bi-functional acrylate has increased. To further investigate this behavior, the influence of MA mixing ratio on the linear expansion rate of the photocured bodies after immersion treatment was evaluated (Fig. 2). The photocured bodies found to expand significantly when the ratio of bifunctional acrylate was high. This suggests that aqueous ammonia solution swells better to the interparticle crosslinks formed from bifunctional acrylate, which facilitates effective polymer decomposition reaction. Fig. 3 presents the surface structure of particles collected after disassembling process. In the system using bifunctional acrylate as the cross-linking resin source, the interparticle crosslinks of the photocured bodies (Fig. 3a) found to successfully disappear upon disassembly treatment (Fig. 3b). We believe that the proposed process should play an important role for recycling prototype printed components.

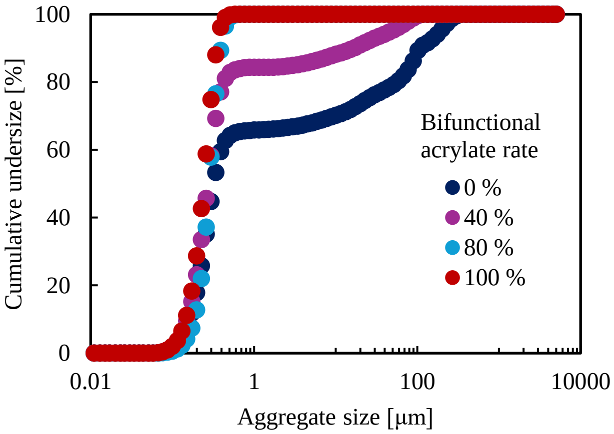

Figure 1. Aggregate size distribution (laser diffraction method) of silica particles disassembled from photocured bodies.

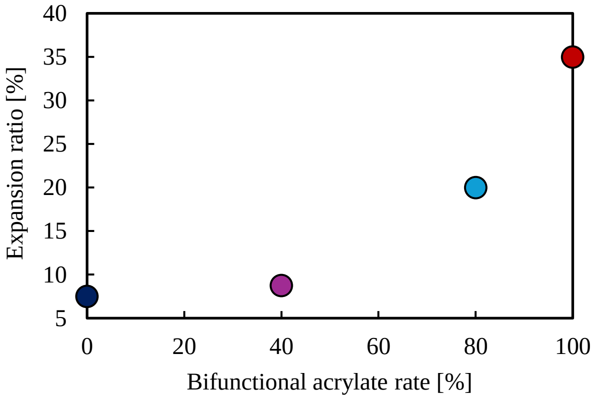

Figure 2. Effect of bifunctional acrylate ratio on the expansion rate of photocured green bodies after immersion in aqueous ammonia solution (5 days).

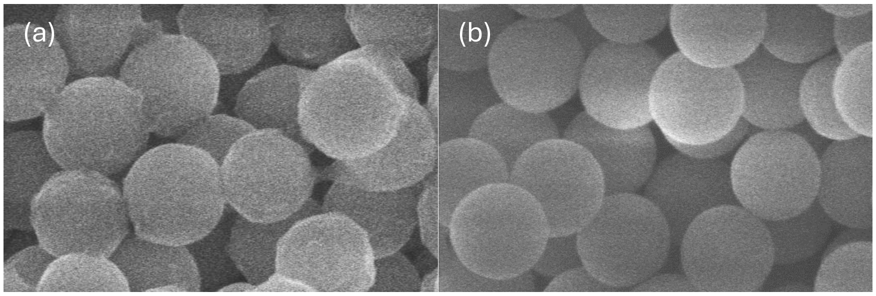

Figure 3. FESEM observation of (a) photocured body and (b) particles collected after disassembling process.

References

[1] F. Kotz, et al., Nature, 554 (2017) 337.
[2] R. Arita, et al., Commun. Mater., 1 (2020) 30.

Reduction of heavy metal content from sewage sludge ash using a Coanda effect-based air classification

Zhou Kun[a], Mauricio Córdova-Udaeta [a], Keishi Oyama [b], Hidehiro Kamiya [a], Chiharu Tokoro [c, *],
Masahiro Ito [d], Kazuhiro, Fujimori [d], Yoshihiro Iwai [d], Eisuke Tamura [d]

[a]Waseda University, Tokyo, Japan
[b] Kyushu University, Fukuoka, Japan
[c] Tokyo University, Tokyo, Japan
[d] Sanki Engineering Co Ltd., Tokyo, Japan
*Corresponding author: tokoro@waseda.jp

Global phosphorus (P) shortage had become a major concern in recent years. Phosphate rock, the main resource of P, is predicted to be exhausted in next 50-100 years [1], while demand of P has increased around the world in recent times, which necessitates alternatives P sources. Sewage sludge ash (SSA) is widely regarded as a potential material due to its high phosphate content (5% - 11% of the dry weight) [2]. Large scale sewage sludge ash combustion plants in Japan have been already put into commercial use for the mass production of SSA, in which heavy metal concentration is strictly limited. However, the conventional P recovery technique from SSA such as thermal and wet chemical methods are not suitable for mass production in terms of energy consumption and waste generation. In this regard, physical separation of heavy metal in solid phase that do not use high temperature or chemical reagents, appears to be promising in SSA mass production with little environmental impact.

In this research work, SSA samples from seven different sources were served to the separation using an air classification based on the Coanda effect: particles inside a fluid jet stay attached to a curved surface based on their inertia moment [3]. Hence, three fractions of separated sample with different particle sizes were obtained after the treatment, including fine (D_{50} = 5.6 µm), medium (D_{50} = 26.5 µm), and coarse fraction (D_{50} = 47.1 µm) while the two cutting angles that divide three fractions are 10 and 50 µm, it's stressed that D_{50} of coarse fraction is smaller than the cutting angle because of the relatively low separation efficiency of elbow jet air classifier, which results in particles either with smaller or larger sizes entering each fraction. All the separated fractions were then digested using a microwave to determine the heavy metal content following the Japanese fertilizer analysis protocol [4]. As displayed in figure 1, the results showed that in some of the samples, the fine fractions tend to have more arsenic (As), cadmium (Cd), lead (Pb), while chromium (Cr) showed the exact opposite tendency. XRF results also showed that P and As, Pb were all mostly concentrated in the fine fractions and remain less in medium and coarse fractions, while Cr shows irregular trends. It could be explained by the combustion process where As, Cd, Pb were vaporized and condensed on the surface of coarser particles because of their low boiling and melting points, thus forming the finer particles and showing the trend. On the contrary, Cr with high boiling point is thermally stable and remain in coarser particles, showing irregular trend. These trends suggest that medium and coarse fraction might be the optimal recovered objects for maintaining balance between heavy metal and P contents, which reduces the heavy metal content compared to the original samples while keeping most of P content. Despite the relatively higher Cr concentration, the concentration of Cr in medium and coarse fraction still satisfies the suggested standard regulation at a value much lower. As conclusion, regardless of fine fraction, medium and coarse fraction could be directly applied for the source of fertilizer after separation.

Finally, the fine fractions of all SSA samples were served to leaching tests with acid (HCl), alkali (NaOH), and distilled water for further heavy metal reduction. Results of the leaching experiments showed that alkali leaching could slightly extract some amount of heavy metal such as Pb, As (less than 0.002% wt.) while causing little loss to P content. On the contrary, acid leaching is generally more effective in dissolving P into solution when compared to alkali and distilled water, at the cost of dissolving small amounts (less than 0.01% wt.) of heavy metals like As, Pb and Cr, suggesting that alkali leaching can be used to further remove the heavy metal from the solid phase. Our results showed that using an air classification method based on the Coanda effect is feasible in reducing the heavy metal from SSA by recovering medium and coarse fractions, suggesting the possibility of using this physical-only method for the recovery of P from SSA with heavy metal concentration lower than the standard.

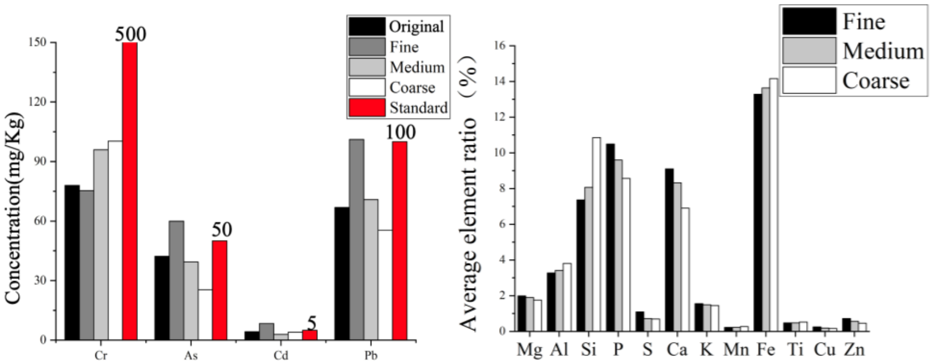

Figure 1. ICP-MS results of heavy metal after microwave digestion with the standard (left) and XRF results (right) in one of the samples

References

[1] Donatello, S. and Cheeseman, C. R. (2013) ‘Recycling and recovery routes for incinerated sewage sludge ash (ISSA): A review’, Waste Management, 33(11), pp.23282340.doi: 10.1016/j.wasman.2013.05.02

[2] G. Boniardi, Assessment of a simple and replicable procedure for selective phosphorus recovery from sewage sludge ashes by wet chemical extraction and precipitation, Chemosphere 285 (2021) 131476, https://doi.org/10.1016/j. chemosphere.2021.131476

[3] Tritton, D.J., Physical Fluid Dynamics, Van Nostrand Reinhold, 1977 (reprinted 1980), Section 22.7, The Coandă Effect.

[4] Fertilizer analysis law – Food and Agricultural Materials Inspection Center（FAMIC）. (n.d.). Retrieved April 19, 2024, from http://www.famic.go.jp/ffis/fert/sub6_data/sub6_analyze.html.

A CFD Study of Gas Solid Flow in a Gas Cyclone Separator for Recycling of Waste Lithium-ion Batteries

Jayden D'Agostin[a,1], Junxian Liu[a,2], Yanyan Zhao[a], Yuqing Feng[b,*]

[a] CSIRO Energy, Victoria 3169, Australia
[b] CSIRO Mineral Resources, Victoria 3169, Australia
[1] Vacation student from Monash University, Victoria 3169, Australia
[2] Vacation student from The Australian National University, ACT 0200, Australia
*Corresponding author: Yuqing.Feng@csiro.au

Lithium-ion batteries (LiB) are becoming increasingly prevalent due to the wide-scale adoption of portable electronics and electric vehicles [1]. Consequently, there has developed a substantial need for efficient and environmentally friendly recycling methods. This paper presents a CFD investigation into the efficiency of a gas cyclone separator for LiB recycling. The separation efficiency of the cyclone for a standard LiB cathode (NMC-811) and anode (Graphite) are investigated across a variety of inlet velocities and dipleg lengths. The findings illustrate the capacity for gas cyclones to separate LiB materials and demonstrate the need for parametric optimization of cyclone geometry for good separation efficiency.

References

[1] B. He, H. Zheng, K. Tang, P. Xi, M. Li, L. Wei & Q. Guan, A Comprehensive Review of Lithium-Ion Battery (LiB) Recycling Technologies and Industrial Market Trend Insights, Recycling; Basel (2024), 9 (1), 9, 9-35.

Hydrogen Reduction of New Zealand Titanomagnetite Ironsand in a Fluidised Bed Reactor for Direct Reduced Iron Production

B. Maisuria[a,*], C.Bumby[a],D. Del Puerto[b]. M.Watson[c], R. Longbottom[d], B. Monaghan[d]

[a]Robinson Research Institute, Victoria University of Wellington, Lower Hutt 5046, New Zealand
[b]Callaghan Innovation, Lower Hutt 5040, New Zealand
[c]University of Canterbury, Christchurch, Canterbury, New Zealand
[d]University of Wollongong, NSW 2522, Australia
*Corresponding author: bavinesh.maisuria@vuw.ac.nz

This study explores the production of direct reduced iron (DRI) from New Zealand titanomagnetite (TTM) ironsand using hydrogen reduction in a fluidised bed reactor. With its natural particle size (100-250 µm), TTM ironsand is well-suited for fluidised bed processing, offering significant advantages over conventional methods. The most notable is eliminating the need for pre-treatment like pelletising and sintering, simplifying the process. A small-scale experimental reactor was designed to reduce H_2 atmospheres at temperatures up to 1050°C. A novel in-situ sampling system allows the extraction of partially reduced material during the batch process for analysis. A pneumatic, solid loading and discharging system is used to conduct multiple experiments within a working day.

The results show no particle sticking occurred during reduction across the temperature range of 750-1000°C. At higher temperatures, sticking was prevented by forming a Ti-rich oxide shell around the partially reduced particles. In contrast, sticking did not occur at lower temperatures without forming this shell. The reduction mechanism varied with temperature: at higher temperatures (950-1000°C), the reduction proceeded through a wüstite phase, with residual TTM showing titanium enrichment. At lower temperatures (750-800°C), TTM was reduced directly to metallic iron, bypassing the wüstite phase. These behaviours were combined at intermediate temperatures (850-900°C), where a brief wüstite phase appeared during reduction.

Pre-oxidation of TTM accelerates reduction rates at temperatures $\leq$ 900°C, enhancing hydrogen diffusion and reduction in later stages. These findings highlight the potential for fluidised bed hydrogen reduction of TTM ironsand to produce DRI, offering a pathway to lower CO_2 emissions in ironmaking.

References

[1] Prabowo, S. W., Longbottom, R. J., Monaghan, B. J., del Puerto, D., Ryan, M. J., & Bumby, C. W. **(2022**). Hydrogen Reduction of Pre-oxidized New Zealand Titanomagnetite Ironsand in a Fluidized Bed Reactor. JOM, 74(3), 885–898. https://doi.org/10.1007/s11837-021-05095-x

[2] Prabowo, S. W., Longbottom, R. J., Monaghan, B. J., del Puerto, D., Ryan, M. J., & Bumby, C. W. (**2022**). Phase transformations during fluidized bed reduction of New Zealand titanomagnetite ironsand in hydrogen gas. Powder Technology, 398. https://doi.org/10.1016/j.powtec.2021.117032

[3] Prabowo, S. W., Longbottom, R. J., Monaghan, B. J., del Puerto, D., Ryan, M. J., & Bumby, C. W. (**2019**). Sticking-Free Reduction of Titanomagnetite Ironsand in a Fluidized Bed Reactor. Metallurgical and Materials Transactions B: Process Metallurgy and Materials Processing Science, 50(4), 1729–1744. https://doi.org/10.1007/s11663-019-01625-w

Numerical simulation of vanadium titanium magnetite (VTM) BF ironmaking process

Yancong Liu,[a,*] Shibo Kuang,[a] Lulu Jiao,[b] Aibing Yu,[a]

[a]ARC Research Hub for Smart Process Design and Control, Department of Chemical and Biological Engineering,
Monash University, VIC 3800, Australia
[b]School of Energy and Environment, Southeast University, Nanjing, 210096, China
*Corresponding author: Yancong.Liu@monash.edu

In an ironmaking blast furnace (BF), ferrous materials melt into liquid in cohesive zone (CZ) and penetrates through coke bed to hearth while interacting with gas and solid flow. The liquid behavior can significantly impact the bed permeability, gas and liquid distributions and associated heat and mass transfer in the lower part of BF, particularly when smelting different ore types. It largely dictates the stability of BF process. However, due to the harsh operating conditions, there remains a lack of effective tools to accurately quantify the liquid flow and its influence on BF performance. Our study aims to address this challenge by further developing the liquid flow model based on our recent Computational Fluid Dynamics (CFD) process model. Specially, our model has been applied to the vanadium titanium magnetite (VTM) BF smelting process by explicitly considering the TiO_2 reduction and its reactant on slag viscosity. The effects of TiO_2 content in ore are investigated to validate the model applicability. Additionally, the top burden distributions are adjusted to improve the bed permeability in the BF lower part. The proposed work extends the predictive capabilities to anticipate the abnormal operations for the VTM smelting process and offers practical solutions for production optimization.

Modeling and Analysis of the Hydrogen Reduction in the Flash Ironmaking Process

Jiayi Wang, [a,b] Shibo Kuang, [a,*] Ning Yang, [b,**] Aibing Yu [a,c]

[a] ARC Research Hub for Smart Process Design and Control, Department of Chemical and Biological Engineering, Monash University, Clayton, Victoria, 3800, Australia

[b] State Key Laboratory of Multiphase Complex Systems, Institute of Process Engineering, Chinese Academy of Sciences, Beijing 100190, PR China

[c] Center for Energy and Environment, Southeast University-Monash University Joint Research Institute, Suzhou, 215123, China

*Corresponding author: shibo.kuang@monash.edu

**Corresponding author: nyang@ipe.ac.cn

After extensive development, blast furnace ironmaking technology has reached a level of maturity. However, the high energy consumption and environmental pollution resulting from emissions remain critical issues that demand attention. To overcome these challenges, a novel ironmaking technology known as flash reduction has emerged in recent years. In comparison to the blast furnace technology, flash reduction eliminates the need for sintering and pelletizing processes. Instead, it employs high-temperature gas to reduce iron ore fines, thereby avoiding complications such as agglomeration or sticking in fluidized beds. Moreover, this process significantly reduces carbon dioxide emissions, lowers energy consumption, exhibits a high rate of heat and mass transfer, and consequently enhances the utilization efficiency of iron ore fines.

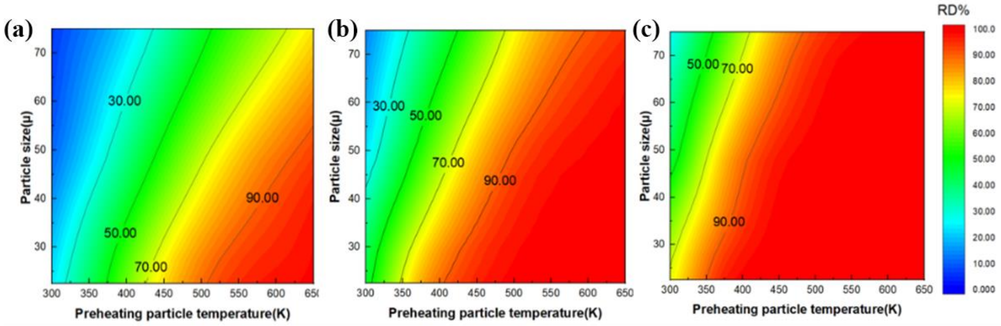

Figure 1 Effect of preheating on flash reduction: Temperature of Reducing gas (H_2) = (a) 1700K, (b) 1800K, (c) 1900K

Flash ironmaking is a reduction process that primarily utilizes hydrogen as the reducing agent. Given that it involves complex processes encompassing both gas and particle phases, intricate chemical reactions, as well as fluid dynamics and heat transfer, computational fluid dynamics (CFD) methods offer an effective research tool for assessing the impacts of various variables and their coupling, compared to experimental studies. In this study, we propose a three-dimensional CFD model using the Ansys Fluent, combined with the Discrete Phase Model (DPM), to effectively simulate and analyze the continuously reducing gas and discrete magnetite particles. Upon validating the proposed model, we propose the concept of preheating both the reducing gas and particles and note that both gas and particle temperatures affect the reduction degree significantly, they must be high enough. The extent of their contributions should be quantified for better optimization. Additionally, the effects of particle size, gas and particle temperatures are quantified, showing intensive interplay. From these results, the significance of preheating in the flash reduction reaction process has been validated.

The project aims to attain a thorough and economically viable comprehension of the flash ironmaking process. The discernments derived from this investigation will furnish significant theoretical underpinnings for prospective industrial implementations and could expedite the refinement and enhancement of flash ironmaking methodologies.

Numerical study on hydrogen-intensive industrial shaft furnaces

Yang Fei,[a,b,]* Shibo Kuang,[a] Xiaoping Guan,[b] Aibing Yu,[a] Ning Yang[b]

[a]ARC Research Hub for Smart Process Design and Control, Department of Chemical and Biological Engineering,
Monash University, Clayton, VIC 3800, Australia
[b]State Key Laboratory of Mesoscience and Engineering, Chinese Academy of Sciences, Beijing 100190, PR China
*Corresponding author: yang.fei1@monash.edu

The steel industry accounts for 6~9% of the global greenhouse gas emissions. The ironmaking blast furnaces and associated processes, which contributed to 70% of steel production, represent 90% of the total CO_2 emissions in integrated steel works. Therefore, reducing CO_2 emissions from the ironmaking process is essential for achieving carbon neutrality by 2050. Various pathways to decarbonize the ironmaking process are taking shape across the global industry to improve the sustainability of the process, e.g., low-carbon blast furnaces, shaft furnaces, and fluidization reduction. We focus on the hydrogen-intensive shaft furnace technology, which uses hydrogen-rich reducing gases to convert iron ore into a purer form of iron, i.e., direct reduction iron. Some exemplary applications include CORREX and Midrex/Energiron shaft furnaces. This work considers the Midrex/Energiron shaft furnace, which are more often adopted in industrial practice. We developed a state-of-the-art CFD model to describe the flow and thermochemical behavior and overall performance of shaft furnaces under different conditions. Following careful model validation, model studies were conducted systematically to understand shaft furnaces and formulate control and optimization strategies to guide shaft furnace applications.

References

[1] Y. Fei, X.P. Guan, S.B. Kuang, A.B Yu, N. Yang, *ACS Engineering Au* **2024**, 4, 145−165.

A novel hybrid free-fall electrostatic separator

Naghmeh Abavi Torghabeh*, Peter M. Ireland, Grant B. Webber

Discipline of Chemical and Renewable Energy Engineering, University of Newcastle, NIER, Vale Street, Shortland
NSW 2308 Australia

*Corresponding author: Naghmeh.abavitorghabeh@uon.edu.au

Electrostatic separation is an attractive method for dry processing in the resources and recycling industries. Free-fall electrostatic separators are a particularly simple and versatile member of this family of technologies. The charging mechanism is an important factor in the performance of free-fall separators, and they are normally used with triboelectric charging. In this work, the effectiveness of a novel hybrid separator (comprising a conductive charging slide and a free-fall separator, with particles injected into the separator at an oblique angle) has been assessed. This design may be more reliable in difficult environments (e.g. extraterrestrial operations) than either rotating drum or triboelectric separators. Separation experiments were conducted on a mixture of glass (non-conductive/ ~350 μm) and aluminium (conductive/ ~50-200 μm) particles of roughly comparable density. The output stream was divided horizontally into bins, allowing their spatial distribution in response to the electric field to be characterized. The influence of different feeding rates from a vibratory feeder (0.5, 2, 8 g/sec), and of varying separator and charger voltages (0, 5, 10, 15, 20, and 25 kV), was investigated. The outputs were analysed using optical microscopy to evaluate the spatial distribution of each component of the original mixture. Deflection of aluminium particles away from the negative plate increased with separator (and charger) voltage, while deflection of glass particles did not increase appreciably. Feed rate had a negligible influence on deflection over the range investigated. This method can in principle separate a mixture of conductive and nonconductive particles.

Numerical simulation of the influence of injection structure on pulverized coal gasification in the dome zone of COREX melter gasifier

Wenchao Zhang[a,b], Heng Zhou[a,b*], Yifan Hu[a,b], Yapu Xing[a,b], Mingyuan Chen[a,b], Mingyin Kou[a,b], Shengli Wu[a,b]

[a] School of Metallurgy and Ecological Engineering, University of Science and Technology Beijing, Beijing 100083, China

[b] State Key Laboratory of Advanced Metallurgy, University of Science and Technology Beijing, Beijing 100083, China

*Corresponding author: zhouheng@ustb.edu.cn

The dome zone is the freeboard at the top of COREX melter gasifier (MG). Changing some oxygen burners (OBs) in the dome zone to oxygen-coal burners (OCBs) can realize the function of pulverized coal gasification. Pulverized coal injection (PCI) in the dome zone of COREX is benefit to increase the amount of reducing gas and improve the metallization rate of the pre-reduction shaft furnace, which can reduce the overall fuel consumption and CO_2 emissions. In this work, a 3-D steady-state mathematical model was developed to study the influence of injection structure on the flow, temperature and species distribution. The results showed that an increase in the opposed deviation angle of the OCBs leads to the formation of a vortex core in the central area, transform the columnar high-temperature area into a leaf shape. An increase in the opposed deviation angle from 0° to 30° results in a rise focal temperature by 189.3K and a 2.82% increase in the effective gas content of the generator gas. However, excessive swirl intensity can lead to the accumulation of pulverized coal at the furnace wall, preventing its full utilization. Therefore, it is advisable to set the opposed deviation angle to 20°. An increase in the diameter of the oxygen pipeline in the OCBs results in a decrease in the velocity of the oxygen jet, which facilitates the water gas conversion reaction and enhances the H_2 content in the generator gas by 1.35%. Moreover, adjusting the OCBs from a downward tilt to a horizontal position shortens the residence time of pulverized coal, thereby limiting the progress of gas-solid reactions and reducing the effective components in the generator gas. Further adjustment of the OCBs to an upward tilt leads to an increase in the amount of unburned pulverized coal.

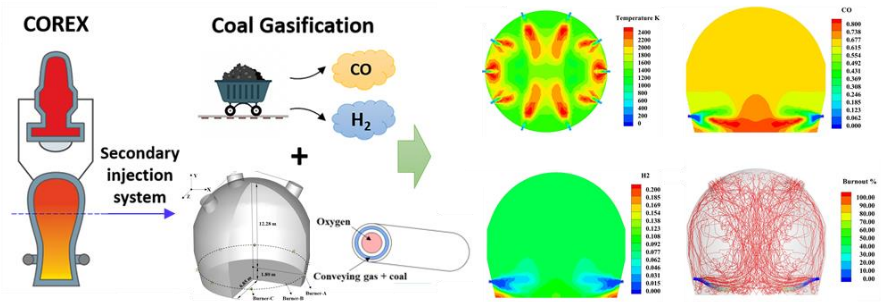

Figure 1. 3-D mathematical model of dome zone

References

[1] Hu Y. F., Zhou H., She X. F., et al. *Ind. Eng. Chem. Res*., 2022, **61**(1): 931-941.

Polymer characterization and pyrolysis mechanism of end-of-life photovoltaic modules

Shangming Wang, Yunan Chen, Bin Chen*

State Key Laboratory of Multiphase Flow in Power Engineering, Xi’an Jiaotong University, Xi’an 710049, China
*Corresponding author: chenbin@mail.xjtu.edu.cn

There are more and more photovoltaic (PV) modules close to the service life (20-30 years) on the market. At present, the main methods of recycling end-of-life (EoL) PV modules are physical, chemical and heat treatment approaches. Heat treatment can effectively separate the components of EoL PV modules through temperature control, which is fast and simple, and is currently the most common and promising recycling technology. Although there have been studies on polymer characterization and pyrolysis study for EoL PV modules, its depolymerization characteristics, kinetic behavior, product formation and other mechanisms under different pyrolysis atmospheres are still unclear. To systematically explore the pyrolysis kinetics, product distribution and mechanism of polymers (including EVA, PET, etc), and lay a foundation for the recovery and utilization of PV modules in the future, this study for the first-time combined experiments with reactive force field molecular dynamics (ReaxFF-MD) simulations to describe the pyrolysis process of polymers under different atmospheres (nitrogen and air). Firstly, pyrolysis kinetic parameters of EVA were evaluated by iso-conversional methods (KAS, FWO, and AIC) based on TG analysis. Subsequently, the pyrolysis process and products were studied by TG-IR, and PyGC/MS analysis. Finally, ReaxFF-MD simulations were used to study the microcosmic reaction pathways of polymers at different temperatures (1700-2900 K, interval of 300K) during the pyrolysis process. All simulations were performed in software LAMMPS by using the 2008_field_cho force field. The constructed model consists of 6 polymers chains with polymerization degree of 60, and 100 oxygen molecules are added to the model to correspond to pyrolysis in air atmosphere. After structural and energy optimized relaxation in NPT ensemble, the model will be subjected to formal pyrolysis simulation for 200 ps in NVT ensemble. Through the analysis of results, the main conclusions are as follows. 1) The pyrolysis process of EVA goes through two stages under both nitrogen and air atmosphere, and the final weight loss rate exceeds 99%. 2) Although EVA has lower apparent activation energy under air atmosphere (as shown in Table 1), its pyrolysis end temperature (about 550 ℃) is higher than that in nitrogen atmosphere (about 500 ℃). 3) The first stage of EVA pyrolysis is deacetylation reaction. In the second stage, the deacetylated carbon atom drives adjacent carbon atom to break bond with parent chain. 4) Oxygen could combine alkyl radicals to form alkyl peroxide, and then peroxy bond breaks to form small molecule products.

Table 1. E_a (kJ/mol) of EVA

Methods	Nitrogen		Air	
	I	II	I	II
KAS	175	260	136	182
FWO	178	264	138	185
AIC	177	273	137	186

References

[1] Tao, J., Yu, S., Sol. *Energy Mater. Sol. Cells* **2015**, 141, 108–124.

Amino Acid-Derived Polynorbornene: Investigating the Shift from Synthetic Polymers to Polymer Interfaces and Interface Bridging with Multi-Wall Carbon Nanotubes

Sutthira Sutthasupa,[a,*] Sirilak Wangnage,[b] Sukanya Thisan,[c] Sarawut Kamphune,[c] Apiwat Pankaew,[d] Weerawut Chaiwat[e]

[a] Division of Packaging Technology, Faculty of Agro Industry, Chiang Mai University, Chiang Mai, Thailand
[b] Office of Research Administration, Chiang Mai University, Chiang Mai, Thailand
[c] Biomedical Engineering and Innovation Research Center, Chiang Mai University, Chiang Mai, Thailand
[d] Mahidol University-Frontier Research Facility, Mahidol University, Salaya, Nakhon Pathom, Thailand
[e] Department of Chemical Engineering, Faculty of Engineering, Mahidol University, Nakhon Pathom, Thailand
*Corresponding author: sutthira.s@cmu.ac.th

Advancements in polymer chemistry are pivotal for crafting polymer interfaces, spanning nano- to micron-sized macromolecular systems ubiquitous in both natural and technological realms. These interfaces, comprising single polymers or assembled polymer chains on support structures, include self-assembly systems driven by individual polymer chains and block copolymers. The assembly of polymers with side-chain functional groups into nanoscale morphologies has proven essential in emerging applications such as drug and gene delivery and nanotechnology [1]. Ring Opening Metathesis Polymerization (ROMP), using the Grubbs catalyst, is a versatile technique capable of creating well-defined polymer structures with diverse functional groups, including aromatics, alkyls, and polar groups. Its high tolerance for polar functionalities like oxygen, nitrogen, or sulfur enables the polymerization of olefins, facilitating the synthesis of polymers with varied chemical structures. ROMP is instrumental in designing advanced materials, such as well-defined block copolymers, micelles for drug delivery, graft copolymers forming amphiphilic nanostructures, and polymeric materials with precise structures and beneficial properties [2]. We have synthesized polymeric materials containing side chain amino acids via ROMP, offering benefits such as stimuli-responsiveness. Examples include pH-sensitive micelles for drug delivery and release [3], temperature-responsive brush block copolymers synthesized via Graft-through ROMP [4], and fluorescent chemosensors based on tryptophan as biomarkers for detecting Fe^{2+} in EA.hy926 cells [5]. The latter work highlights additional opportunities for exploring interesting properties related to polymer interfaces, which we will present in this study.

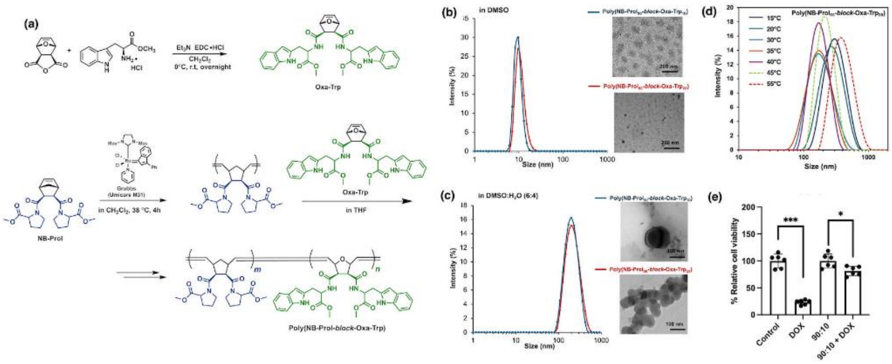

Figure 1. (a) Scheme for monomer synthesis and block copolymerization, Hydrodynamic diameter (D_h)distributions of poly(NB-Prol$_{90}$-*block*-Oxa-Trp$_{10}$) and poly(NB-Prol$_{80}$-*block*-Oxa-Trp$_{20}$) aggregates; TEM images of the aggregates formed in (b) DMSO and (c) the selective solvent DMSO:H_2O (60:40 %v/v) (d) Temperature dependent of hydrodynamic diameter distributions of poly(NB-Prol$_{80}$-*block*-Oxa-Trp$_{20}$) and (e) Cytotoxicity of empty micelles and cancer cell killing activity of the free DOX HCl and poly(NB-Prol$_{90}$-*block*-Oxa-Trp$_{10}$) micelle-loaded DOX HCl.

The synthesized Oxa-Trp monomer exhibits fluorescence emission at 350 nm due to the intrinsic fluorescence of the indole moiety in tryptophan. The proline-derived norbornene monomer (NB-Prol) and its polymer display thermoresponsiveness [4]. Block copolymerization of these monomers, with varying comonomer units, yielded block copolymers with Mw ranging from 5,000 to 7,500 g/mol. The fluorescence properties of the block copolymers confirmed solvent-induced aggregation and core-shell formation, utilizing the intrinsic Trp fluorescence of Poly-Oxa-Trp. In DMSO, Poly(NB-Prol$_{90}$-*block*-Oxa-Trp$_{10}$) and Poly(NB-Prol$_{80}$-*block*-Oxa-Trp$_{20}$) exhibited particles with an average hydrodynamic diameter (D_h) of 11.5–16 nm, attributed to single-chain block copolymers. TEM results showed nano-sized particles and further aggregation in DMSO. [Figure 1(b)] In DMSO:H_2O (60:40 %v/v), a unimodal DLS curve with D_h of 185–210 nm suggested self-assembly into large micelles. [Figure 1(c)] Dh values decreased from 15 °C to 45 °C, slightly from 45 °C to 50 °C, and then increased from 50 °C to 65 °C [Figure 1(d)]. These micelles could load and release DOX HCl, a cancer drug. The empty micelles were non-toxic up to a test concentration of 10 µg/mL. DOX HCl-loaded micelles exhibited antitumor effects on HepG2 cells [Figure 1(e)].

To bridge our tryptophan-derived polynorbornene with Multi wall carbon nanotubes (MWCNTs), we copolymerized it with MWCNT-functionalized norbornene monomers or grafted the polymers onto MWCNTs (Figure 2). The resulting copolymer composites exhibited fluorescence properties and selectively detected Cu^{2+} with fluorescence on-off characteristics. [Figure 2(b)] The addition of amino acids, especially cysteine (Cys), restored the fluorescence intensity. [Figure 2(c)] Intracellular thiols such as cysteine (Cys), homocysteine (Hcy), and glutathione (GSH) are crucial in numerous physiological processes. Imbalanced levels of these biothiols can result in various health issues. [6] Therefore, the synthesized copolymer composites offer a potential fluorescence probe for the selective detection of Cys, Hcy, and GSH.

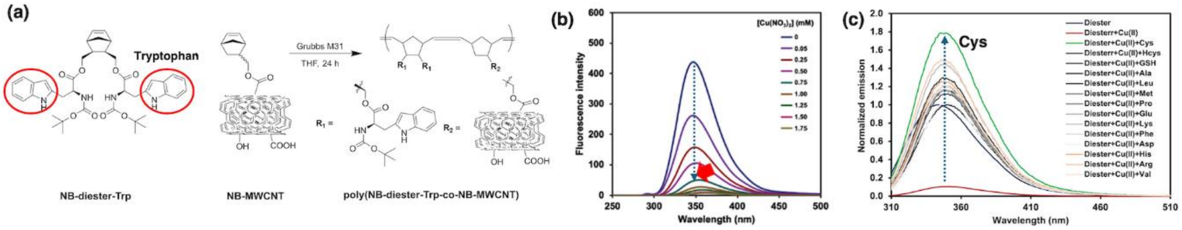

Figure 1. (a) Copolymerization Tryptophan derived norbornene and MWCNT-derived norbornene. (b) Fluorescence titration of Poly(NB-diester-Trp-*co*-NB-MWCNT) (0.1 µM in DMSO) with increasing concentrations of Cu^{2+}. (c) Fluorescence spectra of Poly (NB-diester-Trp-*co*-NB-MWCNT) bound to Cu^{2+} after the addition of various amino acids.

References

[1] C. B. Kowollik, A. S. Goldmann, F. H. Schacher, *Macromolecules.* **2016**, 49, 5001−5016.

[2] C. Slugovc, Synthesis of Homopolymers and Copolymers. In Handbook of Metathesis-Vol. 3: Polymer Synthesis; Wiley-VCH Verlag GmbH & Co. KGaA, **2015**; pp. 123.

[3] S. Sutthasupa, F. Sanda, *Eur. Poly. J*, **2016**, 85, 211–224.

[4] S. Sutthasupa, K. Faungnawakijc, K. B. Wagener, F. Sanda, *Polymer* **2019**, 177, 178–188.

[5] S. Sutthasupa, A. Pankaew, S. Thisan, S. Wangngae, S. Kumphune, *Biomacromolecules* **2024**, 25, 2875−2889.

[6] L. Yang, Y. Su, Y. Geng, Y. Zhang, X. Ren, L. He, X. Song, *ACS Sens.* **2018**, 3, 1863−1869.

AI-based model prediction of respiratory deposition distribution of dry powder inhalation formulations

Lixing Zhang,[a] Zhenbo Tong, [a, b*] Aibing Yu [b,c]

[a] School of Energy and Environment, Southeast University, Nanjing, 210096, PR China
[b] Southeast University-Monash University Joint Research Institute, Suzhou, 215123, PR China
[c] Department of Chemical Engineering, Monash University, Clayton, VIC 3800, Australia
*Corresponding author: z.tong@seu.edu.cn

Understanding the deposition mechanisms of dry powder inhalers in the human respiratory tract is critical to the prediction of aerosol particle deposition in the lungs. In this study, a whole-lung model of a real human respiratory tract was simulated using a coupled computational fluid dynamics-discrete phase method (CFD-DPM). First, an accurate human airway model from the mouth cavity to the tenth-generation bronchi was created based on computed tomography images. Then the CFD-DPM model is validated using the experimental data. Next, the laws of particle size, acoustic gate cross-sectional area, airway curvature, tongue height, and type and depth of inhalation device on the distribution of aerosol particle deposition were investigated at different respiratory flow rates. Finally, a prediction model of aerosol particle deposition distribution was developed based on AI-CFD data. The results indicate that the insertion of an inhalation device significantly alters the structure of the airflow in the respiratory tract and affects the location of aerosol deposition, a non-negligible condition. As the respiratory flow rate increases with particle size, the deposition of particles in the bronchioles decreases and the deep lung content will decrease. The acoustic portal cross-sectional area and tongue height affect the generation as well as the intensity of turbulence in the respiratory tract, which in turn increases the amount of particles deposited at that location. The results predicted by AI model are highly consistent with the CFD numerical simulation results.

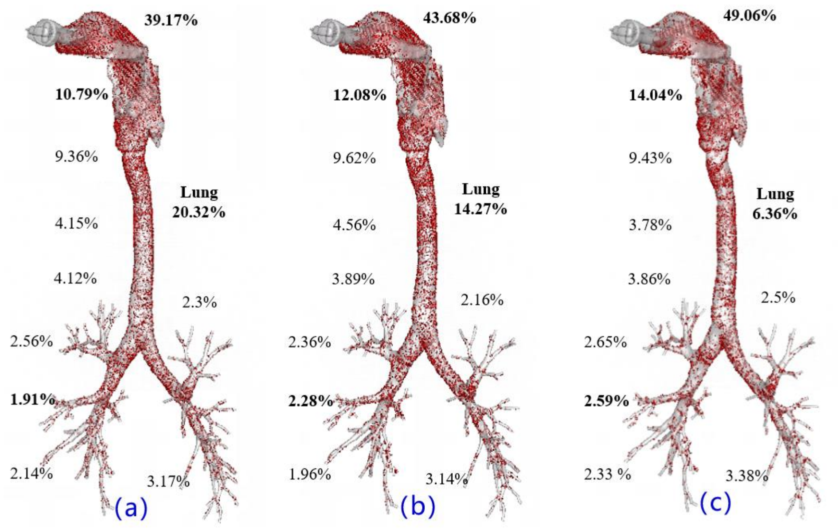

Figure 1. Distribution of aerosol particles of different particle sizes in the respiratory tract at an inspiratory flow rate of 45 L/min. (a) $2\mu m$; (b) $4\mu m$; (c) $6\mu m$

Agglomerate aerosols by ultrasound: its impact on air filter pressure drop

Pengzhan Liu,[a,b,*] Xin Zhang,[a] Guicai Liu,[c] Shi Hao Lim,[a] Man Pun Wan,[b] Grzegorz Lisak,[c,d] Bing Feng Ng[b]

[a]Energy Research Institute @ NTU, Nanyang Technological University, Singapore
[b]School of Mechanical and Aerospace Engineering, Nanyang Technological University, Singapore
[c]Residues and Resource Reclamation Centre, Nanyang Environment and Water Research Institute, Nanyang Technological University, Singapore
[d]School of Civil and Environmental Engineering, Nanyang Technological University, Singapore
*Corresponding author: pengzhan.liu@ntu.edu.sg

Acoustic agglomeration harnesses sound waves to promote the collision of aerosol particulate matter in air, thus enabling the formation of larger particle agglomerates. Here, we employ this acoustics-driven phenomenon for the pre-conditioning of aerosol particles to enhance the filtration efficiency and slow down pressure drop increment of air filters in a ventilation tunnel system. Specifically, we first implement ultrasonic agglomeration of aerosol particles in the main tunnel to transform small particles into larger agglomerates and then deposit them by a cyclone. Benefitting from this process, a downstream air filter receives less particle mass and thus experiences slower pressure drop increment. We also experimentally investigate the influence of some key parameters including the residence time of aerosol particles in the ultrasonic field, sound pressure level, and initial particle number concentration. The findings in the work hold potential for deriving energy savings for fan power in industrial ventilation systems.

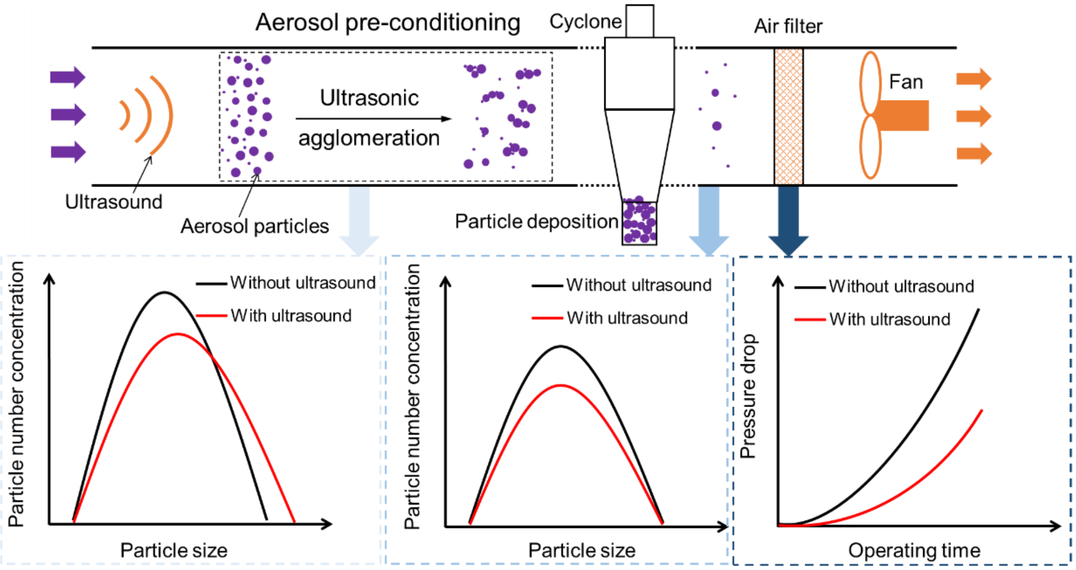

Figure 1. Mechanisms of slowing down increase of air filter pressure drop enabled by ultrasonic aerosol agglomeration [1].

References

[1] P. Liu, X. Zhang, G. Liu, S. Hao Lim, M. Pun Wan, G. Lisak, B. Feng Ng, *Ultrason Sonochem* **2024**, 103, 106774.

Seasonal characteristic variations of PM2.5 chemical components and implications for cloud condensation nuclei activation properties

Yongwei Lu[a], Yunkun Chen[b], Xin Wang[c,*], Bo Ren[a], Biao Li[a], Eric Lichtfouse[a], Yueshe Wang[a,**]

[a] State Key Laboratory of Multiphase Flow in Power Engineering, Xi’an Jiaotong University, Xi’an 710049, Shaanxi, China
[b] Science and Technology on Aerospace Chemical Power Laboratory, Hubei Institute of Aerospace Chemotechnology, Xiangyang, 441003, Hubei, China
[c] School of Chemistry, Xi’an Jiaotong University, Xi’an 710049, Shaanxi, China
* corresponding author: wangxin@mail.xjtu.edu.cn
**corresponding author: wangys@mail.xjtu.edu.cn

The PM2.5 samples were collected from Xi'an city in the summer and winter of 2019, aiming to investigate the characteristic variability of chemical components in atmospheric particles across different seasons, diurnal variations, and pollution levels. The analysis of haze formation in Xi'an and its impact on the activation properties of cloud condensation nuclei was conducted. The findings revealed a significant increase in particulate loading during winter, with SO_4^{2-} showing a rise of 110%, organic materials increasing by 159%, NO_3^- surging by 355%, and Cl^- experiencing an astonishing growth of 2270%. The effect of diurnal variation on the chemical components is negligible. Secondary transformation predominantly contributes to particulate matter, accounting for over 74.97%, primarily originating from local emissions. Motor vehicle exhaust constitutes the primary source of pollution, with exogenous inputs from biomass burning air masses during winter serving as a significant contributor to heightened pollution levels. The atmospheric particles in the city of Xi'an exhibit typical characteristics of continental aerosols, with κ_{ccn} values of 0.26 ± 0.07 during summer and 0.33 ± 0.09 during winter (SS = 0.2%). Seasonal fluctuations in κ_{ccn} are ascribed to the influx of weakly hygroscopic organic air masses from southern forests during the summer period. The occurrence of high κ_{ccn} values is observed during the winter months and periods characterized by elevated pollution levels. Increasing supersaturation leads to a decrease in the critical particle size of particulate matter. When supersaturation reaches levels within convective clouds (SS ≈ 0.7%), both summer and winter particulate matter can be activated in the Aitken nuclei mode.

Particle Engineering: Effective theory for predicting the properties of sprayed products

Alberto Baldelli*

Senior Lecturer, School of Agriculture and Food Sustainability, the University of Queensland
*Corresponding author: a.baldelli@uq.edu.au

Particle engineering is a theory focused on predicting spray-dried powders' chemical and physical properties. Even though the theory is simple and applicable to several fields, such as pharmaceutical and food science, few researchers have employed it in their studies. Moreover, particle engineering is the base behind spraying drying, a technique highly used in several pharmaceutical and food industries, such as dairy, fruit, or fortified foods. Several food products, such as instant coffee, infant formula, whiteners, flavor powders, and fortifying flours, are produced via spray drying. Therefore, the understanding and applicability of particle engineering in controlling the properties of spray-dried powders. The Peclet number is the most important parameter in Particle Engineering. The Peclet number is defined as the ratio between the solvent's evaporation rate divided by the solute's diffusivity. The evaporation rate identifies the speed at which the solvent leaves the evaporating droplet, while the diffusivity identifies the speed at which the solute travels toward the center of the evaporating droplet. Therefore, high Peclet numbers commonly indicate larger microparticles with a crumbled structure. Low Peclet numbers commonly indicate smaller microparticles with the absence of any external and internal voids. However, the Peclet number depends on the drying conditions and the properties of the solution. Higher temperatures lead to a faster evaporation rate, which can lead to a higher one. The density and viscosity of the solutions can influence the diffusivity, which affects the Peclet number. In addition, the particle formation of suspensions, typically, for instance, of dairies, shows a different physics depending on the size of the suspensions. Micro-suspensions and nano-suspensions differ in their diffusivity; the second, having a much smaller size, tends to have a higher diffusivity and, thus, a lower Peclet number.

Microfluidic-based controlled synthesis of cross-linked hyaluronic acid nanoparticles using real-time gas-phase electrophoretic analysis

Po-Yu Lai, Ying-Hsuan Wang, Jen-Huang Huang, De-Hao Tsai*

Department of chemical engineering, National Tsing-Hua University, Hsinchu, Taiwan, R.O.C.
*Corresponding author: dhtsai@mx.nthu.edu.tw

In this study, we demonstrate a microfluidic-based controlled synthesis and characterization of cross-linked hyaluronic acid (HA) using real-time electrospray-differential mobility analysis (ES-DMA). Real-time gas-phase electrophoresis analysis delivers instant nanoparticles size results and microfluidic-based synthesis provides the materials with controlled uniform particle size distributions. The method successfully combines real-time analysis and microfluidic system to acquire specific sizes of HA nanoparticles with high efficiency. Small-angle X-ray scattering and Nuclear Magnetic Resonance spectroscopy (NMR) are performed for complementary analysis of extent of crosslinking and colloidal stability. The work demonstrates a promising approach for synthesis of inorganic and organic functional nanoparticles with high uniformity and traceability.

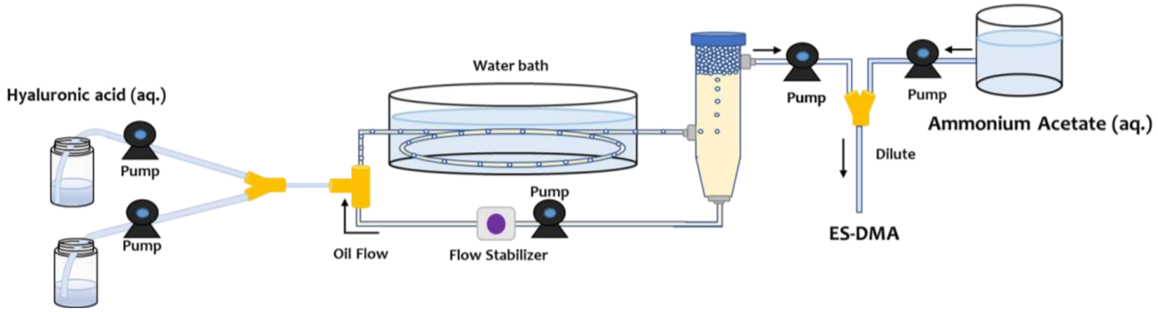

Figure 1 Microfluidic-based synthsis with real-time gas-phase electrophoretic analysis.

Creation of surfactant-free nanopowder emulsions and its interfacial structure

Yuuki YAZAWA,[a,]* Toshihiko EGUCHI[b]

[a]Chiba Institute of Technology, Chiba, JAPAN
[b]AURA TEC Co., Fukuoka, JAPAN
*Corresponding author: yuuki.yazawa@p.chibakoudai.jp

Heterogenous substances that do not dissolve in water will eventually separate into two layers even when thoroughly mixed and left to stand. Emulsions of water and oil also undergo phase separation quickly without the addition of amphiphilic surfactants. We successfully generated nano-sized O/W emulsions that do not separate into oil and water phase phases without the use of surfactants by the ejector-type fine bubble generating nozzle. This study aims to elucidate the presence and its interfacial structure of surfactant-free nano emulsions (SFNE) between the oil (*n*-pentadecane) dispersed phase and the water continuous phase.

Results from the Dynamic Light Scattering (DLS) showed that the oil droplet size was approximately 50 nm immediately after formation but grew to about 200 nm after 100 days (**Figure 1. a)**). The growth rate of the oil droplets was 2.6 x 10^{-28} m^3/s, which is significantly slower than the Ostwald ripening. However, TEM observations using freeze-fracture (FF-TEM) method revealed that the oil droplets had scarcely coalesced and were present as aggregates (Figure 1. b)). The oil droplets, which are less dense than water, floated to the surface over time and aggregated like a powder, but could be easily dispersed with a gentle shake. These reasons are discussed in the negative zeta potential of the nonpolar oil droplets prevents coalescence and causes repulsive forces between the droplets. The O/W interfacial structure of SFNE was quantitatively analysed with solid-liquid phase transitions using the Differential Scanning Calorimetry (DSC). The results indicated that the required hydrophobic hydration number for each bulk oil molecule interacting with water was from 60 to 600, the hydration number necessary for stabilization increased exponentially with increasing the droplets size of SFNE (Figure 1. c)).

Accordingly, it is theoretically suggested that the maximum oil-to-water ratio of SFNE can be up to 20 vol.%. This implies potential applications in a wide range of fields, including pharmaceuticals, cosmetics, pesticides, and energy materials without the need for surfactant, which are often considered impurities.

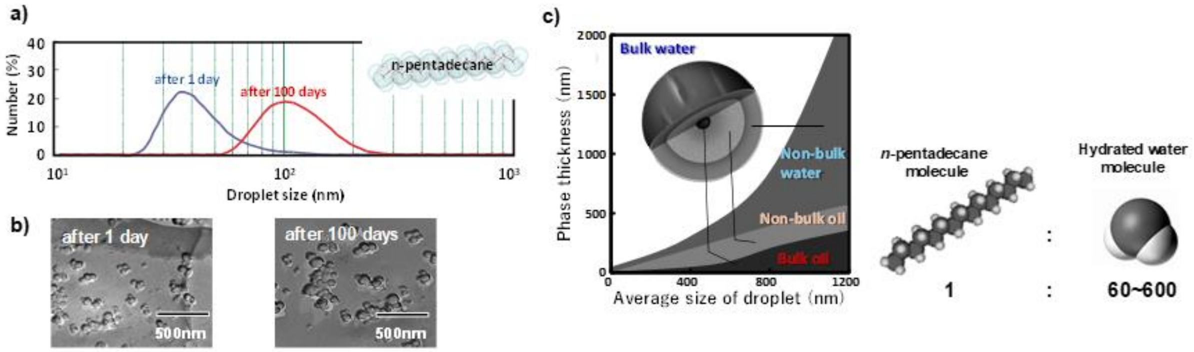

Figure 1. The presences and its interfacial structure of O/W-SFNE (a): oil-droplet sized distribution, b): FF-TEM images, c) stabilized structure *vs.* droplet size).

Investigation of Silane Chemistry for Metal Surface Modification

Yi-Jun Wang,[a] De-Hao Tsai,[a,]* and Chien-Hsun Chen[b]

[a]Department of Chemical Engineering, National Tsing Hua University, Hsinchu, Taiwan, R.O.C.
[b]Highlight Tech Corp. Co., Ltd., No. 32, Guangfu Rd., Hukou Township, Hsinchu County 303036, Taiwan, R.O.C.
*Corresponding author: dhtsai@mx.nthu.edu.tw

Silane chemistry is a specialized field that has gained significant attention in the industry, particularly in surface modification of materials. In this study, we chose tetraethoxysilane (TEOS) as the representative silane to explore surface alkylation and investigate properties such as acid resistance and scratch resistance of material. We began with the mechanism of alcoholysis/hydrolysis, adjusting solute concentration, alcoholysis/hydrolysis reaction time, and ambient temperature. Utilizing innovative analytical methods such as ES-DMA and FTIR, we examined the interaction between reaction parameters through the particle size distribution before film formation and the bonding structure after film formation. This study provides an opportunity to design multifunctional protective coating structure aimed at extending the durability of high-vacuum operation units.

Generation of Acoustic streaming in Closed Field with Ultrasonic Vibration

Kazuki KOINUMA,* Kenji KOFU

Department of Mechanical Engineering, College of Science and Technology, Nihon University, Tokyo, Japan
*Corresponding author: cska23012@g.nihon-u.ac.jp

Kozuka et al. have shown that it is possible to capture microparticles and control their behaviour by using ultrasound in the air and water.[1] If it becomes possible to control particle behaviour using ultrasonic waves, operations such as aggregation and collection can be performed without contact, so the particles will not be damaged, and this can be expected to be applied to technologies such as drug delivery systems.[2] Nonaka et al.[3] said that it was possible to control the behaviour of particles which is larger than several tens micro meter if air velocity is slow and sound pressure is high. On the other hand, in the case of even smaller particles, it was difficult to concentrate at a certain position because they move along with the acoustic streaming. This means it is necessary to know the acoustic streaming if the motion control of small size particle is expected. Therefore, in this study, we measured the sound pressure distribution and acoustic streaming in a closed space. Additionally, it was attempted to simulate the acoustic streaming with COMSOL Multiphysics and compared it with experiments. Figures 1 and 2 show the results of the experiment. In the experiment, a space was filled with smoke and motion was captured with a PIV laser and a high-speed camera. Then, streaming was analysed using image analysis software. In this time, a vibration plate with four nodes was used, the frequency was 20.1 kHz, the vibration amplitude was 10 μm while the distance between vibration plate and the reflector was changed for half or one acoustic wavelengths. It was found that in the case of one wavelength, as in Figure 1, two vertical vortices were observed. Then, in the case of half a wavelength, as in Figure 2, there is only one vertical vortex. It was considered that the number of vertical vortices changes depending on the height. It can also be seen that the maximum flow velocity is almost the same when the amplitude is the same. Figures 3 and 4 show the results of a simulation performed. They show that the number of vortices changes with the gap of plates as well as the experiment.

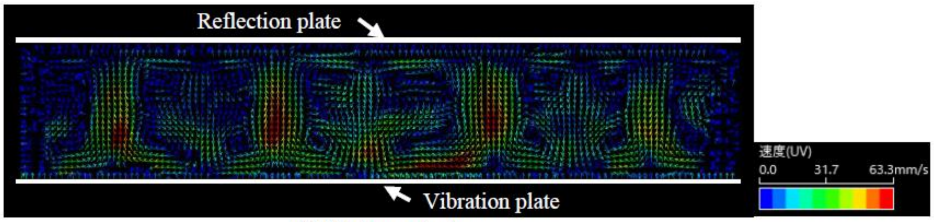

(a) Vector analysis

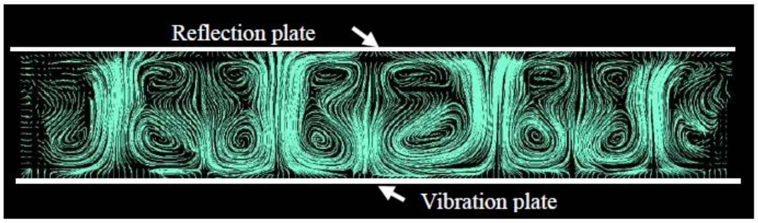

(b) Streamline analysis

Figure 1. Visualizing acoustic streaming (*f*=20.1kHz, node 4, A_m = 10 μm, 1wavelength)

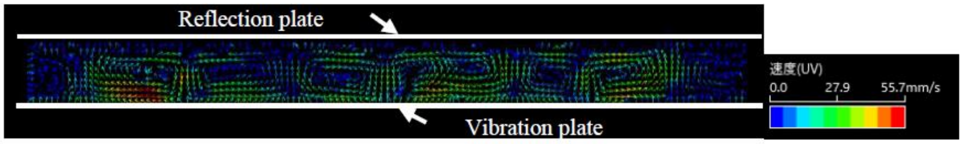

(a) Vector analysis

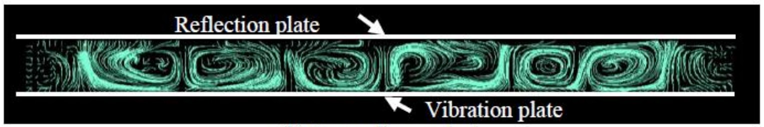

(b) Streamline analysis

Figure 2. Visualizing acoustic streaming (f=20.1kHz, node 4, A_m = 10 μm, 1/2wavelength)

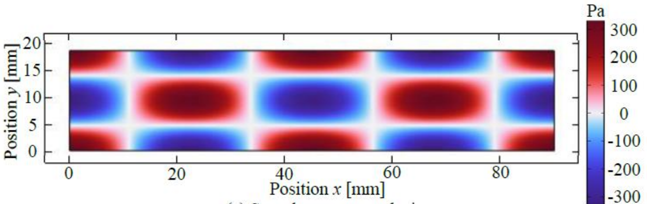

(a) Sound pressure analysis

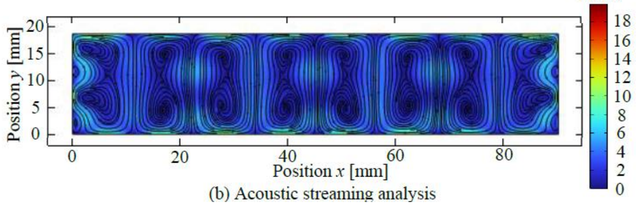

(b) Acoustic streaming analysis

Figure 3. analysis (f = 20 kHz, node 4, A_m = 0.1 μm, H = 18.553 mm)

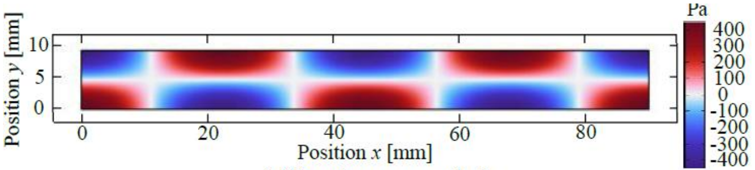

(a) Sound pressure analysis

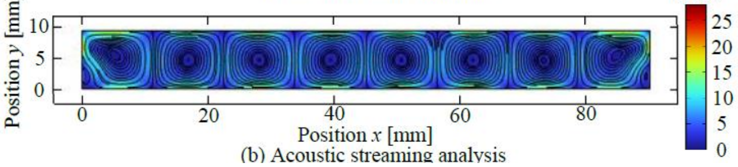

(b) Acoustic streaming analysis

Figure 4. analysis (f = 20 kHz, node 4, A_m = 0.1 μm, H = 9.274 mm)

References

[1] Teruyuki KOZUKA, kyuichi YASUI, Toru TUZIUTI, Atsuya TOWATA, Yasuo IIDA, The IEICE Transactions on fundamentals of electronics, 2008, pp.1156-1160

[2] Koji MASUDA,et. Al, Biocybernetics and Biomedical Engineering, Vol.31, 2011, pp.23-32

[3] Hirofumi NONAKA, Kazuki KOINUMA, Masahiro YAMADA, Kenji KOFU, Preparation of the 59th Symposium on Powder Science and Technology, 2022, pp.23-26

A novel system and method for effectively removing condensable particles using low-temperature condensation combined with adsorption.

Yue Zou, Cheng Zhang, Xian Li, Guangqian Luo, Yi Wang, Yu Qiao, Xiaowei Liu*

State Key Laboratory of Coal Combustion, Huahzong University of Science and Technology 1037 Luoyu Road,
Wuhan 430074, China
*Corresponding author: xwliu@hust.edu.cn

Coal combustion condensable particulate matter (CPM) is a hot topic in the current pollutant research [1]. However, because the generation of CPM involves complex transformations between multi-phase and multi-component systems, existing air pollution control devices are ineffective in removing CPM [2-3]. In this study, based on the characteristics of CPM formation and organic/inorganic components, we designed a CPM removal system including "generation, low-temperature condensation, and physical adsorption", and discussed in detail the efficiency of low-temperature cold condensation and adsorption coupled to remove CPM. This work aims to form the theoretical basis of efficient CPM removal technology.

The system is shown in **Fig. 1**, according to the previous research of our team [4-7], the organic and inorganic fractions and main components of CPM are shown in **Fig. 2**.The dibutyl phthalate in the organic component of CPM and SO_3 in the inorganic component are selected as the main research objects, and both of them are gasified and sequentially removed by low temperature and adsorption to realize the deep removal of CPM. By creating different supersaturated vapor environments, the water vapor in the flue gas is heterogeneously nucleated with ultrafine particles as nuclei to condense and form embryonic droplets to adsorb CPM gaseous precursors. The flue gas after low-temperature desorption was fully contacted and reacted with the adsorbent during the warming process to ensure that the residual CPM gaseous precursors were removed while the flue gas was discharged, and ultimately the deep removal of CPM was realized. The results show that the synergistic effect between condensation and adsorption is effective for CPM removal, in which activated carbon has the best adsorption performance among many adsorption materials in **Fig. 3**.

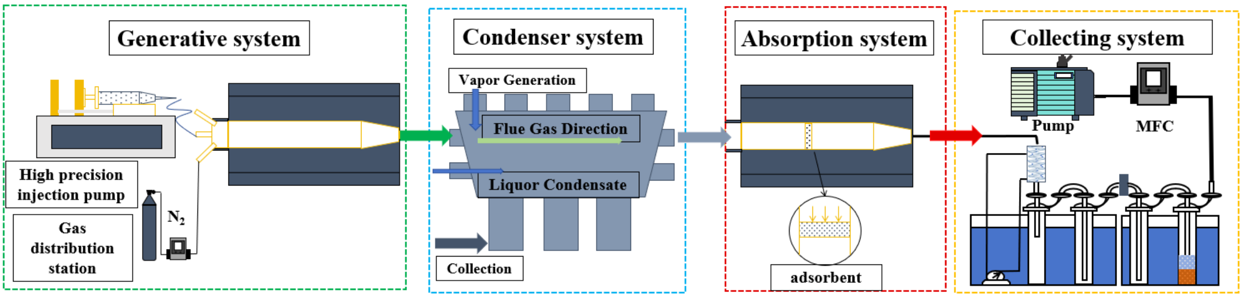

Figure 1. equipment system.

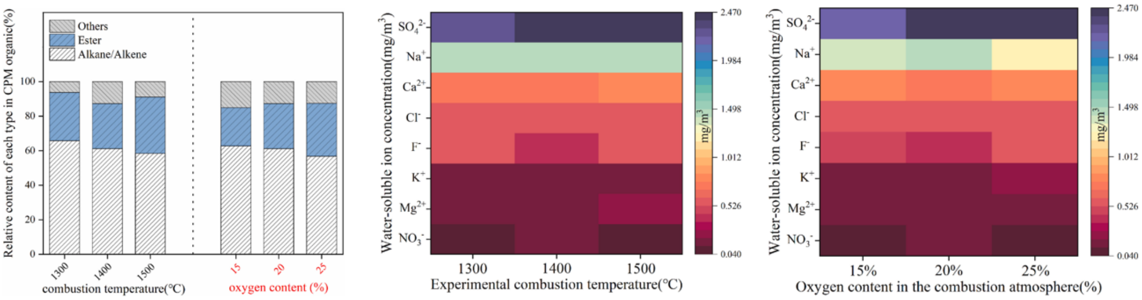

a. Relative content of each type in CPM organic.

b. Water-soluble ions in CPM inorganic.

Figure 2. organic and inorganic fractions and main components of CPM.

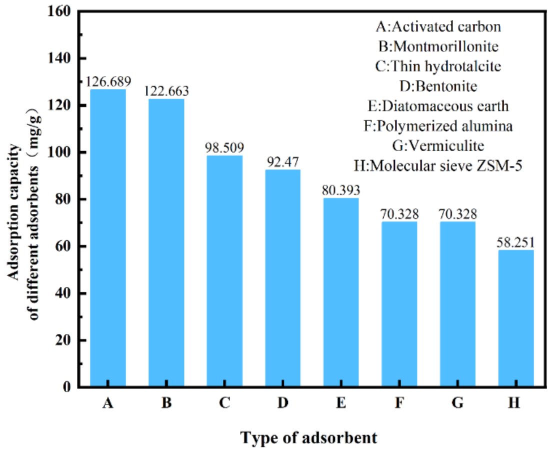

Figure 3. Adsorption capacity of different adsorbents.

References

[1] Lu. Wang, Yuzhong. Li*, Jingwei. Li, *Fuel*, **2022**,325 123807.
[2] Yujia. Wu, Zhenyao. Xu, Shengyong. Lu*, *Fuel*, **2022**,326 125052.
[3] Zhenyao. Xu, Yujia. Wu, Shengyong. Lu*, *Journal of Environmental Chemical Engineering*, **2022**,10 107667.
[4] Yue. Zou, Xiaowei. Liu*, Ku. Wu, *Journal of Hazardous Materials*, **2023**,443 130317.
[5] Yunfei. Zhai, Xiaowei. Liu*, Zijian. Zhou, *Fuel*, **2022**,356 129579.
[6] Yunfei. Zhai, Xiaowei. Liu*, Aoyang. Zhang, *Fuel*, **2022**,329 125492.
[7] Yue. Zou, Xiaowei. Liu*, Ku. Wu, *Chemosphere*, **2024**,353 141638.

Advances in spray drying powders

Meng Wai Woo*

Department of Chemical & Materials Engineering, Faculty of Engineering, Auckland, New Zealand
*Corresponding author: wai.woo@auckland.ac.nz

Spray drying is ubiquitous in the production of powders. This can range from food powder, fine chemical powders to pharmaceutical products. In the first part of this talk, we will examine the potential use of superheated steam as the drying medium replacing hot air. Some of the advantages of using superheated steam are the potential energy saving and in minimizing product oxidation due to the non-presence of oxygen. Superheated steam was also recently found to be a good drying medium to control crystallization in spray dried powder as well as improving the wettability of powders. On the flip side, we will also discuss the complexities of using superheated steam. Along this line, we will discuss the use of antisolvent vapour as the drying medium to produce ultrafine powders. This is a unique technique for utilizing each sprayed droplet in the drying chamber to be a micron-sized precipitating vessel. In the second part of this talk, we will discuss the one-dimensional predictive framework and the Computational Fluid Dynamics (CFD) framework for spray dryer modelling. For the one-dimensional predictive framework, we will examine a few numerical considerations for application in co- and counter-current spray dryer predictions. Agglomeration is at the forefront of CFD modelling and we will discuss the current capabilities and complexities in this area.

Assembly of Hybrid Nanoparticles via Metal Coordination for Disease Treatment

Zi (Sophia) Gu*

School of Chemical Engineering, University of New South Wales, Sydney, NSW 2052, Australia
*Corresponding author: zi.gu@unsw.edu.au

Nanomedicine has emerged as a promising approach for precision treatment of life-threatening diseases such as cancers.[1] Nanomaterial innovation play a key role in driving progress of the field.[2] Nanoparticles synthesized via metal coordination bond have been developed for safe and efficient treatment of diseases.[3,4] In this talk, I will present our recent work on developing programmable nanomedicine formulations by using copolymer-layered double hydroxide hybrid nanoparticles and polyphenol-metal coordination particles. The nanoparticles were constructed via metal coordination chemistry, and demonstrated advantageous properties of sensitive pH responsibility, biodegradability, tunable structure, and biomedical functionalities to deliver therapeutic and diagnostic payloads for targeted delivery, theranostics, drug repurposing, and catalytic nanomedicine. [5-8]

References

[1] Zhang, X.; Centurion, F.; Misra, A.; Patel, S.; Gu, Z. *Adv. Drug Deliv. Rev.* 2023, 114709.
[2] Cao, Z.; Li, B.; Sun, L.; Li, L.; Xu, Z.P.; Gu, Z. *Small Methods* 2019, 1900343.
[3] Cao, Z.; Zhang, L.; Liang, K.; Cheong, S.; Boyer, C.; Gooding, J.J.; Chen, Y.; Gu, Z. *Adv. Sci.* 2018, 1801155.
[4] Q. Zhang, J. Liang, A. Bongers, J.J. Richardson, K. Liang, Z. Gu, *Adv. Sci.* 2023, 2206546
[5] Guo, Z.; Xie, W… Boyer, C., Zhao, L.; Gu, Z. *Chem. Eng. J.* 2022, 137310.
[6] Zhang, H; Cao, Z; Zhang, Q; Xu, J; Yun, SLJ; Liang, K; Gu, Z. *Small* 2020, 16, e2002732
[7] Zhang, H.; Zhang, L.; Cao, Z.; Cheong, S.; Boyer, C.; Wang, Z.; Yun, S.L.Y.; Amal, R.; Gu, Z. *Small* 2022, e2200299.
[8] Z. Cao, L. Zhang, J. Liu, D. Wang, K. Liang, Y. Chen, Z. Gu, *Nanoscale* 2021, 13, 17386-17395

Nasal delivery of encapsulated recombinant ACE2 as a prophylactic drug for SARS-CoV-2

Alberto Baldelli[a], Hale Oguzlu[b], Hui Xin Ong[c], Daniela Traini[c]

[a] School of Agriculture and Food Sustainability, The University of Queensland, Australia
[b] Department of Chemical Engineering, The University of Queensland, Australia
[c] Woolcok Institute of Medical Research, Australia

Covid-19 has caused a global pandemic, and worldwide, the number of deaths exceeded five million. Even though medical research efforts have developed vaccines, vaccination worldwide faces several challenges. As well, several mutations can jeopardize the efficacy of these vaccines. Most research studies the production of a vaccine that uses intravenous (IV) or intramuscular delivery to boost. For such a purpose, one might think that the most logical approach would be to decrease or repress the number of cell receptor ACE2. While as humans, our heart and lung produce soluble ACE2, a recombinant form of the cell receptor Angiotensin-Converting Enzyme2 (rhACE2) version is accessible on the market. rhACE2 can serve as an interceptor of SARS-CoV and other selected coronaviruses by binding to the surface of the viral particle. We aim to develop a non-invasive drug involving the advantages of rhACE2 against SARC-CoV-2. Spray freeze drying (SFD) is the only spraying technique that allows the control over the properties of sprayed powders and the use of low temperatures. The affinity of rhACE2 and the spikes protein of SARS-CoV-2 has already been explored, and the idea of using rhACE2 as a possible treatment of Covid19 has been published in a few research studies. However, the concept of generating an inhalable form of rhACE2 to be delivered to the nasal cavity as prophylactic is new. We encapsulated rhACE2 maintaining its stability and affinity with spike proteins of SARS-CoV-2 at 97 and 82 %, respectively. Using the MTS assay, we demonstrated that rhACE2 protein does not negatively affect Calu-3 and RPMI-2650 cell viability. We ultimately show that the encapsulation procedure enhances the cellular uptake by 93 %.

Inhalable high-loading cannabidiol powders

Waiting Tai[a], Grace Tsz Yan Yau[a], Jonathon Carl Arnold[b,c], Hak-Kim Chan[a], Philip Chi Lip Kwok[a,*]

[a]Advanced Drug Delivery Group, Sydney Pharmacy School, Faculty of Medicine and Health, The University of Sydney, NSW 2006, Australia
[b]Lambert Initiative for Cannabinoid Therapeutics, Brain and Mind Centre, The University of Sydney, NSW 2050, Australia
[c]Discipline of Pharmacology, Sydney Pharmacy School, Faculty of Medicine and Health, The University of Sydney, NSW 2006, Australia
*Corresponding author: philip.kwok@sydney.edu.au

Cannabidiol (CBD) is a non-psychoactive cannabinoid for treating seizures associated with Lennox-Gastaut or Dravet syndromes and tuberous sclerosis complex. An oral solution (Epidiolex®) is available for these indications [1]. However, oral delivery cannot deliver CBD efficiently due to its low bioavailability and slow onset of action. In contrast, pulmonary delivery increased the bioavailability of CBD by 9.1-fold and achieve a 71-fold higher maximum concentration 118 min earlier than Epidiolex in a Phase I clinical trial [2]. These make inhalation an efficient and attractive alternative. Although inhalable CBD powders have been reported in previous studies, most of them contained 20-25% w/w drug and 75-80% excipients [2,3]. Limited attempts have been made to produce powders with high CBD loading for high dose administration.

High-loading CBD powders were produced via wet ball milling in the present study. A total of 60 mg of raw materials (CBD with 0%, 2%, or 5% w/w magnesium stearate (MgSt)) and 3 g of ceramic beads (diameter = 1.4–1.6 mm; Hunan Jeri Precision Ceramics Co. Ltd, Hunan, China) were weighed into a 7 mL stainless steel container (Sartorius Stedim Biotech S.A., Aubagne, France). One hundred and twenty microlitres of ultrapure water was added before shaking at 750 rpm for 60 min using a Mikro-Dismembrator U (Sartorius Stedim Biotech S.A., Aubagne, France). The particles were obtained by suspending the slurry in 150 mL ultrapure water, followed by filtering through a 0.1 µm polycarbonate membrane (Millipore, Massachusetts, United States) and vacuum drying overnight. The aerosol performance of the three powders was investigated using the Next Generation Impactor with the United Stated Pharmacopeia throat (Copley, Nottingham, United Kingdom). The impaction cups were coated with 0.6% w/v Tween 80 in ethanol before use to prevent particle bounce. A Size 3 hydroxypropyl methylcellulose capsule (Capsugel; New South Wales, Australia) was loaded with 5 ± 1 mg of a powder and placed into the inhaler for dispersion. Two inhalers were used in this study, namely, low resistance (LR-RS01; resistance = 0.021 $kPa^{1/2}$ min/L) and high resistance RS01 (HR-RS01; resistance = 0.036 $kPa^{1/2}$ min/L) (Plastiape, S.p.A., Osnago, Italy) [4]. The dispersions were conducted at 56 L/min for 4.3 s and 100 L/min for 2.4 s for HR-RS01 and LR-RS01, respectively. After dispersion, powder deposits on all parts of the setup were thoroughly dissolved for CBD quantification by high performance liquid chromatography. Triplicate runs were conducted.

The aerodynamic particle size distributions of the powders are shown in Figure 1. All powders deposited mostly on Stage 1, regardless of the inhaler used. Without MgSt, the dispersibility of ball milled CBD was poor, with low fine particle fractions (FPFs), as shown in Table 1. Adding MgSt led to higher emitted fractions (EFs) and FPFs, but less inhaler retention and throat deposition was observed with 5% MgSt. This was because MgSt reduced the cohesiveness of the powders and the interaction between CBD and the inner surfaces of the capsules and inhalers [5]. Comparing the two inhalers, the EFs of the three powders were higher when dispersed with the LR-RS01 inhaler because its higher flow rate of 100 L/min during dispersion provided stronger momentum than the HR-RS01 inhaler at 56 L/min for the particles to exit the inhaler [6]. On the other hand, the slightly higher FPF of wet ball milled CBD from the LR-RS01 inhaler than that from the HR-RS01 inhaler could be explained by the stronger turbulent flow generated by the higher flow rate through the LR-RS01 inhaler to deagglomerate the particles [6]. CBD+5% MgSt achieved a lower FPF than CBD+2% MgSt with the LR-RS01 inhaler. On the other hand, MgSt over-coated the CBD particles for CBD+5% MgSt. Thus, the MgSt coating increased the cohesion between particles. When the cohesive powder was dispersed with the LR-RS01 inhaler, the turbulent flow was insufficient to deagglomerate. In contrast, the HR-RS01 inhaler provided a stronger particle-device impaction that dispersed cohesive powders more efficiently, resulting in better aerosol performance of CBD+5% MgSt. For CBD+2 % MgSt, its lower FPF from the HR-RS01 inhaler suggested that the stronger particle-device impaction in the HR-RS01 inhaler could not fully compensate the effect of the lower flow rate.

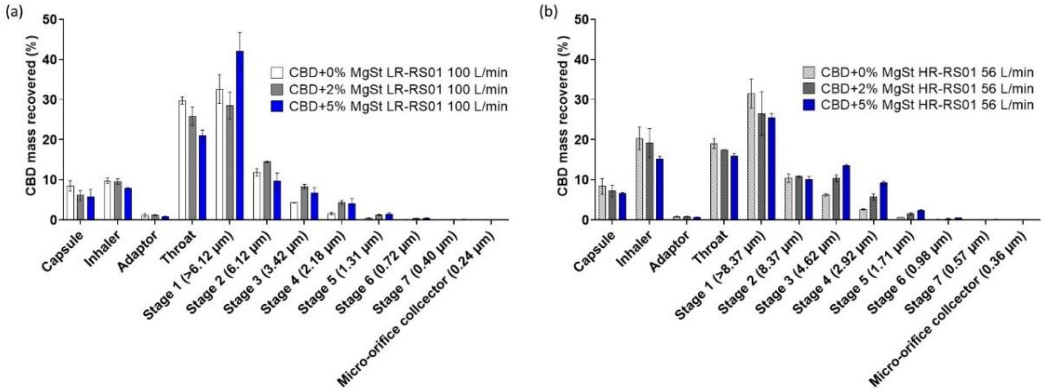

Figure 1. Aerodynamic particle size distributions of the wet ball milled powders dispersed with the (a) low resistance and (b) high resistance RS01 inhalers (mean ± standard deviation, *n* = 3).

Table 1. Emitted fractions and fine particles fractions < 5 μm of wet ball milled powders dispersed with low resistance and high resistance RS01 inhalers (mean ± standard deviation, *n* = 3).

Formulations	Emitted fraction (%)	Fine particle fraction < 5 μm (%)
	Low resistance RS01 (LR-RS01)	
CBD+0% MgSt	81.8 ± 2.0	12.8 ± 1.3
CBD+2% MgSt	84.3 ± 0.6	22.8 ± 1.4
CBD+5% MgSt	86.4 ± 1.8	18.4 ± 3.7
	High resistance RS01 (HR-RS01)	
CBD+0% MgSt	71.3 ± 2.9	10.0 ± 0.7
CBD+2% MgSt	73.6 ± 4.1	17.5 ± 1.8
CBD+5% MgSt	78.2 ± 0.8	23.9 ± 1.1

References

[1] G. T. Y. Yau, W. Tai, J. C. Arnold, H. -K. Chan, P. C. L. Kwok, *Pharm. Res*. **2023**, 40, 1087-1114.

[2] O. Devinsky, K. Kraft, L. Rusch, M. Fein, A. Leone-Bay, *J. Pharm. Sci*. **2021**, 110, 3946-3952.

[3] R. O. Williams, C. Moon, J. J. Koleng, WO2021055672A1. **2021**.

[4] M. Y. Yang, J. Verschuer, Y. Shi, Y. Song, A. Katsifis, S. Eberl, K. Wong, J. D. Brannan, W. Cai, W. H. Finlay, H. -K. Chan, *Int. J. Pharm.* **2016**, 513, 294-301.

[5] M. Lau, P. M. Young, D. Traini, *AAPS PharmSciTech*, **2017**, 18, 2248-2259.

[6] L. C. Almeida, R. Bharadwaj, A. Eliahu, C. R. Wassgren, K. Nagapudi, A. R. Muliadi, *Eur. J. Pharm. Sci*. **2022**, 175, 106226.

Cocrystal preparation of 4-aminosalicylic acid/isoniazid for developing dry powder inhaler formulation of anti-tuberculosis drugs

Yuichi Tozuka,[a]* Yuta Hatanaka,[a] Peiwen Mo,[a] Tero Kämäräinen,[a] Shingo Furukawa,[b] Mai Takase,[b] Shinya Yamanaka,[b] Mitsunobu Doi,[a] Toshio Oguchi,[c] Hiromasa Uchiyama,[a] Kazunori Kadota [a,d]

[a] Osaka Medical and Pharmaceutical University, Takatsuki, Osaka 569-1094, Japan
[b] Muroran Institute of Technology, Muroran, Hokkaido, 050-8585, Japan
[c] University of Yamanashi, Chuo, Yamanashi 409-3898, Japan
[d] Wakayama Medical University, Wakayama, Wakayama 640-8156, Japan
*Corresponding author: yuichi.tozuka@ompu.ac.jp

Cocrystals are crystalline materials composed of two or more different molecular or ionic compounds. Cocrystal engineering is a potent strategy for use in drug formulation design, presenting a multitude of advantages in enhancing drug efficacy, e.g., enhanced drug solubility, improved drug stability, formulation flexibility and commercial viability in the pharmaceutical industry. Concurrently introducing two drugs and realizing simultaneous pharmacological effects at the target site is challenging. We investigated the potential of co-crystallization principles for use in developing dry powder inhaler (DPI) formulations of anti-tuberculosis drugs. The present study focused on the formation of cocrystals of 4-aminosalicylic acid (PAS) and isoniazid (INH), which are crucial components of tuberculosis treatment.

Spray-drying PAS and INH (2 g in total) were dissolved at a molar ratio of 2:1, 1:1, or 1:2 in a mixture of 120 mL of ethanol and 280 mL of distilled water, and the resulting solution was fed to a spray-drying nozzle and spray dried using a B-290 mini. The physical properties of the particles were assessed using powder X-ray diffraction, differential scanning calorimetry, and Raman and infrared spectroscopy. The particle size and morphology obtained via spray drying were examined using scanning electron microscopy and laser diffraction particle size analysis. The inhalation properties of the DPI formulations were evaluated using an Andersen Cascade Impactor, whereas the post-inhalation dissolution behaviours were investigated via in vitro dissolution studies employing transwell inserts.

Via spray drying, we successfully produced spray-dried particles of PAS-INH that exhibited hydrogen bonding interactions between the molecules. **Figure 1** shows the crystal structure of PAS-INH. The PAS-INH crystal is orthorhombic ($Pna2_1$), and the asymmetric unit cell contains two molecules of PAS and two molecules of INH. Two hydrogen bonds mediated by hydrazide groups are formed between the INH molecules. The PAS-INH molecules in the crystal form hydrogen bonds between the amino group of PAS and hydrazide group of INH, and between the pyridyl N atom of INH and the carboxyl O atom of PAS, with these intermolecular interactions establishing the lattice.

On the aerosolization performance evaluation with an Andersen Cascade Impactor (**Figure 2**), the spray-dried particles of PAS and INH exhibit completely different inhalation profiles, indicating the challenge of delivering multiple drugs simultaneously to the infected site, even when the simultaneously inhaled PAS and INH particles are separately prepared using spray drying. The design of inhaled formulations containing multiple drugs is promising for use in efficiently treating diseases, highlighting the potential of our particle design for use in the co-delivery of PAS-INH.

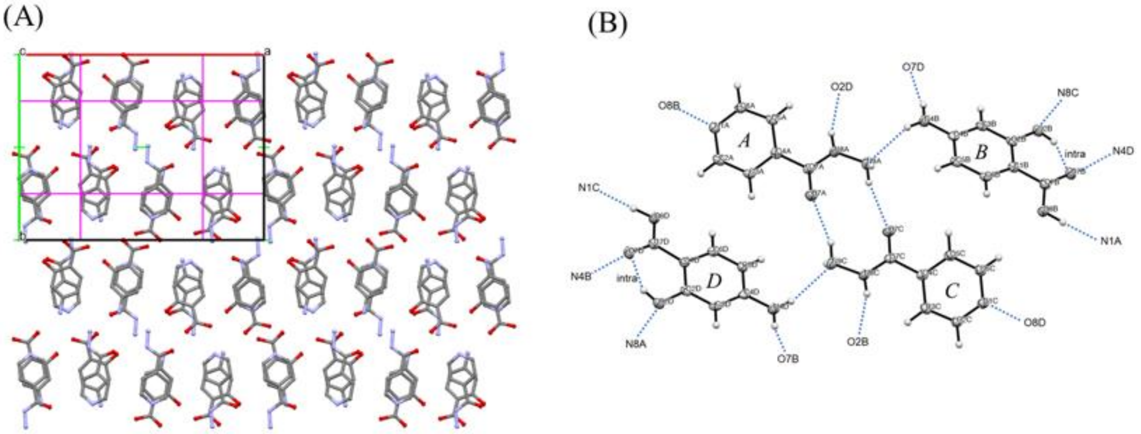

Figure 1. (A) Packing diagram from c-axis projection of PAS-INH cocrystal and **(B)** intermolecular environment of the synthons in PAS-INH crystal.

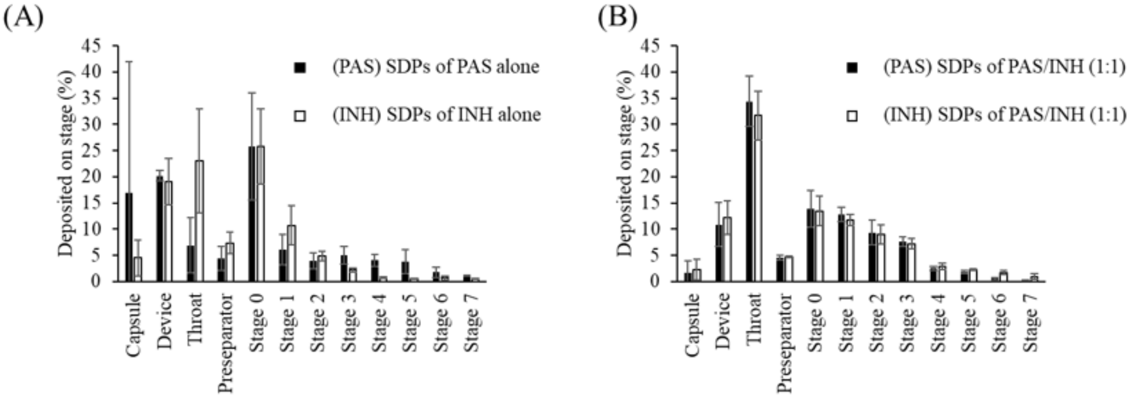

Figure 2. Deposited percentages of **(A)** 4-aminosalicylic acid (PAS) from the spray-dried particles (SDPs) of PAS and PAS/isoniazid (PAS/INH) (1:1) and **(B)** INH from the SDPs of INH and PAS/INH (1:1).

Design of spray-dried supraparticles containing carvedilol using amyloid nanofibrils as binder modifiers for controlled morphology

Yuzuki Nakayama,[a] Tero Kämäräinen,[a] Hiromasa Uchiyama,[a]
Kazunori Kadota,[a,b,]* Yuichi Tozuka[a]

[a] Osaka Medical and Pharmaceutical University, Takatsuki, Japan
[b] Wakayama Medical University, Wakayama, Japan
*Corresponding author: kazunori.kadota@ompu.ac.jp

Nanoparticles have the capability to aggregate into larger structures known as supraparticles (SPs), ranging from micro- to millimeters in size. SPs have garnered significant interest due to their ability to merge modular material designs and functions with easy preparation methods like evaporation-induced self-assembly, enabling the consolidation of materials across mesoscopic length scales. Previously we succeeded in controlling morphology of SPs composed of silica nanoparticles using spray-drying.[1] Incorporating drugs into SPs is anticipated to yield formulations with unique properties compared to conventional products. The SPs with various morphologies were fabricated in this study using silica nanoparticles (SNPs) and amyloid nanofibrils (ANFs), with β-Lactoglobulin (βLG) serving as a binder. Carvedilol (CVD) was employed as a model drug, and its particle characteristics and dissolution behavior were evaluated.

ANF was prepared by self-aggregation of βLG at 90°C for 10 hours.[2] SPs were prepared by spray-drying. The total volume fraction was kept at $\phi = \phi\text{ANF} + \phi\text{SNP} = 0.0005$ and $\phi\text{ANF}/\phi\text{SNP} = 0$, 0.1, and 1. CVD concentration was set to 90 % (High), 50 % (Middle), and 10 % (Low) of the free space according to random close packing (RCP). This procedure involved dissolving CVD in 0.01 M HCl solution, followed by the addition of ANF dispersion with stirring and subsequent sonication for 15 min. SNP suspensions were added dropwise under stirring, and the resulting dispersion was subjected to spray-drying. The particle size and morphology of SPs were evaluated using scanning electron microscopy (SEM). The crystallinity of the drug in SPs was evaluated using a powder X-ray diffractometer (PXRD). The loading capacity in SPs and dissolution behavior in phosphate buffer solution (pH 6.8) were evaluated.

A considerable difference in the morphology of spray-dried βLG control and ANFs was observed, as βLG yielded particles with shallow, dimpled features, whereas ANF resulted in crumpled morphologies as displayed in **Figure 1**. Specifically, the shell thickness of spray-dried SPs was thinner by increasing the ratio of ANF (**Figure 2**). The SPs loaded with CVD showed different particle morphologies compared to those without CVD. The loading capacity of CVD influenced the shell thickness of SPs. According to the results, it can be observed that there is no difference in the CVD concentration between middle and high samples. This indicates that the upper limit of CVD loading capacity is approximately 50% of the free space. In addition, the loading capacity in the SPs depended on the CVD concentration in the precursor solution before spray-drying. Furthermore, it was confirmed that the drug dissolution behavior was also affected. We discovered the potential for controlling particle morphology and dissolution behavior by altering the material ratio.

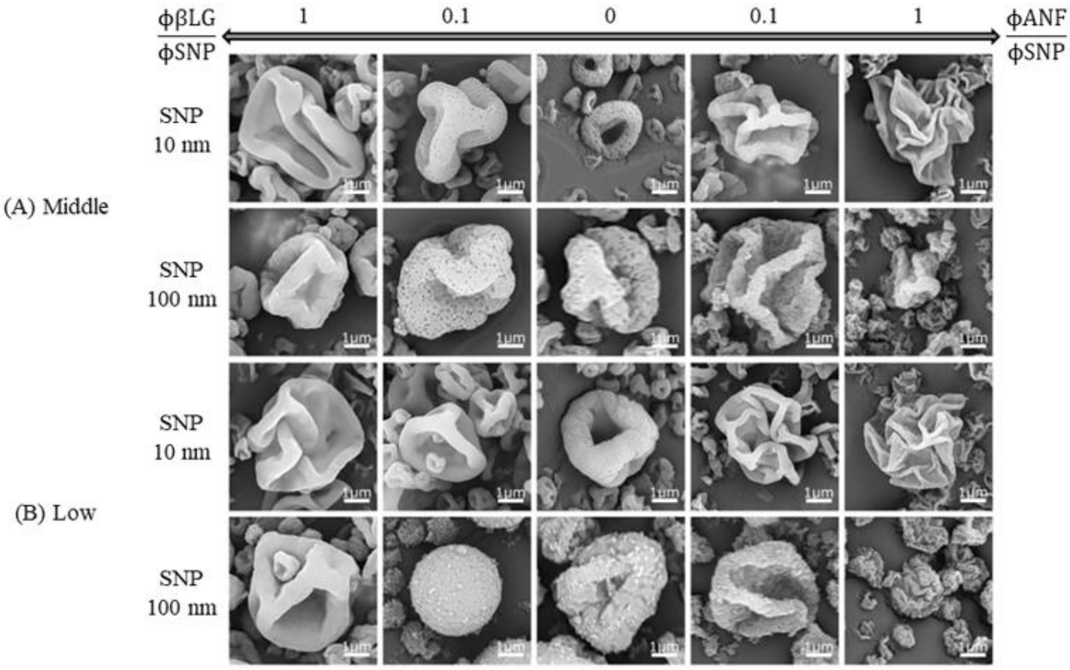

Figure 1. SEM images of SD supraparticles with (A) Middle and (B) Low CVD concentration.

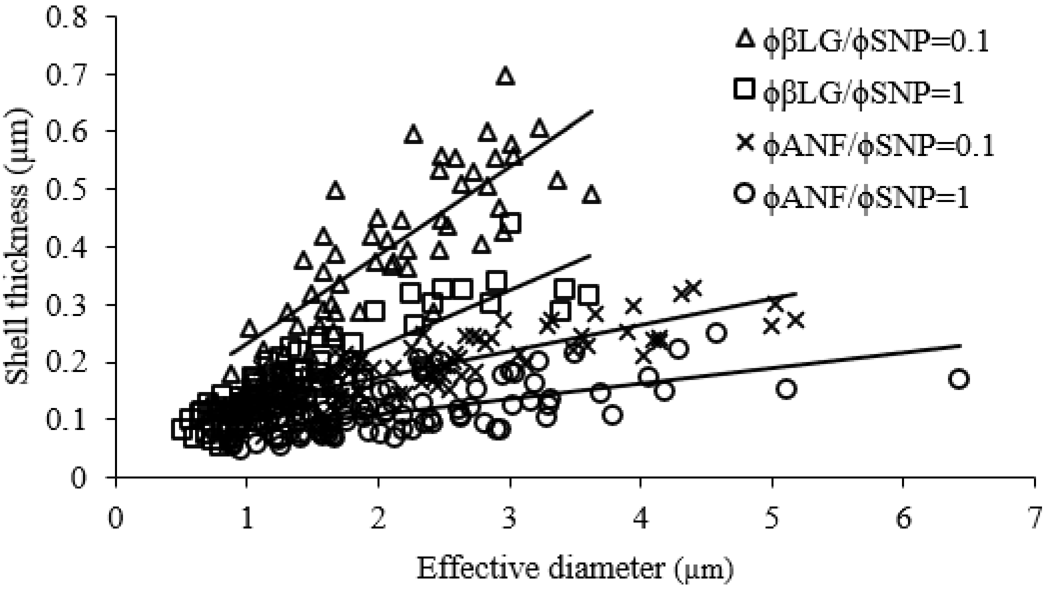

Figure 2. Effect of ANF volume fraction on SD supraparticles.

References

[1] T. Kämäräinen, Y. Nakayama, H. Uchiyama, Y. Tozuka, K. Kadota, *Small*, **in press**

[2] M. Charnley, J. Gilbert, O. G. Jones, et al., *Bio-protocol* **2018**, vol 8, 1-7.

Improvement of drug loading capacity into metal-organic frameworks by electric field application

Soma Omura, Kazuki Oshima, Shuji Ohsaki*, Hideya Nakamura, Satoru Watano

Osaka Metropolitan University, Osaka, Japan
*Corresponding author: shuji.ohsaki@omu.ac.jp

The drug delivery system (DDS) refers to the technology of transporting drugs to the diseased site at the appropriate time by spatial and temporal control. In recent years, metal-organic frameworks (MOFs) have gained attention as carriers in DDS. MOFs are crystalline porous materials formed by self-assembly of metal ions and organic ligands, characterized by a large surface area and the ability to control pore size at the molecular level. In liquid-phase adsorption for drug encapsulation into MOFs, the drug encapsulation ability of MOFs is expected to depend on the balance of molecular interactions among drugs, solvents, and MOFs [1]. Therefore, this study aimed to enhance the drug loading capacity of MOFs by altering the balance of intermolecular forces via the application of an external electric field. The drug loading experiments were conducted using various drugs, MOFs, and solvents in both with and without external electric field.

5-fluorouracil (5FU, 130.08 g/mol), acetaminophen (AAP, 151.16 g/mol), and ibuprofen (IBU, 206.28 g/mol), were selected as model drugs with different molecular weights. UiO-66-NH2 and UiO-66-NO2 were chosen as MOFs. These have different organic ligands. Water was selected as the solvent. The concentration conditions for drug loading experiments were set as follows : 5FU concentration was 1.5 g/L with a MOF to drug mass ratio of 2:3, AAP concentration was 6 g/L with a MOF to drug mass ratio of 1:6, and IBU concentration was 10 mg/L with a MOF to drug mass ratio of 100:1. The solution volume was 50 mL in the non-electric field applied system and 300 mL in the electric field applied system, with stirring for 1 hour. An external electric field was applied by placing the solution in a covered 300 mL beaker with a carbon plate as the electrode, maintaining 4 cm between the plates and 2 cm between the bottom of the beaker and the electrode. The applied voltage was fixed at 1 V. The drug loading amount was calculated based on TG/DTA measurements.

TG/DTA profiles of particles obtained before and after the experiment were measured to calculate the drug loading amount. From the DTA profile of UiO-66-NO2, the onset temperature of MOF decomposition was determined to be 280.3 °C. Beyond this temperature, a mass loss due to the sublimation of organic ligands (a) and the sublimation of encapsulated drugs (b) were observed. [2] Therefore, the drug loading amount [wt.%] was calculated as 100 × a / (a + b). Figure. 1 shows the loading amount of UiO-66-NH2 and UiO-66-NO2 (bottom Figure) and the increase ratio of that by electric field application in water (upper Figure). TG measurements were conducted twice for each loading condition. Then, the calculated loading amount are showed as error bars and the average values are showed as bar graphs. The error bars of the increase ratio represent the ratio of the maximum/minimum loading amount in the electric field applied system to the minimum/maximum loading amount in the non-electric field applied system. When this increase ratio exceeds 1, it is considered as an increase; when it is less than 1, it is considered as a decrease. The loading amount of UiO-66-NH2 did not change for any drug, while the loading amount of UiO-66-NO2 increased for all drugs. Additionally, it was shown that the smaller the size of the drug, the greater the rate of change due to the electric field application. From the results of these loading experiments, it was found that the loading amount could increase with the application of an electric field.

To examine the factors affecting the change in the loading amount, we focused on the functional groups of UiO-66 and the molecular size of the drug. The functional groups of UiO-66 have different charges and polarities. The amino group is electron-donating and positively charged, while the nitro group is electron-withdrawing and negatively charged. Moreover, since the dipole moment of the nitro group is larger than that of the amino group, the induced dipole moment produced by the nitro group is larger than that produced by the amino group. Furthermore, water stabilize against both positive and negative charges by its induced dipole moments. Therefore, the interaction between UiO-66-NO2 with a large dipole moment and solvation of drugs was strengthened in water, leading to an increase in loading amount. Moreover, it is known that smaller drug molecules are more susceptible to changes in polarity due to electric fields. Thus, it was suggested that the smaller the drug molecule, the more stable the solvation. As a result, it was inferred that the change in drug loading amount due to the application of an electric field increased in the order of 5FU > AAP > IBU.

This study performed loading experiments using various combinations of MOFs, drugs, and solvents in both with and without electric field. By applying an electric field, the balance of interactions shifted due to the polarization of each molecule and the inducted dipole moments, leading to an enhancement in the loading amount of UiO-66-NO2 for all drugs in water. Additionally, it was suggested that smaller drug molecules are more susceptible to the influence of electric fields.

References

[1] K. Ohshima et al., Mechanism of Drug Encapsulation in MOFs Focusing on Solvent Dipole, **In preparation**
[2] Hung-Li Wang, Hsin Yeh, Bin-Han Li, Chia-Her Lin, Ta-Chih Hsiao, De-Hao Tsai, ACS Appl. Nano Mater **2019**, 2, 3329–3334.

Evaluation of gadolinium biodistribution and tumor-killing effects of surface-modified gadolinium-loaded chitosan nanoparticles for gadolinium neutron capture therapy

Tooru Andoh[a]*, Ryohei Azuma[a], Yusuke Nagashige[a], Minoru Suzuki[b], Takushi Takata[b], Yoshinori Sakurai[b] and Hideki Ichikawa[a]

[a] Laboratory of Pharmaceutical Technology, Faculty of Pharmaceutical Sciences, Kobe Gakuin University, Japan
[b] Institute for Integrated Radiation and Nuclear Science, Kyoto University, Japan.
*Corresponding author: t.andoh@pharm.kobegakuin.ac.jp

Neutron capture therapy using nonradioactive ^{157}Gd (Gd-NCT) is currently under development as a potential radiation therapy for cancer. Gd-NCT with ^{157}Gd offers several potential advantages over boron (^{10}B) neutron capture therapy (BNCT). The deep tissue penetration (100 μm) of γ-rays from the ^{157}Gd (n, γ) ^{158}Gd reaction is expected to provide tumor-killing efficacy within bulky tumors such as head and neck cancers. Furthermore, oral mucositis caused by BNCT with *p*-boronophenylalanine could be a potential dose-limiting factor in head and neck tumors [1]. Previously, we developed gadolinium-loaded chitosan nanoparticles (Gd-nanoCPs) for controlled Gd delivery in Gd-NCT. These nanoparticles are composed of Gd-diethylenetriaminepentaacetic acid (Gd-DTPA, an MRI contrast agent) and chitosan (a naturally abundant biodegradable polysaccharide with good biocompatibility and bioadhesive characteristics). This study investigates the *in vivo* gadolinium biodistribution and tumor-killing effects of NCT with intratumorally injected nanoparticulate formulations.

Gd-nanoCPs were prepared from chitosan and Gd-DTPA using a previously developed water-in-oil (w/o) emulsion–droplet coalescence technique [2]. Condensation of the amino group present in intact Gd-nanoCP and NHS-activated ester-PEG was carried out to prepare directly PEG-modified Gd-nanoCP (PEG-Gd-nanoCP). A thin-film hydration method was used to modify the surface of Gd-nanoCPs with soybean lecithin and PEG-lipid (PEG-SL-Gd-nanoCP). The mean particle size and zeta potential of the Gd-nanoCPs were measured using a Zetasizer (Malvern). The Gd concentration in the tumor tissue was determined using inductively coupled plasma atomic emission spectrometry (ICP-AES, SPS3100), followed by incineration of each sample. Five-week-old male C3H/HeN mice were used for the NCT. SCC-VII cells (1×10^6 cells/mouse) were injected into the left masseter muscle [3]. The mice were divided into NCT and HOT control groups. Before injection, centrifugation was conducted to concentrate Gd-nanoCPs to 6000 μg Gd/mL. Gd-nanoCPs incorporating 1.2 mg of natural Gd were injected intratumorally twice into the mice. The tumors were exposed to thermal neutron irradiation at the Institute for Integrated Radiation and Nuclear Science, Kyoto University, Japan. The tumor volume ratio before and after neutron irradiation was used to assess the tumor growth-suppressing effects.

The mean particle diameter and zeta potential of Gd-nanoCP, PEG-Gd-nanoCP, and PEG-SL-Gd-nanoCP were 171, 168, and 179 nm and 15, 20, and -6 mV, respectively. In the intratumoral injection test, the Gd concentrations of Gd-nanoCPs, PEG-Gd-nanoCPs, and PEG-SL-Gd-nanoCPs in the tumor tissues were 2337, 1551, and 1533 ppm, respectively. PEG-SL-Gd-nanoCP was not used in Gd-NCT because it showed good permeation, leaked out of the tumor tissue, and accumulated in the normal tissues. In Gd-NCT, the NCT group significantly suppressed tumor growth relative to the HOT control group (Figure 1). Although the Gd concentration in the tumor tissue of the PEG-Gd-nanoCP group was approximately two-third lower than that of the Gd-nanoCP group, the PEG-Gd-nanoCP group showed similar tumor growth suppression to the Gd-nanoCP group. This result was related to the distribution of the Gd preparations within the tumor after administration. Unlike extensive delivery via tumor vasculature, intratumoral injection causes particle diffusion and distribution from the injection site. Therefore, improving the permeability and diffusion of Gd preparations within the tumor tissue after injection is crucial for achieving uniform Gd distribution in the tumor tissue. The improvement in dispersion stability with surface modification possibly led to the homogenization of Gd distribution in the tumor tissue, because the particle sizes of the two types of Gd formulations did not differ significantly.

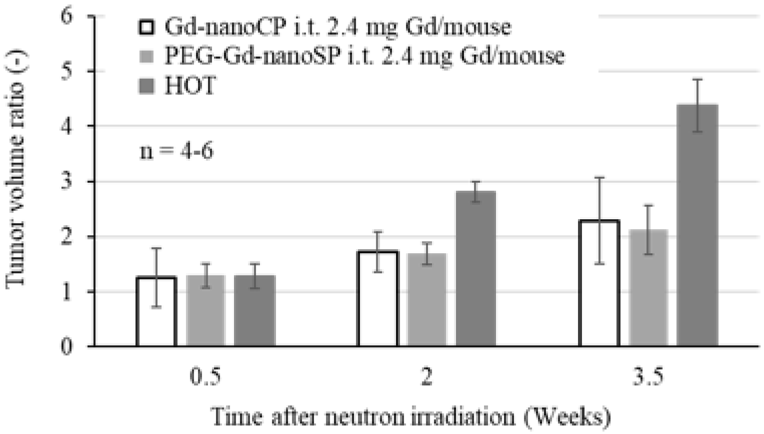

Figure 1. Tumor volumes after thermal neutron beam irradiation of NCT and HOT control groups.

References

[1] J. A. Coderre et al., *Radiat. Res.*, **1999**, 152, 113-118.
[2] H. Tokumitsu et al., *Pharm. Res.*, **1999**, 16, 1830–1835.
[3] T. Nomura et al., 5th Asian Conference on Oral and Maxillofacial Surgery, **2002**, 111-115.

Molecular simulation of multi-drug encapsulation into metal-organic framework with amphiphilic pores

Ayumi Ohashi, Shuji Ohsaki,* Hideya Nakamura, Satoru Watano

Osaka Metropolitan University, Sakai, Japan
*Corresponding author: shuji.ohsaki@omu.ac.jp

In combination therapy, multiple drugs are administered to patients to achieve higher efficacy for cancer therapy, with the expectation of synergistic therapeutic effects and reduction in drug doses. However, the multiple routes for administration can complicate treatment because drug side effects and resistance mechanisms should be considered. Therefore, inclusion of multiple drugs in a single carrier can be expected to reduce the number of routes of drug administration. Recently, metal-organic frameworks (MOFs), which are porous materials composed of metal ions and organic ligands, have been attracting attention as drug carriers. This study focused on γ-CD-MOFs, which are composed of γ-cyclodextrin (γ-CD) and potassium ions. Because γ-CD has a ring structure with hydrophobic interior and hydrophilic exterior, γ-CD-MOF can have hydrophobic and hydrophilic pores. The hydrophobic and hydrophilic pores in γ-CD-MOF have the potential to encapsulate multiple drugs. This study evaluated the applicability of γ-CD-MOF as a multiple drug carrier via experimental and simulation analyses. In drug inclusion experiments, the concentration of γ-CD-MOF was set at 6 g/L and the drug at a predetermined concentration, suspended in ethanol, and stirred for 2 days. 5-fluorouracil (5FU) and ascorbic acid (ASC) were selected as drugs to perform single and simultaneous inclusion experiments. Initial drug concentrations were 1.5 g/L for 5FU and 2 g/L for ASC in single-drug experiments. The grand canonical Monte Carlo (GCMC) method was used to calculate the amount of drug inclusion in γ-CD-MOF using RASPA. The temperature was 298 K, and the drug load was calculated at different pressures (1.0×10−15–1.0×1015 Pa). In addition, the hydrophobic pores of γ-CD-MOF were defined as spheres with a radius of 0.5 nm, and the other areas were defined as hydrophilic pores. The number of drug inclusions in hydrophilic/hydrophobic pores was calculated from the coordinates of the center of gravity of the included drug molecules. In addition to 5FU and ASC, acetaminophen (AAP), indomethacin (IDM), curcumin (CUR), and nifedipine (NIF) were used. The molecular weights of 5FU, ASC, AAP, IDM, CUR, and NIF are 130, 176, 151, 358, 368, and 346 g/mol, respectively.

The single drug inclusion experiments using 5FU/ASC were performed. The loaded amounts of 5FU and ASC were 0.152 g-drug/g-MOF and 0.215 g-drug/g-MOF. The loaded amount of drugs into γ-CD-MOF was calculated by GCMC simulations. It was found that the experimental results for both drugs were comparable to the calculated results at P = 1.0 × 103–105 Pa. Furthermore, the loaded amount in the hydrophilic/hydrophobic pores was calculated. With increasing pressure, the loaded amount of 5FU increased in two steps, whereas the loaded amount of ASC increased in one step with increasing pressure. It was confirmed that 5FU, which was encapsulated in the hydrophobic pore of γ-CD-MOF at low pressure, was also encapsulated in the hydrophilic pore at the high pressure. Comparing this result with the overall inclusion amount, all 5FU was encapsulated in hydrophobic pores when the inclusion amount was low and also in hydrophilic pores when the inclusion amount was high. Meanwhile, ASC was encapsulated in both the hydrophilic and hydrophobic parts even at low pressure. Comparing the drug encapsulation amounts in the experiment and the simulation, it is suggested that 5FU was encapsulated mainly in the hydrophobic pores of γ-CD-MOF in the experiment, while ASC was encapsulated in both pores. From these results, it was found that the pores in which a drug was encapsulated depending on the degree of hydrophilicity of the drug.

The single-drug inclusion simulations using six types of drugs (5FU, AAP, ASC, IDM, CUR, and NIF) were performed to calculate the number of drugs encapsulated in the hydrophobic and hydrophilic pores.

Fig. 1 shows the calculated loading amount of drugs as a function of pressure. Focusing on the low-pressure region (P = 1.0 × 10−3–105 Pa), the number of AAP and ASC was high. This would be because AAP and ASC have the highest hydrophilicity among the six drugs. This suggested that more hydrophilic drugs had a stronger interaction with the hydrophilic pores, being encapsulated in larger amounts in the hydrophilic pores. On the other hand, in the hydrophobic pores, it was found that the inclusion amounts of AAP, 5FU, and ASC were almost the same, while the inclusion amounts of IDM, CUR, and NIF were small. The drugs with a molecular weight were difficult to be included in the hydrophobic pores due to steric hindrance. This suggested that drugs with high hydrophilicity were more likely to be encapsulated in the hydrophilic pores in the low-pressure region. It was also found that there was a difference in the amount of inclusion in the high-pressure region (P > 1.0× 104 Pa). Focusing on the molecular weight of the drug, the small molecular weight of the drug resulted in the large loading amount. Although the simulation at high pressure may be unrealistic, the theoretical maximum loading amount of the drug has been calculated. The trend of loading behaviour of a single drug was different in the low- and high-pressure regions. It was suggested from Fig. 1 that the hydrophilicity of the drug had a large effect on the loading amount of drug in the low-pressure region, whereas the molecular weight of the drug had a large effect on the loading amount of drug in the high-pressure region. Several multiple inclusion simulations using four drugs (5FU, AAP, ASC, IDM) were performed at P = 1.0 × 105 Pa. The total loaded amounts were shown in Fig. 4. Focusing on the combination with IDM in Fig. 4, IDM had the least hydrophilicity among the four drugs, while it had the largest amount of inclusion in hydrophilic pores. Since IDM has the largest molecular weight among the four drugs, the molecular weight also plays a large role in multiple drug inclusion. This study evaluated the encapsulation ability of hydrophobic/hydrophilic drugs in γ-CD-MOF by calculating the encapsulation amount and encapsulation pore size using experiments and simulations. It was found that the molecular weight contributed to encapsulation in the low-pressure region, while the degree of hydrophilicity contributes to encapsulation in the high-pressure region. In the future, the team plans to increase the number of drug types and conduct studies using machine learning, etc.

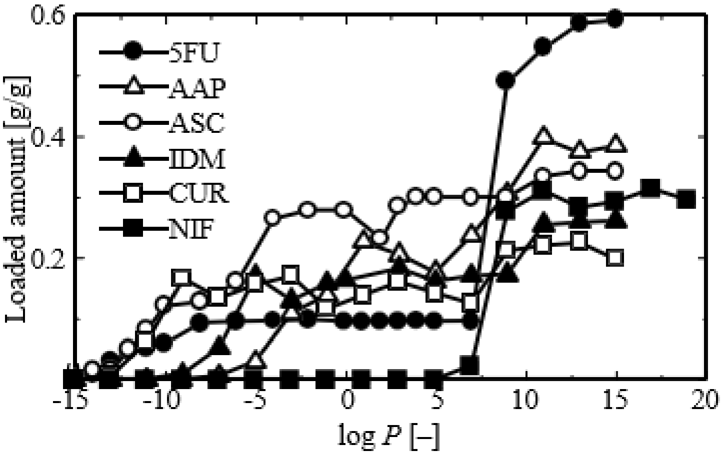

Fig. 1 Loaded amount of each drug.

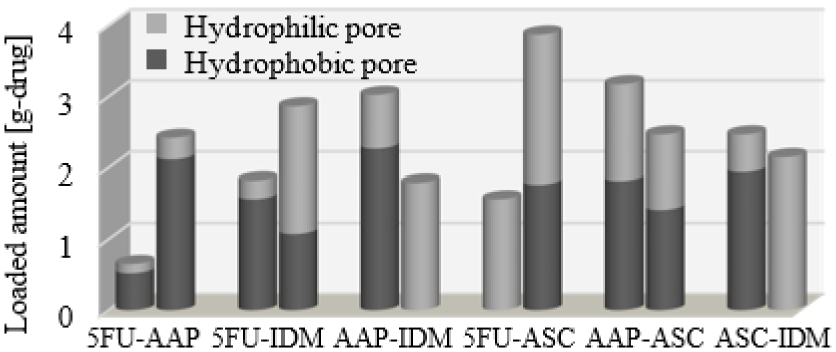

Fig. 2 Loaded amounts of drugs in each pore.

pH-sensitive organic-inorganic hybrid capsules using alginate and aminosilane for sustained release of diclofenac sodium

Sora Imanishi,[a] Yuji Sawano,[b] Fumio Kurayama,[c] Yuichi Shibata,[a] Tatsushi Matsuyama,[b] Junichi Ida[b,]*

[a]Graduate school of Engineering, Soka university, 1-236 Tangi-machi, Hachioji, Tokyo, Japan
[b]Department of Science and Engineering for Sustainable Innovation, Faculty of Science and Engineering, Soka University, 1-236 Tangimachi, Hachioji, Tokyo, Japan
[c]Toyota Technological Institute, 2-12-6, Hisakata, Tenpaku-ku, Nagoya, Aichi, Japan
*Corresponding author: ida@soka.ac.jp

Sodium alginate (AlgNa), a natural polymer with biocompatibility and biodegradability, is often used to prepare drug carriers in drug delivery systems (DDSs)[1]. However, these carriers have limitations in sustained drug release and drug encapsulation efficiency due to their high porosity, large pore sizes, and mechanical and physiological instabilities[2]. Therefore, various research efforts have been made to overcome these problems and improve drug release performance by hybridizing AlgNa with other substances.

This study attempted the development of organic-inorganic hybrid capsules through the hybridization of AlgNa with aminosilanes. Two types of aminosilanes, 3-(2-aminoethylaminopropyl)trimethoxysilane (AAPTS) and 3-aminopropyltriethoxysilane (APTES), were used to improve traditional AlgNa-based capsules. The resulting hybrid capsules, with different aminosilane concentrations (0.05–0.5 M), were used to compare their characterization and applicability for drug delivery systems (DDSs). As a model drug, diclofenac sodium (DCFNa), an antipyretic analgesic drug, was used to investigate the applicability of these capsules for DDSs[3].

The prepared organic-inorganic hybrid capsule was characterized by Fourier transform infrared (FT-IR) spectroscopy, a scanning electron microscope (SEM) observation, and thermogravimetric analysis (TGA). The amino group content in the hybrid capsules was measured by the TNBS method. The mechanical strength of the wet capsules was measured by compression test using a material testing machine. The drug encapsulation efficiency of DCFNa-loaded capsules were measured to compare the loading capacities. The swelling studies and the in-vitro drug release experiment of the capsules were conducted to assess and compare the contribution of aminosilanes in the a physiological environment, using simulated gastric fluid (SGF; pH 1.2, 37℃), simulated intestinal fluid (SIF; pH 7.4, 37℃), as well as continuous gastrointestinal tract with SGF and SIF. Drug release kinetics were analyzed using the Korsmeyer-Peppas model based on drug release behavior in SIF. The result shows that the DCFNa-loaded hybrid capsules were successfully prepared. The encapsulation efficiencies of DCFNa were significantly improved compared to pure AlgNa capsule, and the values ranged from 71.9±1.9 to 92.7±1.1%. In SGF, DCFNa release remained below 40% over 10 h. In contrast, the release rate of DCFNa in SIF were complete release within 10 h. These result indicates its pH-sensitivity across physiological environment. In continuous gastrointestinal tract, the drug leakage from the capsules in SGF was not observed within 2 h, and a desired sustained release was observed in the SIF for both aminosilane cases. Interestingly, the release behavior changed and became slower as aminosilane concentration increases. Good fit were observed for all hybrid capsules (R^2 = 0.9074–0.9922). The rate constant k for APTES capsule and AAPTS capsule was decreased with increasing aminosilane concentration (from 0.5228 to 0.3367 and from 0.5890 to 0.4109, respectively), supporting the change of release behavior of the capsules with different aminosilane concentration. From above results, the hybrid capsule prepared with higher aminosilane concentration showed better drug encapsulation and sustained release. Notably, AlgNa/AAPTS with concentration of 0.5 M exhibited the best sustained release property (>6 h) in SIF. These results suggest the potential of the organic-inorganic hybrid capsules as an effective oral drug carriers.

References

[1] K. Y. Lee, D. J. Mooney, *Progress in Polym. Sci. (Oxford)* **2012**, 37, 106–126.
[2] H. Yadav, R. Agrawal, A. Panday, J. Patel, S. Maiti, *J. Drug Deliv. Sci and Technol.* **2022**, 74. 103753.
[3] A. K. Nayak, D. Pal, *Int. J. Biol. Macromol.* **2011**, 49, 784–793

PEG/DEX aqueous two-phase coacervate for efficient IVT reaction, simultaneous mRNA enrichment and long storage

Shiyi Che,[a,b] Songping Zhang,[a,]* Minsu Liu[b,]**

[a] Institute of Process Engineering in Chinese Academy of Sciences, Beijing, China
[b] Monash University, Melbourne, Australia
*Corresponding author: spzhang@ipe.ac.cn
**Corresponding author: minsu.liu1@monash.edu

The current strategies for IVT synthesis, separation, concentration and storage are inefficient and fragmented, leading to low mRNA yield, lengthy operation times, and tedious procedures. In this study, we integrated and optimized the PEG/DEX aqueous two-phase system (ATPS) to achieve highly efficient mRNA synthesis and enrichment. As the PEG-rich/DEX-rich ratio increased, the DEX-rich phase containing IVT mRNA was more concentrated and finally formed compact coacervates during the reaction. The resulting mRNA coacervates, enriched with mRNA, DEX, Mg^{2+}, and Mg_2PPi particles, but with reduced levels of T7 RNAP and NTP, exhibited enhanced stability against nucleases. Moreover, the freeze-dried mRNA coacervates significantly improved mRNA storage stability at room temperature, maintaining integrity for over two months, whereas the control mRNA degraded within two days. For the post-processing, the mRNA coacervates can either be redissolved directly for the post-capping or compatible with cap analogs for the co-transcriptional capping process. Our findings demonstrate that the ATPS-IVT strategy developed in this study enriches mRNA into spontaneous coacervates without requiring a TFF step, offering a streamlined and continuous platform for high-concentration mRNA production.

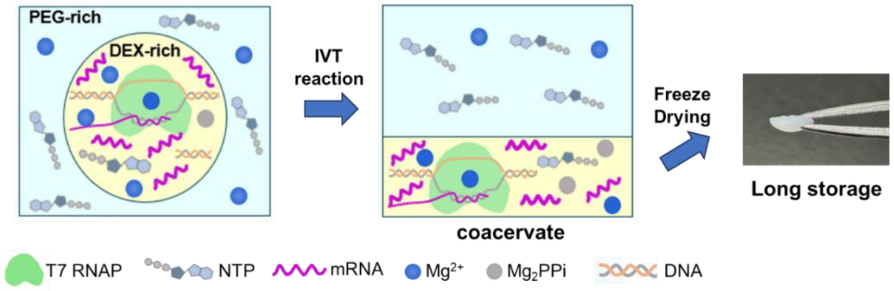

Figure 1. PEG/DEX ATPS for IVT synthesis, mRNA enrichment and long storage proposed in this study.

References

[1] W. Guo, A.B. Kinghorn, Y. Zhang, Q. Li, A.D. Poonam, J.A. Tanner, H.C. Shum, Non-associative phase separation in an evaporating droplet as a model for prebiotic compartmentalization, *Nat Commun* **2021**, 12(1), 3194.

[2] S.F. Banani, H.O. Lee, A.A. Hyman, M.K. Rosen, Biomolecular condensates: organizers of cellular biochemistry, *Nat Rev Mol Cell Biol* **2017**, 18(5), 285-298.

[3] J.E. Henninger, O. Oksuz, K. Shrinivas, I. Sagi, G. LeRoy, M.M. Zheng, J.O. Andrews, A.V. Zamudio, C. Lazaris, N.M. Hannett, T.I. Lee, P.A. Sharp, Cisse, II, A.K. Chakraborty, R.A. Young, RNA-Mediated Feedback Control of Transcriptional Condensates, *Cell* **2021**, 184(1), 207-222.

[4] C.A. Strulson, R.C. Molden, C.D. Keating, P.C. Bevilacqua, RNA catalysis through compartmentalization, *Nat Chem* **2012,** 4(11), 941-946.

[5] F. Luechau, T.C. Ling, A. Lyddiatt, Selective partition of plasmid DNA and RNA in aqueous two-phase systems by the addition of neutral salt, *Sep Purif Technol* **2009**, 68(1), 114-118.

[6] J.A. Asenjo, B.A. Andrews, Aqueous two-phase systems for protein separation: a perspective, *J Chromatogr A* **2011**, 1218(49), 8826-8835.

Preparation of microparticles with coating of poorly water-soluble nanocrystalline drug to improve its dissolution with sugar alcohol

Tooru Andoh*, Chinami Kawane, Keigo Nakano, Kosuke Fukushima, Hideki Ichikawa

Laboratory of Pharmaceutical Technology, Faculty of Pharmaceutical Sciences, Kobe Gakuin University, Japan
*Corresponding author: t.andoh@pharm.kobegakuin.ac.jp

Drug solubility is a crucial factor affecting drug absorption, particularly when drugs are taken orally. Poorly water-soluble drugs face challenges in dissolving in gastrointestinal fluids, which can limit their absorption and reduce their bioavailability. One solution is to decrease the size of drug particles to the submicron range, which can enhance their dissolution and absorption. However, resulting nanosuspensions (NS) are in liquid form, requiring careful attention to ensure stability and ease of use. In a previous study, we developed an NS Spray-Coating System (NSCS) to convert an NS of a poorly water-soluble drug into solid microparticles (NS-MPs), improving drug dissolution. However, NS-MPs produced using this method showed poor redispersibility and inadequate improvement in solubility. In this study, we incorporated sugar alcohol to enhance the redispersibility of NS-MPs, based on findings by Yamamoto et al., who observed immediate dissolution of sugar alcohol from spray-dried particles containing nanoparticles upon water addition, resulting in nanoparticle suspension formation. We hypothesized that sugar alcohol would similarly function in the drug layer on the microparticle surface. Therefore, we investigated the effects of sugar alcohols on this layer. For this purpose, we prepared NS-MPs using erythritol, mannitol, and xylitol, analyzing their redispersibility and dissolution properties.

NS was prepared by wet milling Glibenclamide (GLI, a model drug with a water solubility of 3 μg/mL at 37°C) and hydroxypropyl cellulose (HPC, from Nippon Soda Co., Ltd.) using a planetary ball mill. The resulting NS was then mixed with erythritol, mannitol, or xylitol using a stirrer. To prepare NS-MPs, this mixture was sprayed onto lactose cores (75–106 μm) using a spouted bed coater with a draft tube. The particle size distributions of NS, NS-sugar alcohol mixtures, and resulting dispersions after a dispersibility test with NS-MPs in JP 18 disintegration 2nd fluid (pH 6.8) were measured using dynamic light scattering (LB500, Horiba, Ltd.). Dissolution tests of NS-MPs were conducted using the JP 18 paddle method with dissolution 2nd fluid (pH 6.8) at 37°C.

NS with a mass median diameter ranging between 150-210 nm was obtained via wet milling. The addition of sugar alcohols to NS did not affect colloidal stability. Yields of NS-MPs (HPC), NS-MPs (HPC + Erythritol), NS-MPs (HPC + Mannitol), and NS-MPs (HPC + Xylitol) were 83%, 81%, 89%, and 87%, respectively. In the redispersibility test, GLI nanoparticles dispersed from NS-MPs with sugar alcohol in the 2nd fluid. NS-MPs (HPC + Erythritol), NS-MPs (HPC + Mannitol), and NS-MPs (HPC + Xylitol) redispersed to submicron sizes of 263 nm, 143 nm, and 133 nm, respectively, whereas NS-MPs (HPC) did not redisperse after 10 minutes of sonication. Release studies revealed that the area under the concentration-time curve up to 120 min of NS-MPs (HPC), NS-MPs (HPC + Erythritol), NS-MPs (HPC + Mannitol), and NS-MPs (HPC + Xylitol) were 1365, 1626, 1523, and 2208 μg/mL/min, respectively, indicating an enhancement in GLI dissolution rate from NS-MPs when compared to NS-MPs without sugar alcohol. These results could be attributed to the presence of sugar alcohols in the drug layer of NS-MPs; they can prevent interparticle interaction between GLI nanoparticles and thereby enhance drug dispersibility in the submicron size range, leading to the enhanced GLI dissolution. This effect was particularly pronounced in NS-MPs (HPC + Xylitol), possibly due to the good dispersion characteristics observed in the redispersion test and reflected in the difference in the dissolution-promoting effect of sugar alcohols. These findings suggest that sugar alcohol application enables the formulation of solid particulates with improved dissolution of poorly water-soluble drugs without compromising the characteristics of nanocrystal-coated particles obtained via solidifying process using NSCS.

References

[1] H. Yamamoto, *Earozoru Kenkyu* **2010**, 25(2), 149-154.

Highly stable and pH-universal catalysts for hydrogen evolution reactions

Zhaojun Han*

School of Mechanical, Medical and Process Engineering, Queensland University of Technology, Brisbane, QLD 4000
*Corresponding author: zhaojun.han@qut.edu.au

Green hydrogen production through water electrolysis is a promising method to utilize renewable energy in the context of urgent need to phase out fossil fuels. However, renewable powers such as solar and wind are intermittent, unstable and unpredictable, posing challenges to directly use them for green hydrogen production. In this talk, I will introduce several approaches that can improve the stability and performance of HER electrocatalysts in a range of electrolyte conditions. Specifically, (i) Cr coating was applied on NiMo for alkaline HER under intermittent power supply [1]; (ii) Ru active sites on amorphous Ni-doped MoO_3 nanowires showed pH-universal stability [2]; and (iii) a dual approach of Cr coating and Ca doping boosted the catalytic performance of CoP in alkaline electrolyte. Our approaches deepen the understanding of metal electrocatalysts in HER processes, paving the way for widespread applications of industrial electrolysis under different conditions.

References

[1] ACS Appl. Mater. Interfaces, 2022, 14, 40822.
[2] Small Struct., 2023, 4, 202300194.

Numerical study on the carbonation reaction of CaO with supercritical CO_2 in a fluidized bed reactor for CSP application

Nan Zheng,[a] Shaoxin Chen,[a] Hanqing Liu[a], Jinjia Wei[a,]*

[a] School of Chemical Engineering and Technology, Xi'an Jiaotong University, Xi'an, China
*Corresponding author: jjwei@mail.xjtu.edu.cn

The effect of CO_2 pressure is one of the major controlling parameters in carbonation process which not only affects the final conversion rate of CaO but also determines the integration of the carbonator with a CO_2 power cycle in the CSP application. In our previous studies, we found that using supercritical CO_2 as the fluidizing gas can significantly improve the dispersion of fine particles. Hence, it can be inferred that the use of supercritical fluidization technology could reduce the sintering problem caused by agglomeration of CaO particles during the carbonation process, thereby improving the conversion rate and cyclic stability of $CaCO_3$/CaO reaction pair. In this study, a comprehensive numerical model based on the two-fluid model accompanying with heat transfer and chemical reactions kinetics is developed to simulate the carbonation reaction in a supercritical CO_2 fluidized bed reactor in a temperature range of 873-1173 K. The flow behaviour of supercritical CO_2-partical flow, temperature and reaction rates distribution, gas composition profiles in the bed were predicted and compared with the results obtained based on a normal pressure reactor. The effect of tube bundle arrangement on particle aggregation behaviour and bed-to-tube heat transfer performance were also investigated. The results show that the Ca-based particles show a homogeneous fluidization in supercritical CO_2 fluidized bed reactor. In comparison with the normal pressure reactor, both the conversion rate and bed-to-tube heat transfer coefficient are improved, which provide a theoretical basis for innovation design and optimization of the integration scheme.

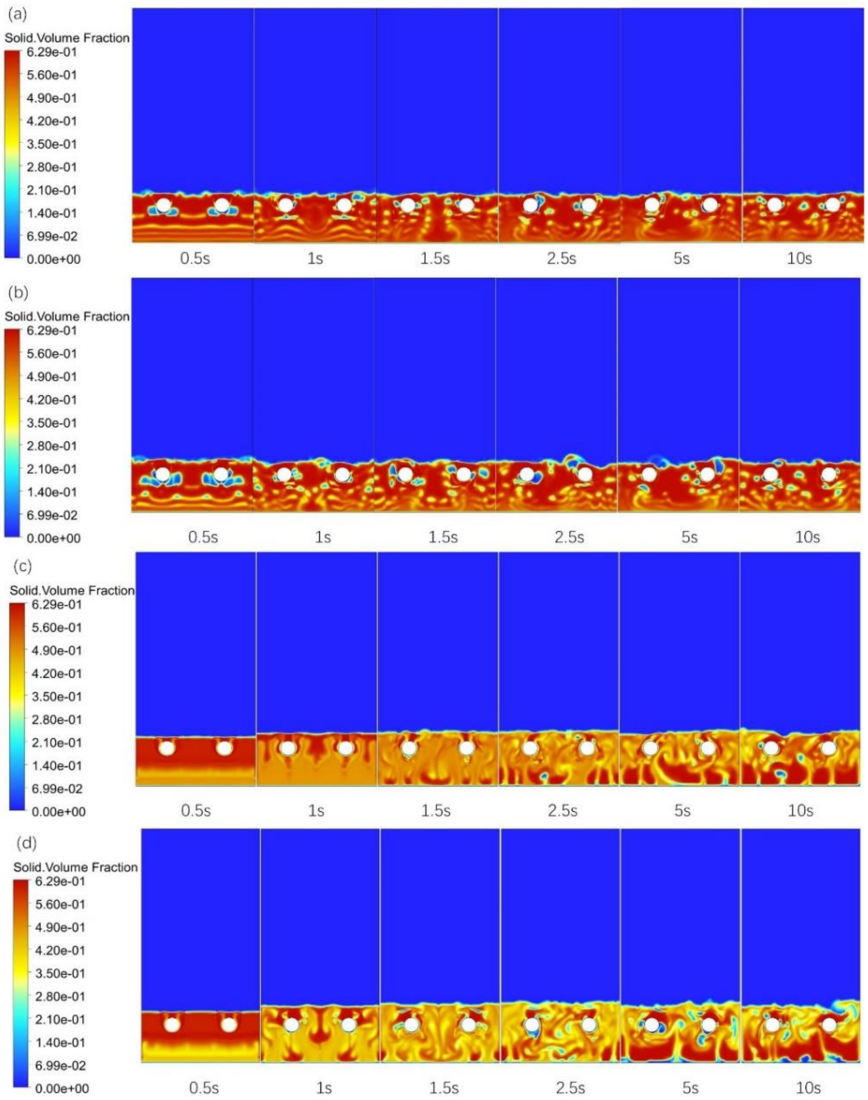

Figure 1. Solid volume fraction in fluidized bed with: (a) normal pressure air, fluidization number of 1.8; (b) normal pressure air, fluidization number of 2.2; (c) supercritical CO_2, fluidization number of 1.8; (d) supercritical CO_2, fluidization number of 2.2.

Nickel ferrite nanoparticles synthesized by the electrochemical method for energy storage applications

Heru Setyawan,* Widiyastuti Widiyastuti, Suci Madhania

Department of Chemical Engineering, Sepuluh Nopember Institute of Technology, Surabaya, Indonesia
*Corresponding author: sheru@its.ac.id

Ferrites have many fascinating properties that make them useful for various energy related applications such as photoelectrochemical cells, photocatalytic CO_2 reduction, batteries, supercapacitors and microbial fuel cells [1]. Spinel ferrites are the most important ferrite for energy-related applications because they are readily available, cheap, stable, eco-friendly and easy to synthesize [2]. They have a cubic structure with a general formula of MFe_2O_4 where M is a doubly charged cation of a transition metal such as Cr, Mn, Fe, Co, Ni, Cu or Zn. Spinel ferrite nanoparticles (NPs) have high surface-area-to-volume ratio that led to unique physicochemical properties due to a large percentage of the atoms in the particle to exist on the surface.

Electrolytic water splitting for hydrogen production and CO_2 electroreduction are considered to become important parts on how chemical industries and other sectors to do decarbonization. One of the problems to adopt this technology comes from the sluggish oxygen evolution reaction (OER). Herein, we propose nickel ferrite ($NiFe_2O_4$) nanoparticles synthesized by the electrochemical method to improve electrocatalytic performance for OER. The nickel ferrite nanoparticles were synthesized by electro-oxidation of iron anode in aqueous nickel sulfate solution. The electrodes were arranged in an alternating monopolar configuration to enhance the productivity of nanoparticles. Detail of the experimental setup has been described elsewhere [3,4].

The nickel ferrite nanoparticles have morphology from nearly spherical to cubic with a size ranging from 4 to 56 nm, depending on the applied voltage (Figure 2a-d). The particles tend to be nearly spherical at lower voltages and changes to cubic at higher voltages. The identified phase in the particles, as indicated by the XRD patterns shown in Figure 2e, consists of only $NiFe_2O_4$ at 9 and 12 V. However, they also contain β-$Ni(OH)_2$ and/or α-Fe_2O_3 at 3 and 6 V. They demonstrated promising electrocatalytic activity for OER in an alkaline solution, with an overpotential of 337 mV at a current density of 10 mA/cm2 and a small Tafel slope of 435 mV/dec. The nickel ferrite also demonstrated its capability to act as bifunctional electrocatalyst for both OER and oxygen reduction reaction (ORR).

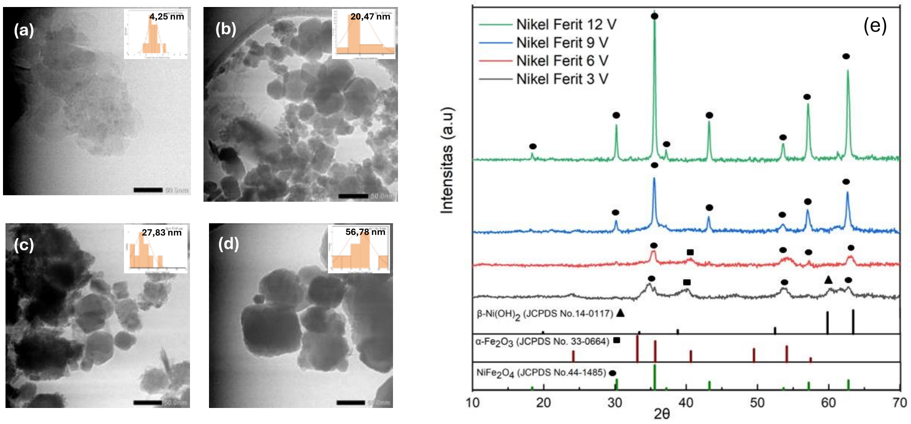

Figure 2. TEM images of particles produced using the electro-oxidation of iron in nickel sulfate solution at a voltage of 3 V (a), 6 V (b), 9 V (c) and 12 V (d), and the XRD patterns of particles produced at various voltages.

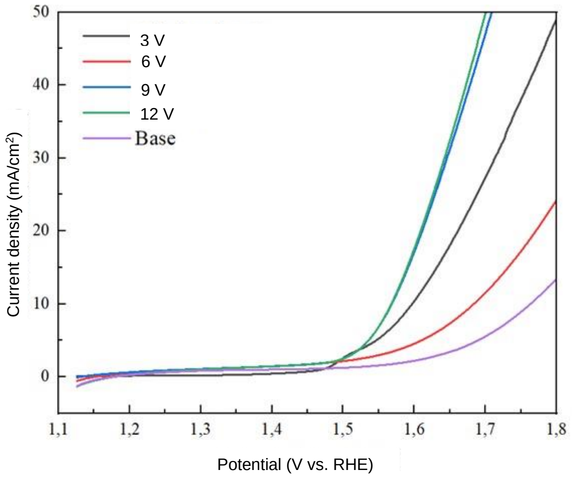

Figure 3. Liner voltammograms of particles prepared using the electro-oxidation of iron at various voltages in 4 M KOH.

References

[1]K.O. Abdulwahab, M.M. Khan, J.R. Jennings, Ferrites and ferrite-based composites for energy conversion and storage applications, Crit Rev Solid State Mater Sci (2023) 1–49. https://doi.org/10.1080/10408436.2023.2272963.

[2]L. Han, S. Dong, E. Wang, Transition-Metal (Co, Ni, and Fe)-Based Electrocatalysts for the Water Oxidation Reaction, Adv Mater 28 (2016) 9266–9291. https://doi.org/10.1002/adma.201602270.

[3]P. Nurlilasari, W. Widiyastuti, H. Setyawan, F. Faizal, M. Wada, I. Wuled Lenggoro, High-throughput production of magnetite nanoparticles prepared by the monopolar arrangement of iron electrodes in water, Chem Eng Sci 201 (2019) 112–120. https://doi.org/10.1016/j.ces.2019.02.027.

[4]P. Nurlilasari, W. Widiyastuti, H. Setyawan, Novel monopolar arrangement of multiple iron electrodes for the large-scale production of magnetite nanoparticles for electrochemical reactors, Adv Powder Technol 31 (2020) 1160–1168. https://doi.org/10.1016/j.apt.2019.12.043.

Integration of Calcium Looping with Methane Bi-reforming via the Ni-Pd Interface: A Combined Experimental and DFT Study

Zhi Xuan Law, Kun-Han Lin, De-Hao Tsai*

Department of Chemical Engineering, National Tsing Hua University, Hsinchu, Taiwan, R.O.C
*Corresponding author: dhtsai@mx.nthu.edu.tw

The urgent need to mitigate greenhouse gas emissions and combat climate change has driven research in carbon capture and utilization (CCU) technologies. Among these, calcium looping (CaL) has emerged as a prominent candidate for CO_2 capture. Previous studies have demonstrated the successful integration of CaL with methane dry reforming (DRM), showcasing high catalytic efficiency in terms of CO_2 conversion and H_2 production. In comparison to DRM, methane bi-reforming (BRM) offers a higher H_2 to CO yield ratio, presenting advantages for downstream applications. However, the introduction of steam into the CaL-BRM system, while using nickel as the active metal, has led to the occurrence of undesired side reactions, such as $Ca(OH)_2$ formation, posing challenges for optimal performance. This study aimed to enhance catalytic performance of CaL-BRM system, primarily through the incorporation of a noble metal, palladium (Pd), to create a Ni-Pd interface. Overall, results indicated promising catalytic performance via the utilization of Ni-Pd as the active metal. Density functional theory (DFT) calculations were employed to elucidate the underlying reasons for the superior performance observed with this bimetal compared to bare nickel.

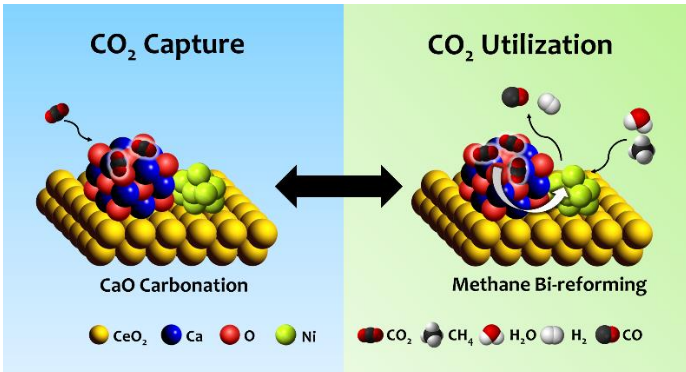

Figure 1. Calcium looping-integrated with methane bi-reforming.

References

[1] Z. X. Law, D. H. Tsai, *ACS Sus. Chem. Eng.* **2023**, 11, 2574-2585.
[2] Z. X. Law, D. H. Tsai, *Langmuir* **2023**, 39, 14782-14790.

Ignition characteristic of coal particle under high pressure

Dongdong Fang, Yuanqiang Duan*, Lunbo Duan**

Key Laboratory of Energy Thermal Conversion and Control, Ministry of Education, School of Energy and
Environment, Southeast University, Nanjing 210096, China
*Corresponding author: 15805174453@163.com (Y. Duan)
**Corresponding author: duanlunbo@seu.edu.cn

Pressurized oxy-fuel combustion is a potential technology to support for carbon capture, utilization and storage (CCUS) for coal power plants. In brief, the benefits of pressurized oxy-fuel combustion include: the size and cost of power plant equipment can be reduced, due to the reduced volume of gas; the convective heat transfer to boiler tubes is increased at higher pressure; the high pressure oxy-fuel flue gases lower the energy and capital costs of carbon capture [1][2], et al. However, there is currently little research on the basic experimental due to the difficulty of experiments, with the predominant focus residing in low-pressure regimes and a dearth of exploration in high-pressure environments. In this work, the ignition characteristics of single particles of bituminous coal and anthracite coal in O_2/CO_2 atmospheres were studied under pressures of 0.1-4 MPa in a visualized high-pressure drop tube furnace. A high-speed camera was employed to capture the combustion process, facilitating the determination of ignition delay time and devolatilization time of single-particle coal (as shown in Figure 1). The results show that a rapid escalation followed by a gradual decrement in the ignition delay time of bituminous coal with increasing operating pressure under the same oxygen volume fraction (Figure 2). The ignition process was homogeneous ignition, where the drastic changes in gas-phase properties (density, specific heat capacity, diffusion coefficients, etc.) and the release of volatile were the main factors for an increased the ignition delay. The augmentation of both the oxygen partial pressure and heat transfer coefficient promoted the ignition of volatile, resulting in a reduction for the ignition delay time. Also, the devolatilization time of bituminous coal showed a positive correlation with pressure. Anthracite coal showed heterogeneous ignition during the ignition process. The changes in gas-phase properties caused by pressure extends the ignition delay time of anthracite. In addition, compared with regular pressure oxygen combustion, pressurized oxy-fuel combustion had a more significant effect on the gasification of the coal particles.

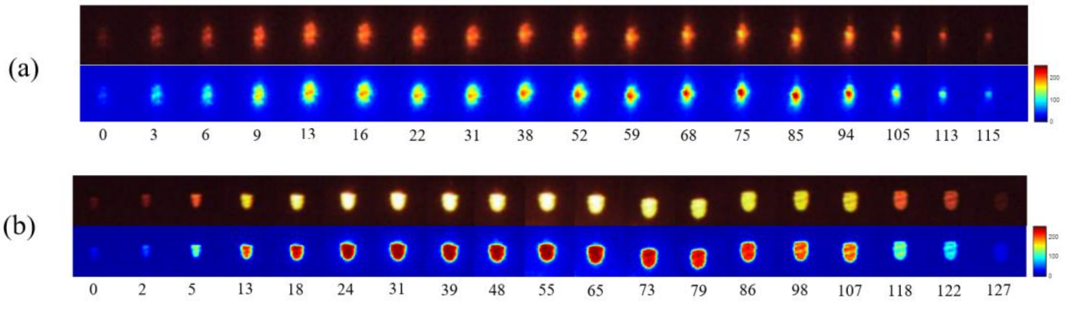

Figure 1. Typical combustion pictures and pseudo-color pictures (50x50 pixels), (a) bituminous coal (b) anthracite

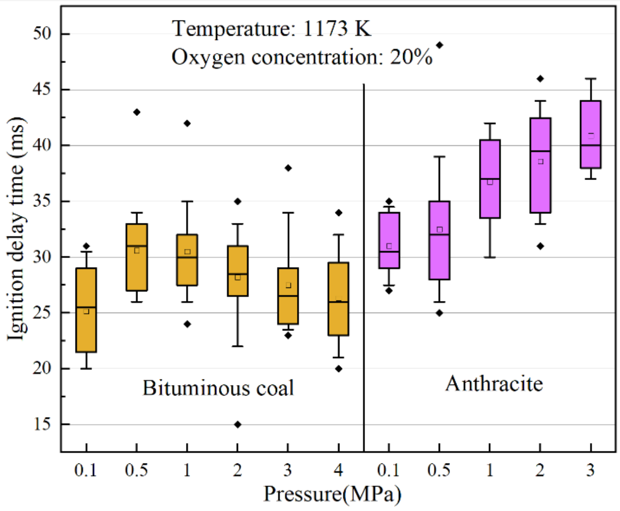

Figure 2. Ignition delay time of bituminous coal and anthracite

References

[1] J. Hong, G. Chaudhry, J. G. Brisson, et al. *Energy*, 2009, 34(9): 1332-1340.
[2] A. Gopan, B. M. Kumfer, J. Phillips, et al. *Applied Energy*, 2014, 125: 179-188.

Gas Penetration and Powder Compression of Powder Bed in Lock-hopper Silo Under High Pressure Dynamic Load

Minghao You, Xin Wang, Liang Cai*

School of Energy and Environment, Southeast University, Nanjing, China
*Corresponding author: liangc@seu.edu.cn

Gas pressurization of powder beds plays an important role in various industrial chemical processes, e.g., the pressure swing adsorption [1], air-assisted discharge of silos [2], and powder transfer in lock hoppers (or called transfer pressure vessels) [3]. The powders in transfer pressure vessels usually need further transport after the pressure rises to a certain value. Moreover, the gas flow in these compressible powders seriously affects the flowability of powders and their subsequent transport. Clearly, there is a need to investigate the gas flow characteristics in the compressible powder bed during gas pressurization more intensively [4, 5].

In this paper, the two-fluid method was used to modelling the powder compression and gas penetration characteristics in a powder bed. Two types of powders, glass powder and coal powder, were chosen for experimentation and simulation. The modified drag force model, which considers particle sphericity and apparent morphology, achieves a high degree of consistency between experiment and simulation. The overall compressibility of the coal powder bed is significantly stronger than that of the glass powder bed. The local compression characteristics in different regions of the powder bed were obtained. The pressure drop across the powder bed increases to a maximum and then decreases during pressurization. The gas penetration time of coal powder bed is longer than of glass powder bed. The association between powder compression and gas penetration characteristics is analysed.

References

[1] R. S. Todd, P. A. Webley, *Ind. Eng. Chem. Res.* **2005**, 44, 7234–7241.
[2] Y. Zhou, P. Y. Lagrée, S. Popinet, P. Ruyer, P. Aussillous, *Phys. Rev. Fluids* **2019**, 4, 124305.
[3] H. Lu, X. Guo, X. Cong, K. Liu, X. Sun, K. Xie, X. Gong, J. Lu, *Ind. Eng. Chem. Res.* **2012**, 51, 13839-13845.
[4] X. Wang, B. Luo, M. You, C. Liang, D. Liu, J. Ma, X. Chen, *Chem. Eng. Sci.* **2023**, 268, 118445.
[5] S. Wang, X. Guo, H. Lu, H. Liu, *Chem. Eng. Sci.* **2022**, 260, 117927.

Experimental and numerical investigation on heat transfer characteristics in a high-temperature particle/molten salt fluidized bed heat exchanger

Hanqing Liu[a], Ziyang Li[a], Shaoxin Chen[a], Nan Zheng[a,]*, Jinjia Wei[a]

School of Chemical Engineering and Technology, Xi'an Jiaotong University, Xi’an, China
*Corresponding author: nanzheng@mail.xjtu.edu.cn

Fluidized bed heat exchanger is one of the core devices in the particle-based high-temperature concentrated solar power (CSP) generation plant, which is responsible for transferring heat from the concentrator (or thermal storage unit) to the power cycle (eg. supercritical CO2 Brayton cycle) efficiently. In the present study, a lab-scale 20 kW particle/molten salt fluidized bed heat exchanger was designed and tested for the first time. Bauxite particles with a mean size of 300 μm and quaternary nitrate mixture are used as the heat transfer fluid on hot side and cold side, respectively. The effect of bed height, gas velocity, gas temperature, particle flow rate and molten salt flowrate on the overall heat transfer coefficient as well as the parasitic energy consumption of the fluidized bed was investigated. Euler-Euler Two-Fluid Model combining with the particle kinetic theory was adopted to simulate heat transfer characteristics between fluidizing particles and immersed horizontal tubes. The distributions of local heat transfer coefficient along the circumference of the tube under various conditions were obtained. Based on the test and simulation data, an empirical correlation for predicting the overall heat transfer coefficient under high-temperature conditions has been proposed. The results indicate that there is an optimal combination of various control parameter to maximize the heat transfer coefficient and minimize the parasitic energy consumption, respectively. In addition, reducing the vertical spacing of the tube bundles and the bed width is beneficial to the heat transfer performance, which provides guidance for the optimization of the geometric structure of fluidized bed heat exchanger.

Figure 1. Experimental setup of particle /molten salt fluidized bed heat exchanger.

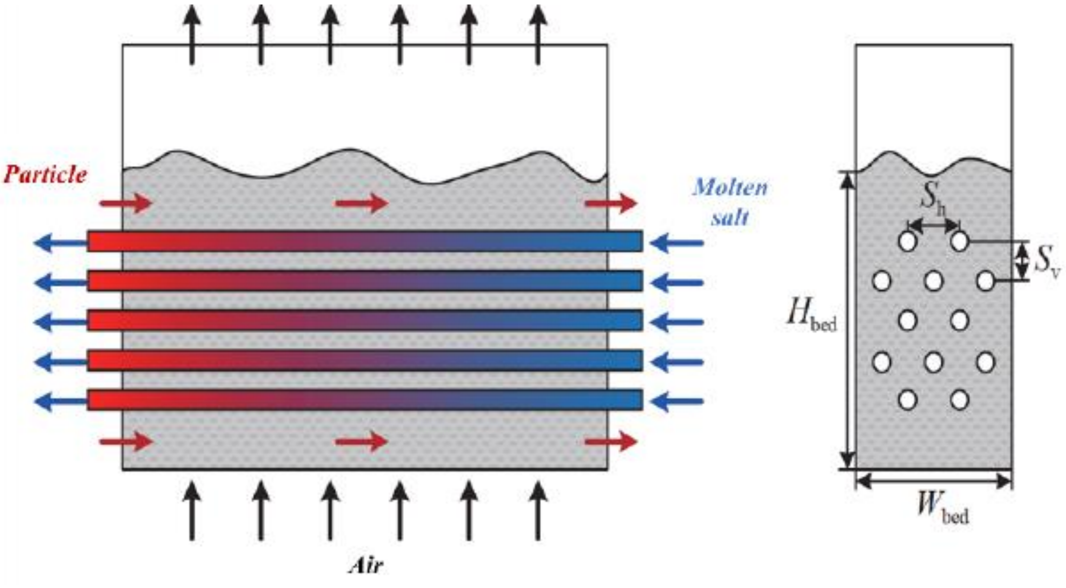

(a)Main view (b) Left view

Figure 2. Schematic diagram of fluidized bed heat exchanger with immersed tubes

Evaluation of the ignitability of a handheld electrostatic powder spray gun using new spark ignition test apparatus

Kwangseok Choi [a], Yuta Endo [a], Takaaki Mizutani [a], and Kenzo Yanagida[b,]*

[a]National Institute of Occupational Safety and Health, Tokyo, Japan
[b]Asahi Sunac Corporation, Aichiken, Japan
*Corresponding author: choiks@s.jniosh.johas.go.jp

This study reports the results of experiments dealing with the ignitability of abnormal discharge occurring from a handheld electrostatic powder spray gun with a new spark ignition test apparatus. The experimental system consists of a small-sized ignition container, a handheld electrostatic powder spray gun and controller, a grounded electrode (25 mm in diameter), test gas (air mixed gas with methane concentration of 12 vol %), a gas concentration meter, and an air compressor. In this study, the voltage applied to the handheld electrostatic powder spray gun was -80 kV, and the setting value of the constant current control circuit inside the electrostatic controller was adjusted in 10 µA increments, ranging from -80 to -140 µA and abnormal discharges gap was set to 4, 9, 14, 16, 18, and 20 mm (for example, Fig.1). As the results of evaluating the ignition hazard of abnormal discharge using the new spark ignition test apparatus, the results with excellent reproducibility were obtained, confirming its validity. None of the abnormal discharges in this study ignited the explosive atmosphere as specified by the EN international standards[1)]. In addition, to estimate the discharge energy, E_{exp} value of abnormal discharge, the methane concentration was changed from 5.0 to 13.0 vol% in 1.0 vol% increments. As the results, the abnormal discharge assumed 0.56 mJ < E_{exp} < 1.07 mJ. In other words, the maximum E_{exp} obtained in this study was 1.06 mJ, which is lower than the standard value of 2 mJ of the EN international standard. These results suggest that the handheld electrostatic spray gun used in this study is extremely safe with no explosion-proof problems.

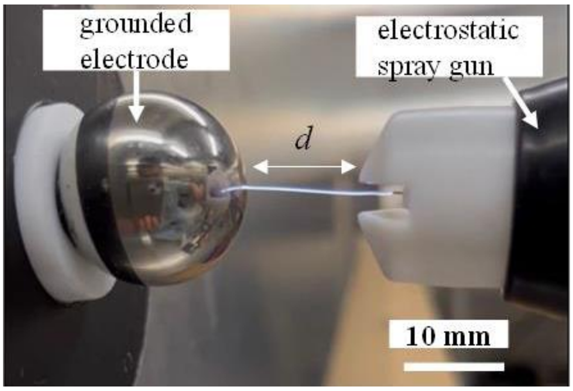

Figure 1. Example of abnormal discharge (Is: 140 µA; d: 18 mm).

References

[1] EN 50050-2, Electrostatic hand-held spraying equipment –Safety requirements– Part 2: Hand-held spraying equipment for ignitable coating powder, 2013.

Hot-melt kneading process of sulfur and porous carbon for all-solid state lithium sulfur batteries

Motoshi Iwao, Hideya Nakamura,* Shuji Ohsaki and Satoru Watano

Department of Chemical Engineering, Osaka Metropolitan University, Sakai, Japan
*Corresponding author: hideyanakamura@omu.ac.jp

All-solid-state lithium sulfur batteries (ASSLSBs) have attracted considerable attention as next generation batteries owing to their high safety and high energy density. Since sulfur (cathode active material of ASSLSBs) has electron and lithium-ion insulating nature, sulfur must be composited with electron conductive additve and solid electrolyte (lithium-ion conductor). As a process to composite sulfur and electron conductive additive, we proposed to utilize a hot-melt kneading process [1]. In this process, particles are exposed to heat and shear force, resulting in melting of the sulfur with lower melting temperature (120 °C) and kneading of molten sulfur with conductive additive. The composite particles prepared from the hot-melt kneading process improved battery performance [1]. When using porous carbon (typical electron conductive additive) to produce composite particles in the hot-melt kneading process, sulfur can exist inside and/or outside the pore of porous carbon in the composite particles. This sulfur-existing region can significantly influence the battery performance. However, a key parameter to control the sulfur-existing region remains unclear. Furthermore, correlation between the sulfur-existing region and battery performance was not well understood. Thus, this study aimed to clarify the aforementioned unclear key parameter and structure-performance correlation.

By adjusting the weight ratio of sulfur to porous carbon, two distinct types of composite particles were prepared; those with almost whole sulfur existing inside the pore and those with a part of sulfur existing outside the pore. This result confirmed that the weight ratio of sulfur to porous carbon was the key parameter to control sulfur-existing region in the composite particles prepared from hot-melt kneading process. Moreover, with increasing the amount of sulfur existing outside the pore, size of composite particles enlarged due to agglomeration of porous carbon as interparticle bridge of the molten sulfur was promoted. These two types of composite particles showed different electrochemical properties. The composite particles with almost all sulfur existing inside the pore exhibited higher initial capacity, whereas the composite particles with a part of sulfur existing outside the pore exhibited higher cycling stability.

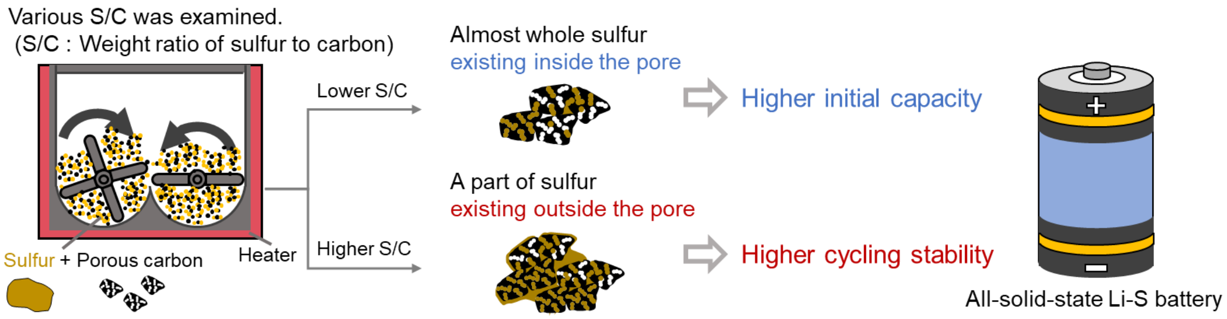

Figure 1. Summary of results in this study.

References

[1] Iwao, M. et al., Advanced Energy and Sustainability Research. (2023) 2200206.

Solubilization of Lignocellulosic Biomass by Milling with Heating

Honami HANABUSA^{a,b}, Toru JOBOJI^{a,}*, Kizuku KUSHIMOTO^{b}

Atsushi FUKUOKA^{c} and Junya KANO^{b,}**

^{a} AISIN CORPORATION, Kariya, Japan
^{b} Institute of Multidisciplinary Research for Advanced Materials, Tohoku University, Sendai, Japan
^{c} Institute for Catalysis, Hokkaido University, Sapporo, Japan
*Corresponding author: toru.joboji@aisin.co.jp
**Corresponding author: kano@tohoku.ac.jp

The utilization of lignocellulosic biomass such as wood and grass are attracting great attention worldwide as a means to break away from dependence on fossil resources, and production of biomaterials and fuels is extensively studied. To utilize lignocellulosic biomass as a raw material, it is necessary to convert natural polymers such as cellulose into monosaccharides in saccharification processes. However, because cellulose has a strong, recalcitrant crystalline structure with many hydrogen bonds in its molecule, conventional chemical processes require large amounts of sulfuric acid, resulting in a high environmental impact 1). Therefore, we investigated a method to solubilize biomass by milling without using chemicals. In this study, we found that cellulose can be solubilized by planetary ball mill with heating (Figure 1). It is confirmed that the milled product turned to amorphous by X-ray diffraction, and that its molecular weight was reduced by gel permeation chromatography. Furthermore, when the milled product was further treated with a reusable solid acid catalyst, a high saccharification yield was obtained, thus showing that these treatments are effective. We believe that this method will enable efficient and environmentally friendly biomass conversion without using chemicals and can contribute to further utilization of lignocellulosic biomass.

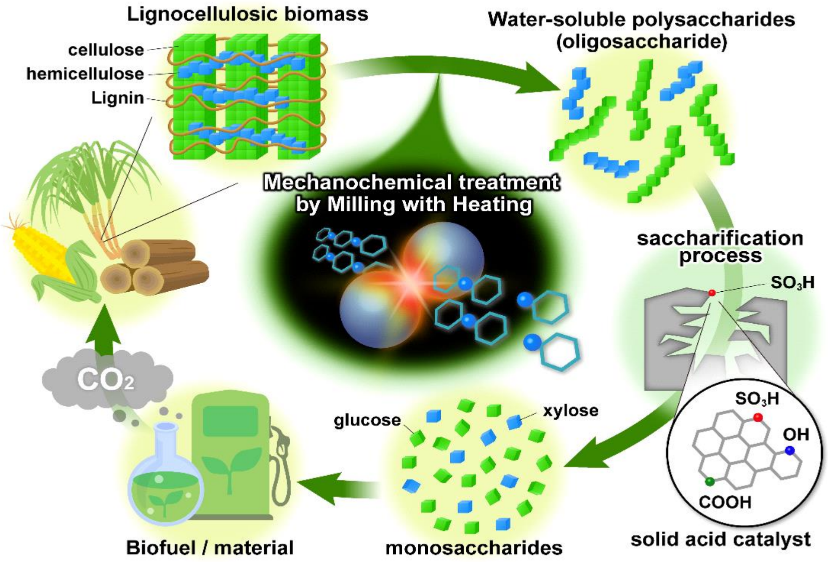

Figure 1. Utilization of biomass in resource circulation.

References

[1] A.Fukuoka, D. L. Dhepe, Angew. *Chem. Int. Ed.*, **2006**,45,5161.

Flare Gases Carbon Nanotubes (CNTs) based Electrode of Supercapacitor and Energy Storage Applications

Sunisa Watcharasing[a], Taradon Piromchart[a], Yaowamarn Chuminjak[b], Chakrit Sriprachuabwong[b]

[a] PTT Exploration and Production Public Company Limited, Bangkok, Thailand
[b]National Science and Technology Development Agency, Pathumthani, Thailand
*Corresponding author: sunisaw@pttep.com

This project aims to synthesize the high-valued CNTs product and explore opportunities to reduce greenhouse gas emissions, developing two key technologies: 1) a fluidized bed chemical vapor deposition (FBCVD) reactor using the remaining process gases as the main feedstock, and 2) the catalyst for converting flare gas to CNTs.

CNTs synthesis from flare gas field trials was first initiated in Thailand, using the remaining process gases as carbon sources for CNTs synthesis. This technology is a part of Carbon Capture and Utilization (CCU) technology which will help reduce CO2 emission into the atmosphere. The prototype-scale CNTs reactor is a low-pressure, isothermal fluidized bed reactor that converts hydrocarbon gas into solid CNTs particles. A catalyst suspended on catalyst bed support is used to promote the conversion of the reactants within the FBCVD. The FBCVD reactor was applied for CNTs synthesis in this project, providing a simultaneous solid/fluid mixture and excellent heat and mass transfer that is great for CNTs reactor unit scale-up. The result shows a promising CNTs yield, and purity. Therefore, CNTs synthesis from the remaining process gases in the field trial test was initiated, by installing the CNTs reactor skid at the PTTEP main gas processing facility. The real process gas stream was routed into the reactor. Referring to actual plant conditions, the changes in the feedstock flowrate, reduction, and reaction temperatures, catalyst loading, and purification methods will be investigated to determine the feasibility of this novel technology. The result of CNTs synthesis shows CNTs purity greater than 95%, with methane conversion over 90% as a Multi-Walled CNTs (MWCNTs) diameter of 25-50 nm. Currently, the CNTs production can be obtained around 10 kg/month. New findings and requirements discovered during the field trial test will be used to iteratively optimize and improve the engineering design of the CNTs reactor for future industrial-scale implementation.

The synthesized CNTs product was further applied as an advanced materials in the real potential applications in the prototype phase of an energy storage. The unique structure of CNTs facilitates high capacity and rate performance of the supercapacitor with promising cycling stability. The preliminary results illustrated that the flare gas based CNTs supercapacitor can provide longer cyclability, and the high energy density compared to the commercial supercapacitor in the market. The key challenge of the CNTs paste for supercapacitor is how to ensure uniform dispersion of CNTs powder with the additive during supercapacitor manufacturing, this is crucial for achieving consistent material properties.

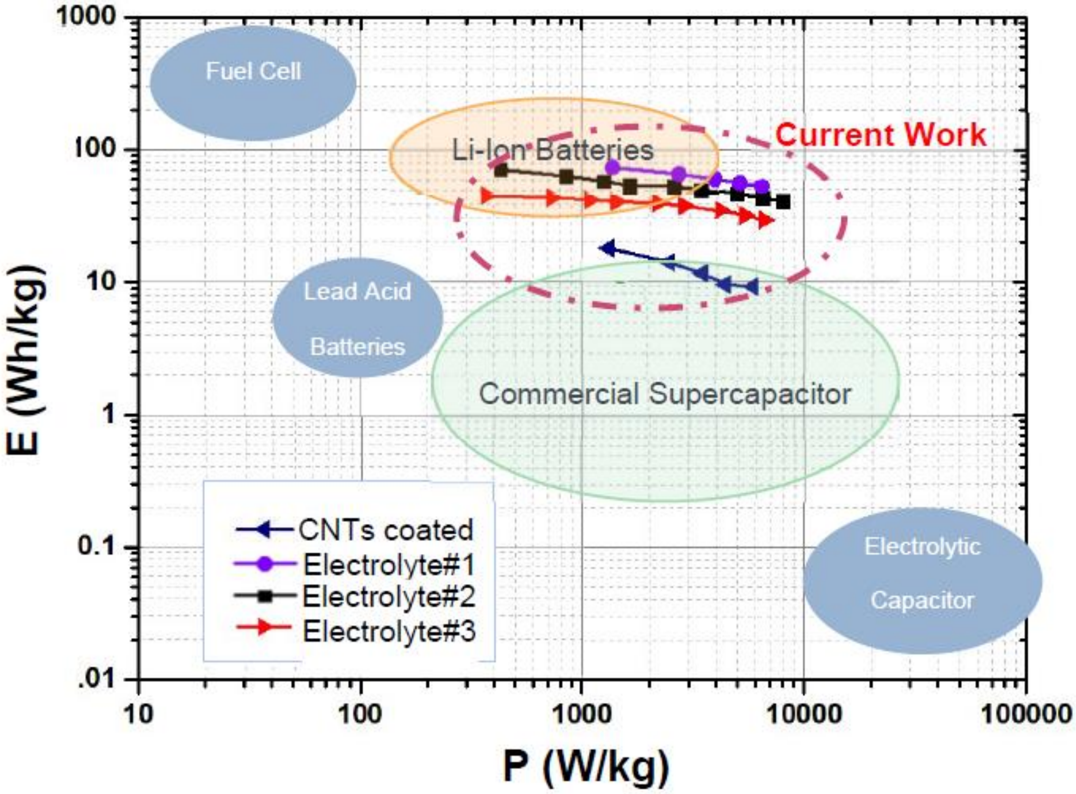
1000
100
10
1
0.1
.01
E (Wh/kg)
10
100
1000
10000
100000
P (W/kg)
Fuel Cell
Li-Ion Batteries
Current Work
Lead Acid Batteries
Commercial Supercapacitor
Electrolytic Capacitor
CNTs coated
Electrolyte#1
Electrolyte#2
Electrolyte#3

PTFE fibrillation by dry powder mixing and its application to electrode fabrication for all-solid-state battery

Hideya Nakamura*, Shota Miyake, Motoshi Iwao, Shuji Ohsaki, Satoru Watano

Osaka Metropolitan University, Sakai, Osaka, Japan
*Corresponding author: hideyanakamura@omu.ac.jp

All-solid-state lithium-ion batteries (ASSLIBs) are highly promising candidates of the advanced secondary batteries for electric vehicles. One of the key challenges regarding ASSLIBs is development of their manufacturing process. Currently, a mainstream process expected for manufacturing ASSLIBs is a wet process [1]. However, the wet process suffers from disadvantages such as high energy consumption and high environmental load. To address this issue, a dry process, in which ASSLIBs can be produced without solvent, has attracted much attention [2]. In the dry process, the raw powders are mixed with binder particles by a dry mixing process, and the electrode sheet is then fabricated from the powder mixture. A key to the fabrication of electrode sheets in the dry process is the use of binder particles. Polytetrafluoroethylene (PTFE) is a typical binder particle. Morphology of the PTFE can be changed from particulate form to fiber by applying external force and/or heat. Once the PTFE fibers are dispersed in the powder mixture, the PTFE can bind the particles together like a spider's web, resulting in a freestanding electrode sheet even without solvent [3]. This PTFE fibrillation mainly proceeds in the dry mixing before sheet fabrication; however, its mechanism is unclear. In particular, key factors to control the PTFE fibrillation are not identified. It is also unclear which dry mixing process, and which specific features, are suitable for the PTFE fibrillation. Furthermore, the relationship between the PTFE fibrillation state and the properties of the final electrode sheet also remains unclear. The objective of this study is to identify the key factors for PTFE fibrillation in dry powder mixing and to clarify the specific features of an optimal mixing process for PTFE fibrillation. Furthermore, electrode sheets and all-solid-state half-cells were fabricated using the powder mixtures with different PTFE fibrillation states. The correlation between the PTFE fibrillation states and physico-electrochemical properties of the electrode sheets was investigated.

We investigated three types of dry mixing equipment, which were horizontal high-shear mixer (HSM), planetary ball mill (PBM), and twin-screw hot kneader (TSHK). Generally, in these processes, the dominant external forces exerting the powder are as follows: shear force in the HSM; shear and compressive forces in the PBM; shear and compressive forces with heat in the TSHK. By comparing these different mixing processes, effects of the type of external forces and processing temperature on the PTFE fibrillation were investigated. A cathode active material (LiNi0.5Co0.2Mn0.3O2), sulfide solid electrolyte, and PTFE were used as experimental materials.

Fig. 1 shows appearance of the powder mixture prepared by each equipment and the fine particle fraction (mass fraction of particles less than 250 μm) in the powder mixture. Appearance of the powder mixture prepared by the HSM was almost same as the original raw powder (Fig. 1b), and large amount of the fine particle fraction still remained (more than 70%) (Fig. 1e). In contrast, the powder mixture prepared by PBM and TSHK exhibited large agglomerates over 0.5 cm and fine particle fraction decreased significantly from the original powder. Among these, the TSHK showed the smallest fine particle fraction. These results indicate that the TSHK is the most effective in fibrillating the PTFE. In other words, it was found that mixing equipment capable of applying shear, compressive force, and heat to the powder is suitable for the fibrillation of PTFE.

Influence of the PTFE fibrillation states on physico-electrochemical properties of the electrode sheets was investigated. The electrode sheets were prepared using a powder mixture prepared by the TSHK under various processing temperatures. Fig. 2 shows the tensile strength of sheet as a function of the number density of PTFE fibers in the prepared mixture. Processing temperature was also displayed at each plot. The tensile strength increased with an increase in the number density of PTFE fibers, indicating that a sheet with high strength can be fabricated by using a powder mixture in which PTFE fibrillation proceeds more. Fig. 3 shows the 2C discharge capacity of the half-cell prepared from each mixture as a function of the number density of PTFE fibers in the mixture. The results exhibited that the maximum electrochemical performance was achieved at 30 mm-2, indicating that the relationship between the number density of PTFE fibres and battery performance is not a simple linear relationship, and there is an optimum fibrillation state which maximizes battery performance. Detailed discussion on this non-linear relationship between the PTFE fibrillation states and battery performance will be presented in the symposium.

In summary, it was found that a dry mixing process which can apply shear force, compressive force, and heat to the powder was suitable for the PTFE fibrillation. It was also determined that temperature during mixing is a key factor in the PTFE fibrillation. The relationship between the PTFE fibrillation state and the physico-electrochemical properties of the electrode sheet was then investigated. The sheet with higher tensile strength was fabricated from the powder mixture in which PTFE fibrillation proceeded more. It was also found that there is an optimum fibrillation state which maximizes the ASSLIB performance.

References

[1] M. Batzer et al., Batter. Supercaps. 2022, 5, e20220032.
[2] Y. Li et al., Mater. Today. 2022, 55, 92–109.
[3] F. Hippauf et al, Energy Stor. Mater. 2019, 21, 390-398.

Comb-shaped anion exchange membrane with segmented hydrophilic/hydrophobic side chain

Kuandi Wang, Jiannan Li, Tiantian Li*

State Key Laboratory of Fine Chemicals, Frontier Science Center for Smart Materials, School of Chemical Engineering, Dalian University of Technology, Dalian, China
*Corresponding author: litiantian@dlut.edu.cn

As a novel efficient and clean power generation device, anion exchange membrane fuel cells (AEMFCs) have attracted more and more attention. Anion exchange membranes (AEMs) as the core part of AWMFCs, directly determine the performances of AEMFCs. The common structure of AEMs is quaternized polymer membrane grafted cationic, which requires excellent ionic conductivity, anti-swelling and mechanical properties. In recently reported literatures, a common strategy to improve the performances of AEMs is to control the hydrophilicity of side chains of AEMs, such as introducing ether bonds to improve the hydrophilicity of side chains or connecting long alkyl hydrophobic tail chains after cationic groups. But these strategies also reduce other properties of AEMs, so that the prepared membranes cannot achieve a balanced and excellent performances.

Based on this, the molecular dynamics simulation was carried out to verify that the segmented hydrophilic/hydrophobic structure is conducive to the formation of the microphase separation structure. And then, this work synthesizes an anion exchange membrane which simultaneously grafts flexible hydrophilic side chain with ether bond and long hydrophobic side chain on the same side chain. The AEMs show high conductivity, mechanical strength and anti- swelling performances. It is found that when the number of ether bonds in the hydrophilic segment is 2, the AEM shows the best performances, which shows a tensile strength of 14.5 MPa and an elongation at break of 78.5%, and a conductivity of 90.4 mScm-1 at 80 oC. The peak power density of the fuel cell with this AEM can reach a 582 mWcm-2. The segmented hydrophobic side chain designed in this work provides a new strategy for improving the performance of AEMs and AEMFCs.

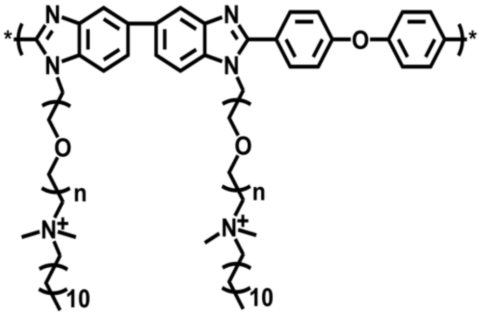

Figure 1. Structure of segmented hydrophilic and hydrophobic membrane materials

Ni-Pd Bimetallic Hybrid Catalyst for Lower-temperature Methane Bi-reforming

Kai-Po Chang, Chuan-Bin Du, De-Hao Tsai*

National Tsing Hua University, Hsinchu, Taiwan, R.O.C
*Corresponding author: dhtsai@mx.nthu.edu.tw

Recently, bi-reforming of methane (BRM) has attracted significant attention in the field of reduced-carbon hydrogen generation. In this work, NiPd@Al_2O_3 hybrid catalyst is successfully synthesized via aerosol-based approach for BRM. To develop superior hydrogen production efficiency, a cyclic reaction scheme is designed, where methane is used as a limiting reactant and excess CO_2 is introduced and recycled. The results show that complete conversion of methane to products can be accomplished at a temperature of > 600 ℃. Hydrogen production maintains at a relatively high value of above 511.6 mmol/h g·cat over multiple cycles. In summary, this research introduces an innovative cyclic reaction design, and the use of high-performance hybrid catalyst achieves a highly efficient pathway for low-temperature reduced-carbon hydrogen production.

Evaluation of the reaction properties of $Ca(OH)_2$ powder and CO_2 at high temperature.

Kunihiro Fukui*, Ayaka Tamaru, Fandi Angga Prasetya, Tomonori Fukasawa, Toru Ishigami

Chemical Engineering Program, Graduate School of Advanced Science and Engineering, Higashi Hiroshima, Japan
*Corresponding author: kfukui@hiroshima-u.ac.jp

$Ca(OH)_2$ powder is used in a bag filter system as an absorbent for hydrogen chloride (HCl) in flue gas discharged from cleaning plants, etc. Simultaneous absorption of CO_2 in flue gas by the bag filter system would contribute to the reduction of greenhouse gases. In this study, the high-temperature reaction characteristics of $Ca(OH)_2$ powder and CO_2 at 180 °C, which is the operation temperature range of the bag filter system, were investigated.

Test gas (H_2O: 0−50 vol%, CO_2: 15−30 vol%, N_2: balance gas) were reacted with 3.0 g of $Ca(OH)_2$ powder in an exposure chamber at 180 °C by continuous gas supply of 0.5 L/min. The conversion of $Ca(OH)_2$ powder to $CaCO_3$ was measured by the neutralisation titration method and the specific surface area of the resulting sample was determined by the BET method.

Fig. 1(a) shows the relationship between the conversion of $Ca(OH)_2$ powder to $CaCO_3$ and the reaction time for H_2O concentration of 50 vol%. For both CO_2 concentrations, the conversion increases rapidly in the early stage, and gradually reaches each constant value. This result indicates that the reaction mechanism changes from a surface reaction control to a diffusion control within the product layer. Because the surface of $Ca(OH)_2$ particle is covered more with a product layer of $CaCO_3$ as the reaction progresses. The higher concentration of CO_2 results in a higher conversion. **Fig. 1(b)** shows the relationship between the specific surface area and the reaction time for H_2O concentration of 50 vol%. The specific surface area decreases with the reaction time in both conditions. This is because the pores in the $Ca(OH)_2$ are more occupied by the generated $CaCO_3$ as the reaction proceeds.

The gas-solid reaction of $Ca(OH)_2$ with CO_2 was analysed using an unreacted core model. The transition from a surface reaction control (reaction time $t = 0$ to t_1) to a diffusion control in the product layer (reaction time $t = t_1$ to t_2^*) was examined. From the respective control models, the relationships between reaction time t and conversion X_B can be calculated by Eqs. (1) for the surface reaction-control region and (2) for the diffusion-control region in the product layer using the reaction completion times t_1^* and t_2^*, the reaction rate constant per unit surface area k_s and the effective diffusion coefficient of CO_2 D_{eA}. where ρ_B and R are the molar density and radius before the reaction of $Ca(OH)_2$ particle, C_{Ab} is the CO_2 concentration in the gas, and X_{Bt1} is the conversion at $t = t_1$.

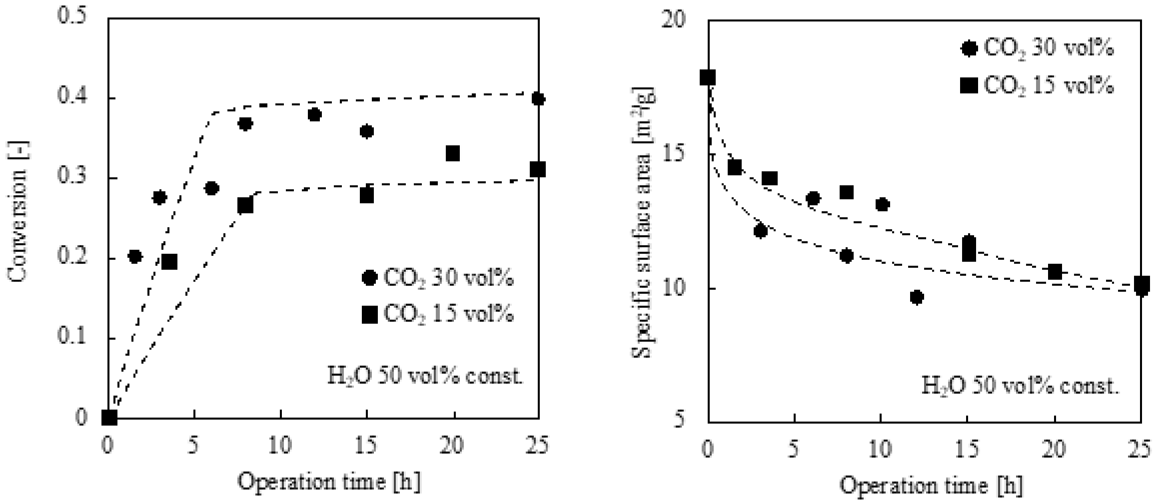

Figure 1. (a) Change in the conversion of $Ca(OH)_2$ powder with reaction time, (b) Change in the specific surface area of obtained sample with reaction time.

Using these equations, the experimental results were fitted using ks, D_{eA}, and X_{Bt1} as parameters to search for values that would best represent the change in the conversion of $Ca(OH)_2$ obtained in the experiments. Under all conditions, the model successfully represented results shown as broken lines in Fig. 1(a). **Table 1** lists the fit-optimized ks, D_{eA}, and X_{Bt1}, and the measured specific surface area S_{BET} and pore volume V at $t = t_1$. The rate constant ks is constant regardless of the CO2 concentration. It can be also observed that the specific surface area S_{BET} and pore volume V decrease with an increase in X_{Bt1}. Furthermore, D_{eA} increases with pore volume V. This is probably because CO_2 gas can diffuse more easily through the product layer when the pore volume increases. The conversion of $Ca(OH)_2$ powder increased with increasing CO_2 concentration. The reaction between $Ca(OH)_2$ particle and CO_2 gas could be represented using the unreacted core model, in which the reaction proceeds from the surface reaction control to a diffusion control in the product layer.

Table 1. Optimal value of reaction rate constant k_s, diffusion coefficient $D_{eA,}$ conversion of $Ca(OH)_2$ X_{Bti} and measured specific surface area S_{BET}, average pore volune V at $t = t_1$

H_2O [vol%]	CO_2 [vol%]	k_s [10^{-8} m/s]	D_{eA} [$10^{-17}m^2/s$]	S_{BET} [cm^2/g]	V [cm^3/g]	X_{Bt1} [-]
50	30	7.70	2.87	11.23	0.11	0.38
50	15	7.70	3.0	13.58	0.12	0.28
30	30	2.81	4.30	17.50	0.13	0.16
0	30	2.14	4.70	17.59	0.14	0.13

References

[1] Vasiliji, M. et al., *Ind. Eng. Chem. Res.* **2010**, 49, 9105-9110.
[2] Jae-Hoon, H. et al., *Journal of the Korean Ceramic Society* **2016**, 53, 429-434.
[3] Shin, M. et al., *Ind. Eng. Chem. Res.* **1999**, 38, 1316-1322.

Temperature-dependent mineral matter vaporization and aerosol formation during low rank fuel combustion

Yankai Huang, Xin Yu, Jingji Zhu, Dunxi Yu*

State Key Laboratory of Coal Combustion, Huazhong University of Science and Technology, Wuhan, China
*Corresponding author: yudunxi@hust.edu.cn

Low rank fuels (e.g., lignite and biomass) have been widely utilized for heat and power generation. However, ash issues are one of the great challenges that have yet to be addressed for safe, efficient and environmentally friendly operation of the combustion units [1]. Low rank fuels usually contain high fractions of alkali and alkaline earth metals (AAEMs), which tend to easily vaporize during combustion. As the temperature of the flue gas gradually decreases, these vaporized materials will homogeneously nucleate to form fine aerosols or heterogeneously condense on existing ash particles/heat exchanger surfaces [2]. These complex processes are the causes of a number of issues such as ash slagging, fouling, corrosion and aerosol emissions. Among them, mineral matter vaporization and aerosol formation are the key processes that have been subject to extensive investigations. It has been identified that the combustion temperature is the critical factor affecting the fate of mineral matter.

Low-load operation of power plants has been widely practiced around the world, in order to accommodate more renewable energy such as solar and wind energy [3]. It is particularly characterized by the feature that the combustion temperature is subject to change in a wide range (e.g., 900-1600 ºC) depending on the loads requried. In these cases, how changes in the combustion temperature (loads) would affect the behavior of mineral matter is an interesting topic of great practical significance. However, there is little work available.

This presentation is expected to report new data on mineral matter vaporization and aerosol formation at combustion temperatures varying in a wide range, as encountered in low-load operation of power plants. A well-controlled entrained flow reactor will be used for the combustion experiments, which allows high flexibility of temperature alteration. Typical lignites and biomasses will be considered, and the results will also be compared to elucidate the effects of fuel properties. The findings obtained in this work are believed to significantly contribute to a further understanding of ash issues in low-load operation of power plants especially firing low rank fuels.

References

[1] R. W. Bryers, *Prog Energ Combust* 1996. 22, 29-120.
[2] E. Raask, Mineral Impurities in Coal Combustion, Behavior, Problems, and Remedial Measures. Hemisphere Publishing, 1985.
[3] M. A. Gonzalez-Salazar, T. Kirsten, L. Prchlik, *Renew Sustain Energy Rev* 2018, 82, 1497-1513.

Efficient separation technology of spent photovoltaic panels for the circular economy

Chiharu Tokoro[a,b,]*

[a] Faculty of Science and Engineering, Waseda University, Tokyo, Japan
[b] Faculty of Engineering, The University of Tokyo, Tokyo, Japan
*Corresponding author: tokoro@waseda.jp

In 2023, total global solar cell installations reached 1 TW and annual production 400 GW; according to the ITRPV (International Technology Roadmap for Photovoltaic), annual production is also expected to reach 0.7-3 TW by 2040. The energy for its production will be supplied by current crystalline silicon solar cells. The energy required to produce these cells is enormous when calculated from current crystalline silicon solar cells. Silicon solar cells are expected to continue to account for a certain share of the market in the foreseeable future, so securing their raw materials and saving manufacturing energy are important for the sustainability of photovoltaics.

The concept of the circular economy, proposed by the European Commission in 2015, has since then received a surge of domestic and international attention as environmental and resource constraints have become more apparent, and is now becoming as important a direction as carbon neutrality. In Japan, recycling laws have been in place since the beginning of 2000 from the viewpoint of the shortage of final disposal sites and the appropriate treatment of waste, and it is fair to say that Japan has led the world in its technology and systems. However, the proper recycling of mass-produced products is not complementary to carbon neutrality, as it requires energy not only for production but also for recovery and separation. Therefore, it is necessary to circulate functions while maximising longevity, maintenance, reuse, repair, direct recycling, upcycling, etc., to create economies in a new resource circulation loop that is also complementary to carbon neutrality and various environmental responses [1].

Currently, three main types of processes have been developed for the recycling of photovoltaic panels, as shown in the Table 1. In any case, the focus for higher efficiency is on the sophistication of powder processing, such as smart milling, physical separation of particles layers and control of heat transfer between particles during heating. The authors have devised a more efficient milling process in the mechanical separation process to physically separate glass, metal and resin [2].

Table 1. Recycling process for photovoltaic panels.

Process	Advantages	Disadvantages
Grinding/Physical separation	low cost	low accuracy
Dismantling	low/middle cost	low throughput
Heating	high accuracy	high cost

We have also proposed a method to separate copper and silvers from resin without chemicals or heating using an electrical pulsed discharge for solar cells obtained by the hot-knife method, which is one of the dismantling process for the spent photovoltaic panels. The electric pulse method can precisely separate the silicon and metals from the resin. In addition, compared to conventional pulverisation methods, this method not only significantly reduces energy consumption as it only uses pulsed electricity in microseconds, but also reduces the risk of hazardous substance dispersal as it is a chemical- and heat-free separation technology that only uses water as the medium [3-7].

In the near future, it will be extremely important to realise a manufacturing-based circular economy by having industry and academic institutions in manufacturing and processing work together to develop easily degradable design-type products that can be economically incorporated into such a new resource circulation loop. Based on such a concept, the authors have started to develop easily degradable adhesives based on the application of electrical pulses[8].

References

[1] S. Murakami, K. Shimizu, C. Tokoro, T. Nakamura, *Sustainability* **2022**, 14(24), 16408.
[2] C. Tokoro, M. Nishi, Y. Tsunazawa, *Advanced Powder Technology* **2021**, 32(3), 841 - 849.
[3] C. Tokoro, S. Lim, Y. Sawamura, M. Kondo, K. Mochidzuki, T. Koita, T. Namihira, Y. Kikuchi, *Int. J. of Automation Technology* **2020**, 14(6), 966 - 974.
[4] S. Lim, Y. Imaizumi, K. Mochidzuki, T. Koita, T. Namihira, C. Tokoro, *IEEE Transactions on Plasma Science* **2021**, 49(9), 2857 - 2865.
[5] Y. Takaya, Y. Imaizumi, T. Koita, C. U. E. Mauricio, C. Tokoro, *Journal of Material Cycles and Waste Management* **2024**, DOI: 10.1007/s10163-024-01951-5
[6] Y. Imaizumi, S. Lim, T. Koita, K. Mochidzuki, Y. Takaya, T. Namihira, C. Tokoro, *EcoDesign for Sustainable Products, Services and Social Systems I* **2024**, 365–380.
[7] A. Heiho, I. Suwa, Y. Dou, S. Lim, T. Namihira, T. Koita, K. Mochidzuki, S. Murakami, I. Daigo, C. Tokoro, Y. Kikuchi, *Resources, Conservation and Recycling* **2023**, 192(5), 106922.
[8] M. Inutsuka, M. Kondo, T. Koita, S. Lim, K. Ota, T. Honda, R. Ogawa, T. Namihira, C. Tokoro, *The Journal of Adhesion* **2023**, DOI: 10.1080/00218464.2023.2167600

Application of particle technology and materials science to biological wastewater treatment

Junichi Ida,[a,*] Stella Chan,[b] Kento Nishi,[a] Kiriko Aramoto,[b] Beatriz Durán,[d] Shinichi Akizuki,[c] Pabel Cervantes Avilés,[e] German,[d] Tatsushi Matsuyama[a]

[a] Department of Environmental Engineering for Symbiosis, affiliation Soka University, Tokyo, Japan
[b] Graduate school of Science and Engineering, Soka University, Tokyo, Japan
[c] Institute of Plankton Engineering, Soka University, Tokyo, Japan
[d] Department of Civil Engineering, University of Guanajuato, Guanajuato, Mexico
[e] Department of Bioengineering, Tecnológico de Monterrey, Monterrey, Mexico
*Corresponding author: ida@soka.ac.jp

Anaerobic Digestion (AD) is a microbial process that produces renewable energy in the form of methane by treating various organic wastes. Recently, it has been reported that the addition of various conductive materials (CMs) into the AD bioreactor could act as a bridge to promote direct interspecies electron transfer (DIET) between exoelectrogenic bacteria and methanogenic archaea which enhances the methane production rate [1]. From the viewpoint of powder technology, bacteria, archaea, and CM are all regarded as particles. Since DIET can only occur when these three kinds of particles are in contact, contact efficiency between the three particles is very important. However, in conventional studies, since bacteria, archaea, and CM are used in a dispersed state, contact efficiency is expected to be low. Another problem with the addition of CM in the continuous anaerobic process is a washout of CM with effluent from the reactor. This may require another recovery process for CM and also result in additional costs to compensate for the lost CM.

To overcome these challenges, we proposed the co-immobilization of anaerobic microbes and CM in hydrogel to achieve improved contact efficiency and to prevent the washout of CM simultaneously. The study demonstrates that co-immobilizing AD sludge and multiwalled carbon nanotube (MWCNT) as CM in polyvinyl alcohol (PVA) hydrogel could enhance the methane production performance, resulting in faster methane production rate (3 times faster as compared to the control), shortening the lag time in the AD process and suppressing washout of MWCNT from the reactor.

Another example is the application of a composite of hydrogel and functional particles to the biological ammonia removal process. Discharge of untreated nitrogen wastewater causes pollution, eutrophication and finally ecosystem destruction in the water environment [2]. Livestock, municipal and food factory wastewaters are known as typical nitrogen-rich wastewaters. Anaerobic digestion effluent is also considered a major nitrogen-rich wastewater source, and the amount discharged increases year by year because the number of anaerobic digestion plants tends to increase around the world [3]. The nitrification–denitrification process is the most commonly used process for nitrogen removal from wastewater. However, it has been known that aeration for nitrification is an energy-intensive and costly operation and may account for 45–75% of energy consumption of the whole process [4]. Therefore, in many developing countries, the nitrification–denitrification method has not been implemented yet, and the development of a more economical and sustainable nitrification process is required. The consortium of microalgae and nitrifying bacteria has attracted attention owing to its advantages, such as energy- and cost-efficiency in terms of using only light irradiation without aeration. However, high light intensity can easily cause photoinhibition of nitrifying bacteria, resulting in process breakdown of the consortium. This challenge limits its practical application in an outdoor environment. To overcome the challenge, we developed a “light-shielding hydrogel” which entrapped nitrifying bacteria in carbon black-added alginate hydrogel beads and confirmed its effectiveness of protecting the nitrifying bacteria from intense light up to 1600 μmol photons m^{-2} s^{-1} [5]. After establishing the advanced light-tolerant microalgae-nitrifying bacteria consortia for stable ammonia removal under strong light irradiation using light-shielding hydrogel in an indoor condition in Japan [6], the effectiveness of the proposed process was examined in an outdoor environment for long-term in Mexico as an example of developing countries where sunlight intensity is very high. Throughout the 77-day experimental period, the average ammonia removal efficiency of 75.2% was obtained. The results showed the effectiveness of the proposed system for stable ammonia removal under strong light irradiation without using a costly aeration system.

References

[1] A. B. Author, C. D. Author, D. E. Author, *Abbreviated Journal Name* **Year**, volume, page.
[1] S. Barua, B.R. Dhar, *Bioresour. Technol.* **2017**, 244, 698–707.
[2] D.J. Conley, H.W. Paerl, R.W. Howarth, D.F. Boesch, S.P. Seitzinger, K.E. Havens, C. Lancelot, G.E. Likens, *Science* **2009**, 323, 1014–1015.
[3] S. Achinas, V. Achinas, G.J.W. Euverink, *Engineering* **2017**, 3, 299–307.
[4] D. Rosso, L.E. Larson, M.K. Stenstrom, *Water Sci. Technol.* **2008**, 57, 973–978.
[5] K. Nishi, S. Akizuki, T. Toda, T. Matsuyama, J. Ida, *Process Biochem.*, **2020**, 94, 359–364.
[6] K. Nishi, S. Akizuki, T. Toda, T. Matsuyama, J. Ida, *Chemosphere* **2022**, 297, 134252.

Multi-scale Modelling and Simulation of Particulate Multiphase Flow Applied in Mineral Processing

Yuqing Feng*, Peter Witt, Phil Schwarz

CSIRO Mineral Resources, Victoria 3169, Australia
*Corresponding author: Yuqing.Feng@csiro.au

Mineral processing involves a sequence of stages encompassing crushing, grinding, classification, concentration, dewatering, and tailings management, each marked by intricate particle flows with complex interactions with fluids (gas and/or liquids). A detailed understanding of particle and fluid flow within each stage are imperative for optimizing mineral recovery and mitigating environmental impact.

Particle sizes range from centimeters upstream to microns downstream. These particles can be either modelled at particle scale using discrete approach, e.g. discrete element method (DEM), which is very computing expensive, or modelled at process scale using continuum approach at the loss of detailed particle dynamics. The ability to feasibly model all important scales simultaneously is a technical challenge that increased computing resources alone will not solve. Using a multi-scale modelling approach, the detailed micro- modelling information of a real system, such as the detailed particle dynamics, can be used to build constitutive correlations to improve macro- or process scale modelling accuracy, and even help to evaluate process efficiency. This multi-scale modelling approach is proved to be promising and powerful, and has received increasing interest in the study of complex multiphase flow systems. CSIRO CFD team has been working on the application of CFD models to new and existing plant in the mineral processing, metal production and energy industries for decades. The broad application of CFD has the potential to save companies many millions of dollars per year.

This paper will present some advancements in developing multi-scale modeling, with a particular focus on linking micro-scale modeling and process-scale modeling to leverage the strengths of each approach effectively. Examples include applications in SAG mills, hydrocyclones, flotation cells, thickeners and coal beneficiation fluidized beds.

References

[1] Wenjie Rong, Yuqing Feng, Phil Schwarz, Peter Witt, Baokuan Li, Tao Song, Junwu Zhou, Numerical study of the solid flow behavior in a rotating drum based on a multiphase CFD model accounting for solid frictional viscosity and wall friction, Powder Technology 361 (2020) 87-98

[2] Shuofu Li, M. Philip Schwarzb, Yuqing Feng, Peter Witt, Chunbao Sun, A CFD study of particle–bubble collision efficiency in froth flotation, Mineral Engineering,

[3] M. Philip Schwarz, Peter T.L. Koh, David I. Verrelli and Yuqing Feng, Sequential multi-scale modelling of mineral processing operations, with application to flotation cells, Minerals Engineering 90 (2016) 2–16.

[4] Qinggong Wang, Yuqing Feng, Junfu Lu, Weidi Yin, Hairui Yang, Peter J. Witt, Man Zhang, Numerical Study of Particle Segregation in a Coal Beneficiation Fluidized Bed by a TFM-DEM Hybrid Model: Influence of Coal Particle Size and Density, Chemical Engineering Journal, 2015, 260:240–257.

[5] Chris Solnordal, Venkatakrishna Kenche, Trevor Hadley , Yuqing Feng , Peter Witt, Seng Lim, Simulation of an Internally Circulating Fluidised Bed using a Multiphase Particle-in-Cell Method, Powder Technology, 2015, 274:123–134.

Gasification of solid wastes for high-purity hydrogen and syngas production with CO_2 capture

Xiuping Liao, Soo Jean Park, Yijiao Jiang*

Macquarie University, Sydney, Australia
*Corresponding author: yijiao.jiang@mq.edu.au

Gasification of carbonaceous wastes offers a promising route for converting waste into valuable resources while addressing waste management challenges[1]. Conventional steam gasification requires significant water and energy inputs to enhance hydrogen production, thus increasing costs and CO_2 emissions[2-3]. In this research, we propose an in-situ steam gasification of biosolids, utilizing its self-contained moisture and spent lime, mainly calcium-oxide (CaO) for CO_2 capture and utilization. This approach demonstrates comparable performance to conventional steam gasification process by consuming a large amount of fresh water and energy for generating steam. It yields high-purity H_2 (70.2 vol%) at Stage I and syngas (93.3 vol%) with a H_2/CO ratio of 2.0 in Stage II. Additionally, the low-energy content of biosolids was compensated by introducing waste plastics as a co-gasification feedstock. When the plastic/biosolid blend ratio is 1:6, a highest syngas yield of 500 NmL/$g_{\text{dry waste}}$ and highest energy recovery efficiency of 43.5% is achieved. By introducing CO_2 into a Stage III, an additional CO production up to 147 NmL/gdry waste was achieved when the CO_2 concentration was 25vol%, confirming that captured CO_2 can be utilized as an efficient gasification agent for maximizing carbon conversion. This process not only enhances the energy recovery efficiency from solid waste but also contributes to negative net CO_2 emissions in waste gasification.

References

[1] J. Watson, Y. Zhang, B. Si, W. T. Chen, and R. de Souza, *Renew. Sust. Energ. Rev,* **2018**, 83, 1-17.
[2] X. Yang, S. Gu, A. Kheradmand, T. Kan, J. He, V. Strezov, R. Zou, A. Yu, Y. Jiang, *Energy,* **2022**, 254, 123904.
[3] X. Yang, T. Kan, A. Kheradmand, H. Xu, V. Strezov, A. Yu, Y. Jiang, *Chem. Eng. J,* **2021**, 404, 126069.

Synergistic effect of heavy metals stabilization during the co-processing of contaminated soil in cement kiln

Ming Gao,[a,b] Lin Li,[a] Xue Liu,[a] Zhipan Ma,[b] Guang Sun,[a] Zhihao Zhou,[a] Bing Li,[b] Lunbo Duan[a,]*

[a]Key Laboratory of Energy Thermal Conversion and Control of Ministry of Education, School of Energy and Environment, Southeast University, Nanjing 210096, China
[b]Jiangsu Academy of Environmental Industry and Technology Corp., Nanjing, 210019, China
*Corresponding author: duanlunbo@seu.edu.cn

Co-processing in cement kiln presents a promising approach for remedying heavy metal-contaminated soil (HMS) [1-2]. Most research primarily focuses on the disposal of organic contaminated soil, with few studies on co-treating HMS in cement kiln. The optimal disposal ratio and operational parameters affecting clinker quality and heavy metal stabilization remain unknown. This study investigates the effect of varying proportions of HMS on clinker characteristics during co-disposal in cement kiln and examines various addition ratios, temperatures, and residence times on heavy metal content in clinker, along with the leaching behavior of prepared clinker. Results show that adding no more than 7.5% HMS to raw materials ($C_{L7.5}$) does not alter clinker's micro-morphology or surface elemental distribution. CaO from HMS assists in the formation of the required crystalline phase C_3S in the clinker without affecting As migration during clinker formation, indicating effective stabilization of these metals from HMS during the calcination process. Minerals from the raw material readily bound Cr and Ni, mitigating their volatilization even at higher temperatures. Residence time minimally affects heavy metal content in clinker, but a 50-minute residence time notably enhances Cr content due to enhanced mineral combination. Leaching concentrations of Cd, Pb, As, Ni, and Cr in clinker C_{L0} and $C_{L7.5}$ are below Chinese national standard limits, despite the exhaustion of acid neutralization, demonstrating effective heavy metal solidification. Co-processing mitigates the leaching of heavy metals for HMS, offering insights for clean disposal and practical cement kiln applications. This study provides a theoretical guidance for the practical application of co-processing heavy metal-contaminated soils in cement kiln, offering a potentially cost-effective and environmentally friendly approach to soil remediation and management.

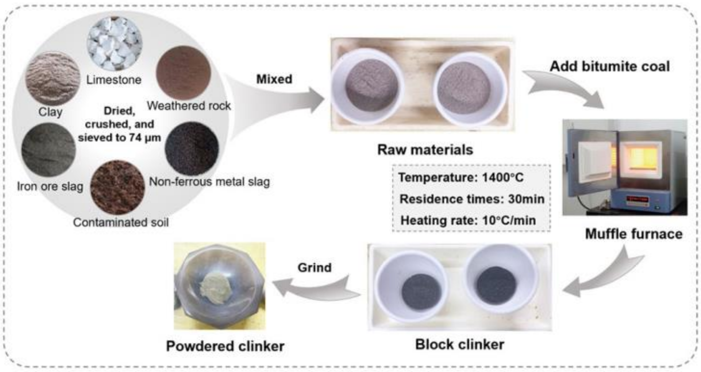

Figure 1. Cement clinker preparation process.

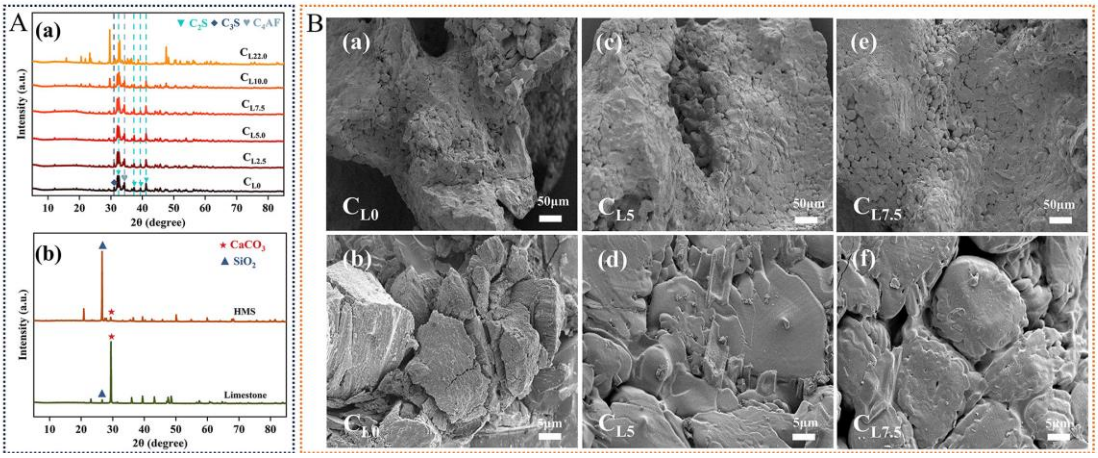

Figure 2 A**)** XRD patterns of (a) all prepared clinker samples, (b) limestone and HMS; B**)** SEM images of clinker samples (a, b) C_{L0}, (c, d) $C_{L5.0}$ and (e, f) $C_{L7.5}$.

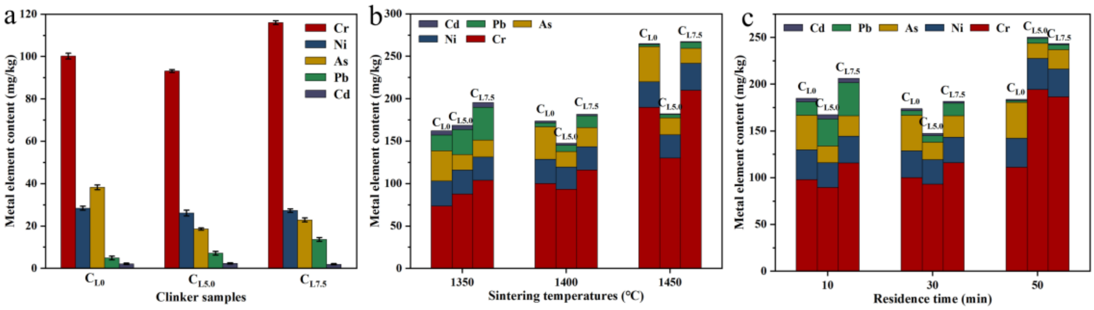

Figure 3. Heavy metals content in clinker samples (C_{L0}, $C_{L5.0}$, $C_{L7.5}$) under different (a) HMS addition levels (0, 5.0, 7.5%), (b) sintering temperature (1350, 1400, 1450 °C) and (c) residence time (10, 30, 50 min).

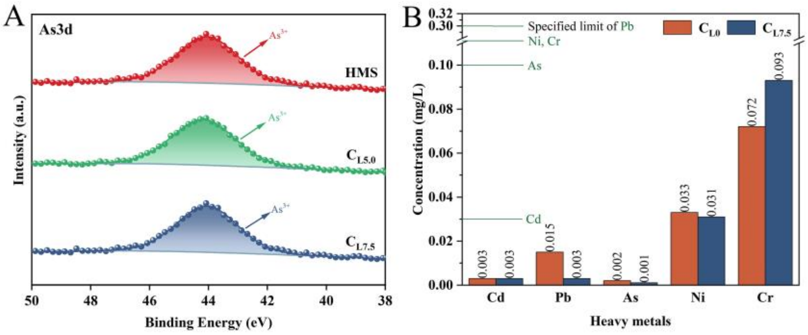

Figure 4 A) XPS spectrum of As in HMS and clinker samples; B) Heavy metal concentrations in leachate from C_{L0} and $C_{L7.5}$.

References

[1] T. Liang, F.H. Yang, A.Z. Ding, F.S. Li, *Sci. Total Environ.* **2022**, 817, 152788.
[2] D.J. Pang, Y.P. Mao, Y. Jin, Z.L. Song, X.J. Wang, J.W. Li, W.L. Wang, *Process. Saf. Environ.* **2023**, 172, 1072-1086.

Design and optimization of oxy-combustion CFB power plant with energy storage system based on particle flow, heat transfer

Xuchen Fu,[a,b] Yuanqiang Duan,[a] Lunbo Duan[a,]*

[a] Key Laboratory of Energy Thermal Conversion and Control, Ministry of Education, School of Energy and Environment, Southeast University, Nanjing 210096, China
[b] Inner Mongolia Power Research Institute Branch, Inner Mongolia Power (Group) Co., Ltd., Huhhot 010020, China
*Corresponding author: duanlunbo@seu.edu.cn

The rapid growth of renewable energy has put forward higher requirements for the peak shaving capacity of coal-fired power plants. Oxy-fuel combustion is one of the most promising technologies for carbon reduction in thermal power plants. This study proposes a novel oxyfuel power plant that is coupled with liquid oxygen storage and cold energy recovery systems to accommodate peak shaving requirements. In this work, a 350 MWe oxy-CFB power plant was selected as the reference power plant. Based on the reference power plant, oxy-CFB power plant with liquid O_2 storage system was proposed. An optimization design is highly necessary for the recovery of the energy during the transformation from liquid O_2 into gaseous one. This work also proposed an oxy-CFB power plant with liquid O_2 storage and cold energy recovery systems. The thermodynamic performance and technical economy of different power plants were compared and analyzed. The thermal efficiency of the boiler is 92.36% and the power generating efficiency of the unit is 38.97% under the BRL condition of air combustion atmosphere. Under the condition of 30%O_2/70%RFG atmosphere, the thermal efficiency of the boiler is 94.68%, and the power generation efficiency of the unit is 39.95%. The results show that the optimal operating oxygen purity is 96%~97%, and the optimal combustion pressure is 1.5~2.0MPa. For the new oxygen-fuel combustion system with liquid oxygen energy storage and peak shaving, the unit can achieve a net power generation efficiency of 38.86% at most during the peak period of electricity consumption. At the same time, in the period of low power consumption, the power supply output of the unit can achieve 0~35% according to the actual demand of the grid, but reducing the power supply output will increase the sacrifice net efficiency of the unit, and the greater the boiler load and power supply output, the greater the sacrifice net efficiency of the unit. Pressurized combustion can lead to a reduction in furnace size and limitations in the arrangement of heating surfaces. Understanding the heat transfer characteristics of the heating surfaces in the fluidized bed is of great significance for the design and operation of pressurized fluidized bed combustion. Based on the experimental data and analysis of the heat transfer coefficient in the previous sections, a conceptual design of an oxy-fuel circulating fluidized bed boiler is carried out under different pressures (0.1, 0.6, 1.0, 1.5 MPa). The heat transfer mechanism of the dense phase and dilute phase inside the boiler is quantitatively analyzed using proposed or validated heat transfer models. As the pressure increases, the overall heat transfer effect also increases, but when the pressure exceeds 1.0 MPa, the contribution of gas convection and radiation to heat transfer is no longer significant. In the dense phase of the circulating fluidized bed, particle convection is still the main way of heat transfer. In the dilute phase, due to the higher partial pressures of CO_2 and H_2O in the fluidized atmosphere, the radiation heat generated by triatomic gases is greater, and radiation becomes the main way of heat transfer. This work provides some reference for the layout and design of pressurized oxy-fuel circulating fluidized bed heat transfer surfaces.

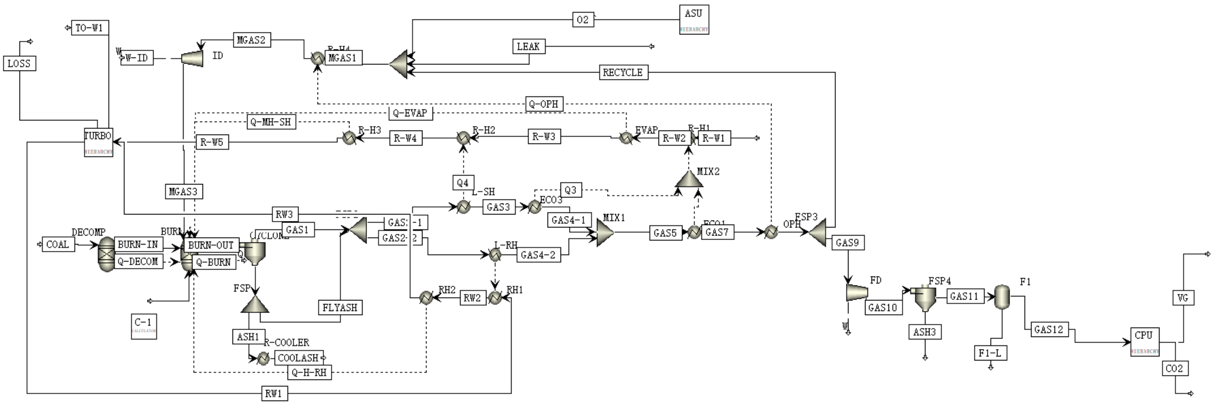

Figure 1 Aspen model of the combustion system of oxy-CFB

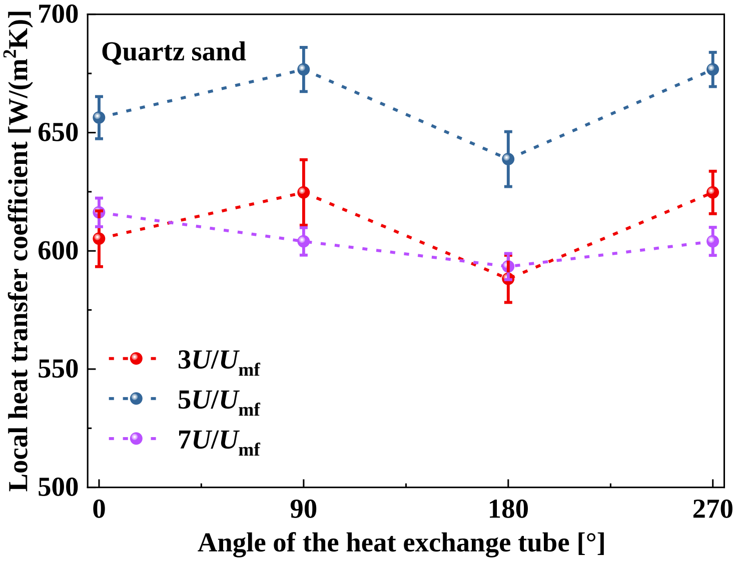

Figure 2 The influence of gas velocity on the local heat transfer coefficient of immersed pipes

References

[1] Duan L, Sun H, Zhao C, et al. Coal combustion characteristics on an oxy-fuel circulating fluidized bed combustor with warm flue gas recycle[J]. Fuel, 2014, 127: 47-51.

[2] Masoumifard N, Mostoufi N, Hamidi A A, et al. Investigation of heat transfer between a horizontal tube and gas–solid fluidized bed[J]. International Journal of Heat and Fluid Flow, 2008, 29(5): 1504-1511.

[3] Barreto G F, Lancia A, Volpicelli G. Heat transfer and fluid dynamic characteristics of gas-fluidized beds under pressure[J]. Powder Technology, 1986, 46(2-3): 155-166.

[4] Kim S W, Ahn J Y, Kim S D, et al. Heat transfer and bubble characteristics in a fluidized bed with immersed horizontal tube bundle[J]. International Journal of Heat and Mass Transfer, 2003, 46(3): 399-409.

A CFD-DEM Approach to Continuous VOC Adsorption in a Countercurrent Fluidized Bed

Wei-Han Jen,[a] Wan-Yi Hsu, [b] Tsuo-Feng Wang, [a] An-Ni Huang,[b],* Hsiu-Po Kuo[a],**

[a] Department of Chemical Engineering, National Taiwan University, Taipei, Taiwan
[b] Green Technology Research Center, Chang Gung University, Taoyuan, Taiwan
*Corresponding author: anhuang@mail.cgu.edu.tw
** Corresponding author: hsiupokuo@ntu.edu.tw

A multi-stage countercurrent fluidized bed with the plate hole size of 2.5 mm and opening ratio of 0.276 is developed for Volatile Organic Compounds (VOCs) adsorption. The system consists of a column with perforated plate segment that allows the activated carbon bead adsorbents to be continuously fed from its top and the MEK adsorbate containing fluid flow from its bottom. Computational Fluid Dynamics coupling Discrete Element Method (CFD-DEM) simulation technique is used to realize the particle and fluid behavior in this system. 700 μm adsorbents show mean residence time of 50 s when the particle feed rate of 0.15 kg/m^{2}s and the fluid velocity of 0.88 m/s. At the inlet MEK concentration of 5100 ppm, the outlet MEK concentration decreases to around 150 ppm for a continues 60-minute run in the single-stage fluidized bed with the particle feed rate of 0.16 kg/m^{2}s and fluid velocity of 1.00 m/s, resulting in the MEK removal efficiency of 96.70%. In the similar two-stage fluidized bed system, the MEK removal efficiency increases to 99.96%.

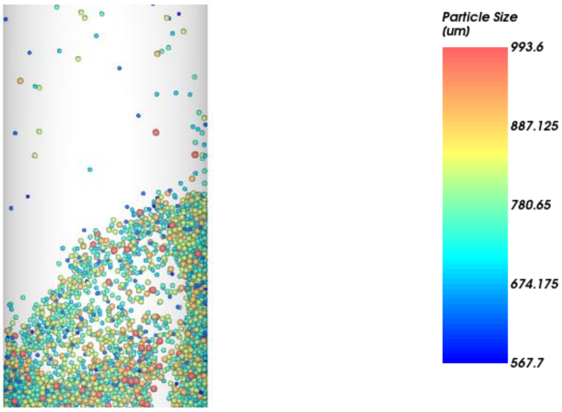

Figure 1. Schematic diagram of countercurrent fluidized bed

References

[1] S. Golshan, R. Sotudeh-Gharebagh, R. Zarghami, N. Mostoufi, B. Blais, J. A. M. Kuipers, *Chem. Eng. Sci.* **2020**; 221, 115646.

Silver Recovery from Crystalline Silicon Photovoltaic Solar Cells using Continuous Stirred-Tank Reactors

Shuang Song, Yuting Zhuo, Qiyuan Li, Yansong Shen*

School of Chemical Engineering, University of New South Wales, Sydney, New South Wales 2052, Australia
*Corresponding author: *ys.shen@unsw.edu.au

Silver can be recycled from the end-of-life (EoL) crystalline silicon (c-Si) photovoltaic (PV), yet the recycling and its technology scale-up are still at an early stage especially in continuously stirred tank reactors (CSTR). In this work, the silver recovery from the solar cells is technically understood and optimised in the CSTR system from the point of view of silver recovery efficiency, through integrating experimental and numerical investigations [1]. Specifically, based on the experiments, a kinetics model is developed, and SEM surface morphology is characterised; and a Computational Fluid Dynamics-Discrete Element Method (CFD-DEM) particle-scale model is integrated with the kinetics model and validated against the fluid-flow pattern and silver leaching performance results from lab measurements. The validated CFD-DEM model is then applied to understand the particle-scale behaviour of silver leaching in the CSTR system in terms of hydrodynamics and AgNO3 distribution under different impeller speeds. The simulation results show that the silver leaching performance is improved in an improved CSTR design with a lower impeller position and doubled impeller layers. This work reveals the effectiveness and underlying hydrodynamics of silver leaching in CSTR systems and lays a foundation for improving silver recovery in PV recycling.

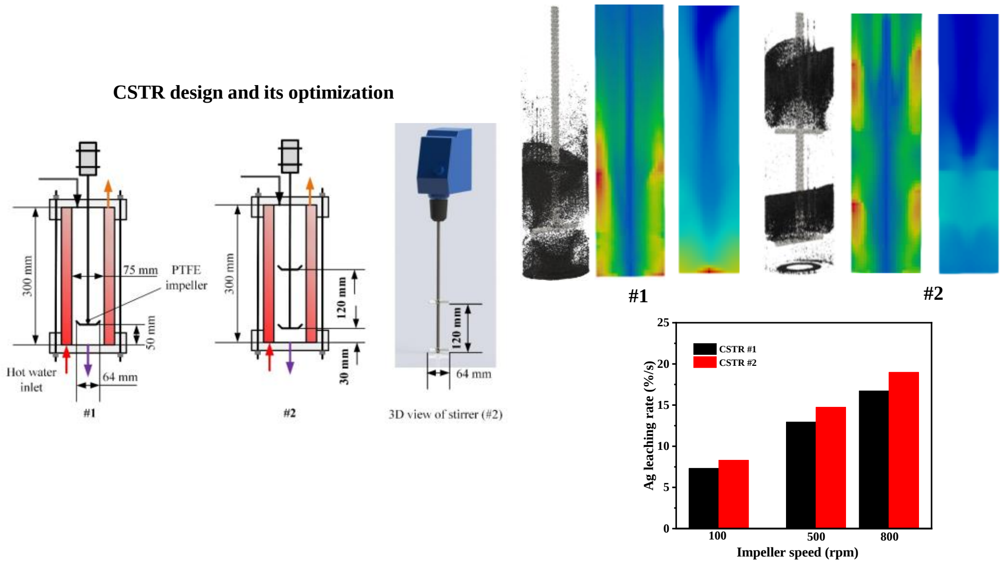

Figure 1. Schematic of the two CSTR design and numerical simulation results of the particle-fluid dynamics and Ag leaching rate in the two CSTR respectively.

References

[1] Song. S., Zhuo. Y., Li. Q. and Shen. Y., *Advanced Materials* **2024**. 2403653.

Investigation on the behavior and mechanism of low-grade magnesite separation enhanced by polycarboxylic acid grinding aid

Wenbao Liu*, Yanbai Shen, Wengang Liu, Sikai Zhao, Qiang Zhao

Northeastern University, Shenyang, China
*Corresponding author: liuwenbao@mail.neu.edu.cn

Low-grade magnesite was not utilized effectively because of its high vein content. A large number of discarded low-grade magnesite will cause waste of resources and serious environmental pollution. In the grinding process, magnesite and calcium-bearing vein mineral dolomite were easy to surface dissolution. The dissolved metal ions will be adsorbed on the surface of the minerals, which will make their surface properties converge and resulting in difficult flotation separation. Based on this, polycarboxylic acid grinding aid (EGTA) was used to optimize the grinding-flotation system of magnesite. The grinding test shows that EGTA can increase the content of –74+23 μm (qualified size) and decrease the content of –23 μm (fine size) in the grinding products of two minerals. Among them, the effect of EGTA on dolomite was more significant. Flotation tests show that adding EGTA to the grinding stage can enhance the flotation separation of magnesite and dolomite. The mechanism study shows that EGTA can selectively adsorb on the surface of dolomite, and has a stronger chelating effect on Ca^{2+} in the slurry. EGTA increased the difference between the surface properties of magnesite and dolomite. Meanwhile, EGTA improved the chemical environment of the flotation slurry. Therefore, EGTA can not only optimize the particle size distribution and improve the grinding effect, but also promote the flotation separation of magnesite and dolomite, which will have great application potential in the flotation separation process of magnesite.

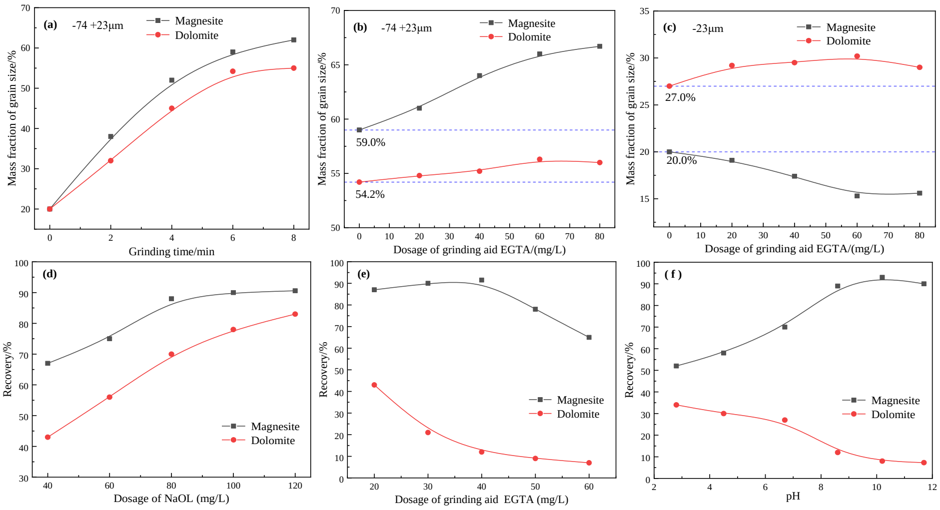

Figure 1 Enhanced magnesite and dolomite grinding-flotation separation by grinding aid EGTA

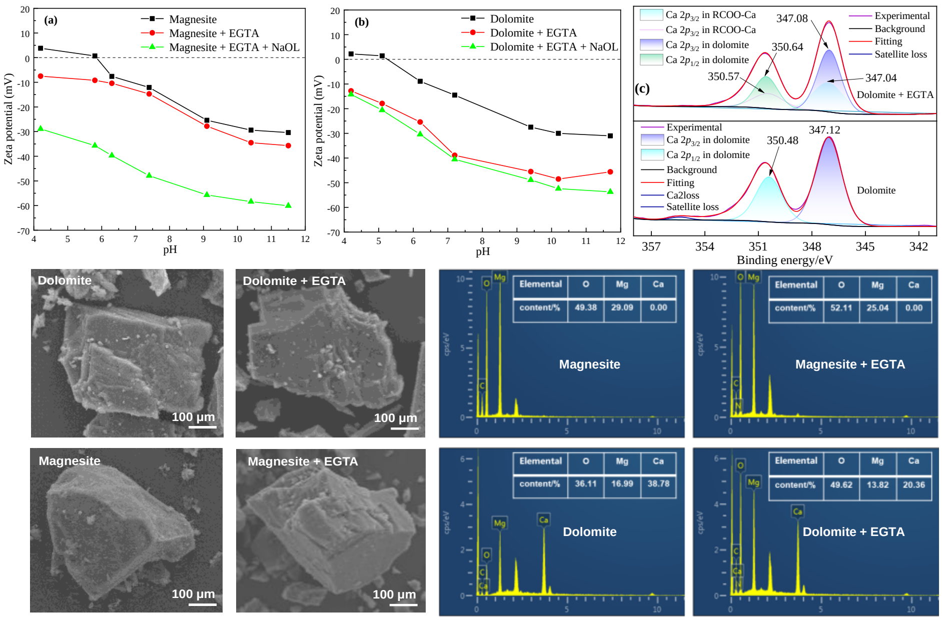

Figure 2 Adsorption mechanism of grinding aid EGTA on the surface of magnesite and dolomite

Magnetic Cleaning of Particulate Materials on Solar Panels

Masato Adachi,* Ryo Goda

Kyoto University, Department of Mechanical Engineering and Science, Kyoto, Japan
*Corresponding author: masato@me.kyoto-u.ac.jp

To fulfill the sustainable development goals, the role of solar power generation is becoming increasingly critical. Optimal operation of solar panels is facilitated by their installation in desert regions, characterized by high solar radiation and minimal rainfall. However, these regions present a unique challenge: sandstorms lead to the accumulation of particles on the solar panels, and the lack of rainfall inhibits their natural removal. This particle deposition impedes the incidence of sunlight onto the solar panels, thereby degrading the power output [1] [2]. A similar issue has also been addressed at industrial sites. Minute iron particles, emitted into the air from the sites, accumulate on the surface of nearby solar panels, resulting in a decrease in power generation. Moreover, such dust-related problems are also prevalent in space environments. Lunar soils on the Moon, called as regolith, cause dust deposition on spacesuits and devices, posing a significant challenge for future long-term space exploration. The common approach is the development of a cleaning technology capable of operating in harsh environments, such as desert areas or on the Moon, and that can be utilized for extended periods without the need for frequent maintenance. Various solutions have been proposed, the majority of which involve the use of mechanical brushing, water jets, or removal solvents. However, these methods have encountered several issues for long-term cleaning processes. Robotic methods that incorporate a brush or solvents can result in wear and damage to solar panels and associated equipment. Furthermore, water is a scarce resource in space and desert environments, limiting its long-term and widespread use.

Therefore, we have developed a novel technology that utilizes magnetic force to remove accumulated particles without contact. The system comprises a multipole permanent magnet roll, a non- magnetic rotating sleeve, a collection part, and a linearly moving mechanism. This cleaning mechanism, previously employed for handling toner particles in a laser printer, enables the continuous capture, transport, and release of magnetic particles. We have applied this mechanism to the cleaning of solar panels. When the device approaches the solar panels and moves across the surface without contact, the permanent magnet roll attracts particles to the sleeve. The non-magnetic sleeve, which can rotate freely on the magnet roll, transports the particles on its surface. In a specific area, the unique magnet roll generates a repulsive magnetic force, releasing the particles. This process eliminates the need for manual cleaning of particles from the sleeve, allowing for the continuous cleaning of solar panels in unmanned operations. This system only requires power for the rotation of the sleeve and movement across the solar panels, and the device can be designed to be compact and lightweight. Importantly, it does not require intermediate fluid materials or contact for cleaning, thereby preventing damage to the solar panels. In this study, we conducted a cleaning demonstration of the system and investigated the effects of system parameters, such as the rotational speed of the sleeve and the magnetic field strength, on the cleaning performance.

Figure 1 shows the experimental setup. The magnetic cleaning system operates on the principle of traversing the surface of solar panels to remove particles. However, for experimental convenience, the panel side was designed to move linearly. A moving plate with a driving mechanism was installed underneath the cleaning assembly, which consisted of a magnet roll, sleeve, and collection box, and particles were dispersed on this plate. This plate simulated a solar panel. The distance between the assembly and the plate was adjusted by a height adjustment screw. The plate and the non-magnetic sleeve could be moved independently by motors, a rack/pinion mechanism, and a timing belt. As an experimental sample, lunar regolith simulant FJS-1, which mimics real regolith and contains some but not large magnetic components, was dispersed on the plate, and the weight of the particles before and after cleaning was evaluated. Figure 2 shows the capturing and releasing performances of the system. The capturing performance refers to the amount of particles removed from the plate to the sleeve, and the releasing performance refers to the amount of captured particles that can be released from the sleeve. As shown in Figure 2, we were able to remove many of the deposited particles using the device. Smaller particles were harder to remove from the plate due to the larger adhesion force. Even for larger particles, some amounts of particles could not be removed. This was because the simulant contained several types of natural minerals, and particles with less permeability tended to remain. We confirmed that a stronger magnetic field generated by another magnetic roll could capture more particles based on a force balance applied to particles. In addition, faster rotation of the sleeve improved the releasing performance simply because a larger centrifugal force was applied. Near the area of particle capture, a larger magnetic force against the adhesion force contributes to the removal of particles from the plate. Meanwhile, a larger centrifugal force against the adhesion force is necessary, along with a suppression of the magnetic field in the release area, for better release performance.

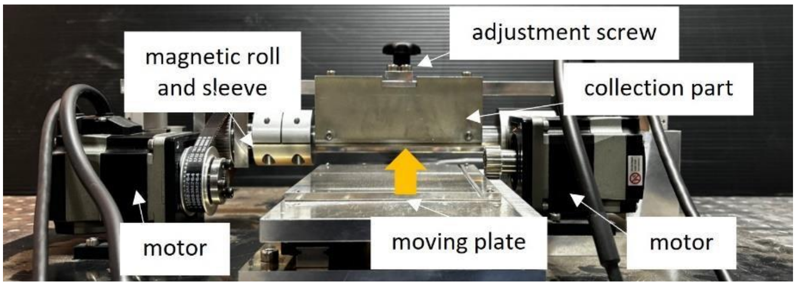

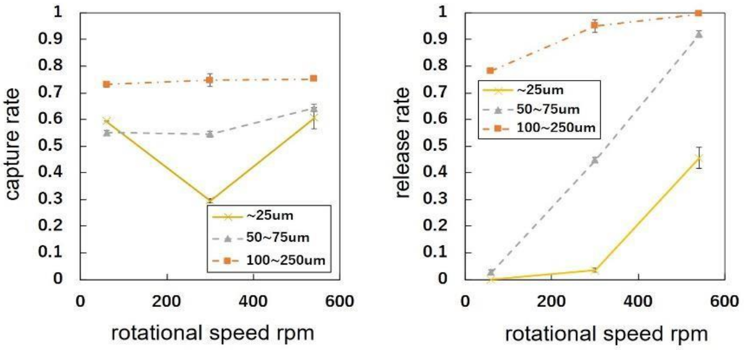

Figure 1. Experimental setup of the magnetic cleaning system.

Figure 2. Cleaning performance of the magnetic system when the rotational speed of the sleeve was varied. The surface velocity of the sleeve equals the speed of the linearly moving plate.

References

[1] A. Sayyah, M. N. Horenstein, and M. K. Mazumder, *Sol. Energy* **2014**, 107, 576–604

[2] B. Guo, W. Javed, B. W. Figgis, and T. Mirza, *First Workshop on Smart Grid and Renewable Energy* **2015**, 1–6

Novel insights into the microscale modelling of bubble-particle collision efficiency in flotation process

Min Sun,[a] Yuqing Feng,[b,]* Peter Witt,[b] Phil Schwarz,[b] Baoyu Cui,[a] Junwu Zhou,[a]

[a]School of Resources and Civil Engineering, Northeastern University, Shenyang, China
[b]CSIRO Mineral Resources, Victoria, Australia
*Corresponding author: Yuqing.Feng@csiro.au

Flotation is an essential and highly effective separation method within the mineral processing field. The flotation process can be divided into three sub-processes: collision, attachment, and detachment, based on the sequence of interactions between the bubbles and particles. The bubble-particle collision sub-process forms the foundation of flotation and is crucial for the successful recovery of particles throughout the flotation process. This study proposes a microscale numerical model of bubble-particle collision efficiency, specifically considering the effect of short-range hydrodynamic resistance as the particle approaches the bubble. The effects of bubble properties, particle size, shape and density on collision efficiency are systematically investigated by conducting the numerical experiments. The numerical results are compared with the predictions of various existing theoretical mathematical models, with an in-depth analysis of the GSE model and the Schulze model. Furthermore, based on the existing theoretical model, a novel mathematical model for collision efficiency is proposed by fitting the numerical experimental results of bubble-particle collision efficiency, which can be employed as a sub-model for bubble-particle collision rate in macro-scale CFD models of flotation cells. This work will provide a comprehensive understanding of key parameters affecting collision efficiency and flotation recovery.

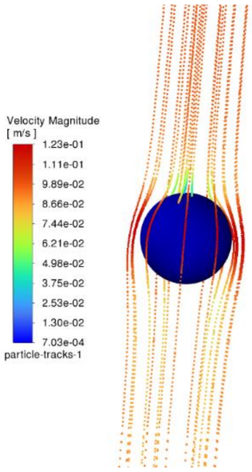

Figure 1. Schematic diagram of bubble-particle collision

Behavioral characteristics of nitrogen during supercritical water gasification of biomass

Shi Liu, Wen Cao, Ruochen Xiong, Libo Lu and Liejin Guo*

State Key Laboratory of Multiphase Flow in Power Engineering (SKLMF), Xi’an Jiaotong University, Xi’an, China
*Corresponding author: lj-guo@mail.xjtu.edu.cn

Nitrogen is an essential element for life and is widely present in biomass waste[1, 2]. Clarifying the behavioral characteristics of potential nitrogenous pollutants in the supercritical water (SCW) environment contributes to the energy and harmless utilization of biomass waste. In this paper, the migration and transformation mechanism of typical nitrogenous functional groups, including NH_3, NO_2^-, NO_3^-, nitrobenzene, and aniline, during the supercritical water gasification (SCWG) process is investigated by combining density functional theoretical and experimental research methods (540°C-700°C). The results show that in the reducing environment of SCW, NH_3 can effectively catalyze the spontaneous reduction of NO and NO_2 to N_2 through multiple pathways, thus avoiding the generation of NO_x. Regarding the NO_3^- from the raw materials that can be spontaneously reduced to NO_2^- in the reducing environment of SCW, the reaction barrier for the consumption pathway of NO_2^- was significantly lower than its generation pathway in the subsequent reaction. As a result, there was no NO_2^- in the gasification product, and the NO_3^- fugacity was also extremely traced. Compared to the pyrolysis process, water molecule clusters unique to SCW environments provided low-energy barrier conversion pathways for the gasification of typical nitrogenous organic functional groups. The study confirmed that nitrogen in biomass waste is converted to inorganic nitrogen in the form of NH_3 and N_2 during SCWG, with no NO_x generation in the dominant conversion pathway.

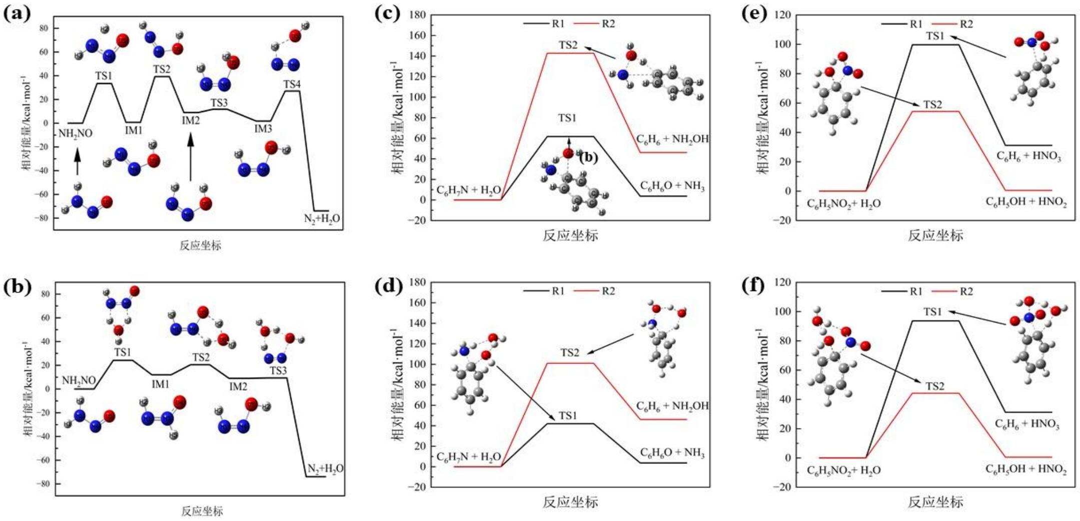

Figure 1. Water molecule clusters unique to SCW lower the reaction energy barriers of typical nitrogenous intermediates.

References

[1] Liu S, Cao W, Wang Y, et al., *Waste Management*, 2022, 153: 240-8.

[2] Liu S, Jin H, Yang Y, et al., *Journal of Molecular Liquids*, 2021, 324: 114769.

Mechanistic Insight into the Decomposition of Phenyl Vinyl Sulfone in Supercritical Water

Libo Lu, Wen Cao, Shi Liu, Liejin Guo*

State Key Laboratory of Multiphase Flow in Power Engineering (SKLMF), Xi’an Jiaotong University, Xi’an, China
*Corresponding author: lj-guo@mail.xjtu.edu.cn

Sulfone is a key sulfur-containing compound that is widely present in coal, crude oil, and organic wastes[1-3]. Revealing the decomposition mechanism of sulfone compounds could provide a basis for the cleaner utilization of these fuels by supercritical water (SCW) treatment. Herein, density functional theoretical calculations and experiments were combined to explore the decomposition of phenyl vinyl sulfone (PVS) in SCW and pyrolysis. The multi-step decomposition pathways that PVS reacted with H_2, H_2O, and free radical (·H/·OH) in SCW and thermal decomposition in pyrolysis were proposed. Energy barrier analysis and thermodynamic analysis showed that H_2O mainly participated in the decomposition of PVS in SCW condition in the role of free radical (·H/·HO) to break the C-S bond and form H_2SO_2, which was further converted by the H_2 generated from gasification of PVS in SCW into H_2S. However, PVS decomposed to generate SO_2 directly via the cleavage of the C-S bond in pyrolysis without H_2O. A series of experiments were carried out to investigate the decomposition performance of PVS in SCW and pyrolysis in a quartz tube reactor system at different temperatures (450°C-700°C). Experimental results showed that PVS could decompose to release mainly H_2S in SCW but SO_2 in pyrolysis.

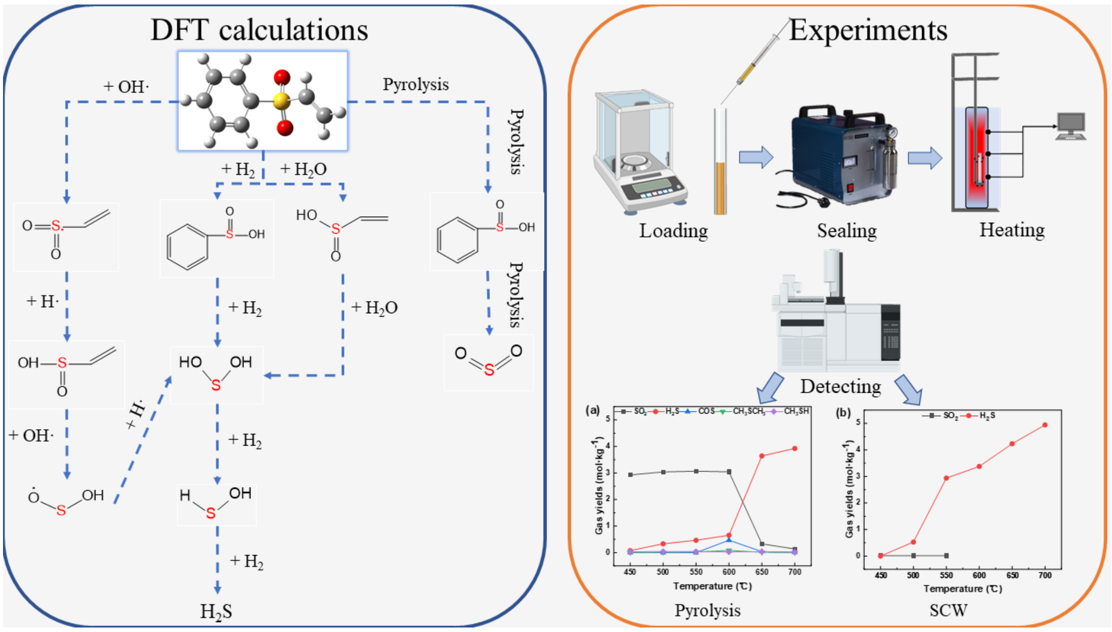

Figure 1. PVS decomposition pathways and characteristics.

References

[1] LU L, WEI W, LIU F, et al. *Fuel*, **2023**, 338: 127333.

[2] YAN M, FENG H, ZHENG R, et al. *Journal of the Energy Institute*, **2021**, 95: 61-8.

[3] MENG N, JIANG D, LIU Y, et al. *Fuel*, **2016**, 186: 394-404.

Powder separation using friction reduction and surface deformation with ultrasonic vibration.

Kenji KOFU*

Nihon University, Tokyo, JAPAN
*Corresponding author: kofu.kenji@nihon-u.ac.jp

In disposal process, products may be pulverized and powder is obtained. In order to separate for size and material of pulverized particle and recycle, some methods are already used, for example, shivering, cyclone, magnetism, mechano-chemicals, fluidization and so on. Authors have researched the ultrasonic vibration method as new technique. In this method, the difference of friction reduction effect between powder and plate by ultrasonic vibration is applied. As a result, the material separation and classification have been already succussed [1]. But the mechanism on friction reduction is unclear. Therefore, it was experimentally clarified in this paper.

In this study, cubes were used instead of particles for the sake of measuring the particle surface deformation with a laser doppler vibrometer. In this experiment, the cube material, cube size, frequency and size of vibration plate were changed. The results showed that inertia force dominates for the friction reduction effect when vibration amplitude is small. In short, the material can not accompany with vibration plate displacement, the gap between them appears, and the friction is reduced. On the other hand, the main factor for friction reduction effect with ultrasonic vibration under large amplitude conditions is revealed as the deformation of the cube. This means the material leaps on the plate by surface deformation.

Furthermore, the effect of the cubic deformation on the detachment of particles adhering to the surface was investigated. As a result, it was found that ultrasonic vibration can peel off adhered particles. Therefore, it is possible to peel off particles adhered to large particles, for example, to improve the separation efficiency.

In short, ultrasonic vibration method can be expected for recycling by making use of the friction reduction effect on cubic deformation and material inertia, and removal effect of adhered powder detachment.

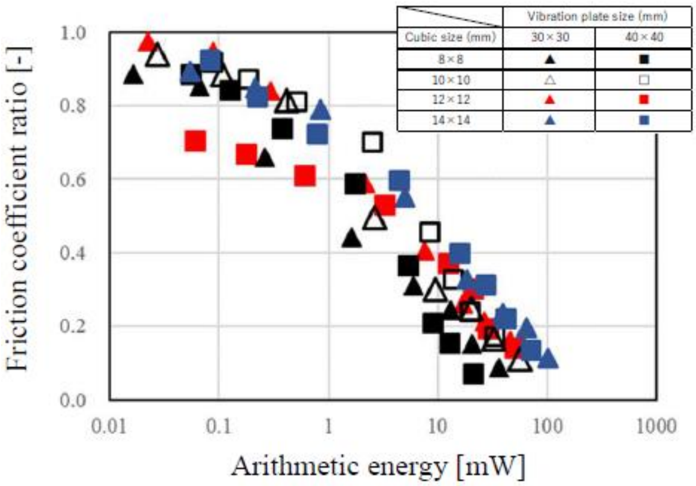

Figure 1. Relation of arithmetic energy and friction coefficient ratio.

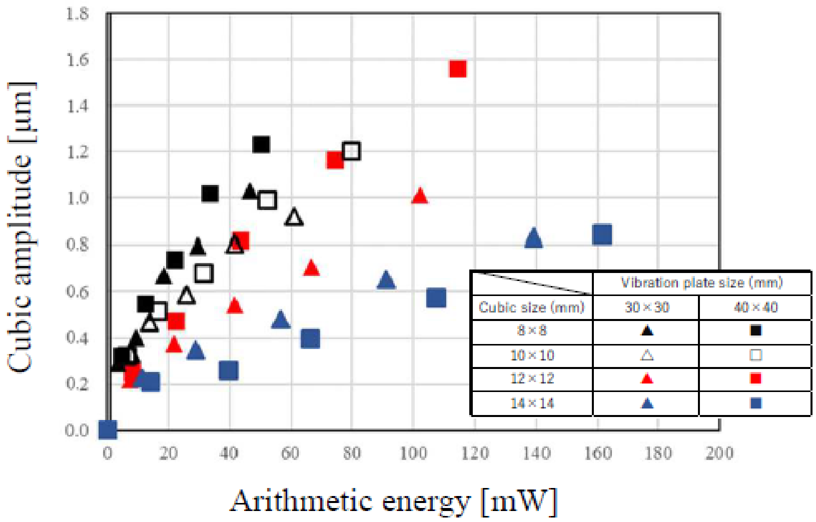

Figure 2. Relation of cubic deformation and friction coefficient ratio.

References

[1] Y. Hatakeyama, K. Inaba, K. Kofu, H. Miura, *J. Soc. Powder Technol., Japan* **2016**, 53, 74-84.

Acceleration Algorithms for Modeling Dense Gas-Solid Reactive Flows

Kun Luo*

State Key Laboratory of Clean Energy Utilization, Zhejiang University, Hangzhou 310027, China
*Corresponding author: zjulk@zju.edu.cn

The Computational Fluid Dynamics-Discrete Element Method (CFD-DEM) is widely used in the multiphase and multi-field simulation of dense gas-solid reactive flows. Research on accelerating its computational theories and methods has garnered significant attention from both academia and industry. We have developed a GPU-based particle acceleration algorithm capable of parallel computation for a large number of particles, significantly enhancing the efficiency of particle-solving processes. This breakthrough enables the rapid simulation of complex multi-physics processes, including turbulence, heat and mass transfer, and chemical reactions, in CFD-DEM frameworks at the hardware level. To address the challenges posed by the computationally intensive and time-consuming nature of particle collisions, we proposed an enhanced coarse-grained CFD-DEM method that improves computational efficiency across spatial and temporal dimensions. This method achieves a remarkable efficiency increase. Furthermore, by coupling the Direct Simulation Monte Carlo (DSMC) algorithm and employing a collision probability model, the computational efficiency of the coarse-grained model is further improved by an additional order of magnitude. The synergistic hardware-software acceleration algorithms and multi-physics coupling models for dense gas-solid reactive flows have been successfully applied to engineering problems in fields such as energy, chemical processing, and metallurgy, delivering significant economic and social benefits.

Numerical Study of Hydrogen Storage Design and Optimisation

Yuting Zhuo, Yansong Shen*

School of Chemical Engineering, University of New South Wales, Sydney, New South Wales 2052, Australia
*Corresponding author: ys.shen@unsw.edu.au

Efficient heat transfer is the key to hydrogen desorption in a metal hydride-based hydrogen storage system. In this study, a three-dimensional transient-state computational fluid dynamics (CFD) model is developed for describing the hydrogen desorption related heat/mass transfer phenomena inside a metal hydride-based hydrogen storage tank. The model involves flow, heat, and mass transfers related to hydrogen desorption in the storage tank. The model is validated against the temperature evolution data reported in the literature. The model is applied to a hydrogen storage tank where $LaNi_5$ is used as a metal hydride. The typical thermochemical phenomena related to the hydrogen desorption process are illustrated, including temperature evolution and hydrogen-to-metal-atomic ratio (H/M) during desorption. Further, several new tank designs are proposed and evaluated, including new heat management system configuration and phase change material application, for promoting heat transfer efficiency and hydrogen absorption/desorption performance. The simulation results indicate that the new design of embedding heating tubes, embedded copper fins, and aluminum foam additives shows the highest desorption performance in terms of both heating rate and hydrogen desorption rate, where the desorption rate is improved by 50% compared to the other designs. The employment of phase change material can make the metal hydride hydrogen storage tank operate as an independent system. This model is a cost-effective tool for designing, optimising, and scaling up hydrogen storage tanks.

Comparative Analysis of Particle Density Effects on Fluidization in Gas-Solid Fluidized Beds

Shuyue Li [a,*], Yongmin Zhang [a], Wenjie Wang [a], Huan Wang [a,b]

[a] State Key Laboratory of Heavy Oil Processing, China University of Petroleum- Beijing, Beijing 102249, PR China
[b] CNNC No. 7 Research and Design Institute Co., Ltd., Taiyuan 030012, PR China
*Corresponding author: Shuyue.li@cup.edu.cn

Gas-solids fluidization technology is commonly used in chemical engineering processes involving high-density particles, often encountering poor defluidization phenomena. However, there is limited research examining the applicability of flow characteristics and empirical correlations established for low-density, easily fluidizable particles in guiding the flow behavior of high-density particles. This knowledge gap poses significant challenges for designing and operating fluidized beds in relevant processes involving high-density particles. This study comprehensively evaluates the effect of particle density on hydrodynamics during the initial fluidization stage using experimental, empirical correlations and simulation methods. Results of preliminary experiments indicate that empirical correlations for predicting U_{mf} may exhibit significant errors of high-density particles. However, the experiments face challenges in eliminating the influence of particle size distribution. In contrast, the simulation results present a high consistency with the experiments after sensitivity analysis. Further simulation results illustrate those empirical correlations for U_{mf} may only yield relatively accurate predictions within the narrow density range. As the particle density increases, the predicted errors tend to increase. During the initial fluidization stage, three distinct fluidization stages can be observed, as revealed by both experiments and simulations. These stages can be attributed to the practical particle size distribution. Furthermore, it is noted that as the particle density increases, the fluidization performance tends to deteriorate. This study endeavors to advance the understanding of the effect of particle density on hydrodynamics during the initial fluidization stage. Nonetheless, more studies are still needed to enhance and deepen the current knowledge of the fluidization of high- density particles.

DEM study on ellipsoidal particle mixing in an industrial mixer

Shintaro Kajiwara,[a],* Mikio Sakai[b],

[a]Kajiwara Inc., Tokyo, Japan
[b]Department of Nuclear Engineering and Management, School of Engineering, The University of Tokyo, Tokyo, Japan
*Shintaro Kajiwara: t161264j@kajiwara.jp

Particle mixing has been widely encountered in a variety of engineering fields and extensively utilized in the field of food, pharmaceutical and chemical engineering. Performance of a mixer or a blender is one of the key factors in the process of mixing as it directly affects the quality of the final product. Hence, detailed information about the mixing performance is required for improvement in the quality. On the other hand, particle mixing for cooking process in the food industry has not been established so far. The Discrete Element Method (DEM) [1] is frequently used in numerical simulation, where the particle shapes are modelled as a spherical body. However, the particles dealt in the food industries are non-spherical shapes in many cases. Hence, the aim of this study is to understand the mixing mechanism of non- spherical mixing system inside an industrial mixer. To simplify the problem, a non-spherical particle is modelled by the ellipsoidal equation, and an industrial mixer with complex structure is modelled using the Signed Distance Function (SDF) [2]. This calculation method is successfully validated through previous studies [3, 4]. For qualitative evaluation, Lacey's mixing index [5] and granular temperature are computed to help understand mixing performance and mechanism of the system. Three types of the particles are selected in the numerical simulation, namely, Sphere (radius: 4 mm), Oblate (axial radii: 4.62 mm × 4.62 mm × 3 mm) and Prolate (axial radii: 5 mm × 3.58 mm × 3.58 mm). Regardless of the particle shape, the particle mass and volume is kept constant. By performing a simulation on a non-spherical particle mixing with a food like physical properties, this study provides significant evidence and novel insights into understanding the mixing mechanism of food products. Particle mixing is illustrated to be most effective when the particle shape is spherical which the clear evidence is observed in the mixing index between the spherical and non-spherical particles. Thus effect of particle shape is shown to be limited. Oblate and prolate spheroids have showed similar mixing performance to each other which reveals that ellipsoid type is minor factor for particle mixing. This study provides new insights into the specific particle mixing mechanism of food products, which will contribute to optimization of the mixer design and operation conditions in the food industries.

References

[1] P.D. Cundall, O. D. L. Strack, *Geotechnique* 1929, 29(1), pp. 47-65
[2] Y. Shigeto, M. Sakai, *Chem. Eng. J.* 2013, 231, pp. 464-476
[3] Y. Mori, M. Sakai, *Chem. Eng. J.* 2022, 429, p. 132415
[4] S. Y. He, J. Q. Gan, D. Pinson, A. B. Yu, Z. Y. Zhou, *Chem. Eng. Sci.* 2021, 235, p. 116491
[5] P. M. C. Lacey, *Chem. Eng. Res. Des.* 1943, 75, S49-S55

DEM-FEM Coupling Simulation for Improved Deformation Prediction in a Hot Isostatic Pressed Part

Wenqing Tian,[a, b, *] Runyu Yang,[a] Cao Cai[b]

[a]School of Materials Science and Engineering, UNSW Sydney, NSW 2052, Australia
[b]State Key Laboratory of Material Processing and Die & Mould Technology and School of Materials Science and Engineering, Huazhong University of Science and Technology, Wuhan, 430074, China
*Corresponding author: wenqing.tian@student.unsw.edu.au

Hot isostatic pressing (HIP) is an advanced manufacturing technique widely employed in aerospace and other industries. The HIP process subjects metal powders to high temperatures and isostatic pressure, yielding materials characterized by minimal porosity and enhanced mechanical properties. During the process, the powders undergoes substantial volumetric reduction, often exceeding 30%, facilitated by the external metal capsule. This significant densification presents considerable challenges in capsule design for near-net-shape component fabrication. Conventional trial-and-error approaches to overcome these challenges often result in increased production costs and extended lead times. The implementation of computational modeling and simulation to analyze powder densification dynamics in HIP offers a promising avenue for accurate deformation prediction and optimized capsule design, potentially enhancing process efficiency and economic viability.

While FEM simulations have traditionally been used to predict forming deviations, they struggle to accurately model the non-uniform shrinkage of powders during the HIP process. This limitation stems from the difficulty in representing the discrete nature and uneven distribution of particles within the capsule. To overcome these challenges, a new simulation approach that couples DEM with FEM has been developed. This integrates 3D particle relative density data into the FEM model, thereby enhancing its ability to capture the nuanced behavior of powder particles during consolidation. The effectiveness of this 3D particle DEM- FEM coupling simulation has been demonstrated through its application to a Ti-6Al-4V part.

The particles in the DEM model were scaled up by a factor of two compared to the original powder dimensions. A validation experiment was initially conducted to assess the accuracy of the DEM model by comparing the repose angle error between experimental and simulation results. The error in repose angles with the DEM model was found to be within 1°, demonstrating high accuracy. Subsequently, a DEM model of characteristic cross-sections of the target part was established to simulate the entire process from powder filling to vibration. The relative density distribution obtained from DEM simulations was integrated into the FEM model. To facilitate the large datasets transferring process, we developed Python scripts capable of efficiently handling cross-platform grid data and automating the assignment of relative density values within ABAQUS.

Compared to traditional FEM simulations, the new approach has significantly improved the prediction of structural deformation. Specifically, it achieved accuracy improvements of 26.47% and 33.75% in angle prediction for two characteristic cross-sections of the manufactured parts. The DEM-FEM coupling simulation not only demonstrates broad applicability in HIP but also introduces a new modeling paradigm for advanced manufacturing techniques that utilize metal particles as raw materials.

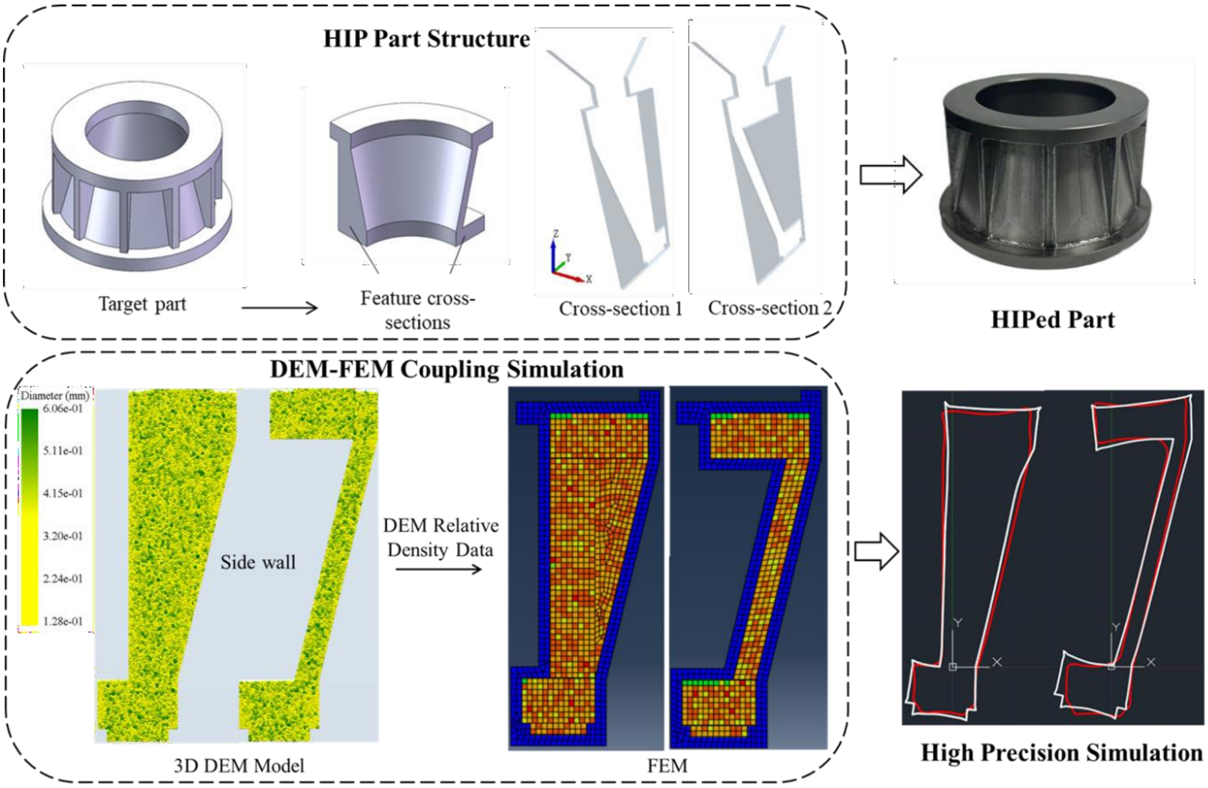

Figure 1. Schematic diagram of the DEM-FEM coupling simulation approach considering the initial particle packing state within the HIP capsule.

References

[1] C. Cai, X. Y. Gao, Q. Teng, et al, Mat Sci Eng A-Struct, 2018, 717, 95-104.
[2] D. D. You, Y. Wang, C. Yang, et al, J Mater Res Technol, 2020, 9, 3091-3108.
[3] S. Riehm, V. Friederici, S. Wieland, et al, Powder Metall., 2021, 64, 295-307.
[4] S. Sobhani, M. Albert, D. Gandy, et al, Journal of Manufacturing and Materials Processing, 2023, 7, 30.
[5] B. Elguezabal, J. M. Martínez-Esnaola, R. Soler, et al, Powder Technol., 2023, 425, 118599.
[6] A. Abena, M. Aristizabal, K. Essa, Adv. Powder Technol., 2019, 30, 2451-2463.
[7] A. Ahmadi, C. Wersäll, S. Larsson, Transp. Geotech., 2024, 47, 101272.

Scaled-up spout fluidized beds for heat release process of thermochemical particles in solar thermal power generation

Yuanhe Yue[a,b,c], Weiwei Zhao[a,b,c], Chenzhen Liu[a,b,c], Zhonghao Rao[a,b,c*]

[a] School of Energy and Environmental Engineering, Hebei University of Technology, Tianjin, 300401, China
[b] Hebei Engineering Research Center of Advanced Energy Storage Technology and Equipment, Hebei University of Technology, Tianjin, 300401, China
[c] Hebei Key Laboratory of Thermal Science and Energy Clean Utilization, Hebei University of Technology, Tianjin, 300401, China
*Corresponding author: raozhonghao@hebut.edu.cn

Bubbling fluidization is commonly used for heat exchange in thermochemical solar storage applications due to its strong heat and mass transfer performance. However, the unstable particle accumulation in the bubbling fluidization will unavoidably cause particle sintering and agglomeration, causing poor cyclability. In this work, we explore the heat release performance of a new configuration, a two-joint spout-fluidized bed, with special attention to particle sintering aspects. This study focuses on achieving scale-up effects of the spouted fluidized bed by allowing multiple deflected spouts to work together. The meso-scale hydrodynamics as well as the underlying mechanism of this new flow pattern is analyzed comprehensively through CFD-DEM approaches. After that, the system was adopted to the thermochemical Fe_3O_4-FeO system. It was demonstrated that this flow pattern has better heat transfer performance and reaction homogeneity. Moreover, the preliminary results show that the particle sintering was greatly alleviated under this system. This could be because the deflected spout provides much horizontal particle transport and needs fundamental study. This work provides some insights into the reactor design of heat exchangers for thermochemical heat storage particles in solar thermal power generation.

Application of Ironmaking Blast Furnace Transient Numerical Model to Study Innovative Operations for Decarbonisation

Ziguang Zhao, Xiaobing Yu, Yansong Shen*

University of New South Wales, Sydney, Australia
*Yansong Shen: ys.shen@unsw.edu.au

The blast furnace (BF) remains the dominant ironmaking reactor and is expected to continue playing a crucial role in the near and medium term. However, high CO_2 emissions present a significant challenge for sustainable BF operations. There is an urgent need for innovative strategies to reduce the carbon footprint of BF ironmaking. A key challenge lies in understanding the full impact of these innovative operations, particularly the time-dependent variations in in-furnace phenomena and potential abnormal performance. This research numerically investigates several decarbonisation strategies, including adjustments to burden properties, top gas recycling, and hydrogen injection, see **Figure 1**. Both steady-state and transient-state industrial-scale BF models are employed to simulate and evaluate these operations, providing a comprehensive assessment of their impact on furnace performance, energy efficiency, and CO_2 emissions.

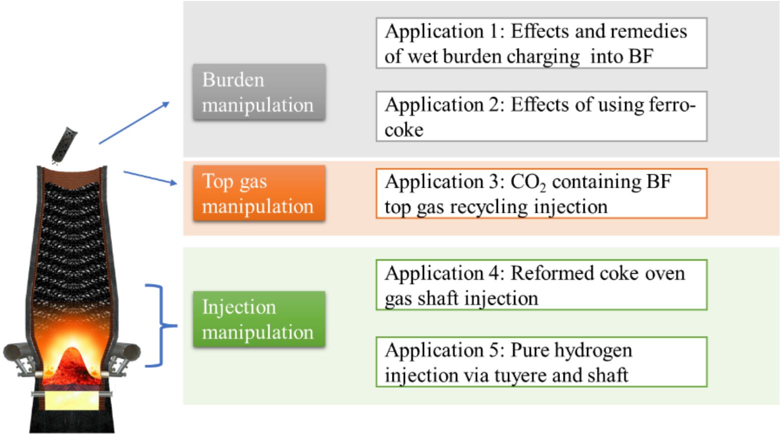

Figure 1. Applications of Ironmaking Blast Furnace Transient Numerical Model to Study Innovative Operations for Decarbonisation

The developed transient blast furnace (TBF) model features a layered burden structure and involves the interactions of flow-thermal-chemical reactions over time to represent the in-furnace phenomena evolution and predict BF performance in a dynamic manner. Time term is considered in the governing equations which is discretised by the finite volume method with implicit method, and SIMPLE method is employed to solve for the velocity-pressure field in a non-orthogonal mesh. The transient-state in-furnace phenomena have been successfully captured in terms of temperature field, fluid flows, key chemical reactions, the movement of the layered burden, dynamic stagnant zone, and the cohesive zone. Besides, the TBF model predicts the BF performance including coke rate, top gas temperature, top gas composition, and overall energy balance. The TBF model thus provides comprehensive insights into transient-state in-furnace phenomena and BF performance.

Moreover, the developed transient BF model attempts to explore innovative BF operations and abnormal BF operations, aiming to assess the feasibility, effects, and remedies for those operations. The specific sub-models are developed within the TBF framework, for these operations including a wet burden charging sub-model [1], a top gas recycling sub-model [2], sub-models for reformed coke oven gas shaft injection [3] hydrogen tuyere shaft co-injection [4] and ferro-coke charging sub-model [5]. The comprehensive analysis of the mentioned operations is conducted qualitatively and quantitatively. Several key findings in these operations include: as for the BF working conditions in this work, in the wet burden operation, the BF thermal conditions can be recovered in approximately 25 hours in terms of the top gas temperature after replacing the wet burden with the dry burden; in the ferro-coke charging operation, the mechanism of using ferro-coke is evaluated using the simulation results combined with the updated RIST diagram, and the coke saving can be achieved by improving the reduction efficiency of wustite-iron by CO inside the decreased temperature of thermal reserve zone; in the operation of the injection of CO2-containing BF top gas, it has the similar effects to blast moisture enrichment operation or oxygen enrichment operation, but with a decreased flame temperature; in the operation of the injection of reformed coke oven gas, it could be a preliminary step towards a hydrogen-enriched BF and the penetration issue requires more attention, while the distributed injection of pure hydrogen via tuyere and shaft aid in maintaining an acceptable BF running condition and achieving coke saving.

In summary, this transient ironmaking BF model contributes to the understanding of innovative and abnormal BF operations with a focus on BF CO_2 deduction and BF’s smooth operation. The TBF model proves to be a cost-effective tool for comprehensively investigating the strategies to maintain the smooth operations of BFs after changing the operating conditions, of which the results offer both theoretical and practical guidance.

References

[1]Z. Zhao, X. Yu, and Y. Shen, "Transient CFD study of wet burden charging on dynamic in-furnace phenomena in an ironmaking blast furnace: Impacts and remedies," *Powder Technology*, vol. 408, p. 117708, 2022.
[2]Z. Zhao, X. Yu, and Y. Shen, "Numerical study of the feasibility of injecting CO2-containing off-gas in an ironmaking blast furnace," *Fuel*, vol. 361, p. 130648, 2024.
[3]Z. Zhao, X. Yu, Y. Shen, Y. Li, H. Xu, and Z. Hu, "Model study of shaft injection of reformed coke oven gas in a blast furnace," *Energy & Fuels*, vol. 34, no. 11, pp. 15048-15060, 2020.
[4]Z. Zhao, X. Yu, Y. Li, J. Zhu, and Y. Shen, "CFD study of hydrogen co-injection through tuyere and shaft of an ironmaking blast furnace," *Fuel*, vol. 348, p. 128641, 2023.
[5]Z.Zhao, X. Yu, and Y.Shen, "Using ferro-coke in an ironmaking blast furnace – a virtual experiment", Submitted.

Low temperature CO_2 methanation using Ni-Al-Ce-La Layer Double Hydroxide catalyst

Haftu Gebretsadik Gebreegziabher[a], Noriaki Sano[b], Sakhon Ratchahat[c],
Tawatchai Charinpanitkul[a]

[a] Department of Chemical Engineering, Faculty of Engineering, Chulalongkorn University
[b] Department of Chemical Engineering, Faculty of Engineering, Kyoto University
[c] Department of Chemical Engineering, Faculty of Engineering, Mahidol University

Many CO_2-rich natural gas reserves in the world are difficult to utilize, as it requires the separation of a huge amount of CO_2. Thus, direct conversion of CO_2 mixed in valuable hydrocarbons to high-value chemicals allows utilizing the CO_2 emissions. From several conversion methods, catalytic decomposition is a promising method as it splits the gases directly into H_2 and carbon through consecutive combined processes of CO_2 methanation via Sabatier reaction (SR) and catalytic decomposition of methane (CDM). The main challenge in the SR is its kinetic favorability at high temperature and low yield of methane. One economical way to address such challenges is developing bi-functional (BF) catalysts, which exhibit both high catalytic capability and water adsorption capability for simultaneously lowering the reaction temperatures and removing the water to shift the reaction towards product. An unprecedented novel ternary composite catalyst for CO_2 methanation will be developed in this work. It is expected that the synergy of the metallic catalyst in nanoscale and the BF support would lead to high water sorption, high CO_2 binding, minimized CO production, and lower reaction temperatures. Meanwhile, CDM is a green process in producing H_2 and CNT, but it is performed at high temperatures and affected by carbon deposition. In this study, Ni-Al-Ce-La Layer Double Hydroxide catalysts will be developed for CO_2 and CH_4 decomposition to CNT and H_2. The main tasks of this work are catalyst synthesis, catalyst performance tests, and theoretical calculations. Through different techniques and DFT calculations, the performance of catalysts and the reaction mechanism will be discussed to provide novel insights into designing bifunctional Ni-Al-Ce-La Layer Double Hydroxide catalyst for simultaneous water adsorption and CO_2 methanation.

Numerical study on particle motion and deposition characteristics inside the film cooling holes of turbine blade

Wenjing Sun,* Jianghan Yu, Yuqiu Zheng, Jingzhou Zhang

Nanjing University of Aeronautics and Astronautics, Nanjing, China
*Corresponding author: wjsun@nuaa.edu.cn

Air pollutant particles will inevitably enter aero engines with the air, and they deposit on the surface of turbine blade, abrade the air film cooling channel, and clog the air film holes, etc. The particle deposition of turbine blade will directly affect the stable operation and cut lifespan of turbine blade, and even threaten the safe operation of engine. This paper focuses on exploring the particle motion and deposition characteristics inside air-film cooling holes. The Realizable k-ε turbulence model for gas flow and DPM model for particle phase, coupled with EI-Batsh particle deposition model are adopted in the numerical simulations. The effects of particle size and cooling air intake way on particle distribution and deposition characteristics in the air collecting chamber and film holes of the blade were systematically studied. The study shows that small particle diameter particles have good flowability and follow the cooling airflow along the leading edge of the film cooling holes, while large particle diameter particles have poor flowability and constantly collide with the wall and flow out of the film cooling holes. As the particle diameter increases, the deposition rate of the particles decreases significantly, and when the particle diameter is larger than 0.8μm, there is almost no deposition in the film cooling holes. Under the condition of double-direction air intake in the air collection chamber, the particles in the single-direction film cooling holes showed the phenomenon of more deposition in the film cooling holes at both ends and less deposition in the middle; under the condition of single-direction air intake, the deposition rate of particles was the largest in the film cooling holes far away from the cooling flow inlet, and there was almost no deposition in the film cooling holes close to the inlet.

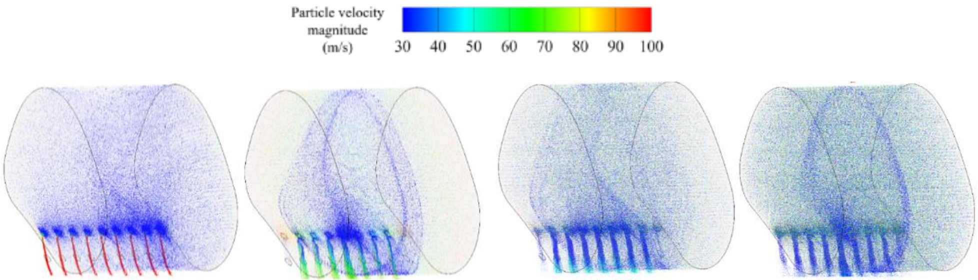

(a) d_p=2.5μm (b) d_p=10μm (c) d_p=17.5μm (d) d_p=25μm

Figure 1. Particle distribution characteristics in gas collection chamber for different particle sizes

Multiscale kinetic theory for heterogeneous granular and gas-solid flows

Bidan Zhao, Junwu Wang*

College of Mechanical and Transportation Engineering, China University of Petroleum, Beijing 102249, P. R. China
*Corresponding author: jwwang@cup.edu.cn

It has been recognized that the particle phase stress model derived from classical kinetic theory is valid only when sufficient scale resolution is offered to explicitly resolve the heterogeneous structures during numerical simulations, however, industrial applications prefer to use coarse computational grids where the heterogeneous structures are not explicitly resolved but implicitly modeled. Unfortunately, in this case a kinetic theory for heterogeneous granular and gas–solid flows is not available yet. To this end, an attempt was made to tracking this challenge: The single particle velocity distribution function at the nonequilibrium stationary state with heterogeneous structures was firstly derived by combining the idea of doubly stochastic Poisson processes or superstatistics with the concept of compromise in competition in the EMMS (Energy Minimization Multi-Scale) theory, the standard Chapman-Enskog method was then used to develop the constitutive relations of heterogeneous continuum theory. It was found that (i) seven state variables are needed to quantify the heterogeneous structures as compared to three for homogeneous systems; (ii) the constitutive relations not only include the contribution from microscale particle–particle interactions but also those due to the interactions between mesoscale structures; and (iii) the resultant constitutive relations are much more complex than those of homogeneous systems due to the simultaneous consideration of microscale and mesoscale contributions and the appearance of cross-coupling effects, but they correctly contain the constitutive relations of homogeneous systems as a limiting case. Finally, the theory was coupled with an EMMS drag model to offer a preliminary validation and to provide a unified EMMS-based constitutive relations for heterogeneous gas–solid flows.

Simulation of the biomass gasification process of cubic particles in a fluidized bed using the superquadric method

Jun Xie,[a,*] Hao Xu,[a] Xinhe Shen[b]

[a] School of Energy and Mechanical Engineering, Nanjing Normal University, Nanjing, PR China
[b]Southeast University, City, Nanjing, PR China
*Corresponding author: xiejun0218@126.com

An efficient biomass gasification process requires a comprehensive understanding of the physical and chemical phenomena occurring at multi-length and time scales. The non-spherical shape of biomass particles increases the difficulty of multi-scale simulation. In this study, a multiscale computational approach was developed and validated for cubic biomass by integrating a superquadric particle method with chemical reaction kinetics and computational fluid dynamics in open-source code MFiX [1]. The recently developed superquadric DEM model was employed to describe the non-spherical particle-particle contact and gas-particle interaction [2]. The De Felice-Holzer/Sommerfeld hybrid model was used to calculate the drag force on particles, and Richter & Nikrityuk correlation was employed for gas-solid heat transfer [3]. Drying, pyrolysis, gasification, combustion, water-gas shift reactions were considered for gasification process. In the particle reaction model, it is assumed that the size of cubic particle shrinks with the constant density and particle shape (same aspect ratio).

The established model was first validated by comparing with experimental data for the combustion of a single cuboid particle. Then the gasification process of cubic biomass in a bubbling fluidized bed is simulated. The cubic biomass particles were continuously fed from the inlet of left wall. The flow pattern, temperature and gas component distributions inside the bed are presented, as shown in Figures 1 and 2. The effects of key operating parameters on product gas compositions are studied in terms of biomass size, bed temperature, and air equivalent ratio. The particle-scale characteristics such as the evolution process of particle size, temperature, and component were emphatically analyzed.

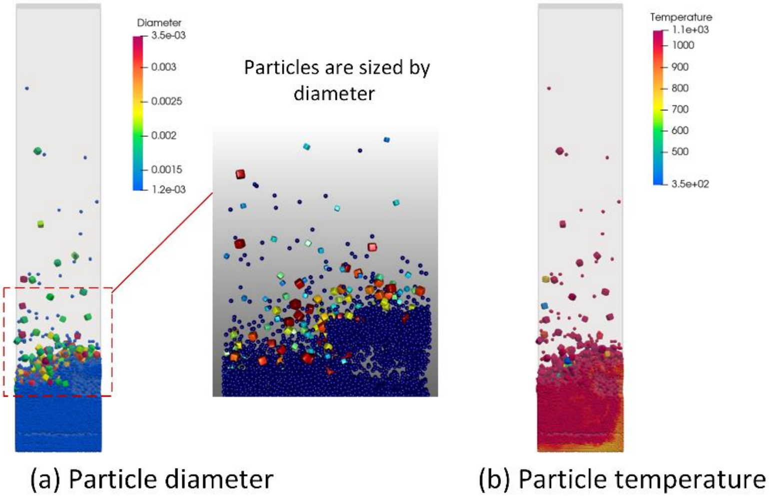

(a) Particle diameter (b) Particle temperature

Figure 1. Particle size and temperature inside the bed.

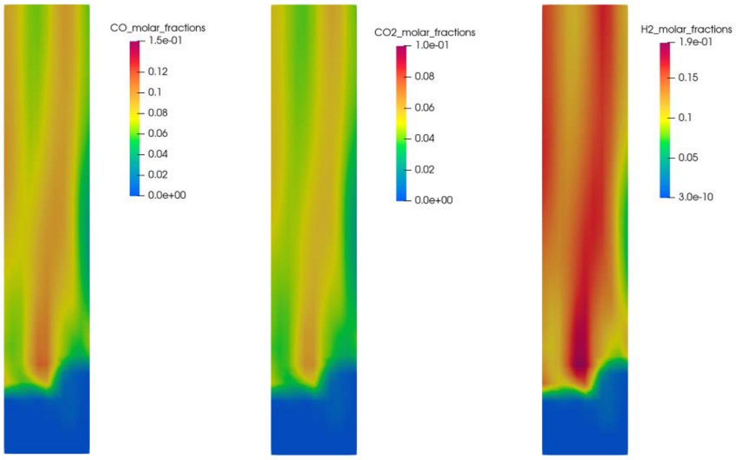

(a) CO (b) CO_2 (c) H_2

Figure 2. Distributions of gas compositions inside the bed.

References

[1]Lu, L., X. Gao, J.-F. Dietiker, et al., MFiX based multi-scale CFD simulations of biomass fast pyrolysis: A review [J]. Chem. Eng. Sci., **2022**, 248: 117131.

[2]Gao, X., J. Yu, L.Q. Lu, et al., Coupling particle scale model and SuperDEM-CFD for multiscale simulation of biomass pyrolysis in a packed bed pyrolyzer [J]. Aiche J., **2021**, 67(4).

[3]Gao, X., J. Yu, L. Lu, et al., Development and validation of SuperDEM-CFD coupled model for simulating non-spherical particles hydrodynamics in fluidized beds [J]. Chem. Eng. J., **2021**, 420: 127654.

An environmentally friendly depressant in the selective flotation of magnesite and calcite: selective inhibition and adsorption mechanism

Yong Mao, Wengang Liu*, Yanbai Shen, Wenbao Liu

Northeastern University, Shenyang, China
*Corresponding author: liuwengang@mail.neu.edu.cn

The similar crystal structures and chemical properties of magnesite and calcite make their effective separation through flotation challenging. This study explores the use of Glutamic acid diacetic acid tetrasodium salt (GLDA), a novel environmentally friendly chelating reagent, to enhance the flotation separation of magnesite and calcite. Flotation test results indicate that in a sodium oleate (NaOL) system, GLDA selectively inhibits the flotation of calcite. Under optimal conditions (slurry pH=9.20, GLDA 15 mg/L, and NaOL 140 mg/L), a flotation concentrate with an MgO grade of 46.21%, CaO grade of 1.39%, and an MgO recovery rate of 73.17% was achieved. GLDA minimally affects the hydrophobicity of magnesite but significantly reduces the hydrophobicity of calcite. The selective inhibition mechanism of GLDA was investigated using zeta potential measurements, FTIR, and XPS analyses. Results show that GLDA selectively reacts with Ca sites on the calcite surface, adsorbing and covering it, thereby preventing NaOL from adsorbing on the calcite. Conversely, GLDA has a minor impact on the Mg sites on the magnesite surface, resulting in a negligible effect on NaOL adsorption by magnesite. Consequently, GLDA enhances the flotation separation efficiency of magnesite and calcite. The research results have potential for application in the purification of low-grade magnesite ore.

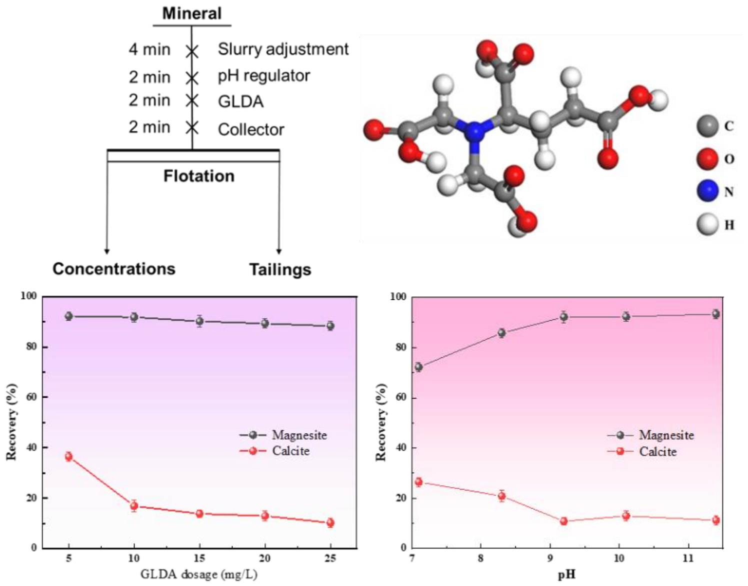

Figure 1 Enhanced magnesite and dolomite flotation separation by GLDA

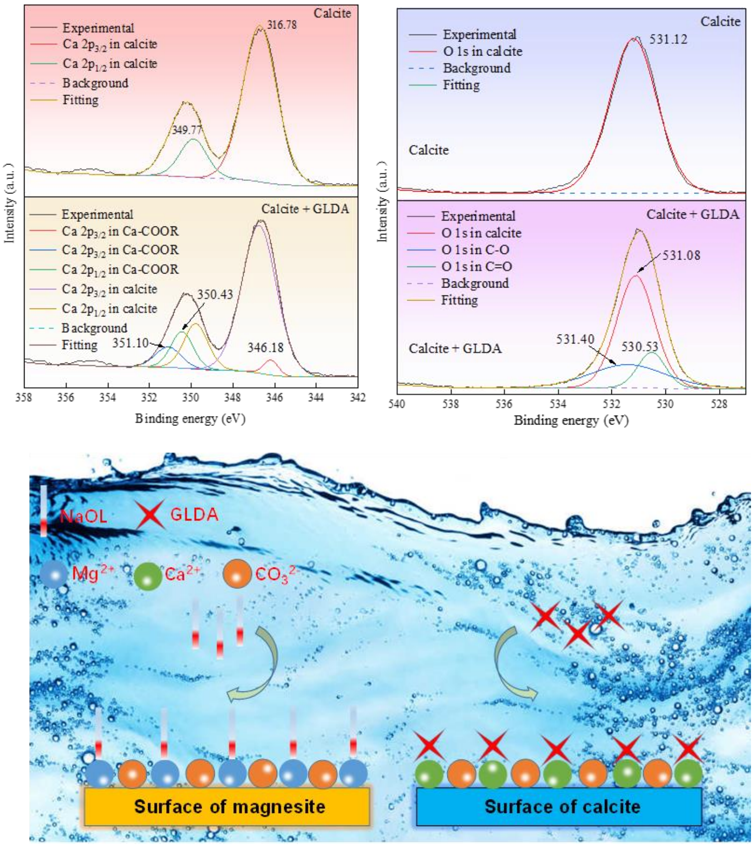

Figure 2 Adsorption mechanism of grinding aid GLDA on the surface of magnesite and dolomite

Numerical study on the influence of cell size and turbulence on the behavior of slurry particles inside a three-dimensional rotating drum

Ikki Adji Dharma,[a,*] Yun-Chi Chung,[a] Li-Shin Lu,[b] Shu-San Hsiau[a]

[a] Department of Mechanical Engineering, National Central University, Taoyuan, Taiwan
[b] Department of Industrial Engineering and Management, National Quemoy University, Kinmen, Taiwan
*Corresponding author: ikkiajidharma@gmail.com

The simulation of complex multiphase flows and other industrial issues often relies on a coupling scheme that integrates the computational fluid dynamics (CFD) and the discrete element method (DEM). This coupling scheme depends on several parameters, particularly cell size and turbulence model selection, significantly influencing result accuracy. However, researchers often need more explicit guidance on these factors when dealing with industrial problems, necessitating the development of guidelines to reduce relative errors. In this study, sensitivity tests were conducted on different types of cell sizes and turbulence models to evaluate the impact of each parameter and determine the optimal options for accurately modeling the slow particle flow of slurry inside a rotating drum. The cell size ranged from 3 to 5 times the particle diameter. The analysis included two turbulence models, laminar and K-ω SST. Additionally, various liquids with different viscosities were chosen as parameters. The simulation was performed in a rotating drum with a diameter of 0.2 meters, containing a specific liquid and 2200 glass beads. To assess the results, the dynamic angles of repose acquired from previous study were compared with the simulation data. The findings reveal that a cell size of three times the particle diameter yields accurate predictions, particularly for low-viscosity scenarios. On the other hand, larger cell sizes demonstrate better results, particularly in scenarios involving higher viscosity levels.

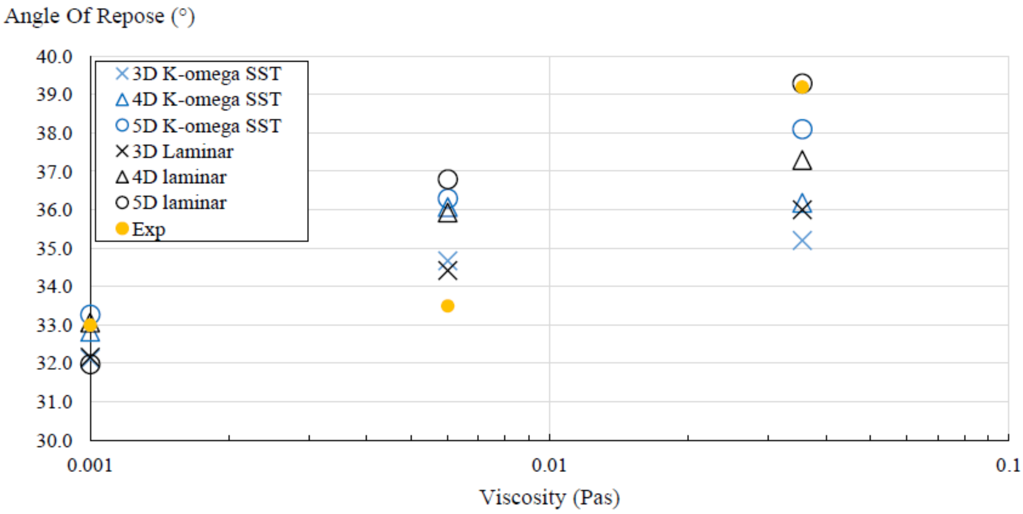

Figure 1. Graph of Angle of Repose at 0.1 rad/s and 0.2 filling degree.

References

[1] F. Marchelli, C. Moliner, B. Bosio, and E. Arato, *Powder Technol* **2019,** vol. 353, pp. 409–425.
[2] S. H. Chou and S. S. Hsiau, *Powder Technol* **2012,** vol. 226, pp. 99–106,

Numerical study and parameters investigation of aerosol droplets in aerosol jet printing process

Xiaojing Bai [a], Minshu Zhan [b], Qijun Zheng [c,*], Aibing Yu [c,d,*]

[a] School of Energy and Environment, Southeast University, Nanjing 210096, China
[b] Institute for Process Modeling and Optimization, Jiangsu Industrial Technology Research Institute, Suzhou 215123, China
[c] Centre for Simulation and Modelling of Particulate Systems, Monash-Southeast University Joint Research Institute, Suzhou, 215123, China
[d] ARC Research Hub for Smart Process Design and Control, Department of Chemical and Biological Engineering, Monash University, Australia
*Corresponding author: qijun.zheng@monash.edu

Aerosol jet printing (AJP) is a direct-write printing technique, which as a type of additive manufacturing that has great potential in the fields of electronics, new energy, microelectronics and micro and nano manufacturing. However, there are also some problems in the application of this technique, such as unstable deposition structure and poor repeatability. Understanding the complex phenomena of gas-liquid interaction in the Aerosol jet printing (AJP) process is critical to improve the quality and production rate of printing devices. In this work a multiphase discrete phase model (DPM) based on computational fluid dynamics (CFD) is utilized to simulate the flowing/depositing behaviors of droplets in the AJP process. The model takes into account the gas-droplet coupling, coalescence, and various contact boundary conditions of droplets on the wall. Good agreements are achieved between the simulation results and the flow field/printed architecture obtained experimentally, providing validation for the model and interpretation of the multiscale dynamics in typical AJP process. The results also show that the initial particle size of aerosol droplets has an important influence on the droplet transport and the final deposition of the AJP process, and thus the products printed. The model provides an in-depth understanding of the mechanism of droplets growth and deposition, which offers a valuable tool for the optimization of AJP process and control of product properties.

Coupling computational fluid dynamics and finite element method (CFD-FEM) for modelling dense particle-fluid flows

Yinghui Wu,[a, b] Qijun Zheng, [a, b,] * Liuyimei Yang,[c] Aibing Yu[a, b]

[a] Department of Chemical Engineering, Monash University, Clayton, Vic 3800, Australia
[b] Southeast University-Monash University Joint Research Institute, Suzhou, 215123, China
[c] Ganjiang Innovation Academy, Chinese Academy of Sciences, Ganzhou, 341119, China
* Corresponding author: Qijun.Zheng@monash.edu

Dense particle-fluid flows are encountered in a variety of natural and industrial processes, in which the particles can exhibit complex flowing or stagnant behaviours. The common Two-Fluid Model (TFM) was built upon the kinetic theory of granular flow and often meets difficulties when the particles become dense. Focused on the dense particle systems, this work proposes a method to couple the computational fluid dynamics (CFD) and the finite element method (FEM), in which the CFD simulates the fluids, and the FEM simulates the dense particles. The FEM allows using a visco-elastoplastic constitutive relationship to describe both the quasi-statics and flow rheology of granular materials. The CFD-FEM is tested in several typical particle-fluid systems, including the packed bed, spouted bed, and granular column collapse. The results demonstrate that this CFD-DEM not only can model the flow of particle-fluid mixture such as bubbles, but also reproduces a truly quasi-static pile of particles and its inherent force transmission. This provides a feasible approach for a wide range of dense particle-fluid flows and will significantly enhance the capacity of particle-fluid modelling in natural and industrial applications.

Predicting Railway In-train Forces from ATO Measurements - a Data-driven Approach

Sheng Zhang, Pu Huang, Wenyi Yan*

Department of Mechanical and Aerospace Engineering, Monash University, Australia
*Corresponding author: Wenyi.yan@monash.edu

Railway in-train forces are an essential element in assessing railway many aspects of rolling stocks. Conventional methods for obtaining the forces, such as field measurements and longitudinal train dynamics simulations (LTSs), can be time-consuming and require significant investment in manpower and domain expertise, while only allowing for the data collection on a single specified service condition at a time. However, automatic train operation (ATO) systems can measure real-time information of trains and tracks by on-board and trackside sensors, which could provide an opportunity for predicting in-train forces. This paper presents a data-driven approach that uses ATO-measured data to predict in-train forces under service conditions. To develop this approach, LTSs for a heavy haul train were conducted to establish the relationship between ATO measurements and specific in-train forces, which was embedded in a large amount of training data. After that, a specially developed self-attention based causal convolutional neural network (SA-CNN) was employed to learn the underlying relationship and predict the in-train force histories by considering the dependencies of current and past time steps. The performance of SA-CNN was compared with four different neural network models, and the predicted results demonstrated that all the well-trained models can accurately predict in-train forces. Furthermore, the generalisation ability of the well-trained SA-CNN model was verified with LTS under four different service conditions. The results showed that the proposed data-driven approach has superior compatibility for any arbitrarily combined inputs with significantly reduced computational time compared to LTSs. This approach has the potential to realise quick and reliable in-situ monitoring of railway in-train forces, which is beneficial to both in-train force related research and industrial applications. This research work has been published in [1].

References

[1] S. Zhang, P. Huang and W. Yan. A Data-driven Approach for Railway In-train Forces Monitoring. *Advanced Engineering Informatics* **2024**, 59, 102258..

Structure characterisation of active particles and comparison with granular particles

Kejun Dong*, Ruizhi Jin, Jigar Modi

School of Engineering, Design and Built Environment, Western Sydney University, Penrith NSW 2751, Australia
*Corresponding author: kejun.dong@westernsydney.edu.au

Active particles are increasingly used as models to study the fundamentals of the collective behaviour of living and non-living systems. Compared with granular particles, active particles can consume energy to *actively* move according to their comprehension of the environment and neighbour particles, and the system can undergo different disorder-order transitions based on the local movement rules of individual particles. Studies in the literature have shown two interesting points: first, the disorder-order transitions of active particles are often associated with specific local structures, and second, some of these structures are comparable to those formed in the disorder-order transitions of granular particles. However, the structure evolution of active particles associated with the disorder-order transitions is not well understood.

In this study, several active particle systems are studied by the classical Vicsek model and a modified model with repulsion and attraction layers considered. In addition, instability in particle interaction is also considered. The disorder-order transitions of these active particle systems are numerically studied under different conditions. In particular, the structures of active particles are characterized by various parameters. The structure signature associated with the disorder-order transitions is analysed and the structure evolution is compared with those in the order transition of granular particles. Through these studies, the disorder-order transitions of active systems can be more clearly understood from the perspective of structure evolution. Furthermore, the common mechanism of the disorder-order transitions of active and passive (granular) particles is explored.

References

[1] Tamás Vicsek, András Czirók, Eshel Ben-Jacob, Inon Cohen, and Ofer Shochet, *Physical review letters* **1995**, 75(6), 1226.
[2] Iain D Couzin, Jens Krause, Richard James, Graeme D Ruxton, and Nigel R Franks, *Journal of theoretical biology* **2002**, 218(1), 1-11.
[3] KJ Dong, RY Yang, RP Zou, XZ An, and AB Yu, *Europhysics Letters* **2009**, 86 (4), 46003.
[4] Jesse L Silverberg, Matthew Bierbaum, James P Sethna, and Itai Cohen, *Physical review letters* **2013**, 110(22), 228701.
[5] Alexandre P Solon, Hugues Chaté, and Julien Tailleur, *Physical review letters* **2015,** 114(6), 068101.
[6] Lucas Barberis, *Physical Review E* **2018**, 98(3), 032607.
[7] R Amirifar, KJ Dong, QH Zeng, XZ An, and AB Yu, *Powder technology* **2021**, 380, 47-58.

Interaction forces of patchy gold nanoparticles derived from molecular dynamics simulation

Pan Yang, Qinghua Zeng*, Kejun Dong and Haiping Zhu

School of Engineering, Design and Built Environment, Western Sydney University, Locked Bag 1797, Penrith, NSW 2751, Australia
*Corresponding author: q.zeng@westernsydney.edu.au

Exploring the interactions forces between nanoparticles is of great significance, yet with many challenges [1-4]. The present work is to calculate the interparticle forces of gold nanoparticles (AuNPs) with a size ranging from 3 to 20 nm by molecular dynamics (MD) simulation and compare their results with those derived from Hamaker equation. Specific attention has been focused on surface patchy AuNPs such as surface metal patches and surfactant modification. Our MD results have generated a fitted interparticle force model, while the Hamaker method obviously underestimates the interparticle forces under short particle separation. Besides, the interactions of AuNPs are independent of the rotated angle as they can still hold the spherical symmetry during their head-on contact. For surface modified AuNPs, those with either Pt or Pd patches are capable to enhance the interactions of two identical AuNPs, while those with either Ni or Ag patches adversely affect their interactions. In addition, AuNP with attached surfactants hamper the interactions of AuNPs due to the early spatial repulsion generated by surfactants. The present investigations and the observed phenomena are valuable not only for generating quantitative force models of patchy nanoparticles but also for opening new ways for guiding nanoparticle self-assembly.

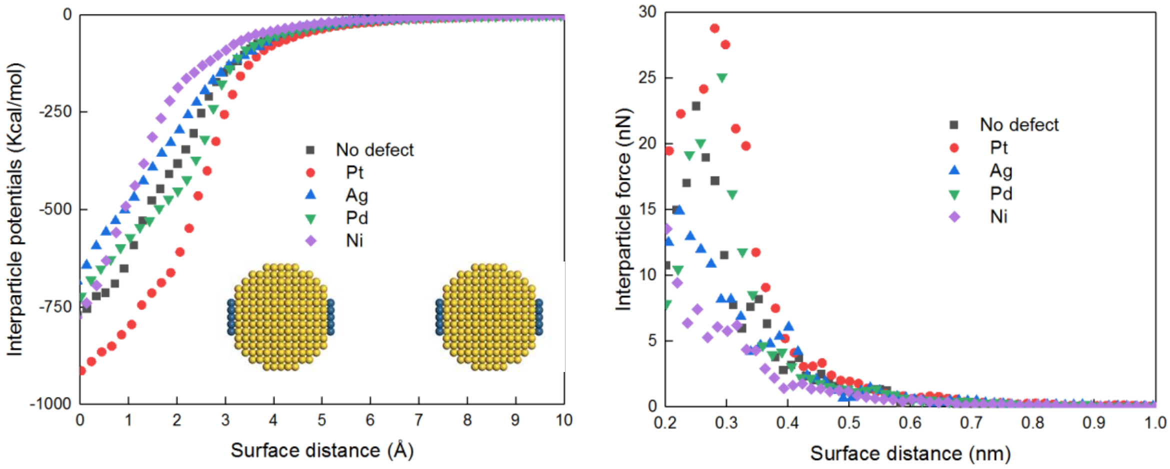

Figure 1. Interactions of a pair of patched AuNPs (d=3 nm) with a single patched layer as a function of surface distance derived from MD simulation: interparticle potentials (left) and interparticle forces (right).

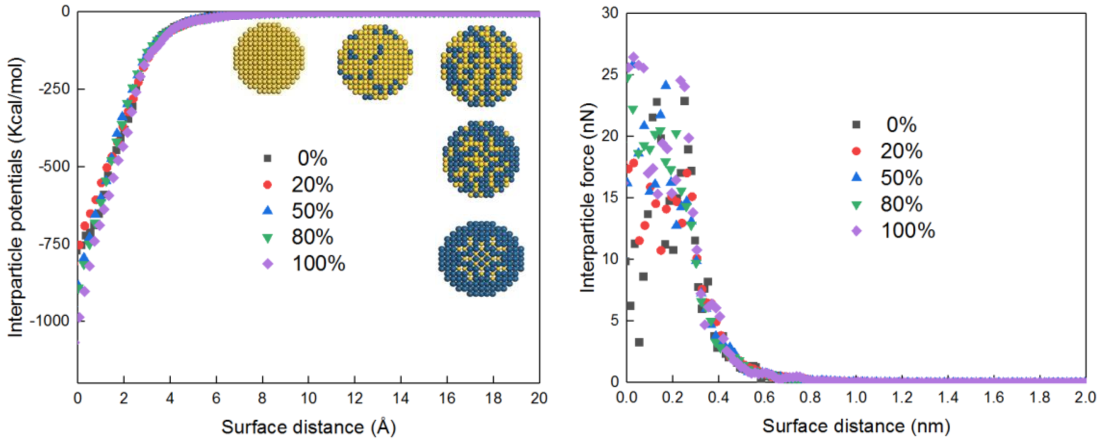

Figure 2. Interactions of a pair of patched AuNPs (d=3 nm) with different percentage of surface patches as a function of surface distance derived from MD simulation: interparticle potentials (left) and interparticle forces (right).

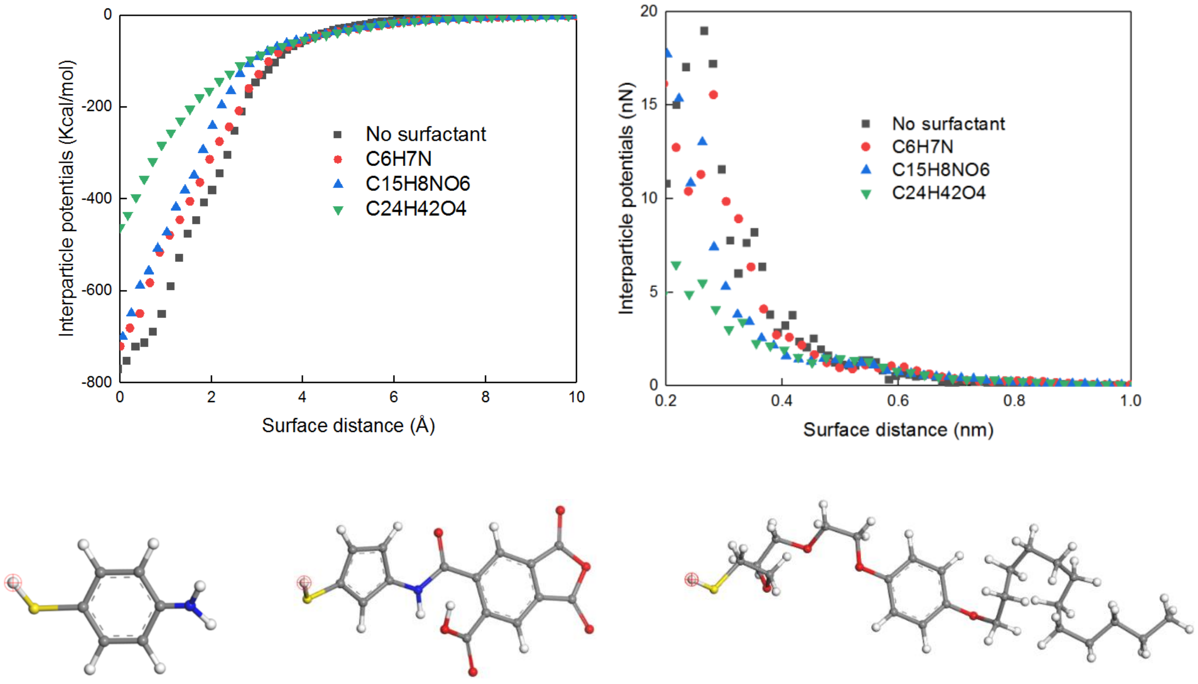

C_6H_7N-S $C_{15}H_8NO_6$-S $C_{24}H_{42}O_4$-S

Figure 3. Interactions of a pair of patched AuNPs (d=3 nm) with different surfactant patches as a function of surface distance derived from MD simulation: interparticle potentials (left) and interparticle forces (right).

References

[1] Q. H. Zeng, A. B. Yu, G. Q. Lu, *Industrial and Engineering Chemistry Research*, **2010**, 49, 12793-12797.
[2] W. F. Sun, Q. H. Zeng, A. B. Yu, *Powder Technology*, **2017**, 314, 2-8.
[3] P. Yang, Q. H. Zeng, K. J. Dong, H. P. Zhu, A. B. Yu, *Nanomaterials*, **2020**, 10, 1293.
[4] P. Yang, Q. H. Zeng, K. J. Dong, H. P. Zhu, *Powder Technology*, **2020**, 362, 501-506.

Fully-Resolved Simulation of Newtonian and non-Newtonian Particle Flows

Mohammad Fazli,[a,b*] Shibo Kuang,[a] Murray Rudman,[b] Aibing Yu [a]

[a] ARC Research Hub for Smart Process Design and Control, Department of Chemical and Biological Engineering, Monash University, VIC, 3800, Australia
[b] Department of Mechanical and Aerospace Engineering, Monash University, VIC, 3800, Australia
*Corresponding author: mohammad.fazli1@monash.edu

Suspensions are widely encountered in engineering applications, including mining and the oil and gas industries. The behaviour of suspension flows in industrial processes, such as transportation and sedimentation, is highly dependent on the interaction between liquid and particles. The presence of multi-sized particles in realistic suspensions, consisting of a mixture of fine particles and a carrier fluid, creates a complex rheological behaviour (e.g., yield-pseudoplastic) for coarse particles, which greatly affects their transportation and sedimentation in particulate systems. This talk presents our efforts to simulate the interaction of particles of different sizes with both Newtonian and non-Newtonian carrier fluids and its influence on transportation and sedimentation rates. In this regard, CFD-DEM simulations are conducted for suspension flows using the Immersed Boundary Method (IBM), as a fully-resolved approach, to accurately capture fluid-particle and particle-particle interactions in these systems. The results clearly demonstrate how particle size distribution and the rheological characteristics of the carrier fluid can affect the behaviour of suspension flows in different engineering processes.

Effect of particle shape on tribocharging in horizontal pneumatic transport

Fayuan Huang,[a] Shibo Kuang,[a,]* Ruiping Zou,[a] Aibing Yu,[a,b]

[a] ARC Research Hub for Smart Process Design and Control, Department of Chemical and Biological Engineering, Monash University, Clayton, Victoria, 3800, Australia
[b] Center for Energy and Environment, Southeast University-Monash University Joint Research Institute, Suzhou, 215123, China
*Corresponding author: Shibo.kuang@monash.edu

The tribocharging phenomenon in pneumatic conveying, resulting from repeated interactions between particles and between particles and the pipe walls, can cause various issues such as particle clustering, adhesion to pipe walls, and potentially fires and explosions. This phenomenon is significantly influenced by particle shape. Investigating tribocharging behaviour during pneumatic conveying, particularly with particles of different shapes, has been challenging due to equipment limitations and the lack of numerical models.

This study presents a numerical investigation of the tribocharging process, focusing on particles with different shapes during pneumatic conveying. The investigation is achieved by integrating computational fluid dynamics (CFD) with the discrete element method (DEM). An in-house CFD-DEM model, developed through continuous efforts, incorporates a condenser model that considers frictional charge. This model accounts for impact charge, frictional charge, and electrostatic interactions between the pipe wall and particles of varying shapes, the working process for the model is illustrated in Figure. 1. The CFD-DEM coupling for non-spherical particles is also achieved and validated.

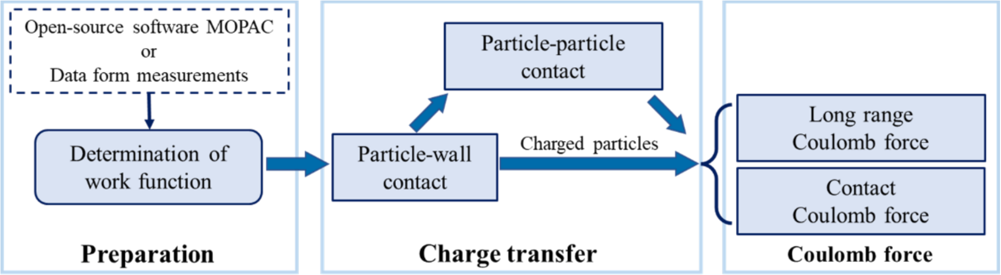

Figure 1. Working process of the charging model.

The charging model and the CFD-DEM coupling for non-spherical particles are validated by comparing simulation results with experimental measurements. Subsequently, the model is used to explore particle tribocharging behaviour under various conditions, including different particle shapes, gas velocities and solid concentrations. The cumulative charge and its effect on the performance of pneumatic conveying are analysed. The charging curves for different particle shapes and operating conditions are shown in Figure 2. Additionally, the flow characteristics are examined to understand the charging phenomena of particles with different shapes.

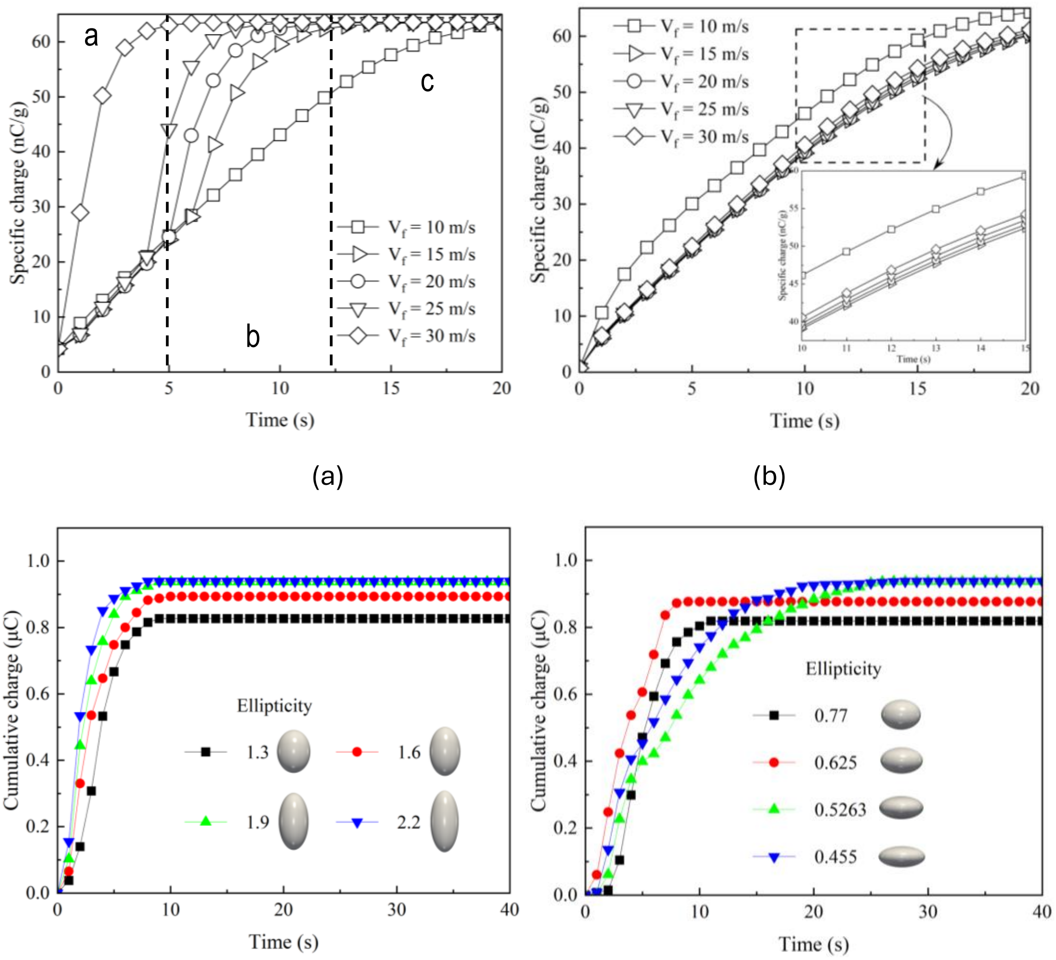

(a) (b)

(c) (d)

Figure 2. The charging profile for spherical ((a) and (b)) and ellipsoid particles ((c) and (d)).

This study underscores the significant impact of tribocharging in pneumatic conveying and provides valuable insights for optimizing pneumatic conveying systems to mitigate these effects.

Numerical simulation study of sludge drying process based on CFD-DEM

Gong Li,[a,b,c] Hao Zhang,[b,d,]* Aibing Yu,[a,c] Zongyan Zhou[e]

[a]ARC Research Hub for Smart Process Design and Control, Department of Chemical and Biological Engineering, Monash University, Melbourne, Australia
[b]Key Laboratory of Energy Thermal Conversion and Control of the Ministry of Education, School of Energy and Environment, Southeast University, Nanjing, China
[c]Southeast University-Monash University Joint Research Institute, Suzhou, China
[d]Key Laboratory for Ecological Metallurgy of Multimetallic Mineral of Ministry of Education, School of Metallurgy, Northeastern University, Shenyang, China
[e]Jiangxi Provincial Key Laboratory for Simulation and Modelling of Particulate Systems, Jiangxi University of Science and Technology, Nanchang, China
*Corresponding author: zhangh@mail.neu.edu.cn

Sludge drying is a crucial part in the sludge treatment and disposal processes, while thermal drying has been a popular choice. In this work, the sludge thermal drying process is numerically simulated using coupled computational fluid dynamics-discrete element method (CFD-DEM) approach. The CFD-DEM model describes the flow and heat transfer in the gas-solid system, while a mass transfer approach is embedded to describe the variation of the moisture content. Firstly, a suitable numerical model to describe the sludge water removal process is developed based on physical experimental data. Quantitative comparisons with experimental data validate the predictive capability of the numerical model for the continuum gas flow field as well as the sludge drying process. Then, five key parameters including velocity, temperature and humidity of the heat source, particle size and sludge pile thickness are discussed so as to obtain the basic laws affecting the sludge drying process, as shown in Figure 1. The pilot dryer is subsequently simulated and a simplified solution for industrial scale simulation is proposed. All the above work is supported by abundant experimental data to demonstrate the capability of the CFD-DEM model.

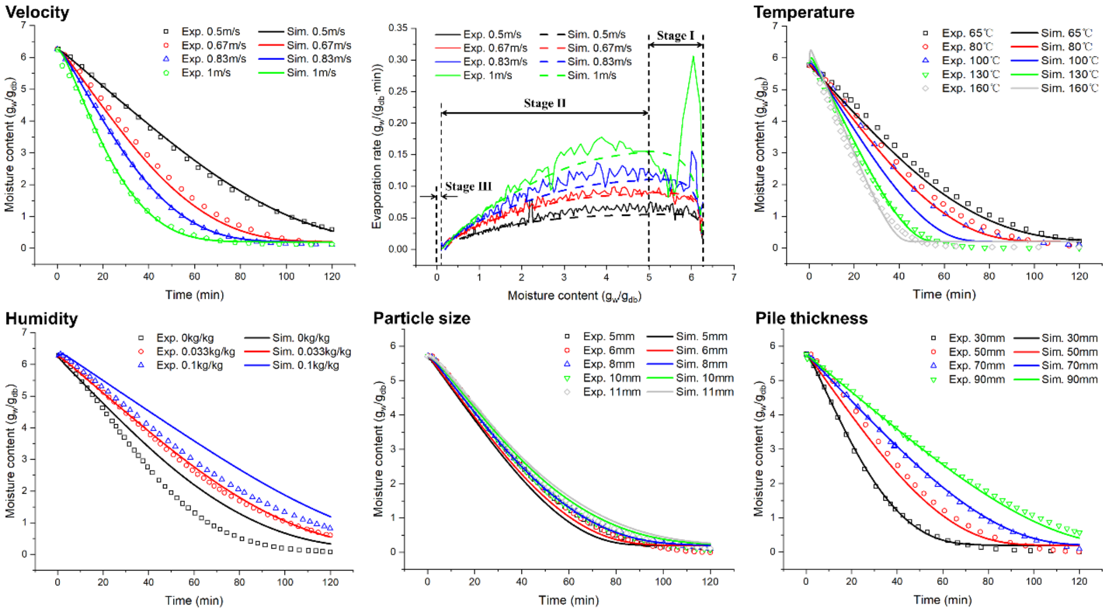

Figure 1. Simulation and experimental results of key parameters affecting sludge drying process.

Finally, based on more CFD-DEM simulations, the critical process parameters such as sludge residence time of each layer and air supply form in the dryer are investigated, as shown in Figure 2.

The optimal operating conditions are determined with flexibility recommendations for dryer design summarized. This work contributes to in-depth understanding of sludge drying characteristics and also facilitates the design and optimization of high-efficiency dryers, which has important practical and theoretical engineering value.

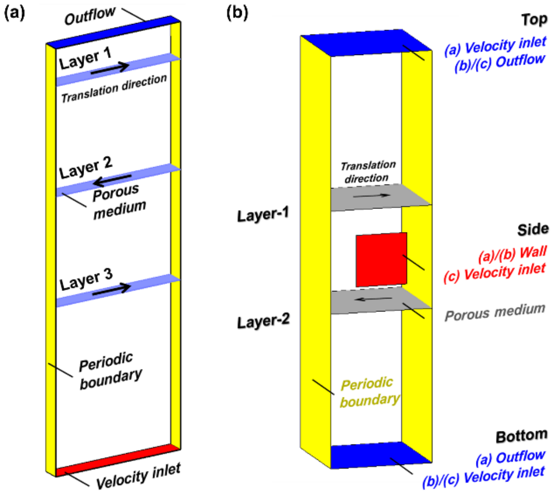

Figure 2. Modelling schematic of the dryer process parameters: (a) sludge residence time of each layer, (b) air supply form.

References

[1] G. Li, H. Zhang, X. Ye, Y. Su, A. Yu, Y. Tan, *IECR* **2023**, 62, 16990-17007.